

NATIONAL AERONAUTICS AND SPACE ADMINISTRATION

065209

**FINAL REPORT
NASA/NAGW-2324***INFRARED IMAGING, SPECTROSCOPIC, &
PHOTOMETRIC STUDIES OF COMETS*

Robert D. Gehrz, Principal Investigator
Department of Astronomy
University of Minnesota
116 Church St. SE
Minneapolis, MN 55455
Telephone: 612-624-7806
E-Mail: gehrz@astro.spa.umn.edu

We have continued our program of infrared (IR) photometric, imaging, spectroscopic, and polarimetric temporal observations of comets to study the properties of comet dust and comet nuclei. During the first two years we digitized our IR data base on P/Halley and other recent comets to facilitate further analysis and comparison with other data bases, and found compelling evidence for the emission of a burst of small grains from P/Halley's nucleus at perihelion. We reported imaging and photometric observations of Comets Austin 1990 V and Swift-Tuttle 1992. The Swift-Tuttle 1992t observations included IR photometry, several 7-14 μm long-slit spectra of the coma and a time-sequence of more than 150 10 μm broadband images of the coma. An analysis of near-IR images of the inner coma of P/Halley obtained on three consecutive nights in 1986 March showed sunward jets. We completed our analysis of IR imaging spectroscopic photometric data on comets. We also obtained observations of Comets Hyakutake 1996 B2 and Hale/Bopp 1995 01.

We obtained infrared imaging, photometric, spectroscopic and polarimetric temporal observations of bright comets using a network of five telescopes, with emphasis on simultaneous observations of comets at many wavelengths with different instruments. Our program offers several unique advantages: 1) rapid observational response to new comets with dedicated infrared telescopes; 2) observations within a few degrees of the sun when comets are near perihelion and 3) access to advanced infrared array imagers and spectrometers. In particular, reduction, analysis, publication and archiving of our Jupiter/s1-9 and Comet Hyakutake infrared data received special emphasis.

Instrumentation development included installation of the latest version of the innovative FORTH telescope control and a data acquisition system that enables us to control three telescopes

remotely by telephone from anywhere in the world for comet observations in broad daylight. We have acquired more than 3000 256x256 images totaling nearly two gigabytes of data detailing the near-IR development of the impact sites of the S-L9 fragments on Jupiter. These data were obtained using the University of Rochester Imaging IR Camera at the cassegrain focus of the 92" at WIRO. The WIRO data set covers 8 days and is, to our knowledge, one of the most extensive observational records of the S-L/Jupiter encounter obtained by any ground-based telescope. This program benefitted from the compilation during these last few months of an upgrade to the data acquisition program at WIRO with support of this NASA contract.

Publications (copies attached):

- "Measurement of Submicron Grains in the Coma of Comet Hale-Bopp C/1995 01 During 1997 February 15-20 UT," D. M. Williams, C. G. Mason, R. D. Gehrz, T. J. Jones, C. E. Woodward, D. E. Harker, M. S. Hanner, D. H. Wooden, F. C. Witteborn, H. M. Butner, 1997, *Ap. J. Letters*, 489, L91.
- "Infrared Observations of Comets," R. D. Gehrz, *Int'l. Comet Quarterly*, Smithsonian Astrophysical Observatory, April, 1997, Vol. 19, No. 2.
- "Ground-Based Near-Infrared Imaging of Comet P/Halley 1986 III," C. E. Woodward, M. A. Shure, W. J. Forrest, T. J. Jones, R. D. Gehrz, T. Nagata, A. T. Tokunaga, 1996, *Icarus*, 124, 651.
- "Mid-Infrared Observations of the Nucleus and Dust of Comet P/Swift-Tuttle," M. N. Fomenkova, B. Jones, R. Pina, R. Puetter, J. Sarnecanic, R. Gehrz, T. J. Jones, October, 1995, *A. J.*, 110, 1866.
- "Infrared Observations of An Outburst of Small Dust Grains from the Nucleus of Comet P/Halley 1986 III at Perihelion," R. D. Gehrz, C. H. Johnson, S. D. Magnuson, E. P. Ney, T. L. Hayward, January, 1995, *Icarus*, 113, 129,
- "Thermal-Infrared High-Resolution Imaging of Comet Austin," M. N. Fomenkova, B. Jones, R. K. Piña, R. C. Puetter, L. A. McFadden, F. Abney and R. D. Gehrz, 1993, *Icarus*, 106, 489.
- "0.7- to 23- μ m Photometric Observations of P/Halley 1986 III and Six Recent Bright Comets," R. D. Gehrz and E. P. Ney, 1992, *Icarus* 100, 162.
- "The Infrared Spectrum of Comet Bradfield (1987s) and the Silicate Emission Features," M. S. Hanner, R. L. Newburn, R. D. Gehrz, T. Harrison, E. P. Ney, T. L. Hayward, 1990, *Astrophys. J.* 348, 312.



2-10-98

MEASUREMENT OF SUBMICRON GRAINS IN THE COMA OF COMET HALE-BOPP C/1995 O1 DURING 1997 FEBRUARY 15–20 UT

D. M. WILLIAMS, C. G. MASON, R. D. GEHRZ, AND T. J. JONES

Astronomy Department, School of Physics and Astronomy, 116 Church Street, S. E., University of Minnesota, Minneapolis, MN 55455

CHARLES E. WOODWARD^{1,2} AND D. E. HARKER²

Wyoming Infrared Observatory, Department of Physics and Astronomy, University of Wyoming, Laramie, WY 82071-3905

M. S. HANNER

Jet Propulsion Lab, Mail Stop 183-601, California Institute of Technology, Pasadena, CA 91109

D. H. WOODEN² AND F. C. WITTEBORN²

NASA Ames Research Center, Space Science Division, Moffet Field, CA 94035-1000

AND

H. M. BUTNER

Department of Terrestrial Magnetism, Carnegie Institution of Washington, and Submillimeter Telescope Observatory, University of Arizona, 933 N. Cherry Avenue, Tucson, AZ 85721

Received 1997 August 14; accepted 1997 September 8; published 1997 October 1

ABSTRACT

We present 1.20–18.5 μm infrared (IR) spectrophotometric measurements of comet C/1995 O1 (Hale-Bopp) during 1997 February 15 and 20 UT. The spectral energy distribution (SED) was dominated by scattering and thermal emission from submicron sized dust grains that were unusually small. Hale-Bopp's surprising brightness may have been largely a result of the properties of its coma grains rather than the size of its nucleus. The thermal emission continuum from the grains had a superheat of $S = T_{\text{color}}/T_{\text{BB}} \approx 1.84$, the peak of the 10 μm silicate emission feature was 1.81 mag above the carbon grain continuum, and the albedo (reflectivity) of the grains was ≈ 0.41 at a scattering angle of $\theta \approx 144^\circ$. These are the highest values for these empirical parameters ever observed in 20 years of optical/IR measurements of bright comets. The observations indicate that the optically important grains dominating the visual scattering and near-IR emission from the coma had an average radius of $a \leq 0.4 \mu\text{m}$. The strong silicate feature is produced by grains with a similar size range. These dust radii are comparable to the radii of the grains that condense in the outflows of some novae ("stardust") but still about 10 times larger than the average radius of the grains that produce the general interstellar extinction.

Subject headings: comets: individual (Hale-Bopp C/1995 O1) — interplanetary medium

1. INTRODUCTION

Dust grains may be a vehicle for the transportation of significant quantities of condensable elements from the circumstellar winds of evolved stars, novae, and supernovae into the parent clouds of young stellar and planetary systems. Whether grains that condense in stellar outflows ("stardust") survive supernova shocks in the ISM (Seab 1987) and high-temperature processing in the solar nebula (Boss 1988) to become the "seed" constituents of planetesimals remains uncertain. If some fraction of these grains survive intact, then analyses of the elemental abundances, mineralogy, and physical characteristics of early solar system grains may be expected to provide direct insight into stellar nucleosynthesis and evolution. Comets, such as Hale-Bopp C/1995 O1, are particularly important to such studies because they are believed to be frozen reservoirs of the most primitive presolar dust grains and ices. Hanner (1983) and Hanner et al. (1985) successfully modeled the infrared (IR) spectral energy distributions (SEDs) of several comets with a size distribution of grains with radii in the range 0.3–0.5 μm . Gehrz & Ney (1992), in an analysis of IR photometric measurements of nine recent bright comets, showed that the SED of the coma can be used to deduce the mineral composition and size distribution of the grains that dominate the coma emis-

sion. They found that the radii of the grains in their sample of comets ranged from 0.5 to 10 μm . Woodward et al. (1996), Gehrz et al. (1995), Hanner et al. (1987), and Tokunaga et al. (1986) found evidence that strong jet activity in comet 1P/Halley 1986 III was correlated with IR emission from grains with radii as small as 0.5 μm , and that the grains were larger when the nucleus was quiescent.

Here we report IR spectrophotometric observations of comet C/1995 O1 (Hale-Bopp) obtained in 1997 February, ≈ 40 days prior to its perihelion passage, showing that the IR emission from its coma was at that time dominated by a population of submicron sized grains. We argue below that these grains were significantly smaller in radius than those observed in any other comet to date.

2. OBSERVATIONS

Five IR photometric measurements of the 1.2–18.5 μm SED of comet Hale-Bopp were obtained on 1997 February 20 UT using a multifilter bolometer (Hanner et al. 1990) mounted at the Cassegrain focus of the University of Minnesota/University of California at San Diego Mount Lemmon Observing Facility (MLOF) 1.52 m telescope. Our filter set included the six IRTF narrowband 7–13 μm "silicate" filters (Tokunaga et al. 1986). The beam was 9"3 in diameter, and the throw between the source and reference beams was $\sim 150''$. The photometric systems, magnitude scales, and absolute flux calibrations for the MLOF bolometer are given by Gehrz & Ney (1992) and Gehrz (1997a, 1997b). Statistical errors were generally much less than

¹ NSF Presidential Faculty Fellow.

² Visiting Astronomer, at the Infrared Telescope Facility, operated by the University of Hawaii, under contract from the National Aeronautics and Space Administration.

TABLE 1
INFRARED MAGNITUDES OF COMET
HALE-BOPP C/1995 O1 ON 1997
FEBRUARY 20 UT

Filter	Average Magnitude
1.2 μm	+4.19 \pm 0.07
1.6 μm	+3.87 \pm 0.08
2.2 μm	+3.71 \pm 0.10
3.60 μm	+1.47 \pm 0.09
4.90 μm	-0.28 \pm 0.10
7.8 μm	-2.74 \pm 0.13
8.7 μm	-3.87 \pm 0.05
9.8 μm	-4.80 \pm 0.06
10.3 μm	-4.86 \pm 0.06
11.6 μm	-4.91 \pm 0.07
12.5 μm	-4.50 \pm 0.08
18.5 μm	-5.67 \pm 0.06

5% (1σ). The comet was variable by a factor of ≈ 1.5 –2 during our observations, but the IR colors remained approximately constant. Average magnitudes, orbital parameters, and physical characteristics of the SED are summarized in Tables 1 and 2 and plotted in Figure 1. The data have not been corrected for coma emission into the reference beam since the effect is only about 1.6% (see Gehrz & Ney 1992).

Confirmation of the presence of a strong 10 μm silicate emission feature in Hale-Bopp during mid-February of 1997 is provided by a preliminary analysis of spectrophotometric measurements of comet Hale-Bopp that we obtained on 1997 February 15.5 UT with the NASA Ames Research Center High-efficiency Faint Object Grating Spectrometer (HIFOGS; Witteborn et al. 1991) at the Cassegrain focus of the 3 m NASA Infrared Telescope Facility (IRTF). The spectrometer entrance aperture was 3" in diameter. The calibrator was α Lyr, for which we have adopted fluxes based on the Kurucz stellar atmosphere model (Walker & Cohen 1992). The HIFOGS data for 1997 February 15.5 UT presented in Figure 1 have been degraded by binning to a resolution of $\lambda/\Delta\lambda \approx 75$ and scaled for heliocentric distance ($r = 1.21$ AU), geocentric distance ($\Delta = 1.73$ AU), and beam diameter using the standard model (Gehrz & Ney 1992) to compare the spectrum with the 1997 February 20 UT photometry. The final analysis of the HIFOGS data will be presented by Wooden et al. (1997).

3. DISCUSSION

The SED derived from our spectrophotometry is presented in Figure 1. Optically thin silicate emission features at 10 and 20 μm are superposed upon a thermal continuum determined by a fitting a blackbody distribution through the 3.6–7.8 μm photometry. Since low-resolution circular-variable filter (CVF) 3–5 μm spectra obtained on 1997 February 21 UT by Mason et al. (1997) show no strong emission features that might be attributed to hydrocarbon or molecular emission, we conclude that it is justifiable to assume that the near-IR continuum (from 3.6–7.8 μm) originates entirely from thermal emission from carbon grains at this epoch (see Gehrz & Ney 1992).

Gehrz & Ney (1992) described three empirical physical parameters derivable from the SED of the coma that are related to the size distribution of comet grains. These are the superheat (S), the strength of the silicate emission feature (Δm_{10}) relative to the extrapolated near-IR blackbody continuum, and the scattering angle dependent albedo [$A(\theta)$]. Gehrz et al. (1995) and Gehrz & Ney (1992) argued that all of these parameters tend to increase with decreasing grain radius, a . Below, we show

TABLE 2
DERIVED PHYSICAL PARAMETERS FOR COMET
HALE-BOPP C/1995 O1

Parameters	Derived Value
r (AU)	1.15
Δ (AU)	1.64
θ (deg)	1.44
T_{color} (K)	≈ 475
T_{BB} (K)	260
S	≈ 1.84
Δm_{10} (mag)	≈ 1.81
$[\lambda F_{\lambda}(\theta)]_{\text{max,scat}}$ (W cm^{-2})	$\approx 1.5 \times 10^{-14}$
$[\lambda F_{\lambda}(\theta)]_{\text{max,IR}}$ (W cm^{-2})	$\approx 2.2 \times 10^{-14}$
$A(\theta)$	≈ 0.41

that the values of these parameters observed for Hale-Bopp on 1997 February 20 UT (Table 2) suggest that its coma was dominated by unusually small grains.

3.1. Superheat as a Grain Size Indicator

The superheat, S , is defined as the ratio of the color temperature of the near-IR carbon grain continuum (T_{color}) to the temperature (T_{BB}) that black conducting spheres would have at the same heliocentric distance r (AU)

$$S = \frac{T_{\text{color}}}{T_{\text{BB}}} = \frac{T_{\text{color}} \sqrt{r}}{278 \text{ K}} \quad (1)$$

We emphasize that S is an empirically determined, model-independent quantity that can be used to compare the near-IR SEDs of comets and to track their temporal development as a function of heliocentric distance. S increases with decreasing grain radius for grain temperatures typical of thermal emission from comets because the emissivity of small grains is a strongly decreasing function of increasing wavelength in the thermal IR. For grains with radii $\approx 0.5 \mu\text{m}$ Gehrz & Ney (1992) showed that $T_{\text{gr}} \leq T_{\text{color}}$ and therefore that $S = (Q_a/Q_e)^{1/4}$, where Q_a and $Q_e(T_{\text{gr}})$ are the grain Planck-mean absorption and emission

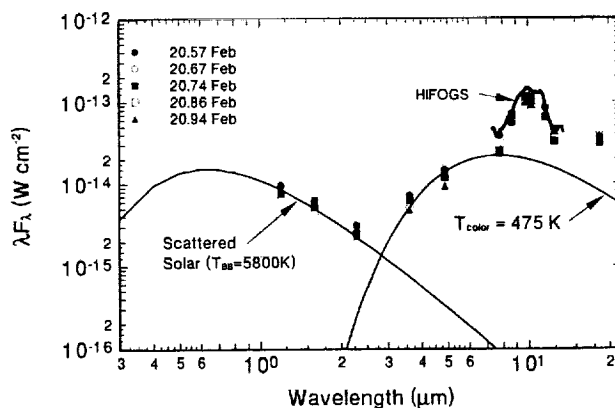


FIG. 1.—SED for comet Hale-Bopp C/1995 O1. The five photometric observations taken on 1997 February 20 UT are indicated in the legend and the statistical averages are presented in Table 1. The continuum fit is the sum of a 5800 K blackbody component due to scattered solar radiation and a 475 K blackbody due to thermal emission from small carbon grains. The 7–13 μm HIFOGS spectrum (heavy solid line) taken on 1997 February 15.5 UT is shown scaled as discussed in the text. The photometric uncertainties in individual measurements and in the HIFOGS spectrum are smaller than the plotted symbols.

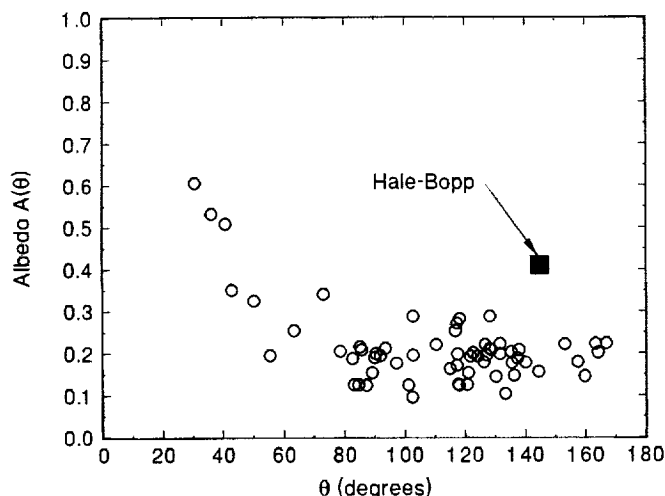


FIG. 2.—Albedo $A(\theta)$ as a function of scattering angle θ for comets previously observed (open circles) by Gehrz & Ney (1992) compared to comet Hale-Bopp C/1995 O1 at a scattering angle of $\theta = 144^\circ$ (black box). The coma grains of Hale-Bopp are substantially brighter than those of the typical comet at this scattering angle.

coefficients respectively of the optically important grains (Gilman 1974) and T_g is the physical grain temperature.

The $3.6\text{--}4.9\text{ }\mu\text{m}$ continuum of Hale-Bopp SED (Fig. 1) has a $T_{\text{color}} \approx 475\text{ K}$, and therefore a superheat $S \approx 1.84$. Our 1997 February 21 UT $3\text{--}5\text{ }\mu\text{m}$ CVF spectra give the same color temperature (Mason et al. 1997). This is the largest value of S yet observed for a comet. If we were to assume that the grain emissivity is not wavelength dependent, then using $S = [Q_{\text{sil}}/Q_{\text{c}}]^{1/4}$ we would derive a grain radius for the optically important grains of $\approx 0.3\text{ }\mu\text{m}$. If we take into account the wavelength dependent emissivity using Mie theory and the optical constants for glassy carbon, we would derive a radius for the optically important grains of $a \approx 0.4\text{ }\mu\text{m}$, although we have not explicitly integrated over a grain size radius distribution function. Employing a broad size distribution of the form used by Hanner et al. (1985), one finds a peak radius of $a \approx 0.15\text{ }\mu\text{m}$, significantly smaller than the $0.3\text{--}0.5\text{ }\mu\text{m}$ peak radius determined for other comets.

3.2. The Strength of the Silicate Emission Feature as a Grain Size Indicator

Many comets show a $10\text{ }\mu\text{m}$ emission feature attributed to radiation from Si-O bond stretching vibrations in a silicate grain component (Gehrz & Ney 1992; Hanner, Lynch, & Russell 1994; Hanner et al. 1987, 1985). Hale-Bopp exhibited an exceptionally strong $10\text{ }\mu\text{m}$ emission feature (Fig. 1).

Gehrz & Ney (1992) have described how the strength of the silicate feature in magnitudes, Δm_{10} , from filter photometry can be measured with respect to the extrapolated near-IR blackbody carbon continuum using the relationship

$$\Delta m_{10} = 2.5 \log_{10} \left[\frac{(\lambda F_{\lambda})_{\text{sil}}}{(\lambda F_{\lambda})_{\text{cont}}} \right], \quad (2)$$

where $(\lambda F_{\lambda})_{\text{sil}}$ and $(\lambda F_{\lambda})_{\text{cont}}$ are the intensities of the emission feature and the extrapolated carbon continuum respectively determined at $\approx 10\text{ }\mu\text{m}$. Laboratory measurement of powdered silicates (Rose 1979) show that the silicate excess, Δm_{10} , increases with decreasing grain size. Thus, measurement of Δm_{10}

in comets can, in principle, provide an estimate of the average silicate grain radius.

We find a value of $\Delta m_{10} \approx 1.81\text{ mag}$ for Hale-Bopp (see Figs. 1 and 3), the largest value ever observed for a comet. In the case of Hale-Bopp, the extrapolated $3\text{--}5\text{ }\mu\text{m}$ continuum falls below the continuum at 7.9 and $12.5\text{ }\mu\text{m}$ so that Δm_{10} as defined above overestimates the actual strength of the silicate feature.

3.3. Albedo as a Grain Size Indicator

A third grain size indicator is the scattering angle (θ) dependent albedo, $A(\theta)$. $A(\theta)$ can be defined as

$$A(\theta) = \frac{f(\theta)}{1 + f(\theta)}, \quad (3)$$

where

$$f(\theta) = \frac{[\lambda F_{\lambda}(\theta)]_{\text{max,scatt}}}{[\lambda F_{\lambda}(\theta)]_{\text{max,IR}}}, \quad (4)$$

and the quantities $[\lambda F_{\lambda}(\theta)]_{\text{max,scatt}}$ and $[\lambda F_{\lambda}(\theta)]_{\text{max,IR}}$ are the apparent intensities measured at the Planckian maxima of the scattered and thermal SEDs respectively as shown in Figure 1. Figure 2 shows the albedo measurements for a collection of previously observed comets, and it is apparent that the albedo of the grains in the coma of comet Hale-Bopp for $\theta = 144^\circ$, $A(\theta) \approx 0.41$, is exceptionally large compared to that of other comets observed at the same scattering angle see Hanner et al. 1985; Tokunaga et al. 1986). One interpretation is that high reflectivity of Hale-Bopp's grains is due to their small size, since small grains scatter sunlight much more efficiently than large grains (see Gehrz & Ney 1992). It is possible that at least part of the effect is due to the mineral composition of the grains as shown by Hanner et al. (1985).

3.4. Comparison to Other Comets

The two most sensitive measured parameters of grain size are S and Δm_{10} . Both indicators increase as grain size decreases. Gehrz & Ney (1992) have found a strong correlation between Δm_{10} and S in a sample of nine comets (see Fig. 3). The correlation suggests that changes in the size distributions of the carbon and silicate components are related, but it does not necessarily imply that superheat and silicate emission originate from the same grain structures. Figure 3 reproduces the data from Gehrz & Ney (1992) along with the 1997 February 20 UT values of $S \approx 1.84$ and $\Delta m_{10} \approx 1.81\text{ mag}$ derived for Hale-Bopp. It is evident that Hale-Bopp lies well beyond the envelope defined by previously measured comets. The large albedo at $\theta = 144^\circ$, $A(\theta) \approx 0.41$, is also significantly larger than has been observed at this scattering angle for other comets and is consistent with the interpretation that the grains are smaller than usual. It is a matter of record that Hale-Bopp is an unusually bright comet, and there has been much speculation that this results from the high mass-loss rate that would be expected from a large nucleus. Our data suggest that the exceptional brightness may be due to the unusual properties of Hale-Bopp's grains.

There are several possible explanations for the differences between Hale-Bopp and previous comets. For example, Hale-Bopp could be an unusually pristine Oort Cloud comet. Alternatively, the submicron grain population could be associated

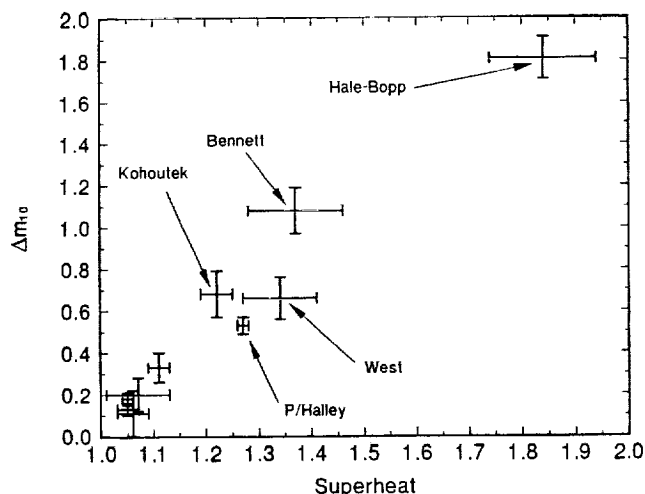


FIG. 3.—Silicate feature excess Δm_{10} as a function of superheat S for comet Hale-Bopp C/1995 O1 and nine comparison comets from Gehrz & Ney (1992). The vertical and horizontal bars represent the standard deviation of the sample ($\sigma_s = N^{1/2}\sigma$) of these parameters for multiple observations of a given comet. Coma emission from comets near the origin is dominated by relatively large grains with radii $a \geq 1 \mu\text{m}$. Coma emission from comets with large values of Δm_{10} and S is dominated by small grains with $a \leq 0.5 \mu\text{m}$. It is evident that Hale-Bopp lies at a new extreme in this diagram relative to previously observed comets, suggesting that its coma grains are significantly smaller.

with Hale-Bopp's exceptionally active jets. Gehrz et al. (1995) found that jet activity in comet P/Halley was correlated with the release of small grains.

4. CONCLUSIONS

Our observations clearly show that comet Hale-Bopp C/1995 O1 contains a population of hot submicron absorbing grains that are unusually small. This submicron grain component is the smallest yet observed for any comet. This grain population produces the large superheat of $S \approx 1.84$. The $10 \mu\text{m}$ silicate emission feature is the strongest yet observed in a comet and indicates an unusually large population of submicron sized grains. The large value of $A(\theta) \approx 0.41$ at $\theta = 144^\circ$ is also consistent with the interpretation that the grains are small. We present arguments showing that the grains have radii $a \leq 0.4 \mu\text{m}$. These dust radii are comparable to the radii of the stardust that condenses in the outflows of some novae (Gehrz 1995) but still about 10 times larger than the average radius of the grains that produce the general interstellar extinction.

Our paper emphasizes the value of having the entire 1–20 μm spectral energy distribution measured simultaneously. We are analyzing similar data sets obtained during 1997 March–June that will allow us to follow the grain properties during Hale-Bopp's perihelion passage.

R. D. G., T. J. J., C. G. M., and D. M. W. thank A. Knutson for his efforts in support of our operations at MLOF and J. Lyke for his assistance in the MLOF data reduction. M. Jura lent helpful suggestions. The UM IR Group was funded for these observations by the NSF, NASA, and the UM Graduate School. C. E. W. and D. E. H. acknowledge support from the NSF (AST94-53354), NASA (GRSP NGT2-52218), and the Office of Research, University of Wyoming. H. M. B. and D. H. W. were supported by NASA.

REFERENCES

- Boss, A. P. 1988, *Science*, 241, 565
- Gehrz, R. D. 1995, in *Proc. Padua (Abano-Terme) Conf. on Cataclysmic Variables*, ed. A. Bianchini, M. Della Valle, & M. Orio (Dordrecht: Kluwer), 29
- . 1997a, in *The International Comet Quarterly*, Vol. 19, ed. D. W. E. Green (Cambridge: Smithsonian Astrophys. Obs.), 55
- . 1997b, in *The International Comet Quarterly Guide to Observing Comets*, ed. D. W. E. Green (Cambridge: Smithsonian Astrophys. Obs.), 117
- Gehrz, R. D., Johnson, C. H., Magnuson, S. D., & Ney, E. P. 1995, *Icarus*, 113, 129
- Gehrz, R. D., & Ney, E. P. 1992, *Icarus*, 100, 162
- Gilman, R. C. 1974, *ApJ*, 28, 397
- Hanner, M. S. 1983, in *Cometary Exploration*, Vol. 2, ed. T. I. Gombosi (Budapest: Hungarian Acad. Sci.), 1
- Hanner, M. S., Lynch, D. K., & Russell, R. W. 1994, *ApJ*, 425, 274
- Hanner, M. S., Newburn, R. L., Gehrz, R. D., Harrison, T. E., Ney, E. P., & Hayward, T. L. 1990, *ApJ*, 348, 312
- Hanner, M. S., et al. 1985, *Icarus*, 64, 11
- Hanner, M. S., Tokunaga, A. T., Golisch, W. F., Griep, D. M., & Kaminski, C. D. 1987, *A&A*, 187, 653
- Mason, C. G., Williams, D. M., Gehrz, R. D., Jones, T. J., & Woodward, C. E. 1997, in preparation
- Rose, L. A. 1979, *A&SS*, 65, 47
- Seab, C. G. 1987, in *Interstellar Processes*, ed. D. J. Hollenbach & H. A. Thronson, Jr. (Dordrecht: Reidel), 491
- Tokunaga, A. T., Golisch, W. P., Griep, D. M., Kaminski, C. D., & Hanner, M. S. 1986, *AJ*, 92, 1183
- Walker, R. G., & Cohen, M. 1992, *An Atlas of selected Calibrated Stellar Spectra*, Final Report Contract NAG 2-13327 (Moffett Field: NASA/Ames Research Center)
- Witteborn, F. C., Bregman, J. D., Rank, D. M., & Cohen, M. 1991, in *Proc. 1991 North American Workshop on Infrared Spectroscopy*, ed. R. E. Stencel (Boulder: Univ. Colorado), 29
- Wooden, D. H., Harker, D. E., Woodward, C. E., Butner, H. M., Witteborn, F. C., & McMurtry, C. M. 1997, in preparation
- Woodward, C. E., Shure, M. A., Forrest, W. J., Jones, T. J., Gehrz, R. D., Nagata, T., & Tokunaga, A. T. 1996, *Icarus*, 124, 651

INTERNATIONAL COMET QUARTERLY

Whole Number 102

APRIL 1997

Vol. 19, No. 2



SMITHSONIAN ASTROPHYSICAL OBSERVATORY
60 Garden Street • Cambridge, MA 02138 • U.S.A.

Infrared Observations of Comets*

Robert D. Gehrz

Department of Astronomy, University of Minnesota

Comets are the "Rosetta Stone" of the solar system; they contain all the refractory and volatile materials that were present in the primitive solar nebula, 4.7 billion years ago during the epoch of formation of the comet nuclei. That material, frozen in its original state for aeons, is released by solar heating to form the comae and tails of comets during the time around perihelion passage, where its composition can be studied by present-day astronomers. Because the thermal emission from comets is primarily emitted in the spectral region 2-30 μm , infrared observations of comets play an especially important role in efforts to reconstruct an accurate picture of the processes that led to the formation of the planets. Infrared observations can be used to determine the composition, mineral structure, and size distribution of cometary dust grains that were the repository for a large fraction of the heavy elements produced by previous generations of massive stars, supernovae, and novae that contributed their ejecta to the solar system. Spectral peculiarities of some of the prominent infrared dust emission features record the processes to which condensable elements were subjected during the formation of the solar system. Infrared studies also provide a basis for defining the relationships between comet grains, grains formed in the outflows of evolved stars, and grains in the interstellar medium. Near-infrared line emission and scattering reveal information about the gas and ice content of cometary material. Variable activity in the infrared dust emission from comets during perihelion passage is related to the physical structure of their nuclei, and observations of the activity provide insight about the physical conditions under which these small bodies were formed.

The historical record of infrared observations of comets originated in the infancy of the field with the measurement of the 1.65- to 10- μm spectrum of the bright comet C/1965 S1 (Ikeya-Seki; O.S. 1965 VIII = 1965f) by infrared pioneers E. E. Becklin and J. A. Westphal [1966]. Maas *et al.* [1970] were the first to demonstrate that infrared observations could be useful for determining the mineralogy of comet dust by detecting the 10- μm silicate-emission peak in the spectrum of comet C/1969 Y1 (Bennett; O.S. 1970 II = 1969i).

E. P. Ney [1974, 1982] was the first infrared astronomer to conduct long-term systematic studies of the temporal development of the infrared spectra of a significant sample of bright comets. His observations and those of subsequent observers demonstrated the importance of infrared observations in determining the mineralogy of comet grains, in specifying the size of the grains, and in assessing physical characteristics of the structure of comet nuclei. The importance of infrared observations in comet research was clearly demonstrated during the recent apparition of comet 1P/Halley (O.S. 1986 III), when extensive temporal infrared photometric, imaging, and spectroscopic coverage was obtained [see Hanner 1988 and the references therein].

Some of the major questions about the physics of comets that are being addressed by current infrared studies of comets are those related to:

- 1) The structure and activity of comet nuclei: How can infrared measures of activity be used to reconstruct information about the structure and composition of the nucleus? What role does nuclear rotation play in variations of the activity of some comets, and in the distribution of material within the inner coma? How heterogeneous are comet nuclei in composition and physical structure? Do the nuclei of pristine and periodic comets differ in any substantial way?
- 2) The structure of comet comae and tails: How are grains of different sizes and mineral compositions distributed in the comae, tails, and anti-tails of comets? What is the origin of the large particles in the comet trails detected by IRAS? How do jets affect the coma surface brightness distribution?
- 3) The properties of comet grains: Why do some comets show silicate-emission features, while others do not? How many comets show the structure in their 10- μm silicate features due to crystalline olivine and enstatite grains? What is the meaning of the time-variable structure and strength of emission features in some comets? Are excess grain temperature (superheat), grain albedo, and silicate-emission strength a function of heliocentric distance? Are comet grains altered by heating at small heliocentric distances?

Table 1 lists the photometric quantities that are measured by infrared observations and the physical parameters that can be derived from them. In section 1.1.1, we use the example of comet C/1973 E1 (Kohoutek; O.S. 1973 XII = 1973f) to show how the photometric properties typically manifest themselves in the spectrum of a comet. Section 1.1.2 outlines how the photometric quantities can be used to derive physical parameters describing behavior of comet comae and nuclei. Finally, we discuss the equipment and techniques used to measure and calibrate the infrared photometric quantities in section 1.1.3. In this work, we have liberally consulted previous extensive reviews and compendia of optical-infrared measurements of comets by Ney [1982], Hanner [1988], Encrenaz and Knacke [1991], Hanner and Tokunaga [1991], Jewitt [1991], Weaver *et al.* [1991], Yeomans and Wimberly [1991], and Gehrz and Ney [1992]. The reader is commended to these sources for more detailed discussions of selected topics.

* This article was written for the *ICQ Guide to Observing Comets*, and appears in the first edition of that publication, pp. 117-132.

Table 1: Photometric properties and Physical Parameters of Comets from Infrared Measurements Assuming the Standard Model

PARAMETERS (units)	DEFINITION	RELATIONSHIPS (units of variables as specified in column one ¹)
$r(\text{cm})$	heliocentric distance	From ephemerides
$\Delta(\text{cm})$	geocentric distance	From ephemerides
$\theta(\text{deg})$	Scattering (Sun-comet-Earth) angle	From ephemerides
$\lambda(\mu\text{m})$	wavelength	Selected by observer
$\phi(\text{arcseconds})$	Photometer diaphragm diameter	Selected by observer
$\psi(\text{arcseconds})$	Angular distance between source and reference beams	Selected by observer
$f_\lambda(\phi, \psi)(W\text{ cm}^{-2}\mu\text{m}^{-1})$	Apparent flux in ϕ for a throw ψ	Measured quantity
$f_\lambda(\phi)$	Apparent flux in ϕ corrected for emission in the reference beam	$f_\lambda(\theta) = 4\psi(4\psi - \phi)f_\lambda(\phi, \psi)$
$f_\lambda(r', \Delta', \phi')$	Predicted apparent flux for the comet at r' and Δ' in a diaphragm ϕ'	$f_\lambda(r', \Delta', \phi') = (\phi'/\phi)(r/r')^4(\Delta/\Delta') \cdot f_\lambda(r, \Delta, \phi)$ (see Gehrz and Ney 1992)
$(\lambda f_\lambda)_{\text{max}}(W\text{ cm}^{-2})$	(λf_λ) in ϕ at Planckian maximum	Inspection of V/IR spectral energy distribution (SED)
$f(W\text{ cm}^{-2})$	Total apparent flux in ϕ	$f = \int_0^\infty f_\lambda(\phi)d\lambda = 1.3586(\lambda f_\lambda)_{\text{max}}$
Q_a, Q_e	Planck mean absorption, emission coefficient	See Gilman (1974)
$T_{BB}(K)$	Temperature of a black sphere at r	$T_{BB} = 278 r^{-1/2}$; r in AU
$T_{gr}(K)$	Observed Grain Temperature	$T_{gr} = (L_\odot Q_a / 16\pi\sigma r^2 Q_e)^{1/4} = 278 r_A^{-1/2} (Q_a/Q_e)^{1/4}$
S	Superheat (Temperature excess)	$S = T_{gr}/T_{BB} = (Q_a/Q_e)^{1/4}$
$f(\theta)$	Ratio of the scattered to the thermal radiation	$f(\theta) = f_{\text{scat}}(\theta)/f_{\text{IR}}(\theta) = [\lambda f_\lambda(\theta)]_{\text{max,scat}}/[\lambda f_\lambda(\theta)]_{\text{max,IR}}$
$A(\theta)$	Bolometric Albedo at θ	$A(\theta) = f(\theta)/[1 + f(\theta)]$
A	Mean Bolometric Albedo	$A = \pi^{-1} \int_0^\pi A(\theta)d\theta$
$\Delta m_{9.7}(\text{mags})$	9.7 μm silicate emission feature excess	Measured off IR SED at $\lambda = 9.7\mu\text{m}$
$dM_D/dt(g\text{ s}^{-1})$	Dust mass loss rate	$dM_D/dt = 7 \times 10^{21} r^2 \Delta \phi^{-1} (\lambda f_\lambda)_{\text{max,IR}}$; r and Δ in AU
grain, gas composition	See Table 1a	IR emission features and spectral lines

¹ Unless otherwise noted in column three

◇ ◇ ◇

1.1.1. Photometric quantities derivable from the infrared spectra of comets

Figure 1 shows the 0.5- to 18- μm spectra of the coma, tail, and anti-tail of comet C/1973 E1 (Kohoutek) [Ney 1974]. Because a spectrum is also a plot of the amount of energy emitted at each wavelength, we often use the term "energy distribution" in the discussion that follows when the spectrum is being used primarily to determine quantities related to energy balance. An important characteristic of the scattered and thermal energy distributions of comets is that they follow the spectral shape of a blackbody (a body that is a perfect absorber and emitter). The blackbody energy distribution $f_\lambda = 2\pi hc^2 \lambda^{-5} [\exp(hc/\lambda kT) - 1]^{-1}$ is called the Planck function after Max Planck, who showed that its characteristic shape can be theoretically predicted from the laws of quantum mechanics. The position in wavelength of the peak of the curve, called the Planckian maximum, was shown by Wien to be related to the temperature of the blackbody. Wien's law is $\lambda_{\text{max}} T = 2898 \mu\text{m K}$ for the f_λ function, and $\lambda_{\text{max}} T = 3670 \mu\text{m K}$ for the λf_λ function. Evaluation of the energetics of comet emission is especially straightforward when the quantity λf_λ is plotted as a function of the wavelength, λ , as shown in section 1.1.2. It should be noted that plots of λf_λ versus λ and plots of λf_ν versus frequency $\nu = c/\lambda$ are equivalent. As discussed in section 1.1.3, the flux f_λ is a quantity that can be directly derived from measurements of comets and standard stars, and it is multiplied by λ to produce the quantity λf_λ plotted in Figure 1.

The scattered solar component of the spectrum is caused by sunlight reflected by dust grains in the coma and tails. This component can be examined by combining observations from the visual and near-infrared regions. The total power (W/cm^2) in the scattered radiation delivered to an observer viewing the comet at a scattering angle θ (the sun-comet-earth angle)² is measured by the quantity $[\lambda f_\lambda(\theta)]_{\text{max,scat}}$, defined by the Planckian maximum of the scattered radiation component (see Table 1). Usually, *VRIJHK* photometry or spectrophotometry will suffice to specify this quantity. This scattered component essentially measures the θ dependence of the albedo, $A(\theta)$, of the comet grains — a measure of their physical size and structure.

Thermal emission from the coma, tail, and anti-tail — produced by the re-radiation of the sunlight absorbed by dust grains — is evaluated by measurements from 3 to 30 μm and beyond. It is evident from Figure 1 that the energy distributions of these structures can contain both a blackbody-continuum-radiation component and broad emission features. The continuum is believed to be caused by an amorphous-carbon-dust component. The total power emitted by the carbon-dust-component of the coma at scattering angle θ is measured by the quantity $[\lambda f_\lambda(\theta)]_{\text{max,IR}}$, the peak of the Planckian maximum of the continuum-radiation component (see Table 1). Additional power contributed by other

² equivalent to the phase angle, usually represented in the *ICQ* and *IAU Circulars* by β .

dust emission features (see the following paragraph) is usually negligible. The total thermal-infrared power is essentially a measure of the dust mass-loss rate dM_{gr}/dt from the nucleus, and can be highly variable. Grain temperature T_g is measured by the wavelength λ_{max} of the peak of the continuum component, using Wien's law. Grain size can be inferred from measurements of this quantity, as we show below. Figure 1 shows that the coma and tail have a much higher temperature than the temperature T_{BB} expected for a black sphere at the same heliocentric distance. This temperature excess, which is termed "superheat", is an indication that these components are made of very small grains. The temperature of the anti-tail is roughly T_{BB} , showing that it is made of very large grains that are efficient radiators. The relationship between grain size and superheat is discussed explicitly in section 1.1.2.1.

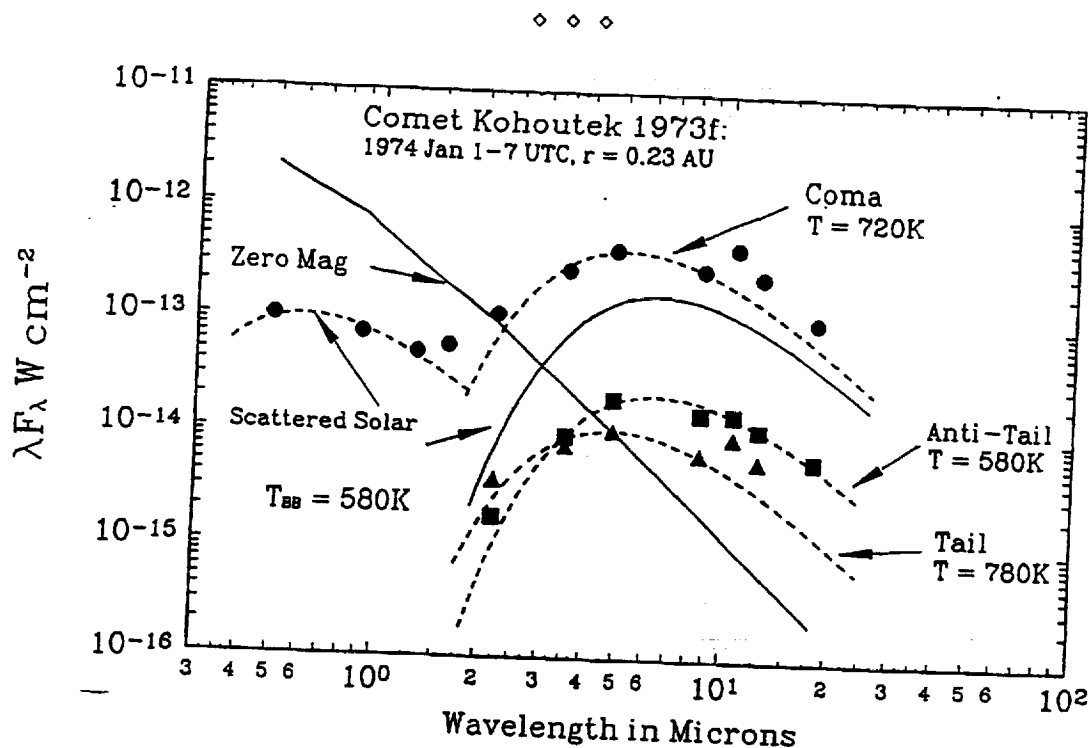


Figure 1. The spectra of the coma, tail, and anti-tail of comet C/1973 E1 (Kohoutek; O.S. 1973 XII = 1973f), showing the various characteristics of cometary emission that can be investigated using infrared observing techniques. Data are from Ney [1974]. The scattered solar component can be compared with the thermal emission to give the albedo. The superheat (temperature excess) of the coma and tail over the low temperature of the anti-tail shows that it is made of large grains. The excess emission in the tail and coma at 10 and 20 μm is caused by emission from small silicate grains.

Broad emission features due to small dust grains are often present in comet spectra, and several of these are evident in the spectra of the tail and coma of comet C/1973 E1 (Kohoutek). Silicate grains can produce strong emission features at 10 and 20 μm caused by the stretching and bending vibrational modes in the SiO_2 molecular bonds, and the Si-C stretch vibration of silicon carbide can produce a feature at 11.3 μm [see Woolf and Ney 1969]. Hydrocarbon emission features in the region 3.2-3.5 μm may be caused by stretch vibrations of the C-H bonds of polycyclic aromatic hydrocarbons (PAHs) or types of hydrogenated hydrocarbons as discussed by Allamandola [1984] and Allamandola *et al.* [1987]. The infrared spectral emission features observed from gas and dust in 1P/Halley and C/1986 P1 (Wilson) are listed in Table 1. The strength and shape of these features can be used to deduce the mineral composition of comet grains. For example, the structure in the 10- μm silicate-emission feature has been interpreted as indicating the presence of the crystalline silicate minerals olivine and enstatite in the grains of some comets [see Hanner 1988; and Hanner *et al.* 1990, 1994a, 1994b].

A very important objective of infrared monitoring of comets is to track activity patterns through long-term temporal observations. Analysis of these variational patterns can be used to infer information about both the physical structure and the rotation rate of the nucleus. Gehrz and Ney [1992] and Gehrz *et al.* [1995] found that the thermal flux from 1P/Halley's coma varied by factors of almost 10 compared to the canonically expected behavior on time scales as short as several hours and as long as several days. The activity variations they observed included significant changes in the grain temperature and albedo, as well as in the shape and strength of the 10- μm silicate-emission feature. Many of these changes were consistent with the hypothesis that jets of small particles can be released by insolation as the nucleus rotates. Recently Fomenkova *et al.* [1995] showed how time-sequences of infrared images can be used to deduce the rotation rate of a comet nucleus through measurements of the positions of prominent jets.

Table A. Infrared Spectral Features and Emission Lines
Observed in Comets 1P/Halley and C/1986 P1 (Wilson)³

λ in μm	PROBABLE SOURCE
1-2.5	CN, H ₂ O
2.63	H ₂ O gas?
2.7	H ₂ O gas, other unknown molecules
2.8	OH
3.0	NH ₃ , HCN, H ₂ O ice
3.15	unidentified
3.29	hydrocarbon grain constituent (PAH?)
3.36	CH stretch in grains
3.52	CH stretch in grains
3.6	H ₂ CO
4.3	CO ₂
4.44	CN
4.6	CO
4.84	OCS
5.2	unidentified
6.8	carbonates
9.7	amorphous silicate dust grains
9.8, 10.5, 11.3	crystalline silicate (Olivine and Pyroxene?)
12.2	unidentified
20	amorphous silicate dust grains
23.8	Olinene?
26.7	unidentified
28.4	Olivine?
34.5	Olivine?
40	Olivine?

³ After data presented in Campins and Tokunaga 1988

◇ ◇ ◇

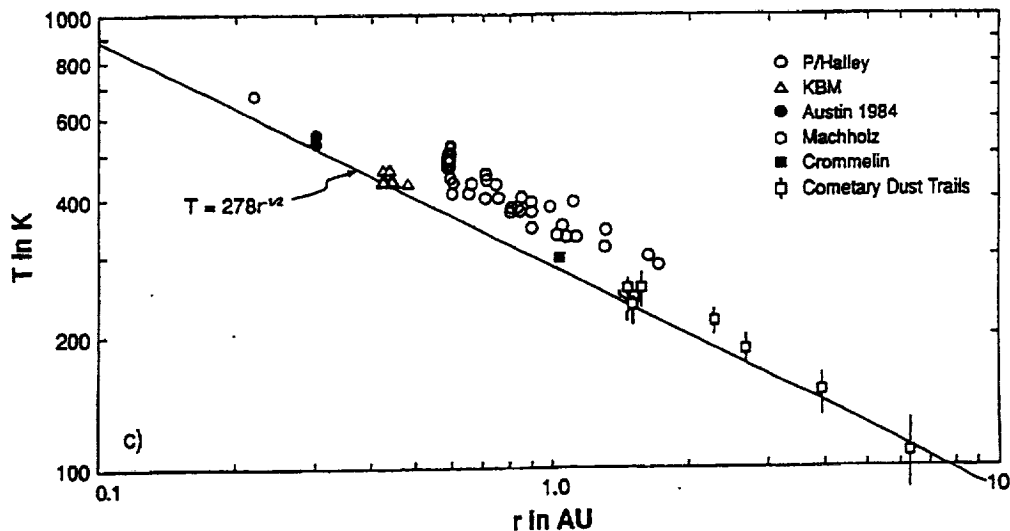


Figure 2. The observed coma continuum temperature, T_{gr} , plotted as a function of heliocentric distance for a sample of recent bright comets. Comet 1P/Halley's grains were superheated. It is also evident that T_{BB} defines the lower limit to the temperature of comet grains. "KBM" indicates comet C/1975 N1 (Kobayashi-Berger-Milon), "Austin 1984" indicates comet C/1984 N1, "Machholz" indicates comet C/1985 K1, "Crommelin" indicates comet 27P, and the dust trails refer to those found by IRAS. Figure from Gehrs and Ney [1992], reproduced by permission of Icarus.

1.2. Derivation of physical properties of comet comae and nuclei from photometric quantities

A straightforward way to gain an elementary understanding of the relationships between measurable infrared photometric quantities and the physical parameters of comets is to consider the steady-state model of nuclear activity [Jewitt 1991; Gehrz and Ney 1992]. For this case, both the scattered and thermal emission from the coma is caused by dust grains ablated from the nucleus at a constant rate dN/dt grains/sec that flow away from the nucleus at constant velocity. Although molecular emission is observed in the infrared as mentioned above, the total energy in this emission is insignificant compared to the dust scattering and emission. We ignore molecular emission in the discussion that follows. Although the standard model does not necessarily apply to periods of high, irregular activity, there are many occasions when a comet has been in a steady state for a long-enough period of time to be adequately characterized by this model. We outline below an analysis deriving some important physical characteristics of the steady-state model. This analysis, originally presented in more detail by Gehrz and Ney [1992], assumes that infrared energy distributions measure the properties of the "optically important" grains. These are defined as the grains that dominate the scattered and emitted radiation. Based upon existing ground- and space-based measurements of the grain-size distribution in comet comae, Jewitt and Meech [1986] and Jewitt [1991] showed that the effective grain radius a for the optically-important grains can be determined by assuming that the differential grain distribution follows a power law of the form $n(a)da = Ka^{-m}da$, where $n(a)$ is the number density of grains of radius a in number of grains cm^{-3} . If, as suggested by existing data, there is a lower limit a_{\min} to the grain radius, the mean grain radius of the optically-important grains can be shown to be between $2a_{\min}$ and $3a_{\min}$, and where m lies between 3 and 4.5 [Gehrz and Ney 1992]. The parameters derived below are defined and their units are given in Table 1.

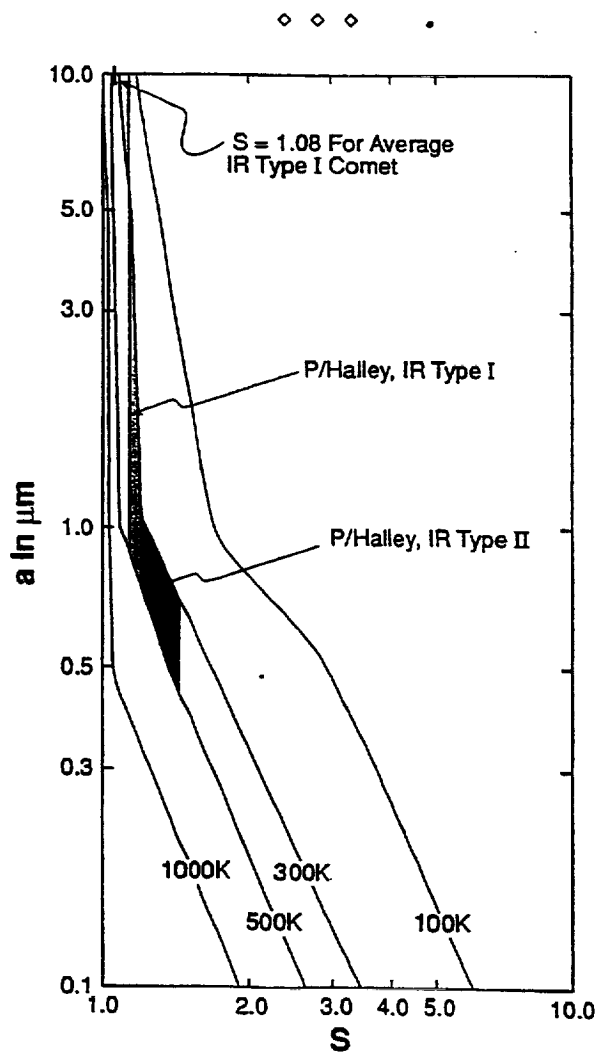


Figure 3. The superheat, S , plotted as a function of grain radius, a , and temperature, T_g , for small carbon grains illuminated by the solar radiation field, assuming that the sun has an effective temperature of 5800 K. Figure from Gehrz and Ney [1992], reproduced by permission of Icarus.

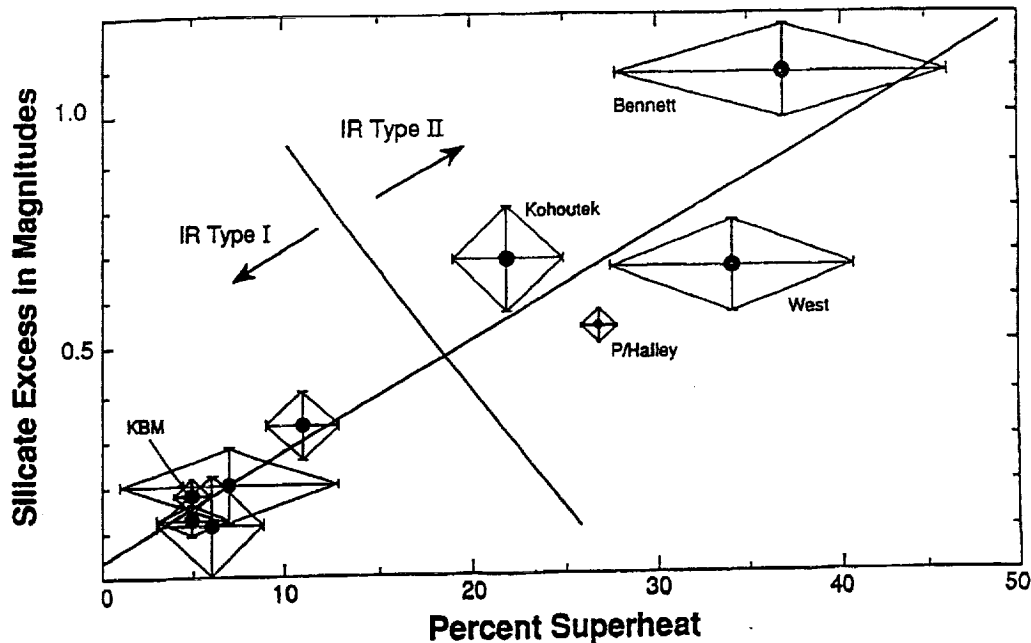


Figure 4. Silicate-emission feature strength (in magnitudes) plotted as a function of percent superheat $[(S - 1) \times 100]$ for recent bright comets. They are correlated, as would be expected, on theoretical grounds. Note that "KBM" indicates comet C/1975 N1 (Kobayashi-Berger-Milon), "Kohoutek" indicates comet C/1973 E1, "Bennett" indicates C/1969 Y1, and "West" indicates comet C/1975 V1. Figure from Gehrz and Ney [1992], reproduced by permission of *Icarus*.

◇ ◇ ◇

1.1.2.1. Superheat and silicate emission features: their relationship to grain size

Many comets have a coma-grain temperature considerably higher than the black-sphere temperature appropriate to the comet's heliocentric distance, probably because the coma grains are too small to radiate effectively. A quantitative relationship between the grain radius, a , and the grain temperature, T_{gr} , results from equating the power absorbed by the grain from insolation⁴ to the power emitted by the grain in the infrared:

$$\frac{L_{\odot}}{4\pi r^2 \pi a^2 Q_a} = 4\pi a^2 Q_e \sigma T_{gr}^4, \quad (1)$$

where r is the heliocentric distance in cm, a is the grain radius in cm, $L_{\odot} = 3.826 \times 10^{33}$ erg/s is the solar luminosity, $\sigma = 5.6696 \times 10^{-5}$ erg cm⁻² deg⁻⁴ is the Stefan-Boltzmann constant, and $Q_a(a, T)$ and $Q_e(a, T)$ are the Planck mean absorption and emission coefficients. Q_a is the absorption efficiency of the grain averaged over the spectrum of the illuminating source (the sun), and Q_e is the thermal emission efficiency of the grain at T_{gr} . Solving equation (1) for the grain temperature yields

$$T_{gr} = \left[\frac{L_{\odot} Q_a}{16\pi \sigma r^2 Q_e} \right]^{1/4}, \quad (2)$$

which gives the black-sphere temperature,

$$T_{BB} = \frac{278}{\sqrt{r}} \text{ deg K}, \quad (3)$$

in the case when $Q_a = Q_e = 1$, where r in equation (3) is the heliocentric distance expressed in AU (1 AU = 1.4960×10^{13} cm).

The black-sphere condition defines the temperature that would be expected for rather large grains that have a very low reflectivity, and therefore T_{BB} is also expected to define the lower limit to the temperature of comet grains. For small grains ($Q_e < Q_a$), the grain temperature must be higher than the black-sphere temperature when the grain is in radiative equilibrium. The grain temperatures for a sample of recent bright comets and comet tails are shown in Figure

⁴ absorbed by the grain from sunlight

2. The temperature excess can be quantified by defining the superheat $S = T_{gr}/T_{BB}$ as the ratio of the grain temperature to the temperature of a perfectly-conducting black sphere at the same heliocentric distance. Assuming that the infrared color temperature of the grains measures the physical temperature of the grain T_{gr} , it is seen that S measures the fourth root of the ratio of Q_a to Q_e :

$$S = \frac{T_{gr}}{T_{BB}} = \left[\frac{Q_a}{Q_e} \right]^{1/4}, \quad (4)$$

where the right-hand side is unity for large grains, and becomes progressively larger as the grain size decreases (see Figure 3). The physical grain temperature and the grain-color temperature are equivalent in cases where the grain emissivity does not vary significantly over the spectral region that is used to define the color temperature. The strength of the 10- and 20- μm silicate features is also an indicator of grain size. As discussed by Gehrz and Ney [1992], the features should be strongest for grains that are much smaller than a few microns in radius, and should become very weak for grains that approach or exceed radii of 10 μm . This has been confirmed for the 10- μm silicate-emission feature in laboratory experiments conducted by Rose [1979].

Since the arguments that we have outlined above show that both S and silicate-emission strength should increase as grain size decreases, one might expect that S and silicate-emission strength should be correlated in comets. Figure 4 shows that this is, indeed, the case.

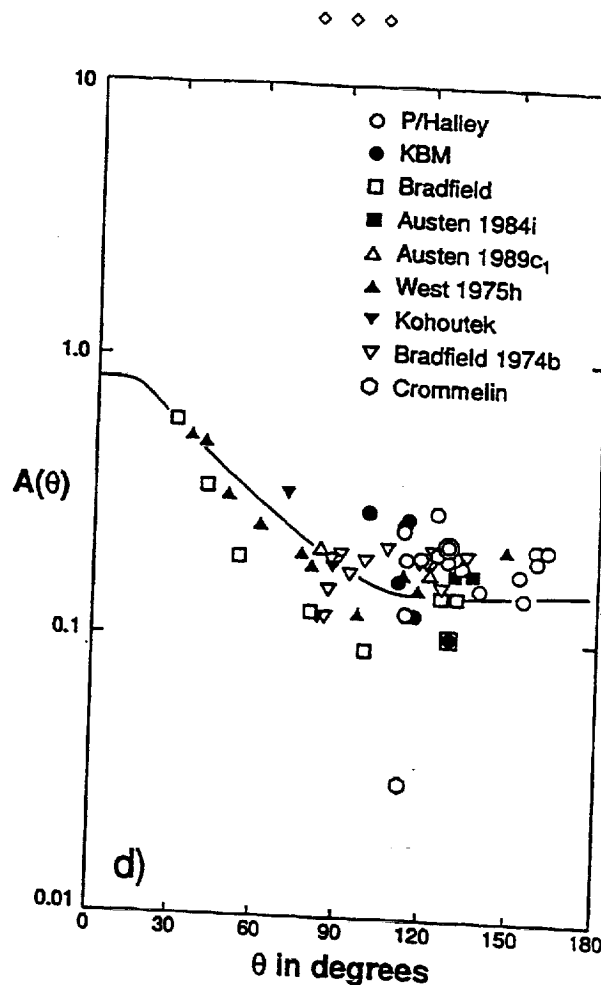


Figure 5. The albedo of comet grains as a function of scattering angle, as measured by the ratio of the scattered to the re-emitted (absorbed) radiation. The forward scattering peak and shape of the curve show that the grains are fluffy aggregates. Note that "KBM" indicates comet C/1975 N1 (Kobayashi-Berger-Milon), "Kohoutek" indicates comet C/1973 E1, "Bradfield" indicates comet C/1980 Y1, "Bradfield 1974b" indicates comet C/1974 C1, "Crommelin" indicates comet 27P, "Austen 1984i" indicates comet C/1984 N1 (Austin), "Austen 1989c1" indicates comet C/1989 X1 (Austin), and "West 1975h" indicates comet C/1975 V1. Figure from Gehrz and Ney [1992], reproduced by permission of *Icarus*.

1.1.2.2. Total power in the scattered and thermal energy distributions

The determination of the total power f radiated by a blackbody (see Table 1) is particularly straightforward when the continuum emission from the dust approximates that of a blackbody. This is essentially true for all comets, since emission features contribute a negligible amount to the total power in either the scattered or thermal energy distributions. In this case, the ratio of the maximum of the λf_λ function to the total blackbody emission f is given by

$$\frac{(\lambda f_\lambda)_{\max}}{f} = \frac{2\pi hc^2}{\sigma(\lambda_m T)^4} \left[\frac{1}{e^{hc/k(\lambda_m T)} - 1} \right] = \frac{1}{1.3586}, \quad (5)$$

where λ_m is the wavelength of maximum emission in λf_λ ; $\lambda_m T = 0.3670$ cm deg is Wien's law for λf_λ ; $h = 6.626 \times 10^{-27}$ c.g.s.; $c = 2.9979 \times 10^{10}$ cm/s; $\sigma = 5.6696 \times 10^{-5}$ c.g.s.; and $k = 1.3806 \times 10^{-16}$ c.g.s. Thus, for example, the apparent infrared intensity f_{IR} of the coma is given by

$$f_{IR} = 1.3586(\lambda f_\lambda)_{\max, IR}, \quad (6)$$

where $(\lambda f_\lambda)_{\max, IR}$ is the observed apparent emission maximum of the thermal-infrared continuum.

1.1.2.3. Albedo of comet dust and the structure of the grains

The bolometric (total-power) albedo, A , for a comet's coma is a measure of the ratio of the light scattered by the grains to that absorbed and re-emitted; A can be defined by the relationship

$$\frac{f_{\text{scat}}}{f_{IR}} = \frac{A}{1 - A}, \quad (7)$$

where the left-hand side is the ratio of the energy scattered in all directions to the total energy absorbed from the sun; f_{scat} is the observed scattered power (in units of W cm^{-2}) integrated over all scattering angles, and f_{IR} (in W cm^{-2}) is the observed thermal emission due to re-radiation of the absorbed radiation. For small grains, f_{scat} must be derived from measurements of the visible/near-infrared energy distribution of the coma at all scattering (sun-comet-Earth) angles, because the scattering function is strongly angle-dependent (see Figure 5). This can be accomplished to some extent for any given comet by observing it at as many phase angles as possible, as the viewing aspect changes during the orbit. In practice, since no single comet necessarily presents all scattering angles, the "typical" comet scattering function shown in Figure 5 must be obtained by piecing together measurements of many comets. It can be seen that much more data are still required for scattering angles near 0° and 180° . The sunlight that is absorbed and re-emitted in the infrared by the grains as f_{IR} can be determined by measurements of the thermal-infrared energy distribution of the coma. The albedo, $A(\theta)$ for a scattering angle θ is defined by analogy to equation (7), above, as

$$A(\theta) = \frac{f(\theta)}{1 + f(\theta)}, \quad (8)$$

where:

$$f(\theta) = \frac{f_{\text{scat}}(\theta)}{f_{IR}(\theta)} = \frac{[\lambda f_\lambda(\theta)]_{\max, \text{scat}}}{[\lambda f_\lambda(\theta)]_{\max, IR}}. \quad (9)$$

In equation (9), $f_{\text{scat}}(\theta)$ and $f_{IR}(\theta)$ are the integrated apparent intensities of the scattered and thermal energy distributions of the coma, respectively, for the scattering angle θ .

The mean bolometric albedo, A , averaged over all scattering angles is then given by

$$A = \frac{1}{\pi} \int_0^\pi A(\theta) d\theta. \quad (10)$$

Since the scattered and thermal energy distributions of comets can be closely approximated by blackbody energy distributions, the result obtained in section 1.1.2.2 (above) can be used to determine $f_{\text{scat}}(\theta)$ and $f_{IR}(\theta)$ from the directly measurable quantities $[\lambda f_\lambda]_{\max, \text{scat}}$ and $[\lambda f_\lambda]_{\max, IR}$. The $A(\theta)$ curve defined by infrared observations of a number of comets (see Figure 5) shows that there is a fairly strong forward scattering peak near $\theta \approx 0^\circ$ and is consistent with the interpretation that the grains are fluffy aggregates [Gehrz and Ney 1992].

1.1.2.4. Dependence of a comet's apparent infrared luminosity on r , Δ , and beam size

For a coma that is optically thin to thermal infrared radiation, as is always the case in the thermal infrared, the apparent infrared intensity f_{IR} of a coma composed of N dust grains is:

$$f_{IR} = \frac{L_{IR}}{4\pi\Delta^2} = \frac{4\pi N a^2 Q_e \sigma T_{gr}^4}{4\pi\Delta^2} = \frac{N a^2 Q_e \sigma T_{gr}^4}{\Delta^2}, \quad (11)$$

where L_{IR} is the coma luminosity. Assuming an isotropic grain distribution for a spherically symmetric coma within a radius R of the nucleus, then N is given by

$$N = 4\pi \int_0^R n(R) R^2 dR = \frac{dN}{dt} t = \frac{dN}{dt} \frac{R}{V_0}, \quad (12)$$

where $t = R/V_0$ is the time required for grains to flow at constant velocity V_0 out to radius R , and $n(R)$ is the radial number density distribution of grains in the coma. It therefore follows that the radial grain density distribution for the steady-state model must be

$$n(R) = \frac{1}{4\pi R^2 V_0} \frac{dN}{dt}. \quad (13)$$

Integrating $n(R)$ over the cylindrical volume V of the coma that is intercepted by a photometer beam of angular diameter ϕ , to obtain the number N_ϕ of grains emitting into the beam, yields — with the help of equation (11) — an apparent infrared intensity $f_{\phi,IR}$ in the beam of

$$f_{\phi,IR} = \frac{a^2 Q_e \sigma T_{gr}^4}{\Delta^2} N_\phi = \frac{a^2 Q_e \sigma T_{gr}^4}{\Delta^2} \iiint_V n(R) d^3R = \left[\frac{\pi a^2 Q_e \sigma T_{gr}^4}{4V_0} \right] \frac{\phi}{\Delta} \frac{dN}{dt}, \quad (14)$$

where the result on the extreme-right-hand side is for the case where the angular diameter of the beam is much smaller than the angular diameter of the coma. It can be seen from equation (14) that $f_{\phi,IR} \propto \phi/\Delta$, leading to the correction terms specified in Table 1 and discussed in section 1.1.3.7, below.

◇ ◇ ◇

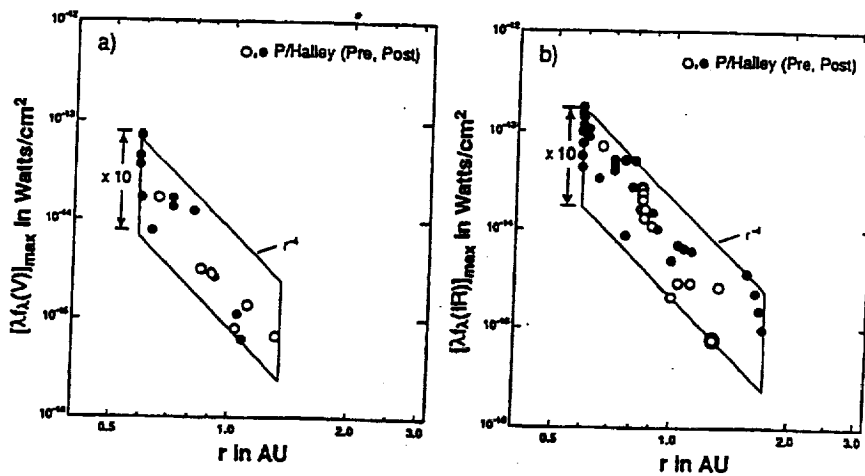


Figure 6. The activity of the nucleus of 1P/Halley as a function of heliocentric distance at visible (a) and infrared (b) wavelengths, as measured by variations of the apparent intensities $[\lambda f_\lambda(V)]_{\max} = (\lambda f_\lambda)_{\max, \text{scat}}$ and $[\lambda f_\lambda(IR)]_{\max} = (\lambda f_\lambda)_{\max, IR}$, respectively. Figure from Gehrz and Ney [1992], reproduced by permission of Icarus.

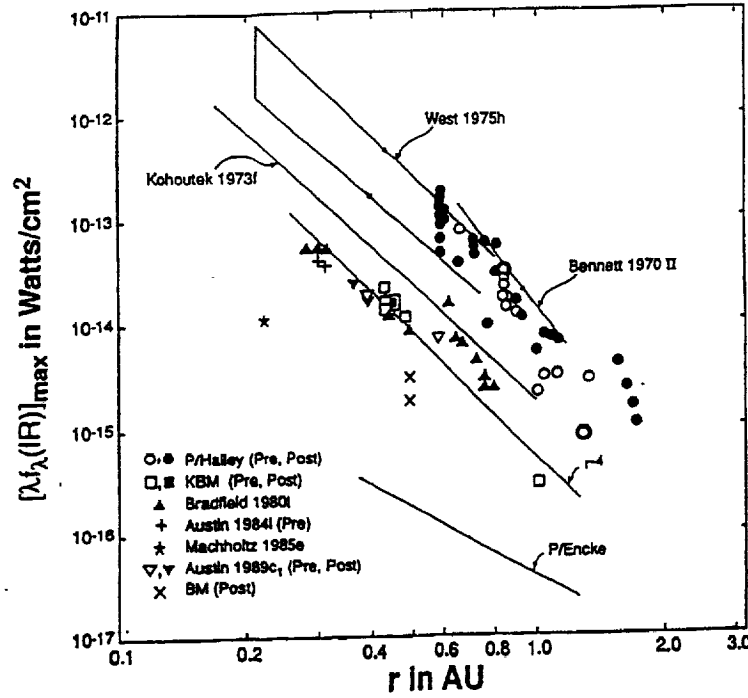


Figure 7. The infrared activity of the nuclei recent bright comets as a function of heliocentric distance, as measured by variations in the quantity $[\lambda f_\lambda(IR)]_{\max} = (\lambda f_\lambda)_{\max, IR}$. Figure from Gehrz and Ney [1992], reproduced by permission of *Icarus*.

◇ ◇ ◇

1.1.2.5. Activity in comet nuclei

The apparent infrared intensity $f_{\phi, IR}$ of an optically-thin cometary coma in a beam of angular diameter ϕ radians that is much smaller than the angular extent of the coma is

$$f_{\phi, IR} = 1.3586(\lambda f_\lambda)_{\max, IR} = \left[\frac{\pi a^2 Q_e \sigma T_{gr}^4}{4V_o} \right] \frac{\phi}{\Delta} \frac{dN}{dt} = \left[\frac{a^2 Q_e L_\odot}{64V_o} \right] \frac{\phi}{r^2 \Delta} \frac{dN}{dt}. \quad (15)$$

If the grain production rate as a function of r , $dN(r)/dt$, is directly proportional to the insolation of the nucleus:

$$\frac{dN(r)}{dt} = \frac{dN(q)}{dt} \left[\frac{q}{r} \right]^2, \quad (16)$$

where q is the perihelion distance and $dN(q)/dt$ is the grain production rate in grains/sec at perihelion. Therefore, the apparent coma intensity is

$$f_{\phi, IR} = \left[\frac{a^2 Q_e L_\odot}{64V_o} \right] \frac{\phi q}{r^4 \Delta} \frac{dN(q)}{dt} \propto \frac{\phi}{r^4 \Delta}. \quad (17)$$

In cases where the luminosity of the coma is generated by emission from very small silicate grains, for which $Q_e \propto a$, the apparent infrared intensity of the coma is directly proportional to the total mass, M_{gr} , of the grains:

$$f_{\phi, IR} \propto \frac{M_{gr} \phi}{r^4 \Delta}. \quad (18)$$

From equation (18), it is apparent that the approximation quantified in equation (16) implies a dependence of r^{-4} for both the scattered and thermal energy distributions of comets. The quantity $[\lambda f_\lambda]_{\max, IR}$ is a better measure of a comet's intrinsic brightness than is $[\lambda f_\lambda]_{\max, scat}$ because of the rather strong variation in albedo with phase angle (see Figure 5). Figures 6 and 7 summarize the activity of the nuclei of 1P/Halley and other recent bright comets. Clearly, the activity in most comets is proportional to r^{-4} as predicted by the theory outlined above both preceding and following perihelion passage. There are, as noted elsewhere in this review, substantial superimposed variations for some comets due to nuclear activity that is most probably associated with nuclear rotation.

1.1.2.6. Dust mass-loss rates of comet nuclei

The dust mass-loss rate dM_D/dt caused by the ablation of dN/dt grains/sec from a comet nucleus, assuming that each grain has a density ρ_{gr} and radius a , is

$$\frac{dM_D}{dt} = m_{gr} \frac{dN}{dt} = \frac{4\pi}{3} \rho_{gr} a^3 \frac{dN}{dt} \quad (19)$$

where $m_{gr} = 4\pi\rho_{gr}a^3/3$ is the mass of a single grain. From the discussion above, it follows that

$$\frac{dM_D}{dt} = [1.3586(\lambda f_\lambda)_{\max,IR}] \frac{256\pi}{3} \frac{a\rho_{gr}}{L_\odot Q_a} V_o \frac{r^2 \Delta}{\phi}, \quad (20)$$

where V_o is the grain ejection velocity and $(\lambda f_\lambda)_{\max,IR}$ is obtained by correcting the observed intensity for diaphragm-size and reference beam throw effects (see Table 1). Grains accelerated to terminal velocity by momentum coupling to the gas will have V_o given by

$$V_o = 5 \times 10^4 \left[\frac{T_{BB}}{278} \right]^{1/2} = \frac{5 \times 10^4}{r^{1/4}} \text{ cm/s} \approx 0.5 \text{ km/s}, \quad (21)$$

Since V_o depends only weakly upon r [expressed in equation (21) in AU], we henceforth use $V_o \approx 0.5 \text{ km/s}$. Assuming that $a \approx 1 \mu\text{m} = 10^{-4} \text{ cm} = 1000 \text{ nm}$, $\rho_{gr} \leq 1 \text{ g/cm}^3$, and $Q_a = 1$, then the dust mass-loss rate becomes

$$\frac{dM_D}{dt} = 7 \times 10^{21} (\lambda f_\lambda)_{\max,IR} \frac{r^2 \Delta}{\phi} \text{ g/s} \propto r^{-2}, \quad (22)$$

where r and Δ in equation (22) are expressed in units of AU. We emphasize that this mass-loss rate refers only to the emission from the optically-important particles. Since a considerable amount of the dust mass may be in large particles that do not contribute significantly to the infrared emission, the mass-loss rate given by equation (22) should be considered to be a lower limit.

1.1.3. Measurement and calibration of photometric and spectroscopic quantities

We describe in this section how typical infrared observations of the crucial quantities $(\lambda f_\lambda)_{\text{cat}}$, $(\lambda f_\lambda)_{IR}$, and their derivatives are obtained and calibrated using infrared photometers, spectrophotometers, and imagers. Until recently, state-of-the-art infrared instrumentation and infrared-optimized telescopes were sufficiently complex and costly as to be ordinarily beyond the resources of even the most wealthy amateur astronomers. From the founding of modern infrared astronomy in the early 1960s until well into the 1980s, most of the existing infrared instruments were constructed and used by a small handful of professionally-trained experimental physicists and astronomical instrumentation specialists. However, nearly all major national, and most large private, observatories now own and operate a fairly complete complement of infrared spectrophotometers, imagers, and imaging spectrometers. More readily than ever before, the non-specialist can gain access to robust and well-supported infrared instruments. The price of small CCD cameras that respond in the very near-infrared ($\lambda \leq 1.2 \mu\text{m}$) is now so low that even many amateurs are acquiring them. We present here, as an aid to comet observers at all levels, a summary of the generic types infrared of instruments that are appropriate for various types of infrared observations, brief comments on the observational techniques that should be used for these observations, and tables providing typical calibration data required to reduce infrared measurements.

1.1.3.1. Basics of infrared telescopes and measurements

Sensitive infrared measurements, especially at wavelengths longer than $3 \mu\text{m}$ — where thermal (heat) emission is the dominant contribution to the background — must be obtained with telescopes and instrumentation that have been optimized to minimize thermal emission from the telescope and optics using techniques designed to facilitate the cancellation of background radiation from the telescope and the sky. Low and Rieke [1974] and Gehrz *et al.* [1992] have previously described infrared telescope, instrumentation, and observing techniques in detail, and we present here only a very brief summary of the essentials to guide the interested reader in consulting these more extensive discussions.

In general, infrared optimized telescopes have high-reflectivity, low-emissivity coatings on the optical surfaces to minimize thermal emission, and they have "chopping" secondary mirrors for canceling the telescope and sky background. A "chopping" secondary mirror is one that is mounted on a flexural-pivot hinge so that it can be moved back and forth (chopped) by means of a servo-motor system. The resulting motion causes the footprint, or "beam" seen by the detector to sweep across the sky. A field stop (Lyot stop) is an aperture that defines the focal ratio of an optical system by limiting the divergence angle of the rays that can be seen from the focal plane. In a telescope, this type of stop can be thought of as preventing an instrument in the focal plane from seeing either blank sky around the secondary mirror or any of the telescope structure that lies beyond the edge of the primary mirror. Cold Lyot stops in IR detection systems prevent the detectors from seeing any thermal emission from the sky around the secondary and from the telescope walls. The stop must be cold so that it does not emit thermal radiation onto the detector. A Lyot stop can be placed anywhere an image of the telescope's primary mirror (a "pupil" image) is formed, and it is a blackened aperture whose diameter is equal to that of the image of the primary.

Cooling is easily provided since all of the infrared detectors used in the observations described herein must be operated at either liquid-nitrogen or liquid-helium temperatures using a dewar (a vacuum-jacketed vessel, much like a thermos bottle, that is designed hold cold liquefied gases) that contains a window to facilitate the transmission of the light path to the detector. Since a pupil image is also uniformly illuminated, it is usually customary to place the infrared filters, which must also be cooled and uniformly illuminated, as close to the Lyot stop as possible. In cases where this is mechanically impossible due to space limitations, a second pupil image may have to be provided for the filters. Pupil images are formed where needed within the dewar using small lenses or mirrors placed in the optical path. A detector in the focal plane will view a beam upon the sky whose size is determined by the magnification of the optical system. Single detectors in infrared photometers typically have beams with angular diameters of 3"-20". Gehrz, Grasdalen, and Hackwell [1992] have described infrared dewars (see their Figure 3) and cooled optical systems (see their Figure 4) in detail.

The usual background cancellation technique is to rock (chop) the secondary mirror about its pivot with a square-wave motion at a fixed frequency of f_0 cycles per second, so that the detector alternately views two discrete sky positions called beam A and beam B. Each beam will nominally contain the same amount of background power. The detector alternately views each beam for a dwell-time, $t_0 = 1/(2f_0)$ sec during a chop cycle, and the time actually required to move the secondary from one beam to the other is negligible compared to the dwell time, t_0 . Typical values for f_0 are 5 to 20 cps, and for t_0 are therefore 0.025 to 0.1 sec. When an astronomical point source is placed in one of the beams (now designated the "source" beam), the power emitted by the source into that beam is added to the background power level. The background power in the other beam (now designated the "reference" beam) remains unaltered. A filtered synchronous amplifier tuned to the frequency f_0 will detect the source signal as an AC signal that has a nominal phase angle of either 0° or 180° with respect to the initiation of the chop cycle, depending upon whether beam A or beam B is the source beam. Gehrz *et al.* [1992] have described the square-wave chopping process and the expected signal forms in detail (see their Figure 5). Under "Background Limited Incident Power" (BLIP) conditions, the detector noise is negligible compared to the noise on the signal due to the photon ("shot") noise in the background power. If the background power is negligible, the noise on the signal will be due to the intrinsic electrical noise of the detector and amplification systems. These two conditions are termed background-noise-limited and detector-noise-limited, respectively. If the two beams view the optics of the detection system and the telescope from slightly different aspects, the amount of residual thermal emission into each beam will be different for the two beam positions, and a "false" AC source signal will be produced whose phase remains constant when the astronomical source is switched from one beam to the other.

Data is typically obtained by taking a number of A-B, B-A beam-switched pairs. The source is first centered in beam A, so that beam B is the sky-reference beam, and the signal is integrated for a time t . The telescope is then moved so that the source is centered in beam B, with beam A becoming the sky-reference beam, and the signal is integrated for the same time interval. The second half of the A-B, B-A cycle is conducted by reversing the process. It can be shown that the A-B, B-A cycle eliminates the false AC signal component from the telescope to first order. Signal-to-noise is improved by statistically co-adding the results of many A-B, B-A pairs. Although the most accurate background cancellation can be obtained if the beams are tangent (that is, the angular distance, or "throw", between the beams is equal to their diameter), larger throws are needed for comets because they are extended sources of emission.

Chopped, beam-switched elimination of the telescope emission and sky background is essential for any infrared photometric, imaging, or spectroscopic observation where strong or variable background radiation is a significant issue. This includes almost any observations where the thermal background is high ($\lambda \geq 3 \mu\text{m}$), but can also apply to observations at shorter wavelengths where cancellation of rapid upper-atmospheric air-glow line-emission fluctuations is required. Correction of the data for the effects of atmospheric extinction (absorption) is described in section 1.1.3.6. Because the angular distance between the source and reference beams cannot be arbitrarily large, due to the mechanical limitations of chopping secondary mirrors, the reference beam may still fall on a portion of a source that has a large angular extent. This is almost always the case for comets, and we describe how to correct the source-beam flux for source emission in the reference beam in section 1.1.3.7, below.

1.1.3.2. Infrared photometry of comets

Infrared photometry may be defined as the measurement of monochromatic intensities using broad filter bandpasses, ordinarily with widths given by $30 \geq \lambda_0/\Delta\lambda \geq 1$, where λ_0 is the effective wavelength of the center of the bandpass and $\Delta\lambda$ is the nominal Full Width of the bandpass at Half Maximum intensity (FWHM). Usually, individual cold thin-film interference filters are placed in the incident radiation beam by mounting them in a slide or wheel that is fastened to the cold work surface within the dewar. In computing λ_0 , the instrumental transmission function, $\Phi(\lambda)$; the atmospheric transmission curve $\tau(\lambda)$; and the energy distribution of the source under observation, f_λ , must all be taken into account using

$$\lambda_0 = \frac{\int_0^\infty \lambda \Phi(\lambda) \tau(\lambda) f_\lambda d\lambda}{\int_0^\infty \Phi(\lambda) \tau(\lambda) f_\lambda d\lambda}. \quad (23)$$

The function $\Phi(\lambda)$ includes the transmission function of the filters, the transmission efficiency of the telescope/instrument optical system, and the response curve of the detector. Bolometers (total energy detectors) are the detector of choice for ground-based photometric measurements of comet infrared-energy distributions, because they have a quantum efficiency ≈ 1 from V (0.55 μm) to 33 μm and have detector noises lower than the BLIP noise for photometric bandpasses. The most popular of these in the 1990s are the Ga:Ge and Ga:Si devices available through Infrared Laboratories, Inc., in Tucson, AZ. Photoconductive and photovoltaic solid-state detectors are used in some photometric systems, but these

have a long-wavelength cutoff beyond which they do not respond because the photon energy is too low to move carriers into the conduction band; they also have lower quantum efficiency and a less-uniform response curve than bolometers. Photoconductors have an additional noise factor of $2^{1/2}$ compared to bolometers, because of the random recombination of electron-hole pairs as the carriers are de-excited. In:Sb detectors can be used from 1 to 5 μm , and As:Si are useful in the 7- to 20- μm region. Hg:Cd:Te detectors are an alternative for the 1- to 2.5- μm systems.

Several standard sets of photometric filters are currently in use for ground-based observations. Table 2 summarizes the effective wavelengths and FWHM bandpasses of the three systems that are now used for almost all infrared observations of comets. The absolute flux densities for a zero-magnitude star at the top of the earth's atmosphere are given in Table 3. For interpolating the fluxes given in column 3 of Table 3 to obtain zero-magnitude fluxes to within a few percent accuracy at other effective wavelengths between 1.2 and 33 μm on the Minnesota/Wyoming system, one may use the relationship:

$$F_{\lambda} = \left[\frac{1.903 \times 10^{-12}}{\lambda^5} \right] \left[\frac{1}{e^{1.439/\lambda} - 1} \right], \quad (24)$$

where λ is in μm , F_{λ} has units of $\text{W cm}^{-2} \mu\text{m}^{-1}$, and F_{λ} and F_{ν} are related by

$$F_{\nu} = (3.33 \times 10^{11}) \lambda^2 F_{\lambda}, \quad (25)$$

with F_{ν} in units of $\text{W m}^{-2} \text{Hz}^{-1/2}$. Several private and national infrared telescopes are equipped with state-of-the-art helium-cooled bolometers and with standard filters on the infrared photometric systems similar to those defined in Tables 2 and 3. The filter sets for these systems usually include *V*, *R*, *I*, *J*, *H*, *K*, *M*, various *N* (10- μm) and *Q* (20- μm) filters, and the IRTF "silicate filters" (which respond at $\lambda_0 = 7.8, 8.7, 9.8, 10.3, 11.6$, and $12.5 \mu\text{m}$, having bandwidths of ≈ 10 percent).

The magnitude of an unknown source may be calculated from a measurement of a standard star, using the fact that the magnitude difference between two stars whose apparent fluxes are $f_1(\lambda)$ and $f_2(\lambda)$ is given by

$$\Delta m = -2.5 \log \left[\frac{f_1}{f_2} \right], \quad (26)$$

The minus sign indicates that the magnitude of the brighter of the two stars has a smaller value than that of the fainter star. Stars brighter than magnitude zero have negative magnitudes. Table 4 lists the infrared magnitudes of the bright primary standard stars on the Wyoming photometric system. It should be noted that we have used the convention recently adopted by most infrared observers where Vega (α Lyrae) is arbitrarily defined to have an apparent magnitude of zero at all infrared wavelengths. The stars in Table 4 will be suitable for calibrating bolometer systems. These detectors, used on a 2- to 3-meter-class ground-based telescope, can typically measure (at a signal-to-noise level of 3 or better) magnitudes as faint as +10 at *K*, +5 at *N*, and +2 at *Q*. Bright comets inside $r = 1.5$ AU typically will be this bright in a beam or 5" angular diameter centered on the coma. In:Sb spectrophotometers containing *JHKKLLM* photometric filters and 1-percent resolution, 2- to 4- μm Circular Variable Filter Wheels (CVFWs) are much more sensitive than bolometers at wavelengths from 1 to 2.5 μm where the background power is negligible; they can measure objects with *J-K* magnitudes fainter than 15-17, depending upon telescope aperture size. The calibration of the InSb systems requires the use of a network of much fainter standards, and linearity issues must be addressed by observing standards having a brightness comparable to that of the unknown source. We give lists of selected intermediate brightness (Table 5) and faint (Table 6) United Kingdom Infrared Telescope (UKIRT) standards to facilitate near-infrared observations with In:Sb systems.

1.1.3.3. Infrared spectroscopy

Infrared spectroscopy is performed at higher resolutions than photometry, and is usually characterized by spectral resolutions of $10^6 \geq \lambda/\Delta\lambda \geq 30$. Moderate-resolution spectroscopy ($\lambda/\Delta\lambda \leq 100$) for $\lambda \leq 20 \mu\text{m}$ is often accomplished using cooled circular variable thin-film interference filters (CVFs), for which the wavelength transmitted is a function of angle around the wheel. These are mounted within the dewar as described above for photometry, and are rotated in front of the detector to scan the wavelength interval of interest. Still-higher spectral resolutions, and applications beyond 20 μm , require the use of dispersive optical elements such as reflection gratings or prisms constructed of infrared-transmitting materials. The highest spectral resolutions ($\lambda/\Delta\lambda \geq 10^4$) require Michelson or Fabry-Perot interferometers and heterodyne detection techniques such as are used in radio astronomy. The detectors of choice for most infrared spectroscopic measurements are the photoconductive and photovoltaic detectors described in section 1.1.3.2 (above), since the thermal background is very low at these high resolutions. Despite their superiority at high backgrounds, bolometers suffer from excessive detector noise at lower backgrounds. The calibration data and stars cited in Tables 2-6 are also suitable for calibrating spectra, and the background removal techniques are basically the same as for photometry. In spectrometers that have large format arrays (see section 1.1.3.4, below), the spectra of both the source and sky can be obtained on a single frame along the slit. Even in this case, beam switched AB/BA pairs are usually required to eliminate variable background emission and telescope effects. Wavelength calibration can be obtained using telluric water, ozone, and CO absorption lines and numerous near-infrared airglow emission lines. Extinction corrections such as those described in section 1.1.3.6 can be fine-tuned by iteratively applying equation (27) to null out the telluric emission and absorption features. In general, spectroscopy of sufficiently high spectral resolution ($\lambda/\Delta\lambda = 50-100$) to study the mineralogy of dust grains (using the 10- μm feature) limits such studies to bright comets that are near or inside $r = 1$ AU.

Table 2: Infrared Photometric Bandpasses Commonly in Use for Infrared Observations of Comets¹

Filter	Minnesota/Wyoming Systems				NASA IRTF System ²				Arizona Systems ²			
	Gehrz et al. 1974		Gehrz et al. 1992		Gehrz 1997 (This work) ³		Tokunaga 1986		Johnson 1965		Campius et al. 1985	
	λ_0 (μm)	$\Delta\lambda_0$ (μm)	λ_0 (μm)	$\Delta\lambda_0$ (μm)	λ_0 (μm)	$\Delta\lambda_0$ (μm)	λ_0 (μm)	$\Delta\lambda_0$ (μm)	λ_0 (μm)	$\Delta\lambda_0$ (μm)	λ_0 (μm)	$\Delta\lambda_0$ (μm)
R	-	-	0.9	0.2	-	-	1.2	0.3	1.25	0.37	1.26	0.20
J	-	-	1.2	0.2	-	-	1.6	0.3	-	-	1.60	0.36
H	-	-	1.6	0.3	-	-	2.2	0.4	2.2	0.6	2.22	0.52
K	2.3	0.7	2.2	0.4	-	-	3.55	1.05	3.5	1.0	3.54	0.97
L	3.6	1.2	3.6	1.2	-	-	3.78	0.57	-	-	-	-
L'	-	-	-	-	3.8	0.4	4.7	0.57	5.0	1.2	4.8	0.60
M	4.9	0.7	4.9	0.7	-	-	10.5	5.	10.2	5.6	10.6	5.
N	10.0	5.8	10.0	5.8	-	-	-	-	-	-	-	-
N7	-	-	-	-	7.91	0.76	-	-	-	-	-	-
N8	8.7	1.0	8.7	1.0	8.81	0.87	-	-	-	-	-	-
N9	-	-	-	-	9.80	0.95	-	-	-	-	-	-
N10	-	-	-	-	10.27	1.00	-	-	-	-	-	-
N11	11.4	2.0	11.4	2.0	11.70	1.11	-	-	-	-	-	-
N12	12.6	0.8	12.6	0.8	12.49	1.16	-	-	-	-	21.0	11.0
Q	19.5	5.8	19.5	5.8	18	5	20.6	9.	-	-	-	-
Q23	-	-	23	6	-	-	-	-	-	-	-	-
Q33	-	-	33	22	-	-	-	-	-	-	-	-

¹ Filter bandwidths are Full Width at Half Maximum (FWHM)² As cited in Hanner and Tokunaga 1991³ The G-filter NASA IRTF silicate interference filter set ($\lambda_0 = 7.91, 8.81, 9.80, 10.27, 11.70$, and $12.49 \mu\text{m}$) has been installed in several Minnesota/Wyoming Bolometers since June of 1987.Table 3: Absolute Flux Densities for 0 Magnitude¹

Filter	Minnesota/Wyoming Systems ²				IRTF/Arizona Systems ³			
	λ_0 (μm)	F_λ ($\text{W cm}^{-2} \mu\text{m}^{-1}$)	F_ν ($\text{W m}^{-2} \text{Hz}^{-1}$)	F_ν (Jy) ¹	λ_0 (μm)	F_λ ($\text{W cm}^{-2} \mu\text{m}^{-1}$)	F_ν ($\text{W cm}^{-2} \mu\text{m}^{-1}$)	F_ν (Jy) ¹
R	0.9	8.9×10^{-13}	2.40×10^{-23}	2405	-	-	-	-
J	1.2	3.3×10^{-13}	1.72×10^{-23}	1720	1.26	3.03×10^{-13}	1.60×10^{-23}	1600
H	1.6	1.2×10^{-13}	1.02×10^{-23}	1025	1.6	1.25×10^{-13}	1.07×10^{-23}	1067
K	2.2	4.2×10^{-14}	6.78×10^{-24}	678	2.2	4.11×10^{-14}	6.64×10^{-24}	664
K	2.3	3.39×10^{-14}	5.98×10^{-24}	598	-	-	-	-
L	3.6	6.43×10^{-15}	2.78×10^{-24}	278	3.54	6.83×10^{-15}	2.86×10^{-24}	286
L'	3.8	5.25×10^{-15}	2.53×10^{-24}	253	3.80	5.29×10^{-15}	2.55×10^{-24}	255
M	4.9	1.99×10^{-15}	1.59×10^{-24}	159	4.8	2.19×10^{-15}	1.68×10^{-24}	168
N	10.0	1.23×10^{-16}	4.10×10^{-25}	41.0	10.10	1.18×10^{-16}	4.02×10^{-25}	40.2
N7	7.91	3.08×10^{-16}	6.43×10^{-25}	64.3	-	-	-	-
N8	8.7	2.12×10^{-16}	5.35×10^{-25}	53.5	-	-	-	-
N8	8.81	2.02×10^{-16}	5.23×10^{-25}	52.3	-	-	-	-
N9	9.8	1.33×10^{-16}	4.26×10^{-25}	42.6	-	-	-	-
N10	10.27	1.11×10^{-16}	3.91×10^{-25}	39.1	-	-	-	-
N11	11.4	7.35×10^{-17}	3.19×10^{-25}	31.9	-	-	-	-
N11	11.70	6.63×10^{-17}	3.03×10^{-25}	30.3	-	-	-	-
N12	12.49	5.13×10^{-17}	2.76×10^{-25}	27.6	-	-	-	-
N12	12.6	4.96×10^{-17}	2.63×10^{-25}	26.3	-	-	-	-
Q	18	1.21×10^{-17}	1.31×10^{-25}	13.1	-	-	-	-
Q	19.5	8.84×10^{-18}	1.12×10^{-25}	11.2	20.0	7.88×10^{-18}	1.05×10^{-25}	10.5
Q23	23	4.58×10^{-18}	8.08×10^{-26}	8.08	-	-	-	-
Q33	33	1.09×10^{-18}	3.96×10^{-26}	3.96	-	-	-	-

¹ $1 \text{ Jy} = 10^{-26} \text{ W m}^{-2} \text{ Hz}^{-1}$ ² Interpolated using the flux scales given by Gehrz, Hackwell and Jones (1974) and Gehrz, Graedel, and Hackwell (1992)³ Calculated for the Vega fluxes and magnitudes given by Hanner and Tokunaga 1991

Table 4: Magnitudes of Selected Bright Infrared Standard Stars on the Minnesota/Wyoming Photometric System¹

Filter	λ_0	α Lyr ² A0V	α Boo K2IIIp	α Tau K5III	β Peg M2II-III	β And M0III	β Gem K0III	μ UMa M0III	α Sco M1Ib	α CMa A1V	γ Cru M3III
I	0.9	0.00	-1.67	-1.31	-0.40	-0.19	-0.11	+0.81	-1.70	-1.43	-
J	1.2	0.00	-2.17	-1.83	-1.09	-0.81	-0.48	-0.08	-3.10	-1.43	-
H	1.6	0.00	-2.91	-2.70	-2.07	-1.75	-1.05	-0.68	-3.80	-1.43	-
K	2.2	0.00	-3.00	-2.84	-2.24	-1.90	-1.12	-0.86	-3.80	-1.43	-
K	2.3	0.00	-3.00	-2.84	-2.24	-1.90	-1.12	-0.86	-3.80	-1.43	-3.08
L	3.6	0.00	-3.11	-2.95	-2.43	-2.06	-1.18	-1.00	-4.10	-1.43	-3.08
L'	3.8	0.00	-3.11	-2.95	-2.43	-2.06	-1.18	-1.00	-4.10	-1.43	-3.24
M	4.9	0.00	-2.97	-2.78	-2.27	-1.86	-1.09	-0.75	-3.90	-1.43	-3.24
N	10.0	0.00	-3.12	-2.94	-2.48	-2.03	-1.16	-0.92	-	-1.43	-3.03
N7	7.91	0.00	-3.12	-2.95	-2.43	-2.01	-1.19	-0.90	-	-1.43	-
N8	8.7	0.00	-3.13	-2.95	-2.43	-2.01	-1.19	-0.90	-4.30	-1.43	-3.26
N8	8.81	0.00	-3.13	-2.95	-2.43	-2.01	-1.19	-0.90	-4.30	-1.43	-3.26
N9	9.8	0.00	-3.13	-2.95	-2.44	-2.01	-1.19	-0.90	-4.80	-1.43	-3.39
N10	10.27	0.00	-3.13	-2.95	-2.47	-2.02	-1.19	-0.92	-4.80	-1.43	-3.40
N11	11.4	0.00	-3.19	-3.02	-2.54	-2.11	-1.19	-1.01	-4.80	-1.43	-3.44
N11	11.7	0.00	-3.19	-3.03	-2.55	-2.07	-1.19	-1.01	-4.80	-1.43	-3.45
N12	12.49	0.00	-3.20	-3.03	-2.55	-2.07	-1.17	-1.01	-4.80	-1.43	-3.51
N12	12.6	0.00	-3.20	-3.04	-2.56	-2.02	-1.16	-1.01	-4.80	-1.43	-3.52
Q	18.0	0.00	-3.17	-3.13	-2.77	-2.08	-1.16	-1.01	-4.80	-1.43	-3.40
Q	19.5	0.00	-3.17	-3.13	-2.77	-2.08	-1.16	-1.01	-4.80	-1.43	-3.40
Q23	23	0.00	-3.17	-3.13	-2.77	-2.08	-1.21	-1.01	-4.80	-1.43	-3.40
Q33	33	0.00	-3.17	-3.13	-2.77	-2.08	-1.21	-1.01	-4.80	-1.43	-3.40

¹ Magnitudes interpolated from data given by Gehrz and Ney (1972), Gehrz, Hackwell, and Jones (1974), Gehrz, Grasdalen, and Hackwell (1992), and Gehrz and Ney (unpublished).

² The currently accepted convention is to derive zero points for magnitude scales by assuming that the infrared colors of Vega (α Lyr) and other "average" A0 stars are all equal to zero, and to arbitrarily define Vega to be magnitude zero at all infrared wavelengths (see Bessell and Brett 1988). Normalization between systems can be made by comparing the magnitudes given for Vega. Magnitudes for Vega at 18-23 μ m assume a negligible contribution from the debris disk in the small beams typically used in ground-based photometry.

Table 5: Magnitudes of Selected Faint Infrared Standard Stars Suitable for Calibrating InSb JKLL'M Photometers and Imagers

Star	Spectrum	RA(1950) h m s	δ (1950) ° ' "	J (1.2 μ m)	H (1.6 μ m)	K (2.2 μ m)	L (3.5 μ m)	L' (3.8 μ m)	M (4.8 μ m)	Reference ²
HD 1160	A0	00 13 23.1	+03 58 24	7.060	7.051	7.040	7.05	7.04	-	1, 3
HD 2811	A3 V	00 28 53.0	-43 52 58	7.178	7.093	7.067	7.040	-	-	1, 3
BS 696	B2 Iae	02 21 43.1	+56 23 04	5.587	5.499	5.443	5.37	5.33	5.31	1, 3
HD 19904	A4 III-IV	03 08 49.1	-39 14 24	6.727	6.662	6.642	6.62	-	-	1, 3
HD 22686	A0	03 36 18.7	02 36 07	7.196	7.190	7.185	7.20	7.19	-	1, 3
BS 1552	B2 III	04 48 32.4	+05 31 16	4.029	4.087	4.138	4.18	4.18	4.15	1, 3
HD 38921	A0 V	05 45 41.0	-38 14 51	7.572	7.551	7.536	7.53	-	-	1, 3
HD 40335	A0	05 55 37.6	+01 51 09	6.555	6.473	6.452	6.43	6.43	6.41	1, 3
BD +0°1694	K5	06 52 07.3	+00 00 52	5.750	4.857	4.606	4.43	4.43	-	1, 3
HD 75223	A1 V	08 45 29.8	-39 36 54	7.329	7.296	7.281	7.260	-	-	1, 4
HD 77281	A2	08 59 05.4	-01 16 45	7.111	7.052	7.031	7.00	7.06	6.97	1, 3
HD 84800	A2	09 45 35.9	+43 53 56	7.592	7.549	7.538	7.55	7.54	7.58	1, 3
HD 101452	A2	11 37 45.1	-38 52 09	7.018	6.890	6.848	6.81	-	-	1, 3
HD 106965	A2	12 15 24.0	+01 51 10	7.380	7.337	7.316	7.30	7.34	7.30	1, 3
HD 129655	A2	14 41 11.0	-02 17 38	6.826	6.724	6.692	6.67	6.68	-	1, 3
HD 130163	A0 V	14 44 36.2	-39 43 04	6.856	6.846	6.835	6.81	-	-	1, 3
HD 136754	A0	15 19 24.3	+24 31 19	7.155	7.146	7.135	7.14	7.14	-	1, 3
HD 161743	B9 IV	17 45 31.8	-38 06 11	7.620	7.620	7.615	7.61	-	-	1, 3
HD 161903	A2	17 45 43.3	-01 47 34	7.172	7.059	7.023	6.99	7.01	7.14	1, 3
HD 162208	A0	17 46 20.7	+39 59 40	7.223	7.141	7.112	7.09	7.14	7.12	1, 3
BS 7773	B9.5 V	20 17 53.5	-12 55 04	4.825	4.859	4.859	4.86	4.86	-	1, 3
HD 201941	A2	21 10 13.6	+02 26 12	6.696	6.657	6.626	6.60	6.61	-	1, 3
HD 205772	A5 IV-V	21 35 33.6	-41 16 26	7.775	7.688	7.657	7.634	-	-	1, 3
BS 8541	B9 Iab	22 22 29.0	+49 13 21	4.305	4.267	4.235	4.23	4.22	4.22	1, 3
BS 8551	K0 III-IV	22 25 19.6	+04 26 39	2.956	2.378	2.312	2.25	2.24	2.32	1, 3

¹ 1) Walther 1996; 2) Elias et al. 1982; 3) spectral type from the Walther 1996; 4) spectral type from SIMBAD

Table 6: Magnitudes of Selected UKIRT Faint
Infrared Standard Stars for Calibrating
JHK Photometers and Imagers

Star	RA(1950)			δ (1950)			J	H	K
	h	m	s	°	'	"	(1.2 μ m)	(1.6 μ m)	(2.2 μ m)
FS 01	00	31	22.7	-12	24	29	13.429	13.048	12.967
FS 02	00	52	36.0	+00	26	58	10.713	10.504	10.466
FS 03	01	01	46.6	+03	57	34	12.600	12.725	12.822
FS 04	01	52	03.7	+00	28	20	10.556	10.304	10.264
FS 05	01	52	04.7	-07	00	47	12.335	12.340	12.342
FS06	02	27	39.2	+05	02	34	13.239	13.305	13.374
FS 07	02	54	47.2	+00	06	39	11.105	10.977	10.940
FS 08	02	55	12.9	+00	04	04	7.547	8.184	8.313
FS 09	02	55	38.8	+00	58	54	7.382	8.108	8.266
FS 10	03	46	17.4	-01	07	38	14.749	14.870	14.919
FS 11	04	50	25.4	-00	19	34	11.354	11.294	11.278
FS 12	05	49	34.8	+15	52	37	13.681	13.807	13.898
FS 13	5	54	33.8	+00	00	53	10.517	10.182	10.135
FS 14	07	21	41.2	-00	27	10	14.108	14.182	14.261
FS 15	08	48	2.9	+11	55	02	12.778	12.420	12.360
FS 16	08	48	31.0	+12	00	36	12.971	12.669	12.631
FS 17	08	48	35.4	+12	03	26	12.681	12.343	12.270
FS 19	10	31	14.5	-11	26	08	13.565	13.654	13.796
FS 20	11	05	27.6	-04	53	04	13.353	13.404	13.473
FS 21	11	34	27.6	+30	04	35	12.948	13.031	13.132
FS 33	12	54	35.1	+22	18	08	14.017	14.162	14.240
FS 23	13	39	25.7	+28	44	59	12.997	12.446	12.374
FS 24	14	37	33.3	+00	14	36	10.904	10.772	10.753
FS 25	15	35	59.9	+00	24	03	10.231	9.826	9.756
FS 26	16	34	26.3	-00	28	39	8.830	8.127	7.972
FS 27	16	38	54.2	+36	26	56	13.494	13.181	13.123
FS 35	18	24	44.5	+04	01	17	12.231	11.846	11.757
FS 34	20	39	41.9	-20	15	21	12.819	12.919	12.989
FS 29	21	49	53.0	+02	09	16	13.175	13.271	13.346
FS 30	22	39	11.3	+00	56	55	11.923	11.979	12.015
FS 31	23	09	50.4	+10	30	46	13.798	13.919	14.039
FS 32	23	13	38.2	-02	06	58	13.459	13.576	13.664

Magnitudes from Casali and Hawarden 1992

♦ ♦ ♦

1.1.3.4. Infrared imaging

As far as is known, the dust emission from comet comae and tails probably conforms to the area covered by the structures seen in visual light. It is merely the relatively low sensitivity of infrared detection systems that has prevented extensive studies of the distribution of infrared emission in the outer coma and tails. The situation is changing. Until the late 1980s, infrared images of extended sources such as comet comae and tails were constructed by scanning or point-wise mapping with a single detector. Recent advances in solid-state technology have fostered the industrial development of large-format infrared detector arrays of photoconductive and photovoltaic detectors suitable for the low-background conditions attending high-resolution infrared spectroscopy and narrow-band infrared photometry. Sensitive, high-quality In:Sb , As:Si , and Hg:Cd:Te array detectors are now widely available. They have formats of 16×64 , 64×64 , 128×128 , and 256×256 pixels — and formats as large as 1024×1024 pixels are anticipated for the near-infrared in a few years. The stable of available arrays can cover the 1- to 20- μ m spectral region. Some are charge-coupled devices (CCDs), but the best signal-to-noise is obtained with the Direct ReadOut (DRO) devices produced by the Aerojet Corporation, Rockwell International, and Santa Barbara Research Corporation (SBRC). Most of the funding for the development of these arrays came from military-related research funded by the United States' Department of Defense, but NASA's Space InfraRed Telescope Facility (SIRTF) Program has had a substantial impact on the most recent infrared array detector

innovations.

Infrared array detectors are now available in infrared imaging cameras and spectrometers at many national (and some private) observatories. Data acquisition and calibration techniques using both imagers and imaging spectrometers follows the arguments outlined in sections 1.1.3.1, 1.1.3.2, and 1.1.3.3 (above), with several caveats. First, since the instrumental response over the spatial field-of-view may be affected by vignetting, adequate background removal requires the acquisition of observations of "flat" intensity fields. These can be obtained either by viewing blank sky or a uniformly-illuminated portion of the telescope dome. Second, the linearity of the response of the pixels must be determined by viewing a calibration lamp that illuminates the array at several light levels covering the dynamic range of the observations. Third, the dark-current (false signal due to creation of carriers in an unilluminated detector) may vary from pixel-to-pixel, so that dark "flats" must be obtained. The calibration sources cited in Tables 2-6 will suffice to deal with infrared imager and imaging-spectrometer data over the range of signal levels required to evaluate detector linearity.

1.1.3.5. Infrared polarimetry

Infrared polarimetry of comets can be a valuable technique for determining the physical properties of the coma and tail material. Since all of the grains and gas molecules in the coma have exactly the same scattering geometry with respect to the sun and earth, regardless of their distance from the nucleus, the percent polarization will be determined only by the size distribution and optical constants of the grains, and by the gas emission. The near-infrared covers the range from almost pure scattering in the J (1.22- μm) band to a combination of scattering and molecular-band emission in the K (2.2- μm) band, to predominately thermal dust emission in the L' (3.8- μm) band. Spectropolarimetry can be used to distinguish the contributions from the gas and dust in various emission features. Observations using both photometers and imagers equipped with wire-grid polarizers and half-wave plates have been employed in recent measurements [see Hanner and Tokunaga 1991]. Calibration and analysis of polarimetric data involves both flux calibration, using objects cited in Tables 2-6, and observations of standard stars whose intrinsic polarization is well known. A standard calibration technique to eliminate the instrumental and interstellar polarization from measurements of a comet is to measure the intrinsic polarizations of faint A-, F-, and G-type stars lying in the same direction in the sky, and whose interstellar polarization component should be nearly zero.

1.1.3.6. Correction for atmospheric extinction

First-order corrections for atmospheric extinction are ordinarily applied to infrared photometric measurements using the relationship

$$f_{\lambda}(1.00) = f_{\lambda}(x) \times 10^{0.4A_{\lambda}(x-1.00)}, \quad (27)$$

where $f_{\lambda}(1.00)$ is the apparent flux from the source that would be observed through the first airmass at the zenith, $f_{\lambda}(x)$ is the apparent flux observed for the source through x air masses, and A_{λ} is the extinction coefficient in magnitudes per airmass. Provided that observations are made at altitude angles above about 10° , the atmospheric path length can be determined with sufficient accuracy by assuming that the atmosphere is a plane parallel slab, so that x for an observation at an altitude angle θ_{alt} is given by:

$$x = \frac{1}{\sin \theta_{alt}}. \quad (28)$$

Note that equation (28) yields a value of 1.00 at the zenith ($\theta_{alt} = 90^{\circ}$). The value of A_{λ} is ordinarily determined by repeated observations of the calibration standards during the night, as they rise and set. In the case of spectroscopic measurements, the corrections are somewhat more complex, since the atmospheric absorption is dominated by a plethora of atomic and molecular lines that are individually resolved at the higher spectral resolutions. The attenuation of a signal having a value at the top of the atmosphere of $f_{\lambda}(0)$ along a path length x can be written as

$$f_{\lambda}(x) = f_{\lambda}(0)e^{-\kappa_{\lambda}x}, \quad (29)$$

where $f_{\lambda}(x)$ is the signal observed at x , as determined by equation (28), and κ_{λ} is the linear absorption coefficient of the atmosphere as a function of wavelength in units of cm^{-1} . In principle, telluric absorption lines can be removed from a spectrum using equation (29). As in the case of photometry, κ_{λ} can be determined empirically by repeated observations of standard stars. Alternatively, one can use model-atmosphere calculations such as those described in Cohen *et al.* [1992] or measured values such as those available in Allen [1973].

Atmospheric absorption in the infrared can be highly variable between nights, and on time scales of several hours on any given night. Average extinction coefficients based on many nights of observing can be used as a last resort to obtain corrections, but it is always better to measure the extinction coefficients for each night upon which a comet is observed. The very best extinction compensation can be obtained when both the comet and the calibration star are measured at nearly the same airmass as closely in time as possible.

1.1.3.7. Normalization of photometric quantities for beam-size, throw, and distance

Comet comae and tails ordinarily have such a large angular extent that it is often mechanically impossible to throw the reference beam far enough from the source so that it falls on completely blank sky. Therefore, the standard beam-switching technique used for background cancellation also reduces the full signal that one would expect from a compact source, centered in the source beam, by the residual amount that an extended source emits into the reference beam. The reconstruction of the full source signal requires a detailed understanding of the surface brightness distribution of the source. We describe here the correction factors applicable to measurements centered on the coma of a comet that obeys the standard model (defined in section 1.1.2, above). The total emission from an optically-thin steady-state coma into a beam or pixel with angular diameter ϕ is proportional to the number of coma grains intercepted by the beam. We described this model in section 1.1.2, above, and concluded (see equation 14) that it leads to a ϕ^{+1} dependence of the coma brightness upon angular radius, and a Δ^{-1} dependence of the coma brightness on geocentric distance. Thus, it follows that the true intensity f_{∞} that would be measured in ϕ for a throw sufficiently large for the reference beam to reach blank sky can be recovered from the apparent intensity, f_{ψ} , observed in ϕ with a throw of angular distance ψ by

$$f_{\infty} = \left[\frac{4\psi}{4\psi - \phi} \right] f_{\psi}. \quad (30)$$

The apparent intensities f_1 and f_2 measured in diaphragms with angular diameters ϕ_1 and ϕ_2 at geocentric distances Δ_1 and Δ_2 are related by

$$f_2 = \left[\frac{\phi_2 \Delta_1}{\phi_1 \Delta_2} \right] f_1. \quad (31)$$

Equations (30) and (31) are useful for normalizing measurements made at different times and/or with different detection systems, so that brightness variations caused by the intrinsic activity of the comet nucleus can be evaluated.

REFERENCES

- Allamandola, L. J. (1984). in *Galactic and Extragalactic Infrared Spectroscopy*, ed. by M. F. Kessler and J. P. Phillips (Dordrecht: Reidel), 5.
- Allamandola, L. J.; A. G. G. M. Tielens; and J. R. Barker (1987). in *Interstellar Processes*, ed. by D. J. Hollenbach and H. A. Thronson, Jr. (Dordrecht: Reidel), 471.
- Allen, C. W. (1973). *Astrophysical Quantities*, 3rd ed. (London: Athlone Press).
- Becklin, E. E.; and J. A. Westphal (1966). *A.J.* **145**, 445.
- Bessell, M. S.; and J. M. Brett (1988). *P.A.S.P.* **100**, 1134.
- Campins, H.; G. H. Rieke; and M. J. Lebofsky (1985). *A.J.* **90**, 896.
- Campins, H.; and A. Tokunaga (1988). in Hanner (1988), 1-15.
- Casali, M. M.; and T. G. Hawarden (1992). "Provisional Faint Standards on the UKIRT System", in *JCMT-UKIRT Newsletter*, No. 3, Aug.; see also the UKIRT Web site at http://www.jach.hawaii.edu/UKIRT/astronomy/calib/faint_stds.html.
- Cohen, M.; R. G. Walker; M. J. Barlow; and J. R. Deacon (1992). *A.J.* **104**, 1650.
- Elias, J. H.; J. A. Frogel; K. Matthews; and G. Neugebauer (1982). *A.J.* **87**, 1029.
- Encarnaz, T.; and R. Knacke (1991). in Newburn *et al.* (1991), 1, 107.
- Fomenkova, M. N.; B. Jones; R. Pina; R. Puetter; J. Sarmecanic; T. J. Jones; and R. D. Gehrz (1995). *A.J.* **110**, 1866.
- Gehrz, R. D.; G. L. Grasdalén; and J. A. Hackwell (1992). in *The Encyclopedia of Physical Science and Technology* (New York: Academic Press), 2, 125.
- Gehrz, R. D.; J. H. Hackwell; and T. W. Jones (1974). *Ap.J.* **191**, 675.
- Gehrz, R. D.; C. H. Johnson; S. D. Magnuson; and E. P. Ney (1995). *Icarus* **113**, 129.
- Gehrz, R. D.; and E. P. Ney (1972). *PASP* **84**, 162.
- Gehrz, R. D.; and E. P. Ney (1992). *Icarus* **100**, 162.
- Gilman, R. C. (1974). *Ap.J. Suppl. Ser.* **28**, 397.
- Hanner, M. S., ed. (1988). *Infrared Observations of Comets Halley and Wilson and Properties of the Grains* (NASA Conference Publication 3004). Washington, DC: NASA Scientific and Technical Information Division. 186 pages.
- Hanner, M. S.; J. A. Hackwell; R. W. Russell; and D. K. Lynch (1994a). "Silicate Emission Feature in the Spectrum of Comet Mueller 1993a", *Icarus* **112**, 490.
- Hanner, M. S.; D. K. Lynch; and R. W. Russell (1994b). *Ap.J.* **425**, 274.
- Hanner, M. S.; R. L. Newburn; R. D. Gehrz; T. Harrison; E. P. Ney; and T. L. Hayward (1990). *Ap.J.* **348**, 312.
- Hanner, M. S.; and A. T. Tokunaga (1991). "Infrared Techniques for Comet Observations", in Newburn *et al.* (1991), 1, 67.
- Jewitt, D. (1991). "Cometary Photometry", in Newburn *et al.* (1991), 1, 19ff.
- Jewitt, D.; and K. Meech (1986). *A.J.* **93**, 1542.
- Johnson, H. L. (1965). *Comm. Lunar Plan. Lab.* **3**, 73.
- Low, F. J.; and G. H. Rieke (1974). *Methods. Exp. Phys.* **12A**, 415.

- Maas, R. W.; E. P. Ney; and N. J. Woolf (1970). *Ap.J.* **160**, L101.
 Ney, E. P. (1974). *Ap.J.* **189**, L141.
 Ney, E. P. (1982). "Optical and Infrared Observations of Bright Comets in the Range 0.5 μm to 20 μm ", in Wilkening (1982), 323.
 Rose, L. A. (1979). *Astrophys. Space Sci.* **65**, 47.
 Tokunaga, A. T. (1986). *The NASA Infrared Telescope Facility Photometry Manual*.
 Walther, D. (1996). in UKIRT Standards: Revised list MMC 3/3/92, see the UKIRT Homepage at http://www.jach.hawaii.edu/UKIRT/astrometry/calib/ukirt_stds.html.
 Weaver, H. A.; M. J. Mumma; and H. P. Larson (1991). in Newburn *et al.* (1991), 1, 93.
 Woolf, N. J.; and E. P. Ney (1969). *Ap.J.* **155**, L181.
 Yeomans, D. K., and R. N. Wimberly (1991). in Newburn *et al.* (1991), 2, 1281.

Φ Φ Φ

DESIGNATIONS OF RECENT COMETS

Listed below, for handy reference, are the last 30 comets to have been given designations in the new system. The name, preceded by a star (*) if the comet was a new discovery (compared to a recovery from predictions of a previously-known short-period comet). Also given are such values as the orbital period (in years) for periodic comets, date of perihelion, T (month/date/year), and the perihelion distance (q , in AU). Four-digit numbers in the last column indicate the *IAU Circular* (4-digit number) containing the discovery/recovery or permanent-number announcement. Not included below are nine recently-discovered comets observed only with the ESA/NASA Solar and Heliospheric Observatory (SOHO) spacecraft that are presumed to be Kreutz sungrazers that are no longer in existence (*IAUC* 6653, 6669, 6676): C/1996 B3, C/1996 Q2, C/1996 Q3, C/1996 S3, C/1996 X1, C/1996 X2, C/1996 Y1, C/1997 B2, and C/1997 K1. [This list updates that in the January 1997 issue, p. 52.]

<i>New-Style Designation</i>	<i>P</i>	<i>T</i>	<i>q</i>	<i>IAUC</i>
* C/1995 Y1 (Hyakutake)		2/24/96	1.05	6279
* P/1996 A1 (Jedicke)	19.3	8/15/95	4.1	6287
* C/1996 B1 (Szczepanski)		2/6/96	1.45	6296
* C/1996 B2 (Hyakutake)		5/1/96	0.23	6299
* C/1996 E1 (NEAT)		7/27/96	1.36	6341
125P/1996 F1 (Spacewatch)	5.6	7/14/96	1.54	6349
* C/1996 J1 (Evans-Drinkwater)		12/30/96	1.30	6397
* C/1996 N1 (Brewington)		8/3/96	0.93	6428
* P/1996 N2 (Elst-Pizarro)	5.6	4/18/96	2.63	6456
126P/1996 P1 (IRAS)	13.3	10/29/96	1.70	6446
* C/1996 P2 (Russell-Watson)		3/1/96	2.01	6448
* C/1996 Q1 (Tabur)		11/3/96	0.84	6455
* C/1996 R1 (Hergenrother-Spahr)		8/29/96	1.90	6470
* P/1996 R2 (Lagerkvist)	7.3	1/18/97	2.62	6473
* C/1996 R3		5/30/96	1.8	6564
127P/1996 S1 (Holt-Olmstead)	6.3	2/6/97	2.15	6475
128P/1996 S2 (Shoemaker-Holt 1)	9.5	11/20/97	3.05	6477
129P/1996 U1 (Shoemaker-Levy 3)	7.2	3/4/98	2.82	6494
* C/1997 A1 (NEAT)		6/19/97	3.16	6532
* P/1997 B1 (Kobayashi)	25.2	3/2/97	2.05	6553
* C/1997 BA ₆ (Spacewatch)		11/26/99	3.4	6561
* P/1997 C1 (Gehrels)	17.4	1/29/96	3.6	6549
* C/1997 D1 (Mueller)		10/11/97	2.25	6562
55P/1997 E1 (Tempel-Tuttle)	33.2	2/27/98	0.98	6579
* P/1997 G1 (Montani)	21.8	4/26/97	4.2	6622
* C/1997 G2 (Montani)		4/15/98	3.1	6626
130P/1997 H1 (McNaught-Hughes)	6.7	2/23/98	2.1	6640
* C/1997 J1 (Mueller)		5/3/97	2.3	6642
* C/1997 J2 (Meunier-Dupouy)		3/9/98	3.0	6648
* C/1997 H2 (SOHO)		5/2/97	0.14	6650

Tabulation of Comet Observations

ERRORS AND PROBLEMS WITH CONTRIBUTED DATA

When a bright, well-observed comet such as C/1995 O1 (Hale-Bopp) comes along, many new observers suddenly appear. Some will continue to observe other comets, and others will not be heard from again; a few may even become among the best and most prolific observers of comets. So encouragement and help is often required, and this is one purpose of the *ICQ*.

But your Editor has been overwhelmed with correspondence in recent months — not only because of the large numbers of daily e-mail messages that each contain only 1 or 2 observations from a single observer, but also because of the return e-mail necessitated by errors in the sending of data. If one takes a “file” to be all of the data sent by a single contributor (whether an Observation Coordinator or a single observer) for a 3-month *ICQ* publication period, I would guess that around 90 percent of all such “files” contributed by e-mail for the *ICQ* have problems. These problems come in three ways: (a) column-formatting errors (where data are placed in the wrong columns); (b) abbreviation/unit errors (where the wrong key letters or the wrong units are used); and (c) outright errors in the actual data. I estimate that roughly 50-60 percent of all such files actually have column-formatting errors, even from experienced contributors — which means that the data are *not* being properly checked before sending to the *ICQ*. Corresponding with so many contributors on so many problems is a huge reason why this issue is delayed by two months.

An especially big problem causing delays is that of the descriptive information; a quick perusal at the published descriptive information in the *ICQ* should immediately suggest that there are standard ways of providing this information, and yet many contributors ignore this fact. Descriptive information should be given chronologically, with the date spelled out and abbreviated (Jan., Feb., Mar., Apr., May, June, July, Aug., Sept., Oct., Nov., Dec.), with the year given for the first observation only per comet, and with the date given to 0.01 date (UT) as with the tabulated data. A colon then follows the date, with abbreviation standards along the lines of standard *ICQ*-coded abbreviations (see Keys in *ICQ Guide to Observing Comets* and on *ICQ* Web pages). Information within each date by a single observer is separated by commas, semi-colons, and parentheses, as appropriate (but never by periods, which indicate an end of the descriptive information by that particular observer on that particular date). Each observation ends with the observer's three-letter, 2-digit *ICQ* code given in square brackets, followed by a period. Start the next date of descriptive information on a new line. Things *not* to include in descriptive information: limiting naked-eye stellar magnitude; observing location; *suspected* faint tails, jets, and outer coma. Also, any tabulated information that lacks a magnitude estimate should *only* be included as descriptive information, unless the other categories (coma diameter, DC, tail length, *and* position angle) are all measured and available (if these four quantities are all available in the absence of m_1 data, it is permissible to include them on one line as a tabulated observation).

Observation Coordinators (OCs) need to check and double check every byte of data sent to the *ICQ*. I have said much about care and checking in the pages of the *ICQ* over the years, but this point can not be overstated: the quality of the entire archive depends on carefully checking all of the data at every step, whether at the telescope or contributing data to OCs or sending data to the *ICQ*. The number of simple errors that I find is alarming. This includes the wrong designation, the wrong year, month, date, or fraction of a date; this includes reference codes that do not exist, blatantly-wrong instrumentation (as with the 80-cm, 20× naked-eye data that I got recently), and wrong observer codes. We do our best to catch the problems beforehand, both via visual inspection and automatic computer programs to scan the data for obvious problems, with corrections made prior to publication both with and without consulting the contributors (as deemed appropriate); but many mistakes do get through in published form, and both contributors to and users of this archive need to be aware of this fact. Contributors need to understand that their efforts may be in vain if they do not take the time and care to check data and sort out problems before sending observations to the *ICQ*.

PROPER USE OF KEY LETTERS/ABBREVIATIONS, AND NEW ADDITIONS TO THE KEYS

An example of a subtle problem appears in the pages of this issue, one that I caught in the course of preparing these final pages for printing, therefore deciding to include the observations herein and remark on the problem: Under the “Key to Magnitude Methods”, we have for some years listed the letter ‘G’, intended to indicate that eyeglasses were used to defocus comet and/or comparison stars; however, this is not really a “method” and has now been moved to the “Special Notes Key” (as we will probably do for a few more letters in the near future). One still needs to provide a method when noting code ‘G’, and none of the corresponding observations in this issue do this properly; I elected to keep the ‘G’ observations that appear in this issue because they were all made of C/1995 O1 when it was quite bright with a rather small coma, meaning that I assume they were all made with the VBM method (code ‘B’).

In connection with this, I have also added a related special-notes code, ‘f’, which denotes the use of a single 50-mm binocular lens to defocus the comet and comparison star, also used when C/1995 O1 was brighter than mag +1. Yet another special-notes key, ‘%’, has been added to denote that a conversion was made for comparison stars from V to visual magnitude, using the B-V color and either the formula by Howard and Bailey (1980, *JBAA* 90, 265) or that by Stanton (1981, *JAAVSO* 10, 1), both of which are given in the first edition of the *ICQ Guide to Observing Comets*, page 65; when making such an application, the cited reference for comparison stars should also be used (meaning that really only actual catalogues can be used, as opposed to charts with magnitudes inscribed thereon).

With bright comets, some observers have attempted m_1 estimates visually either with camera lenses alone or a camera lens attached to a camera (viewing the comet and comparison stars on the camera's viewing screen); in such cases, for the standard ICQ tabulation, use instrument code letter 'A' for camera lens and insert a '0' (zero) under magnification, so that columns 44-47 read '0'.

Again, time has not permitted observations contributed on paper to be entered into the computer; such observations should appear in the July issue. — D. W. E. Green

Descriptive Information, to complement the Tabulated Data (all times UT):

◊ *Comet 46P/Wirtanen* \Rightarrow 1997 Feb. 25.73: possible outburst of ~ 0.7 mag [BAR06]. Mar. 1.77: clear enhancement w/ Lumicon SB Filter [MEY]. Apr. 15.13: central cond. of mag 13.4 and dia. $\sim 3''$; coma, although strongly asymmetrical toward p.a. 85° , gave only a slight hint of the possible beginning of a short, recognizable tail [ROQ].

◊ *Comet 81P/Wild 2* \Rightarrow 1997 Jan. 13.16: extremely obvious object; strong cond.; faint outer coma opens towards WNW, possible tail; T Cnc AAVSO seq. (1986); star of mag 4.7 some $20'$ away [PER01]. Jan. 15.02: comet easy, but star of mag 4.7 some $10'$ away; T Cnc AAVSO seq. (1986) [PER01]. Feb. 1.08: "sequence AAVSO U Gem (this applies to all of my 81P obs.)" [GRA04]. Feb. 3.03: U Gem AAVSO seq.; central cond. not as sharp as two weeks ago, yet still quite strong, looking like a fuzzy star; tail pointing E suspected but not confirmed [PER01]. Feb. 3.49: w/ 25.4-cm L (71 \times), comet appeared very condensed; fainter using Swan Band filter [SEA]. Feb. 3.97: coma opens towards W (i.e., sunwards); comet close to star of mag 5.4; U Gem AAVSO seq. [PER01]. Feb. 3.97: circular coma with prominent central cond.; U Gem AAVSO seq. [VIT01]. Feb. 4.42: most light from a condensed central region of dia. $\approx 2'$; this appeared to be surrounded by a fainter outer coma with a difficult-to-define boundary [SEA]. Feb. 5.47: comet near star; outer coma not visible and inner region appeared very small [SEA]. Feb. 9.02: with MM = S, $m_1 = 10.2$; outer coma edges ill-defined; looks more diffuse, still strong cond. but not so dominating; completely different from the relatively sharp-edged coma plus strong starlike central cond. seen in previous obs.; U Gem AAVSO seq. [PER01]. Feb. 9.96: coma edges ill-defined; still nearly starlike central cond.; U Gem AAVSO seq. [PER01]. Feb. 10.91: photometry w/ 36-cm f/6.7 T + V filter + CCD [MIK]. Feb. 15.94: coma edges ill-defined; still 12th-mag, weak, nearly-starlike nucleus; moonlight, moon nearby; U Gem AAVSO seq.; coma could be as large as 2'2 [PER01]. Feb. 27.94: U Gem AAVSO seq.; coma edges ill defined; very faint, 13th-mag starlike nucleus; central cond. like a globular cluster superimposed on a large diffuse coma [PER01]. Mar. 1.86: w/ 0.33-m L, $m_2 = 13.8$ [SZE02]. Mar. 3.46: estimate influenced by nearby star; w/ 25.4-cm L (114 \times), elongation or short tail in p.a. $\approx 110^\circ$; central cond. did not appear as sharply defined as it had in early Feb. [SEA]. Mar. 3.88: central cond. offset towards p.a. $\sim 320^\circ$; fan-shaped outer coma suspected; U Gem AAVSO seq. [PER01]. Mar. 9.83: w/ 20-cm T (166 \times), false nucleus of mag 13.5 in a well-condensed coma [KAM01]. Mar. 11.46 and 12.42: comet appeared fainter through Swan-band filter on Mar. 12 [SEA]. Mar. 11.79: elongated coma [MEY]. Mar. 31.88: comet involved with stars [PER01 and VIT01]. Apr. 1.80: at 230 \times , 8' dust tail in p.a. 75° [SAR02]. Apr. 1.85: disk-like inner coma dia. 3'5, fan-like outer coma dia. 6' [BAR06]. Apr. 7.88: comet involved w/ 12th-mag star [BOU]. Apr. 29.90: coma opens towards ESE; very faint stellar pseudo-nucleus offset towards WNW; T Cnc AAVSO seq. [PER01].

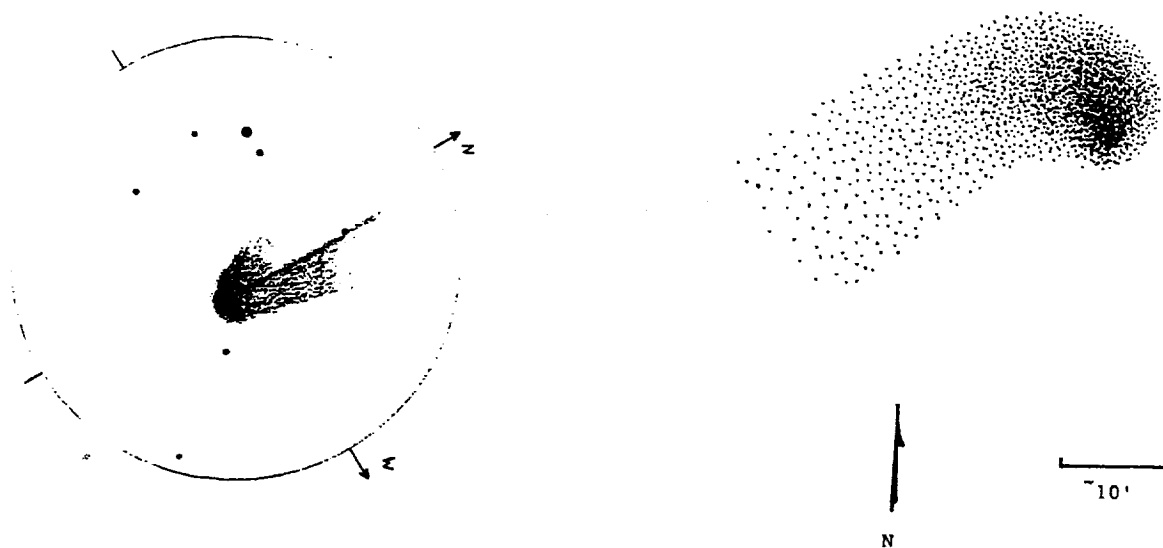
◊ *Comet 109P/Swift-Tuttle* \Rightarrow 1992 Nov. 27.78: w/ 10 \times 50 B, $m_1 = 4.8$, 3' coma, DC = 7, $0^\circ 20'$ tail in p.a. 57° [DOH]. 1992 Nov. 28.77: w/ 15-cm f/2 T (25 \times), 3' coma, DC = 5, $m_1 = 4.8$ (MM = S), $0^\circ 25'$ tail in p.a. 55° [DOH].

◊ *Comet 118P/Shoemaker-Levy 4* \Rightarrow 1997 Feb. 3.46: not seen using Swan Band filter [SEA].

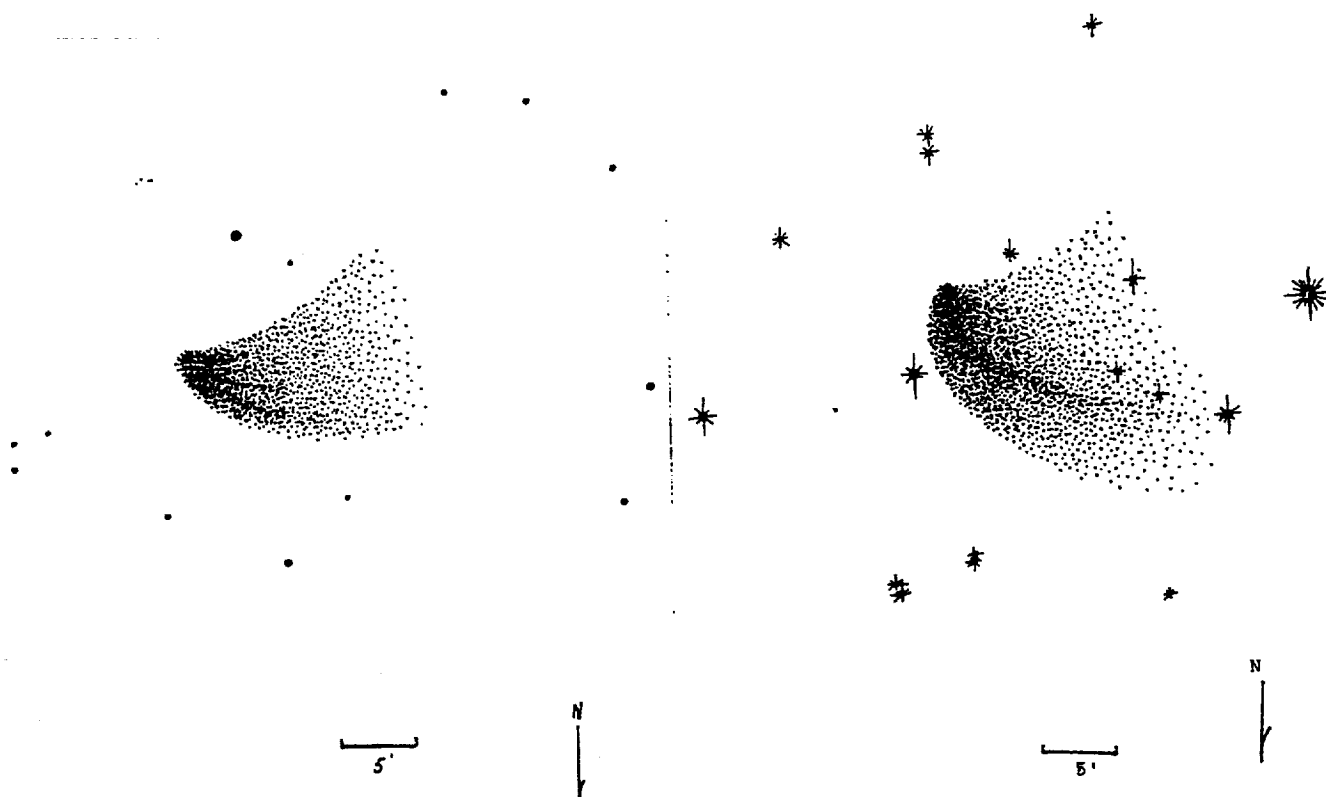
◊ *Comet C/1995 O1 (Hale-Bopp)* \Rightarrow 1996 June 7.98: w/ 20-cm T (51 \times), $m_1 = 7.6$ (Ref: S); at 225 \times , $m_1 \approx 8.3$ [NIE01 = Detlev Niechoy, Goettingen, Germany]. June 9.03: w/ 20-cm T (170 \times), $m_1 \approx 8.3$ [NIE01]. June 14.01: w/ 20-cm T (51 \times), $m_1 \approx 8.0$ [NIE01]. June 15.01: w/ 20-cm T (51 \times), $m_1 \approx 7.8$ [NIE01]. July 15.98, 16.94, and 17.98: w/ 10 \times 50 B, $m_1 = 5.8, 5.5$, and 5.7 (MM = S; Ref = PPM Star Catalogue, Röser and Bastian 1991, unacceptable for visual magnitude work); 20' coma, DC = 3 [MCK]. Aug. 2.82: w/ 25.4-cm T, comet appears extremely condensed, w/ coma extending broadly towards the NNE [TAN02]. Aug. 3.81: fanned eastward [TAN02]. Aug. 10.85: w/ 20 \times 70 B, broad tail $0^\circ 6'$ long in p.a. 107° [TAN02]. Sept. 4.78: coma elongated toward the NE or NNE [TAN02]. Sept. 6.78: coma elongated toward E [TAN02]. Sept. 7.80: w/ 20 \times 70 B, coma dia. 12', DC = 5, coma fanned for 16' toward p.a. 50° [TAN02]. Sept. 30.79: w/ 20 \times 70 B, tail $0^\circ 9'$ long in p.a. 71° ; broad fan seen adjacent to the main tail, $0^\circ 4'$ long in p.a. 43° [TAN02]. Oct. 8.78: w/ 20 \times 70 B, $1^\circ 2'$ tail in p.a. 70° ; comet near 6th-mag star; bright appendage to tail, $0^\circ 9'$ long in p.a. 83° [TAN02]. Oct. 16.45: three tails visible w/ a 20-cm f/9 L (45 \times) — $1^\circ 4'$ long in p.a. 50° - 55° , $1^\circ 2'$ long in p.a. 85° - 115° , and $40'$ long in p.a. 95° - 105° , $25'$ long in p.a. 80° , and $40'$ long in p.a. 100° - 110° [NAG04]. Nov. 7.74: w/ 20 \times 70 B, $1^\circ 4'$ tail in p.a. 72° [TAN02]. Dec. 14.37: w/ 20.0 f/9 C (45 \times), coma dia. 3'1, DC = 7, tail $\sim 2^\circ$ long [NAG04].

1997 Jan. 12.21: w/ 11 \times 80 B, $0^\circ 5'$ tail in p.a. 78° [ELT]. Jan. 16.27: w/ 13 \times 60 B, $m_1 \approx 4.5$ (ref = AA), 3' coma, DC = 6, $0^\circ 5'$ tail in p.a. 345° [HEN]. Jan. 25.25: w/ 13 \times 60 B, $m_1 \approx 4.0$ (ref = AA) [HEN]. Jan. 26.84: broad dust tail, $1^\circ 0'$ long in p.a. 275° and $0^\circ 8'$ long in p.a. 25° [SHI]. Jan. 30.84: broad dust tail, $1^\circ 2'$ long in p.a. 265° and $0^\circ 3'$ long in p.a. 10° [SHI].

Feb. 1.23: w/ 25.6-cm f/5 L (84 \times), stellar nucleus of mag 6.8; main jets between p.a. 160° and 240° , curving towards p.a. 280° , w/ fainter narrow jet in p.a. 27° [BIV]. Feb. 1.23: "w/ 10 \times 50 B, the m_2 refers the the bright, nearly-stellar central cond. (this applies to all of my m_2 estimates w/ 10 \times 50 B); the comet remained visible until the true solar alt. was $-5^\circ 7'$ (civil twilight); w/ 25.4-cm L (108 \times), central cond. was detectable until solar alt. $-3^\circ 0'$ " [GRA04]. Feb. 1.24 and 3.23: w/ 7 \times 50 B, 15' coma, DC = 7, 4° tail [SKI]. Feb. 2.22-2.23: w/ 10 \times 50 B, tail was clearly seen for $\sim 1^\circ$, difficult after $\sim 2^\circ$; there was also a shorter tail $0^\circ 5'$ - $1^\circ 0'$ long, oriented $\sim 30^\circ$ W of the main tail; the sunward part of

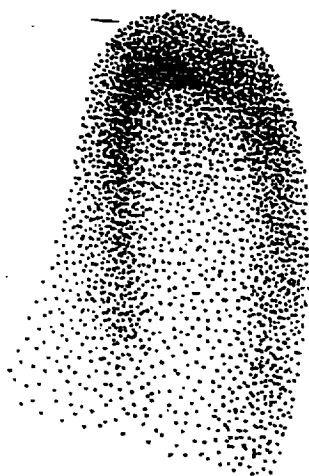


Four drawings of comet C/1995 O1 (Hale-Bopp) in 1996. Clockwise from upper left: (1) Observation by Martin Lehký (Hradec Králové, Czech Republic) with a 20-cm refractor at 140 \times on 1996 June 7.96; the northward jet was some 8' long. (2) Stipple drawing by John E. Bortle (Stormville, NY) with 10 \times 50 and 20 \times 100 binoculars on Aug. 11.10. (3) Drawing by Bortle on Sept. 15.04 with a 41-cm reflector at 70 \times . (4) Drawing by Bortle on 1996 Oct. 31.99 with a 41-cm reflector at 70 \times .



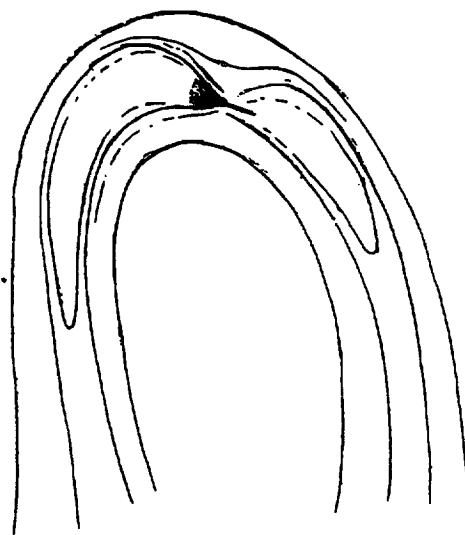


Above: drawings of C/1995 O1 by Richard Didick (code DID) with a 25-cm $f/4.5$ L at $46\times$ on 1997 Jan. 12 (left) and at $162\times$ on Jan. 29.43 (right); the Jan. 29 drawing shows a field $10'$ across, and west is to the lower left. Below: stipple (left) and pseudo-isophoto-contour (right) drawings of C/1995 O1 by John Bortle (code BOR) from his visual observations with a 41-cm L ($56\times$ - $114\times$) on Jan. 29.44.



N

$\sim 2'$



N

$\sim 2'$

◇ ◇ ◇

Comet C/1995 O1 (Hale-Bopp) [text continued from page 75] \Rightarrow

coma had a parabolic outline; observing somewhat hampered by clouds and twilight [GRA04]. Feb. 2.23: in 7×50 DC = 8; besides faint 3° gas tail in p.a. 330° , very complex, broad dust tail; most material in a fan spanning p.a. 5° - 290° , but maybe extending as far as p.a. 240° (longest $1^\circ 4$ in p.a. 315°) [BOU]. Feb. 2.49: tail was fan-shaped, w/ first $\sim 1^\circ$ of tail spanning p.a. $\sim 330^\circ$ - 270° ; the main tail component was distinctly yellow in color, and may have

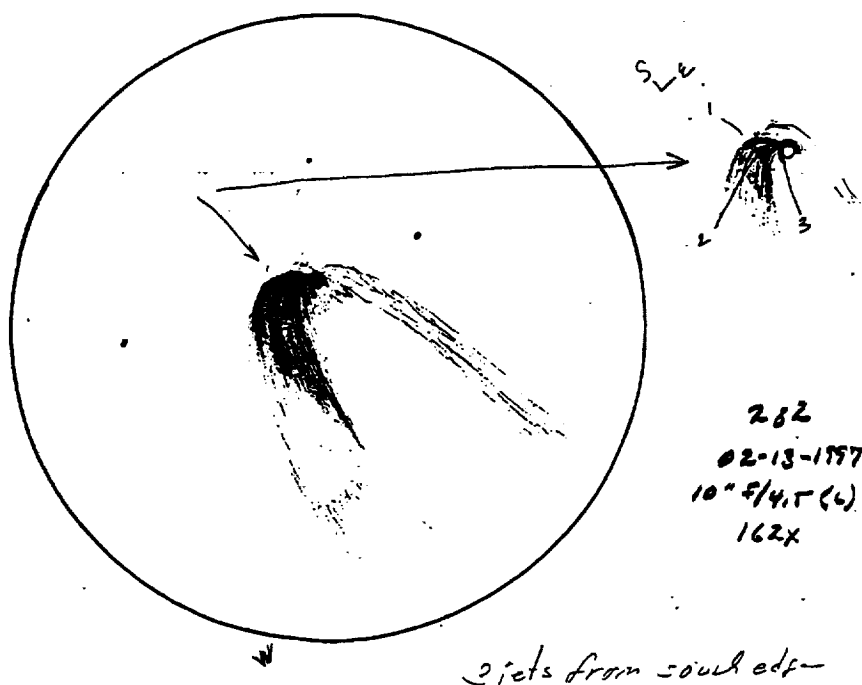
◊ Comet C/1995 O1 (Hale-Bopp) [text continued from page 77] ⇒

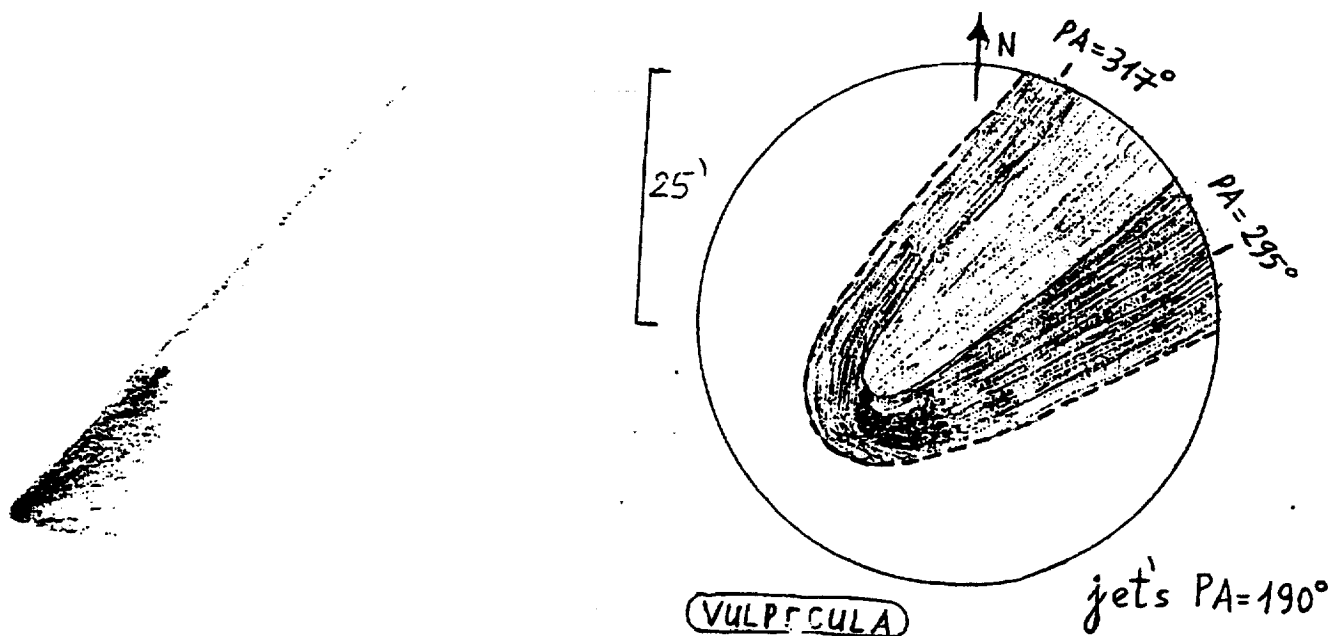
extended beyond the 3° listed; in 7×50 B, the head was roughly parabolic in outline, w/ the near-stellar central cond. offset slightly to the S side; moonlight [ADA03]. Feb. 3.13 and 5.14: w/ 8.0-cm f/10 R (40×), coma dia. 15'6-16', DC = S7 [GER01]. Feb. 3.17: w/ naked eye, second tail 2° long, visible as a faint fan [MAN01]. Feb. 3.19: photometry w/ 180-mm-f.l. f/2.8 lens + V filter + CCD; two YF standard stars inside the comet field used [MIK]. Feb. 3.20 and 4.21: photometry w/ 90-mm-f.l. f/4 lens + V filter + ST-6 CCD; two YF standard stars inside the comet field used [MIK]. Feb. 3.20: diffuse dust tail in p.a. ~ 215°-320°, ion tail at least ~ 3° long in p.a. ~ 320°; w/ naked eye, straight tail ~ 12° long in p.a. ~ 330° [MIK]. Feb. 3.20: second tail 0.6° in p.a. 300° [HOR02]. Feb. 3.23: w/ 7×50 B, 15' coma, DC = 7/, 4° tail [SKI]. Feb. 4.14: w/ 12×80 B, several ray-like extensions 1.5-2° long visible in coma and tail [BAR06]. Feb. 4.18, 7.21, 8.19, and 10.19: photometry w/ 180-mm-f.l. f/2.8 lens + V filter + CCD; one YF standard star inside the comet field used [MIK]. Feb. 4.21: diffuse dust tail in p.a. ~ 215°-320°, ion tail at least ~ 3° long in p.a. ~ 320° [MIK]. Feb. 4.23: w/ 7×50 B, tail was at least 4° long; coma was parabolic; several jets seen near the central cond., and the central cond. and coma appeared yellowish against the bright morning sky; w/ naked eye, the comet was visible until solar alt. was -6°9 [SKI]. Feb. 4.23: w/ 7×50 B, 15' coma, DC = 7, 4° tail [SKI]. Feb. 4.72: evening obs.; alt. 6°; comet was visible to naked eye [GRA04]. Feb. 4.88: image taken w/ 60-cm Y + CCD (two 5-sec exp. co-added) and enhanced w/ rotational gradient filter shows three bright jets in p.a. 31°, 166°, and 209°, and two faint ones in p.a. 88° and 320° [NAK01].

Feb. 5.19: a N component to the tail is seen (1.3° long in p.a. 328°); w/ 20×70 B, two curving jets are seen issuing from the 'nucleus' (the N one is 6' long, while the other is 11' long) [TAN02]. Feb. 5.22: w/ naked eye, the comet was visible until solar alt. was -6°9; w/ 7×50 B, 15' coma was parabolic, DC = 7/, 5° tail; the first 2° of the tail was fan-shaped and relatively bright, the rest of it was faint [SKI]. Feb. 5.23-5.24: w/ 10×50 B, the coma showed a parabolic outline in sunward direction; there was no clear distinction between coma and tail (the 'coma' size has been measured ⊥ to radius vector and through the central cond.); the first part of the tail was broad and fan-shaped [GRA04]. Feb. 6.19: N component to tail 1.9° long in p.a. 325°; the two jets seen yesterday are visible (the N one is shorter and barely detectable; the S jet is very evident, measuring 21') [TAN02]. Feb. 6.22: w/ 10×50 B, the central cond. was bright and nearly stellar (dia. < 1'); the coma had a parabolic outline towards the sun; tail bright for 1°, the rest being faint; w/ 20.3-cm T (123×), two tail components were seen, the W part was strongly curved; in the central cond., there was a bright jet directed towards p.a. ~ 250° (clearly curved, apparently towards the W tail); there was an obvious darkness behind the inner coma and between the tail components [GRA04]. Feb. 6.22: w/ 7×50 B, 15' coma, DC = 7/, 5° tail [SKI]. Feb. 6.25: w/ 25.6-cm f/5 L (169×), stellar nucleus with bright material at 15" from p.a. 160° to 210°, giving a '?'-like shape; bright jets in p.a. 30°, 160°, 190°, and 210° [BIV]. Feb. 7.12: second 'dust' tail 1° in p.a. 300° [PLS]. Feb. 7.20: w/ 9×63 B, broad dust tail ~ 1.0° long spanning p.a. 270°-330° and ion tail 3.5° long in p.a. 327°; central cond. of mag ~ 4.5; w/ 9-cm T (56×), false nucleus of mag ~ 6 w/ a broad fan of bright material at p.a. 215° and a faint jet at p.a. ~ 25°; immediately behind the false nucleus the brightness of the coma dropped significantly; coma resembled a parabola [KAM01]. (text continued on next page)

◊ ◊ ◊

Below: drawing of comet C/1995 O1 by Richard Didick (Taunton, MA) with a 25-cm f/4.5 L (162×) on 1997 Feb. 13. West is to the lower left, and south is to the upper left.





Above: Drawings of C/1995 O1. At left is a sketch of the field seen in 7x35 B by Margareta Westlund (Uppsala, Sweden) at daybreak on 1997 Feb. 17.19. At right is a drawing on Feb. 17.18 by Attila Kósa-Kiss (Salonta, Romania), from his view through a 6.3-cm Zeiss R (52x).

♦ ♦ ♦

♦ Comet C/1995 O1 (Hale-Bopp) [text continued from page 78] ⇒

Feb. 7.21, 8.19, and 10.19: V CCD imaging w/ 180-mm-f.l. $f/2.8$ lens shows an ion tail at least $\sim 3^\circ$ long in p.a. $\sim 320^\circ$ and a diffuse fan-like dust tail in p.a. $\sim 240^\circ$ - 320° [MIK]. Feb. 7.22: w/ 7x50 B, the tail was quite bright for 3° , certainly seen for 6° , and possibly visible to 7° [SKI]. Feb. 7.73: evening obs.; alt. 7° ; w/ naked eye, comet was clearly visible, and despite similar viewing conditions much easier than during evening obs. in late Jan.; w/ 10x50 B, the comet was bluer and much brighter than nearby γ Sge [GRA04]. Feb. 8.17: w/ 12x80 B, 35' coma, DC = S6 [BAR06]. Feb. 8.20: dust tail 1° in p.a. 280° [KYS]. Feb. 8.21: w/ naked eye, γ Sge was located close to the comet, but the objects were clearly separated; w/ 7x50 B, 15' coma, DC $\approx 7/$, 7° tail [SKI]. Feb. 8.22: in 7x50 B, DC = 8; besides 5° gas tail in p.a. 322° , very complex, broad dust tail; most material in a fan spanning p.a. 335° - 275° (longest $\sim 2^\circ$ in p.a. 305°) [BOU]. Feb. 8.22-8.24: w/ 10x50 B, two tails were seen, one being $0^\circ 7'$ long in p.a. 276° ; w/ 20.3-cm T (123x), there was a bright, fan-shaped jet directed from the bright central cond. at p.a. $\sim 250^\circ$ (its width was $\sim 30^\circ$ and it was curved towards the preceding tail component); a fainter and more diffuse jet was seen at nearly the opposite direction (p.a. $\sim 60^\circ$); both tail components appeared strongly curved; there was an obvious darkness between the tail components (mean p.a. of this dark area was 325°); the central cond. was very small, but not quite stellar; the comet formed a beautiful pair w/ γ Sge, though the comet was much bluer than this red-orange star [GRA04]. Feb. 8.74: evening obs.; alt. $5^\circ 5'$; w/ 10x50 B, the surface brightnesses of inner coma (excluding the bright central cond.) and inner tail (at $\sim 0^\circ 5'$ from central cond.) were estimated as ~ 14.0 and 17.5 mag/arcsec 2 ; as a comparison, the surface brightness of the central region of M31 was estimated as ~ 19.5 mag/arcsec 2 ; comet was clearly visible to naked eye [GRA04]. Feb. 9.17: w/ 12x80 B, star-like nucleus $m_2 \approx 5$, fan-shaped dust tail more than 2° long in p.a. 300° - 260° (brightest part in p.a. 290°) [MAN01]. Feb. 9.19: excellent conditions; the dust tail is shorter but wider, and extends for $2^\circ 3'$ (its trailing edge points toward p.a. 293°); a short ($0^\circ 6'$) but very wide (spreading from p.a. 279° to 241°) fan is visible w/ averted vision; the two jets seen in the last few days are again visible in 20x70 B — they curve upwards to form the tail; the S jet is longest and most distinct, extending for $22'$; also extending toward the SW is a wide and bright fountain [TAN02]. Feb. 9.26: in 25.3-cm L (58x), central cond. is a minute planetary-like disk near the resolution limit; from this disk emerges a very bright, extremely prominent fountain, strongly curving anti-clockwise into the tail; the coma has a distinct blue tint; the shape is somewhere between parabolic and pear-shaped; a bright envelope includes the fountain on its W side, the inner border of this envelope being sharply defined and passing through the false-nucleus; just inside of this envelope, there is a striking 'hollow'; the $2'$ - $3'$ fountain leaving the nucleus to the SW was still visible ~ 15 min before sunrise; the nucleus was lost 1 or 2 min before sunrise (at sunrise, γ Sge at $m_v \sim 3.5$ was still easy); with 9x34 B, DC = 8, parabolic hollow tail spanning p.a. 280° - 335° ; central cond. like a fuzzy star near focus of parabola [PER01]. Feb. 9.26: in 25.3-cm L $f/5.6$ (58x), a bright prominent fountain (initially to the WSW) was present, curving anti-clockwise back into the tail; both the fountain and the false-nucleus, were distinctly blue colored; this false nucleus looked like a very bright small disk with

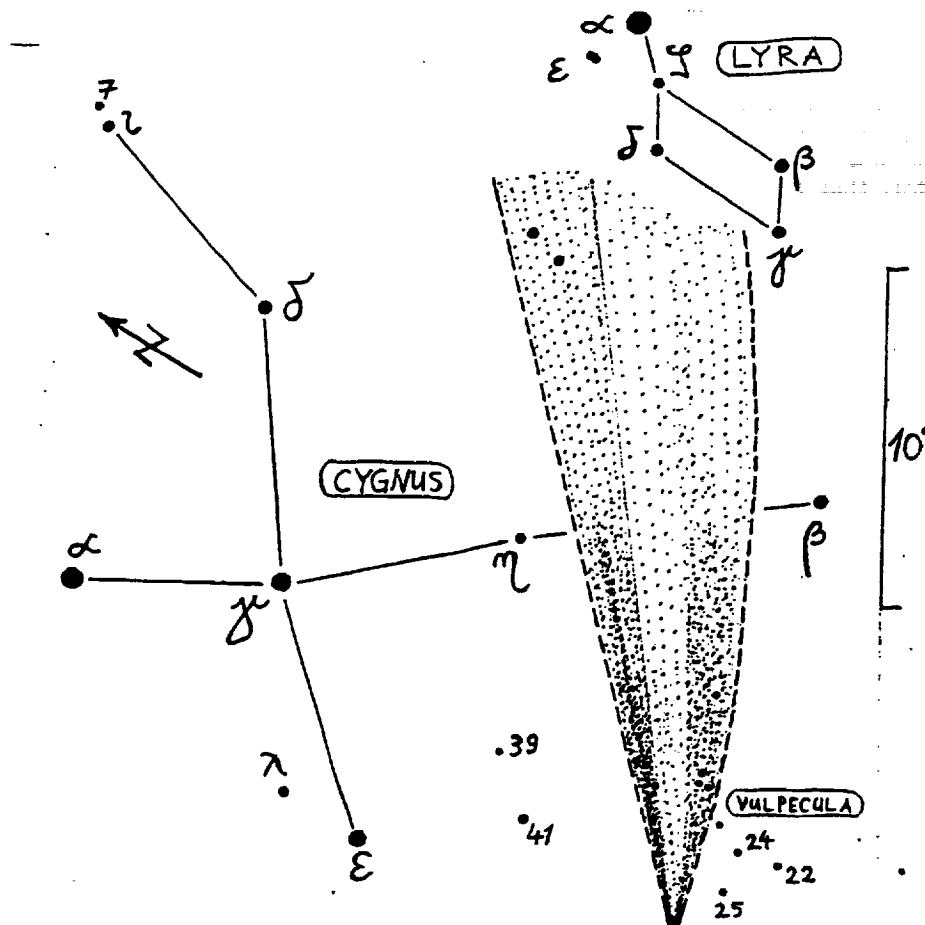
◊ Comet C/1995 O1 (Hale-Bopp) [text continued from page 79] ⇒

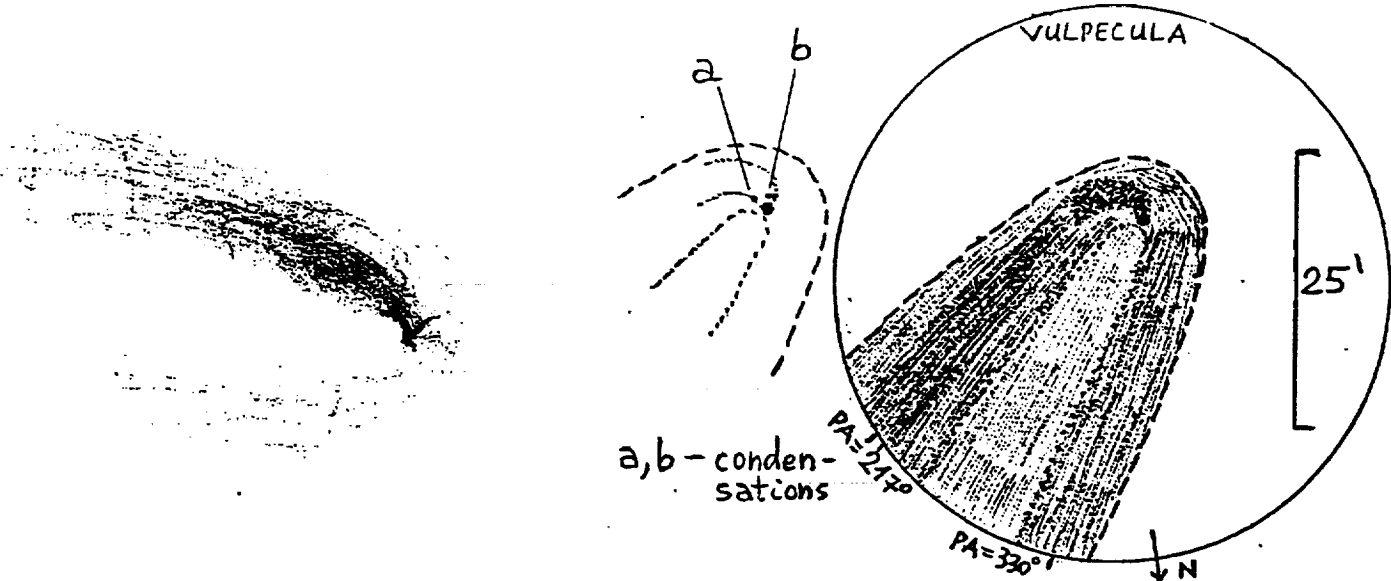
well-defined limits; the coma had a near-parabolic shape and showed a slightly brighter zone (or envelope) surrounding and including the fountain and the false nucleus; a large teardrop-shaped area inside the coma was very dark (the outline of this area was quite contrasting, grazing the false-nucleus and the curved fountain); the dark area, though gradually not so well-defined, continues through the tail, making its outer parts seem more prominent [VIT01]. Feb. 9.74: evening obs.; alt. 6°; mag uncertain due to thin clouds, some auroral light, and corrections for extinction; w/ 7×50 B, DC = 8, 1°5 tail [SKI]. Feb. 9.84: w/ 8×56 B, coma dia. 17', DC = 8, tail > 5° long [OKA05]. Feb. 9.87: image taken w/ 60-cm Y + CCD (two 3-sec exp. co-added) and enhanced w/ rotational gradient filter shows three bright jets in p.a. 31°, 171°, and 219°, and two faint ones in p.a. 92° and 315° [NAK01].

Feb. 10.18: excellent conditions; the tail looks essentially the same as on Feb. 9; the dust tail extends for 2°3, w/ its S edge now pointing toward p.a. 280°; the short fan is less pronounced today; the jets on both sides of the 'nucleus' give a 'U' shape to the coma; the S jet is 0°5 long [TAN02]. Feb. 10.24: quite bright sky in nautical twilight (solar alt. -11°6); w/ naked eye, comet was visible until solar alt. -6°3; w/ 7×50 B, 15' coma, DC = 7/, 2° tail [SKI]. Feb. 10.26: in 25.3-cm L f/5.6 (58×), the fountain seemed not so strongly curved than in previous obs.; next to central cond., there was clearly a small bright 'spot' towards N-NE; coma brightness definitely asymmetric, as a brighter zone incl. the fountain and the first deg/minutes of tail on its W side; in 9×34 B, the coma showed a very narrow parabolic shape, the central cond. being slightly offset towards SW; DC = 7; slight green tint [VIT01]. Feb. 11.18: w/ naked eye, 8° tail in p.a. 312°; the dust tail is best seen w/ 12×50 B and measures 4° in length (its trailing edge points toward p.a. 288°) [TAN02]. Feb. 11.21: poor sky w/ heavy cloud; w/ 10×50 B, DC = 7, 2° tail in p.a. 318° [GRA04]. Feb. 11.21: in 7×50 B, DC = 7-8; besides 5°5 gas tail in p.a. 318°, broad dust tail spanning p.a. 325°-275° (longest ~ 1°7 in p.a. 300°) [BOU]. Feb. 11.74: evening obs.; alt. 5°5; comet clearly visible to naked eye [GRA04]. Feb. 11.74: evening obs.; alt. 6°; comet was clearly brighter and easier to see than two evenings ago; w/ 7×50 B, DC = 7/, 3° tail [SKI]. Feb. 11.79: w/ 20×125 B, coma dia. 20', DC = 8, tail 0°6 long in p.a. 310° [TOY]. Feb. 11.82: broad dust tail, 1°5 long in p.a. 290° and 0°8 long in p.a. 330° [SHI]. Feb. 12.06: w/ 11-cm L (32×), $m_2 \sim 6$ [IVA03]. Feb. 12.16: w/ 6.7-cm f/1.8 A, 1-min exp. on 100 ASA film shows narrow tail 3°6 long in p.a. 324° and second fan-like tail 2°0 long spanning p.a. 320°-300° [FIL05]. Feb. 12.18: dust tail stretches for 3° in p.a. 288°; ion tail glimpsed momentarily w/ the naked eye; the S jet is very evident; it seems to be the main source of the dust tail; obs. made through gaps in the clouds [TAN02]. Feb. 12.20:

◊ ◊ ◊

Below: drawing of comet C/1995 O1 by Atilla Kósa-Kiss (code KOS) on 1997 Feb. 17.18, using 7×50 B.





Above: Drawings of C/1995 O1. At left is a sketch of the field seen visually in a 25-cm f/4 L (44×) on 1997 Feb. 20.43 by Daniel W. E. Green from Middlesex County, MA; intensely bright jets emanated from the nuclear region into a very yellowish side of the coma (upward in this view), whereas the coma below the nucleus in this view (from whence the ion tail ran) was very blue in color. At right is a drawing by Atilla Kósa-Kiss made on Feb. 23.17 w/ a 6.3-cm Zeiss R (52×).

♦ ♦ ♦

Comet C/1995 O1 (Hale-Bopp) [text continued from page 80] ⇒

7×50 B, dia. 15'-20'; the tail was divided in two parts near the coma, the length and p.a. referring to the long and the narrow gas component; the W tail appeared somewhat curved and ended in a fainter glow towards W (mean p.a. 280°); w/ 10.2-cm R (60×), coma was clearly shaped like a parabola; a broad jet was radiating towards W from the nucleus [SKI]. Feb. 12.21: w/ 20.3-cm T (123×), the comet showed two tail components, the inner part of the W appearing slightly brighter than the inner portion of the E component; in the heart of comet, there was a bright false nucleus that looked like a short streak ~ 5" long, oriented along p.a. ~ 60°-240°; a bright and wide fountain (1'-2' long) spanning ~ 40° in p.a.) was radiating from this nucleus in mean p.a. ~ 230°; it curved towards the W tail; the N boundary of the fountain was considerably sharper than on the S side [GRA04]. Feb. 12.74: evening obs.; alt. 6°5; comet easily visible to naked eye as a diffuse star, its visibility comparable to mag-3 stars overhead [GRA04]. Feb. 13.20: thin jets in front of comet; w/ 7×50 B, DC = 7/, 3° tail [SKI]. Feb. 13.23: w/ 10×50 B, tail 6° long [HAS02]. Feb. 14.18: 7×50 B, 2°7 tail in p.a. 288° [SHA02]. Feb. 14.24: w/ 9×63 B, 1°75 tail [ENT]. Feb. 14.83: w/ 8×56 B, coma dia. DC = 8, tail 5° long [OKA05]. Feb. 14.84: 4° dust tail in p.a. 285°, 3° long in p.a. 315° [SHI]. Feb. 15.13-15.15: w/ 10×50 B, two tail components were seen, one being 1°5 long in p.a. 290°; the surface brightness of the inner portion of tail (at ~ 0°5 from coma, before the splitting of the tails) was estimated as 17.7 mag/arcsec²; 25.4-cm L (108×), in the bright central cond., there were two cond. separated by ~ 3"; a bright and wide fountain radiated W from the central cond. and curved apparently towards the dust tail; some interference from clouds; temp. 1° C [GRA04]. Feb. 15.17: w/ 11-cm L (50×), strong nuclear cond. and very bright fountain w/ two or three jets pointing SW of the false nucleus and curving counter-clockwise towards dust tail; several other nearly-straight jets in various directions [BAR06]. Feb. 15.17: w/ naked eye, 2° tail in p.a. 294° [SHA02]. Feb. 15.18: dust tail is wide and ends for 4°5; its trailing edge points toward p.a. 277° [TAN02]. Feb. 15.24: w/ naked eye, 3° tail in p.a. 294° [SHA02]. Feb. 15.25: w/ 25.6-cm f/5 L (169×), stellar nucleus w/ a new shell of bright material at 15" from p.a. 200° to 240°; radial (2-4) condensations are seen on the jets, every 15"-20" (p.a. 35°, 75°-90°, 150°, 165°, and 200°-240°), which seem to appear every 8-9 days [BIV]. Feb. 15.74: evening obs.; alt. 8°; w/ 7×50 B, DC = 7/, 3° tail [SKI]. Feb. 15.77: evening in moonlight; alt. 5° [GRA04]. Feb. 16.18-16.19: w/ 10×50 B, two tails were seen, one being 2°5 long in p.a. 280°; W dust component was broader and more diffuse than the gas tail and was quite bright for ~ 2°; it apparently curved slightly towards S; the gas tail was clearly seen for 6°, but the rest of it was difficult due to the Milky Way background in Cyg (width 0°5-1°); the surface brightness of the merged tail at ~ 0°5 from central cond. was estimated as 7.6 mag/arcsec²; the tails separated at ~ 0°8 from the central cond.; temp -22° C [GRA04]. Feb. 16.19: w/ 7×50 B, DC = 7/, tail 8° long in p.a. 319°; two tail components were seen; the W dust tail had a somewhat higher surface brightness and was easier to detect to the naked eye than the longer ion tail; several streamers were seen; the ion tail was clearly seen for 5°-6°, the rest of it was faint; air temp at observing site was -20° C [SKI]. Feb. 16.19: second 'dust' tail 7° in p.a. 315° [ZNO]. Feb. 16.19: 4°2 ion tail in p.a. 315°; 1°2 dust tail in p.a. 300° [VAN06]. Feb. 16.21, 19.20, 21.19, 28.82, 30.82, Apr. 1.82, and 6.84: tab. tails are apparently gas tail; respective dust tail lengths and position

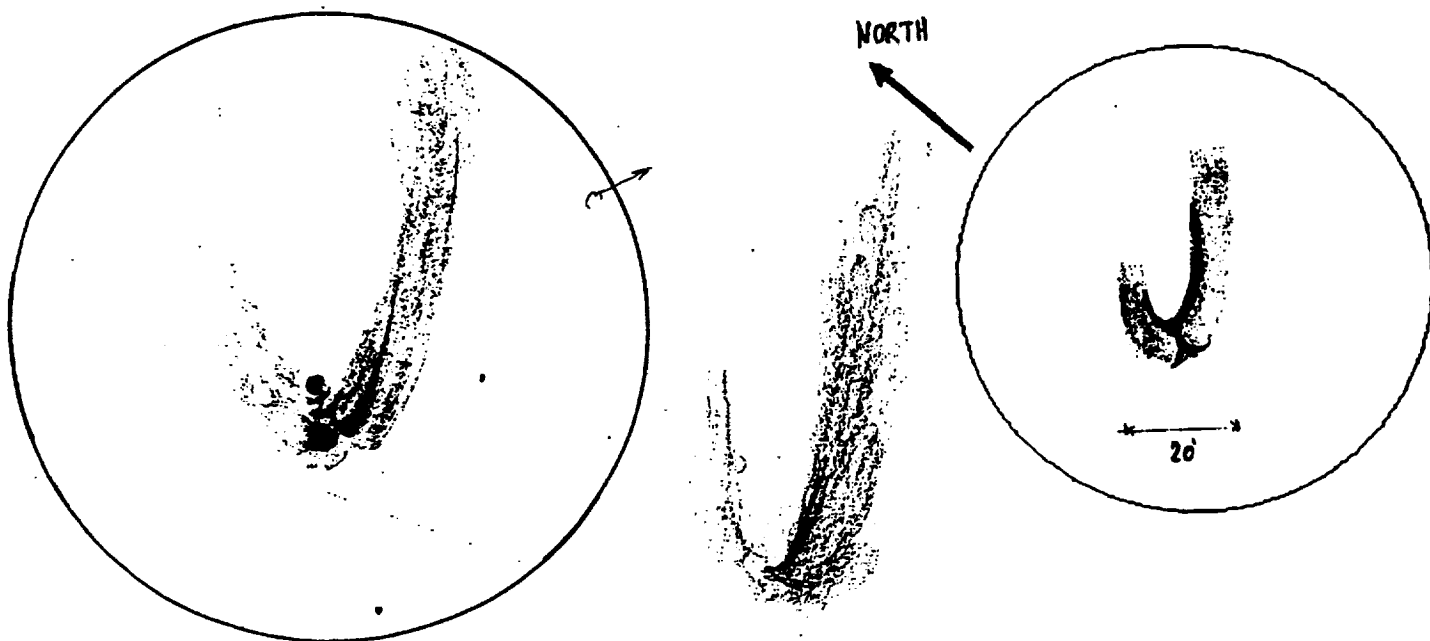
◊ Comet C/1995 O1 (Hale-Bopp) [text continued from page 81] ⇒

angles were $\sim 3^\circ$ in 280° , 2° in 295° , 10° in 320° , 8° in 0° , 14° in 0° , 12° in 345° , and 16° in 355° [GLI]. Feb. 16.83: w/ 8×56 B, coma dia. $17'$, DC = 9, tail 1° long [OKA05]. Feb. 17.18-Apr. 17.80: "naked-eye brightness estimation done using a doublet achromat of focal length 36 cm (and in some cases, another doublet w/ a focal length of 30 cm); on Mar. 9.75 and Apr. 8.77, I employed the VSS and Morris methods w/ the help of these same lenses for defocusing images; for C/1996 B2 last year, I used a doublet w/ focal length 18 cm" [MIL02]. Feb. 17.24: to the naked eye, also dust tail $\sim 4.5^\circ$ long near p.a. 290° ; comparison basically w/ α Cyg + γ Cyg; α Aql and α Cep also used, but too far from the comet's alt. ($\sim 20^\circ$); in 9×34 B, parabolic tail over 4° spanning p.a. 290° - 310° ; W side of tail much brighter; parabolic envelope; a strongly-curved fountain p.a. $\sim 260^\circ$ is seen bending back into the tail; dark spine clearly offset towards the E part of the tail; in 25.3 -cm L $f/5.6$ ($58\times$), strongly-curved fountain initially spanning p.a. $\sim 170^\circ$ - 210° close to the starlike nucleus, then bending back towards the tail, along p.a. $\sim 290^\circ$; parabolic 'hollow' inside the tail, touching the nucleus; two hoods are seen, one involving the curved fountain, the other one (fainter) involves the former, but begins towards the NE, then strongly bends counter-clockwise through the sunward part of the coma, to follow the W part of the tail; thin cirrostratus likely to have interfered; $m_1 = 1.7$ w/ 1.4×35 monocular; w/ a divergent lens used, an in-focus estimate yields $m_1 = 1.7$ [PER01]. Feb. 18.16: dust tail 1.4° long in p.a. 305° [KOZ]. Feb. 18.17: second tail 3.5° in p.a. 295° [HOR02]. Feb. 18.18: second 'dust' tail 2° in p.a. 295° [PLS]. Feb. 18.195: wide-field 5-min exp. taken w/ $3.5/65$ -mm lens, CCD, and narrow-band H_2O^+ filter, centered at 620 nm (FWHM = 10 nm) shows ion tail at least 7° long in p.a. $\sim 315^\circ$ [MIK]. Feb. 18.20: 3.3° ion tail; 1.3° dust tail in p.a. 315° [VAN06]. Feb. 18.85: tail spans p.a. 260° - 310° [MIY01]. Feb. 19.13: w/ 8 -cm R ($28\times$), second fan tail $\sim 2^\circ$ long spanning p.a. 250° - 300° ; w/ 8 -cm R ($40\times$), fan spans p.a. 300° - 270° ; star-like nucleus brighter than mag 5 [MAN01]. Feb. 19.14: narrow tail is 7.5° long in p.a. 325° , second fan-like tail 2.0° long spans p.a. 315° - 300° [FIL05]. Feb. 19.16: bluish ion tail is 6° long in p.a. 313° , yellowish fan-like dust tail 1.8° long spans p.a. 272° - 302° , dust tail is brighter than ion tail; w/ 12×80 B, $30'$ coma, tail 6° long in p.a. 313° [BAR06]. Feb. 19.84: w/ 10×50 B, coma dia. $9'$, DC = 9, tail 3° long [OKA05]. Feb. 19.85: tail spans p.a. 260° - 300° [MIY01]. Feb. 19.85: w/ 7×35 B, coma dia. $25'$, DC = 7, tail 6° long [WAS].

Feb. 20.20: in 7×50 B, DC = 8; besides 6° gas tail in p.a. 320° , broad (slightly curved) dust tail spanning p.a. 320° - 283° (longest 2.4° in p.a. 296°); moon 4° over NW horizon [BOU]. Feb. 20.23: w/ 7×50 B, 2° tail in p.a. 302° [SHA02]. Feb. 20.24: w/ 9×63 B, $m_1 = 1.7$ (MM = S), $30'$ coma, DC = D7, 2.5° tail [LAN03]. Feb. 20.4 and 24.4: w/ 25 -cm $f/4$ L at low power, bright jets toward SE are in very yellowish coma, whereas the coma on the NE side of the nucleus shows a faint but deep blue color; the SE jets are easily visible in 12×50 B; for all subsequent naked-eye m_1 estimates of this comet utilizing comparison stars where m_s differed from V by ≥ 0.1 mag, corrections were made on page 74 of this issue (last paragraph) [GRE]. Feb. 20.75: evening obs.; alt. 9.5° ; w/ 10×50 B, two tails seen (one being 1.5° long in p.a. 320°); the W dust tail was easier to detect than the gas component [GRA04]. Feb. 20.76: evening obs.; alt. 8° ; listed tail lengths refer to the dust tail; w/ 7×50 B, DC = 7, tail 3° long; w/ naked eye, the comet was first located w/ solar alt. -6.3° [SKI]. Feb. 20.83: dust tail 2.7° long in p.a. 275° and 1.8° long in p.a. 320° [SHI]. Feb. 20.84: w/ 10×50 B, coma dia. $9'$, DC = 8, tail 2° long [OKA05]. (text continued on next page)

◊ ◊ ◊

Below: drawings of comet C/1995 O1, oriented so that west is toward the upper right and north toward the upper left. At left is a drawing by Richard Didick on 1997 Feb. 23, as seen through his 25 -cm $f/4.5$ L ($127\times$). At center is a sketch by Daniel W. E. Green on Feb. 24.43 with his 25.4 -cm $f/4$ L ($44\times$), in which two bright jets were seen, and the right side of the coma in this view was very yellowish (toward which the dust tail ran), while the left side of the coma was very bluish (toward which the ion tail ran). At right is a drawing by Sandro Baroni (Milan, Italy), made using 20×80 B on Feb. 23.20; the line indicates $20'$.



N
E $\begin{array}{|c|} \hline 1^\circ \times 1^\circ \\ \hline \end{array}$
(B 7x35)



Above: Drawings of comet C/1995 O1 by Margareta Westlund as seen with 7x35 B on 1997 Mar. 3.81 (left) and 10.12 (right).

♦ ♦ ♦


♦ Comet C/1995 O1 (Hale-Bopp) [text continued from page 82] ⇒

Feb. 21.20 and 22.18: photometry w/ 90-mm-f.l. $f/4$ lens + V filter + ST-6 CCD; one YF standard star inside the comet field used for photometry [MIK]. Feb. 21.20: ion tail at least $\sim 5^\circ$ long in p.a. $\sim 320^\circ$; diffuse dust tail $\sim 3^\circ$ long in p.a. $\sim 250^\circ$ - 320° [MIK]. Feb. 21.20: w/ naked eye, the listed tail refer to the dust tail; gas tail glimpsed for a couple of deg; despite a nearly full moon, parts of the Milky Way were visible in Cyg; w/ 7x50 B, coma dia. $\sim 15'$, DC = 7/, and the gas tail was visible for over 5° , but the surface brightness of the dust tail was higher near the head of the comet; the p.a. of the dust tail was $\sim 300^\circ$ [SKI]. Feb. 21.83: w/ 8x56 B, coma dia. 8', DC = 9, tail 3° long [OKA05]. Feb. 22.21: w/ 7x50 B, 2° tail in p.a. 327° [SHA02]. Feb. 23.69: obs. in the evening sky; w/ naked eye, coma dia. $\sim 30'$, DC = 5 [KUS]. Feb. 23.75: evening obs.; alt. 12° ; comet was only observable for a couple of min, due to rapidly drifting clouds (first detected w/ the naked eye under better skies w/ solar alt. $-6^\circ 0$) [SKI]. Feb. 24.51: central cond. of mag 7.1 and dia. almost $5''$; although the tail, as tab., extended to the CCD frame edge, its major fan-shaped form was readily followed for at least 3° using binoc.; prominent, diffuse jets imaged at p.a. 23° and 67° through Kron-Cousins filters at wavelengths 650 (R), 550 (Y), and 440 nm (B), where they maintained approx. equal relative intensities in all three bands [ROQ]. Feb. 24.84: brightest part of dust tail 4° long in p.a. 285° [SHI]. Feb. 25.21: w/ naked eye, 2.5° tail in p.a. 293° [SHA02]. Feb. 25.83: dust tail in p.a. 270° - 305° ; brightest part in p.a. 295° (6° long) [SHI]. Feb. 26.14-26.15: w/ naked eye, the comet was a prominent object w/ a nearly-stellar head and a clearly visible dust tail; w/ 10x50 B, two tails were seen (one being 3.5° long in p.a. 290°); the E ion tail was the longer one, but until 2° from the head, the dust tail was clearly brighter than the gas tail; a distinct jet, $\sim 1^\circ$ long, was seen in the middle of the dust tail; w/ 20.3-cm T (123x), there was a nearly-stellar pseudo-nucleus, not more than $3''$ in size, in the head of comet; a bright, wide fountain was radiating from this nucleus in p.a. 175° - 245° (the fountain curved strongly towards the jet in the dust tail); a lot of detail seen in and near the fountain, incl. several small dark knots and rifts; the head showed a distinct golden yellow hue, w/ nearby star HR 8084 (spectral type F7) considerably bluer; first morning obs. since Feb. 16 after an extended period w/ poor weather [GRA04]. Feb. 26.17: w/ 8x50 B, $28'$ coma, DC = 7, 2.3° tail [DIE02]. Feb. 26.19: w/ 7x50 B, two tails were seen; the E gas tail was visible for 5° until it disappeared behind a cloud layer; surface brightness of dust tail was higher than that of the gas tail, this tail was also visible to the naked eye; interference from clouds [SKI]. Feb. 26.26: w/ 8x30 B, $14'$ coma, DC = 8, 2° tail [ENT]. Feb. 26.78: evening obs.; alt. 10.5° ; heavy cloud (even still, the dust tail was clearly seen for 2°) [GRA04]. Feb. 27.15-27.19: w/ naked eye, the comet showed a bright and nearly-stellar head and an easily visible tail; w/ 10x50 B, two tails were seen (one being 3° long in p.a. 239°); the W dust tail curved towards S and was considerably brighter than the gas tail until 2° from the head; the mean surface brightness of the dust tail estimated as $16.4 \text{ mag/arcsec}^2$ at 0.5° , and $16.9 \text{ mag/arcsec}^2$ at 1.0° from the nucleus; ion tail clearly visible to 7° from the head (width $\sim 0.8^\circ$); in the dust tail, there was a jet $\sim 0.8^\circ$ long; w/ 20.3-cm T (123x), the pseudo-nucleus was small, but nonstellar; it looked like a bar that was $\sim 4''$ long and

◊ Comet C/1995 O1 (Hale-Bopp) [text continued from page 83] ⇒

directed along p.a. 5° - 185° ; from this nucleus, there was a bright fountain, $\sim 1'$ long and spanning p.a. 155° - 225° (in this fountain, there were two dark rifts located $\sim 15''$ and $\sim 30''$ from the nucleus; the surface brightness of the fountain was $14.3 \text{ mag/arcsec}^2$); the head of the comet was yellow and bluer than the K5-star HR 8005; in moonlight, Milky Way faintly visible [GRA04]. Feb. 27.16: second tail 5° in p.a. 285° [HOR02]. Feb. 27.19: second tail $2^{\circ}2$ in p.a. 290° [PLS]. Feb. 28.05: w/ 11-cm L ($32\times$), $m_2 \sim 5.3$ [IVA03]. Feb. 28.16: w/ 11×80 B, coma dia. $15'$ and $3^{\circ}5$ tail in p.a. 310° [STO]. Feb. 28.16: w/ 9×63 B, ion tail displayed at at least two bright streamers; bright dust tail 3° long centered at p.a. 290° and spanning $\sim 30^{\circ}$; tail $> 5^{\circ}$ long in p.a. 307° ; DC = S8; extremely bright central cond.; obs. under severe moonlight [KAM01]. Feb. 28.19: ion tail at least $\sim 5^{\circ}$ long in p.a. $\sim 325^{\circ}$; dust tail at least 3° long in p.a. $\sim 260^{\circ}$ - 305° [MIK]. Feb. 28.19: in 7×50 B, DC = 8; besides $6^{\circ}5$ gas tail in p.a. 322° , slightly-curved dust tail (longest $3^{\circ}3$ in p.a. 303°); very strong nuclear cond. of slightly yellowish color; comet impressive despite moonlight [BOU]. Feb. 28.20: w/ 8×30 B, 2° tail [ENT]. Feb. 28.73: w/ 80×12 (B), ion tail 12° long and dust tail 4° long; shadow between two tails [BAR06].

1997 Mar. 1, 3, 9 and 10: three shells near the cometary nucleus were observed w/ 0.7-m L; on Mar. 3.14, distances of shells from nucleus were: 2nd shell, $7''$; 3rd shell, $9''$ (diameters of shells were $22''$ and $25''$) [CHU]. Mar. 1.17: dust tail 4° in p.a. 305° [KYS]. Mar. 1.18: dust tail 2° in p.a. 305° [KYS]. Mar. 1.19: in 7×50 B, DC = 8; besides $6^{\circ}6$ gas tail in p.a. 324° , broad slightly-curved dust tail spans p.a. 283° - 307° (longest $4^{\circ}0$ in p.a. 299°); w/ 15×80 B and 0.16-m L (at $29\times$, $102\times$), broad fountain-like structure visible in p.a. $\sim 220^{\circ}$, curving back (anti-clockwise) into the main tail and forming bright streamer some $1^{\circ}5$ long near the N side of the tail in p.a. 305° ; very strong central cond., yellowish in color [BOU]. Mar. 1.19: w/ 7×50 B, $26'$ coma, DC = 7, 4° tail [DIE02]. Mar. 1.22: w/ 9×63 B, 3° tail [ENT]. Mar. 1.22-1.23: to the naked eye, besides the 9° gas tail near p.a. 320° , there is also a broad, slightly curved clockwise 7° dust tail spanning p.a. $\sim 280^{\circ}$ - 305° ; strong disk-like central cond.; in 9×34 B, conspicuous fountain, initially to the SW, then strongly bending anti-clockwise into the dust tail; a prominent streamer flowing from the nucleus along p.a. $\sim 280^{\circ}$ can be traced for at least 2° into the dust tail; there is a dark area very close to the nucleus, and between the N edge of the fountain and this streamer; gas tail is less well defined and fainter than the dust tail; dark spine separating the two tails clearly offset towards the gas tail (i.e., to the NE of two tails' axes); in 25.3-cm $f/5.6$ L ($58\times$), even at such low power, the inner-coma structure is extremely complex and intricate; non-stellar nucleus, just above the resolution limit; huge fountain spanning p.a. $\sim 160^{\circ}$ - 220° near-nucleus, now presenting sharp inner detail; four plumes, two on each side of the giant fountain, plus a bright cloud of material in a short circular arc (separated from the fountain, and towards p.a. $\sim 100^{\circ}$, some $30''$ - $60''$ from the nucleus), all combine to give the impression of two concentric layers, estimated at $\sim 30''$ intervals; the dark 'hollow' tailwards of the pseudo-nucleus is much less pronounced and rather narrow-shaped now; the coma is strikingly asymmetric in brightness; the thick large stream of material in the continuation of the fountain makes the whole 'trailing' side of the coma look markedly brighter than the 'leading' edge, the transition being quite dramatic through p.a. $\sim 120^{\circ}$ from the nucleus; this gives the coma an almost-dichotomous phase aspect; the gas tail looks less defined; obs. made through a veil of cirrostratus, thought to have not affected m_1 significantly (i.e., estimates made at times when the veil was looking homogeneous, both at the comp. stars and at the comet); w/ 1.4 \times 35 monocular, $m_1 = +0.2$ [PER01]. Mar. 2.07: w/ 11-cm L ($32\times$), $m_2 = 5.3$ [IVA03]. Mar. 2.09: w/ 7×50 B, dust tail 7° long in p.a. 310° [VEL03]. Mar. 2.14: second tail 5° in p.a. 285° [HOR02]. Mar. 2.16: w/ naked eye, dust tail 8° long in p.a. 310° ; $m_2 = 1.8$ [SAR02]. Mar. 2.16: dust tail 9° long in p.a. 310° [SZE02]. Mar. 2.17: ion tail at least $\sim 5^{\circ}$ long in p.a. $\sim 323^{\circ}$; dust tail at least 3° in p.a. ~ 260 - 305° [MIK]. Mar. 2.17: curved dust tail $2^{\circ}8$ long [MEY]. Mar. 2.19: $4^{\circ}8$ ion tail in p.a. 325° ; $2^{\circ}6$ dust tail in p.a. 290° [VAN06]. Mar. 2.45: w/ naked eye, 4° gas tail at p.a. 326° , and broad 3° dust tail spanning p.a. 285° - 310° ; in 7×50 B, the gas tail was traced to $\sim 5^{\circ}5$ and it curved slightly counter-clockwise to \sim p.a. 330° ; there was a dark lane w/ a spine-like tip separating the two tails; the central cond. was an elongated disk w/ axis pointing in p.a. $\sim 285^{\circ}$, and w/ a bright streamer extending from the nucleus $\sim 1^{\circ}$ into the dust tail at p.a. $\sim 305^{\circ}$; the gas tail and NE side of the coma had a definite bluish tint, giving way to a yellow color on the other side of the coma and into the dust tail [ADA03]. Mar. 2.67: "w/ 4-inch R, hoods are fabulous, like luminous arcs or interference patterns just like George Bond's drawings of comet Donati in 1858; jets form a 30° wedge, w/in which are three parabolic hoods that appear to be illuminated as w/ a flashlight beam *only w/in this 30° wedge!*; outside of this wedge, the hoods are much fainter" [OME]. Mar. 3.10: dust tail $2^{\circ}5$ long in p.a. 305° [KOZ]. Mar. 3.11: w/ naked eye, 5° tail in p.a. 310° [SHA02]. Mar. 3.17: also dust tail $4^{\circ}7$ long in p.a. 300° [BOU]. Mar. 3.23: w/ 8×30 B, $2^{\circ}5$ tail [ENT]. Mar. 3.6: "nuclear cond. of C/1995 O1 was still easily visible well after sunrise at Apache Point Observatory, as viewed w/ the 60-cm Sloan Digital Sky Survey 'Monitor Telescope' and a 55-mm eyepiece; three concentric shell fragments and a huge jet, which had been visible around the nucleus in dawn twilight, were astounding!" [John W. Briggs, Apache Point Observatory, Sunspot, NM]. Mar. 4.06: w/ 11-cm L ($50\times$), two bright and one faint shells, w/ best visibility towards fountain in the SW quadrant from the false nucleus; bright narrow jet $3'$ long sunward; w/ naked-eye, ion tail 15° long was blue in color and dust tail 6° long in p.a. 270 - 298 was yellow; coma had bluish color [BAR06]. Mar. 4.08: w/ 7×50 B, dust tail 5° long in p.a. 300° [VEL03]. Mar. 4.18: also slightly-curved dust tail $5^{\circ}0$ long in p.a. 304° [BOU]. Mar. 4.23: to the naked eye, 12° -long, broad, slightly-curved dust tail spanning p.a. $\sim 290^{\circ}$ - 310° ; also 11° gas tail near p.a. 325° ; comet looks more diffuse; in 9×34 B, nearly-parabolic edges less well defined; gas tail near p.a. 310° much fainter than dust tail that spans p.a. 280° - 300° ; nearly-stellar nucleus; strongly-curved fountain, initially towards p.a. $\sim 240^{\circ}$, seems to be feeding the trailing edge of a bright streamer inside the dust tail along p.a. $\sim 295^{\circ}$; this streamer now looks much broader than in previous obs., the leading edge leaving the nucleus tailwards, almost w/o bending; dark spine offset towards the gas tail; overall, the comet resembles a 'hockey stick' surrounded by a fainter parabolic envelope; in 25.3-cm $f/5.6$ L ($58\times$), dust tail much brighter than gas tail; dark area tailwards of the nucleus not so conspicuous, more contrasty near the inner edge of the dust tail; three hoods spanning p.a. $\sim 135^{\circ}$ - 260° inside huge fountain, spaced by roughly $0^{\circ}5$ difference, surround the nucleus; a bright jet (like a narrow 20° open fan) is centered near p.a. 200° inside a broad fountain, extending $\sim 0^{\circ}2$ from the nucleus; another weaker fountain-like structure leaves the nucleus towards



Above: Three sketches of the coma of comet C/1995 O1 by Daniel W. E. Green, showing the dust 'hoods' or 'haloes' emanating from the nuclear region. In each view, the yellowish dust tail (and coma) is above the nuclear region, and the bluish ion tail (and coma) is below. From left to right, the drawings were made at the telescope on 1997 Mar. 7.42 (25.4-cm f/4 L, 44× and 64×), Mar. 9.38 (81-cm f/4 L, 100×), and Mar. 13.98 (23-cm f/12 R, 86×).

◇ ◇ ◇

◇ Comet C/1995 O1 (Hale-Bopp) [text continued from page 84] ⇒

p.a. ~ 120°, then strongly bends counter-clockwise through the sunward coma to join the trailing edge of the comet; as twilight advanced, the nucleus became separated from the bright jet, nevertheless remaining non-stellar just above the resolution limit, its dia. estimated as < 3"; w/ L, the brighter inner hood remained visible up until 15 min before sunrise [PER01]. Mar. 4.23: also 8° gas tail near p.a. 325° [VIT01]. Mar. 4.26: w/ 10×50 B, 1°4 tail in p.a. 298° [TAY]. Mar. 4.80: brightest part of dust tail in p.a. 285° (5° long) [SHI]. Mar. 4.82: tail spans p.a. 295°-325° [MIY01].

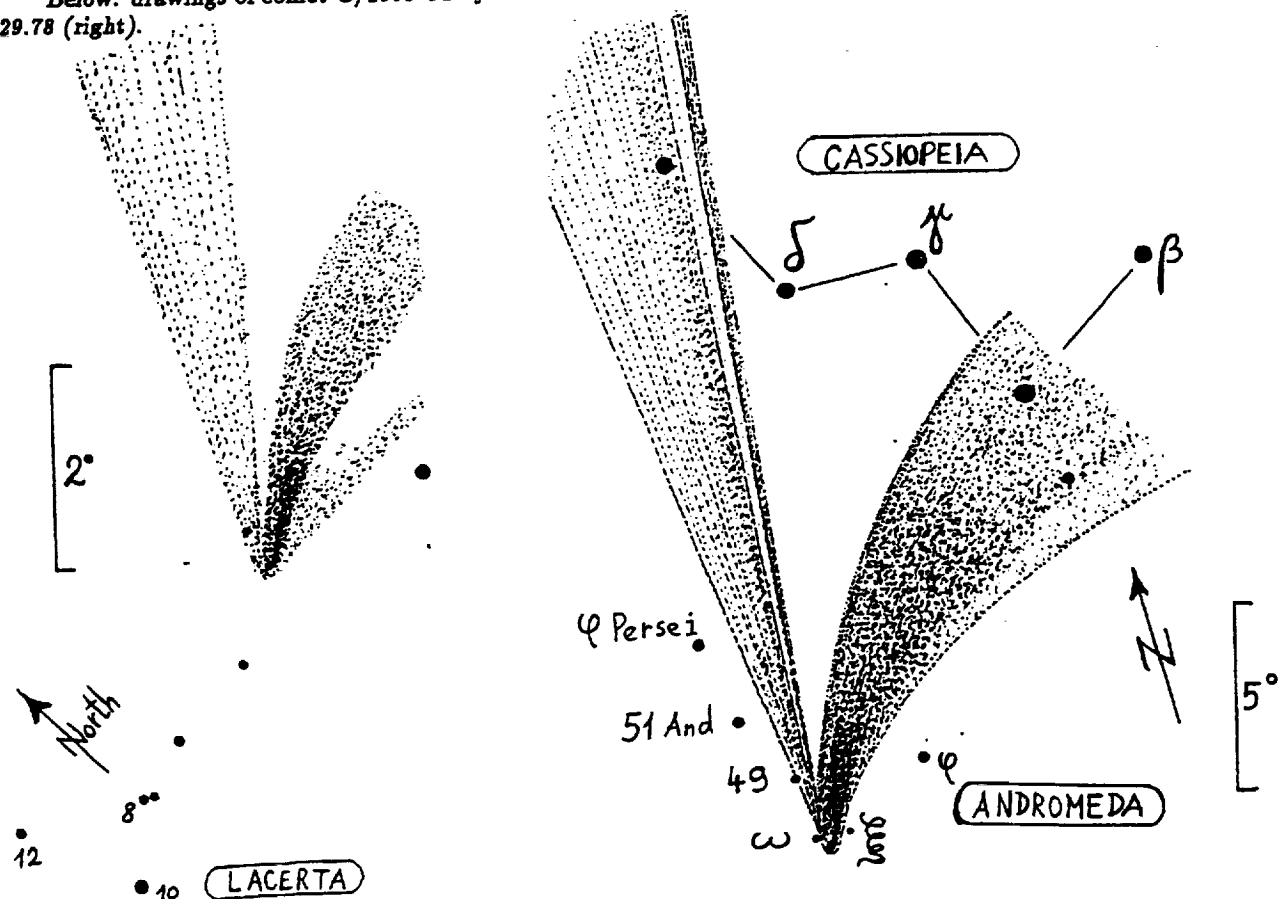
Mar. 5.06: shells are wider than on day before [BAR06]. Mar. 5.14: dust tail 2°5 long in p.a. 309° [KOZ]. Mar. 5.14 and 8.13: dust tail 4°5 long [MEY]. Mar. 5.15: second tail 10° in p.a. 285° [HOR02]. Mar. 5.16: second tail 6° in p.a. 300° [PLS]. Mar. 5.17: also slightly curved dust tail 5°1 long in p.a. 300° [BOU]. Mar. 5.25: w/ 10×50 B, 2°5 tail in p.a. 295° [TAY]. Mar. 5.75: w/ 7×50 B, dust tail 6° long in p.a. 303° [VEL03]. Mar. 5.83: tail spans p.a. 295°-320° [MIY01]. Mar. 6.08: w/ 11-cm L (32×), $m_2 = 4.8$ [IVA03]. Mar. 6.13: gas tail 13° long in p.a. 332° and dust tail 4° long in p.a. 313° [CHE03]. Mar. 6.14: dust tail 6°5 [KON06]. Mar. 6.14: dust tail 2°5 long [CHV]. Mar. 6.15: w/ naked eye, 5° dust tail in p.a. 300°; curved slightly towards W [SAR02]. Mar. 6.15: second tail 12° in p.a. 290° [HOR02]. Mar. 6.15: w/ 7×50 B, dust tail 6° long in p.a. 301° [VEL03]. Mar. 6.23: w/ 10×50 B, 3°5 tail [ENT]. Mar. 6.23: "w/ naked eye and 9×63 B, tails 14° (gas), 7° (dust); the tails had a comparable surface brightness at 3° from the nucleus; the area between the two tails seemed as dark as the sky background; m_1 estimated by taking off eyeglasses (this applies to all of my obs. of C/1995 O1 during Mar. 6-12" [Håkon Dahle = DAH, Observatorio del Roque de Los Muchachos, La Palma, Canary Is., Spain]. Mar. 6.46: a fan-shaped dust tail spanning p.a. 290°-309° started out straight for ~ 4° and then gently curved to end near τ Cyg (total length ~ 8° in p.a. 280°); the NW edge of the dust tail showed a bright spine of material extending for ~ 4° in 7×50 B [ADA03]. Mar. 6.92: tail was broad and diffuse [HEE]. Mar. 7.14: dust tail 5° [KON06]. Mar. 7.18: w/ naked eye, curved dust tail 6° long, central cond. of mag ~ 1.5; w/ 9×63 B, bright streamer on E border of dust tail; w/ 20-cm T (111×), false nucleus of mag ~ 3.0, w/ curved jet and three bright envelopes (which were the origin of the bright streamer); sunward jet fan spanning ~ 120°; in tailward direction, much darker area; false nucleus is not at the apex of the parabola, but positioned a bit to the NW [KAM01]. Mar. 7.18: besides gas tail, slightly curved dust tail in p.a. 288°-310° (longest 6°3 in p.a. 300°); strong cond., yellowish in color [BOU]. Mar. 7.18: due to slight coma increase, the aperture size was enlarged accordingly [MIK]. Mar. 7.26: w/ naked eye and 9×63 B, tails 13° (gas), 5° (dust); gas tail lost in the Milky Way; m_1 uncertain due to clouds [DAH]. Mar. 7.44: comet's alt. same as that of comparison star (Capella) [CRE01]. Mar. 8.06: w/ 7×50 B, dust tail 5° long in p.a. 312° [VEL03]. Mar. 8.13: w/ 63-cm f/16 L (130×), 'waving stream' seen from the nucleus, w/ jet pointing towards p.a. 170°; three elongated concentric rings/brightenings in section w/ p.a. ~ 170°-280° [CHE03]. Mar. 8.14: w/ naked eye, 10° dust tail in p.a. 310°; curved towards W [SAR02]. Mar. 8.15: dust tail 8° [KON06]. Mar. 8.15: second tail 10° long in p.a. 290° [HOR02]. Mar. 8.16: second tail 5° long in p.a. 305° [PLS]. Mar. 8.17: 12° ion tail in p.a. 330°; 4° dust tail in p.a. 310° [VAN06]. Mar. 8.17: dust tail 7° [FLA]. Mar. 8.17: second tail 10° in p.a. 300° [ZNO]. Mar. 8.26: w/ naked eye and 11×80 B, tails 14° (gas), 5° (dust); coma had distinctly yellow color; the N edge of the dust tail was much sharper and more well-defined than the S edge, which was very diffuse; several faint streamers seen in the gas tail [DAH]. Mar. 8.46: main (gas) tail showed possible extension to 15°5; fan-shaped dust tail spanning p.a. 275°-310° had maximum confirmed length of 6° in p.a. 300°, but may have had faint extension to ~ 10° in p.a. 275°; the dust tail showed more curvature than in my previous obs., and the tail spine was still visible, but was not as bright; light fog formed toward end of observing session [ADA03]. Mar. 8.53: "a pretty twin-tailed comet!"; very noticeable w/ naked eye; in 7×50 B, the S dust tail (yellow) is very broad (over 2° wide), over 7° long in p.a. 310°; narrow 10° plasma tail in p.a. 330° [SPR]. Mar. 8.82: brightest part of dust tail in p.a. 290° (5° long) [SHI]. Mar. 9.10: dust tail 6° long [MOR04]. Mar. 9.07: w/ 11-cm L (32×), $m_2 = 4.3$ [IVA03]. Mar. 9.10: w/ 4-cm R (8×), dust tail 7° long in p.a. 282°-295°; w/ naked-eye, ion tail 15° long in p.a. 333° [BAR06]. Mar. 9.14: 10° dust

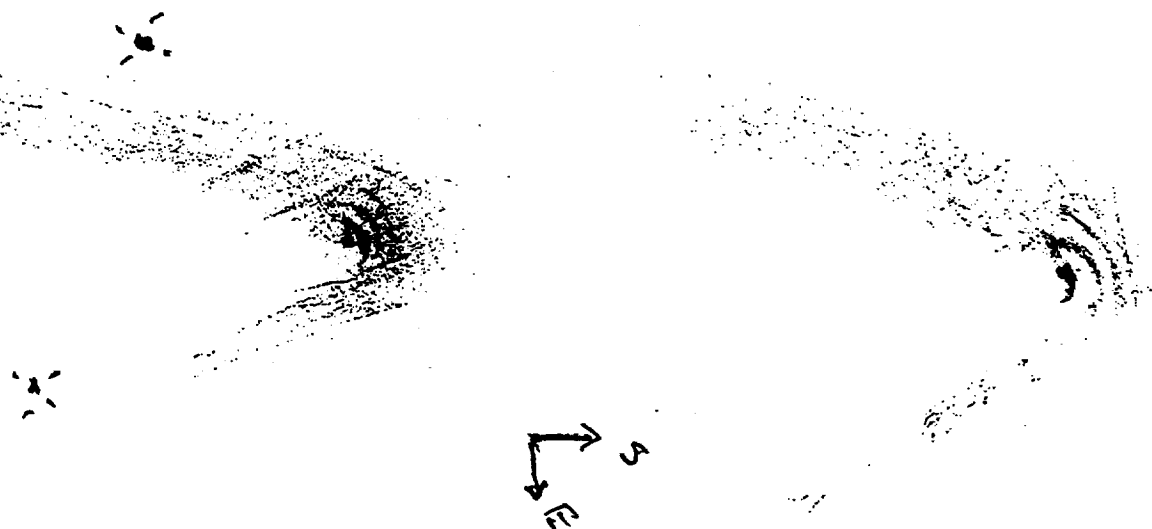
◊ Comet C/1995 O1 (Hale-Bopp) [text continued from page 85] ⇒

tail in p.a. 315°, curved towards W [SAR02]. Mar. 9.15: second tail 10° long in p.a. 295° [HOR02]. Mar. 9.16: 13° ion tail in p.a. 330°; 5° dust tail in p.a. 310° [VAN06]. Mar. 9.17: also slightly-curved dust tail spans p.a. 296°–318° (longest 6°5 in p.a. 305°); strong cond., yellowish in color; w/ 7×50 B, the head looks like an inverted 'J', w/ a broad fountain roughly centered in p.a. 210°, curving back anti-clockwise into the dust tail [BOU]. Mar. 9.24: to the naked eye, broad, slightly-curved dust tail spans p.a. 290°–310°, longest towards p.a. 310°; 7°–8° gas tail near p.a. 330°; the bright fountain and streamer are perceived; 0°5 tail still seen 30 min before sunrise; still visible to naked eye 20 min before sunrise; in 9×34 B, very strong central cond.; a huge fountain continues as a broad bright streamer along the inner or leading edge of the dust tail (the inside boundary just tailwards of the nucleus being ve sharply defined); inside this broad streamer, there is a brighter, narrow streamer that leaves the pseudo-nucleus towards p.a. 260°, then curving slightly tailwards; dust tail is better defined than gas tail; in 25.3-cm f/5.6 L (58×), wide open fountain initially spanning p.a. 180°–295°; four hoods inside this fountain, the first being linked to the nucleus by a 'V'-shaped wedge of bright material that leaves the nucleus towards p.a. 320°, then sharply turns back to touch the first hood near p.a. 295°; another weaker fountain-like structure leaves the nucleus towards p.a. 100°, then strongly curves counter-clockwise through the sunward part of the coma to join the outer edge of the great fountain; broad bright streamer flowing from the great fountain along the inner part of the dust tail, the inner or leading edge being sharply defined; the dark void tailwards of the nucleus is no longer prominent, there being a gradual brightness increase from the sharp inner edge of the dust tail to the outer, leading edge of the gas tail (the inner, trailing edge of the gas tail is ill-defined); as twilight advances, the nucleus remains stellar, while a knot of bright material is suspected very roughly 0°5 to the NW; 15 min before sunrise, the first hood is still visible, whilst the nucleus itself could be followed until 4 min to sunrise, still w/ some diffuseness around; slight mist at the beginning of obs., conditions improving thereafter [PER01]. Mar. 9.26: w/ naked eye and 11×80 B, tails 14° (gas), 7° (dust); the dust tail is a wide fan beautifully curved towards the S, w/ a sharply-defined N edge and a very diffuse S edge; the gas tail was lost in the Milky Way, but there is a hint (stronger than yesterday) that the tail is emerging from the Milky Way into the N-galactic hemisphere, which would increase the quoted tail length by ~ 10° [DAH]. Mar. 9.31–9.44: comet viewed from its rising around 2:45 a.m. local time until in deep twilight around 5:30 a.m. local time (nearly 3 hr); forked tail (ion vs. dust) was really remarkable from a dark sky w/ 12×50 B; w/ 32-inch L (100×), remarkable structure in inner coma w/ 3 irregular hoods/shells and a faint outer fourth shell strongly suspected; as before, the SE side of the coma w/ the strong dust jets/shells is very yellowish, while the other side of the coma (where the ion tail commences) is very bluish; even from a very dark mountain site under crystal-clear winter skies, naked-eye ion tail is seen w/ difficulty to 10° (the outermost few deg extremely faint and tenuous), and the dust tail is seen to only ~ 5° or so [GRE, w/ B. Volz and M. Motta, Center Harbor, NH]. Mar. 9.78: w/ 4-cm R (8×), dust tail 8° long in p.a. 300°; w/ naked eye, ion tail 15° long in p.a. 326° [BAR06]. (text continued on next page)

◊ ◊ ◊

Below: drawings of comet C/1995 O1 by Atilla Kósa-Kiss via 7×50 B on 1997 Mar. 10.15 (left) and Mar. 29.78 (right).





Above: Two sketches of the coma of comet C/1995 O1 by Daniel W. E. Green, showing the changing dust 'hoods' or 'haloes' emanating from the nuclear region in 24 hours, as seen with the Harvard College Observatory 9-inch f/12 R (86 \times). The view at left was on 1997 Mar. 16.00 and that at the right was on Mar. 16.98. A new shell appears to be forming in the right picture.

♦ ♦ ♦

♦ Comet C/1995 O1 (Hale-Bopp) [text continued from page 86] \Rightarrow

Mar. 10.06: w/ 7 \times 50 B, dust tail 6 $^\circ$ long in p.a. 314 $^\circ$ [VEL03]. Mar. 10.11: dust tail 3 $^\circ$ 6 long in p.a. 340 $^\circ$ [CHV]. Mar. 10.14: second tail 10 $^\circ$ long in p.a. 295 $^\circ$ [HOR02]. Mar. 10.14: dust tail 5 $^\circ$ long [MEY]. Mar. 10.15: w/ naked eye, curved dust tail 6 $^\circ$ long spanning p.a. 265 $^\circ$ -310 $^\circ$; central cond. of mag \sim 1.0; w/ 9 \times 63 B, coma dia. 15', DC = S8/; bright streamer on E border of dust tail; w/ 20-cm T (111 \times), false nucleus of mag \sim 3.0; again visible is a curved (comma-shaped) jet and three bright envelopes; sunward jet fan spans \sim 120 $^\circ$; tailward is a much darker area; false nucleus not at the apex of the parabola, but positioned a bit to the NW [KAM01]. Mar. 10.16: 13 $^\circ$ ion tail in p.a. 330 $^\circ$, 3 $^\circ$ 5 dust tail in p.a. 305 $^\circ$ [VAN06]. Mar. 10.17: also slightly-curved dust tail, longest 6 $^\circ$ 5 in p.a. 306 $^\circ$; strong cond., yellowish in color [BOU]. Mar. 10.23: to the naked eye, gas tail ends a little S of α Cep; dust tail < 10 $^\circ$ long, lost in Milky Way, spanning p.a. 290 $^\circ$ -320 $^\circ$, the trailing edge being slightly curved clockwise; in 25.3-cm f/5.6 L (58 \times), overall appearance similar to previous night (however, the wedge of material linking the nucleus to the first hood looks slightly broader, centered at p.a. 280 $^\circ$); dark void tailwards of the nucleus slightly more prominent again [PER01]. Mar. 10.25: w/ naked eye, tails 24 $^\circ$ (gas), 13 $^\circ$ (dust); the gas tail is for the first time definitely seen to extend beyond the Milky Way; dust tail was lost in the Milky Way; both tails seem to have higher surface brightness than on previous mornings [DAH]. Mar. 10.74: w/ 7 \times 50 B, dust tail 6 $^\circ$ long in p.a. 320 $^\circ$ [VEL03]. Mar. 10.76: dust tail 9 $^\circ$ [KON06]. Mar. 10.77: second tail 7 $^\circ$ in p.a. 295 $^\circ$ [HOR02]. Mar. 10.82: brightest part of dust tail in p.a. 295 $^\circ$ (7 $^\circ$ long) [SHI]. Mar. 11.11: w/ 7 \times 50 B, dust tail 6 $^\circ$ long in p.a. 312 $^\circ$ [VEL03]. Mar. 11.13: w/ 63-cm L (130 \times), two bright concentric rings; bright jet towards p.a. 260 $^\circ$; on Neopan 1600 film, 1- and 3-sec exp. w/ 63-cm L show four rings elongated w/in 3' of the photometric nucleus; dust tail in the section p.a. 295 $^\circ$ -308 $^\circ$; ion tail is suspected to length of 23 $^\circ$ [CHE03]. Mar. 11.13: dust tail 6 $^\circ$ long in p.a. 305 $^\circ$ [KOZ]. Mar. 11.14: dust tail 6 $^\circ$ long [MEY]. Mar. 11.15: second tail 10 $^\circ$ in p.a. 295 $^\circ$ [HOR02]. Mar. 11.16: 13 $^\circ$ ion tail in p.a. 330 $^\circ$, 6 $^\circ$ dust tail in p.a. 310 $^\circ$ [VAN06]. Mar. 11.20: w/ 10 \times 50 B, 4 $^\circ$ tail [ENT]. Mar. 11.24: w/ naked eye and 9 \times 63 B, tails 17 $^\circ$ (gas), 9 $^\circ$ (dust); m_1 uncertain due to clouds [DAH]. Mar. 11.51: twin tails very noticeable; in 7 \times 50 B, coma very elongated and bright yellow in color; plasma tail seen w/ naked eye to stretch to 4 $^\circ$ in p.a. 31 $^\circ$; dust tail to 8 $^\circ$ in p.a. 32 $^\circ$ [SPR]. Mar. 11.70: dust tail 6 $^\circ$ long [MOR04]. Mar. 11.77: dust tail 4 $^\circ$ 6 long [CHV]. Mar. 11.77: second tail 8 $^\circ$ in p.a. 300 $^\circ$ [HOR02]. Mar. 11.77: second tail 10 $^\circ$ in p.a. 300 $^\circ$ [PLS]. Mar. 11.78: dust tail 9 $^\circ$ [KON06]. Mar. 11.99: w/ 11-cm L (32 \times), $m_2 = 4.2$ [IVA03]. Mar. 12.12: dust tail 5 $^\circ$ 6 long [CHV]. Mar. 12.14: dust tail 3 $^\circ$ 5 long [MEY]. Mar. 12.14: second tail 10 $^\circ$ in p.a. 300 $^\circ$ [HOR02]. Mar. 12.15: second tail 7 $^\circ$ in p.a. 300 $^\circ$ [PLS]. Mar. 12.15: second tail 9 $^\circ$ in p.a. 295 $^\circ$ [ZNO]. Mar. 12.16: w/ naked eye, curved dust tail 6 $^\circ$ long spanning p.a. 280 $^\circ$ -315 $^\circ$; central cond. of mag 0.7; w/ 20-cm T (111 \times), spectacular sight — false nucleus again showed the comma-shaped jet, starting in NW and creating the innermost envelope; this and a second envelope today were broader and more diffuse than on the preceding days; a ring-like feature (at first glance resembling one of the impact sites of comet D/1993 F2 = 1993e only a few hours after impact) surrounded the false nucleus, which was positioned a bit to the SE of the center of this feature; a closer inspection showed the feature to be most probably the result of a rotating jet; on the sunward side, it was identical w/ the innermost envelope, while on the tailward side, it started at the SE end of the envelope and then looped around the false nucleus w/ a radius of \sim 1'; the NE segment was weakest, while to the N and NW, it brightened again and got broader and more diffuse; w/ 9 \times 63 B, coma dia. 15', DC = S8/ [KAM01]. Mar. 12.20: w/ 10 \times 50 B, 4 $^\circ$ tail [ENT]. Mar. 12.23: to the naked eye, also 12 $^\circ$ dust fan spans p.a. 290 $^\circ$ -320 $^\circ$; in 25.3-cm f/5.6 L (58 \times), broad

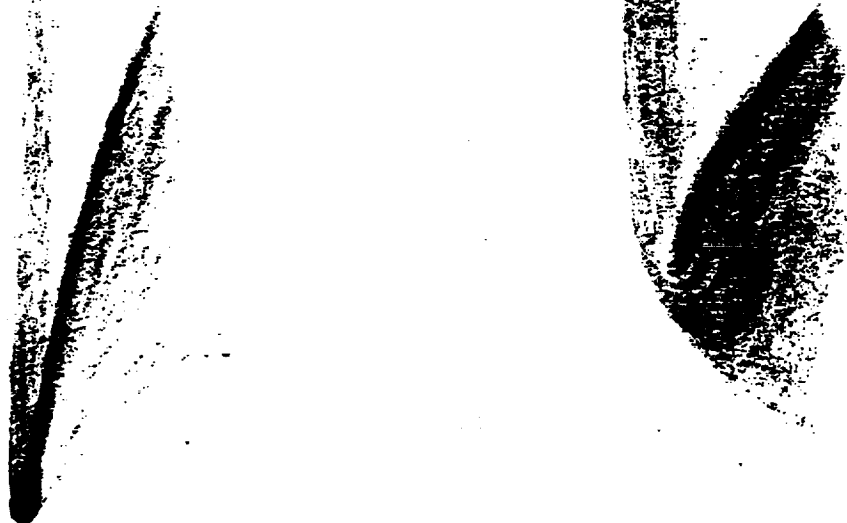
◊ Comet C/1995 O1 (Hale-Bopp) [text continued from page 87] ⇒

fountain seems to be weakening, spanning p.a. 185°-295°; nucleus looks like a 0.2 beam aligned towards p.a. 205°; broad wedge of material leaves the nucleus towards p.a. 270°, then abruptly turns 90° to S to 'start' the first hood, some 0.5 from nucleus; the hood looks broken near the edge of the fountain at p.a. 180°, then reappears as a parabolic arc going through the sunward coma until p.a. 70°, where there is another abrupt turn, the hood going through tailwards of the nucleus to touch the beginning of the second hood at p.a. 295° (i.e., the hoods appear as a spiral made of ogival arcs!); this second hood also breaks at p.a. 185°, reappearing weakly as a short arc to p.a. 160°-180°; a new hood seems to be forming W of the p.a. 205° 'nucleus beam'; third hood spanning p.a. ~ 185°-295°; fourth hood much fainter, spanning p.a. 245°-285° [PER01]. Mar. 12.51: "both tails wider, longer, and more distinct; S side of comet more yellow; impressive sight!" [SPR]. Mar. 12.77: dust tail 9° [KON06]. Mar. 12.77: second tail 8° in p.a. 300° [HOR02]. Mar. 12.77: second tail 10° in p.a. 300° [PLS]. Mar. 13.10: dust tail 6° long [MOR04]. Mar. 13.10: w/ 11-cm L (32×), distinct starlike nucleus dia. 1.5; coma observed as a small spherical triangle containing three or four bright arcs [MOS03]. Mar. 13.14: second tail 8° in p.a. 300° [HOR02]. Mar. 13.23: to the naked eye, 28° gas tail leaving the nucleus towards p.a. 335°, very slightly curving counter-clockwise after ~ 9°, ending close to β Cep; 9° dust fan spans p.a. 295°-315°; comp. stars Vega and Deneb; in 25.3-cm f/5.6 L (240×), stellar nucleus; 0.2 jet towards p.a. 200°; fountain spanning p.a. 190°-290°; first hood 0.5 from nucleus, spanning SSE-WNW, linked to the fountain by a broad bridge spanning p.a. 220°-270°; third hood spans p.a. 200°-270°, some 1.1 from nucleus; at 58×, nucleus as a beam towards p.a. 190°-200°; weakening fountain now spans p.a. 170°-285°; void tailwards of the nucleus more prominent again, appearing as a narrow parabolic dark area; first hood spans the full fountain fan, fading at the p.a. 170° edge, then reappearing as a short arc to the SE; second hood also spans the full fountain fan, fading at the p.a. 170° edge, to reappear immediately as a parabolic arc that could be traced clockwise until p.a. 60°; third hood much weaker, as a short arc to the W; fourth hood only glimpsed towards p.a. 270°-290°; overall, the coma continues strongly dichotomized, the trailing part being prominently brighter; broad bright streamer inside dust tail as in recent obs. [PER01]. Mar. 13.39: "it *really* makes a HUGE difference seeing this comet in a dark sky, just as w/ C/1996 B2!!; naked-eye ion tail curves beautifully past the Milky Way — no doubt about it, more than 20° long; we both felt that the ion tail was both much longer and of much higher surface brightness this morning than four mornings earlier from the same site (both under clear conditions, near 0° F); dust tail curves about 8° in right fork (ion tail forming the left fork) — stunning via naked eye, in 12×50 B, and in 32-inch f/4 L; comet still visible at this latitude (+44°) for 1.5 hr prior to the commencement of astronomical twilight; words can hardly describe the beauty of this comet this morning" [GRE, w/ M. Motta, near Center Harbor, NH]. Mar. 13.99: w/ 11-cm L (32×), $m_2 = 4.1$ [IVA03]. Mar. 14.16: the end of the ion tail is superimposed on the Milky Way, clearly seen up to 18°; "I suspect a possible further extension up to 20°, but as it is superimposed on a bright star cloud, I cannot be sure it is real" [MIL02]. Mar. 14.50: both tails are growing larger; in the 7×50 B, the twin tails both extend to over 10° [SPR]. (text continued on next page)

◊ ◊ ◊

Below: drawings of comet C/1995 O1 by Margareta Westlund. At left, broad view of tails with 7×35 B on 1997 Mar. 18.10. At right, view of coma with 20-cm f/10 T (125×) on Mar. 22.82, in moonlight.

N
E $\begin{array}{|c|} \hline 1^\circ \times 1^\circ \\ \hline (B\ 7\times 35) \end{array}$





Above: Two sketches of the coma of comet C/1995 O1 by Daniel W. E. Green, showing the changing dust 'hoods' or 'haloes' emanating from the nuclear region, as seen with a 25.4-cm f/4 L (39 \times and 85 \times). The view at left was on 1997 Mar. 16.4 and that at the right was on Mar. 18.4. The right side of the coma (from whence issues the ion tail) was very bluish, while the left side of the coma (from whence issues the main part of the dust tail) was very yellowish in color. Numerous splintered streamers and rays were easily visible in the ion tail within a degree of the nucleus.

◇ ◇ ◇

◇ Comet C/1995 O1 (Hale-Bopp) [text continued from page 88] ⇒

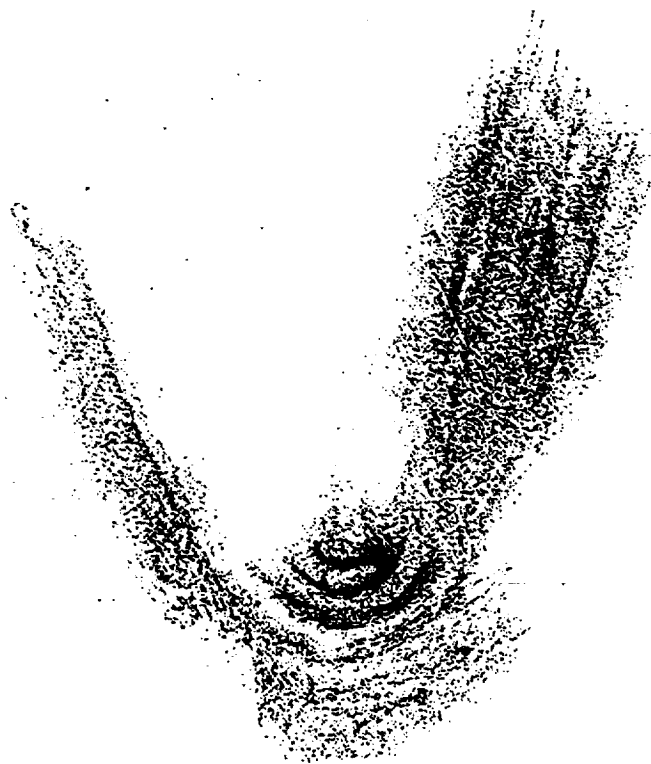
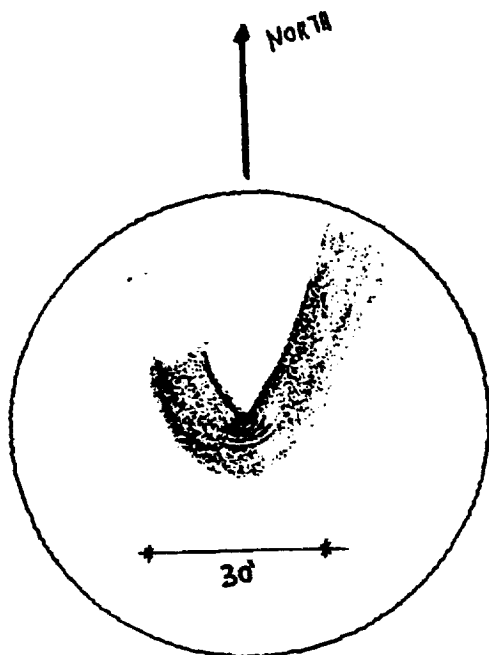
Mar. 15.45: dust tail 8° long in p.a. ~ 310°, spanning p.a. 290°-315° [ADA03]. Mar. 15.49: comet lower but very impressive; twin tails seem to have 'merged' somewhat, as they now are more 'blended' together (wider); tail length over 10° in p.a. 32° [SPR]. Mar. 16.10: w/ naked eye, tails 14° (ion) and 8° (dust); the gas tail was nearly straight; in 7 \times 50 B, gas tail 14° — easily seen for 10°; w/ 10.2-cm f/15 R (60 \times), the nucleus appeared round; two bright arcs (hoods) spanning ~ 120° were seen in the fountain that originated from the nucleus, the innermost hood being brightest [SKI]. Mar. 16.12: w/ naked eye, tails 13° in p.a. 340° (ion), 7° in p.a. 318° (dust); the dust tail was very bright until ~ 3° from central cond., and it showed a strong curvature towards S; the intensity of the gas tail was comparable to the Cyg Milky Way until 6°-7° from the head; in 10 \times 50 B, tails 13° (ion), 7.5° (dust) [GRA04]. Mar. 16.18: in 20.3-cm f/10 T (123 \times), a bright fountain was seen near the false nucleus, spanning p.a. ~ 170°-270°; 3-4 bright arcs (hoods) were seen in this fountain; these hoods were separated by dark lanes; observed in nautical twilight [GRA04]. Mar. 16.24: to the naked eye, slightly-curved 16° dust fan spans p.a. 290°-330°; also 14° gas tail near p.a. 350°; in 25.3-cm f/5.6 L (240 \times), stellar nucleus; broad bridge of material leaving the nucleus towards W, then abruptly turning clockwise to start the first hood, which spans p.a. 190°-270°; 2nd hood spans p.a. ~ 200°-270°; third hood spans p.a. 230°-270°; the distance between two first hoods is larger than the distance between second and third hoods; at 58 \times , 'nuclear beam' towards p.a. ~ 320°; broad, weak fountain spans p.a. 190°-270°; four hoods starting to convey the impression of layers; first hood linked to the 'nuclear beam' by a broad bridge of material due-W of the nucleus; strongly dichotomized coma, the trailing part being much brighter [PER01]. Mar. 16.75: w/ 7 \times 50 B, dust tail 4° long in p.a. 320° [VEL03]. Mar. 16.83: w/ naked eye, tails 13° in p.a. 340° (ion), 7.5° in p.a. 322° (dust) [GRA04]. Mar. 16.97: only the dust tail was seen; moonlight [SKI]. Mar. 16.99: in 20.3-cm f/10 T (123 \times), from the pseudo-nucleus there was a wide, bright fountain spanning p.a. ~ 160°-270°; three arcs (hoods) were visible in the fountain (the two innermost were bright and easily seen); the intensity of the inner part of the dust tail was considerably higher than the nearby planetary nebula NGC 7662 [GRA04]. Mar. 17.13: dust tail 6° long in p.a. 354° [KOZ]. Mar. 17.17: w/ naked eye, 8° tail in p.a. 320° [SHA02]. Mar. 17.23: w/ 7 \times 50 B, dust tail 6° long in p.a. 325° [VEL03]. Mar. 17.24: to the naked eye, ~ 10° gas tail near p.a. ~ 345°; also ~ 10° dust fan spanning

◊ Comet C/1995 O1 (Hale-Bopp) [text continued from page 89] ⇒

p.a. 290°-310°; in 25.3-cm f/5.6 L (58×), stellar nucleus; broad bridge of material towards W links the nucleus to the first hood; the spiral structure of the four hoods like ogival arcs; first three hoods can be traced from W through S, to E; second hood also continues faintly from W to N, while the third hood has an ill-defined extension from W to NW; the fourth hood only spans WSW-W; there are clear breaks/dimmings in the hoods, both at p.a. 160° and 270°; narrow parabolic dark void tailwards of the nucleus, clearly offset towards the leading edge of the tail system — the contrast at the dust-tail leading edge being stronger than at the gas-tail trailing edge; strongly dichotomized coma, as in recent obs.; the 'terminator' along p.a. ~ 160° is slightly concave towards the leading part of the coma [PER01]. Mar. 17.38: the ion tail seems again fainter in surface brightness and not as obvious through Milky Way as during last obs. at this dark-sky site; can the ion tail be oscillating in brightness as did the ion tail of C/1996 B2?; crisp, clear (and cold! — 0° F) conditions near Center Harbor, NH [GRE]. Mar. 17.79: second tail 7° in p.a. 305° [ZNO]. Mar. 17.82: w/ naked eye, tails 7° (gas), 5° (dust); dust tail bright for 3°; moonlight and thin clouds; in 7×50 B, tails 8° (gas), 6° (dust) [SKI]. Mar. 17.84: w/ 7×50 B, DC = 8, tails 10° in p.a. 330° (gas), 5° in p.a. 310° (dust); both tails appeared curved; weak aurora borealis near comet [HEE]. Mar. 18.01: w/ naked eye, only the dust tail was seen; moonlight [GRA04]. Mar. 18.09: dust tail 7° long [MOR04]. Mar. 18.15: second tail 9° in p.a. 315° [HOR02]. Mar. 18.15: ion tail 4° in p.a. 325° [DVO]. Mar. 18.24: to the naked eye, dust tail spanning p.a. 300°-330° and 9° gas tail near p.a. 345°; in 25.3-cm f/5.6 L (240×), nearly-stellar nucleus; broad spiral arm initially leaves the nucleus towards p.a. ~ 280°, then strongly bends clockwise ~ 0.3-0.4 from the nucleus to form the first hood; near the opposite side of where this spiral arm leaves the nucleus, there is another weaker and smaller spiral arm leaving the nucleus towards p.a. ~ 110°, then strongly bending clockwise some 0.2 from the nucleus, but it couldn't be traced much farther after the bend; the second hood spans p.a. ~ 180°-270°, some 0.5 from nucleus; at 58×, hint of new hood or spiral arm very close and to the E side of the nucleus; the bridge or spiral arm linking the nucleus to the first hood, on the W side, is much weaker now, as if the detachment of the first hood was near completion; three hoods seen, all spanning p.a. ~ 110°-280°, there being a conspicuous weakening near p.a. 190°; overall, the hoods do not convey so strongly the impression of ogival arcs as previously, but rather the shape of wide parabolic arcs; narrow parabolic dark void tailwards of the nucleus [PER01]. Mar. 19.05: w/ naked eye, dust tail 6°; in 10×50 B, tails 9° in p.a. 347° (ion), 7° in p.a. 328° (dust) [GRA04]. Mar. 19.09: dust tail 8° long [MOR04]. Mar. 19.13: w/ 7×50 B, dust tail 5° long in p.a. 332° [VEL03]. Mar. 19.16: w/ naked eye, tails 7° (gas), 6° (dust); dust tail curved strongly towards W; observed in morning twilight; in 7×50 B, tails 10° (gas), 7° (dust) [SKI]. Mar. 19.84: w/ naked eye, tail 12° in p.a. 346° (ion), 7° (dust); the gas tail was quite easily seen for 7°; the comet was first detected when the solar alt. was -4°1; in 7×50 B, tails 12° (gas) and 8° (dust) long [SKI]. (text continued on next page)

◊ ◊ ◊

Below: drawings of comet C/1995 O1. At left, sketch by Sandro Baroni as viewed through 20×80 B on 1997 Mar. 20.78; the line is 30' in length. At right, sketch by Daniel W. E. Green as viewed through the Harvard College Observatory 9-inch f/9 Clark R on Mar. 24.98.



◊ Comet C/1995 O1 (Hale-Bopp) [text continued from page 90] ⇒

Mar. 20.04: w/ 11-cm L (32×), $m_2 = 3.7$ [IVA03]. Mar. 20.17-20.18: w/ naked eye, only dust tail seen; in 20.3-cm f/10 T (123×), extending from the nucleus was a bright fountain spanning p.a. $\sim 160^\circ$ - 270° ; four hoods were visible in the fountain near the nucleus, three of them easily seen; observed in strong morning twilight [GRA04]. Mar. 20.45: plasma tail very faint but traced for length of 10° in p.a. 350° ; the dust tail, of length 9° in p.a. 320° , was much brighter and more broad, spanning p.a. 305° - 323° ; both tails were lost in the Milky Way; m_1 estimates w/ 1×50 monocular continue to be significantly fainter than naked-eye estimates [ADA03]. Mar. 20.7: tab. tail refers to the type-I tail; 1.7 type-II tail in p.a. 305° ; twilight [FOG]. Mar. 21.06: w/ naked eye, only the dust tail was seen for 5° (being bright despite the moonlight) [SKI]. Mar. 21.12: in 10×50 B, tails 12° in p.a. 352° (ion) and 6° in p.a. 335° (dust); despite the moonlight (3 days from full moon) the gas tail was clearly seen [GRA04]. Mar. 21.80: in 10×50 B, tail 6° in p.a. 354° (ion), 6° in p.a. 336° (dust); moonlight [GRA04]. Mar. 22.14: slightly curving dust tail spans p.a. 318° - 340° (longest 11° in p.a. 328°); strong cond., clearly yellowish in color [BOU]. Mar. 22.20: very strong moonlight; in 7×50 B, the S dust tail is a little more intense, stretching over 12° in length [SPR]. Mar. 22.81: central cond. of mag 0.3 [KAM01]. Mar. 22.82: moon and clouds interfered, ion tail not visible [ZNO]. Mar. 22.88: w/ naked eye, tails 7° (dust), 3.5 (gas); gas tail was faint; comet first detected at w/ sun at alt. -3.7° ; in 7×50 B, tails 8° (dust), 7° (gas); gas tail clearly seen for 5° [SKI]. Mar. 22.91: w/ 10.2-cm f/15 R (60×), three arcs (hoods) were seen (the innermost was bright and resembled a spiral outward from the nucleus; the next one was fainter but clearly visible, while the outermost was faint and best seen w/ averted vision); the distance between the arcs were clearly larger than nearly a week ago [SKI]. Mar. 23.00: w/ 10×50 B, tails 5° in p.a. 355° (ion) and 5° in p.a. 342° (dust); strong moonlight [GRA04]. Mar. 23.15: ion tail 6° [KYS]. Mar. 23.16: ion tail 6° [KYS]. Mar. 23.74: w/ 7×50 B, dust tail $\sim 4^\circ$ long in p.a. 343° [VEL03]. Mar. 23.77: dust tail 7° in p.a. 320° [ZNO]. Mar. 24.18: moon partially eclipsed [SPR]. Mar. 24.86: only the dust tail was seen w/ the naked eye; full moon and hazy sky; in 10×50 B, tails 5° in p.a. 7° (ion) and 6° in p.a. 345° (dust) [GRA04]. Mar. 24.86: only the dust tail was seen (easily seen for 4°); full moon and thin clouds [SKI].

Mar. 25.07: in 20.3-cm f/10 T (123×), a diffuse, fan-shaped fountain was seen on the preceding side on the pseudo-nucleus, spanning p.a. $\sim 200^\circ$ - 320° ; four hoods were seen in this fountain [GRA04]. Mar. 25.12: dust tail $> 6^\circ$ long in p.a. 343° - 350° [BAR06]. Mar. 25.80: dust tail $> 4^\circ$ long in p.a. 334° - 344° [BAR06]. Mar. 25.84: only dust tail seen clearly, due to full moon; the tail was curved; w/ 15.2-cm f/8 L (80×), $30'$ coma, DC = 8, three arcs seen SW of nucleus at p.a. 170° - 280° [THO03]. Mar. 26.77: w/ 7×50 B, dust tail 7° long in p.a. 352° [VEL03]. Mar. 26.84: w/ 15.2-cm f/8 L (80×), $30'$ coma, DC = 8, three arcs seen SW of nucleus at p.a. 170° - 280° (they were a bit wider than yesterday and seem to expand over a period of 1-2 hr) [THO03]. Mar. 26.85: w/ the naked eye and 7×50 B, tails 16° in p.a. 1° (gas) and 11° in p.a. $\sim 335^\circ$ (dust); the width of the gas tail increased outwards [SKI]. Mar. 26.85: excellent conditions (zodiacal light is glaringly obvious); comparison basically w/ α Aur, β Ori, and Sirius; the comet rivals Mars, but this wasn't used because of color; to the naked eye, strongly-curved-clockwise dust fan spanning p.a. 340° - 350° ; 10° gas tail near p.a. 5° ; dust tail much brighter than gas tail [PER01]. Mar. 26.86-26.87: w/ naked eye, tails 15° in p.a. 7° (ion) and 14° in p.a. 336° (dust); very impressive sight, observed before moonrise; w/ 10×50 B, tails 15° (ion) and 11° (dust); the dust tail was very bright for 3° - 4° ; the gas tail was much weaker, its intensity comparable to the Cyg-Cas Milky Way; there was a possible bend in the gas tail at $\sim 4^\circ$ from the head [GRA04]. Mar. 26.93: in 10.2-cm f/15 R (60×), two arcs were seen near the nucleus, the innermost arc clearly seen despite a turbulent atmosphere; the width of the area between the arcs was comparable to the width of the arcs [SKI]. Mar. 27.06: ion tail 14° long, dust tail 11° long [CRE01]. Mar. 27.14: slightly-curved dust tail spans p.a. 328° - 346° (longest 9.5° in p.a. 337°); head clearly yellowish in color [BOU]. Mar. 27.16: w/ 20-cm T (101×-185×), the greenish-tinged coma shows a complex structure of 3 hoods; one hood comes from the comet's SW side and curves around some 110° from the false nucleus towards the solar vector; two other fainter hoods are very visible; the false nucleus and intense hood make the comet look like a giant comma [SPR]. Mar. 27.76: dust tail 11° long in p.a. 335° [BAR06]. Mar. 27.76: w/ 7×50 B, dust tail 9° long in p.a. 346° [VEL03]. Mar. 27.83-Apr. 18.80: ion tail $> 7^\circ$ long, dust tail $> 6^\circ$ long [MIK]. Mar. 27.85: to the naked eye, 10° dust fan strongly curved clockwise; also 10° ion tail; in 25.3-cm f/5.6 L (240× and 58×), bright 'nuclear beam' ~ 1.5 towards p.a. 290° ; possibly what was once the great fountain is now seen in the background of the hoods as a broad $\sim 1'$ fan spanning p.a. 160° - 270° ; new thin hood is seen, no more than 0.1 from the nucleus, spanning p.a. $\sim 130^\circ$ - 250° ; the gap between this new hood and the nucleus is also very thin, the two structures being linked at the WSW end; the second hood has still some ill-defined, weak bridge linking it to the nucleus at the W end; this second hood spans p.a. 120° - 305° , some 0.5 from the nucleus; third hood $\sim 1'$ from nucleus spans p.a. 120° - 305° ; fourth hood better defined towards SW-WNW; along p.a. 320° , a sharp contrast is seen — the W coma being much brighter than the N coma, tailwards of the nucleus; dark void no longer seen; all hoods are roughly parabolic-shaped now [PER01]. Mar. 27.89: "w/ naked eye, ion tail 15° , dust tail 11° ; w/ 7×50 B, several streamers were seen in the gas tail; the width of this tail at $\sim 10^\circ$ from the head was $\sim 2^\circ$; the dust tail was broad and bright for $\sim 7^\circ$; by now, I can imagine how Comet Donati looked like in 1858!" [SKI]. Mar. 27.90: "w/ naked eye, tails 15° in p.a. 5° (ion) and 13° in p.a. 341° (dust); the dust tail was clearly more prominent than 1-2 weeks ago; in 10×50 B, tails 13° (ion) and 10° (dust); the comet was clearly visible w/ reversed 10×50 B, and I est. total mag ~ -1.9 (ref: Mars)" [GRA04]. Mar. 28.05: ion tail 15° long, dust tail 12° long [CRE01]. Mar. 28.07: w/ 20.3-cm f/10 T (123×), comparison star ϕ And (spec. type B7) was clearly bluer than the nucleus, while ξ And (spec. type K0) was redder; there was a $\sim 120^\circ$ -wide sector (spanning p.a. $\sim 160^\circ$ - 280°) of bright material originating from the false nucleus; in this sector there were at least three hoods separated by dark arcs [GRA04]. Mar. 28.77: ion tail 12° [KYS]. Mar. 28.80: ion tail 12° in p.a. 5° [HOR02]. Mar. 28.81: dust tail 18° [KON06]. Mar. 28.81: ion tail 20° in p.a. 5° [PLS]. Mar. 28.81: dust tail 16° in p.a. 335° [ZNO]. Mar. 28.84: also slightly-curved dust tail, longest 12° in p.a. 336° [BOU]. Mar. 28.85, 30.84, and 31.85: w/ naked eye, 14° tail in p.a. 343° , 14° , and 13° [SHA02]. Mar. 28.854: w/ naked eye, 8.8 tail in p.a. 10° [HAS02]. Mar. 28.89: w/ naked eye, ion tail 15° in p.a. 6° , dust tail 13° in p.a. 343° ;

Below: drawings of comet C/1995 O1 by Margareta Westlund (Uppsala, Sweden), as seen through 7×35 B. At left is the view in moonlight on 1997 Mar. 27.91; at right is the view on Mar. 29.96.

N
E $\begin{array}{|c|} \hline 1^\circ \times 1^\circ \\ \hline \end{array}$
(B 7×35)

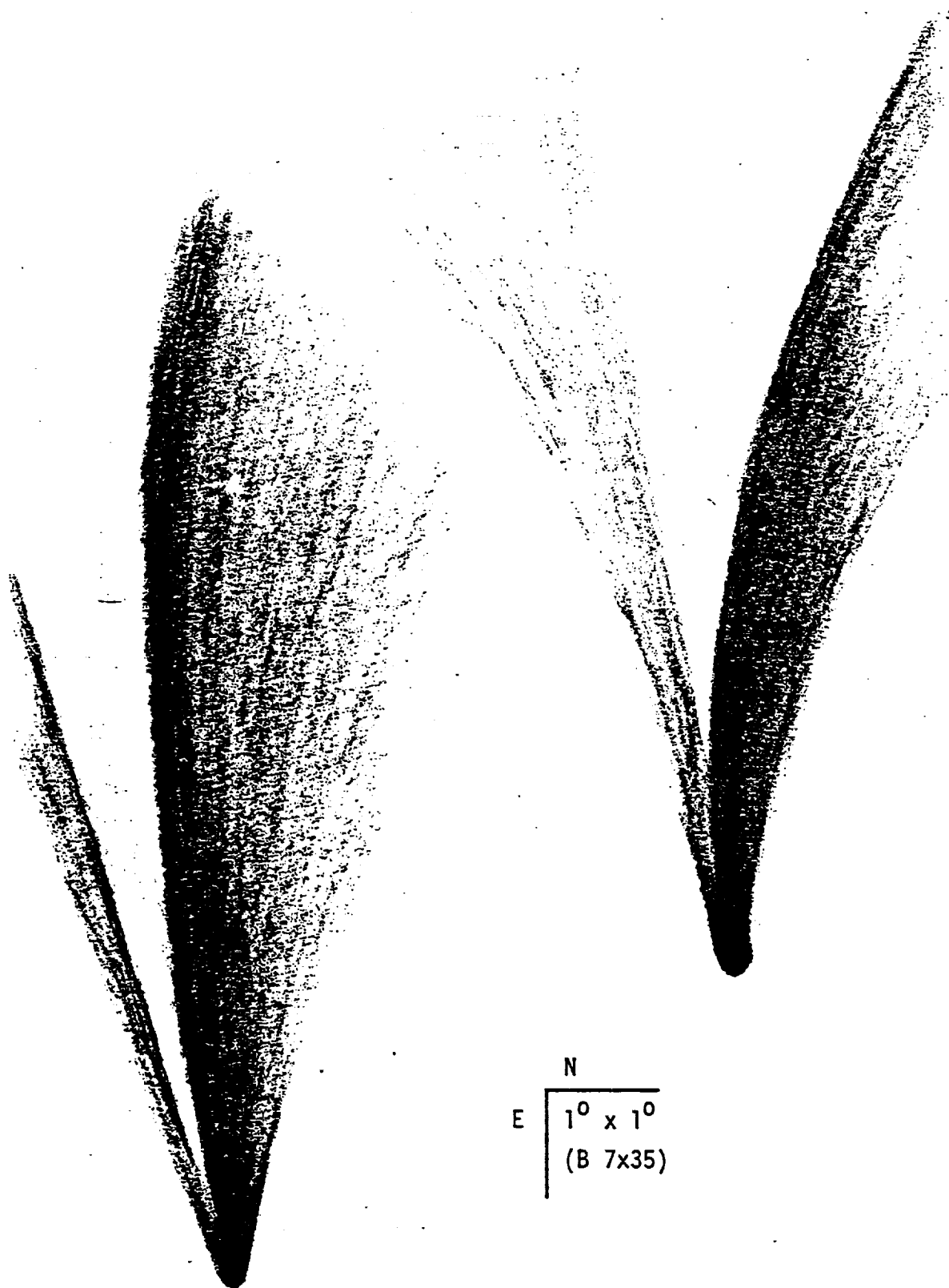


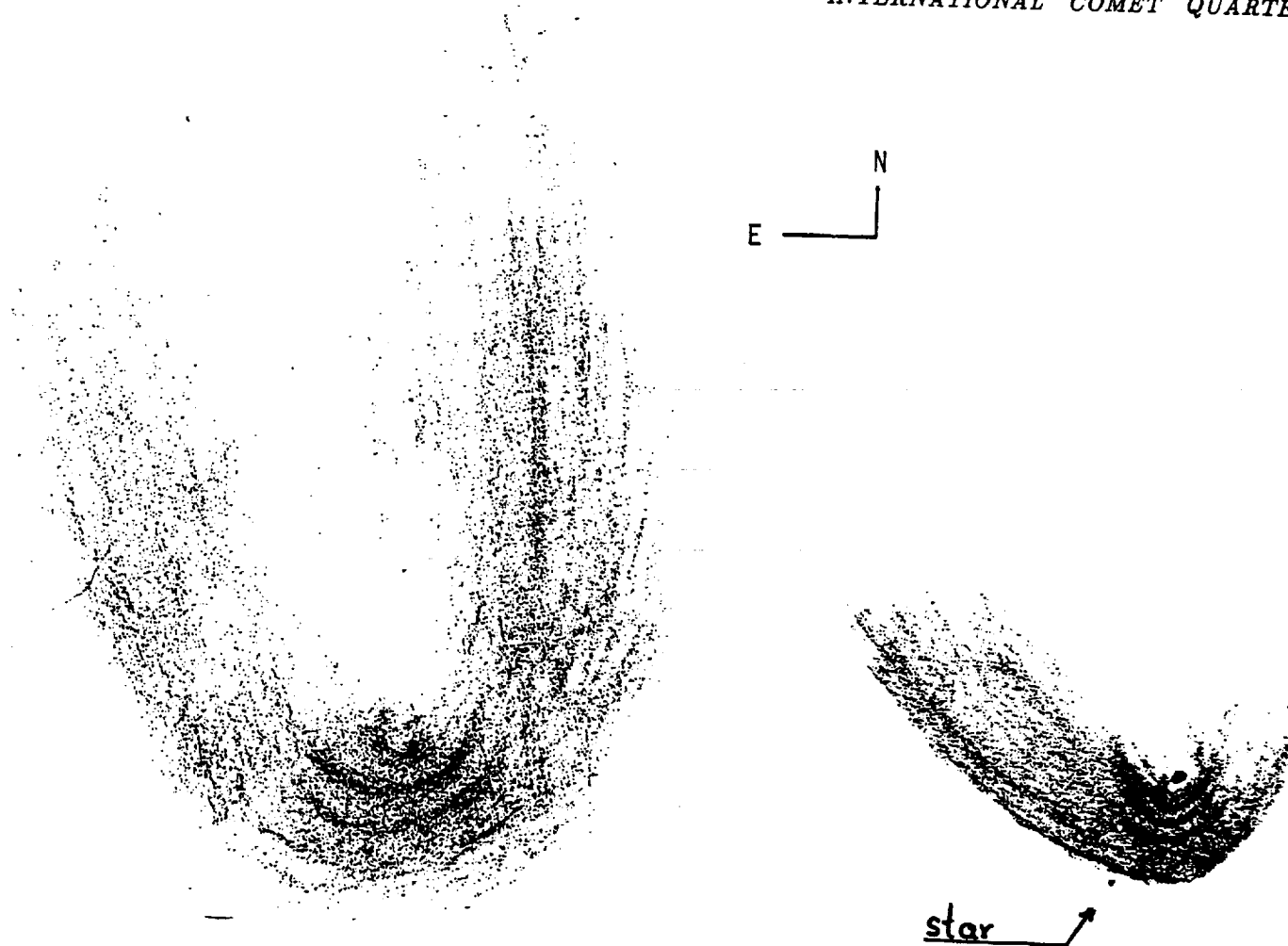
◊ Comet C/1995 O1 (Hale-Bopp) [text continued from page 91] ⇒

favorable conditions; w/ 10×50 B, both tails visible for 13°, at p.a. 6° (ion) and 350° (dust); gas tail was clearly split in two components, separated by 0°5-1°; a streamer was seen in the dust tail [GRA04 = Bjørn H. Granslo]. Mar. 28.94: w/ naked eye, ion tail 15°, dust tail 11°; favorable conditions, but aurora below the comet; w/ 7×50 B, several streamers were seen in the gas tail [SKI]. Mar. 28.98: w/ 20.3-cm f/10 T (123×), four hoods were visible on the SW side of the nucleus (p.a. 170°-310°), these hoods were separated by dark arcs [GRA04]. Mar. 29.76: w/ 7×50 B, DC = D8, 13° tail in p.a. 7° [VEL03]. Mar. 29.79: w/ naked eye, 10° long curved dust tail in p.a. 340° [SAR02]. Mar. 29.85: tab. tail is ion; also dust tail ~ 10° long [PAL02]. Mar. 29.85: dust tail 16° in p.a. 335° [ZNO]. Mar. 29.88: ion tail 12° in p.a. 5° [HOR02]. Mar. 29.96: w/ naked eye, both the dust and gas tails were seen for 10°; conditions not ideal due to thin clouds [SKI]. Mar. 30.13: gas tail not visible w/ naked eye; the sky was covered by thin clouds, in morning twilight; w/ 10×50 B, gas tail 8° in p.a. 8°, dust tail 7° in p.a. 351°; comet not seen w/ reversed 10×50 B [GRA04]. Mar. 30.15: w/ 20.3-cm f/10 T (123×), a bright fountain was seen on the preceding side of the false nucleus, spanning p.a. 180°-310°; at least three hoods were seen in this fountain [GRA04]. Mar. 30.77: dust tail 16° in p.a. 330° [ZNO]. Mar. 30.78 and Apr. 1.78: w/ 20×60 B, large envelope as diffuse outer coma, ~ 20' in dia. [CHE03]. Mar. 30.78: dust tail 15° [KYS]. Mar. 30.79: ion tail 6° [DVO]. Mar. 30.80: w/ 7×50 B, dust tail 11° long in p.a. 333° [VEL03]. Mar. 30.80: photometry w/ 90-mm-f.l. f/2.8 lens + V filter + CCD; the exposure time is listed as 1 sec, although the exp. are recently only 0.3-0.5 sec long [MIK]. Mar. 30.83: "also slightly curving dust tail, longest 13°5 in p.a. 337°; in 15.6-cm L (102×), strong cond., yellowish in color; in sunward direction, sort of knot attached to small jet (new hood forming?); three concentric hoods visible, brightest in sunward direction, the inner two rather sharply defined, and the outer one very diffuse (some 1'-1'5 in dia.)" [BOU]. Mar. 30.85: dust tail 18° [KON06]. Mar. 30.86: w/ naked eye, both the dust and ion tail were seen for 13°, directed toward p.a. 348° and 14°, respectively; observing affected by thin clouds; w/ 10×50 B, 11° dust tail in p.a. 355°, 10° ion tail in p.a. 14°; "for all of my obs. in Mar., the m_2 values refer to the nearly-stellar central cond. (dia. < 2'); the comet was clearly visible w/ reversed 10×50 B, at total mag -1.7, using Mars as a comparison object" [GRA04]. Mar. 30.97: dust tail 13° in p.a. 330° [HOR02]. Mar. 30.97: dust tail 15° in p.a. 335° [PLS]. Mar. 31.00: w/ naked eye, tails 15° (gas) and 12° (dust); w/ 7×50 B, two streamers easily seen on each side of the gas tail; a bright streamer was seen for ~ 2° w/in dust tail (another streamer was curved and formed the E edge of this tail); in reversed 7×50 B, the comet was as bright as Mars; w/ 10.2-cm f/15 R (84×), three hoods were seen on the SW side of the false nucleus — the innermost started near the nucleus and formed an outward spiral (the next one was fainter and formed a bright arc spanning 120° in p.a., while the outermost was faint but more sharply defined on its inner side) [SKI]. Mar. 31.07: plasma tail 7° long in p.a. 9°; an ~ 7° dust tail was also seen [ADA03]. Mar. 31.79: dust tail 12° in p.a. 330° [HOR02]. Mar. 31.795: w/ naked eye, 15°4 tail in p.a. 13° [HAS02]. Mar. 31.80: dust tail [KYS]. Mar. 31.81: w/ 10.2-cm f/15 R (84×), three bright arcs were seen (the innermost was brighter and closer to the nucleus than on the preceding evening; the next one was nearly as bright, while the outermost was fainter, but still easily seen); the separation between arcs 2 and 3 were slightly less than between the two innermost arcs [SKI]. Mar. 31.83: w/ naked eye, curved dust tail 10° long (initially directed to p.a. 350°); ion tail fainter than on Mar. 12, but decidedly broader; central cond. of mag 0.5; w/ 9×63 B, very complex coma, which can roughly be divided into 3 regions — a region directed towards the ion tail, a considerably brighter region from which the dust tail emanates (which again is dominated by the dust streamer on the leading edge), and a diffuse-looking region immediately to the E of the trailing edge of the dust tail; w/ 20-cm T (80×), the false nucleus still showed the comma-shaped jet, starting in NW and creating the innermost of three envelopes [KAM01]. Mar. 31.84: "also slightly curving dust tail, longest 12° in p.a. 340°; strong cond. w/ clear yellow color; w/ 25.4-cm L (88×, 115×), new hood forming at end of small sunward jet; w/in 2' of nucleus, three more concentric hoods visible, brightest in sunward direction, the outer one being very diffuse; at moments of good seeing, several more very diffuse hoods suspected, but this may have been an illusion" [BOU]. Mar. 31.86: w/ naked eye, tails 14° in p.a. 16° (ion) and 16° in p.a. 358° (dust); w/ 10×50 B, tails 12° in p.a. 16° (ion) and 13° in p.a. 3° (dust); two streamers visible in the ion tail, forming its W and E boundaries; a diffuse streamer was seen in the dust tail; the comet was easily seen and appeared brighter than Mars in reversed 10×50 B (the estimated mag was -1.9, which apparently includes parts of the dust tail) [GRA04]. Mar. 31.86: w/ naked eye, both the dust and gas tails were visible for 14°; w/ 7×50 B, same tail lengths as w/ the naked eye; the width of the dust tail reached nearly 2°5; the gas tail was 2° wide at ~ 7° from the central cond.; in the dust tail, there was a bright streamer that originated from the nuclear region; the E edge of the dust tail was sharply defined, and much more diffuse on its other side; several streamers and structures were seen in the gas tail; the W edge of the gas tail was straight and more sharply defined than its E side [SKI].

1997 Apr. 1.05: ion and dust tails 15° and 10° long [CRE01]. Apr. 1.14: plasma tail faint, but also traced to 8° (extension to ~ 10° was suspected) in p.a. 9°; main dust tail spanned p.a. 338°-355° [ADA03]. Apr. 1.17: w/ 7×50 B, there is a distinctly-curved yellow tail stretching for over 14° in p.a. 34°; plasma tail much fainter; hints of 'veiled structure' in the main dust tail, w/ a bright narrow middle section curving outwards from the coma [SPR]. Apr. 1.79: dust tail 15° [KYS]. Apr. 1.80: dust tail 10° in p.a. 330° [HOR02]. Apr. 1.80 and 2.78: w/ naked eye, 12° curved dust tail in p.a. 345° and 350° [SAR02]. Apr. 1.81: ion tail 15° [KON06]. Apr. 1.82: dust tail 12° in p.a. 335° [ZNO]. Apr. 1.833: w/ naked eye, 15°7 tail in p.a. 17° [HAS02]. Apr. 1.84: also slightly curving dust tail, longest 15° in p.a. 340°; nearly-stellar cond., yellowish in color [BOU]. Apr. 1.84: w/ naked eye, curved dust tail 12° long (initially directed to p.a. 355°); ion tail fainter and broader than yesterday; central cond. of mag 0.7; w/ 9×63 B, very complex coma of dia. 15' and DC = S8/ (overall appearance as yesterday); highly structured ion tail w/ several streamers; w/ 20-cm T (80×), the innermost envelope showed a spiral-like appearance, one streamer emanating from the leading edge of the coma to the NE [KAM01]. Apr. 1.87: w/ naked eye, gas tail 14° in p.a. 14°; the outer portion of the gas tail was slightly easier to detect than on the previous evening; w/ reversed 7×50 B, total mag -1.3 (comparison w/ Mars); the comet was easily seen in 7×50 B when first detected w/ solar alt. -2°7 [SKI]. Apr. 1.88: w/ naked eye, tails each 14° long in p.a. 18°

Below: drawings of comet C/1995 O1 by Margareta Westlund (Uppsala, Sweden), as seen through 7×35 B. At left is the view on 1997 Apr. 1.09; at right is the view on Apr. 4.89.





Above: Two sketches of the coma of comet C/1995 O1 in 1997 April. At left, drawing by Daniel W. E. Green on Apr. 11.06 UT at the Harvard College Observatory's 9-inch $f/12$ Clark R (261 \times , and lower magnifications). At right, drawing by Margareta Westlund with a 20-cm $f/10$ T (125 \times) on Apr. 20.82, in moonlight.

◊ ◊ ◊

◊ Comet C/1995 O1 (Hale-Bopp) [text continued from page 93] \Rightarrow

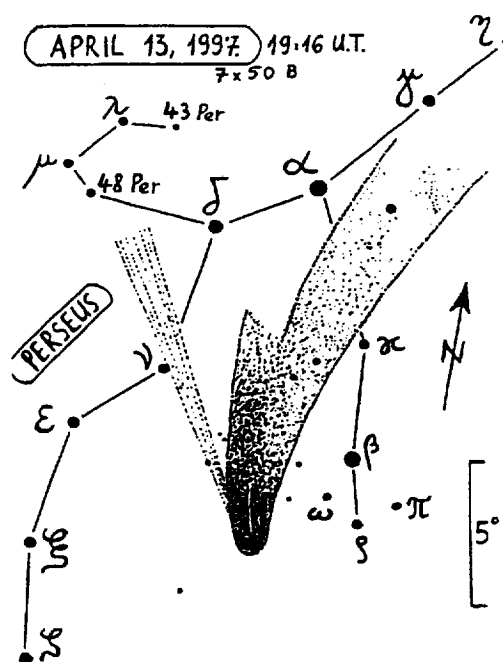
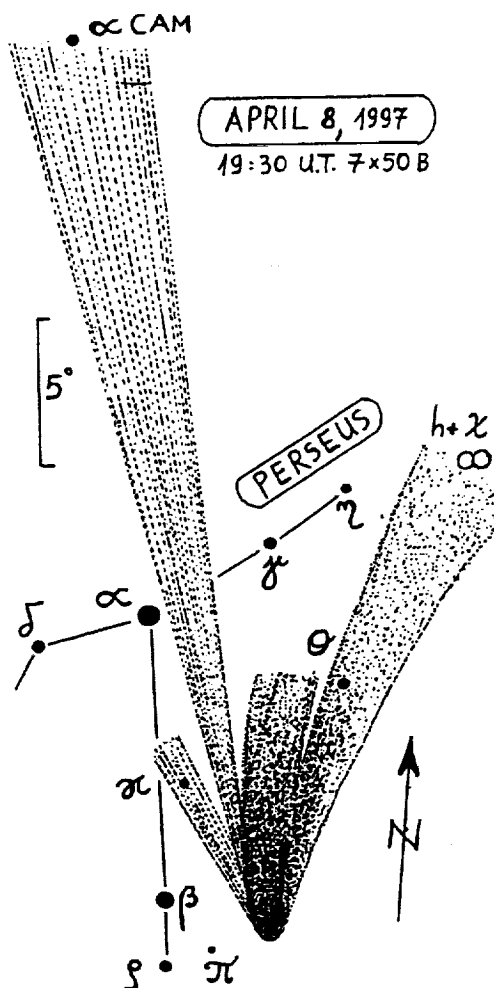
(ion) and 0° (dust); in 10 \times 50 B, tails 14° in p.a. 22° (ion) and 13° in p.a. 6° (dust); several streamers were seen both in the ion and dust tails [GRA04]. Apr. 2.0-2.1: from a dark-sky site, this comet looks to the naked eye very similar to Bond's drawings of comet C/1858 L1 (Donati), w/ the curved dust tail and the ion tail streaming off to form a the 'upper branch' of the 'V'-shaped comet; the ion tail has considerable width $\sim 5^\circ$ - 10° from the comet's head; at our latitude ($+44^\circ$), the comet was observed for some 4 hr (and for more than 3 hr in a dark sky after the end of twilight); again, one must get to a really dark sky (away from any artificial sky glow) to appreciate the true splendor of this comet [GRE, w/ Andy Chaikin, observing near West Rumney, NH, at the edge of the White Mountains National Forest]. Apr. 2.06: ion and dust tails 18° and 11° long [CRE01]. Apr. 2.08: in 20.3-cm $f/10$ T (123 \times), the false nucleus was small, but not quite stellar (its size was not more than 3"-4", as compared w/ the nearby double star γ And); there was a region of enhanced brightness SW of the nucleus (p.a. $\sim 160^\circ$ - 300°), in which three, possibly four, hoods were seen; the comet's head was much more evenly illuminated than in Feb. [GRA04]. Apr. 2.18: w/ 20-cm T (101 \times), the yellow-green-tinged coma shows a complex structure of 3 hoods; one hood comes from the comet's SW side and curves around some 100° + from the false-nucleus towards the solar vector; two other fainter hoods are very visible; the false nucleus and intense inner hood make the comet look like a giant comma or 'S'-shaped spiral nebula [SPR]. Apr. 2.78: w/ 15-cm $f/15$ R (65 \times), bright inner coma of dia. 12', outer coma of dia. 18'; nucleus offset w/ respect to geometric center of the outer coma; curved dust tail in p.a. 330° - 350° , gas tail has sharp wavy structure w/ in 7° of nucleus [CHE03]. Apr. 2.79: dust tail 14° in p.a. 340° [ZNO]. Apr. 2.80: dust tail 12° in p.a. 345° [HOR02]. Apr. 2.80: dust tail 13° in p.a. 350° [PLS]. Apr. 2.83: ion tail 5° [LIB]. Apr. 2.85: tab. tail is ion; also dust tail $\sim 6^\circ$ long [PAL02]. Apr. 3.78 and 4.78: w/ naked eye, 14° and 20° curved dust tail in p.a. 350° [SAR02]. Apr. 3.79: ion tail 9° [KON06]. Apr. 3.83: ion tail 4° [LIB].

Apr. 3.85: also slightly curving dust tail (longest 15° in p.a. 350°); strong, nearly-stellar cond., yellow in color [BOU]. Apr. 3.86: w/ naked eye, 9° tail in p.a. 22° [SHA02]. Apr. 4.18: w/ 7×50 B, the tail is a complex fabric of material (brighter up the middle section, but w/ a 'hook' or twist part way, giving the comet a 'tadpole' effect); the faint plasma tail extends for 8° whilst the dust tail can be traced well over 17° [SPR]. Apr. 4.83: w/ naked eye, $12^\circ 0'$ tail in p.a. 348° and $12^\circ 5'$ tail in p.a. 28° [HAS02]. Apr. 4.85: tab. tail is ion; also dust tail $\sim 9^\circ$ long [PAL02]. Apr. 4.86: to the naked eye, excellent conditions (the zodiacal light is strikingly conspicuous); dust fan at least 12° long, centered near p.a. 0° ; ion tail at least 8° long, near p.a. 35° ; in 9×34 B, two parabolic streamers flowing from the nucleus, symmetric to the ion-tail axis; broad dust fan curving clockwise, significantly sharper at the leading edge, the trailing edge being ill-defined; in $25.3\text{-cm } f/5.6$ L ($240\times$), non-stellar nucleus; first hood appears as a spiral arm, leaving the nucleus as a narrow fountain towards p.a. 270° , then strongly curving clockwise $\sim 21''$ from the nucleus, going through the sunward coma until p.a. 155° ; the second hood also originates from the same narrow westward fountain, then strongly curving clockwise some $36''$ from the nucleus; it was possible to trace the second hood through the sunward coma until p.a. 155° ; hint of a weak new hood being formed as a narrow $9''$ spiral arm touching the nucleus nearly S, but directed along ESE; at $58\times$, new hood is clearly seen, as well as four more hoods, the first two spanning p.a. 155° - 270° ; third hood spans p.a. 170° - 270° ; fourth hood as a short arc towards the SW — not concentric w/ the three inner hoods (i.e., more linear, not-so-strongly curving clockwise); parabolic coma w/ axis near p.a. 30° - 35° ; dust tail is seen w/ the trailing edge along NNW [PER01]. Apr. 4.87: dust tail 18° in p.a. 345° [ZNO].

Apr. 5.19: w/ 7×50 B, the faint plasma tail extends for 10° whilst the dust tail can be traced for 15° [SPR]. Apr. 5.79: w/ $5\text{-cm } R$ ($20\times$), $m_2 = 2.6$ [BAR06]. Apr. 6.79: tab. tail refers to type-I tail; type-II tail in p.a. 25° [FOG]. Apr. 6.84: w/ naked eye, curved dust tail 14° long (initially directed toward p.a. 5°); weak, broad ion tail; central cond. of mag 0.8; w/ 9×63 B, very complex coma of dia. $25'$ and $DC = S8$; highly structured ion tail, dominated by several streamers, the brightest one at the leading edge; w/ $20\text{-cm } T$ ($80\times$), false nucleus nearly at the apex of the paraboloid coma; three envelopes, more diffuse than six days ago; bright streamer easily visible as a conspicuous streak emanating from the brighter parts of the coma [KAM01]. Apr. 6.84: ion tail 5° [LIB]. Apr. 6.84: also slightly curving dust tail, longest 19° in p.a. 348° ; strong, nearly-stellar cond., yellowish in color [BOU]. (text continued on next page)

◇ ◇ ◇

Below: drawings of comet C/1995 O1 by Attila Kósa-Kiss via 7×50 B, showing how the ion tail shortened and faded rapidly in April. At left, 1997 Apr. 8.81; at right, Apr. 13.80 UT.



◊ Comet C/1995 O1 (Hale-Bopp) [text continued from page 96] ⇒

Apr. 6.87: w/ naked eye, 14°1 tail in p.a. 335° and 12°1 tail in p.a. 25°; w/ 10×50 B, coma dia. 20', DC = 8 [HAS02]. Apr. 7.79: dust tail [DVO]. Apr. 7.81: 15° dust tail in p.a. 350° [HOR02 and HYN]. Apr. 7.81: 6° ion tail [LIB]. Apr. 7.82: w/ naked eye, 10°8 tail in p.a. 26°; w/ 10×50 B, coma dia. 9'3, DC = 8 [HAS02]. Apr. 7.82: 21° dust tail in p.a. 345° [ZNO]. Apr. 7.82: 16° ion tail [KON06]. Apr. 7.84: w/ naked eye, curved dust tail 14° long (initially directed toward p.a. 5°); weak, broad ion tail, which could not be traced beyond the line α - γ Per, although the limiting mag at the comet's position was 5.3 and the zodiacal light well visible; central cor. of mag 0.6; w/ 9×63 B, 22' coma, DC = 8.8, highly-structured ion tail, streamers not as dominating as the night before; the part of the ion tail very near the coma looked like a DE (of the leading part) [KAM01]. Apr. 7.84: w/ naked eye, 6° tail in p.a. 28° [SHA02]. Apr. 7.85: also slightly curving dust tail, longest 20° in p.a. 349° [BOU]. Apr. 7.88: 16° dust tail in p.a. 350° [HOR02]. Apr. 8.06: ion and dust tails 8° and 12° long [CRE01]. Apr. 8.77: w/ naked eye, dust tail 13° long in p.a. 335°; w/ 5-cm R (20×), $m_2 = 2.3$ [BAR06]. Apr. 8.80: 6° ion tail [LIB]. Apr. 8.80: 13° dust tail in p.a. 355° [HOR02]. Apr. 8.83: 16° ion tail [KON06]. Apr. 8.85: 17° dust tail in p.a. 350° [ZNO]. Apr. 8.86: w/ naked eye, 13°6 tail in p.a. 349° and 11°1 tail in p.a. 30° [HAS02]. Apr. 8.90: tab. tail is ion; also dust tail ~ 12° long [PAL02]. Apr. 9.81: 7°5 dust tail in p.a. 0° [HYN]. Apr. 9.89: w/ naked eye, 5° tail in p.a. 32° [SHA02].

Apr. 10.85: w/ naked eye, 5° tail in p.a. 29° [SHA02]. Apr. 11.79: 16° ion tail in p.a. 50° [ZNO]. Apr. 11.82: 12° ion tail [KON06]. Apr. 11.85: w/ 9×63 B, ion tail at p.a. 40°; interfering moonlight [KAM01]. Apr. 11.85: also 5° ion tail near p.a. 40°; moonlight [PER01]. Apr. 11.88: w/ naked eye, 10°8 tail in p.a. 353° and 10°7 tail in p.a. 30° [HAS02]. Apr. 12.19: moonlight starting to 'wash out' tail; Algol (near minimum) 2°5 away [SPR]. Apr. 12.84: 10° ion tail [KON06]. Apr. 13.79: 12° ion tail in p.a. 50° [ZNO]. Apr. 13.80: 4° ion tail [LIB]. Apr. 13.84: w/ naked eye, curved dust tail traced to 10°; central cond. of mag 0.8; interfering moonlight [KAM01]. Apr. 14.85: moonlight; to the naked eye, dust tail could be as long as 12°, there being a sharp clockwise bend in the leading edge some 2°-3° from the head; in 9×34 B, hint of 'lobes' in the dust tail, as in recent two weeks; both the sharp leading edge and the diffuse trailing edge are slightly curved clockwise; in 25.3-cm f/5.6 L (240×), stellar nucleus w/ weak narrow jet towards W; newly-formed hood appears as a 'cumulonimbus anvil' fan spanning p.a. 130°-250°, the outer edge leaving the nucleus towards W, then strongly curving clockwise, reaching an average distance of 6" from the nucleus; the second hood leaves the nucleus towards the W, then strongly bends clockwise through the sunward coma, w/ the outer edge ~ 19" from the nucleus; third hood not clearly linked to the nucleus, but emerges at some distance Wwards, then strongly bending clockwise until S (the outer edge reaching ~ 31" from the nucleus); at 58×, both edges of the tail curve slightly clockwise; the new 'anvil-shaped' hood gives the impression of having a faint extension going clockwise tailwards of the nucleus; the hood's edge towards W is involved in diffuseness; second hood spans p.a. 135°-260°; third hood spans p.a. 155°-260°; a fourth, weaker hood spans p.a. 185°-250°; parabolic-shaped, weakly-pronounced dark void tailwards of the nucleus; the leading part of the coma is now clearly brighter than the trailing part [PER01].

Apr. 15.85: 9° ion tail [KON06]. Apr. 15.85: w/ naked eye, 6° tail in p.a. 45° [SHA02]. Apr. 17.83: naked-eye estimate made w/ different pairs of comparison stars than 10×50 B estimate [GLI]. Apr. 17.85 and 21.85: w/ naked eye, central cond. of mag 1.1 and 1.2; strong moonlight [KAM01]. Apr. 19.89-29.89: comparison stars α Aur, β Ori, α Tau [DES01]. Apr. 20.82: estimates employed Capella and Procyon as comparison stars [GLI]. Apr. 20.85: only comp. star used (α Lyr) had the same zenith distance as the comet [GLI]. Apr. 24.19: w/ 7×50 B, the comet shows a very broad and distinctly-curved dust tail some 8°+ in length [SPR]. Apr. 24.81: ion tail > 5° long, dust tail > 6° long [MIK]. Apr. 27.21: w/ 7×50 B, the plasma tail is much more evident than in recent days; the dust tail shows a distinct filamentary structure to it [SPR]. Apr. 28.87: comparison stars α Aur, α CMi, β Gem, and α Vir [PER01]. Apr. 29.78: w/ naked eye, 10° dust tail and 16° ion tail; $m_2 = 1.3$ [MIL02]. Apr. 30.78: 12° ion tail, 8° dust tail [MIL02].

◊ Comet C/1996 B2 (Hyakutake) ⇒ 1996 Apr. 5.46: w/ 20.0 f/9 C (45×), 5'8, DC = 8; ion tail 2°5 long in p.a. 60° [NAG04]. Apr. 12.45: another tail in p.a. 50° [NAG04]. Apr. 13.47: another tail in p.a. 70° (> 1° long); w/ 20.0-cm f/9 C (60×), 6'3 coma, DC = 7 [NAG04]. Apr. 22.44: w/ 10×70 B, DC = 7, tail 13°5 long in p.a. 40° [NAG04].

◊ Comet C/1996 N1 (Brewington) ⇒ 1996 Sept. 5.88 and 6.88: w/ 20.0-cm f/6 L (38×), $m_1 = 8.7$ and 9.5 (MM = S; Ref = PPM Star Catalogue, Rösner and Bastian 1991, unacceptable for visual magnitude work); coma dia. 6' and 4'; DC = 4 and 3 (respectively) [GIL01]. Oct. 2.88: w/ 20.0-cm f/6 L (38×), $m_1 \approx 10.2$ (see his data above for Sept. 5 and 6); coma dia. 6', DC = 2 [GIL01].

◊ Comet C/1996 Q1 (Tabur) ⇒ 1996 Oct. 16.81: another faint narrow tail, 1°1 long in p.a. 290° [NAG04]. Oct. 23.83: other faint tails in p.a. 303° (1°25 long), 5° (60'), and 350° (33') [NAG04].

◊ Comet C/1997 D1 (Mueller) ⇒ 1997 Mar. 4.94: starlike central cond. suspected [MEY]. Mar. 5.20: central cond. of dia. 2" and mag 15.0; tail, as tab., although somewhat faint and irregular in shape, nevertheless was readily apparent [ROQ]. Mar. 9.27: central cond. of dia. 5" and mag 15.4; inner coma region generally symmetrical [ROQ]. Mar. 9.84: photometry w/ 36-cm f/6.7 T + V filter + CCD [MIK]. Mar. 9.85: comet similar in appearance to nearby NGC 3824, but slightly smaller and rounder [BOU]. Mar. 13.15: central cond. of mag 14.6 and dia. 3"; coma was asymmetrical, as expected, in the direction of the tail; tail's structure and visibility appeared consistent on exposure-calibrated images made in V, R, and unfiltered [ROQ]. Mar. 18.16: central cond. of mag 15.7 and dia. ~ 4" [ROQ]. Mar. 20.20: central cond. of dia. 4" and mag 15.0 [ROQ]. Mar. 27.14: central cond. of dia. 2" and mag 13.7; tail showed two distinct components — a tapering inner "core" extending 40" at p.a. 108°, which was immersed in a fainter, diffuse component extending almost 100" at p.a. 104° [ROQ]. Mar. 30.13: central cond. of dia. ~ 2" and mag 14.6; tail showed no sub-structure w/in its main, diffuse body such as was evident three days previously [ROQ]. Apr. 13.15: central cond. of dia. 3" and mag 15.1; image processing showed no sub-structure w/in the coma or tail [ROQ].

TABULATED DATA

The headings for the tabulated data are as follows: "DATE (UT)" = Date and time to hundredths of a day in Universal Time; "N" = notes [* = correction to observation published in earlier issue of the *ICQ*; an exclamation mark (!) in this same location indicates that the observer has corrected his estimate in some manner for atmospheric extinction (prior to September 1992, this was the standard symbol for noting extinction correction, but following publication of the extinction paper — July 1992 *ICQ* — this symbol is only to be used to denote corrections made using procedures different from that outlined by Green 1992, *ICQ* 14, 55-59, and in Appendix E of the *ICQ Guide to Observing Comets* — and then only for situations where the observed comet is at altitude $> 10^\circ$); '&' = comet observed at altitude 20° or less with no atmospheric extinction correction applied; '\$' = comet observed at altitude 10° or lower, observations corrected by the observer using procedure of Green (*ibid.*); for a correction applied by the observer using Tables Ia, Ib, or Ic of Green (*ibid.*), the letters 'a', 'w', or 's', respectively, should be used].

"MM" = the method employed for estimating the total (visual) magnitude; see article on page 186 of the Oct. 1996 issue [B = VBM method, M = Morris method, S = VSS or In-Out method, I = in-focus, C = unfiltered CCD, c = same as 'C', but for 'nuclear' magnitudes, V = electronic observations — usually CCD — with Johnson V filter, etc.]. "MAG." = total (visual) magnitude estimate; a colon indicates that the observation is only approximate, due to bad weather conditions, etc.; a left bracket ([) indicates that the comet was not seen, with an estimated limiting magnitude given (if the comet IS seen, and it is simply estimated to be fainter than a certain magnitude, a "greater-than" sign (>) must be used, not a bracket). "RF" = reference for total magnitude estimates (see pages 98-100 of the October 1992 issue, and Appendix C of the *ICQ Guide to Observing Comets*, for all of the 1- and 2-letter codes). "AP." = aperture in centimeters of the instrument used for the observations, usually given to tenths. "T" = type of instrument used for the observation (R = refractor, L = Newtonian reflector, B = binoculars, C = Cassegrain reflector, A = camera, T = Schmidt-Cassegrain reflector, S = Schmidt-Newtonian reflector, E = naked eye, etc.). "F/" and "PWR" are the focal ratio and power or magnification, respectively, of the instrument used for the observation — given to nearest whole integer (round even); note that for CCD observations, in place of magnification is given the exposure time in seconds (see page 11 of the January 1997 issue).

"COMA" = estimated coma diameter in minutes of arc; an ampersand (&) indicates an approximate estimate; an exclamation mark (!) precedes a coma diameter when the comet was not seen (i.e., was too faint) and where a limiting magnitude estimate is provided based on an "assumed" coma diameter (a default size of 1' or 30" is recommended; cf. *ICQ* 9, 100); a plus mark (+) precedes a coma diameter when a diaphragm was used electronically, thereby specifying the diaphragm size (i.e., the coma is almost always larger than such a specified diaphragm size). "DC" = degree of condensation on a scale where 9 = stellar and 0 = diffuse (preceded by lower- and upper-case letters S and D to indicate the presence of stellar and disklike central condensations; cf. July 1995 issue, p. 90); a slash (/) indicates a value midway between the given number and the next-higher integer. "TAIL" = estimated tail length in degrees, to 0.01 degree if appropriate; again, an ampersand indicates a rough estimate. Lower-case letters between the tail length and the p.a. indicate that the tail was measured in arcmin ("m") or arcsec ("s"), in which cases the decimal point is shifted one column to the right. "PA" = estimated measured position angle of the tail to nearest whole integer in degrees (north = 0° , east = 90°). "OBS" = the observer who made the observation (given as a 3-letter, 2-digit code).

A complete list of the Keys to abbreviations used in the *ICQ* is available from the Editor for \$4.00 postpaid (available free of charge via e-mail); these Keys are also now available in the new *Guide to Observing Comets* and via the *ICQ's* World Wide Web site. Please note that data in archival form, and thus the data to be sent in machine-readable form, use a format that is different from that of the Tabulated data in the printed pages of the *ICQ*; see pages 59-61 of the July 1992 issue, p. 10 of the January 1995 issue, and p. 100 of the April 1996 issue for further information [note correction on page 140 of the October 1993 issue]. Further guidelines concerning reporting of data may be found on pages 59-60 of the April 1993 issue, and in the *ICQ Guide to Observing Comets*.

◇ ◇ ◇

Key to observers with observations published in this issue, with 2-digit numbers between Observer Code and Observer's Name indicating source [07 = Comet Section, British Astronomical Assn.; 16 = Japanese observers (c/o Akimasa Nakamura, Kuma, Japan); 23 = Czech group (c/o P. Pravec and V. Znojil); 32 = Hungarian group (c/o K. Sarneczky); 37 = Ukrainian Comet Section (c/o A. R. Baransky and K. I. Churyumov); 42 = Belarus observers, c/o V. S. Nevski, Vitebsk; 43 = Slovenian observers, c/o Herman Mikuz, Ljubljana; etc.]. Those with asterisks (*) preceding the 5-character code are new additions to the Observer Key:

ADA03	Brian Adams, IA, U.S.A.	BOR04 37	Sergiy A. Borysenko, Ukraine
AND03 17	Krasimir Andreev, Bulgaria	BOR05 34	Galin Borisov, Bulgaria
ANZ	Fabio Anzellini, Italy	BOU	Reinder J. Bouma, Netherlands
*APE 07	Cornel Apetroaei, Romania	BRL 12	Pal Brlas, Budapest, Hungary
BAK01 32	Gaspar Bakos, Budapest, Hungary	*BR006	Xavier Bros, Barcelona, Spain
BAN 18	Jaroslav Bandurowski, Poland	BRU 42	Ivan S. Brukhanov, Belarus
BAR	Sandro Baroni, Italy	BUS04 32	Sandor Busa, Hungary
BAR06 37	Alexandr R. Baransky, Ukraine	CAN04	P. Candy, Viterbo, Italy
BEA 07	Sally Beaumont, Cumbria, England	*CHA02 34	Neofit Chanev, Bulgaria
BIV	Nicolas Biver, France	CHE03 33	Kazimieras T. Cernis, Lithuania
BOJ01 34	Eva Bojurova, Bulgaria	CH001 18	Franciszek Chodorowski, Poland
*BON01 37	Anton Bondarenko, Ukraine	*CHR 18	Antoni Chrapek, Pikulice, Poland

CHU Klim Churyumov, Kiev, Ukraine
 *CHV 37 V. V. Chvak, Ukraine
 CNO 18 Ryszard Cnota, Poland
 CDD02 Tim P. Cooper, South Africa
 CRE01 Phillip J. Creed, OH, U.S.A.
 CSU 32 Matyas Csukas, Salonta, Romania
 DAB 24 Haakon Dahle, Norway
 DAM 36 Matteo Damiani, Italy
 DER 18 Oskar Deren, Poland
 DES01 Jose G. de Souza Aguiar, Brazil
 DIE02 Alfons Diepvens, Belgium
 DINO1 07 E. L. Dinham, Plymouth, England
 *DOB 32 Szabolcs Dobra, Hungary
 DOH 07 Paul B. Doherty, England
 *DRA02 18 Michal Drahos, Krakow, Poland
 DVO 23 Denisa Dvorakova, Czech Repub.
 ELT Maurizio Eltri, Italy
 ENT 07 L. Entwisle, England
 FAJ 18 Tomasz Fajfer, Torun, Poland
 *FIA 23 Karolina Fialova, Czech Republic
 FIL04 18 Marcin Filipek, Poland
 FIL05 37 Alexander V. Filatov, Ukraine
 *FIL06 34 Peter Filkov, Bulgaria
 FOG Sergio Foglia, Italy
 *FRE01 45 Jose Rodriguez Freitas, Uruguay
 FUK01 16 Hiromi Fukushima, Japan
 *FUK02 16 Hideo Fukushima, Japan
 *GEN 34 Maria Genkova, Bulgaria
 *GEN01 34 Ivajlo Genov, Bulgaria
 GER01 37 O. N. Geraschenko, Ukraine
 GIL01 11 G. Gilein, Netherlands
 GLI Gunnar Glitscher, Germany
 GOL 19 Vladimir A. Golubev, Belarus
 *GOL02 07 Steven Goldsmith, Kent, U.K.
 *GON05 Juan Jose Gonzalez, Spain
 GRA04 24 Bjoern Haakon Granslo, Norway
 GRA07 34 Ivan Gradinarov, Bulgaria
 GRE Daniel W. E. Green, U.S.A.
 GRO04 18 Jaroslav Grolik, Poland
 GUB Herbert Gubo, Germany
 HAL04 23 Karel Halir, Czech Republic
 HAN04 34 Hristo Handjijski, Bulgaria
 HAR09 37 Sergiy V. Harchuk, Ukraine
 HAS02 Werner Hasubick, Germany
 HAS08 16 Yuji Hashimoto, Hiroshima, Japan
 HAV Roberto Haver, Italy
 HEE 24 Lars Trygve Heen, Norway
 HEN 07 Michael J. Hendrie, England
 HOM 37 Vasyl M. Homyak, Ukraine
 HOR 12 Tibor Horvath, Hungary
 IOR02 23 Kamil Hornoch, Czechoslovakia
 IYN 23 Petr Hynek, Czech Republic
 ILI 34 Georgi Iliev, Bulgaria
 *ISH03 37 Andriy S. Ishchenko, Ukraine
 *IVA03 37 Vladimir Ivanov, Russia
 *JAR01 18 Marcin Jarski, Poland
 *JOR01 34 Ivajlo Jordanov, Bulgaria
 *JAM01 Andreas Kammerer, Germany
 AT01 16 Taichi Kato, Kyoto, Japan
 ES01 Sandor Keszthelyi, Hungary
 ID01 18 Krzysztof Kida, Elblag, Poland
 IN 16 Kazuo Kinoshita, Japan
 IS02 32 Laszlo Kiss, Szeged, Hungary
 DB01 16 Juro Kobayashi, Kumamoto, Japan
 DJ01 34 Michail Kojchev, Bulgaria
 JNO6 23 Jiri Konecny, Czech Republic
 JS Attila Kosa-Kiss, Romania
 JZ 37 Vladimir A. Kozlov, Ukraine

KRY02 Washington Kryzanowski, Uruguay
 KWI 18 Maciej Kwinta, Krakow, Poland
 KYS 23 J. Kysely, Czech Republic
 LAN02 32 Zsolt Lantos, Budapest, Hungary
 LEH01 37 Kostayntyn S. Lehman, Ukraine
 *LIB 23 Jan Libich, Czech Republic
 LOU 35 Romualdo Lourencon, Brazil
 LUK04 37 Igor Lukyanyk, Ukraine
 MAI 37 Alexander S. Maidic, Ukraine
 MAN01 37 Vladimir Man'ko, Ukraine
 MAR02 13 Jose Carvajal Martinez, Spain
 MAR12 18 Leszek Marcinek, Poland
 MAR19 34 Alexander Marinov, Bulgaria
 MAR20 38 Fernando Martin, Madrid, Spain
 MAT06 18 Leslaw Materniak, Poland
 MCK 07 Richard McKim, England
 MEN03 07 Haldun I. Menali, Turkey
 MEY 28 Maik Meyer, Germany
 MIK Herman Mikuz, Slovenia
 MILO2 Giannantonio Milani, Italy
 MIY01 16 Osamu Miyazaki, Japan
 MOE Michael Moeller, Germany
 MOR04 37 Vladimir G. Mormyl, Ukraine
 MOS03 37 Yuriy A. Moskalenko, Ukraine
 NAG02 16 Takashi Nagata, Akashi, Japan
 NAG04 16 Kazuro Nagashima, Japan
 NAG08 16 Yoshimi Nagai, Matsumoto, Japan
 NAK01 16 Akimasa Nakamura, Kuma, Japan
 *NAN02 Kouji Naniwada, Tokyo, Japan
 NAU 37 Alexandr V. Naumov, Ukraine
 NEV 42 Vitali S. Nevski, Belarus
 OHM 16 Fumihiko Ohmori, Japan
 OKA05 16 Takuma Oka, Tokyo, Japan
 OKS 07 Gabriel Oksa, Slovak Republic
 OLE 18 Arkadiusz Olech, Poland
 OME Stephen O'Meara, MA, U.S.A.
 PAL02 43 Rok Palcic, Kamnik, Slovenia
 PAR03 18 Mieczyslaw L. Paradowski, Poland
 *PEN 34 Svetlana Peneva, Bulgaria
 PER01 Alfredo J. S. Pereira, Portugal
 PI001 18 Marek Piotrowski, Poland
 PLE01 18 Janusz Pleszka, Poland
 PLS 23 Martin Plsek, Czech Republic
 POD 23 M. Podzorny, Czech Republic
 POP01 34 Kostadin Popanastasov, Bulgaria
 POR05 40 Joao Porto, Azores Is., Portugal
 RAD01 17 Veselka Radeva, Bulgaria
 RED 37 Sergei Red'ko, Kiev, Ukraine
 RES 18 Maciej Reszelski, Poland
 RDO01 13 Diego Rodriguez, Spain
 ROGO2 John H. Rogers, England
 ROM 42 Aleksandr M. Romancev, Belarus
 ROQ Paul Roques, AZ, U.S.A.
 ROT01 23 Michal Rottenborn, Czech Repub.
 *SAL01 42 Mihail Saltanov, Minsk, Belarus
 SAN04 38 Juan M. San Juan, Madrid, Spain
 SAN07 32 Gabor Santa, Hungary
 SAR02 32 Krisztian Sarneczky, Hungary
 *SCH14 34 Vladislav Schiderov, Bulgaria
 SCI Tomasz Sciezor, Poland
 *SCU 07 Virgil V. Scurtu, Romania
 SEA 14 David A. J. Seargent, Australia
 SEA01 14 John Seach, Australia
 SER 42 Ivan M. Sergey, Belarus
 SEA02 07 Jonathan D. Shanklin, England
 SHI 16 Hiroyuki Shioi, Yachiyo, Japan
 SIW 18 Ryszard Siwiec, Poland
 SIW01 18 Michal Siwak, Tuchow, Poland

SKI	24	Oddleiv Skilbrei, Norway	TSUO2	16	Mitsunori Tsumura, Japan
*SLI01	37	Bogdan V. Slipachok, Ukraine	TUB	12	Vince Tuboly, Hungary
SMI08	15	T. Smith, Keetmanshoop, Namibia	*VAL01	34	Taschko Valchev, Bulgaria
SOC	18	Krzysztof Socha, Poland	VANO6		Gabriele Vanin, Italy
SPE01	18	Jerzy Speil, Poland	*VAS03	34	Valcho Vasilev, Bulgaria
SPR		Christopher E. Spratt, Canada	VELO2	17	Valentin Velkov, Bulgaria
*SRA	32	Marta Sragner, Pecs, Hungary	VELO3	37	Peter Velestschuk, Ukraine
STO		Enrico Stomeo, Italy	VETO1	15	Marie Vetrovcova, Czech Republic
SWI	18	Mariusz Swietnicki, Poland	VITO1	40	Catarina Vitorino, Portugal
SZA		Sandor Szabo, Sopron, Hungary	*WAL02	07	Richard Walters, Switzerland
*SZA05	18	Konrad Szaruga, Telatyn, Poland	WAS	16	Shinsyo (Shinsho) Washi, Japan
SZE02	32	Laszlo Szentasko, Hungary	WLO	18	Robert Wlodarczyk, Poland
*TAK06	16	Shin Takeda, Habikino, Japan	YOS	16	Shigeru Yoshida, Japan
TAN02		Tony Tanti, Malta	YOS02	16	Katsumi Yoshimoto, Japan
TAY	07	Melvyn D. Taylor, England	YOS04	16	Seiichi Yoshida, Ibaraki, Japan
TH003	24	Steinar Thorvaldsen, Norway	ZAN		Mauro Vittorio Zanotta, Italy
TOD	16	Hiroyuki Toda, Okayama, Japan	*ZEK		Hans Zekl, Einhausen, Germany
*TOL	07	Alin Tolea, Romania	*ZIF	23	Michal Zifcak, Czech Republic
*TOY	16	Takehiro Toyoshima, Japan	ZNO	23	Vladimir Znojil, Czech Republic
TRI		Josep M. Trigo Rodriguez, Spain			

◇ ◇ ◇

Comet C/1992 F1 (Tanaka-Machholz)

DATE (UT)	N	MM	MAG.	RF	AP.	T	F/	PWR	COMA	DC	TAIL	PA	OBS.
1992 05 03.03		S	8.5	SC	6.0	R	10	30	3		0.04		MAN01
1992 05 10.03		S	7.3	SC	6.0	R	10	30	3				MAN01
1992 05 23.88		S	8.6	SC	6.0	R	10	30	3.5				MAN01

Comet C/1994 J2 (Takamizawa)

DATE (UT)	N	MM	MAG.	RF	AP.	T	F/	PWR	COMA	DC	TAIL	PA	OBS.
1996 12 03.64		C	17.9	GA	60.0	Y	6	a240	0.35				NAK01
1997 01 11.58		C	17.4	GA	60.0	Y	6	a480	0.75				NAK01

Comet C/1995 01 (Hale-Bopp)

DATE (UT)	N	MM	MAG.	RF	AP.	T	F/	PWR	COMA	DC	TAIL	PA	OBS.
1995 07 28.94		S	10.3	NP	44.5	L	5	100	5	5			MAR02
1995 07 30.96		S	10.4	NP	44.5	L	5	100	4	4			MAR02
1995 07 30.96		S	10.5	NP	44.5	L	5	100	4	4			ROD01
1996 04 12.74		B	8.6	S	20.0	C	9	90	1.7	3			NAG04
1996 04 21.77		B	8.5	S	20.0	C	9	60	2.5	3			NAG04
1996 04 27.76		B	8.3	S	20.0	C	9	60	2.1	4			NAG04
1996 06 16.76		B	7.1	S	3.5	B		7					NAG04
1996 06 17.90		S	6.6	S	20	L	8	83		6			COO02
1996 06 20.41		S	7.3	AA	21.0	L	6	48	3	3			KRY02
1996 06 21.09		S	7.0	AA	21.0	L	6	48	4	4			KRY02
1996 06 24.05		S	7.0	AA	21.0	L	6	48	4	2			KRY02
1996 07 05.80		S	6.5	S	20	L	8	83		5			COO02
1996 07 14.90		B	6.0	S	15	L	9	50	15	5			SMI08
1996 07 15.83		S	6.3	S	20	L	8	83		5			COO02
1996 07 19.96		S	6.3	S	10	B	4	25		9			HAL04
1996 07 19.97		S	6.7	TI	10	B	4	25	10				VETO1
1996 07 20.01		B	6.0	S	15	L	9	50	16	5			SMI08
1996 07 20.89		S	6.7	TI	10	B	4	25	10	5			VETO1
1996 07 20.91		S	6.3	S	10	B	4	25	6	7	0.13	40	HAL04
1996 07 21.87		S	6.3	S	10	B	4	25	6	6	0.13	10	HAL04
1996 07 22.88		S	6.2	S	10	B	4	25	6	6	0.13	10	HAL04
1996 07 22.89		S	6.1	TI	7.0	B	4	10	10	5/			VETO1
1996 08 01.86		S	6.5	S	10	B	4	25	6	7			HAL04
1996 08 05.85		S	6.0	S	10	B	4	25	10	7	0.25	10	HAL04
1996 08 06.70		S	5.6	S	20	L	8	83	5.0	6			COO02
1996 08 08.86		S	6.8	S	10	B	4	25	12	6			HAL04
1996 08 08.87		M	5.6	S	15	L	9	80	18	6	1.0	130	SMI08

101

Comet C/1995 01 (Hale-Bopp) [cont.]

DATE (UT)	N	MM	MAG.	RF	AP.	T	F/	PWR	COMA	DC	TAIL	PA	OBS.
1996 08 10.05		S	6.2	AA	3.0	B		8					FRE01
1996 08 10.85		S	5.5	TI	10	B	4	25	15	7			VET01
1996 08 13.81		S	5.4	S	20	L	8	83		5			C0002
1996 08 13.87		B	5.5	S	15	L	9	80	18	6	1.2	130	SMI08
1996 08 15.86		S	6.8	S	10	B	4	25	12	6			HAL04
1996 08 17.83		S	6.5	S	10	B	4	25	15				HAL04
1996 08 18.87		S	6.3	S	10	B	4	25	15				HAL04
1996 08 19.85		S	6.2	S	10	B	4	25	19				HAL04
1996 08 20.58					20.0	C	9	45	5.9	8	45	m 115	NAG04
1996 08 20.58		B	5.9	AA	7.0	B		10					NAG04
1996 08 20.88		S	6.2	S	10	B	4	25	20				HAL04
1996 08 21.08		S	6.5	AA	21.0	L	6	48	4	4			KRY02
1996 08 24.08		S	6.2	AA	3.0	B		8					FRE01
1996 08 29.81		S	6.6	TI	10	B	4	25	5.0	5			ROT01
1996 08 30.81		S	6.4	TI	10	B	4	25	5.0				ROT01
1996 08 31.82		S	5.0	S	5.0	B		10		6			C0002
1996 09 01.78		S	5.7	AA	5.0	B		12		5			TAN02
1996 09 03.80		S	5.3	S	15	L	9	80	11	7	2.0	125	SMI08
1996 09 04.78		M	6.1	AA	7.0	B		20	8	6			TAN02
1996 09 04.80		S	5.9	AA	5.0	B		12	11	5/			TAN02
1996 09 05.80		S	5.2	S	5.0	B		10		6			C0002
1996 09 06.05		S	6.4	AA	3.0	B		8					FRE01
1996 09 06.78		S	5.7	AA	5.0	B		12	13	5			TAN02
1996 09 06.96		S	6.3	AA	3.0	B		8					FRE01
1996 09 07.09		S	6.0	AA	21.0	L	6	48		5			KRY02
1996 09 07.79		M	5.9	AA	5.0	B		12	15	5/			TAN02
1996 09 08.83		S	5.1	AA	0.0	E		1	12				HAV
1996 09 09.09		S	5.8	AA	21.0	L	6	48		7			KRY02
1996 09 13.80		S	5.3	S	15	L	9	80	10	7	2.0	130	SMI08
1996 09 14.77		M	6.0	AA	5.0	B		12		5/			TAN02
1996 09 14.77		S	5.5	S	5.0	B		10		4			C0002
1996 09 14.83		S	5.1	AA	0.0	E		1					HAV
1996 09 16.83		S	5.7	SC	15	R	13	40	2.5	7			HEN
1996 09 17.80		S	5.6	SC	15	R	13	40	2.5	7			HEN
1996 09 17.87		S	5.6	S	5.0	B		10	12				ENT
1996 09 19.80		S	5.3	TI	10	B	4	25	12	4			VET01
1996 09 19.81		S	6.1	TI	10	B	4	25	7.0	5			ROT01
1996 09 29.75		S	5.6	S	5.0	B		10		4			C0002
1996 09 30.77		M	5.6	AA	5.0	B		12		6/			TAN02
1996 09 30.77		S	5.6	S	10	B	4	25	15	4	0.40	70	HAL04
1996 09 30.79		S	5.3	TI	10	B	4	25	10		0.25		VET01
1996 09 30.80		S	5.7	TI	10	B	4	25	7.0				ROT01
1996 10 02.80		S	5.0:	SC	15	R	13	80	2	6			HEN
1996 10 03.77		S	5.2	TI	10	B	4	25	10	5	0.33		VET01
1996 10 03.77		S	5.7	TI	10	B	4	25	9.0				ROT01
1996 10 05.76		M	5.7	AA	5.0	B		12		5			TAN02
1996 10 05.95		S	6.0	AA	3.0	B		8					FRE01
1996 10 06.77		M	5.6	AA	5.0	B		12		5/			TAN02
1996 10 06.97		S	5.9	AA	3.0	B		8					FRE01
1996 10 07.75		S	5.2	AA	11	L	7	32		4			IVA03
1996 10 08.67		S	5.2	AA	11	L	7	32		4			IVA03
1996 10 08.77		M	5.5	AA	5.0	B		12	22	5/			TAN02
1996 10 09.66		S	5.1	AA	11.0	B		20		5			IVA03
1996 10 10.67		S	5.2	AA	11	L	7	32		5			IVA03
1996 10 10.69		S	5.0	AA	3.0	R	5	6	8	5			IVA03
1996 10 11.66		S	5.1	AA	11	L	7	32		5			IVA03
1996 10 11.69		S	5.1	AA	3.0	R	5	6	8	5/			IVA03
1996 10 11.69		S	5.1	AA	3.0	R	5	6	8	5/			IVA03
1996 10 11.74		S	5.7	TI	10	B	4	25	9.0	5			ROT01
1996 10 11.75		S	5.2	TI	10	B	4	25	12	6	0.37		VET01
1996 10 12.69		S	5.1	AA	11	L	7	32		5/			IVA03
1996 10 13.66		S	5.0	AA	11	L	7	32		6			IVA03
1996 10 14.74		S	5.7	TI	10	B	4	25	12	5			ROT01
1996 10 14.80		S	5.2	TI	10	B	4	25	12	5/	0.45		VET01
1996 10 15.75		S	4.9	S	5.0	B		10		5			C0002

Comet C/1995 01 (Hale-Bopp) [cont.]

DATE (UT)	N	MM	MAG.	RF	AP.	T	F/	PWR	COMA	DC	TAIL	PA	OBS.
1996 10 15.75		S	5.3:	SC	15	R	13	40	2	6	0.50	50	HEN
1996 10 15.80		S	4.7:	SC	5.0	B		10	20	6			MCK
1996 10 15.80		S	5.8	S	5.0	B		10					ENT
1996 10 16.45		B	6.2	AA	7.0	B		10					NAG04
1996 10 16.75		M	5.4	AA	5.0	B		12	17	5/			TAN02
1996 10 17.66		S	4.9	AA	11	L	7	32		6			IVA03
1996 10 19.74		S	5.4	TI	10	B	4	25	10	5			ROT01
1996 10 21.38		S	4.7	AA	5.0	B		10	9	2			SEA01
1996 10 23.76		S	6.9	S	10	B	4	25	7	5	0.40	85	HAL04
1996 10 25.40		S	5.2	AA	5.0	B		10	7	4	10 m		SEA01
1996 10 26.39		S	5.1	AA	5.0	B		10	5	3			SEA01
1996 10 27.71		S	4.8	S	5.0	B		10		5			C0002
1996 11 01.75		S	4.7	AA	0.0	E		1	12				HAV
1996 11 02.72		S	4.6	S	5.0	B		10		4			C0002
1996 11 04.41		S	5.8	AA	7.0	B		10					NAG04
1996 11 07.73		M	5.0	AA	5.0	B		12	19	6			TAN02
1996 11 09.41		S	4.7	AA	5.0	B		10	6	S6	1.4	80	SEA01
1996 11 11.63		S	4.6	AA	3.0	R	5	6	8	6			IVA03
1996 11 11.63		S	4.6	AA	11	L	7	32		6			IVA03
1996 11 13.76		S	5.0:	SC	15	R	13	100	2	6			HEN
1996 11 14.63		S	4.5	AA	11	L	7	32		6			IVA03
1996 11 14.64		S	4.5	AA	3.0	R	5	6	8	6			IVA03
1996 11 15.63		S	4.5	AA	11	L	7	32		4			IVA03
1996 11 21.69		S	4.9	TI	10	B	4	25	20	7	0.42	280	ROT01
1996 11 22.63		S	4.4	AA	3.0	R	5	6	6	5	0.5		IVA03
1996 11 22.63		S	4.4	AA	11	L	7	32		4			IVA03
1996 11 22.69	a	M	4.4	S	5.0	B		10	15	6/	1	70	HOR02
1996 11 22.70	a	M	3.9	S	0.0	E		1	20	4			HOR02
1996 11 24.72	!	S	4.5	AA	5.0	B		10	7.5	6			HAV
1996 11 30.64		S	4.5	AA	11	L	7	32	7	6	0.47		IVA03
1996 11 30.72		B	4.6	AA	0.0	E		1					VAN06
1996 11 30.72	—	M	4.9	AA	5.0	B		10	8	5	0.3	80	VAN06
1996 12 01.63		S	4.4	AA	3.0	R	5	6	11	6	0.5		IVA03
1996 12 01.63		S	4.5	AA	11	L	7	32	7	6	0.47		IVA03
1996 12 01.70		S	4.5	Y	10.0	C	10	40	10	5	0.5	75	HOR
1996 12 01.72		M	4.8	AA	5.0	B		10	8	5	0.5	67	VAN06
1996 12 01.72	!	S	4.1	AA	5.0	B		10	9	6	0.4	60	HAV
1996 12 01.73		S	4.0	Y	7.2	R	7	20	15	4	0.5	24	TUB
1996 12 02.72		B	4.6	AA	0.0	E		1					VAN06
1996 12 02.72		M	4.8	AA	5.0	B		10	6	6	0.4	60	VAN06
1996 12 03.37		B	5.2	AA	7.0	B		10					NAG04
1996 12 03.40					20.0	C	9	45	5.3	7	1.8	42	NAG04
1996 12 04.63		S	4.4	AA	3.0	R	5	6	12	6	0.5		IVA03
1996 12 04.69		S	4.3	S	10	B	4	25	5	6	0.67	55	HAL04
1996 12 04.70		S	4.7	TI	10	B	4	25	15	7	0.42	280	ROT01
1996 12 04.71		S	4.5	Y	10.0	C	10	40	10	5	0.5	70	HOR
1996 12 04.73		M	4.7	AA	5.0	B		10	6	7	0.5	65	VAN06
1996 12 04.75		S	5.5:	AA	6.0	B		13	2.5	6	0.50	40	HEN
1996 12 04.76		M	4.4	AA	5.0	B		12	21	6	2.4	58	TAN02
1996 12 05.63		S	4.2	AA	3.0	R	5	6	12	6	0.5		IVA03
1996 12 05.72		S	5.0:	AA	15	R	13	100		7			HEN
1996 12 05.73		S	4.0	AA	5.0	B		8	20	6	0.67	30	BEA
1996 12 07.64		S	4.2	AA	3.0	R	5	6	12	6	0.5		IVA03
1996 12 07.72	!	S	4.2	AA	8.0	B		20	11	7	1.5	50	HAV
1996 12 08.37		B	4.5:	AA	7.0	B		10			>1		NAG04
1996 12 12.62		S	4.1	AA	3.0	R	5	6	12	6	0.6		IVA03
1996 12 13.73		S	4.7	AA	6.0	B		13	3	6	>0.5	50	HEN
1996 12 14.37		B	4.2	AA	7.0	B		10					NAG04
1996 12 14.62		S	4.1	AA	3.0	R	5	6	14	6	0.9		IVA03
1996 12 16.66		B	4.2	AA	5.0	R	5	7	8	6			KOZ
1996 12 16.69		S	4.7	AA	3.0	B		8	12	S5	5	58	CSU
1996 12 20.60		S	3.9	AA	3.0	R	5	6	14	6	0.9		IVA03
1996 12 26.67		S	3.7	SC	8.0	B		12	14	S5/	0.8	13	ISH03
1996 12 27.66		B	4.6:	AA	5.0	B		7		5			HOM
1996 12 28.66		S	3.6	SC	8.0	B		12	14	S5/	0.8	10	ISH03

Comet C/1995 01 (Hale-Bopp) [cont.]

DATE (UT)	N	MM	MAG.	RF	AP.	T	F/	PWR	COMA	DC	TAIL	PA	OBS.
1996 12 28.67		B	4.7:	AA	5.0	B		7	6				HOM
1996 12 28.69		a O	4.4:	Y	5.0	B		7	10	4			KYS
1996 12 28.70		a S	3.6	AA	5.0	B		10	11	6	0.8		MEY
1996 12 30.68		a O	4.0:	Y	5.0	B		7	10				KYS
1997 01 06.69		a M	3.2	S	8.0	B		10	11	5	1.0		HOR02
1997 01 07.14		B	3.5	HD	5.0	B		7	8	6	0.4		MOR04
1997 01 07.26		S	3.7	AA	5.0	B		8	40	6	1.20	30	BEA
1997 01 08.14		B	3.5	HD	5.0	B		7	8	6	0.4		MOR04
1997 01 08.21		M	3.5	Y	5.0	B		10	15	s7	0.5	0	SAN07
1997 01 09.88		S	3.5:	AA	7.0	B		10	5	6			TAK06
1997 01 10.87		S	3.5:	AA	17.0	L	5	45	5	6			TAK06
1997 01 12.14		B	3.4	HD	5.0	B		7	10	7	0.4	10	MOR04
1997 01 12.21					5.0	B		10	6	7	0.5	65	VAN06
1997 01 12.21		M	3.0	AA	3.6	B		4					VAN06
1997 01 12.88		S	3.3	AA	17.0	L	5	36	12	7	25	m 30	TAK06
1997 01 13.14		B	3.4	HD	5.0	B		7	10	7	0.5	10	MOR04
1997 01 13.21		B	2.7	AA	0.0	E		1					ELT
1997 01 14.21					8.0	B		11	7	4	1.5	325	STO
1997 01 14.21		B	2.7	AA	0.0	E		1					STO
1997 01 14.21	w	B	2.7	AA	0.0	E		1					VAN06
1997 01 14.22					8.0	B		20	5	8	0.3	360	VAN06
1997 01 14.23		S	2.7	S	10	B	4	25	6	7	0.67	40	HAL04
1997 01 14.25		a S	2.9	SC	5.0	B		7	11	7	0.8	350	OKS
1997 01 14.28		S	3.1	AA	5.0	B		8	40	6	1	30	BEA
1997 01 16.20		a M	2.8	AA	5.0	B		12		5/	2.0	332	TAN02
1997 01 16.21		a M	2.9	S	5.0	B		7	25	5	2.0		POD
1997 01 16.23		S	2.3	S	10	B	4	25	10	7	0.43	20	HAL04
1997 01 16.28		S	3.5	AA	0.0	E		1	40	7			DIE02
1997 01 16.87		S	3.1	AA	17.0	L	5	36	7	6	15	m 30	TAK06
1997 01 17.14		B	3.3	HD	5.0	B		7	10	7	0.5	350	MOR04
1997 01 17.20		a M	2.8	AA	5.0	B		12	20	5/	2.0	336	TAN02
1997 01 17.21	w	B	2.5	AA	0.0	E		1					VAN06
1997 01 17.22					8.0	B		20	5	8	0.4	345	VAN06
1997 01 18.20		a B	2.8	AA	0.6	E		1					MEY
1997 01 18.20		a M	2.9	AA	5.0	B		10	11	D5/	1.6		MEY
1997 01 18.84		I	3.0	S	0.0	E		1					TOY
1997 01 19.20		a M	3.0	AA	5.0	B		12		5/	1.5	343	TAN02
1997 01 19.28		S	3.1	AA	5.0	B		8	40	6	1	350	BEA
1997 01 19.88		S	3.3	AA	5.0	B		7	10				TOD
1997 01 20.20		a M	2.8	AA	5.0	B		12	17	6			TAN02
1997 01 20.86		B	3.0	HS	3.5	B		7		6			OHM
1997 01 20.86		S	3.1	AA	17.0	L	5	36	8	6	20	m 10	TAK06
1997 01 21.20		a M	2.8	AA	5.0	B		12	15	6			TAN02
1997 01 21.25		S	2.7	YF	3.0	B		8	18	7	2.5	345	ENT
1997 01 21.25		S	3.0	AA	5.0	B		8	40	7	1	350	BEA
1997 01 22.22		a S	2.6	SC	5.0	B		7	10	7/	1.0	340	OKS
1997 01 22.22		a M	2.5	S	0.0	E		1	30	7	0.5	325	PLS
1997 01 22.26	!	M	2.8	S	5.0	B		12	6	S7/	1		GON05
1997 01 22.27		S	3.0:	SC	3.0	B		8	15	7	1.08	10	DIN01
1997 01 22.84		I	3.3	S	7.0	B		10					TOY
1997 01 23.15	!	B	3.4	SC	5.0	B	6	7	12	4	0.4	2	FIL05
1997 01 23.15	!	S	3.4	SC	5.0	B	6	7	12	4	0.4	2	FIL05
1997 01 23.16		B	2.9	AA	5.0	B		7	9	3	0.3		HOM
1997 01 23.16	!	B	3.5	SC	7.0	R	6	60	15	4	0.5	357	FIL05
1997 01 23.19		B	3.7	AA	5.0	B		7	13	S7	1.5	330	VEL03
1997 01 23.19		G	3.5	AA	0.0	E		1		4			VEL03
1997 01 24.25		S	2.6	SC	6.3	B		9	8	8	0.42	350	DIN01
1997 01 24.84		S	3.3	S	3.5	B		7					TOY
1997 01 24.87		B	3.0	HS	3.5	B		7		7			OHM
1997 01 25.16		B	2.8	AA	2.0	B		2	12	8			KOZ
1997 01 25.16		B	2.9	AA	5.0	R	5	7	10	7			KOZ
1997 01 25.17		B	3.0	AA	10.0	B	4	12	9	7	1.2	336	KOZ
1997 01 25.19		B	3.3	AA	5.0	B		7	13	D7	1.5	321	VEL03
1997 01 25.19		G	3.3	AA	0.0	E		1					VEL03
1997 01 25.19		S	2.7	AA	5.0	B		10		S8	1		SCU

Comet C/1995 01 (Hale-Bopp) [cont.]

DATE (UT)	N	MM	MAG.	RF	AP.	T	F/	PWR	COMA	DC	TAIL	PA	OBS.	
1997 01 25.30		B	3.2	SC	0.7	E		1	15	5	0.5		ROG02	
1997 01 26.14		B	3.2	HD	5.0	B		7	10	7	0.5	335	MOR04	
1997 01 26.17		S	2.8	SC	8.0	B		12	15	S6	0.6	340	ISH03	
1997 01 26.18		M	2.5	Y	5.0	B		10	10	S8	2	310	SAN07	
1997 01 26.18		S	2.9	SC	0.0	E		1	10	S6	0.6	340	ISH03	
1997 01 26.19		B	3.3	AA	5.0	B		7	13	S7	1.0	331	VEL03	
1997 01 26.19		G	3.3	AA	0.0	E		1					VEL03	
1997 01 26.19		M	2.5	Y	6.0	B		20	25	s4	2		LAN02	
1997 01 26.19		S	2.5	Y	0.0	E		1	25	s4	2		LAN02	
1997 01 26.19		S	3.0	AA	5.0	B		7	14	S9	8	320	KOS	
1997 01 26.19	a	M	3.1	Y	5.0	B		7	12	7	>3	335	KYS	
1997 01 26.21	a	M	2.4	S	0.0	E		1	25	7/	3.5	330	PLS	
1997 01 26.21	a	M	2.4	S	3	R		2	25	7/			HOR02	
1997 01 26.21	a	O	2.6	SP	0.0	E		1	25	5/	1.8		ZNO	
1997 01 26.22	a	M	2.3	TI	5.0	B		7	20	6	1.0		DVO	
1997 01 26.23	a	M	2.6	Y	10	B		25	15	5/	0.7		HYN	
1997 01 26.25		S	3.0:	AA	6.0	B		13	3		>0.5		HEN	
1997 01 26.26		S	3.0	YF	5.0	B		10	14	7	2.0		ENT	
1997 01 26.26		S	3.2	AA	7.0	B		16	8	3	0.13	357	TAY	
1997 01 26.30		B	3.3	SC	0.7	E		1	15	5			ROG02	
1997 01 26.85		S	3.2	S	3.6	B		12					TOY	
1997 01 26.87		B	2.9	HS	3.5	B		7		7			OHM	
1997 01 26.89		S	2.9	AA	5.0	B		7					TAK06	
1997 01 27.14		B	3.1	HD	5.0	B		7	10	7	0.5	335	MOR04	
1997 01 27.16		B	2.5	AA	5.0	B		7	9	6	0.5		HOM	
1997 01 27.17		S	2.7	AA	5.0	B		10		S8	1		SCU	
1997 01 27.17		S	4.0	AA	0.7	E		1	12	S3	2	294	CSU	
1997 01 27.18		S	3.0	AA	6.3	R	13	52	14	S9	10	320	KOS	
1997 01 27.19		B	3.3	AA	5.0	B		7	13	S7	1.5	330	VEL03	
1997 01 27.19		G	3.2	AA	0.0	E		1	14	S5			VEL03	
1997 01 27.19		S	2.0	S	10	B	4	25	8	7	0.67	340	HAL04	
1997 01 27.20	—	M	2.5	Y	5.0	B		10	7	S8	1	320	SAN07	
1997 01 27.20		S	2.4	TI	10	B	4	25	22	7	0.60	330	ROT01	
1997 01 27.84		S	3.3	S	3.6	B		12					TOY	
1997 01 28.16		B	1.8:	AA	3.0	B		7		7	0.3		CHV	
1997 01 28.18		B	2.9	SC	5.0	B		10					VEL02	
1997 01 28.18		M	2.5	SC	11.0	B		20	22	4	1.5		BAR06	
1997 01 28.19		S	2.7	AA	5.0	B		10		S8	1		SCU	
1997 01 28.20	a	M	2.7	AA	5.0	B		12	20	6			TAN02	
1997 01 28.23		S	2.7	YF	3.0	B		8	12	7	2.5	355	ENT	
1997 01 28.26		S	2.6	AA	5.0	B		8	45	7	1.30	320	BEA	
1997 01 29.14		B	3.0	HD	5.0	B		7	13	7	0.5	336	MOR04	
1997 01 29.15		B	2.9	SC	5.0	B		10		7			RAD01	
1997 01 29.16		B	2.9	SC	5.0	B		10		5			BOR05	
1997 01 29.16		B	3.2	SC	5.0	B		10		8			BOJ01	
1997 01 29.17		B	1.2:	AA	5.0	B		7	14	7	0.7		HOM	
1997 01 29.17		S	2.4	SC	0.0	E		1	30	3	2		BAR06	
1997 01 29.18					4	R	7	20	7	8	0.28	310	TOL	
1997 01 29.18		M	2.8	Y	0.0	E		1	5	7			KES01	
1997 01 29.18		S	2.8	Y	0.0	E		1	5	7			KES01	
1997 01 29.19		B	2.5	SC	5.0	B		10		7			GRA07	
1997 01 29.19		S	2.9	SC	5.0	B		7	10	7	0.67	320	TOL	
1997 01 29.20		S	2.5	Y	0.0	E		1	25	s4	2	350	LAN02	
1997 01 29.20	a	M	2.8	AA	5.0	B		12		6/			TAN02	
1997 01 29.87		S	2.5	AA	5.0	B		7	12	6	50	m	310	TAK06
1997 01 30.13	z	S	2.8	S	5.0	R	8	20	24	D6	1.6	330	BOR04	
1997 01 30.17		S	2.5	SC	8.0	B		12	18	S6	1.0	330	ISH03	
1997 01 30.18		B	2.6	AA	2.0	B		2	14	7			KOZ	
1997 01 30.18		B	2.8	AA	5.0	R	5	7	12	7			KOZ	
1997 01 30.18		M	2.8	Y	5.0	B		10	8	S8	1	330	SAN07	
1997 01 30.18		S	2.8	Y	5.0	B		10	25	S8	1	330	SAN07	
1997 01 30.20	a	M	2.5	AA	5.0	B		12		7/	2.5	327	TAN02	
1997 01 30.21	w	B	2.5	AA	0.0	E		1					VAN06	
1997 01 30.22					8.0	B		20	5	6	0.4	3	VAN06	
1997 01 30.85		S	3.3	S	3.5	B		7					TOY	

Comet C/1995 01 (Hale-Bopp) [cont.]

DATE (UT)	N	MM	MAG.	RF	AP.	T	F/	PWR	COMA	DC	TAIL	PA	OBS.
1997 01 31.15		B	1.8	SC	8.0	B		8		8			RAD01
1997 01 31.17		B	1.5	SC	8.0	B		8		6			BOR05
1997 01 31.17		B	1.9	SC	8.0	B		8					BOJ01
1997 01 31.18		B	2.6	SC	5.0	B		10					VEL02
1997 01 31.19		B	1.7	SC	8.0	B		8		6			GRA07
1997 01 31.85		I	2.9	S	7.0	B		10					TOY
1997 01 31.87		S	2.5	AA	5.0	B		7	9	6	1	310	TAK06
1997 02 01.14		B	3.0	HD	5.0	B		7	13	7	0.5	320	MOR04
1997 02 01.15		M	2.7	AA	3.0	R	4	7	10	5	0.5		MAI
1997 02 01.16		B	2.7	AA	2.0	B		2	14	8			KOZ
1997 02 01.16		B	2.8	AA	5.0	R	5	7	12	8			KOZ
1997 02 01.17		B	1.8	AA	3.0	B		7		7	0.5	337	CHV
1997 02 01.17		B	2.8	AA	10.0	B	4	12	10	8	1.3	327	KOZ
1997 02 01.17		G	2.8	AA	0.0	E		1		8			KOZ
1997 02 01.18		S	2.4	Y	0.0	E		1	7	7	0.3	300	KES01
1997 02 01.18		S	2.7	AA	5.0	B		10		S8	0.8		SCU
1997 02 01.19		B	3.0	AA	5.0	B		7	18	S7		325	VEL03
1997 02 01.19		G	3.0	AA	0.0	E		1	20	S5	1		VEL03
1997 02 01.19		S	2.4	AA	5.0	B		10	9	8	3	320	MOE
1997 02 01.20	a	M	2.2	TI	5.0	B		7	20	6/	2.5		DVO
1997 02 01.20	a	M	2.3	S	3	R		1	30	7/	2.5	330	HOR02
1997 02 01.21	a	M	2.1	S	3	R		1	25	7	2.5	330	PLS
1997 02 01.23		M	2.2	YG	0.7	E		1	12	7	2.5	321	GRA04
1997 02 01.23		N	4.9	YG	5.0	B		10	12	7/	4.5	321	GRA04
1997 02 01.24		B	2.7	SC	0.0	E		1	15	8			BIV
1997 02 01.24		S	2.2	YG	0.7	E		1			1		SKI
1997 02 01.24	a	M	2.2	Y	10	B		25		6	1.2	320	HYN
1997 02 01.85					12.5	B		20	10	8	1	330	TOY
1997 02 01.85		I	2.6	YG	0.0	E		1	<20	8			YOS04
1997 02 01.85		S	2.5	S	3.5	B		7					TOY
1997 02 01.85		S	2.5	YG	2.4	B		10	18	7	0.6	330	YOS04
1997 02 02.14		B	1.7	AA	3.0	B		7		7	0.7	338	CHV
1997 02 02.17		B	1.3	SC	5.0	B		10					BOR05
1997 02 02.17		B	1.9	SC	8.0	B		8					BOJ01
1997 02 02.17		B	2.2	SC	5.0	B		10					VEL02
1997 02 02.17		S	2.5	SC	4	R	7	20	12.5	8	0.58	300	TOL
1997 02 02.17	!	B	2.0	Y	0.0	E		1	&15	S8	7	330	SAR02
1997 02 02.18		B	1.3	SC	8.0	B		8		7			GRA07
1997 02 02.18		B	2.9	AA	5.0	B		7	14	S8	1.5	317	VEL03
1997 02 02.18		G	2.9	AA	0.0	E		1	18	S6	1		VEL03
1997 02 02.18		S	2.5	AA	5.0	B		10		S8	1		SCU
1997 02 02.18		S	2.5	AA	6.3	R	13	52	14	S9	13	345	KOS
1997 02 02.19					5.0	B		7	6	7	0.60	300	TOL
1997 02 02.19		B	2.2	AA	0.0	E		1	&15	7	1.5	325	CHE03
1997 02 02.19		S	2.3	AA	5.0	B		10	11	8	2.5	325	MOE
1997 02 02.19	a	M	2.1	S	3	R		1	25	7	2	335	PLS
1997 02 02.19	a	M	2.2	AA	5.0	B		12	22	8/	3	322	TAN02
1997 02 02.19	a	M	2.3	AA	0.6	E		1		8	0.6		MEY
1997 02 02.19	a	M	2.5	AA	5.0	B		10	13	S8	2.7		MEY
1997 02 02.20		B	1.8	S	0.0	E		1	20	7	1.75	315	HAL04
1997 02 02.20		S	2.1	TI	10	B	4	25	20	7	0.67	330	ROT01
1997 02 02.20		S	3.0	AA	0.7	E		1	17	S3/	7	313	CSU
1997 02 02.20	a	M	2.2	S	3	R		1	30	7/	2.5	330	HOR02
1997 02 02.20	a	O	2.3	TI	0.0	E		1	30	7	2.8		KON06
1997 02 02.21					8.0	B		20	4	8	1.1	315	VAN06
1997 02 02.21		S	2.1	YG	0.7	E		1	&15	7	1.5		SKI
1997 02 02.21	w	B	2.3	AA	0.0	E		1					VAN06
1997 02 02.22		M	2.1	YG	0.7	E		1	12	7			GRA04
1997 02 02.23					5.0	B		10	5.3	6	1.0	320	HAS02
1997 02 02.23		N	4.7	YG	5.0	B		10	14	7/	4.0	325	GRA04
1997 02 02.23		S	2.2	AA	0.7	E		1					BOU
1997 02 02.25		K	2.5	SC	3.0	B		8			&6	312	WAL02
1997 02 02.25		M	2.8	SC	5.0	B		10		7/	&0.5		GLI
1997 02 02.49	w	M	2.2	YF	0.0	E		1		9	&1.5	312	ADA03
1997 02 02.49	w	M	2.3	YF	5.0	B		7	&15	S8	&3.0	312	ADA03

Comet C/1995 01 (Hale-Bopp) [cont.]

DATE (UT)	N	MM	MAG.	RF	AP.	T	F/	PWR	COMA	DC	TAIL	PA	OBS.
1997 02 02.55		M	2.2	SC	0.0	E		1			5		OME
1997 02 03.13		G	2.6	AA	0.0	E		1					GER01
1997 02 03.14		S	2.0	SC	0.0	E		1	30	3	2		BAR06
1997 02 03.15		B	2.4	AA	5.0	B		7	& 7	7	0.7		HOM
1997 02 03.15		B	2.7:	SC	3.5	R	5	30	4	7	0.13	322	APE
1997 02 03.16		B	1.5	AA	3.0	B		7		7	0.7	339	CHV
1997 02 03.16		B	2.1	SC	6.0	L	10	25	20	S6	1.3	315	ISH03
1997 02 03.16		M	2.5	Y	11.0	L	8	36		S6			HOR
1997 02 03.16		S	2.5	Y	0.0	E		1	7	S8	5	330	SAN07
1997 02 03.17		B	1.9	SC	0.0	E		1	30	3	2		BAR06
1997 02 03.17		B	2.0:	SC	0.0	E		1	&30	D4	&2	320	MAN01
1997 02 03.17	w	I	2.0	SC	0.0	E		1			0.6		FIL05
1997 02 03.17	w	S	2.3:	SC	5.0	B	6	7	& 7	4	0.9		FIL05
1997 02 03.18		B	2.6	AA	5.0	B		7	14	S8	4	320	VEL03
1997 02 03.18		G	2.5	AA	0.0	E		1		S6	3	320	VEL03
1997 02 03.18		S	3.0	AA	0.7	E		1	17	S3/	11	309	CSU
1997 02 03.18	a	M	2.1	AA	5.0	B		12	18	8	2.3	321	TAN02
1997 02 03.19	!	V	2.0	YF	6.4	A	3 a	5	&50	7	&2.5	320	MIK
1997 02 03.19	a	O	2.2	TI	0.0	E		1	30	7	3		KON06
1997 02 03.20		B	2.3	S	0.0	E		1	17	7	1.20	310	HAL04
1997 02 03.20		K	2.5	SC	25	L	4	40			10	315	WAL02
1997 02 03.20		S	2.5:	AA	0.7	E		1	15	5	1.5		GIL01
1997 02 03.20	!	V	2.0	YF	2.3	A	4 a	30	&60	7	&3	320	MIK
1997 02 03.20	a	M	2.3	S	3	R		2	25	7/	3	330	HOR02
1997 02 03.21	a	O	1.9	SP	0.0	E		1	15	6/	2.0		ZNO
1997 02 03.22		S	1.9	TI	10	B	4	25	18	7	0.60	335	ROT01
1997 02 03.22	a	M	2.3	TI	5.0	B		7	20	6	2		DVO
1997 02 03.23		S	2.0	YG	0.7	E		1			1.5		SKI
1997 02 03.23	!	S	2.3	AA	5.0	B		7	5	8	2	319	SHA02
1997 02 03.24		S	2.3	SC	6.3	B		9	10	8	1.25	315	DIN01
1997 02 03.24	!	S	2.5	AA	0.7	E		1	4	8			SHA02
1997 02 03.24	a	S	2.0	SC	0.6	E		1	15	7	5.5	330	OKS
1997 02 03.25		G	2.6	SC	6.0	B		13		7	>1.5	320	HEN
1997 02 03.27		S	2.5	AA	7.0	B		16	9	D3	1.2	330	TAY
1997 02 03.28		B	2.1	S	5.0	B		7	40	6			TRI
1997 02 03.30		B	2.4	SC	0.7	E		1	24	5	&1.5		ROG02
1997 02 03.46	a	G	2.2:	SC	0.0	E		1	10	8/			CRE01
1997 02 03.84					15.0	B		25	>60	5	>2.5	325	FUK02
1997 02 03.84		B	2.3	YG	0.0	E		1					KAT01
1997 02 03.84		B	2.5	YG	3.5	B		7	14	7	1.5	300	OHM
1997 02 03.84		G	2.3	S	0.0	E		1					FUK02
1997 02 03.85		B	2.3	YG	0.0	E		1	<20	S5	1	310	YOS04
1997 02 03.85		I	2.6	S	0.0	E		1					TOY
1997 02 03.85		S	2.1	YG	2.4	B		10	12	7	1.6	310	YOS04
1997 02 03.86		S	2.1	YG	0.0	E		1	15	7/	1.5	300	NAG08
1997 02 04.13	&	B	2.6	S	5.0	R	8	20	24	D6	1.6	325	BOR04
1997 02 04.14		B	2.9	HD	5.0	B		7	15	7	1	305	MOR04
1997 02 04.14		S	1.8	SC	0.0	E		1	40	3	3		BAR06
1997 02 04.16		B	1.5	AA	3.0	B		7		7	1	340	CHV
1997 02 04.16		S	2.3	AA	5.0	B		10		S8	2		SCU
1997 02 04.17		B	1.9	SC	0.0	E		1	30	D4	&2	320	MAN01
1997 02 04.17		S	3.0	AA	0.7	E		1	17	S3/	11	301	CSU
1997 02 04.17	w	I	2.0	SC	0.0	E		1			1.0		FIL05
1997 02 04.17	w	S	2.2:	SC	5.0	B	6	7	10	4	1.3		FIL05
1997 02 04.18		B	2.1	AA	0.0	E		1	&13	7	1.0	325	CHE03
1997 02 04.18		B	2.6	AA	5.0	B		7	12	S8	3	317	VEL03
1997 02 04.18		G	2.5	AA	0.0	E		1		S5			VEL03
1997 02 04.18		S	2.0	AA	5.0	B		7	14	S9	15	320	KOS
1997 02 04.18	!	V	1.9	YF	6.4	A	3 a	2	&50	7	&2.5	320	MIK
1997 02 04.18	w	B	1.5	SC	0.0	E		1		8	1		BOR05
1997 02 04.21	!	V	1.9	YF	2.3	A	4 a	20	&60	7	&3	320	MIK
1997 02 04.22					8.0	B		20	6	7	1	305	VAN06
1997 02 04.22	w	B	2.1	AA	0.0	E		1					VAN06
1997 02 04.23		S	1.9	YG	0.7	E		1		8	1.5		SKI
1997 02 04.25		M	2.2	S	5.0	B		12	12	S8	2.5		GON05

Comet C/1995 01 (Hale-Bopp) [cont.]

DATE (UT)	N	MM	MAG.	RF	AP.	T	F/	PWR	COMA	DC	TAIL	PA	OBS.
1997 02 04.29		B	1.8	S	0.0	E		1		8			TRI
1997 02 04.29		B	2.0	S	5.0	B		7	50	6	3	340	TRI
1997 02 04.31		M	2.2	SC	5.0	B		10	&45	6/	&1.0	315	POR05
1997 02 04.65		M	2.0	SC	0.0	E		1			5		OME
1997 02 04.72	!	M	2.1	YG	5.0	B		10	10	7			GRA04
1997 02 04.72	!	N	4.4	YG	5.0	B		10					GRA04
1997 02 04.83		I	2.4	S	0.0	E		1					TOY
1997 02 04.84		B	2.5	YG	0.0	E		1	<15	S5			YOS04
1997 02 04.84		S	2.4	YG	2.4	B		10	12	7	0.8	320	YOS04
1997 02 04.85		B	2.5	AA	4.2	B		7		7			HAS08
1997 02 04.85		S	2.1	YG	0.0	E		1	&12	7/			NAG08
1997 02 04.86		G	2.2	AA	0.0	E		1					YOS02
1997 02 04.86		M	2.3	AA	3.5	B		7	15	7	1.6	310	YOS02
1997 02 04.86		S	2.2	AA	0.0	E		1		8			HAS08
1997 02 04.86		S	2.3	AA	7.0	B		10		7			FUK01
1997 02 04.86	a	B	2.3	YG	0.0	E		1					NAK01
1997 02 05.10	&	B	2.7	S	5.0	R	8	30	24	D5/	1.5	325	BOR04
1997 02 05.11		M	2.3	AA	3.0	R	4	7	12	5	0.5		MAI
1997 02 05.12		B	2.8	HD	5.0	B		7	15	7	1	305	MOR04
1997 02 05.14		G	2.4	AA	0.0	E		1					GER01
1997 02 05.15		S	2.3	AA	5.0	B		10		S8			SCU
1997 02 05.15	w	B	2.3	SC	5.0	B		10		8			VEL02
1997 02 05.17	w	B	1.5	SC	5.0	B		10		8	1.5		BOR05
1997 02 05.17	w	B	1.7	SC	0.0	E		1		8			GRA07
1997 02 05.17	w	B	2.2	SC	0.0	E		1		6			BOJ01
1997 02 05.18	w	B	2.0	SC	5.0	B		10		7			MAR19
1997 02 05.19	a	M	1.9	AA	5.0	B		12	19	8	2.5	318	TAN02
1997 02 05.22		S	1.8	YG	0.7	E		1		8	1.5		SKI
1997 02 05.23		M	2.0	YG	0.7	E		1	12	7			GRA04
1997 02 05.24					5.0	B		10	10	7/	3.0	320	GRA04
1997 02 05.25		S	2.2	SC	6.3	B		9	9	8	1.25	315	DIN01
1997 02 05.25	!	S	1.9	AA	5.0	B		7	12	8	1.3	314	SHA02
1997 02 05.25	T	S	2.1	AA	0.7	E		1	12	7	1.3	315	SHA02
1997 02 05.26		G	2.5	SC	0.7	E		1	10	7	>1.5	320	HEN
1997 02 05.27		B	1.7	S	0.0	E		1	30	8		310	TRI
1997 02 05.28		B	1.9	S	5.0	B		7	50	6	3	310	TRI
1997 02 05.87		S	2.2	AA	5.0	B		7	10	6	1	310	TAK06
1997 02 06.19	a	M	2.1	AA	5.0	B		12	16	9	3	311	TAN02
1997 02 06.20		B	2.1	S	0.0	E		1	20	7	1.30	300	HAL04
1997 02 06.22		M	2.0	YG	0.7	E		1	12	7			GRA04
1997 02 06.22		N	4.4	YG	5.0	B		10	10	7/	4.0	324	GRA04
1997 02 06.22		S	1.8	YG	0.7	E		1			2		SKI
1997 02 06.22		S	2.0	TI	10	B	4	25	20	6			ROT01
1997 02 06.22	s	M	1.7	SC	0.0	E		1	& 8	7/	&2.0	325	GLI
1997 02 06.24		B	2.5	SC	0.0	E		1	15	7			BIV
1997 02 06.25		B	1.8	S	0.0	E		1	30	8	1	300	TRI
1997 02 06.25		B	2.0	S	5.0	B		7	40	6	2	300	TRI
1997 02 06.25		M	2.1	S	5.0	B		12	10	S8/	3		GON05
1997 02 06.31		M	1.9	SC	5.0	B		10	&35	7	&1.2	320	POR05
1997 02 06.83		B	2.2	S	2.5	B		8			0.8	320	TOY
1997 02 06.85		B	2.2	YG	0.0	E		1	<30	S5	1	310	YOS04
1997 02 06.85		S	1.9	AA	0.0	E		1	20	7	2	310	NAG08
1997 02 06.85		S	2.1	YG	2.4	B		10	14	7	0.6	300	YOS04
1997 02 07.12		B	2.7	HD	3.5	B		7	15	S7/	2	315	HAR09
1997 02 07.12		B	2.7	HD	5.0	B		7	18	S7/	3	320	MOR04
1997 02 07.12		M	2.2	AA	3.0	R	4	7	12	5	0.5		MAI
1997 02 07.16	!	B	1.5	Y	0.0	E		1	&20	S8	20	315	SAR02
1997 02 07.18		S	2.0	Y	0.0	E		1	14	8	0.9	290	KES01
1997 02 07.19		M	2.0	S	3	R		1	35	7	3	335	PLS
1997 02 07.19		S	1.6	TI	0.8	E		1	20	7/	0.5		VET01
1997 02 07.20					6.3	B		9	15	S8	3.5	327	KAM01
1997 02 07.20	a	M	1.9	S	3	R		1	25	7/	2	330	HOR02
1997 02 07.20	w	G	1.7	AA	0.6	E		1					KAM01
1997 02 07.21	!	V	1.8	YF	6.4	A	3 a	2	&40	7	&3	320	MIK
1997 02 07.21	a	M	1.9	TI	5.0	B		7	20	6/	3		DVO

Comet C/1995 01 (Hale-Bopp) [cont.]

DATE (UT)	N	MM	MAG.	RF	AP.	T	F/	PWR	COMA	DC	TAIL	PA	OBS.
1997 02 07.22					5.0	B		7	15	7/	6	319	SKI
1997 02 07.22		S	1.7	YG	0.7	E		1		8	2.5		SKI
1997 02 07.22		S	2.0	TI	10	B	4	25	20	6	1.00		ROT01
1997 02 07.22	w	M	1.9	SC	0.0	E		1	&10	7/	&4	325	GLI
1997 02 07.23		B	1.7	S	0.0	E		1	30	8	1	315	TRI
1997 02 07.23		B	1.8	S	5.0	B		7	40	6	2.5	315	TRI
1997 02 07.25		B	1.8	S	5.0	B		7	50	6	4	350	ROD01
1997 02 07.25		B	2.4	SC	0.0	E		1	20	7			BIV
1997 02 07.26	s	B	1.9	S	5.0	B		7	40	8	1.5	290	MAR20
1997 02 07.41	a	B	1.6	AA	0.0	E		1		8/	&1		GRE
1997 02 07.73	!	M	1.8:	YG	5.0	B		10	10	7/	0.6		GRA04
1997 02 07.75	!	S	2.6	AA	7.0	B		16	7	3			TAY
1997 02 08.12		B	2.6	HD	3.5	B		7	15	S7/	3	315	HAR09
1997 02 08.15	w	B	2.0	SC	0.0	E		1		8			RAD01
1997 02 08.16		S	1.7	SC	0.0	E		1	40	3	3		HAR06
1997 02 08.16		S	1.7	SC	8.0	B		12	25	S6	2.1	318	ISH03
1997 02 08.17		B	1.7	S	0.0	E		1	12	7	0.70	300	HAL04
1997 02 08.17		S	1.5	SC	0.0	E		1	40	3	3		CHU
1997 02 08.17		S	2.0	AA	5.0	B		10	9	8	4.5	330	MOE
1997 02 08.17	w	B	1.9	SC	5.0	B		10		8			RAD01
1997 02 08.18	!	S	1.5	AA	0.8	E		1	15	7	4	318	SHA02
1997 02 08.19	!	V	1.7	YF	6.4	A	3 a	2	&40	7	&3	320	MIK
1997 02 08.19	a	M	1.9	Y	0.0	E		1	15	7			KYS
1997 02 08.19	a	O	1.7	S	0.0	E		1	30	5	5		POD
1997 02 08.20		S	1.5:	AA	0.0	E		1					ANZ
1997 02 08.20		S	1.6	AA	5.0	B		10			6		ANZ
1997 02 08.20	a	M	1.8	Y	5.0	B		7	15	8	8	320	KYS
1997 02 08.21		B	1.7	SC	8.0	B		11		D6			BR006
1997 02 08.21		S	1.6	YG	0.7	E		1		8	2		SKI
1997 02 08.21	w	M	1.6	Y	0.0	E		1	20	D7	4	300	CAN04
1997 02 08.22		B	1.8	S	5.0	B		7	40	6	2.5	315	TRI
1997 02 08.22	—	M	1.8	YG	0.7	E		1	10	8			GRA04
1997 02 08.22		N	4.3	YG	5.0	B		10	10	7/	4.5	321	GRA04
1997 02 08.22	a	B	1.6	AA	0.7	E		1					BOU
1997 02 08.23					3.2	B		8	4.4	4	4.8	330	HAS02
1997 02 08.23		B	1.6	S	0.0	E		1	30	8	1	315	TRI
1997 02 08.27		M	1.9:	SC	5.0	B		10	&45	6/	&2.3	320	POR05
1997 02 08.74	!	M	1.9:	YG	5.0	B		10	10	7	0.8	323	GRA04
1997 02 08.81		S	1.9:	AA	0.0	E		1	&20	7/	1	310	NAG08
1997 02 08.83		I	1.8	S	0.0	E		1					TOY
1997 02 08.85		S	1.7	S	15.0	R	5	25	15	6	1.4		NAG02
1997 02 08.86		I	2.3	YG	0.0	E		1		8			YOS04
1997 02 08.86		S	2.0	YG	2.4	B		10	25	7			YOS04
1997 02 08.87		M	1.9	YG	3.0	B		8	20	6	0.8	300	KAT01
1997 02 08.87		M	2.1	AA	3.5	B		7	&15	7	1.2	320	YOS02
1997 02 08.88		S	2.0:	AA	5.0	B		7	12	7	1		TAK06
1997 02 09.12		B	1.7	SC	0.0	E		1	30	S6	5	320	MAN01
1997 02 09.12		B	2.5	HD	5.0	B		7	19	S7/	4	315	MOR04
1997 02 09.12		B	2.6	HD	3.5	B		7	16	S7/	4	320	HAR09
1997 02 09.13		M	2.0	AA	3.0	R	4	7	11	5	0.6		MAI
1997 02 09.15		B	1.4	AA	3.0	B		7		7	0.8	338	CHV
1997 02 09.15		S	1.5	SC	0.0	E		1	42	3			LUK04
1997 02 09.15	w	B	1.9	SC	0.0	E		1		8	1.5		AND03
1997 02 09.16					8.0	B		12	40	S6	4.5	324	BAR06
1997 02 09.16		S	1.6	SC	0.0	E		1	42	3	3.5	320	BAR06
1997 02 09.16	w	B	1.3	SC	0.0	E		1		8			RAD01
1997 02 09.16	w	B	1.6	SC	0.0	E		1		7			BOJ01
1997 02 09.17	w	B	1.3	AA	0.0	E		1	&25	6	5	317	CHE03
1997 02 09.17	w	B	1.5	SC	5.0	B		10		8			GRA07
1997 02 09.17	w	B	1.5	SC	5.0	B		10		8			RAD01
1997 02 09.18		S	1.5	AA	8.0	B		20			6.5		ANZ
1997 02 09.18		S	1.7:	AA	0.0	E		1					ANZ
1997 02 09.18	w	B	1.4	SC	5.0	B		10		8	4.5		BOR05
1997 02 09.19	a	M	1.6	AA	5.0	B		12	24	8/	5	316	TAN02
1997 02 09.21					8.0	B		20	5	7	3	310	VAN06

Comet C/1995 01 (Hale-Bopp) [cont.]

DATE (UT)	N	MM	MAG.	RF	AP.	T	F/	PWR	COMA	DC	TAIL	PA	OBS.
1997 02 09.21	w	B	1.7	AA	0.0	E		1					VAN06
1997 02 09.21	w	M	1.5	Y	0.0	E		1	20	D7	7	325	CAN04
1997 02 09.22		B	1.4	S	6.0	B		10	8	7	0.75	315	SAN04
1997 02 09.22		B	1.7	S	5.0	B		7	40	6	1.5	320	TRI
1997 02 09.23					3.2	B		8	6.6	3	5.8	340	HAS02
1997 02 09.23		B	1.6	S	0.0	E		1	30	8	1	300	TRI
1997 02 09.25		B	2.3	SC	0.0	E		1	20	7			BIV
1997 02 09.25		M	1.9	S	5.0	B		12	10	S8/	4		GON05
1997 02 09.25	s	B	1.7	S	5.0	B		7	40	8	2	300	MAR20
1997 02 09.26	a	I	2.1	AT	0.0	E		1			&7	320	VIT01
1997 02 09.27	a	I	1.8	AT	0.0	E		1			&4.5	320	PER01
1997 02 09.46	a	I	1.5	SC	0.0	E		1	10	9	3	320	CRE01
1997 02 09.74	!	S	1.7:	YG	0.7	E		1		8/			SKI
1997 02 09.84		B	1.6	AA	0.0	E		1					OKA05
1997 02 09.84		I	2.2:	AA	0.0	E		1					TSU02
1997 02 09.84		S	1.5	S	15.0	R	5	25	15	6/	1.5		NAG02
1997 02 09.85		I	1.8	AA	0.0	E		1					WAS
1997 02 09.85		M	2.1	AA	3.5	B		7	15	7	2.0		WAS
1997 02 09.85		S	2.3	AA	5.0	B		7	10	7	1.2	300	TAK06
1997 02 09.86		B	2.2	YG	3.5	B		7	11	8	2.0	310	OHM
1997 02 09.86		I	2.2	YG	0.0	E		1		8			OHM
1997 02 09.86		M	2.2	AA	5.0	B		7	20				TOD
1997 02 09.86		S	2.1	AA	0.0	E		1					TAK06
1997 02 09.97		B	3.2:	AA	5.0	B		7		7			HOM
1997 02 10.11		B	2.4	HD	3.5	B		7	16	S7/	4	315	HAR09
1997 02 10.11		M	1.9	AA	3.0	R	4	7	13	5	0.7		MAI
1997 02 10.12		B	2.3	HD	5.0	B		7	19	S7/	4	315	MOR04
1997 02 10.14	w	B	1.8	SC	5.0	B		10	30	8	4		AND03
1997 02 10.15	w	B	1.9	SC	0.0	E		1		8	1.5		AND03
1997 02 10.16		S	1.6	SC	5.0	B		7	7	9	1.50	315	TOL
1997 02 10.16	w	B	1.5	SC	5.0	B		10		8	4		GRA07
1997 02 10.16	w	B	1.8	SC	0.0	E		1		8			RAD01
1997 02 10.17	w	B	1.4	SC	0.0	E		1		8			BOJ01
1997 02 10.17	w	B	1.5	SC	5.0	B		10		8			BOR05
1997 02 10.18		B	2.0	S	0.0	E		1	10	6	0.70	305	HAL04
1997 02 10.18	a	M	1.4	AA	5.0	B		12	23	8	6	321	TAN02
1997 02 10.19	!	V	1.6	YF	6.4	A	3 a	1	&40	7	&3	320	MIK
1997 02 10.20					8.0	B		20	3	7	3.3	315	VAN06
1997 02 10.21	w	M	1.4	Y	0.0	E		1	25	D7	7.5	325	CAN04
1997 02 10.23					5.0	B		10	13.2	3	4.0	330	HAS02
1997 02 10.24		B	1.5	S	0.0	E		1	30	8	0.5	300	TRI
1997 02 10.24		B	1.6	S	5.0	B		7	35	6	1	315	TRI
1997 02 10.24		S	1.6	YG	0.7	E		1		8/			SKI
1997 02 10.25		S	2.0	SC	6.3	B		9	6	7	1.92	315	DIN01
1997 02 10.25	s	B	1.7	S	5.0	B		7	40	8	2	290	MAR20
1997 02 10.26	a	I	1.9	AT	0.0	E		1			&4.5	302	VIT01
1997 02 10.27	a	B	1.9	AT	0.0	E		1		7/	&6.5	290	PER01
1997 02 10.27	a	I	1.6	AT	0.0	E		1		7/	&6.5	290	PER01
1997 02 10.27	a	S	1.6	AT	0.0	E		1		7/	&6.5	290	PER01
1997 02 10.76	!	S	1.4:	AA	5.0	B		7	6	6			SHA02
1997 02 10.84		S	1.3	S	15.0	R	5	25	15	6/	1.5		NAG02
1997 02 10.86		M	1.6	YG	3.0	B		8	20	7	0.6	300	KAT01
1997 02 11.15		B	1.4	AA	3.0	B		7		6	1.5	339	CHV
1997 02 11.15		B	1.6	AA	3.0	B		8		6	1.5		SLI01
1997 02 11.15		B	1.6	AA	3.0	B		8		6	2.5		SLI01
1997 02 11.15	w	B	1.6	SC	0.0	E		1		8	1.5		VEL02
1997 02 11.15	w	B	1.7	SC	5.0	B		10		8	4.5		AND03
1997 02 11.16		S	1.5	SC	4	R	7	20	6	9	1.6	320	TOL
1997 02 11.16		S	1.6	AA	6.3	R	13	52	14	S9	19	320	KOS
1997 02 11.16	w	B	1.3	SC	0.0	E		1		8	2		BOR05
1997 02 11.16	w	B	1.6	SC	5.0	B		10		8			RAD01
1997 02 11.17	w	B	1.4	SC	0.0	E		1		8			RAD01
1997 02 11.17	w	B	1.5	SC	0.0	E		1		8			BOJ01
1997 02 11.18	a	M	1.3	AA	5.0	B		12	23	7/			TAN02
1997 02 11.19					15.0	R	8	30	22	7	1.2	330	DIE02

Comet C/1995 01 (Hale-Bopp) [cont.]

DATE (UT)	N	MM	MAG.	RF	AP.	T	F/	PWR	COMA	DC	TAIL	PA	OBS.
1997 02 11.19		S	1.9	AA	0.0	E		1					DIE02
1997 02 11.21		M	1.5:	YG	0.7	E		1	&12				GRA04
1997 02 11.21	a	S	1.5	AA	0.7	E		1					BOU
1997 02 11.22			1.4:	AA	0.6	E		1	15	5	2.0	320	GIL01
1997 02 11.22		B	1.7	SC	0.7	E		1	22	5	&5		ROG02
1997 02 11.22		S	1.3	SC	5.0	B		10	25	8	3.5	312	MCK
1997 02 11.22	w	M	1.7	SC	0.0	E		1	&10	7/	&4	315	GLI
1997 02 11.23	!	S	1.9	AA	5.0	B		7	5	8	2	310	SHA02
1997 02 11.23	!	S	2.0	AA	0.7	E		1	10	8	2	310	SHA02
1997 02 11.23	!	S	2.3	AA	8.0	B		20	4.9	8	2	310	SHA02
1997 02 11.24		B	1.7	S	5.0	B		7	35	6			TRI
1997 02 11.24		S	1.7	SC	6.3	B		9	8	7	3.5	320	DIN01
1997 02 11.24	a	S	1.5	SC	0.6	E		1	20	8	>8	320	OKS
1997 02 11.74	!	M	1.6	YG	5.0	B		10	11	7/	1.2		GRA04
1997 02 11.74	!	S	1.5	YG	0.7	E		1		8			SKI
1997 02 11.81		I	1.8	S	0.0	E		1					TOY
1997 02 11.82	!	S	1.3	SC	0.0	E		1	20	S8	9	320	SHI
1997 02 11.82	!	S	1.6	SC	3.0	B		10	13	D7	6	320	SHI
1997 02 11.84		B	2.0	YG	3.5	B		7	15	8	3.2	300	OHM
1997 02 11.84		I	1.8	YG	0.0	E		1	<20	S4	1.5	310	YOS04
1997 02 11.84		S	1.6	YG	2.4	B		10	15	7	2.0	320	YOS04
1997 02 11.85		S	1.8	AA	0.0	E		1	20	7	1	310	NAG08
1997 02 11.86		G	1.5	AA	0.0	E		1			2		YOS02
1997 02 11.86		M	1.7	AA	3.5	B		7	15	7	1.8	320	YOS02
1997 02 12.06		S	2.2	AA	11.0	L	7	32	17	6	1.5		IVA03
1997 02 12.12		B	2.4:	AA	5.0	B		7	5	6	3		HOM
1997 02 12.13		B	1.8	SC	7.0	B		40			2.0		PEN
1997 02 12.14		B	1.5	AA	3.0	B		7		6	1	340	CHV
1997 02 12.14		B	1.8	SC	7.0	B		40			2.0		CHA02
1997 02 12.14		S	1.3	SC	0.0	E		1		5			LUK04
1997 02 12.14	w	B	1.3	SC	0.0	E		1		8			VEL02
1997 02 12.15					8.0	B		12	34	S6	6	324	BAR06
1997 02 12.15		B	2.1	AA	5.0	B		7	10	S8	4	315	VEL03
1997 02 12.15		G	1.9	AA	0.0	E		1	14	S6			VEL03
1997 02 12.15		S	1.4	SC	0.0	E		1	40	3/			BAR06
1997 02 12.15	w	I	1.2	SC	0.0	E		1		4	3	325	FIL05
1997 02 12.16	w	B	1.3	SC	0.0	E		1		8			BOJ01
1997 02 12.16	w	B	1.5	SC	5.0	B		10		8			RAD01
1997 02 12.17	w	B	1.3	SC	0.0	E		1		8	2		BOR05
1997 02 12.17	w	B	1.4	SC	0.0	E		1		8			RAD01
1997 02 12.18	a	M	1.3	AA	5.0	B		12	16	8	7	315	TAN02
1997 02 12.20					5.0	B		7	&18	7/	7.5	320	SKI
1997 02 12.20		S	1.3	YG	0.7	E		1		8	3		SKI
1997 02 12.21		M	1.5	YG	0.7	E		1	12	8	2		GRA04
1997 02 12.21		N	4.0	YG	5.0	B		10	11	7/	6.5	322	GRA04
1997 02 12.24		B	1.5	S	0.0	E		1	30	8	1	300	TRI
1997 02 12.24		B	1.6	S	5.0	B		7	35	6	1	335	TRI
1997 02 12.25	s	B	1.8	S	5.0	B		7	40	8	2	300	MAR20
1997 02 12.65	a	M	1.6	SC	0.0	E		1			15		OME
1997 02 12.74	!	M	1.7	YG	5.0	B		10	10	7/	1.0	305	GRA04
1997 02 12.83					5.0	B		7	15	8	3.0	320	NAG08
1997 02 12.83		I	1.6	S	0.0	E		1					TOY
1997 02 12.83		S	1.6	AA	0.0	E		1	20	7/	1.5	310	NAG08
1997 02 12.84		B	1.5	YG	0.0	E		1	<20	S4	1	310	YOS04
1997 02 12.84		S	1.4	YG	2.4	B		10	15	s6	1.2	310	YOS04
1997 02 12.86		M	2.0	AA	5.0	B		7	20				TOD
1997 02 12.86		S	1.2	S	15.0	B	5	25	18	7	2.0		NAG02
1997 02 12.87		S	2.2	AA	5.0	B		7					TAK06
1997 02 13.16	w	B	1.5	SC	0.0	E		1		8			RAD01
1997 02 13.20		S	1.4	YG	0.7	E		1		8			SKI
1997 02 13.20	w	M	1.3	Y	0.0	E		1	30	D7	15	325	CAN04
1997 02 13.22			1.5:	AA	0.6	E		1	15	5	1.5	315	GIL01
1997 02 13.24		B	1.5	S	5.0	B		7	35	6	0.5	330	TRI
1997 02 13.41	w	B	1.3	AA	0.0	E		1		8	&4		GRE
1997 02 13.46	a	M	1.5	SC	5.0	B		7	8	9	4.5	315	CRE01

Comet C/1995 01 (Hale-Bopp) [cont.]

DATE (UT)	N	MM	MAG.	RF	AP.	T	F/	PWR	COMA	DC	TAIL	PA	OBS.
1997 02 13.65	a	M	1.3	SC	0.0	E		1			15		OME
1997 02 13.81		I	1.6	S	0.0	E		1					TOY
1997 02 13.82		B	1.5	YG	0.0	E		1	<20	S4	2	310	YOS04
1997 02 13.82		S	1.6	YG	2.4	B		10	18	7	1.5	310	YOS04
1997 02 13.83		M	1.1	YG	3.0	B		8	20	7	1.5	310	KAT01
1997 02 13.83		S	1.2	S	15.0	R	5	25	18	6/	2.0		NAG02
1997 02 13.83		S	1.6	AA	0.0	E		1	20	7/	2	310	NAG08
1997 02 13.84		B	1.8	YG	3.5	B		7		8	4	340	OHM
1997 02 13.84		I	1.4	AA	0.0	E		1					TSU02
1997 02 13.84		I	1.9	YG	0.0	E		1		8			OHM
1997 02 13.85		B	1.4	AA	0.0	E		1			2		YOS02
1997 02 13.85		B	1.8	AA	0.0	E		1					TOD
1997 02 13.85		M	2.0	AA	5.0	B		7	15				TOD
1997 02 13.86					5.0	B		7	12	7	1	310	TAK06
1997 02 13.86		S	2.0	AA	0.0	E		1					TAK06
1997 02 14.18					15.0	R	8	30	23	7	1.35	320	DIE02
1997 02 14.18		S	1.7	AA	0.0	E		1					DIE02
1997 02 14.18	!	G	1.1	AA	0.8	E		1	12	8	11	323	SHA02
1997 02 14.18	!	M	1.1	AA	5.0	B		7	9	8	6	323	SHA02
1997 02 14.18	a	M	1.4	AA	5.0	B		12	20	8			TAN02
1997 02 14.19	a	S	1.4	SC	0.6	E		1	15	8	3	315	OKS
1997 02 14.20	w	M	1.3	Y	0.0	E		1	30	D7	15	325	CAN04
1997 02 14.22			1.6:	AA	0.6	E		1	15	5	0.5	315	GIL01
1997 02 14.24		B	1.5	SC	0.7	E		1		5	&1		ROG02
1997 02 14.24		S	1.8	YF	6.3	B		9	18	8	3		ENT
1997 02 14.25		S	1.2	AA	7.0	B		16	12	D3	1.1	316	TAY
1997 02 14.83					5.0	B		7	15	7/	7.0	320	NAG08
1997 02 14.83		B	1.1	S	0.0	E		1	&20	5	&6	325	FUK02
1997 02 14.83		B	1.8	AA	0.0	E		1					OKA05
1997 02 14.83		S	1.4	AA	0.0	E		1	20	7/	3	320	NAG08
1997 02 14.84	!	S	1.2	SC	0.0	E		1	20	S7	9	315	SHI
1997 02 15.15		M	1.4	YG	0.7	E		1	12	8			GRA04
1997 02 15.15	—	N	3.5	YG	5.0	B		10	12	7/	6.5	317	GRA04
1997 02 15.15	w	B	1.3	SC	8.0	B		8		8			GRA07
1997 02 15.15	w	B	1.3	SC	8.0	B		8		8			RAD01
1997 02 15.16		S	1.5	SC	4	R	7	20	5	9	0.40	330	TOL
1997 02 15.17		S	1.1	SC	0.0	E		1	25	4	4	319	BAR06
1997 02 15.17		S	1.1	SC	0.0	E		1	30	S6	6	319	ISH03
1997 02 15.17	!	G	0.9	AA	0.8	E		1	12	8	5	329	SHA02
1997 02 15.17	w	B	1.3	SC	5.0	B		10		8			BOR05
1997 02 15.18	a	M	1.3	AA	5.0	B		12	22	8	10	320	TAN02
1997 02 15.20		B	1.9	SC	0.0	E		1	30	8			BIV
1997 02 15.23		B	1.4	S	0.0	E		1	35	8	1.5	315	TRI
1997 02 15.23		B	1.5	S	5.0	B		7	35	6	1.5	315	TRI
1997 02 15.23		S	1.4	AA	5.0	B		8	45	8	2	315	BEA
1997 02 15.23		S	1.4	AA	12.5	R	5	20	45	8	2	315	BEA
1997 02 15.23	s	B	1.2	S	0.0	E		1		8	1	300	MAR20
1997 02 15.23	s	B	1.5	S	5.0	B		7	35	8	3	295	MAR20
1997 02 15.23	s	B	1.6	SC	0.0	E		1	10	8		310	GLI
1997 02 15.24		B	1.3	SC	0.7	E		1		5	4		ROG02
1997 02 15.24	G	1.5	AA	0.8	E			1	12	8	9	329	SHA02
1997 02 15.25		S	1.2	AA	7.0	B		16	15	D3	1.3	313	TAY
1997 02 15.25	a	I	1.4	AT	0.0	E		1		7/	&5	310	PER01
1997 02 15.25	a	I	1.5	AT	0.0	E		1					VIT01
1997 02 15.74	!	S	1.5	YG	0.7	E		1		8			SKI
1997 02 15.77	!	M	1.6:	YG	5.0	B		10	10	7/	1.0		GRA04
1997 02 16.13		M	1.7	AA	3.0	R	4	7	14	6	2		MAI
1997 02 16.14					8.0	R	10	28	12	S7	0.8	305	GER01
1997 02 16.14		G	1.8:	AA	0.0	E		1					GER01
1997 02 16.15	w	B	1.1	SC	0.0	E		1		8			GRA07
1997 02 16.15	w	B	1.3	SC	8.0	B		8		8			RAD01
1997 02 16.16	w	B	1.2	SC	0.0	E		1		8	6.5		BOR05
1997 02 16.17	w	B	1.2	AA	0.0	E		1	25	6/	5	322	CHE03
1997 02 16.18		N	3.4	YG	5.0	B		10	12	7/	10	321	GRA04
1997 02 16.19					8.0	B		20	4	7	4.2	315	VAN06

Comet C/1995 01 (Hale-Bopp) [cont.]

DATE (UT)	N	MM	MAG.	RF	AP.	T	F/	PWR	COMA	DC	TAIL	PA	OBS.
1997 02 16.19		M	1.3	YG	0.7	E		1	&12	8	5		GRA04
1997 02 16.19		S	1.1	YG	0.7	E		1		8	3.5		SKI
1997 02 16.19	a	O	1.1	SP	0.0	E		1	45	7	12	340	ZNO
1997 02 16.19	w	B	1.4	AA	0.0	E		1					VAN06
1997 02 16.21	s	B	1.5	SC	0.0	E		1	12	8	>8	310	GLI
1997 02 16.21	w	B	1.0	S	0.0	E		1		8	3	290	SAN04
1997 02 16.22	w	B	1.2	S	0.0	E		1		8/	5	315	MAR02
1997 02 16.23		B	1.3	S	0.0	E		1	35	8	1.5	315	TRI
1997 02 16.23		B	1.8	SC	0.0	E		1	20	8			BIV
1997 02 16.23	s	B	1.1	S	0.0	E		1		8	1	300	MAR20
1997 02 16.23	s	B	1.5	S	5.0	B		7	35	8	3	290	MAR20
1997 02 16.23	w	M	1.4	S	3.0	B		6	20	7	5	320	MAR02
1997 02 16.24		B	1.4	S	5.0	B		7	35	6	1.5	315	TRI
1997 02 16.42	w	B	1.3	AA	0.0	E		1		8			GRE
1997 02 16.65	a	M	1.4	SC	0.0	E		1			12		OME
1997 02 16.81		I	1.2	S	0.0	E		1					TOY
1997 02 16.82		S	1.3	AA	0.0	E		1	&20	7/	2	320	NAG08
1997 02 16.83		B	1.7	AA	0.0	E		1					OKA05
1997 02 17.08		S	1.3	AA	11.0	L	7	32	20	6	1.8		IVA03
1997 02 17.14	!	G	2.7:	AA	0.7	E		1	6	7			SHA02
1997 02 17.14	!	M	3.2:	AA	8.0	B		10	6	7	0.33	317	SHA02
1997 02 17.16					5.0	B		7	16	S7	6	315	VEL03
1997 02 17.16	G	1.3	AA	0.0	E			1	20	S5	3	318	VEL03
1997 02 17.16	S	1.3	AA	8.0	B			20	20		8.5	320	ANZ
1997 02 17.17		B	1.4	S	0.0	E		1	18	6	1.20	310	HAL04
1997 02 17.17		S	1.1	AA	0.0	E		1					ANZ
1997 02 17.17	w	B	1.2	AA	0.0	E		1	25	6	6	322	CHE03
1997 02 17.17	w	M	1.2	Y	0.0	E		1	30	D7	&15	310	CAN04
1997 02 17.18		M	1.5	Y	6.3	R	13	33		S6	9	310	HOR
1997 02 17.18		S	0.8	AA	6.3	R	13	52	14	S9	23.3	295	KOS
1997 02 17.18	a	B	1.3	AT	0.0	E		1					MIL02
1997 02 17.18	a	M	1.0	S	5	R		1	35	7/			HOR02
1997 02 17.21	a	O	1.1	SP	0.0	E		1	35	7			ZNO
1997 02 17.23		B	1.4	S	5.0	B		7	30	6	1	310	TRI
1997 02 17.24		M	1.2	S	5.0	B		7	12	S8/	6		GON05
1997 02 17.24	a	B	1.7	AT	3.5	R		1					PER01
1997 02 17.24	a	I	1.5	AT	0.0	E		1		8	&9	310	PER01
1997 02 17.24	s	B	1.5	S	5.0	B		7	<40	8	2	285	MAR20
1997 02 17.47	G	1.1:	SC	0.0	E			1	11	7	1.0	315	CRE01
1997 02 17.65	a	M	1.5	SC	0.0	E		1			10		OME
1997 02 17.83		S	1.1	S	15.0	R	5	25	20	7	2.8		NAG02
1997 02 17.85		B	1.3	YG	3.5	B		7	20	8	6	320	OHM
1997 02 18.11		B	1.5	HD	5.0	B		7	20	S7/	6	318	MOR04
1997 02 18.11		B	1.9	HD	3.5	B		7	17	S7/	5	310	HAR09
1997 02 18.12		S	0.7	SC	0.0	E		1	35	S6	7	320	ISH03
1997 02 18.14		S	0.9	SC	8.0	B		12	30	S6	6	320	ISH03
1997 02 18.16		B	1.5	AA	2.0	B		2	13	7			KOZ
1997 02 18.16		S	1.2	Y	0.0	E		1	11	S7/	7	313	SAN07
1997 02 18.16	w	M	1.1	AA	0.0	E		1	30	6	7	322	CHE03
1997 02 18.17		S	0.6	AA	6.3	R	13	52	14	S9	25	295	KOS
1997 02 18.17	!	G	1.2	AA	0.7	E		1	5	7			SHA02
1997 02 18.17	!	M	1.4	AA	5.0	B		7	4	8	1.5	303	SHA02
1997 02 18.17	a	M	0.8	S	5	R		1	40	7/	6	325	HOR02
1997 02 18.18		B	1.1	Y	0.0	E		1	20	S8	5	300	SAR02
1997 02 18.18		B	1.4	S	0.0	E		1	12	7	0.75	305	HAL04
1997 02 18.18		S	1.2	Y	0.0	E		1	10	8	1.5	290	KES01
1997 02 18.18	a	M	1.1	S	5	R		1	30	7/	4	325	PLS
1997 02 18.18	a	O	1.6	SP	0.0	E		1	25	6	4		POD
1997 02 18.19	!	V	1.0	YF	6.4	A	3 a	1	&40	8			MIK
1997 02 18.20	a	M	0.8	TI	5	R		1	25	7	4		DVO
1997 02 18.20	a	O	1.1	SP	0.0	E		1	35	7	11		ZNO
1997 02 18.20	w	B	1.4	AA	0.0	E		1					VAN06
1997 02 18.22		S	1.4	SC	6.3	B		9	2	7	3	320	DIN01
1997 02 18.24		B	1.3	S	5.0	B		7	30	6	1	320	TRI
1997 02 18.76		B	1.8	AA	7.0	B		16	8	D6			TAY

Comet C/1995 01 (Hale-Bopp) [cont.]

DATE (UT)	N	MM	MAG.	RF	AP.	T	F/	PWR	COMA	DC	TAIL	PA	OBS.
1997 02 18.76		S	0.6	AA	7.0	B		16	8	D6			TAY
1997 02 18.77		M	1.4	AA	5.0	B		7	7	7	0.33	350	SHA02
1997 02 18.85		B	0.9	AA	0.0	E		1			5		YOS02
1997 02 18.85		B	1.4:	AA	0.0	E		1	&20	6	&3	310	MIY01
1997 02 18.85		B	1.6:	AA	5.0	B		7	20	D7	7	310	MIY01
1997 02 18.85		I	1.3	AA	0.0	E		1					TSU02
1997 02 18.85		M	1.1	AA	3.5	B		7	20	8	7	325	YOS02
1997 02 18.86		B	1.3	AA	0.0	E		1					TOD
1997 02 18.86		I	1.5	S	0.0	E		1					TOY
1997 02 18.86		M	1.0	Y	0.0	E		1	25	7	9	320	KOB01
1997 02 19.10		G	1.3	Y	0.0	E		1		S8			MOS03
1997 02 19.11		B	1.7	HD	3.5	B		7	17	S7/	6	320	HAR09
1997 02 19.12					8.0	R	10	28	10	S6	>1.3	326	GER01
1997 02 19.12		B	1.5	HD	5.0	B		7	20	S7/	7	318	MOR04
1997 02 19.12		G	1.7:	AA	0.0	E		1					GER01
1997 02 19.12	w	I	0.9	SC	0.0	E		1		4	5		FIL05
1997 02 19.13		B	1.3:	SC	0.0	E		1	&25	S6	&3	320	MAN01
1997 02 19.13	w	B	1.1	SC	0.0	E		1		8	3.5		VEL02
1997 02 19.14		S	0.8	SC	0.0	E		1	40	4	4	313	BAR06
1997 02 19.15		S	0.8	SC	0.0	E		1	40	5	4		LUK04
1997 02 19.15	w	B	1.2	SC	0.0	E		1		8			BOJ01
1997 02 19.16	w	B	1.2	SC	0.0	E		1		8			RAD01
1997 02 19.16	w	B	1.2	SC	0.0	E		1		8	6.5		BOR05
1997 02 19.18	w	B	1.0:	AA	0.0	E		1	22	6	4	323	CHE03
1997 02 19.20	w	B	1.4	SC	0.0	E		1	12	8	>8	325	GLI
1997 02 19.21		S	1.3	AA	0.0	E		1	16	7	3	300	BAR
1997 02 19.21	w	B	1.2	S	0.0	E		1	25	7/	4	310	MAR02
1997 02 19.22			1.3:	AA	0.6	E		1	12	7	2.0	315	GIL01
1997 02 19.22	w	B	1.3	S	3.0	B		6	30	7	6	320	MAR02
1997 02 19.23		B	1.1	S	0.0	E		1	30	8	2	310	TRI
1997 02 19.23		B	1.2	S	5.0	B		7	25	7	4	320	TRI
1997 02 19.24		M	1.1	S	5.0	B		7	12	S8/	8		GON05
1997 02 19.24	s	B	1.1	S	0.0	E		1		8	1	290	MAR20
1997 02 19.24	s	B	1.4	S	5.0	B		7	30	8	3	270	MAR20
1997 02 19.82		I	1.2	S	0.0	E		1					TOY
1997 02 19.83		B	1.1	YG	0.0	E		1	&20	S5	3	310	YOS04
1997 02 19.83		S	1.0	S	15.0	R	5	25	22	7	3.0		NAG02
1997 02 19.83		S	1.1	AA	0.0	E		1	&20	7/	3	320	NAG08
1997 02 19.84		B	1.4	AA	0.0	E		1					OKA05
1997 02 19.84		I	1.1	AA	0.0	E		1					WAS
1997 02 19.84		S	1.3	YG	2.4	B		10	15	S6	3	320	YOS04
1997 02 19.85		B	1.4:	AA	0.0	E		1	&20	6	5	300	MIY01
1997 02 19.85		B	1.6:	AA	8.0	B		11	20	D7	7	300	MIY01
1997 02 19.85		I	0.8	AA	0.0	E		1					TSU02
1997 02 19.86		B	1.2	YG	0.0	E		1					NAK01
1997 02 19.86		C	1.0	YF	2.5	A	2		41		7.5	319	NAK01
1997 02 19.86		M	0.9	YG	3.0	B		8	20	7	1.5	310	KAT01
1997 02 19.87		B	1.3	AA	0.0	E		1					TOD
1997 02 20.09		G	1.0	AA	0.0	E		1	18	9	0.8	320	SER
1997 02 20.11		M	1.5	AA	3.0	R	4	7	14	6	2.5		MAI
1997 02 20.12		B	1.4	HD	5.0	B		7	20	S8	7	320	MOR04
1997 02 20.13	w	I	0.8	SC	0.0	E		1		5			FIL05
1997 02 20.14		S	0.7	SC	0.0	E		1	50	4			BAR06
1997 02 20.14	w	S	0.6	SC	0.0	E		1	50	4			BAR06
1997 02 20.15		S	1.1	Y	0.0	E		1	9	S8	3	315	SAN07
1997 02 20.17					5.0	B		8	25	7	1.5	313	DIE02
1997 02 20.17		S	1.5	AA	0.0	E		1					DIE02
1997 02 20.20			1.2	AA	0.6	E		1	12	8	2.5	315	GIL01
1997 02 20.20	a	B	1.0	AA	0.7	E		1					BOU
1997 02 20.21		S	1.2	AA	5.0	B		10	30	6	4	290	FOG
1997 02 20.22		B	1.4	S	0.0	E		1	8	7	0.75	300	HAL04
1997 02 20.23		B	1.0	S	0.0	E		1	30	8	3	310	TRI
1997 02 20.23		B	1.2	S	5.0	B		7	25	7	6	320	TRI
1997 02 20.23		G	1.1	AA	0.7	E		1	18	8	2	304	SHA02
1997 02 20.23		I	1.0	AA	0.8	E		1					HAS02

Comet C/1995 01 (Hale-Bopp) [cont.]

DATE (UT)	N	MM	MAG.	RF	AP.	T	F/	PWR	COMA	DC	TAIL	PA	OBS.
1997 02 20.23		M	1.1	AA	5.0	B		7	7	8	3.5	322	SHA02
1997 02 20.23	w	B	1.2	SC	0.0	E		1		8			GLI
1997 02 20.25		B	1.3	SC	0.7	E		1		5	3.5		ROG02
1997 02 20.40	Gw	B	1.1	AA	0.0	E		1		8	&2		GRE
1997 02 20.45		G	1.0	SC	0.0	E		1	11	8	2.0	315	CRE01
1997 02 20.45		M	1.1	SC	5.0	B		10	9	9	5	315	CRE01
1997 02 20.75	!	M	1.2:	YG	0.7	E		1	12	8			GRA04
1997 02 20.75	!	N	3.2	YG	5.0	B		10		8	2	290	GRA04
1997 02 20.76	!	S	0.9:	YG	0.7	E		1		8/	1.5		SKI
1997 02 20.81		I	1.5	S	0.0	E		1					TOY
1997 02 20.83	!	S	1.1	SC	0.0	E		1	17	S8	7	320	SHI
1997 02 20.84		B	1.5	AA	0.0	E		1					OKA05
1997 02 20.84		I	1.5	YG	0.0	E		1		8	1	300	YOS04
1997 02 20.84		S	1.5	YG	2.4	B		10	&15	s7	1	310	YOS04
1997 02 21.12		B	1.4	HD	5.0	B		7	18	S8	6	320	MOR04
1997 02 21.14		B	1.9:	AA	5.0	B		7	5	6	2		HOM
1997 02 21.14		M	1.5	AA	3.0	R	4	7	14	6	3		MAI
1997 02 21.16		B	0.5	Y	5.0	B		10	20	S6	8	325	BUS04
1997 02 21.17		M	1.3	Y	6.0	B		20					TUB
1997 02 21.17		S	1.0	Y	0.0	E		1	10	S8	4	320	SAN07
1997 02 21.17	a	B	1.2	AT	0.0	E		1					MIL02
1997 02 21.18		B	1.5	AA	0.0	E		1	20		4.5	308	STD
1997 02 21.20		S	1.0	SC	0.7	E		1	30	7/			MCK
1997 02 21.20		S	1.0	YG	0.7	E		1		8	2.5		SKI
1997 02 21.20	!	V	0.9	YF	2.3	A	4 a	5	&40	8	&5	320	MIK
1997 02 21.23		B	0.9	S	0.0	E		1	30	8	0.5	330	TRI
1997 02 21.23		B	1.0	S	5.0	B		7	25	7	3	320	TRI
1997 02 21.67		M	1.3	SC	0.0	E		1					OME
1997 02 21.73		I	1.2	AA	0.7	E		1					MOE
1997 02 21.81		I	1.3	S	0.0	E		1					TOY
1997 02 21.83		B	1.3	AA	0.0	E		1					OKA05
1997 02 21.84	—	B	1.2	YG	0.0	E		1	&20	S5	1.5	310	YOS04
1997 02 21.84		S	0.8	S	15.0	R	5	25	20	7	3.0		NAG02
1997 02 21.84		S	1.3	YG	2.4	B		10	&18	s7	2	320	YOS04
1997 02 22.11		M	1.5	AA	3.0	R	4	7	14	6	3		MAI
1997 02 22.18	!	V	0.9	YF	2.3	A	4 a	10	&35	8			MIK
1997 02 22.20		S	1.1	SC	0.7	E		1					MCK
1997 02 22.21		M	1.4:	AA	5.0	B		7	7	8	2	307	SHA02
1997 02 22.21		S	1.2:	AA	0.7	E		1	10	8	1	300	SHA02
1997 02 22.65		M	1.1	SC	0.0	E		1					OME
1997 02 22.82		B	1.0	YG	0.0	E		1		8	1	305	YOS04
1997 02 22.82		S	1.1	YG	2.4	B		10	15	s7	1.5	315	YOS04
1997 02 22.85		B	1.0	YG	0.0	E		1					NAK01
1997 02 22.85		I	1.1	S	0.0	E		1					TOY
1997 02 23.14		M	1.2	Y	6.0	B		20	40	4	5		TUB
1997 02 23.15		M	0.9	Y	0.0	E		1	11	S6/	2	300	SAN07
1997 02 23.16					5.0	B		10	11.5	8	2.0	300	HAS02
1997 02 23.16					5.0	B		10	11.5	8	4.0	315	HAS02
1997 02 23.16	s	B	1.2	AA	0.6	E		1		S8	0.6		MEY
1997 02 23.16	s	M	1.4	AA	5.0	B		10	9.5	S7	1.8		MEY
1997 02 23.17		B	1.2	S	0.0	E		1	12	7	0.67	320	HAL04
1997 02 23.17		S	0.4	AA	6.3	R	13	52	14	S9		297	KOS
1997 02 23.17		S	1.3	AA	0.7	E		1	17	S2	15.5	304	CSU
1997 02 23.18		I	0.9	AA	0.8	E		1					HAS02
1997 02 23.18		M	1.2:	S	3	R		1	30	7/	2	320	PLS
1997 02 23.19	!	V	0.8	YF	2.3	A	4 a	5	&30	8			MIK
1997 02 23.19	a	M	0.7	TI	5	R		1	30	7	5		DVO
1997 02 23.19	a	O	0.8	SP	0.0	E		1	40	7/	13		ZNO
1997 02 23.41	Gw	B	0.9	AA	0.0	E		1		8	&2.5		GRE
1997 02 23.69	w	B	0.8:	SC	0.0	E		1	&30	3			BAR06
1997 02 23.75	!	S	0.9	YG	0.7	E		1		8/	1		SKI
1997 02 23.81		I	1.2	S	0.0	E		1					TOY
1997 02 23.85		B	1.1	AA	0.0	E		1					TOD
1997 02 23.85		B	1.3:	AA	0.0	E		1	&20	6	&2	290	MIY01
1997 02 23.85		B	1.4:	AA	5.0	B		7	20	D7	3	290	MIY01

Comet C/1995 01 (Hale-Bopp) [cont.]

DATE (UT)	N	MM	MAG.	RF	AP.	T	F/	PWR	COMA	DC	TAIL	PA	OBS.
1997 02 23.85		M	0.9	YG	3.0	B		8	20	7	2.0	300	KAT01
1997 02 23.86		S	0.5	S	15.0	R	5	25	25	7/	3.5		NAG02
1997 02 24.13		B	1.2	HD	5.0	B		7	18	S8			MOR04
1997 02 24.14		B	0.5	SC	0.0	E		1	35	4	5	338	BAR06
1997 02 24.14		S	0.3	SC	0.0	E		1	35	4			LUK04
1997 02 24.14		S	0.5	SC	0.0	E		1	35	S6	5	340	ISH03
1997 02 24.16		S	1.3	AA	0.7	E		1	17	S2	15.5	311	CSU
1997 02 24.17		S	0.4	AA	6.3	R	13	52	14	S9			KOS
1997 02 24.20		S	1.2	Y	0.0	E		1	10	8			SRA
1997 02 24.23		B	0.7	S	0.0	E		1	20	8			TRI
1997 02 24.23		B	0.8	S	5.0	B		7	25	7	2	320	TRI
1997 02 24.25		S	1.3	SC	3.0	B		8	3.5	7	3		DIN01
1997 02 24.42	W	B	0.8	AA	0.0	E		1		8	&1.5		GRE
1997 02 24.69	W	S	0.8:	SC	8.0	B		12	&15	7			BAR06
1997 02 24.82		B	1.1	YG	0.0	E		1		8			YOS04
1997 02 24.82		I	1.1	S	0.0	E		1					TOY
1997 02 24.82		S	1.1	YG	2.4	B		10	12	s7	0.6	305	YOS04
1997 02 24.83		I	0.9	AA	0.0	E		1	&15	8	1	330	NAG08
1997 02 24.83		I	1.1	AA	0.0	E		1					YOS
1997 02 24.84		B	1.1	AA	0.0	E		1					TOD
1997 02 24.84		S	0.7	SC	0.0	E		1	18	D8	7	325	SHI
1997 02 25.06		S	0.9	AA	11.0	L	7	32	20	6	2		IYA03
1997 02 25.08		M	1.4	AA	3.0	R	4	7	15	6	3		MAI
1997 02 25.11					8.0	R	10	28	10	S6	>1.2	310	GER01
1997 02 25.11		G	1.5:	AA	0.0	E		1					GER01
1997 02 25.13		I	0.4	SC	0.0	E		1	28	S6	6.5	338	ISH03
1997 02 25.14		B	0.5	SC	0.0	E		1	35	4/			BAR06
1997 02 25.14	W	B	0.9	SC	5.0	B		10		8			BOR05
1997 02 25.14	W	G	0.2	SC	0.0	E		1		6			LUK04
1997 02 25.14	W	G	0.3	SC	0.0	E		1	35	4/			BAR06
1997 02 25.15	W	B	1.1	SC	0.0	E		1		8			RAD01
1997 02 25.17		M	1.0	Y	0.0	E		1	20	7	4		BRL
1997 02 25.21		G	0.7	AA	0.7	E		1	10	8	3	321	SHA02
1997 02 25.23		B	0.5	SC	0.7	E		1		5	&6		ROG02
1997 02 25.23		B	-0.4	SC	6.3	R		53		7	4		POP01
1997 02 25.24		S	1.0	SC	6.3	B		9	3.5	7	3	320	DIN01
1997 02 25.43	Gw	B	0.7	AA	0.0	E		1		8	&2.5		GRE
1997 02 25.44		G	0.8	SC	0.0	E		1	10	8	2.0	310	CRE01
1997 02 25.78		B	2.0	AA	7.0	B		16	10	7	1.5	330	TAY
1997 02 25.81		I	1.0	S	0.0	E		1			1	310	TOY
1997 02 25.81		I	1.0	S	0.0	E		1			1	310	TOY
1997 02 25.83		B	1.2	AA	0.0	E		1		8	1		OKA05
1997 02 25.83		S	0.7	SC	0.0	E		1	20	D8	8	320	SHI
1997 02 25.84		B	0.8	YG	0.0	E		1	15	S4	1	310	YOS04
1997 02 25.84		S	0.9	YG	2.4	B		10	15	s7	1.5	310	YOS04
1997 02 26.13	W	B	0.9	SC	0.0	E		1		8			RAD01
1997 02 26.14		M	0.8	YG	0.7	E		1		8/	3		GRA04
1997 02 26.14		N	2.8	YG	5.0	B		10	10	8	7.0	319	GRA04
1997 02 26.14	W	B	0.9	SC	0.0	E		1		8			BOR05
1997 02 26.15		N	5.6:	YG	20.3	T	10	123					GRA04
1997 02 26.15	W	B	0.9	SC	0.0	E		1		8	3.5		BOJ01
1997 02 26.15	W	B	1.0	SC	0.0	E		1		8			JOR01
1997 02 26.17		S	1.1	AA	0.0	E		1					DIE02
1997 02 26.19		S	0.8	YG	0.7	E		1		8	3		SKI
1997 02 26.21		S	1.1:	AA	0.6	E		1	12	8	2.5	315	GIL01
1997 02 26.23		B	-0.7	SC	6.3	R		53		7	4.5		POP01
1997 02 26.23		S	0.7	SC	0.7	E		1					MCK
1997 02 26.78	!	G	1.1	AA	0.7	E		1	12	8	1	296	SHA02
1997 02 26.78	!	M	0.9:	YG	5.0	B		10	12	7/	2		GRA04
1997 02 26.82		S	0.4	S	15.0	R	5	25	22	7	4		NAG02
1997 02 26.84		I	1.1	AA	0.0	E		1					YOS
1997 02 27.07		S	0.6	AA	11.0	L	7	32	15	5/	2.2		IYA03
1997 02 27.13		B	1.2	SC	7.0	B		40			5		CHA02
1997 02 27.15		M	0.7	YG	0.7	E		1		8/	3		GRA04
1997 02 27.15		N	2.8	YG	5.0	B		10	10	7/	10	321	GRA04

Comet C/1995 01 (Hale-Bopp) [cont.]

DATE (UT)	N	MM	MAG.	RF	AP.	T	F/	PWR	COMA	DC	TAIL	PA	OBS.
1997 02 27.15		S	0.9	AA	5.0	B		10	12	7	4	330	MOE
1997 02 27.16	a	M	0.5	S	5	R		1	25	8	10	315	HOR02
1997 02 27.18		M	0.6	Y	10	B		25	25	7	2.5	345	HYN
1997 02 27.18		S	0.7	AA	0.0	E		1	20	8	5.5	297	BAR
1997 02 27.19		N	5.8	YG	20.3	T	10	123					GRA04
1997 02 27.19	a	M	0.3	TI	5	R		1	25	7/	4		DVO
1997 02 27.19	a	M	0.4	S	3	R		1	40	7/	8	310	PLS
1997 02 27.20	a	O	0.6	SP	0.0	E		1	25	8			ZNO
1997 02 27.21	a	B	0.6	AA	0.7	E		1		8			BOU
1997 02 27.23		B	-0.8	SC	6.3	R		53		7	4.5		POP01
1997 02 27.24		S	1.0	YF	3.0	B		8	12	8	7		ENT
1997 02 27.24		S	1.1	AA	5.0	B		8	20	8	1	315	BEA
1997 02 27.75		I	1.0	AA	0.7	E		1	10	8	3	320	MOE
1997 02 28.05		S	0.6	AA	11.0	L	7	32	14	5/	2.2		IYA03
1997 02 28.12		B	1.2	AA	5.0	B		7	10	S8	10	314	VEL03
1997 02 28.14		S	0.6	AA	6.0	B		20		8			SCU
1997 02 28.15	w	M	0.7	Y	0.0	E		1	35	D8	8	315	CAN04
1997 02 28.16		B	0.5	Y	0.0	E		1	15	S8	10	310	SAR02
1997 02 28.16		B	1.0	AA	0.0	E		1					STO
1997 02 28.16		M	0.6	Y	0.0	E		1	15	s8	5	315	SAN07
1997 02 28.16	a	G	0.8	AA	0.6	E		1		8			KAM01
1997 02 28.17					5.0	B		7	24	7	4	307	DIE02
1997 02 28.17		M	0.6	Y	10	B		25	25	7	3		HYN
1997 02 28.17		S	0.8	AA	0.7	E		1	17	S2	15	300	CSU
1997 02 28.17		S	1.4	AA	0.0	E		1					DIE02
1997 02 28.17	a	B	0.5	AT	0.0	E		1					MIL02
1997 02 28.18		S	1.1	Y	0.0	E		1	8	7	2	305	SRA
1997 02 28.18	a	B	0.5	AA	0.7	E		1					BOU
1997 02 28.19		I	0.6	AA	0.8	E		1					HAS02
1997 02 28.19		S	0.6	AA	0.0	E		1	25	8/	6	300	ZAN
1997 02 28.19	!	V	0.5	YF	2.3	A	4 a	3	+29	8	4.5	325	MIK
1997 02 28.19	a	M	0.5	S	5	R		1	25	8	4	285	HOR02
1997 02 28.20		S	1.0	YF	3.0	B		8		8	6		ENT
1997 02 28.20	a	O	0.6	S	0.0	E		1	25	8	2		LIB
1997 02 28.20	a	O	0.6	SP	0.0	E		1	25	7/	>8		ZNO
1997 02 28.70	w	S	0.5	SC	0.0	E		1	45	4/			BAR06
1997 02 28.73		B	0.5	SC	8.0	B		12	40	6	12		BAR06
1997 02 28.74	a	M	0.8:	Y	5.0	B		7	10	8	>2		KYS
1997 02 28.83		I	0.8	S	0.0	E		1			0.5	300	TOY
1997 02 29.09					5.0	B		7	11	S8	7.5	321	VEL03
1997 02 29.13		I	0.0	SC	0.0	E		1	28	S6	9.5	330	ISH03
1997 03 01.07		B	1.0	SC	7.0	B		40			5		CHA02
1997 03 01.08		G	0.6	Y	0.0	E		1		S8			MOS03
1997 03 01.11	!	G	0.0	AA	0.7	E		1	12	8	1	304	SHA02
1997 03 01.13		S	0.8	AA	6.0	B		20		8			SCU
1997 03 01.13	w	B	0.6	SC	0.0	E		1		8			BOR05
1997 03 01.15		S	0.8	AA	0.7	E		1	17	S2			CSU
1997 03 01.16		B	1.5	SC	3.5	R	5	30	4.5	8	0.25	30	APE
1997 03 01.16		S	0.0	AA	6.3	R	13	52	12	S9		337	KOS
1997 03 01.16	w	M	0.5	Y	0.0	E		1	25	D8	8	315	CAN04
1997 03 01.17	a	M	0.7	Y	5.0	B		7	15	9	10	335	KYS
1997 03 01.17	a	O	0.6	SP	0.0	E		1	30	6	5		POD
1997 03 01.17	w	B	0.7	SC	0.0	E		1		8			VEL02
1997 03 01.18		B	0.5	S	0.0	E		1	12	7	1.75	300	HAL04
1997 03 01.18	a	O	0.1	Y	0.0	E		1	10	8	10	335	KYS
1997 03 01.19		S	1.0	AA	0.0	E		1					DIE02
1997 03 01.19	a	B	0.5	AA	0.7	E		1					BOU
1997 03 01.20		B	0.3	SC	0.7	E		1		5	6		ROG02
1997 03 01.21		S	0.8	SC	0.7	E		1	20	8	5		MCK
1997 03 01.22		S	0.7	YF	6.3	B		9	12	8	5	330	ENT
1997 03 01.22	s	G	0.4	AT	0.0	E		1					PER01
1997 03 01.22	s	I	0.4	AT	0.0	E		1		D8	4.9	320	PER01
1997 03 01.22	s	I	0.5	AT	0.0	E		1			4.7	325	VIT01
1997 03 01.23	s	B	0.2	AT	3.5	R		1					PER01
1997 03 01.23	s	G	0.5	AT	0.0	E		1					VIT01

Comet C/1995 01 (Hale-Bopp) [cont.]

DATE (UT)	N	MM	MAG.	RF	AP.	T	F/	PWR	COMA	DC	TAIL	PA	OBS.
1997 03 01.72		B	0.3	SC	0.0	E		1	35	4/	14		BAR06
1997 03 01.72	w	G	0.1	SC	0.0	E		1	35	4/	14		BAR06
1997 03 01.81		B	0.9	AA	0.0	E		1		9	4		OKA05
1997 03 01.82		B	0.6	YG	0.0	E		1	20	S4	3	300	YOS04
1997 03 01.82		S	0.7	YG	2.4	B		10	15	s7	3	290	YOS04
1997 03 01.83		S	0.3	S	15.0	R	5	25	22	7	5		NAG02
1997 03 01.84		M	0.0	AA	0.0	E		1			3.0	330	TSU02
1997 03 02.07		B	1.0	SC	7.0	B		40			5		CHA02
1997 03 02.07		S	0.4	AA	11.0	L	7	32	17	6	4.5		IYA03
1997 03 02.09		G	0.7	AA	0.0	E		1	21	S7	4	310	VEL03
1997 03 02.13	w	B	0.6	SC	0.0	E		1		8			VEL02
1997 03 02.14	a	M	0.3	S	5	R		1	35	7	5	315	HOR02
1997 03 02.15		S	0.8	AA	0.7	E		1	17	S2	15	297	CSU
1997 03 02.15	w	B	0.5	SC	0.0	E		1		8			BOR05
1997 03 02.16		B	0.3	Y	0.0	E		1	20	S7	17	320	SAR02
1997 03 02.16		B	0.4	Y	0.0	E		1	25	S7	13	325	SZE02
1997 03 02.16		S	-0.1	AA	6.3	R	13	52	12	S9		340	KOS
1997 03 02.16	a	O	0.5	SP	0.0	E		1	30	7	12		ZNO
1997 03 02.16	w	B	0.7	SC	0.0	E		1		8			RAD01
1997 03 02.17	!	V	0.4	YF	2.3	A	4 a	3	+29	8	&5	323	MIK
1997 03 02.17	a	M	0.2	TI	5	R		1	25	7	2.5		DVO
1997 03 02.17	s	M	0.6	AA	5.0	B		10	15	S8			MEY
1997 03 02.17	s	S	0.3	AA	0.6	E		1		S8	7		MEY
1997 03 02.18	a	M	0.5	S	0.0	E		1	30	8	5		KUN06
1997 03 02.19					5.0	B		7	26	7	5	320	DIE02
1997 03 02.19		S	0.6	AA	0.0	E		1					DIE02
1997 03 02.19	s	M	0.2	SC	0.0	E		1	20	7/	10	290	GLI
1997 03 02.19	w	B	0.5	AA	0.0	E		1		8	4.8	325	VAN06
1997 03 02.20		I	0.6	AA	0.8	E		1					HAS02
1997 03 02.20	a	O	0.6	S	0.0	E		1	25		2		LIB
1997 03 02.22		M	0.4	S	5.0	B		7	12	S8/	6		GON05
1997 03 02.23		S	0.8	SC	3.0	B		8		7	6		DIN01
1997 03 02.45	w	B	0.2	YF	0.0	E		1	&15	8/	4	326	ADA03
1997 03 02.45	w	M	0.2	YF	5.0	R		1					ADA03
1997 03 02.67	w	M	0.5:	SC	0.0	E		1					OME
1997 03 02.78		S	1.1	SC	0.7	E		1		9			MCK
1997 03 02.80		S	0.3	AA	5.0	B		10	14	7	6	320	MOE
1997 03 02.80	!	B	0.4	YF	0.5	E		1		8			ENT
1997 03 03.08		I	0.4	AA	0.8	E		1	12	8	9	330	MOE
1997 03 03.10		B	0.5	AA	2.0	B		2	10	7			KOZ
1997 03 03.10		B	0.9	SC	7.0	B		40			6		CHA02
1997 03 03.10		S	0.3	AA	6.0	B		20		8			SCU
1997 03 03.10	w	B	0.5	SC	0.0	E		1		8			SCH14
1997 03 03.10	w	B	0.6	SC	0.0	E		1		8			JOR01
1997 03 03.11					8.0	R	10	28	11	S6	>1.3	312	GER01
1997 03 03.11		B	1.1	HD	5.0	B		7	20	S8	7	330	MUR04
1997 03 03.11		G	0.7:	AA	0.0	E		1					GER01
1997 03 03.11	!	G	0.1	AA	0.8	E		1	10	8	10	325	SHA02
1997 03 03.12		B	0.7	AA	5.0	R	5	7	10	7			KOZ
1997 03 03.12		G	0.2	SC	0.0	E		1	35	5	16		BAR06
1997 03 03.13		I	0.0	SC	0.0	E		1	30	S6	10	325	ISH03
1997 03 03.14	w	B	0.4:	AA	0.0	E		1	30	6/	8	315	CHE03
1997 03 03.15	a	S	0.5	AA	0.7	E		1	25	8	2.5	300	MEN03
1997 03 03.15	w	B	0.5	SC	0.0	E		1		8			RAD01
1997 03 03.16		S	-0.3	AA	6.3	R	13	52	12	S9		315	KOS
1997 03 03.16	w	B	0.4	SC	0.0	E		1		8			VEL02
1997 03 03.17	a	B	0.3	AA	0.7	E		1		8	9.5	324	BOU
1997 03 03.19		S	0.3	AA	5.0	B		8	40	8	4	320	BEA
1997 03 03.20		B	0.0:	SC	0.7	E		1		5	6		ROG02
1997 03 03.23	!	B	0.4	YF	0.5	E		1	8	8	6		ENT
1997 03 03.78		I	0.6	AA	0.8	E		1	11	8	3.5	330	MOE
1997 03 03.80		S	0.4	AA	0.0	E		1	&15	7/	3	330	NAG08
1997 03 03.81		S	0.3	AA	5.0	B		8	40	8	4	320	BEA
1997 03 03.85	\$	M	0.1	YG	0.0	E		1	20	7	10	335	KOB01
1997 03 04.06		B	0.0	SC	0.0	E		1	45	5	15	323	BAR06

Comet C/1995 01 (Hale-Bopp) [cont.]

DATE (UT)	N	MM	MAG.	RF	AP.	T	F/	PWR	COMA	DC	TAIL	PA	OBS.
1997 03 04.06	w	G	-0.1	SC	0.0	E		1	45	5	15	323	BAR06
1997 03 04.08		B	0.6	AA	5.0	B		7	12	D8	6	323	VEL03
1997 03 04.08		B	0.8	SC	7.0	B		40			6		CHA02
1997 03 04.08		G	0.6	AA	0.0	E		1	17	S7	5	323	VEL03
1997 03 04.11	a	S	0.6	AA	0.7	E		1	25	8	1.5	300	MEN03
1997 03 04.12		B	1.0	HD	5.0	B		7	20	S8	7	330	MOR04
1997 03 04.14		M	0.6	AA	3.0	R	4	7	17	6	4		MAI
1997 03 04.15		S	-0.3	AA	6.3	R	13	52	12	S9		317	KOS
1997 03 04.18	a	B	0.3	AA	0.7	E		1		8	10	325	BOU
1997 03 04.21		S	0.1	AA	5.0	B		8	40	8	4	320	BEA
1997 03 04.22	!	B	0.4	YF	0.5	E		1		8	6	325	ENT
1997 03 04.23	a	B	0.5	AT	3.5	R		1					PER01
1997 03 04.23	a	G	0.4	AT	0.0	E		1					PER01
1997 03 04.23	a	G	0.6	AT	0.0	E		1					VIT01
1997 03 04.23	a	I	0.3	AT	0.0	E		1		6	12	300	PER01
1997 03 04.23	a	I	0.6	AT	0.0	E		1			15	295	VIT01
1997 03 04.24	a	B	0.6	AT	3.5	R		1					VIT01
1997 03 04.26		S	0.7	AA	5.0	B		10	35	D7	2.5	312	TAY
1997 03 04.67	w	M	0.4	SC	0.0	E		1			25.5		OME
1997 03 04.68		B	1.0	HD	5.0	B		7	18	S8	4		MOR04
1997 03 04.74	a	O	0.5	S	0.0	E		1	30		2.5		LIB
1997 03 04.74	w	B	-0.1	AA	0.0	E		1		7	9	318	CHE03
1997 03 04.78		S	0.2	AA	5.0	B		10	14	7	10	330	MOE
1997 03 04.80	!	S	0.5	SC	0.0	E		1	21	D8	7	320	SHI
1997 03 04.82		B	0.6	AA	0.0	E		1	15	7	10	320	MIY01
1997 03 04.82		B	0.6:	AA	5.0	B		7	10	S7	10	320	MIY01
1997 03 04.82		I	0.6	S	0.0	E		1			0.5	310	TOY
1997 03 04.82		S	0.3	AA	0.0	E		1	15	7/	7	300	NAG08
1997 03 04.85	a	B	0.2	YG	0.0	E		1			4	300	NAK01
1997 03 04.85	a	B	0.3	AA	0.0	E		1					YOS02
1997 03 05.00		S	0.3	AA	11.0	L	7	32	16	6	5		IYA03
1997 03 05.06		I	0.2	AA	0.8	E		1	15	8	13	330	MOE
1997 03 05.06	w	S	-0.2	SC	0.0	E		1	50	5	14		BAR06
1997 03 05.10		G	0.6	AA	0.0	E		1	21	9	6	350	SER
1997 03 05.10		S	0.5	AA	6	R	10	16	18	6	3.5	295	ROM
1997 03 05.13		S	0.1	SC	0.6	E		1	15	8	7	310	OKS
1997 03 05.13	w	B	0.0	AA	0.0	E		1		6/			CHE03
1997 03 05.14		B	0.6	AA	2.0	B		2	9	8			KOZ
1997 03 05.14	a	M	0.0	AA	0.6	E		1		S8	14		MEY
1997 03 05.14	a	M	0.3	AA	5.0	B		10	13	S8			MEY
1997 03 05.15		S	-0.4	AA	6.3	R	13	52	12	S9		330	KOS
1997 03 05.15	a	M	0.0	S	5	R		1	40	7/	25	320	HOR02
1997 03 05.17	a	B	0.2	AA	0.7	E		1		8	9	324	BOU
1997 03 05.18		M	0.3	Y	10	B		25	20	6	1.5		HYN
1997 03 05.19					5.0	B		7	28	7	5	315	DIE02
1997 03 05.19		S	0.4	AA	0.0	E		1					DIE02
1997 03 05.19	!	V	0.2	YF	2.3	A	4 a	3	+29	8	>6	323	MIK
1997 03 05.25		S	0.2	AA	5.0	B		10	25	D7	5.5	320	TAY
1997 03 05.68		B	0.7	HD	5.0	B		7	15	S8	5		MOR04
1997 03 05.72		S	-0.1	SC	0.0	E		1	50	5	14		BAR06
1997 03 05.73	a	O	0.1	SP	0.0	E		1	35	6/	>8		ZNO
1997 03 05.74	w	B	-0.2	AA	0.0	E		1		6/	13	332	CHE03
1997 03 05.75					5.0	B		7	12	S7	10	322	VEL03
1997 03 05.81		S	0.0	AA	5.0	B		8	45	8	5	320	BEA
1997 03 05.82		I	0.6	S	0.0	E		1			0.5	310	TOY
1997 03 05.82	w	M	-0.1	YG	0.0	E		1			15	320	KIN
1997 03 05.83		B	0.6	AA	0.0	E		1	10	7	25	315	MIY01
1997 03 05.83		B	0.6:	AA	5.0	B		7	10	S7	10	315	MIY01
1997 03 05.83	w	B	0.5	YG	0.0	E		1	15	8	1.5	310	YOS04
1997 03 05.83	w	S	0.5	YG	2.4	B		10	15	S6	1.5	310	YOS04
1997 03 06.08		B	0.6	SC	7.0	B		40			8		CHA02
1997 03 06.08		G	0.2	AA	0.0	E		1		S7	12	323	VEL03
1997 03 06.08		S	0.3	AA	11.0	L	7	32	20	6	6		IYA03
1997 03 06.09		B	0.6	SC	7.0	B		40			7		PEN
1997 03 06.09		B	0.6	SC	7.0	B		40			9		GEN

Comet C/1995 01 (Hale-Bopp) [cont.]

DATE (UT)	N	MM	MAG.	RF	AP.	T	F/	PWR	COMA	DC	TAIL	PA	OBS.
1997 03 06.10		B	0.6	SC	7.0	B		40			8		GEN01
1997 03 06.10		I	-0.3	SC	0.0	E		1	32	S6	10	325	ISH03
1997 03 06.10	w	B	-0.2	AA	0.0	E		1	45	5	14		BAR06
1997 03 06.13		G	0.5	AA	0.0	E		1	20	8	6	319	GOL
1997 03 06.13		S	0.3	AA	6	R	10	16	19	6	6	305	ROM
1997 03 06.13		S	-1.0:	AA	6.0	B		20		8			SCU
1997 03 06.13	!	G	0.2	AA	0.7	E		1	14	8	3	306	SHA02
1997 03 06.13	w	B	-0.1	AA	0.0	E		1		6/	4	313	CHE03
1997 03 06.14		B	0.5	AA	3.0	B		7		6	6	339	CHV
1997 03 06.14		M	0.5	AA	3.0	R	4	7	18	6	5		MAI
1997 03 06.14	a	M	0.2	S	0.0	E		1	25	8	8		KON06
1997 03 06.15		B	0.2	Y	0.0	E		1	20	S7	20	330	SAR02
1997 03 06.15		B	0.6:	AA	5.0	B		7	10	D7	14	323	VELO3
1997 03 06.15		G	0.3	AA	0.0	E		1					VELO3
1997 03 06.15		S	-0.5	AA	6.3	R	13	52	14	S9		325	KOS
1997 03 06.15	a	M	-0.1	S	5	R		1	40	7/	25	330	HOR02
1997 03 06.15	w	B	0.9	SC	0.0	E		1		9			VELO2
1997 03 06.17		S	0.7	AA	0.7	E		1	17	S2			CSU
1997 03 06.18	a	M	-0.1	TI	5	R		1	25	8	5		DVO
1997 03 06.19	a	O	0.2	SP	0.0	E		1	30	7	>5	320	ZNO
1997 03 06.21		B	-0.2	SC	0.7	E		1		5	10		ROG02
1997 03 06.21		S	-0.1	AA	5.0	B		8	50	8	10	330	BEA
1997 03 06.23		B	-0.2:	YG	0.7	E		1		8	14		DAH
1997 03 06.23		B	-1.2	SC	6.3	R		53		7	9.5		POP01
1997 03 06.23	!	B	0.3	YF	0.5	E		1	16	8	8		ENT
1997 03 06.46	w	B	-0.1	YF	0.0	E		1	&15	S9	18	328	ADA03
1997 03 06.75	w	B	-0.2	AA	0.0	E		1	45	5	14		BAR06
1997 03 06.78		S	0.1	AA	5.0	B		10	13	8	9	330	MOE
1997 03 06.79			0.3	AA	0.6	E		1	20	9	3.0	325	GIL01
1997 03 06.81		I	0.5	S	0.0	E		1			1.5	310	TOY
1997 03 06.81		S	0.3	SC	0.7	E		1	15	9	3		MCK
1997 03 06.83	w	B	0.3	YG	0.0	E		1	&20	8	2	310	YOS04
1997 03 06.83	w	S	0.2	YG	2.4	B		10	15	S6	2	310	YOS04
1997 03 06.92					5.0	B		7	7	9	3.0	305	HEE
1997 03 06.92		S	0.5	YG	0.7	E		1					HEE
1997 03 07.01		B	0.6	SC	7.0	B		40			7		CHA02
1997 03 07.07		S	0.3	AA	11.0	L	7	32	20	6	6		IVA03
1997 03 07.11		B	0.6	SC	7.0	B		40			4		HAN04
1997 03 07.12		B	0.6	SC	7.0	B		40			7		GEN01
1997 03 07.13	a	S	0.4	AA	0.7	E		1	25	8	3.5	305	MEN03
1997 03 07.18	!	V	0.1	YF	2.3	A	4 a	5	+32	8	>6	325	MIK
1997 03 07.18	a	B	0.1	AA	0.7	E		1		8	12	325	BOU
1997 03 07.18	a	G	0.2	AA	0.6	E		1		S8/	8	325	KAM01
1997 03 07.19	s	M	0.0	SC	0.0	E		1	12	8			GLI
1997 03 07.22	w	G	-0.2	YF	0.0	E		1	&12	S9	11	70	ZEK
1997 03 07.26		B	0.0:	YG	0.7	E		1		8	13		DAH
1997 03 07.39	Gw	B	0.0	AA	0.0	E		1		8/	&5		GRE
1997 03 07.44	&	G	-0.1	SC	0.0	E		1	15	8	13	305	CRE01
1997 03 07.74	a	O	-0.1	SP	0.0	E		1	35	6/	14	325	ZNO
1997 03 07.74	w	B	-0.1	AA	0.0	E		1		6/	12	324	CHE03
1997 03 07.76	a	M	0.1	Y	0.0	E		1	20	7	3	330	HYN
1997 03 07.76	a	M	0.1	Y	10	B		25	20	7	4	330	HYN
1997 03 07.76	a	O	-0.3	Y	0.0	E		1	10	9	4		KYS
1997 03 07.77	a	O	0.4	S	0.0	E		1	30		3		LIB
1997 03 07.77	s	M	0.0:	SC	0.0	E		1					GLI
1997 03 07.78		S	0.0	AA	5.0	B		10	13	8	7	330	MOE
1997 03 07.81	a	M	0.3	S	0.0	E		1	25	8	8		KON06
1997 03 07.82	!	S	0.0	AA	0.0	E		1	&15	7/	10	330	NAG08
1997 03 07.84	a	B	-0.2	AA	0.0	E		1			12	330	YOS02
1997 03 07.99	w	B	-0.2	Y	0.0	E		1		8			GRE
1997 03 08.03		G	-0.5	AA	0.0	E		1	25	9	5	280	SER
1997 03 08.06		B	0.6	AA	5.0	B		7	11	D8	13	324	VELO3
1997 03 08.08		G	-0.1	AA	0.0	E		1	17	S8	13	324	VELO3
1997 03 08.09		G	-0.5	AA	0.0	E		1		8	5	322	GOL
1997 03 08.10		B	-0.3	AA	0.0	E		1	50	5	15		BAR06

Comet C/1995 01 (Hale-Bopp) [cont.]

DATE (UT)	N	MM	MAG.	RF	AP.	T	F/	PWR	COMA	DC	TAIL	PA	OBS.
1997 03 08.12		M	0.4	AA	3.0	R	4	7	18	6	5		MAI
1997 03 08.13	!	S	-0.7:	AA	0.0	E		1			10		ANZ
1997 03 08.13	a	M	-0.1	AA	0.6	E		1		S8	11		MEY
1997 03 08.13	w	B	-0.2	AA	0.0	E		1	22	6	6	308	CHE03
1997 03 08.14		B	-0.2	Y	0.0	E		1	15	S7,	25	330	SAR02
1997 03 08.14		S	-0.8	AA	6.3	R	13	52	14	S9		312	KOS
1997 03 08.15	a	M	0.1	S	0.0	E		1	20	8	10		KON06
1997 03 08.16		B	0.4	AA	0.0	E		1					ST0
1997 03 08.16	a	M	0.3	S	0.0	E		1	30	9	7		ZIF
1997 03 08.16	a	M	-0.1	TI	5	R		1	25	8	15		DV0
1997 03 08.16	w	M	-0.2	Y	0.0	E		1	30	D8	15	340	CAN04
1997 03 08.17	a	M	0.3	S	0.0	E		1	25	8	11		FIA
1997 03 08.17	a	0	0.0	SP	0.0	E		1	30	7	16	335	ZNO
1997 03 08.17	w	B	0.1	AA	0.0	E		1		8	12	330	VAN06
1997 03 08.18	w	M	0.3	SC	0.0	E		1	12	7/	9		GLI
1997 03 08.19		S	-0.4	AA	5.0	B		8	40	8	10	330	BEA
1997 03 08.20		S	0.8	SC	6.3	B		9	4	7	6		DIN01
1997 03 08.21		M	0.1	Y	10	B		25	25	7	2	320	HYN
1997 03 08.22		M	-0.2	S	5.0	B		7	15	S8/	9		GON05
1997 03 08.25		B	0.5	SC	8.0	B		11		D6			BR006
1997 03 08.26		B	-0.1	YG	0.7	E		1		8	14		DAH
1997 03 08.45	w	M	0.0	YF	5.0	R		1					ADA03
1997 03 08.46	w	B	-0.1	YF	0.0	E		1	&18	S9	12	323	ADA03
1997 03 08.53	w	S	0.0	AA	5.0	B		7	8	8/	7	325	SPR
1997 03 08.70		B	0.2	HD	5.0	B		7	15	S8	4	330	MOR04
1997 03 08.78		S	-0.4	AA	5.0	B		8	40	8	10	330	BEA
1997 03 08.79	w	M	-0.2	Y	0.0	E		1	30	D8	3.5	320	CAN04
1997 03 08.80		B	-0.3	AA	0.0	E		1	50	5	15		BAR06
1997 03 08.81		I	0.0	S	0.0	E		1			8	330	TOY
1997 03 08.82					2.4	B		10	15	S6	4	305	YOS04
1997 03 08.82		B	0.0	AA	4.0	R		8	25	S7	9		BAR06
1997 03 08.82	+	S	0.0	SC	0.0	E		1	27	D7	9	325	SHI
1997 03 08.82	w	B	0.1	YG	0.0	E		1	&20	8	4	305	YOS04
1997 03 09.01		B	1.1	HD	5.0	B		7	20	S8	10	330	MOR04
1997 03 09.07		S	0.2	AA	11.0	L	7	32	25	6	7		IVA03
1997 03 09.10		B	0.0	HD	5.0	B		7	15	S7	10	331	LEH01
1997 03 09.10		M	0.0	AA	4.0	R		8	25	S7	9	333	BAR06
1997 03 09.12		B	-0.2	AA	0.0	E		1	45	6	14		BAR06
1997 03 09.12	w	B	-0.3	AA	0.0	E		1	45	6	14		BAR06
1997 03 09.13	w	M	-0.3	AA	0.0	E		1	30	6	12	324	CHE03
1997 03 09.14		B	-0.3	Y	0.0	E		1	12	S8	20	340	SAR02
1997 03 09.14	!	S	-0.4:	AA	0.0	E		1			13		ANZ
1997 03 09.16	w	B	0.0	AA	0.0	E		1		8	13	330	VAN06
1997 03 09.17	a	B	-0.1	AA	0.7	E		1		8	13	328	BOU
1997 03 09.17	a	M	-0.2	TI	5	R		1	25	8	6		DV0
1997 03 09.17	w	B	-0.2	S	0.0	E		1		9	12	335	MAR02
1997 03 09.18	!	V	-0.1	YF	2.3	A	4 a	3	+32	8	>6	325	MIK
1997 03 09.18	w	B	0.1	S	3.0	B		6		9	8.5	335	MAR02
1997 03 09.18	w	B	-0.1	S	0.0	E		1		9	9	330	SAN04
1997 03 09.21					5.0	B		7	20	7	4.5	320	DIE02
1997 03 09.21		S	0.1	AA	0.0	E		1					DIE02
1997 03 09.22		M	-0.4	S	5.0	B		7	15	S8/	13		GON05
1997 03 09.22	s	I	0.4	AT	0.0	E		1			10	310	VIT01
1997 03 09.23	s	G	0.6	AT	0.0	E		1					PER01
1997 03 09.23	s	G	0.6	AT	0.0	E		1					VIT01
1997 03 09.23	s	I	0.3	AT	0.0	E		1			18	310	PER01
1997 03 09.26	!	B	-0.2	YG	0.7	E		1		9	14		DAH
1997 03 09.38	w	B	-0.3	Y	0.0	E		1		8/	10		GRE
1997 03 09.40	&	G	-0.2	SC	0.0	E		1	15	8	10	305	CRE01
1997 03 09.74	w	B	-0.3	AA	0.0	E		1	25	6	6	312	CHE03
1997 03 09.75		B	0.6	AA	5.0	B		7	10	D8	12	327	VEL03
1997 03 09.75	a	B	-0.3	AA	0.0	E		1			5		MIL02
1997 03 09.75	a	M	-0.4	AA	0.0	E		1			5		MIL02
1997 03 09.76	a	0	-0.3:	Y	0.0	E		1	10	8	>3		KYS
1997 03 09.77		I	-0.5	SC	0.0	E		1	30	S7	13	330	ISH03

Comet C/1995 01 (Hale-Bopp) [cont.]

DATE (UT)	N	MM	MAG.	RF	AP.	T	F/	PWR	COMA	DC	TAIL	PA	OBS.
1997 03 09.77	w	B	-0.3	AA	0.0	E		1	45	6	14		BAR06
1997 03 09.78		S	-0.3	SC	8.0	B		12	30	S7	10	330	ISH03
1997 03 09.78	w	B	0.0	AA	4.0	R		8	25	S7	9	326	BAR06
1997 03 09.80		S	0.0	AA	5.0	B		7	13	8	8	330	MOE
1997 03 09.80	w	M	-0.2	Y	0.0	E		1	30	D8	3.5	320	CAN04
1997 03 09.81		I	0.2	S	0.0	E		1			2	330	TOY
1997 03 09.82	!	S	-0.1	AA	0.0	E		1	&15	7/	11	330	NAG08
1997 03 09.83					2.4	B		10	18	S6	4	305	YOS04
1997 03 09.83	w	B	-0.1	YG	0.0	E		1	&20	8	5	305	YOS04
1997 03 10.06		B	0.0	AA	5.0	B		7	13	D8	15	327	VEL03
1997 03 10.06		G	-0.1	AA	0.0	E		1			15	327	VEL03
1997 03 10.06		S	0.2	AA	11.0	L	7	32	25	6/	7		IYA03
1997 03 10.10		B	-0.1	HD	5.0	B		7	15	S7	10	333	LEH01
1997 03 10.11		B	0.3	AA	3.0	B		7		6	6.6	346	CHV
1997 03 10.12		B	0.5	AA	3.0	B		8	25	8/	4	322	SAL01
1997 03 10.13	w	B	-0.3	AA	0.0	E		1		6/	14	328	CHE03
1997 03 10.14		S	-1.0	AA	6.3	R	13	52	14	S9		340	KOS
1997 03 10.14	a	M	-0.2	AA	0.6	E		1		S8	12		MEY
1997 03 10.14	a	M	-0.4	S	5	R		1	35	7/	13	330	HOR02
1997 03 10.15	w	G	-0.4	AA	0.6	E		1		S8/	14	332	KAM01
1997 03 10.16	a	O	-0.1	SP	0.0	E		1	30	7	9	335	ZNO
1997 03 10.16	w	B	-0.4	AA	0.0	E		1	15	8	13	330	VAN06
1997 03 10.17	a	B	-0.1	AA	0.7	E		1		8	12	331	BOU
1997 03 10.17	a	B	-0.2	AT	0.0	E		1			6		MIL02
1997 03 10.17	w	G	-0.5	YF	0.0	E		1	&12	S9	11	70	ZEK
1997 03 10.18	!	V	-0.1	YF	2.3	A	4 a	3	+32	8	>6	325	MIK
1997 03 10.22	a	I	0.5	AT	0.0	E		1			12	310	VIT01
1997 03 10.23	a	G	0.7	AT	0.0	E		1					VIT01
1997 03 10.23	a	I	0.1	AT	0.0	E		1	>30	7	25	330	PER01
1997 03 10.24	a	G	0.4	AT	0.0	E		1					PER01
1997 03 10.25	!	B	-0.3	YG	0.7	E		1		9	24		DAH
1997 03 10.40	a	G	-0.4	SC	0.0	E		1	18	8	>5	300	CRE01
1997 03 10.70		B	0.2	HD	3.5	B		7	18	S7/	9	332	HAR09
1997 03 10.71		G	-1.0	Y	0.0	E		1		8			MOS03
1997 03 10.74					5.0	B		7	17	D8	&8	329	VEL03
1997 03 10.74	w	M	-0.5	AA	0.0	E		1		6/	8	301	CHE03
1997 03 10.75		B	0.4	AA	3.0	B		7		7	6.5	342	CHV
1997 03 10.76	!	S	-0.4	AA	0.0	E		1					ANZ
1997 03 10.76	a	M	0.0	S	0.0	E		1	20	8	14		KON06
1997 03 10.77	a	M	-0.3	S	5	R		1	30	7/	8	330	HOR02
1997 03 10.77	a	O	0.3	S	0.0	E		1	35		3		LIB
1997 03 10.78		S	-0.2	AA	5.0	B		10	15	8	11	335	MOE
1997 03 10.79		S	-0.2	SC	0.7	E		1	15		>4		MCK
1997 03 10.79	!	G	0.9	AA	0.7	E		1	9	8	0.5	305	SHA02
1997 03 10.80		S	1.2	AA	7.0	B		16	10	6	1.2	340	TAY
1997 03 10.81					2.4	B		10	15	S6	3	310	YOS04
1997 03 10.81		I	0.6	S	0.0	E		1			1	310	TOY
1997 03 10.81	a	B	0.2	YG	0.0	E		1	&15	8	3	310	YOS04
1997 03 10.82	!	S	-0.3	SC	0.0	E		1	32	D7	9	330	SHI
1997 03 11.00		S	0.2	AA	11.0	L	7	32	25	6/	7		IYA03
1997 03 11.07		B	-0.2	HD	5.0	B		7	15	S8	7	335	MOR04
1997 03 11.08		S	0.2	AA	6	R	10	16	19	7	6	305	ROM
1997 03 11.10		B	-0.2	HD	5.0	B		7	15	S7	10	334	LEH01
1997 03 11.11		B	0.4	AA	3.0	B		8	23	9	4	322	SAL01
1997 03 11.11		B	0.4	AA	5.0	B		7		D8	15	330	VEL03
1997 03 11.11		S	-0.8	AA	6.0	B		20		8			SCU
1997 03 11.12		M	0.3	AA	3.0	R	4	7	18	6	5		MAI
1997 03 11.12	w	B	0.0	AA	4.0	R		8	30	S7	10		BAR06
1997 03 11.12	w	B	-0.3	AA	0.0	E		1	45	5	16		BAR06
1997 03 11.13		B	0.0	AA	2.0	B		2	9	8	10.5	336	KOZ
1997 03 11.13	w	B	-0.5	AA	0.0	E		1	24	6/	18	333	CHE03
1997 03 11.14		S	-1.1	AA	6.3	R	13	52	14	S9		352	KOS
1997 03 11.14	!	B	-0.3	Y	0.0	E		1	13	S7/	3	305	SAR02
1997 03 11.14	a	G	-0.2	AA	0.8	E		1			6.6	325	HAS02
1997 03 11.14	a	I	-0.4	AA	0.8	E		1			13.8	335	HAS02

Comet C/1995 01 (Hale-Bopp) [cont.]

DATE (UT)	N	MM	MAG.	RF	AP.	T	F/	PWR	COMA	DC	TAIL	PA	OBS.
1997 03 11.14	a	M	-0.1	AA	0.6	E		1		S8	13		MEY
1997 03 11.15	a	M	-0.4	S	5	R		1	35	7/	13	330	HOR02
1997 03 11.16		M	-0.2	Y	10	B		25	35		3.5		HYN
1997 03 11.16		S	0.3	AA	0.7	E		1	17	S2	13	346	CSU
1997 03 11.16	w	B	-0.6	AA	0.0	E		1	15	8	13	330	VAN06
1997 03 11.17	!	V	-0.1	YF	2.3	A	4 a	3	+32	8	>6		MIK
1997 03 11.17	a	O	-0.3	SP	0.0	E		1	25	8	12	335	ZNO
1997 03 11.20	!	B	0.2	YF	0.5	E		1	18	8	7	325	ENT
1997 03 11.21		B	1.0	AA	4.0	B		8	15	6	2.2	330	TAY
1997 03 11.21		B	-0.5	SC	0.7	E		1		5	6		ROG02
1997 03 11.24		B	-0.3	YG	0.7	E		1		8	17		DAH
1997 03 11.42	a	G	-0.4	SC	0.0	E		1	12	9	15	320	CRE01
1997 03 11.51	w	S	0.1	AA	5.0	B		7	9	8/	8	325	SPR
1997 03 11.70		B	0.0	HD	3.5	B		7	15	S7/	6	333	HAR09
1997 03 11.72		I	-0.6	SC	0.0	E		1	30	S7	15	335	ISH03
1997 03 11.74	a	M	-0.3	Y	0.0	E		1			3		HYN
1997 03 11.74	w	B	-0.4	AA	0.0	E		1		6/			CHE03
1997 03 11.76		B	0.2	AA	0.0	E		1					STO
1997 03 11.76	a	O	-0.3	SP	0.0	E		1	25	8	16	335	ZNO
1997 03 11.77		B	0.4	AA	3.0	B		7		6	8		CHV
1997 03 11.77	a	M	-0.3	S	5	R		1	30	7/	13	340	HOR02
1997 03 11.77	a	M	-0.3	S	5	R		1	40	7/	15	335	PLS
1997 03 11.77	a	O	0.2	S	0.0	E		1	40		4		LIB
1997 03 11.78	a	M	0.0	S	0.0	E		1	20	8	14		KON06
1997 03 11.78	w	B	-0.2	AA	0.0	E		1	50	5	16		BAR06
1997 03 11.79		S	0.0	SC	0.7	E		1	20	9	>5		MCK
1997 03 11.79	w	M	0.0	AA	4.0	R		8	30	S7	10		BAR06
1997 03 11.80	!	G	0.3	AA	0.7	E		1	4	8	4	308	SHA02
1997 03 11.81	!	S	-0.2	AA	0.0	E		1	15	7/	5	300	NAG08
1997 03 11.81	w	M	-0.3	Y	0.0	E		1	25	D8	4	320	CAN04
1997 03 11.85	a	B	-0.3	YG	0.0	E		1			3	325	NAK01
1997 03 11.99	—	S	0.2	AA	11.0	L	7	32	25	6/	7		IVA03
1997 03 12.07		B	-0.3	HD	5.0	B		7	18	S8	5	336	MOR04
1997 03 12.08		S	0.2	AA	6	R	10	16	20	6	7	315	ROM
1997 03 12.10		B	-0.3	HD	5.0	B		7	15	S7	10	335	LEH01
1997 03 12.10		B	-0.3	HD	5.0	B		7	20	S8	10	335	MOR04
1997 03 12.10	w	B	-0.3	AA	0.0	E		1	50	5	16		BAR06
1997 03 12.10	w	M	-0.1	AA	4.0	R		8	35	S7	10		BAR06
1997 03 12.11		M	0.3	AA	3.0	R	4	7	20	6	5		MAI
1997 03 12.12		B	0.5	AA	3.0	B		7		6	9.5		CHV
1997 03 12.12		S	-0.5	AA	6.0	B		20		8			SCU
1997 03 12.13	w	B	-0.9	SC	0.0	E		1		8			RAD01
1997 03 12.14		S	-0.1	SC	0.6	E		1	12	8/	10	300	OKS
1997 03 12.14	a	M	-0.1	AA	0.6	E		1		S8	8		MEY
1997 03 12.14	a	M	-0.4	S	5	R		1	40	7/	17	340	HOR02
1997 03 12.15	a	G	-0.2	AA	0.8	E		1			5.9	330	HAS02
1997 03 12.15	a	I	-0.4	AA	0.8	E		1			12.5	350	HAS02
1997 03 12.15	a	M	-0.3	S	5	R		1	35	7/	10	335	PLS
1997 03 12.15	a	O	-0.3	SP	0.0	E		1	30	8	17	335	ZNO
1997 03 12.16	a	B	-0.4	AA	0.0	E		1		8	15		MIL02
1997 03 12.16	s	G	-0.5	AA	0.6	E		1		S8/	11	326	KAM01
1997 03 12.17	!	V	-0.2	YF	2.3	A	4 a	3	+32	8	>6		MIK
1997 03 12.20	!	B	-0.1	YF	0.5	E		1	18	8	7	322	ENT
1997 03 12.22		M	-0.6	S	5.0	B		7	15	S8/	13		GON05
1997 03 12.23	a	B	0.4	AT	3.5	R		1					PER01
1997 03 12.23	a	B	0.4	AT	3.5	R		1					VIT01
1997 03 12.23	a	G	0.3	AT	0.0	E		1					PER01
1997 03 12.23	a	G	0.6	AT	0.0	E		1					VIT01
1997 03 12.23	a	I	0.3	AT	0.0	E		1			18	310	VIT01
1997 03 12.23	a	I	-0.1	AT	0.0	E		1			16	330	PER01
1997 03 12.41	w	B	-0.2	Y	0.0	E		1		8/	15		GRE
1997 03 12.51	s	S	0.0	AA	0.0	E		1	10	9	8	320	SPR
1997 03 12.70		B	-0.3	HD	5.0	B		7	19	S8	10	340	MOR04
1997 03 12.75	a	O	-0.3	SP	0.0	E		1	22	8/	15	335	ZNO
1997 03 12.75	w	B	-0.7	SC	0.0	E		1		9			VAL01

April 1997

123

INTERNATIONAL COMET QUARTERLY

Comet C/1995 01 (Hale-Bopp) [cont.]

DATE (UT)	N	MM	MAG.	RF	AP.	T	F/	PWR	COMA	DC	TAIL	PA	OBS.
1997 03 12.75	w	B	-0.8	SC	0.0	E		1		9			RAD01
1997 03 12.77	a	M	0.0	S	0.0	E		1	20	8	14		KON06
1997 03 12.77	a	M	-0.5	S	3	R		1	40	7/	8	335	PLS
1997 03 12.77	a	M	-0.5	S	5	R		1	30	7/	10	340	HOR02
1997 03 12.77	a	M	-0.5	Y	10	B		25	30	6	4	325	HYN
1997 03 12.77	a	0	0.1	S	0.0	E		1	35		4		LIB
1997 03 12.77	w	B	-0.2	AA	0.0	E		1	50	5	16		BAR06
1997 03 12.78	w	M	0.0	AA	4.0	R		8	35	S7	9		BAR06
1997 03 12.79	S	-0.5	SC	0.7	E			1	30	6	3		MCK
1997 03 12.80	!	G	0.3	AA	0.7	E		1	6	8	3.5	320	SHAO2
1997 03 12.80	a	0	-0.2:	Y	0.0	E		1	15	9	>2		KYS
1997 03 12.83	w	B	-0.5:	AA	0.0	E		1		6/			CHE03
1997 03 12.99	w	B	-0.5	Y	0.0	E		1		8			GRE
1997 03 13.05	S	0.1	AA	11.0	L		7	32	30	6/	9		IYA03
1997 03 13.07	B	0.5	SC	7.0	B			40			5		CHA02
1997 03 13.08	B	1.6:	AA	5.0	B			7	9	6	3.3		HOM
1997 03 13.10	B	-0.3	HD	5.0	B			7	17	S7	10	340	LEH01
1997 03 13.10	B	-0.3	HD	5.0	B			7	19	S8	10	340	MOR04
1997 03 13.10	G	-1.5:	Y	0.0	E			1		8			MOS03
1997 03 13.11	M	0.3	AA	3.0	R		4	7	20	6	5		MAI
1997 03 13.13	B	0.4	SC	7.0	B			40			6		HAN04
1997 03 13.13	B	0.5	SC	7.0	B			40			6		GEN01
1997 03 13.14	a	M	-0.4	S	5	R		1	40	7/	17	340	HOR02
1997 03 13.15	!	S	-0.4	AA	0.0	E		1			13		ANZ
1997 03 13.15	w	M	-0.4	Y	0.0	E		1	30	D8	18	325	CAN04
1997 03 13.17	!	V	-0.3	YF	2.3	A	4 a	3	+32	8	>6		MIK
1997 03 13.20	B	-0.5	SC	0.7	E			1		5	7.5		ROG02
1997 03 13.23	B	-1.5	SC	6.3	R			53		7	10.5		POP01
1997 03 13.23	a	B	0.3	AT	3.5	R		1					PER01
1997 03 13.23	a	B	0.4	AT	3.5	R		1					VIT01
1997 03 13.23	a	G	0.2	AT	0.0	E		1					PER01
1997 03 13.23	a	G	0.4	AT	0.0	E		1					VIT01
1997 03 13.23	a	I	0.1	AT	0.0	E		1			24	335	VIT01
1997 03 13.23	a	I	-0.2	AT	0.0	E		1			28	335	PER01
1997 03 13.39	fw	B	-0.4	Y	0.0	E		1		8	&20		GRE
1997 03 13.66	a	M	-0.3	SC	0.0	E		1			20		OME
1997 03 13.70	B	-0.3	HD	5.0	B			7	15	S8	6	345	MOR04
1997 03 13.72	a	S	0.2	AA	0.7	E		1	20	8	3	320	MEN03
1997 03 13.75	w	B	-0.7	SC	0.0	E		1		9			RAD01
1997 03 13.82	S	-0.3	AA	5.0	B			10	15	8	7	345	MOE
1997 03 13.82	S	-0.5	SC	0.7	E			1	30	6	5		MCK
1997 03 13.99	S	0.1	AA	11.0	L		7	32	30	6/	9		IYA03
1997 03 13.99	fs	B	-0.5:	Y	0.0	E		1					GRE
1997 03 14.09	B	0.5	SC	7.0	B			40			5		HAN04
1997 03 14.10	B	-0.4	HD	5.0	B			7	15	S7	11	339	LEH01
1997 03 14.12	B	0.5	SC	7.0	B			40			6		GEN01
1997 03 14.16	a	B	-0.5	AA	0.0	E		1		8	18		MIL02
1997 03 14.22	S	0.6	SC	6.3	B			9	6	7	4		DINO1
1997 03 14.50	s	S	-0.0	AA	0.0	E		1	11	9	10	325	SPR
1997 03 14.70	B	-0.2	HD	3.5	B			7	15	S7/	6	338	HAR09
1997 03 14.70	B	-0.3	HD	5.0	B			7	15	S8			MOR04
1997 03 14.80	w	M	-0.4	Y	0.0	E		1	30	D8	4	325	CAN04
1997 03 15.10	B	-0.4	HD	5.0	B			7	16	S7	11	340	LEH01
1997 03 15.45	w	B	-0.5	YF	0.0	E		1		S8/	15	338	ADA03
1997 03 15.45	w	M	-0.3	YF	5.0	R		1					ADA03
1997 03 15.49	s	S	-0.3	AA	0.0	E		1	12	9/	10	325	SPR
1997 03 15.70	B	-0.3	HD	3.5	B			7	15	S7/	5	340	HAR09
1997 03 15.79	!	G	0.6	AA	0.7	E		1	10	8	2		SHAO2
1997 03 15.85	!	B	-0.1	AA	4.0	B		8	25	6	4	354	TAY
1997 03 15.88	S	-0.4	AA	5.0	B			10	16	8	12	350	MOE
1997 03 15.95	w	B	-0.7	AA	0.0	E		1		6/	8	330	CHE03
1997 03 15.99	fw	B	-0.5	Y	0.0	E		1		8	&2		GRE
1997 03 16.06	S	0.0	AA	11.0	L		7	32	30	6/	10		IYA03
1997 03 16.10	!	B	-0.6	YG	0.7	E		1		8/	14		SKI
1997 03 16.12	!	B	-0.2	YG	0.7	E		1		8/	13	340	GRA04

Comet C/1995 01 (Hale-Bopp) [cont.]

DATE (UT)	N	MM	MAG.	RF	AP.	T	F/	PWR	COMA	DC	TAIL	PA	OBS.
1997 03 16.12	!	N	1.8	YG	5.0	B		10	17	8	13		GRA04
1997 03 16.16	!	S	0.0	AA	0.7	E		1	25	8	3	320	MEN03
1997 03 16.17	!	S	-0.5	AA	0.0	E		1					ANZ
1997 03 16.17	!	V	-0.3	YF	2.3	A	4 a	3	+32	8	>6		MIK
1997 03 16.22	a	B	0.1	AT	3.5	R		1					VIT01
1997 03 16.22	a	G	0.3	AT	0.0	E		1					PER01
1997 03 16.22	a	G	0.3	AT	0.0	E		1					VIT01
1997 03 16.23	a	B	0.3	AT	3.5	R		1					PER01
1997 03 16.23	a	I	-0.4	AT	0.0	E		1			12	310	VIT01
1997 03 16.23	ra	I	-0.4	AT	3.4	B		9					PER01
1997 03 16.23	a	I	-0.6	AT	0.0	E		1			16	310	PER01
1997 03 16.38	w	B	-0.6	Y	0.0	E		1		8	15		GRE
1997 03 16.75					5.0	B		7	14	D7	&7	339	VELO3
1997 03 16.80	w	M	-0.5	Y	0.0	E		1	30	D8	6	320	CAN04
1997 03 16.83	!	B	-0.2	YG	0.7	E		1		8/	13	340	GRA04
1997 03 16.88	!	B	0.4	AA	7.0	B		16	10	D6	5	334	TAY
1997 03 16.97	!	B	-0.7:	YG	0.7	E		1		8/	5		SKI
1997 03 16.99	!	N	1.7	YG	5.0	B		10	15	7/			GRA04
1997 03 16.99	!	N	4.8	YG	20.3	T	10	123					GRA04
1997 03 16.99	w	B	-0.4	Y	0.0	E		1		8			GRE
1997 03 17.03	a	G	-0.6:	SC	0.0	E		1	15	9	4	330	CRE01
1997 03 17.08		B	0.8:	AA	5.0	B		7	9	6	6.7		HOM
1997 03 17.08	w	B	-0.5	AA	0.0	E		1	60	5	16		BAR06
1997 03 17.09	w	M	-0.2	AA	4.0	R		8	35	S7	10		BAR06
1997 03 17.10	w	M	-0.8	AA	0.0	E		1	25	7	14	350	CHE03
1997 03 17.13		B	-0.3	AA	2.0	B		2	12	8	9	354	KOZ
1997 03 17.13		G	-0.2	AA	0.0	E		1	19	D8	14	342	VELO3
1997 03 17.15	!	G	0.5	LN	0.7	E		1	10	8	2	314	SHA02
1997 03 17.15	a	B	-0.4	AA	0.7	E		1		8			BOU
1997 03 17.17	!	G	0.3	LN	0.8	E		1	12	8	10	341	SHA02
1997 03 17.20		B	-0.9	SC	0.7	E		1		5	7		ROG02
1997 03 17.22	a	B	0.4	AT	3.5	R		1					VIT01
1997 03 17.22	a	G	0.2	AT	0.0	E		1					PER01
1997 03 17.22	a	G	0.3	AT	0.0	E		1					VIT01
1997 03 17.22	a	I	-0.5	AT	0.0	E		1					VIT01
1997 03 17.22	a	I	-0.5	AT	0.0	E		1			10	300	PER01
1997 03 17.23		B	-0.2	AA	5.0	B		7	12	D8	15	342	VELO3
1997 03 17.23	a	B	0.3	AT	3.5	R		1					PER01
1997 03 17.23	ra	I	-0.5	AT	3.4	B		9					PER01
1997 03 17.38	fw	B	-0.6	Y	0.0	E		1		8/	&15		GRE
1997 03 17.70		B	-0.4	HD	3.5	B		7	15	S7/	5	340	HAR09
1997 03 17.70	w	B	-0.9	SC	0.0	E		1		9			RAD01
1997 03 17.74					5.0	B		7	12	D8	&6	346	VELO3
1997 03 17.74		G	0.0	HD	0.0	E		1	20	8	6		BRU
1997 03 17.75		B	-0.5	HD	5.0	B		7	19	S8	5	340	MOR04
1997 03 17.79	a	M	-0.7	S	5	R		1	30	7/	8	320	HOR02
1997 03 17.79	a	O	-0.1	S	0.0	E		1	40		5		LIB
1997 03 17.79	a	O	-0.5	SP	0.0	E		1	40	8	11	345	ZNO
1997 03 17.80	w	B	-0.7	AA	0.0	E		1	60	5	16		BAR06
1997 03 17.80	w	M	-0.6	Y	0.0	E		1	30	D8	6.5	320	CAN04
1997 03 17.81	!	S	-0.4	AA	0.0	E		1	&15	7/	12	350	NAG08
1997 03 17.81	w	M	-0.3	AA	5.0	B		7	35	S7	10		BAR06
1997 03 17.82		S	-0.5	AA	5.0	B		10	16	8	11	350	MOE
1997 03 17.82	!	B	-0.6	YG	0.7	E		1		8	7		SKI
1997 03 17.83		M	-0.6	AA	0.0	E		1	&20	8	&4	320	PAL02
1997 03 17.84	!	S	-0.5	YG	0.7	E		1					HEE
1997 03 18.01	!	B	-0.3	YG	0.7	E		1		8/	6	330	GRA04
1997 03 18.09		B	-0.5	HD	5.0	B		7	16	S8	11	340	MOR04
1997 03 18.10		S	0.0	AA	6	R	10	16	21	8	7	310	ROM
1997 03 18.13		S	-1.5	AA	6.3	R	13	52	15	S9		353	KOS
1997 03 18.14	w	M	-0.7	Y	0.0	E		1	25	D8	20	320	CAN04
1997 03 18.15	a	M	-0.6	S	5	R		1	30	7/	15	345	HOR02
1997 03 18.15	a	M	-0.6	TI	5	R		1	35	8	8	295	DVO
1997 03 18.20		S	0.0	SC	3.0	B		8		7	10	45	DIN01
1997 03 18.21		M	-0.7	S	5.0	B		7	20	S8/	15		GON05

April 1555

125

INTERNATIONAL COMET QUARTERLY

Comet C/1995 01 (Hale-Bopp) [cont.]

DATE (UT)	N	MM	MAG.	RF	AP.	T	F/	PWR	COMA	DC	TAIL	PA	OBS.
1997 03 18.22	a	B	-0.2	AT	3.5	R		1					PER01
1997 03 18.22	a	G	0.2	AT	0.0	E		1					PER01
1997 03 18.22	a	I	-0.6	AT	0.0	E		1					PER01
1997 03 18.22	ra	I	-0.6	AT	3.4	B		9			11	315	PER01
1997 03 18.38	a	B	-0.6	Y	0.0	E		1					PER01
1997 03 18.72	!	B	-0.5	AA	0.7	E		1	20	8/	&5		GRE
1997 03 18.74		B	0.6:	AA	3.0	B		7		8	2.5	325	MEN03
1997 03 18.75		B	0.3	SC	3.5	R	5	30	5.5	6			CHV
1997 03 18.76	a	O	-0.5:	Y	5.0	B		7	15	8/	2.67	319	APE
1997 03 18.84	a	B	-0.7	AA	0.0	E		1	20	8	>3		KYS
1997 03 19.05	!	B	-0.4	YG	0.7	E		1		7	9	345	CHE03
1997 03 19.05	!	N	1.6	YG	5.0	B		10	&15	8	6		GRA04
1997 03 19.08		B	-0.6	HD	5.0	B		7	16	7/	9	347	GRA04
1997 03 19.10		S	-0.1	AA	6	R	10	16	21	S8	12	352	MOR04
1997 03 19.13		G	-0.5	AA	0.0	E		1		8	7	310	ROM
1997 03 19.16	!	B	-0.5	YG	0.7	E		1			15	344	VELO3
1997 03 19.19		S	-1.0	AA	5.0	B		8	40	8/	7		SKI
1997 03 19.80	!	G	0.2	SC	0.7	E		1	12	8	10	335	BEA
1997 03 19.80	!	G	0.6	SC	5.0	B		7	12	8	2	323	SHA02
1997 03 19.80	w	M	-0.8	Y	0.0	E		1	30	8	2.2	323	SHA02
1997 03 19.81	a	B	-0.8	AA	0.0	E		1	22	D8	7	325	CAN04
1997 03 19.84	!	B	-0.3	AA	4.0	B		8	12	7	6	308	CHE03
1997 03 19.84	!	B	-0.7	YG	0.7	E		1		D6	3.2	315	TAY
1997 03 19.91		S	-1.0	AA	5.0	B		8	40	8/	12	346	SKI
1997 03 19.99	fs	B	-0.5:	Y	0.0	E		1		8	5	335	BEA
1997 03 20.04		S	-0.2	AA	11.0	L	7	32	30	8	&2.5		GRE
1997 03 20.17	!	B	-0.3	YG	0.7	E		1		6/	7		IVA03
1997 03 20.17	!	N	1.7	YG	5.0	B		10		8/	4		GRA04
1997 03 20.18	!	N	5.0	YG	20.3	T	10	123		8	12		GRA04
1997 03 20.45	w	B	-0.9	AE	0.0	E		1					GRA04
1997 03 20.45	w	M	-0.6	AE	5.0	R		1		S9	10	350	ADA03
1997 03 20.77		S	-0.2	AA	5.0	B		10	50	7	1.1	325	FOG
1997 03 20.78	a	O	-0.7	SP	0.0	E		1	35	8/	8	315	ZNO
1997 03 20.80	w	B	-0.6	AA	0.0	E		1	70	5			BAR06
1997 03 20.81	w	M	-0.3	AA	4.0	R		8	40	S7	8		BAR06
1997 03 20.90		I	-0.6	AA	0.8	E		1	15	8	7	340	MOE
1997 03 20.90		S	-1.1	AA	5.0	B		8	40	8	10	335	BEA
1997 03 21.04	s	G	-0.8	SC	0.0	E		1	20	9	5	330	CRE01
1997 03 21.06	!	B	-0.9	YG	0.7	E		1		8/	5		SKI
1997 03 21.10	a	I	-0.5	AA	0.8	E		1					HAS02
1997 03 21.10	w	M	-0.3	AA	4.0	R		8	40	S7	8		BAR06
1997 03 21.11	!	B	-0.3	YG	0.7	E		1		8	6		GRA04
1997 03 21.12	!	N	1.6	YG	5.0	B		10	15	8	12	352	GRA04
1997 03 21.12	w	B	-0.6	AA	0.0	E		1	70	5			BAR06
1997 03 21.21		M	-0.8	S	5.0	B		7	20	S8/	12		GON05
1997 03 21.38	w	B	-0.8	Y	0.0	E		1		8	&5		GRE
1997 03 21.75	!	M	-0.6	Y	0.0	E		1	13	S7	4	340	SAR02
1997 03 21.75	w	B	-0.5	AA	0.0	E		1	60	5			BAR06
1997 03 21.76	a	B	-0.7	AA	0.0	E		1			5		MIL02
1997 03 21.76	a	M	-0.7:	AA	0.0	E		1		6/			CHE03
1997 03 21.78		G	-0.1	AA	0.0	E		1	25	9	4	330	SER
1997 03 21.80		G	0.3:	SC	0.7	E		1	10	8	&2		SHA02
1997 03 21.80	!	S	-0.6	AA	5.0	B		10	16	8	8	340	MOE
1997 03 21.80	!	B	-0.4	YG	0.7	E		1		8/	6		GRA04
1997 03 21.80	!	N	1.6	YG	5.0	B		10	15	7/	6	336	GRA04
1997 03 21.80	a	M	-0.7	SC	0.0	E		1	15	8	4	315	GLI
1997 03 21.80	w	M	-0.3	AA	4.0	R		8	40	S7	9		BAR06
1997 03 21.80	w	M	-1.0	Y	0.0	E		1	25	D8	8	330	CAN04
1997 03 21.82		S	-1.2	AE	5.0	B		8	40	8	5	340	BEA
1997 03 21.84					5.0	B		7	15	7	5.5	332	DIE02
1997 03 21.84	S	-0.3	AA	0.0	E			1					DIE02
1997 03 21.84	a	B	-0.6	AA	0.7	E		1		8			BOU
1997 03 22.10	w	M	-0.2:	AA	4.0	R		8	40	S7	10		BAR06
1997 03 22.12	w	B	-0.5:	AA	0.0	E		1	60	5			BAR06
1997 03 22.14	a	B	-0.7	AA	0.7	E		1		8	11	328	BOU

Comet C/1995 01 (Hale-Bopp) [cont.]

DATE (UT)	N	MM	MAG.	RF	AP.	T	F/	PWR	COMA	DC	TAIL	PA	OBS.
1997 03 22.16	s	M	-0.5	SC	0.0	E		1	15	8	15	320	GLI
1997 03 22.20	a	S	-0.7	AA	0.0	E		1	7	9	14	325	SPR
1997 03 22.21		M	-0.6	S	5.0	B		7	20	S8/	7		GON05
1997 03 22.76	a	G	-0.2	AA	0.0	E		1	20	9			NEV
1997 03 22.79		I	-0.9	SC	0.0	E		1	35	S7	>10	15	ISH03
1997 03 22.79		S	-0.5	AA	5.0	B		10	18	8	8	340	MOE
1997 03 22.79	s	M	-0.7	SC	0.0	E		1	12	8	7	330	GLI
1997 03 22.81	a	G	-0.4	AA	0.6	E		1		S8/	&6	326	KAM01
1997 03 22.81	w	M	-1.1	Y	0.0	E		1	25	D8	7	325	CAN04
1997 03 22.82	a	O	-0.7	SP	0.0	E		1	30	8/	6	320	ZNO
1997 03 22.83	a	M	-0.9	AA	0.0	E		1	22	6/			CHE03
1997 03 22.88	!	B	-0.6	YG	0.7	E		1		8/	7		SKI
1997 03 22.89	!	B	0.3	AA	4.0	B		8	18	D6	3	351	TAY
1997 03 23.00	!	M	-0.7	YG	0.7	E		1		8/	5		GRA04
1997 03 23.00	!	N	1.5	YG	5.0	B		10	15		5	355	GRA04
1997 03 23.08	w	M	-0.1	AA	4.0	R		8	40	S7	10		BAR06
1997 03 23.11	w	B	-0.4	AA	0.0	E		1	50	5			BAR06
1997 03 23.15	a	O	-0.2	Y	5.0	B		7	15	9	8		KYS
1997 03 23.16	a	O	-0.6	Y	0.0	E		1	15	9	8		KYS
1997 03 23.38	w	B	-0.8	Y	0.0	E		1		8	&5		GRE
1997 03 23.73	w	B	-0.4	SC	0.0	E		1		8			RAD01
1997 03 23.74					5.0	B		7	13	D8	&6	351	VELO3
1997 03 23.74		G	-0.7	AA	0.0	E		1	18	D8			VELO3
1997 03 23.76	a	O	-0.4	S	0.0	E		1	40		8		LIB
1997 03 23.77	a	O	-0.7	SP	0.0	E		1	25	8	11	2	ZNO
1997 03 23.78	w	B	-0.5	AA	0.0	E		1	50	5			BAR06
1997 03 23.79	a	M	-0.8	S	5	R		1	30	7/	5	340	PLS
1997 03 23.80	w	M	-0.2	AA	4.0	R		8	40	S7	9		BAR06
1997 03 23.83	a	M	-0.6	TI	5	R		1	30	7	3	295	DVO
1997 03 24.02	w	B	-0.6	Y	0.0	E		1		8	&2.5		GRE
1997 03 24.04	w	G	-0.8	SC	0.0	E		1	20	9	6	340	CRE01
1997 03 24.07	w	M	-0.2	AA	4.0	R		8	30	S7	9		BAR06
1997 03 24.18	a	S	-0.5	AA	0.0	E		1	10	9	9	320	SPR
1997 03 24.38	a	B	-0.6	Y	0.0	E		1		8	&4		GRE
1997 03 24.78		S	0.3	AA	0.7	E		1	17	S2/	32	342	CSU
1997 03 24.80		I	-1.0	SC	0.0	E		1	35	S7	>10	17	ISH03
1997 03 24.84	!	B	0.2	AA	4.0	B		8	24	D6	3.2	12	TAY
1997 03 24.86	!	B	-0.3	YG	0.7	E		1		8	5.5		SKI
1997 03 24.86	!	M	-0.6	YG	0.7	E		1		8/	6		GRA04
1997 03 24.86	!	N	1.7	YG	5.0	B		10	20	8	6	345	GRA04
1997 03 24.97	!	G	-0.3	SC	0.7	E		1	10	8	2.6	349	SHA02
1997 03 25.00	fw	B	-0.6	Y	0.0	E		1		8	&4		GRE
1997 03 25.07		N	4.9	YG	20.3	T	10	80					GRA04
1997 03 25.12	a	B	-0.5	AA	0.0	E		1	40	6			BAR06
1997 03 25.12	a	M	-0.4	AA	4.0	R		8	20	S7			BAR06
1997 03 25.74	w	B	-0.5	SC	0.0	E		1		9			VELO2
1997 03 25.75	a	G	-0.2	AA	0.0	E		1	23	9	8	357	NEV
1997 03 25.75	w	B	-0.6	SC	0.0	E		1		9			RAD01
1997 03 25.77	a	B	-1.0	AA	0.0	E		1			4		MIL02
1997 03 25.79	a	B	-0.6	AA	0.0	E		1	40	5			BAR06
1997 03 25.79	a	M	-1.2	AA	0.0	E		1		7	15	0	CHE03
1997 03 25.80		M	-0.8	AA	0.0	E		1	&20	8	&5	320	PAL02
1997 03 25.80	a	M	-0.4	AA	4.0	R		8	23	S8			BAR06
1997 03 25.84		M	-1.1	S	5.0	B		7	20	S8/	10		GON05
1997 03 25.84		S	-0.5	S	0.7	E		1			6	348	THO03
1997 03 26.12	a	B	-0.5	AA	0.0	E		1	35	6			BAR06
1997 03 26.12	a	M	-0.3	AA	4.0	R		8	22	S7			BAR06
1997 03 26.12	w	M	-1.0	Y	0.0	E		1	25	D8	6	330	CAN04
1997 03 26.75	a	G	0.0	AA	0.0	E		1	23	9	8	358	NEV
1997 03 26.75	w	B	-0.6	SC	0.0	E		1		8			RAD01
1997 03 26.76	a	B	-0.6	AA	0.0	E		1	40	6			BAR06
1997 03 26.76	a	M	-0.5	AA	4.0	R		8	20	S7			BAR06
1997 03 26.77					5.0	B		7	18	D8	10	4	VELO3
1997 03 26.77		G	-0.9	AA	0.0	E		1					VELO3
1997 03 26.77		S	0.0	AA	0.7	E		1	17	S2/			CSU

Comet C/1995 01 (Hale-Bopp) [cont.]

DATE (UT)	N	MM	MAG.	RF	AP.	T	F/	PWR	COMA	DC	TAIL	PA	OBS.
1997 03 26.79	a	S	-0.7	SC	0.6	E		1	20	8/	>10	345	OKS
1997 03 26.81	a	M	-1.2	AA	0.0	E		1	20	7	8	343	CHE03
1997 03 26.83		B	-0.8	S	0.0	E		1	15	9	10	5	MAR02
1997 03 26.84		S	-0.5:	S	0.7	E		1			6	345	THD03
1997 03 26.84	!	B	-0.4	AA	4.0	B		8	21	7	3.5	345	TAY
1997 03 26.84	w	G	-0.9	AT	0.0	E		1					PER01
1997 03 26.84	w	I	0.0	AT	0.0	E		1			10	10	VIT01
1997 03 26.85		M	-1.1	S	5.0	B		7	20	S8/	14		GON05
1997 03 26.85		S	-1.4	AE	5.0	B		8	40	8	11	350	BEA
1997 03 26.85	!	B	-0.7	YG	0.7	E		1		8	16	1	SKI
1997 03 26.85	w	B	-0.4	AT	3.5	R		1					VIT01
1997 03 26.85	w	B	-0.5	AT	3.5	R		1					PER01
1997 03 26.85	w	G	-1.1	AT	0.0	E		1					VIT01
1997 03 26.85	rw	I	-1.0	AT	3.4	B		9					PER01
1997 03 26.85	w	I	-1.3	AT	0.0	E		1			10	5	PER01
1997 03 26.85	w	M	-1.1	Y	0.0	E		1	25	D8	9	330	CAN04
1997 03 26.86	!	M	-0.6	YG	0.7	E		1		8/	15	7	GRA04
1997 03 26.87	!	N	1.5	YG	5.0	B		10	27	8	15		GRA04
1997 03 26.91	!	G	-0.2	SC	0.7	E		1	10	7	5.5	347	SHA02
1997 03 27.06	a	G	-0.8	SC	0.0	E		1	20	9	14	0	CRE01
1997 03 27.14	a	B	-0.8	AA	0.7	E		1		8	9.5	337	BOU
1997 03 27.16	a	S	-0.8	AA	0.0	E		1	18	9	14	330	SPR
1997 03 27.26	w	M	-0.7	SC	0.0	E		1			20		OME
1997 03 27.74		B	-0.7	SC	6.3	R		34			3		HAN04
1997 03 27.74		B	-1.0	AA	8.0	B		12	15	9	2.5	340	MEN03
1997 03 27.75		B	-0.7	SC	6.3	R		34			4		FIL06
1997 03 27.75		B	-0.7	SC	6.3	R		34			4		GEN
1997 03 27.76		G	-0.8	AA	0.0	E		1	15	D8	11	2	VELO3
1997 03 27.76	a	B	-0.6	AA	0.0	E		1	40	6	15	5	BAR06
1997 03 27.76	a	M	-0.5	AA	4.0	R		8	20	S7			BAR06
1997 03 27.81		M	-1.0	AA	0.0	E		1	&20	8	10	320	PAL02
1997 03 27.81		S	-0.6	AA	5.0	B		10	22	8	14	10	MOE
1997 03 27.82	w	M	-1.2	Y	0.0	E		1	25	D8	11	335	CAN04
1997 03 27.83		B	-1.8	SC	6.3	R		53		7	12.5		POP01
1997 03 27.83	!	V	-0.5	YF	3.2	A	3 a	1	+34	8	>7		MIK
1997 03 27.85		B	-1.0	S	0.0	E		1	20	9	16	5	MAR02
1997 03 27.85		M	-1.1	S	5.0	B		7	20	S8/	16		GON05
1997 03 27.85	a	B	-0.6	AT	3.5	R		1					VIT01
1997 03 27.85	a	B	-0.7	AT	3.5	R		1					PER01
1997 03 27.85	a	G	-1.2	AT	0.0	E		1					PER01
1997 03 27.85	a	G	-1.2	AT	0.0	E		1					VIT01
1997 03 27.85	ra	I	-0.8	AT	3.4	B		9					PER01
1997 03 27.85	a	I	-1.0	AT	0.0	E		1			10		VIT01
1997 03 27.85	a	I	-1.5	AT	0.0	E		1			10		PER01
1997 03 27.86		B	-0.7	SC	6.3	R		34			4		KOJ01
1997 03 27.89	!	B	-0.9	YG	0.7	E		1		8	15		SKI
1997 03 27.89	a	O	-0.3	S	0.0	E		1	40		3		LIB
1997 03 27.90	!	M	-0.8	YG	0.7	E		1		8/	15	5	GRA04
1997 03 27.90	!	N	1.5	YG	5.0	B		10	26	8	13		GRA04
1997 03 27.97	!	B	0.2	AA	5.0	B		10	12	7	2.2	355	TAY
1997 03 28.02	fw	B	-0.8	Y	0.0	E		1		8	&13		GRE
1997 03 28.05	a	G	-0.8	SC	0.0	E		1	20	9	15	5	CRE01
1997 03 28.07	!	N	4.5	YG	20.3	T	10	123					GRA04
1997 03 28.12	!	G	-0.1	SC	0.7	E		1	10	8	6	339	SHA02
1997 03 28.74		B	-0.7	SC	6.3	R		34			9		CHA02
1997 03 28.74		B	-0.7	SC	6.3	R		34			9		KOJ01
1997 03 28.76		B	-1.0	AA	8.0	B		12	15	9	2.5	330	MEN03
1997 03 28.76		B	-1.9	SC	6.3	R		53		7	12		POP01
1997 03 28.76		S	-0.8	SC	0.6	E		1	12	9	10	350	OKS
1997 03 28.77	a	M	-0.7	Y	0.0	E		1	20	9	15		KYS
1997 03 28.80	a	M	-1.1	S	5	R		1	50	8	16	325	HOR02
1997 03 28.81	a	M	-0.6	S	0.0	E		1	25	9	24		KON06
1997 03 28.81	a	M	-1.0	S	5	R		1	45	7/	16	340	PLS
1997 03 28.81	a	O	-0.9	SP	0.0	E		1	25	8	21	12	ZNO
1997 03 28.82		S	-0.6	AA	5.0	B		10	23	8	15	10	MOE

Comet C/1995 01 (Hale-Bopp) [cont.]

DATE (UT)	N	MM	MAG.	RF	AP.	T	F/	PWR	COMA	DC	TAIL	PA	OBS.
1997 03 28.82	!	B	-0.3	AA	4.0	B		8	18	7	3	358	TAY
1997 03 28.82	w	M	-0.9	SC	0.0	E		1	12	8	12	340	GLI
1997 03 28.84	a	B	-0.8	AA	0.7	E		1		8	15	10	BOU
1997 03 28.85					5.0	B		7	12	7	10	355	DIE02
1997 03 28.85		S	-0.7	AA	0.0	E		1					DIE02
1997 03 28.85	!	G	-0.4	AE	0.8	E		1	10	8	15	12	SHA02
1997 03 28.85	a	G	-1.3	AA	0.8	E		1			8.0	330	HAS02
1997 03 28.85	a	I	-1.4	AT	0.0	E		1			8		VIT01
1997 03 28.88		B	-0.9	S	0.0	E		1	12	9	15	5	MAR02
1997 03 28.88		S	-1.1	AE	5.0	B		8	50	8	12	350	BEA
1997 03 28.89		B	-1.3	S	0.0	E		1		9	20	3	SAN04
1997 03 28.89	!	M	-0.8	YG	0.7	E		1		8/	15	6	GRA04
1997 03 28.89	!	N	1.6	YG	5.0	B		10	25	8	13	350	GRA04
1997 03 28.89	a	O	-0.5	S	0.0	E		1	40		7		LIB
1997 03 28.94	!	B	-0.6	YG	0.7	E		1		8	15		SKI
1997 03 28.98	!	N	4.5	YG	20.3	T	10	123					GRA04
1997 03 29.76		G	-0.9	AA	0.0	E		1			11	7	VEL03
1997 03 29.76		S	0.0	AA	0.7	E		1	17	S2/			CSU
1997 03 29.77		B	-0.5	AA	5.0	B		10	50	8	2.8		FOG
1997 03 29.77		S	-1.8	AA	6.3	R	13	52	25	S9		15	KOS
1997 03 29.78	a	B	-0.4	AA	0.0	E		1			16		MIL02
1997 03 29.79	!	B	-0.9	Y	0.0	E		1	12	S8	13	10	SAR02
1997 03 29.81		G	0.0:	SC	0.7	E		1	10	8	1	360	SHA02
1997 03 29.82		S	-0.6	AA	5.0	B		10	24	8	17	15	MOE
1997 03 29.82	a	M	-0.9	Y	0.0	E		1	20	9	>15		KYS
1997 03 29.83		B	-1.0	S	0.0	E		1	10	9	19	10	MAR02
1997 03 29.83	!	V	-0.4	YF	3.2	A	3 a	1	+34	8	>7		MIK
1997 03 29.83	w	M	-1.2	Y	0.0	E		1	25	D8	15	330	CAN04
1997 03 29.85		M	-0.9	AA	0.0	E		1	25	8	15	330	PAL02
1997 03 29.85		M	-1.1	S	5.0	B		7	20	S8/	19		GON05
1997 03 29.85		S	-1.0	AE	5.0	B		8	40	8	8	355	BEA
1997 03 29.85	a	B	-0.7	AT	3.5	R		1					PER01
1997 03 29.85	a	B	-0.8	AT	3.5	R		1					VIT01
1997 03 29.85	a	G	-1.0	AT	0.0	E		1					PER01
1997 03 29.85	a	G	-1.1	AT	0.0	E		1					VIT01
1997 03 29.85	ra	I	-1.0	AT	3.4	B		9					PER01
1997 03 29.85	a	I	-1.1	AT	0.0	E		1					PER01
1997 03 29.85	a	I	-1.1	AT	0.0	E		1					VIT01
1997 03 29.85	ra	I	-1.3:	AT	3.4	B		9					VIT01
1997 03 29.85	a	O	-0.9	SP	0.0	E		1	25	8/	18	9	ZNO
1997 03 29.86	!	B	-0.6	AA	4.0	B		8	19	7	4.2	360	TAY
1997 03 29.88	a	M	-1.1	S	5	R		1	45	8	12	330	HOR02
1997 03 29.89	a	B	-0.9	Y	10	B		25	40	7	6	345	HYN
1997 03 29.96	!	B	-0.5	YG	0.7	E		1			10		SKI
1997 03 30.13	!	M	-0.7	YG	0.7	E		1		8	9	351	GRA04
1997 03 30.13	!	N	1.7	YG	5.0	B		10	20	7/	8	8	GRA04
1997 03 30.15	!	N	4.7	YG	20.3	T	10	123					GRA04
1997 03 30.75	a	B	-0.8	AA	0.0	E		1	40	6	15		BAR06
1997 03 30.75	a	G	-0.9	AA	0.0	E		1	40	6	15		BAR06
1997 03 30.76		G	-0.9	AA	0.0	E		1					VEL03
1997 03 30.76	a	G	0.0	AA	0.0	E		1	26	9	11	5	NEV
1997 03 30.77	a	M	-1.2	AA	0.0	E		1	30	7	17	14	CHE03
1997 03 30.77	a	O	-0.8	SP	0.0	E		1	20	7	20	8	ZNO
1997 03 30.78		S	-1.8	AA	6.3	R	13	52	25	S9		15	KOS
1997 03 30.78	a	B	-0.4	AA	0.0	E		1			12		MIL02
1997 03 30.78	a	M	-0.8	Y	0.0	E		1	20	9	17		KYS
1997 03 30.79		B	-0.8	AA	0.0	E		1					STO
1997 03 30.79		S	-0.6	AA	5.0	B		10	50	8	3.0	10	FOG
1997 03 30.79		S	-0.7	SC	0.6	E		1	15	8/	9	350	OKS
1997 03 30.79	a	M	-1.1	S	5	R		1	45	7/	19	7	HOR02
1997 03 30.79	a	M	-1.1	S	5	R		1	45	7/	20	5	PLS
1997 03 30.79	a	M	-1.2	TI	5	R		1	40	7/	12		DVO
1997 03 30.80	!	V	-0.5	YF	3.2	A	3 a	1	+34	8	>7		MIK
1997 03 30.81	a	O	-0.6	S	0.0	E		1	35		8		LIB
1997 03 30.82	s	M	-0.9	SC	0.0	E		1	12	8	14	335	GLI

Comet C/1995 01 (Hale-Bopp) [cont.]

DATE (UT)	N	MM	MAG.	RF	AP.	T	F/	PWR	COMA	DC	TAIL	PA	OBS.
1997 03 30.83	a	B	-0.8	AA	0.7	E		1		8	21	12	BOU
1997 03 30.83	w	M	-1.2	Y	0.0	E		1	25	D8	11	330	CAN04
1997 03 30.84	!	G	-0.3	AE	0.8	E		1	9	8	14.5	360	SHA02
1997 03 30.85		M	-1.1	S	5.0	B		7	20	S8/	18		GON05
1997 03 30.85	!	B	-0.2	AA	4.0	B		8	21	8	1	15	TAY
1997 03 30.85	a	M	-0.6	S	0.0	E		1	20	9	24		KON06
1997 03 30.86	!	M	-0.6	YG	0.7	E		1		8	13	348	GRA04
1997 03 30.86	!	N	1.8	YG	5.0	B		10	25	7/	11	355	GRA04
1997 03 30.87					5.0	B		7	12	7	8	355	DIE02
1997 03 30.87	S		-0.7	AA	0.0	E		1					DIE02
1997 03 30.87	a	I	-0.9	AA	0.8	E		1	25	8	11	330	MOE
1997 03 31.00	!	B	-0.8	YG	0.7	E		1			15		SKI
1997 03 31.01	fs	B	-0.5	Y	0.0	E		1		8	17		GRE
1997 03 31.07	w	B	-0.6	AE	0.0	E		1		S9	7	9	ADA03
1997 03 31.78	S		-2.0	AA	6.3	R	13	52	26	S9		20	KOS
1997 03 31.79	a	M	-1.1	S	5	R		1	45	8	14	10	HOR02
1997 03 31.80	a	G	-1.2	AA	0.8	E		1			12.9	332	HAS02
1997 03 31.80	a	O	-0.6	Y	0.0	E		1	20	9	>3		KYS
1997 03 31.83	a	B	-0.9	Y	10	B		25	40	7	10	350	HYN
1997 03 31.83	a	G	-0.5	AA	0.6	E		1		S8/	15	10	KAM01
1997 03 31.83	a	O	-0.5	S	0.0	E		1	35		8		LIB
1997 03 31.83	a	O	-0.7	SP	0.0	E		1	18	8	14		ZNO
1997 03 31.84					5.0	B		7	12	7	8	355	DIE02
1997 03 31.84	S		-0.7	AA	0.0	E		1					DIE02
1997 03 31.84	!	B	-0.1	AA	4.0	B		8	12	8	4.2	15	TAY
1997 03 31.84	a	B	-0.9	AA	0.7	E		1		8	14	14	BOU
1997 03 31.84	a	S	-0.9	AA	5.0	B		10	23	8	17	20	MOE
1997 03 31.85		B	-1.0	S	0.0	E		1	20	9	14	15	MAR02
1997 03 31.85		M	-1.1	S	5.0	B		7	20	S8/	16		GON05
1997 03 31.85	S		-1.0	AE	5.0	B		8	40	8	8	360	BEA
1997 03 31.85	!	G	-0.7	AE	0.8	E		1	12	8	16	350	SHA02
1997 03 31.85	a	G	-0.9	AT	0.0	E		1					PER01
1997 03 31.85	a	G	-1.0	AT	0.0	E		1					VIT01
1997 03 31.85	ra	I	-0.8	AT	3.4	B		9					PER01
1997 03 31.85	a	I	-1.1	AT	0.0	E		1			15	20	PER01
1997 03 31.85	a	I	-1.2	AT	0.0	E		1					VIT01
1997 03 31.86	!	B	-0.6	YG	0.7	E		1		8	14		SKI
1997 03 31.86	!	M	-0.9	YG	0.7	E		1	20	8	16	358	GRA04
1997 03 31.86	!	N	1.6	YG	5.0	B		10	22	7/	13	3	GRA04
1997 03 31.86	a	B	-0.3	AT	3.5	R		1					VIT01
1997 03 31.86	a	B	-0.4	AT	3.5	R		1					PER01
1997 03 31.87	a	B	-0.8	AA	0.0	E		1	45	6	15		BAR06
1997 03 31.95	!	B	0.6	SC	5.0	B		7	18	8			SHA02
1997 04 01.05	w	G	-0.6	SC	0.0	E		1	21	9	15	10	CRE01
1997 04 01.10	a	B	-0.8	AA	0.0	E		1	40	6	16		BAR06
1997 04 01.14	w	B	-0.7	AE	0.0	E		1		S9	8	350	ADA03
1997 04 01.17	a	S	-0.5	AA	0.0	E		1	21	9	12	340	SPR
1997 04 01.76	a	G	0.3	AA	0.0	E		1	24	9	12	9	NEV
1997 04 01.77	a	G	-1.0	AA	0.0	E		1	38	6	16		BAR06
1997 04 01.78	a	B	-0.3	AA	0.0	E		1			6		MIL02
1997 04 01.78	a	M	-1.3	AA	0.0	E		1	30	7	15	345	CHE03
1997 04 01.78	a	M	-1.3	TI	5	R		1		7/	4		DVO
1997 04 01.79	a	M	-0.6	Y	0.0	E		1	20	9	17		KYS
1997 04 01.80	!	M	-1.0	Y	0.0	E		1	12	S8	25	15	SAR02
1997 04 01.80	a	M	-1.1	S	5	R		1	40	8	5	10	HOR02
1997 04 01.80	a	O	-0.7	SP	0.0	E		1	18	8	16	10	ZNO
1997 04 01.81	a	M	-0.8	S	0.0	E		1	25	8/	23		KON06
1997 04 01.82	s	M	-0.9	SC	0.0	E		1	10	8	15	20	GLI
1997 04 01.83	a	G	-1.1	AA	0.8	E		1			12.0	341	HAS02
1997 04 01.83	a	O	-0.4	S	0.0	E		1	35		7		LIB
1997 04 01.84	a	B	-0.9	AA	0.7	E		1		8	22	15	BOU
1997 04 01.84	a	G	-0.3	AA	0.6	E		1		S8/	13	15	KAM01
1997 04 01.85		M	-1.1	S	5.0	B		7	20	S8/	20		GON05
1997 04 01.85	a	S	-0.8	AA	5.0	B		10	20	8	8	320	MOE
1997 04 01.87					5.0	B		7	11	7	8	358	DIE02

Comet C/1995 01 (Hale-Bopp) [cont.]

DATE (UT)	N	MM	MAG.	RF	AP.	T	F/	PWR	COMA	DC	TAIL	PA	OBS.
1997 04 01.87		S	-0.6	AA	0.0	E		1					DIE02
1997 04 01.87	!	B	-0.5	YG	0.7	E		1		8	14	14	SKI
1997 04 01.88	!	B	-0.6	YG	0.7	E		1		8	14	18	GRA04
1997 04 01.88	!	N	1.7	YG	5.0	B		10	23	7/	14	22	GRA04
1997 04 02.04	a	B	-0.7:	AA	0.0	E		1	35	6	16		BAR06
1997 04 02.04	fw	B	-0.7	Y	0.0	E		1		8	&20		GRE
1997 04 02.06	w	G	-0.6	SC	0.0	E		1	15	9	18	10	CRE01
1997 04 02.08	!	N	4.3	YG	20.3	T	10	123					GRA04
1997 04 02.18	a	S	-0.3	AA	0.0	E		1	20	9	10	340	SPR
1997 04 02.78	!	M	-0.9	Y	0.0	E		1	12	S8	24	20	SAR02
1997 04 02.78	a	B	-0.4	AA	0.0	E		1			4		MILO2
1997 04 02.78	a	B	-0.9	AA	0.0	E		1	40	6	15		BAR06
1997 04 02.78	a	G	0.2	AA	0.0	E		1	21	9	14	15	NEV
1997 04 02.78	a	M	-0.9	AA	0.0	E		1	18	7	14	18	CHE03
1997 04 02.79	!	V	-0.5	YF	3.2	A	3	a	1	+34	>7		MIK
1997 04 02.79	a	O	-0.7	SP	0.0	E		1	18	7/	16	12	ZNO
1997 04 02.80	a	B	-1.0	Y	10	B		25	30	7	8	360	HYN
1997 04 02.80	a	M	-0.8	AA	4.0	R		8	25	S8			BAR06
1997 04 02.80	a	M	-0.9	S	5	R		1	40	7/	10	25	HOR02
1997 04 02.80	a	M	-1.1	S	5	R		1	50	7/	10	20	PLS
1997 04 02.80	a	M	-1.2	TI	5	R		1	30	8	3		DVO
1997 04 02.83	a	O	-0.7	S	0.0	E		1	35		9		LIB
1997 04 02.84					5.0	B		7	11	7	8	0	DIE02
1997 04 02.84		S	-0.6	AA	0.0	E		1					DIE02
1997 04 02.85		M	-0.6	AA	0.0	E		1	&25	8	&8		PAL02
1997 04 02.85		M	-0.9	S	5.0	B		7	20	S8/	18		GON05
1997 04 02.96	a	M	-0.9	AA	0.0	E		1		7	12	333	CHE03
1997 04 03.05	fw	B	-0.7	Y	0.0	E		1		8/	&15		GRE
1997 04 03.78	!	M	-1.2	Y	0.0	E		1	14	S8	30	15	SAR02
1997 04 03.78	a	B	-0.4	AA	0.0	E		1			5		MILO2
1997 04 03.79	a	B	-0.8	AA	0.0	E		1	55	6	16		BAR06
1997 04 03.79	a	G	-0.9	AA	0.0	E		1	50	6	16		BAR06
1997 04 03.79	a	M	-0.6	S	0.0	E		1	20	8/	20		KON06
1997 04 03.80	a	M	-1.0	S	5	R		1	30	7/	12	345	HOR02
1997 04 03.83	a	O	-0.5	S	0.0	E		1	35		7		LIB
1997 04 03.83	w	M	-1.1	Y	0.0	E		1	25	D8	12	330	CAN04
1997 04 03.85					5.0	B		7	11	7	8	358	DIE02
1997 04 03.85		S	-0.6	AA	0.0	E		1					DIE02
1997 04 03.85	a	B	-0.7	AA	0.7	E		1		8	16	20	BOU
1997 04 03.86		M	-0.8	S	5.0	B		7	20	S8/	20		GON05
1997 04 03.86	!	G	-0.5	AE	0.7	E		1	12	8	12	8	SHA02
1997 04 03.88	a	S	-0.8	AA	5.0	B		10	22	8	12	30	MOE
1997 04 03.90		S	-1.1	AE	5.0	B		8	40	8	12	15	BEA
1997 04 04.18	a	S	-0.8	AA	0.0	E		1	22	9	14	340	SPR
1997 04 04.78	!	M	-1.1	Y	0.0	E		1	14	S8	35	15	SAR02
1997 04 04.81	a	B	-0.9	AA	0.0	E		1	48	6	16		BAR06
1997 04 04.81	a	M	-0.9	AA	4.0	R		8	20	D7/	15		BAR06
1997 04 04.82	a	S	-0.5	AA	5.0	B		10	20	8	12	25	MOE
1997 04 04.85	!	M	-0.8	AA	0.0	E		1	&25	8	&15		PAL02
1997 04 04.85	a	B	-0.4	AT	3.5	R		1					PER01
1997 04 04.85	a	B	-0.6	AT	3.5	R		1					VIT01
1997 04 04.85	a	G	-0.8	AT	0.0	E		1					VIT01
1997 04 04.85	a	I	-1.5	AT	0.0	E		1					VIT01
1997 04 04.86	a	G	-0.9	AT	0.0	E		1					PER01
1997 04 04.86	a	I	-1.1	AT	0.0	E		1			12	0	PER01
1997 04 04.86	ra	I	-1.1	AT	3.4	B		9					PER01
1997 04 04.87	a	O	-0.8	SP	0.0	E		1	35	6/	20	11	ZNO
1997 04 04.88		B	-0.9	S	0.0	E		1	25	9	13	340	MAR02
1997 04 05.05	a	M	-0.9	AA	0.0	E		1	18	7	15	18	CHE03
1997 04 05.07	fw	B	-0.7	Y	0.0	E		1		8	&15		GRE
1997 04 05.19	a	S	-0.7	AA	0.0	E		1	22	9	12	345	SPR
1997 04 05.78	a	G	0.5	AA	0.0	E		1	20	9			NEV
1997 04 05.79	a	B	-0.8	AA	0.0	E		1	55	6	14		BAR06
1997 04 05.79	a	M	-0.7	AA	4.0	R		8	21	D7/	15		BAR06
1997 04 05.81		B	-0.2	SC	6.3	R		34			18		CHA02

April 1997

131

INTERNATIONAL COMET QUARTERLY

Comet C/1995 01 (Hale-Bopp) [cont.]

DATE (UT)	N	MM	MAG.	RF	AP.	T	F/	PWR	COMA	DC	TAIL	PA	OBS.
1997 04 05.82		B	-0.2	SC	6.3	R		34			11		HAN04
1997 04 05.82		B	-1.2	SC	3.5	R	5	30	6	8	3.10	352	APE
1997 04 05.83		B	-0.7	S	0.0	E		1	20	9	14	340	MAR02
1997 04 05.86		M	-0.8	S	5.0	B		7	20	S8/	14		GON05
1997 04 06.78	a	B	-0.4	AA	0.0	E		1			8		MIL02
1997 04 06.79		S	-0.7	AA	5.0	B		10	50	8	4.0	32	FUG
1997 04 06.82	!	V	-0.6	YF	3.2	A	3 a	1	+34	8	>7		MIK
1997 04 06.84	a	B	-0.5	AA	0.7	E		1		8	19	29	BOU
1997 04 06.84	a	G	-0.2	AA	0.6	E		1		S8/	11	23	KAM01
1997 04 06.84	a	O	-0.6	S	0.0	E		1	35		10		LIB
1997 04 06.84	a	S	-0.6	AA	5.0	B		10	20	8	14	330	MOE
1997 04 06.84	w	M	-0.2	SC	0.0	E		1	10	8	10	25	GLI
1997 04 06.85					5.0	B		7	10	7	7	345	DIE02
1997 04 06.85		S	-0.6	AA	0.0	E		1					DIE02
1997 04 06.86		M	-0.7	S	5.0	B		7	20	S8/	11		GON05
1997 04 07.20	a	S	-0.3	AA	0.0	E		1	20	9	10	340	SPR
1997 04 07.77		B	0.5	SC	6.3	R		34			13		GEN
1997 04 07.78	!	S	-0.8	AA	0.0	E		1					ANZ
1997 04 07.78	a	G	0.4	AA	0.0	E		1	21	9	10	29	NEV
1997 04 07.78	a	O	-0.8	SP	0.0	E		1	40	7	17	15	ZNO
1997 04 07.79	a	M	-1.0	TI	5	R		1	35	8	9		DVO
1997 04 07.80	a	B	-0.7:	AA	0.0	E		1	45	6			BAR06
1997 04 07.80	a	M	-0.7:	AA	4.0	R		8	18	8			BAR06
1997 04 07.81		B	0.5	SC	6.3	R		34			11		CHAO2
1997 04 07.81	!	V	-0.5	YF	3.2	A	3 a	1	+34	8	>7		MIK
1997 04 07.81	a	B	-1.1	Y	10	B		25	30	7	15	20	HYN
1997 04 07.81	a	M	-1.0	S	5	R		1	40	7/	10	35	HOR02
1997 04 07.82	a	O	-0.8	S	0.0	E		1	35		11		LIB
1997 04 07.82	a	G	-0.8	AA	0.8	E		1			15.3	340	HAS02
1997 04 07.84	a	M	-0.6	S	0.0	E		1	20	8/	21		KON06
1997 04 07.84		B	-0.4	AE	0.8	E		1	15	8	16	13	SHA02
1997 04 07.84	a	S	-0.6	AA	5.0	B		10	21	8	15	330	MOE
1997 04 07.84	w	G	-0.4	AA	0.6	E		1		S8/	11	27	KAM01
1997 04 07.85	a	B	-0.3	AT	3.5	R		1					VIT01
1997 04 07.85	a	B	-0.4	AT	3.5	R		1					PER01
1997 04 07.85	a	B	-0.5	AA	0.7	E		1		8	16	30	BOU
1997 04 07.85	a	G	-0.7	AT	0.0	E		1					VIT01
1997 04 07.85	a	G	-0.8	AT	0.0	E		1					PER01
1997 04 07.85	a	I	-0.5	AT	0.0	E		1					VIT01
1997 04 07.85	a	I	-0.6	AT	0.0	E		1					PER01
1997 04 08.03	fa	B	-0.5	Y	0.0	E		1					PER01
1997 04 08.06	w	G	-0.5	SC	0.0	E		1		8/	&7		GRE
1997 04 08.75		B	0.7	SC	6.3	R		34	18	9	12	0	CRE01
1997 04 08.76		B	0.7	SC	6.3	R		34			11		GEN01
1997 04 08.76	a	M	-0.6	AA	4.0	R		8	25	S7	>13		CHAO2
1997 04 08.76	a	S	-0.7	AA	0.0	E		1	45	S7	>12		BAR06
1997 04 08.77	a	I	-0.8	AA	0.0	E		1	37	S8	>12		BAR06
1997 04 08.77	a	S	-0.6	AT	0.0	E		1			4		BAR06
1997 04 08.78	a	B	-0.5	AT	0.0	E		1			4		MIL02
1997 04 08.78	a	G	0.4	AA	0.0	E		1			4		MIL02
1997 04 08.80	a	M	-1.0	S	5	R		1	24	9	12	351	NEV
1997 04 08.80	a	O	-0.8	S	0.0	E		1	40	7/	5	35	HOR02
1997 04 08.83	a	M	-0.6	S	0.0	E		1	35		12		LIB
1997 04 08.85	a	O	-0.6	SP	0.0	E		1	25	8	23		KON06
1997 04 08.90	!	M	-0.9	AA	0.0	E		1	35	7	12	20	ZNO
1997 04 09.06	fa	B	-0.5	Y	0.0	E		1	&20	8	&8		PAL02
1997 04 09.20	a	S	-0.5	AA	0.0	E		1		8	&4		GRE
1997 04 09.21		S	-1.0	AE	5.0	B		1	20	9	10	345	SPR
1997 04 09.75		B	1.1	SC	6.3	R		8	30	8	5	25	BEA
1997 04 09.76		B	1.1	SC	6.3	R		34			10		GEN
1997 04 09.77	a	B	-0.3	AT	0.0	E		1					VAS03
1997 04 09.78	a	I	-0.8	AA	0.0	E		1	38	S7/	>13		MIL02
1997 04 09.79	a	G	0.5	AA	0.0	E		1	23	9	16	349	BAR06
1997 04 09.79	a	M	-0.7	AA	4.0	R		8	18	S7	>13		NEV
1997 04 09.81	!	S	-0.6	AA	0.0	E		1					BAR06
													ANZ

Comet C/1995 01 (Hale-Bopp) [cont.]

DATE (UT)	N	MM	MAG.	RF	AP.	T	F/	PWR	COMA	DC	TAIL	PA	OBS.
1997 04 09.81	a	B	-1.2	Y	10	B		25	25	7	8	25	HYN
1997 04 09.83		B	1.1	SC	6.3	R		34			11		CHA02
1997 04 09.83	a	S	-0.4	AA	5.0	B		10	18	8	14	330	MOE
1997 04 09.89	!	B	0.3	SC	0.8	E		1	15	8	25	22	SHA02
1997 04 09.91	w	M	-0.4	SC	0.0	E		1	12	8	>8	0	GLI
1997 04 09.92		S	-1.0	AE	5.0	B		8	40	8	10	25	BEA
1997 04 10.06	fw	B	-0.7	Y	0.0	E		1		8	&15		GRE
1997 04 10.46	a	S	-1.0:	YG	0.0	E		1	&15	8/	15	350	NAN02
1997 04 10.75		B	1.1	SC	6.3	R		34			5		GEN
1997 04 10.76		B	1.1	SC	6.3	R		34			5		ILI
1997 04 10.76		B	1.1	SC	6.3	R		34			6		VAS03
1997 04 10.76		B	1.1	SC	6.3	R		34			11		CHA02
1997 04 10.83	!	V	-0.7	YF	3.2	A	3 a	1	+34	8	>7		MIK
1997 04 10.85		B	-0.3	AE	0.8	E		1	20	8	20	15	SHA02
1997 04 10.86		M	-0.7	S	5.0	B		7	15	S9	15		GON05
1997 04 10.88		S	-1.0	AE	5.0	B		8	40	8	12	30	BEA
1997 04 10.89	a	S	-0.5	AA	5.0	B		10	17	8	11	35	MOE
1997 04 11.05	fa	B	-0.6	Y	0.0	E		1		8	&7		GRE
1997 04 11.21	a	S	-0.3	AA	0.0	E		1	20	9	10	345	SPR
1997 04 11.57		B	1.1	SC	6.3	R		34			8		CHA02
1997 04 11.75		B	1.1	SC	6.3	R		34			7		GEN
1997 04 11.76		B	1.1	SC	6.3	R		34			5		ILI
1997 04 11.76		B	1.1	SC	6.3	R		34			6		GEN01
1997 04 11.79		B	1.1	SC	6.3	R		34			8		HAN04
1997 04 11.79	a	O	-0.5	SP	0.0	E		1	40	6/	32	3	ZNO
1997 04 11.82	a	M	-0.3	S	0.0	E		1	25	8	19		KON06
1997 04 11.84	a	B	-0.7	Y	10	B		25	20	7	8	20	HYN
1997 04 11.84	s	M	0.0	SC	0.0	E		1	8	8/	10	10	GLI
1997 04 11.85	a	B	-0.3	AT	3.5	R		1					PER01
1997 04 11.85	a	B	-0.7	AT	3.5	R		1					VIT01
1997 04 11.85	a	G	-0.2	AA	0.6	E		1		S8/			KAM01
1997 04 11.85	a	G	-0.7	AT	0.0	E		1					PER01
1997 04 11.85	a	G	-0.7	AT	0.0	E		1					VIT01
1997 04 11.85	a	I	-0.8	AT	0.0	E		1			14	30	PER01
1997 04 11.85	a	I	-0.9	AT	0.0	E		1					VIT01
1997 04 11.85	a	S	-0.4	AA	5.0	B		10	16	8	10	35	MOE
1997 04 11.86	!	B	-0.4	AE	0.7	E		1	20	8	17	29	SHA02
1997 04 11.88		S	-0.8	AE	5.0	B		8	30	8	6	30	BEA
1997 04 12.03	fs	B	-0.4:	Y	0.0	E		1		8	&5		GRE
1997 04 12.19	a	S	-0.2	AA	0.0	E		1	20	9	6	345	SPR
1997 04 12.42	s	S	-0.7	YG	0.0	E		1	&15	8/	2	0	NAN02
1997 04 12.78	a	B	-0.5	AT	0.0	E		1			8		MILO2
1997 04 12.78	a	I	-0.8	AA	0.0	E		1	38	S7	>14		BAR06
1997 04 12.84	a	M	-0.3	S	0.0	E		1	25	8	19		KON06
1997 04 12.84	a	S	-0.2	AA	5.0	B		10	16	8	11	335	MOE
1997 04 13.77	a	B	-0.6:	AT	0.0	E		1			4		MILO2
1997 04 13.78	a	I	-0.8	AA	0.0	E		1	38	S7	>14		BAR06
1997 04 13.79	a	M	-0.8	AA	4.0	R		8	20	S7	>13		BAR06
1997 04 13.79	a	O	-0.3	SP	0.0	E		1	40	7	21	0	ZNO
1997 04 13.80	a	O	-0.6	S	0.0	E		1	30		8		LIB
1997 04 13.83	s	M	-0.2	SC	0.0	E		1	10	8	11	15	GLI
1997 04 13.84	a	G	-0.2	AA	0.6	E		1		S8/			KAM01
1997 04 13.85		B	0.6	SC	0.7	E		1	15	7	4	28	SHA02
1997 04 14.79	a	B	-0.6	AT	0.0	E		1			2		MILO2
1997 04 14.83	a	S	-0.1	AA	5.0	B		10	16	8	8	340	MOE
1997 04 14.85	!	B	-0.7	AE	0.8	E		1	20	8	10	18	SHA02
1997 04 14.85	a	B	-0.4	AT	3.5	R		1					VIT01
1997 04 14.85	a	B	-0.6	AT	3.5	R		1					PER01
1997 04 14.85	a	G	-0.5	AT	0.0	E		1					VIT01
1997 04 14.85	a	G	-0.6	AT	0.0	E		1					PER01
1997 04 14.85	a	I	-0.6	AT	0.0	E		1			>8	30	PER01
1997 04 14.85	a	I	-0.7	AT	0.0	E		1					VIT01
1997 04 14.88		M	-0.3	S	5.0	B		7	15	S9	13		GON05
1997 04 15.04	fa	B	-0.5	Y	0.0	E		1		8	&6		GRE
1997 04 15.06	a	G	-0.3	SC	0.0	E		1	15	9	4	20	CRE01

April 1997

133

INTERNATIONAL COMET QUARTERLY

Comet C/1995 01 (Hale-Bopp) [cont.]

DATE (UT)	N	MM	MAG.	RF	AP.	T	F/	PWR	COMA	DC	TAIL	PA	OBS.
1997 04 15.82	!	V	-0.4	YF	3.2	A	3	a	1	+34	8	>7	MIK
1997 04 15.84	a	M	0.3	SC	0.0	E			1	10			GLI
1997 04 15.84	a	M	-0.6:	AA	4.0	R			8	18			BAR06
1997 04 15.84	a	S	-0.2	AA	5.0	B		10	15	8			MOE
1997 04 15.85	!	B	-0.4	AE	0.8	E		1	15	8	8	340	SHA02
1997 04 15.85	a	M	-0.2	S	0.0	E		1	25	8	14	9	KON06
1997 04 16.04	fa	B	-0.6	Y	0.0	E		1		8	14		GRE
1997 04 16.43	s	M	0.2	YG	5.6	B		8	&12	8/	&4		NAN02
1997 04 16.78	a	B	-0.6	AA	0.0	E		1	35	S7	2	5	BAR06
1997 04 16.78	a	M	-0.5	AA	4.0	R		8	19	S7			BAR06
1997 04 16.83	a	G	-0.6	AA	0.8	E		1					HAS02
1997 04 16.84	a	S	-0.2	AA	5.0	B		10	15	8			MOE
1997 04 16.85	a	B	-0.5	AT	3.5	R		1			13	350	PER01
1997 04 16.85	a	G	-0.4	AT	0.0	E		1					PER01
1997 04 16.85	a	I	-0.1	AT	0.0	E		1					PER01
1997 04 16.85	a	M	0.1:	SC	0.0	E		1	10	7/	>7.5	28	GLI
1997 04 16.87	a	B	0.0	AT	3.4	B		9	&10	7/			PER01
1997 04 17.02	fs	B	-0.5	Y	0.0	E		1		8	&4		GRE
1997 04 17.45	s	S	0.2	YG	5.6	B		8	&12	8/	2	10	NAN02
1997 04 17.80	a	B	-0.2	AT	0.0	E		1			>3		GLI
1997 04 17.83	w	M	0.4	SC	0.0	E		1	10	8	5	30	KAM01
1997 04 17.85	a	G	0.0	AA	0.6	E		1		S8			MOE
1997 04 17.85	a	S	-0.1	AA	5.0	B		10	15	8	11	350	PER01
1997 04 17.86	a	G	-0.1	AT	0.0	E		1					PER01
1997 04 17.87	a	B	0.4	AT	3.4	B		9	&14	7/			PER01
1997 04 17.87	a	B	-0.3	AT	3.5	R		1					PER01
1997 04 17.87	a	I	-0.3	AT	0.0	E		1					PER01
1997 04 17.87	w	B	0.5	SC	5.0	B		10			>7	25	GLI
1997 04 17.91	!	B	0.2	AA	0.8	E		1	23	8	13	27	SHA02
1997 04 18.80	!	V	-0.3	YF	3.2	A	3	a	1	+34	8	>7	MIK
1997 04 18.84	s	M	-0.1	SC	0.0	E		1	10	8	5	30	GLI
1997 04 18.85	a	S	-0.1	AA	5.0	B		10	13	8	10	350	MOE
1997 04 19.06	a	G	-0.1	SC	0.0	E		1	15	9	8	30	CRE01
1997 04 19.79	a	B	-0.4	AA	0.0	E		1	36	S6			BAR06
1997 04 19.79	a	M	-0.3	AA	4.0	R		8	21	S7			BAR06
1997 04 19.85	a	M	-0.5	AA	0.0	E		1	10	7	5	26	CHE03
1997 04 19.86	a	S	-0.1	AA	5.0	B		10	13	8	8	350	MOE
1997 04 19.89	s	-0.3	AA	8.0	B		11	25	7	7	>4	40	DES01
1997 04 20.05	a	G	-0.1	SC	0.7	E		1	12	9	6	35	CRE01
1997 04 20.82	a	G	-0.3	AA	0.0	E		1	32	6			BAR06
1997 04 20.82	w	B	0.1	SC	0.0	E		1	8	8/	&8	35	GLI
1997 04 20.83	a	B	-0.3	Y	10	B		25	35	8	3	45	HYN
1997 04 20.85	B	0.0	SC	0.0	E		1						GLI
1997 04 20.85	a	B	0.0	AT	3.5	R		1					PER01
1997 04 20.85	a	G	0.0	AT	0.0	E		1					PER01
1997 04 20.85	a	I	0.1	AT	0.0	E		1					PER01
1997 04 20.85	a	S	0.0	AA	5.0	B		10	13	8	>7.5	40	MOE
1997 04 20.86	a	G	0.1	AT	0.0	E		1			8	0	VIT01
1997 04 20.87	!	B	1.0	AA	0.7	E		1	18	8	7	33	SHA02
1997 04 20.87	a	B	0.2	AT	3.4	B		9	&6	7/			PER01
1997 04 20.87	a	B	0.9	AT	3.4	B		9	&10				VIT01
1997 04 20.87	a	I	0.3	AT	0.0	E		1					VIT01
1997 04 21.78	a	B	-0.3	AA	0.0	E		1	32	6			BAR06
1997 04 21.78	a	M	-0.2	AA	4.0	R		8	20	S7			BAR06
1997 04 21.82	w	B	0.1	SC	0.0	E		1	8	9	>8	35	GLI
1997 04 21.85	a	G	0.1	AA	0.6	E		1		S7/			KAM01
1997 04 21.90	S	-0.1	AA	8.0	B		11	25	8	8	>4	40	DES01
1997 04 22.86	a	S	-0.1	AA	5.0	B		10	12	8	7	10	MOE
1997 04 22.87	!	B	0.7	SC	0.7	E		1	15	7	2	42	SHA02
1997 04 23.02	fs	B	-0.3	Y	0.0	E		1		7/	&2		GRE
1997 04 23.44	a	S	0.3	YG	0.0	E		1	&10	8/	2		NAN02
1997 04 23.78	a	B	-0.2	AA	0.0	E		1	30	6			BAR06
1997 04 23.78	a	M	-0.0	AA	4.0	R		8	20	S7			BAR06
1997 04 23.81	a	B	-0.2	Y	10	B		25	18	8	2	45	HYN
1997 04 23.81	a	B	-0.4	AA	0.0	E		1	12	7	4	28	CHE03

Comet C/1995 01 (Hale-Bopp) [cont.]

DATE (UT)	N	MM	MAG.	RF	AP.	T	F/	PWR	COMA	DC	TAIL	PA	OBS.
1997 04 23.83	a	B	0.1	SC	0.0	E		1	10	8/	>5	35	GLI
1997 04 23.83	a	O	-0.1	S	0.0	E		1	25		5		LIB
1997 04 23.85	!	B	1.0	SC	0.7	E		1	20	7	3.5	41	SHA02
1997 04 23.86		M	-0.2	S	5.0	B		7	10	S9	4		GON05
1997 04 24.19	a	S	-0.1	AA	0.0	E		1	18	9	7	340	SPR
1997 04 24.78	a	B	-0.2	AA	0.0	E		1	35	6			BAR06
1997 04 24.81	!	V	-0.1	YF	3.2	A	3 a	1	+30	8	>5		MIK
1997 04 24.81	a	O	0.1	S	0.0	E		1	25		5		LIB
1997 04 25.44	a	S	0.3	YG	0.0	E		1	&10	8/	3		NAN02
1997 04 25.83	\$	B	0.0	AA	0.0	E		1	12	7	7	40	CHE03
1997 04 25.86	a	B	0.5	AT	3.5	R		1					VIT01
1997 04 25.86	a	G	0.2	AT	0.0	E		1					PER01
1997 04 25.86	a	G	0.5	AT	0.0	E		1					VIT01
1997 04 25.86	a	I	0.3	AT	0.0	E		1					VIT01
1997 04 25.86	a	M	1.1	AT	3.4	B		9	&11	7/			PER01
1997 04 25.87	a	B	0.5:	AT	3.4	B		9					VIT01
1997 04 25.87	a	I	0.2	AA	0.8	E		1	10	8	7	30	MOE
1997 04 25.87	a	I	-0.2	AT	0.0	E		1			13	40	PER01
1997 04 26.46	s	S	0.1	YG	0.0	E		1	&10	8/	10	25	NAN02
1997 04 26.78	a	B	-0.1	AA	0.0	E		1	35	6			BAR06
1997 04 26.87	a	S	0.1	AA	5.0	B		10	14	8	11	35	MOE
1997 04 26.89			0.2	AA	0.0	E		1	20	6/	>4	40	DES01
1997 04 26.91			0.0	AA	0.0	E		1	20	9	5	40	LOU
1997 04 27.04	fa	B	-0.3	Y	0.0	E		1		7/	&3.5		GRE
1997 04 27.21	a	S	-0.0	AA	0.0	E		1	14	9	5	345	SPR
1997 04 27.78	a	B	-0.1	AA	0.0	E		1	35	6			BAR06
1997 04 27.79	a	B	0.0	SC	0.0	E		1		9			RAD01
1997 04 27.84	\$	B	0.3	AA	0.0	E		1	10	7	5	40	CHE03
1997 04 27.85	a	B	0.1	SC	0.0	E		1	8	9	>6		GLI
1997 04 27.90			0.2	AA	0.0	E		1	20	7	>4	40	DES01
1997 04 27.91			0.0	AA	0.0	E		1	20	9	>5	40	LOU
1997 04 28.79	a	B	0.0	SC	0.0	E		1		9			RAD01
1997 04 28.79	a	B	0.2:	AA	0.0	E		1	30	6			BAR06
1997 04 28.86	a	G	0.4	AT	0.0	E		1					PER01
1997 04 28.86	a	I	0.3	AT	0.0	E		1			12		VIT01
1997 04 28.87	a	I	0.2	AT	0.0	E		1			12	40	PER01
1997 04 28.88	a	G	0.4	AT	0.0	E		1					VIT01
1997 04 28.91			0.1	AA	0.0	E		1	25	7/	>4	40	DES01
1997 04 29.85		B	0.1	S	0.0	E		1		7/	14	9	MAR02
1997 04 29.87	a	G	0.2	AT	0.0	E		1					PER01
1997 04 29.87	a	G	0.2	AT	0.0	E		1					VIT01
1997 04 29.87	a	M	0.6	AT	3.4	B		9	&11	7			PER01
1997 04 29.88	a	B	0.8	AT	3.4	B		9					VIT01
1997 04 29.88	a	I	0.1	AT	0.0	E		1			12	50	PER01
1997 04 29.88	a	I	-0.2	AT	0.0	E		1					VIT01
1997 04 29.88	a	M	0.8	AT	3.4	B		9					VIT01
1997 04 29.89			0.3	AA	0.0	E		1	25	7/	>4	40	DES01
1997 04 30.04	fa	B	-0.1	Y	0.0	E		1		7	&3.5		GRE
1997 04 30.87		M	0.1	S	5.0	B		7	10	S9	15		GON05

Comet C/1995 Q1 (Bradfield)

DATE (UT)	N	MM	MAG.	RF	AP.	T	F/	PWR	COMA	DC	TAIL	PA	OBS.
1995 10 06.83		B	8.9	S	20.0	C	9	60		3			NAG04
1995 11 03.81		B	8.9	S	20.0	C	9	60	2.3	1			NAG04

Comet C/1995 Y1 (Hyakutake)

DATE (UT)	N	MM	MAG.	RF	AP.	T	F/	PWR	COMA	DC	TAIL	PA	OBS.
1996 02 22.84		B	8.5	S	20.0	C	9	60	1.9	3			NAG04
1996 02 28.85		B	9.0	S	25	H	3	45	1.5	3			NAG04

April 1997

135

INTERNATIONAL COMET QUARTERLY

Comet C/1996 B1 (Szczepanski)

DATE (UT)	N	MM	MAG.	RF	AP.	T	F/	PWR	COMA	DC	TAIL	PA	OBS.
1996 02 28.79		B	8.5	S	25	H	3	45	3.5	2			NAG04
1996 03 13.65		B	9.1	AA	16	H	3	28	4.6	1			NAG04

Comet C/1996 B2 (Hyakutake)

DATE (UT)	N	MM	MAG.	RF	AP.	T	F/	PWR	COMA	DC	TAIL	PA	OBS.
1996 02 22.81		B	8.1	S	20.0	C	9	60	3.5	7			NAG04
1996 02 28.83		B	7.3	S	25	H	3	45	4.7	7	20 m	275	NAG04
1996 02 29.11		S	6.3	AA	8.0	B		12		5			BON01
1996 03 04.83		B	6.2	AA	10.0	R	4	20	3.0	7			NAG04
1996 03 13.67		B	4.6	AA	10.0	R	4	20	11.3	7	1.1	280	NAG04
1996 03 20.15		M	2.3	AA	0.8	E		1					GUB
1996 03 23.63		B	-0.1	AA	0.7	E		1	58	7	16.5	225	NAG04
1996 03 23.94		M	0.2	AA	0.8	E		1			28	220	GUB
1996 03 25.87		M	0.0	AA	0.8	E		1					GUB
1996 03 25.94		G	-0.5:	SP	0.7	E		1	45	8	4		HEN
1996 03 26.04		M	-0.2	AA	0.8	E		1	70	1	50	205	GUB
1996 03 26.80					7.0	B		10	27	8	15	170	NAG04
1996 03 26.80		S	0.0	Y	0.7	E		1					NAG04
1996 03 27.82					7.0	B		10	22	8	6	60	NAG04
1996 03 27.82		B	0.8	Y	3.5	R		7					NAG04
1996 03 27.83		G	-0.5:	SP	0.7	E		1		8	4		HEN
1996 03 28.14		M	0.4	AA	0.8	E		1			27	290	GUB
1996 03 29.08		G	-0.3:	SP	0.7	E		1	30	7			HEN
1996 03 29.81		G	0.0:	SP	0.7	E		1		6	5		HEN
1996 03 30.83		G	0.5	SP	0.7	E		1		8			HEN
1996 03 30.84		M	2.0	AA	0.8	E		1					GUB
1996 04 01.88		G	1.9	SP	0.7	E		1		6	4		HEN
1996 04 02.87		G	1.9	SP	0.7	E		1		8			HEN
1996 04 03.96		G	2.5	SP	0.7	E		1		7	5		HEN
1996 04 04.83		G	2.1	SP	0.7	E		1		7			HEN
1996 04 05.46		B	2.1	Y	7.0	B		10			4.5	55	NAG04
1996 04 05.88		G	2.3	SP	0.7	E		1		7	7		HEN
1996 04 12.45		B	3.0	Y	7.0	B		10		8	6	45	NAG04
1996 04 13.47		B	3.0	Y	7.0	B		10			5.5	40	NAG04
1996 04 13.87		S	3.5:	SP	3.5	B		9		8	2		HEN
1996 04 17.88		G	2.3	SP	0.7	E		1		7	7		HEN
1996 04 23.87		G	2.0:	SP	3.5	B		9		6	4		HEN
1996 06 18.15		S	5.7	S	11	L	8	72		7	0.3		C0002
1996 07 16.16		S	7.6	S	11	L	8	72		5			C0002
1996 07 17.14		M	7.5	S	15	L	9	80	4.9	5			SMI08
1996 07 19.14		S	8.0	S	15	L	9	80	4.7	5			SMI08
1996 08 06.20		S[10	:	S	20	L	8	83					C0002
1996 08 13.20		S[10	:	S	20	L	8	83					C0002

Comet C/1996 N1 (Brewington)

DATE (UT)	N	MM	MAG.	RF	AP.	T	F/	PWR	COMA	DC	TAIL	PA	OBS.
1996 07 16.76		S	9.0	S	15	L	9	50	4.8	2			SMI08
1996 08 13.74		S	8.1	S	15	L	9	80	4.0	3			SMI08
1996 08 18.91		B	7.2	YF	5.0	B		15	8	D3			FAJ
1996 08 19.90		B	7.4	YF	5.0	B		15	7	D4			FAJ
1996 08 20.91		B	7.8	YF	5.0	B		15	6	D4			FAJ
1996 08 21.91		B	8.0	YF	5.0	B		15	9	D2			FAJ
1996 08 24.90		B	8.2	YF	5.0	B		15	4	DO/			FAJ

Comet C/1996 P2 (Russell-Watson)

DATE (UT)	N	MM	MAG.	RF	AP.	T	F/	PWR	COMA	DC	TAIL	PA	OBS.
1997 02 09.44		a C	16.7	GA	60.0	Y	6		0.65			305	NAK01

Comet C/1996 Q1 (Tabur)

DATE (UT)	N	MM	MAG.	RF	AP.	T	F/	PWR	COMA	DC	TAIL	PA	OBS.
1996 09 04.08		S	8.7:	AC	5.0	B		10	& 4	3			RES

Comet C/1996 Q1 (Tabur) [cont].

DATE (UT)	N	MM	MAG.	RF	AP.	T	F/	PWR	COMA	DC	TAIL	PA	OBS.
1996 09 05.08		S	8.6	AC	5.0	B		10	3.1	1			RES
1996 09 09.05		S	7.7	AA	8.0	B		15	11	4			HAV
1996 09 09.08		S	8.2	S	5.0	B		10	8.6	0/			RES
1996 09 12.08		B	7.0:	S	10	M	10	56	3	2			MAR12
1996 09 12.12	&	S	8.2	S	11	L	7	32	& 3.5	d3			CH001
1996 09 14.09		S	7.9	S	15	L	9	80	6	4			SMI08
1996 09 14.12	\$	S	7.7	S	6.6	B		20	6	s4			PLE01
1996 09 14.97		S	7.4	S	20	L	8	83		4			C0002
1996 09 15.05		B	7.5:	S	8.0	B		20	6.6	s4			SPE01
1996 09 15.08		S	6.9	AA	8.0	B		15	10	5	0.4	275	HAV
1996 09 15.11		S	7.3:	S	5.0	B		10	& 7	0/			RES
1996 09 15.72		S	8.2	S	20.0	C	9	45	3.75	3			NAG04
1996 09 15.94		B	7.0	S	15.0	L	6	30	9.5	s2/			PI001
1996 09 16.04		S	6.6	S	5.0	B		10	5.8	1			RES
1996 09 16.08		S	6.3	S	0.0	E		1	& 7	0/			RES
1996 09 17.09		S	7.5	S	20	L	8	83	4	3			C0002
1996 09 17.12	\$	B	7.4	S	6.6	B		20	6	s4			PLE01
1996 09 18.06		S	6.7	S	5.0	B		10	4	0/			RES
1996 09 18.10	&	S	8.0	S	11	L	7	32	& 3.5	d3			CH001
1996 09 19.09		I	7.5:	S	5	R	6	20	& 6	2			WLO
1996 09 19.10	!	B	7.0	S	5.0	B		7	7	s4/			PLE01
1996 09 19.98		B	7.5:	S	7.0	B		25	& 2	s1			SOC
1996 09 21.03		B	7.7:	S	6.6	B		20	& 7	4			FIL04
1996 09 21.07		M	6.9	S	8	R	7	35	8	5			KWI
1996 09 21.09		B	7.2	S	5	R	6	20	& 8	2			WLO
1996 09 22.04		S	6.6	S	5.0	B		10	8.1	0/			RES
1996 09 22.05		B	7.0	S	5.0	B		10	4	2			MAR12
1996 09 22.06		B	7.0	S	6.4	R	6	20	& 8	d4			CNO
1996 09 22.08		S	7.0	S	5.0	B		10	& 9	1			OLE
1996 09 23.00		B	6.5	S	6.4	R	6	20	& 8	d4			CNO
1996 09 23.02		S	6.5	S	7.0	B		25	&13	2/			OLE
1996 09 23.04	—	S	6.5	S	5.0	B		10	11	1/			RES
1996 09 23.11	!	B	6.1	S	5.0	B		7	7	s4/			PLE01
1996 09 24.00		S	6.4	S	5.0	B		10	&10	3			OLE
1996 09 27.08		S	6.2	S	5.0	B		10	6	1			RES
1996 09 27.11		B	6.0	S	5.0	B		15	15	S3	0.2	210	FAJ
1996 09 27.13		B	6.8	S	8.0	B		20	8.3	s5			SPE01
1996 09 29.08		S	5.7	S	5.0	B		10	& 7	2			RES
1996 09 29.09		I	6.0:	S	4.0	B		12	&10	3/			WLO
1996 09 30.13	a	B	5.5	S	5.0	B		7	10	s5			PLE01
1996 10 01.06		B	5.5	S	5.0	B		10	7	3			MAR12
1996 10 01.07		M	5.7	S	8	R	7	35	8	5			KWI
1996 10 01.10		I	6.0:	S	4.0	B		12	&10	3/			WLO
1996 10 01.94		B	6.7:	S	6.5	R	6	28	& 3	1			SWI
1996 10 02.09		B	5.4	S	5.0	B		10	11	3			SIW01
1996 10 02.10		I	5.5:	S	4.0	B		12	&10	4			WLO
1996 10 02.13		B	5.5	S	5.0	B		10	8	3			MAR12
1996 10 02.17		I	7.5:	S	4.0	B		12	& 5	6			WLO
1996 10 02.94		B	4.9	S	5.0	B		15	25	S2	0.4	80	FAJ
1996 10 03.94		S	5.9	S	5.0	B		10	&13	6/			OLE
1996 10 03.96		B	6.1	S	5.0	B		7	& 9	5			BAN
1996 10 04.05		B	5.9	S	5.0	B		7	&10	d4			CNO
1996 10 04.06	&	S	5.5	S	11	L	7	32					CH001
1996 10 04.10		B	6.2	S	8.0	B		20	11	S5			SPE01
1996 10 04.11		B	5.5	S	5.0	B		10	9	3			MAR12
1996 10 04.12		B	5.2	S	4.0	B		12	&12	5			WLO
1996 10 04.13	&	M	6.0	S	5.0	B		10	25	2/			GR004
1996 10 04.86		M	5.4	S	5.0	B		7	10	d4			PAR03
1996 10 04.93		S	5.9	S	5.0	B		10	&22	5/			OLE
1996 10 04.95	!	B	6.3	S	6.8	R	12	40	15	d4			CHR
1996 10 04.98		B	6.0	S	5.0	B		7	& 9	5			BAN
1996 10 05.05		B	5.8	S	5.0	B		10	9	4			MAR12
1996 10 05.10		B	5.1	S	4.0	B		12	&15	5			WLO
1996 10 05.13		S	6.2	YF	5.0	B		10	12				ENT
1996 10 05.15		B	5.8	S	5.0	B		7	&10	d4			CNO

Comet C/1996 Q1 (Tabur) [cont].

INTERNATIONAL COMET QUARTERLY

DATE (UT)	N	MM	MAG.	RF	AP.	T	F/	PWR	COMA	DC	TAIL	PA	OBS.
1996 10 06.75	S	5.3:	S	5.0	B			10	& 8	5			RES
1996 10 06.92	S	5.0	S	5.0	B			10	&10	3/			RES
1996 10 07.89	B	6.5:	S	5.0	B			15	18	S1/	0.3	190	FAJ
1996 10 07.91	& B	5.3	S	5.0	B			10	12	3/			SIW01
1996 10 08.11	B	5.9	S	5.0	B			10	10	9			MAR12
1996 10 08.12	I	5.2:	S	4.0	B			12	&12	4/			WLO
1996 10 08.20	M	5.2	S	8	R	7		35	11	5	0.6	290	KWI
1996 10 08.96	B	6.6	S	7.0	B			25	& 3	s2			SOC
1996 10 08.99	S	5.6	AA	0.0	E			1					IWA03
1996 10 09.08	B	6.4:	S	5.0	B			7	&10	d5			CNO
1996 10 09.13	B	6.4	S	5.0	B			10	8	4			MAR12
1996 10 10.00	S	5.5	AA	0.0	E			1					IWA03
1996 10 10.13	& M	5.8	S	5.0	B			10	30	3			GR004
1996 10 10.15	S	5.7	YF	5.0	B			10	9				ENT
1996 10 10.75	B	5.6	S	5.0	B			15	20	S2	1.4	115	FAJ
1996 10 10.75	S	4.7	S	0.0	E			1	&15	7			RES
1996 10 10.76	B	6.1	S	6.0	B			20	12	2			KID01
1996 10 10.76	S	4.9	S	5.0	B			10	&15	4/	0.50	310	RES
1996 10 10.82	a B	5.3	S	10.0	B			25	15	S5/	0.7	305	PLE01
1996 10 10.94	& S	7.0	S	11	L	7		32	& 5	d			CHO01
1996 10 10.98	S	5.9:	S	5.0	B			10	&13	4			OLE
1996 10 11.13	B	6.4:	S	5.0	B			10	& 6	3/			MAR12
1996 10 11.74	B	6.5	S	5.0	B			10	9	2			DER
1996 10 11.75	S	5.6	S	6.0	B			20	5	6			SZA05
1996 10 11.75	B	4.9	S	5.0	B			10	&15	1	0.33	310	RES
1996 10 11.78	& O	5.8:	NP	5	R	6		20	3	s2/	&0.07		JAR01
1996 10 11.83	& B	5.3	S	5.0	B			10	12	3/			SIW01
1996 10 11.92	B	6.5	S	6.6	B			20	8	4	&0.37	325	FILO4
1996 10 11.92	! B	6.6	S	6.8	R	12		40	14	d3			CHR
1996 10 11.94	S	6.1:	S	5.0	B			10	&14				OLE
1996 10 12.00	& S	6.9	S	11	L	7		32					CHO01
1996 10 12.10	B	6.7	S	5.0	B			10	& 6	4			MAT06
1996 10 12.10	S	6.3:	AA	8.0	R	10		40	6.3	4			GER01
1996 10 12.13	B	5.3	S	4.0	B			12	&12	5			WLO
1996 10 12.13	B	5.8	S	6.0	B			20	&10	6	0.25	320	SCI
1996 10 12.73	B	6.4	S	5.0	B			10	7	4			MAR12
1996 10 12.73	B	5.7	S	6.0	B			20	5	6			SZA05
1996 10 12.75	M	5.9	S	5.0	B			7	10	d4			PAR03
1996 10 12.76	B	6.5	S	5.0	B			7	7.2	S4			SPE01
1996 10 12.77	B	6.6	S	5.0	B			10	12	2			DER
1996 10 12.77	S	5.2	S	8.0	B			20	11.7	S4			SPE01
1996 10 12.79	& O	6.3	NP	5.0	B			10	&15	1/			RES
1996 10 12.96	M	5.7	S	9	L	10		70	1.5	s2	&0.05		JAR01
1996 10 13.00	B	6.7	S	8	R	7		35	11	5	0.8	320	KWI
1996 10 13.09	S	6.3:	AA	5.0	B			7	& 7	3			BAN
1996 10 13.10	B	6.7	S	8.0	R	10		40	6.8	5/			GER01
1996 10 13.12	B	6.5	S	5.0	B			10	& 6	4			MAT06
1996 10 13.13	B	6.5	S	5.0	B			10	6	4			MAR12
1996 10 13.21	I	5.4:	S	4.0	B			12	&12	4/			WLO
1996 10 13.70	M	5.9	S	8	R	7		35	12	6	0.8	316	KWI
1996 10 13.73	B	6.4:	AA	8.0	R	10		40	6.5	5/			GER01
1996 10 13.73	B	6.5	S	5.0	B			10	4	3			SWI
1996 10 13.75	M	6.0	S	5.0	B			7	10	d4			PAR03
1996 10 13.75	B	6.4	S	5.0	B			7	7.7	S4			SPE01
1996 10 13.75	S	5.7	S	5.0	B			10	& 5	3	0.40	310	RES
1996 10 13.76	& O	6.3	AA	6.0	B			20	&10	d3			SIW
1996 10 13.78	B	6.6	NP	5	R	6		20	2.5	s2/	&0.07		JAR01
1996 10 13.89	& S	6.4	AA	5.0	B			10	&10				SIW
1996 10 13.98	B	7.5	S	11	L	7		32	& 5	d0			CHO01
1996 10 14.00	S	5.9	S	5.0	B			10	8	4			SIW01
1996 10 14.09	B	5.4	AA	0.0	E			1					IWA03
1996 10 14.11	B	6.4:	AA	8.0	R	10		40	6.3	4/			GER01
1996 10 14.13	B	5.9:	S	6.0	B			20	& 6	6	0.83	330	SCI
1996 10 14.13	B	5.5	S	4.0	B			12	&10	5			WLO
1996 10 14.13	B	6.3	S	5.0	B			10	5	3/			MAR12

Comet C/1996 Q1 (Tabur) [cont].

DATE (UT)	N	MM	MAG.	RF	AP.	T	F/	PWR	COMA	DC	TAIL	PA	OBS.
1996 10 14.20		B	6.5	S	5.0	B		10	& 6	4			MAT06
1996 10 14.72		B	6.1	S	15.0	L	6	30	10.4	s2/			PID01
1996 10 14.72		S	5.9	S	6.0	B		20	15	s3			DRA02
1996 10 14.73	&	M	5.6	S	5.0	B		10	30	3			GRO04
1996 10 14.75		B	5.6:	S	5.0	B		15	10	S2/	0.2	100	FAJ
1996 10 14.75		B	5.8	S	6.0	B		20	5	6			SZA05
1996 10 14.75		S	5.4	S	5.0	B		10	& 8	2/			RES
1996 10 14.75	&	0	6.6	NP	5	R	6	20	2.5	s3/			JAR01
1996 10 14.76	&	B	5.5	S	5.0	B		10	9				SIW01
1996 10 14.79		S	6.3	AA	6.0	B		20	&10				SIW
1996 10 14.82	!	B	6.5	S	6.8	R	12	40	12	D4			CHR
1996 10 14.84	a	B	5.7	S	5.0	B		7	15	S6	1.0	320	PLE01
1996 10 15.11		B	6.1	S	5.0	B		10	16	3			DER
1996 10 15.13		B	5.9	S	6.0	B		20	&10	6	0.50	350	SCI
1996 10 15.13		B	6.1	S	5.0	B		10	6	5			MAR12
1996 10 15.14		B	5.6	S	4.0	B		12	& 9	6			WLO
1996 10 15.20		B	6.4	S	5.0	B		10	& 7	5			MAT06
1996 10 15.73		B	6.2	S	15.0	L	6	30	13	s0			PID01
1996 10 15.74		B	6.2	S	5.0	B		10	5	3			SWI
1996 10 15.74	&	0	6.6	NP	5	R	6	20	3	s3			JAR01
1996 10 15.75		B	5.8	S	6.0	B		20	6	6/			SZA05
1996 10 15.75		B	6.7	S	7.0	B		25	& 3	S2			SOC
1996 10 15.77		B	6.1	S	6.0	B		20	7	2			KID01
1996 10 15.79		S	5.7	YF	5.0	B		10	9				ENT
1996 10 15.80		S	5.7:	SC	5.0	B		10	16	3/			MCK
1996 10 15.82	!	B	6.6	S	6.8	R	12	40	12	D4			CHR
1996 10 15.84	a	B	5.8	S	5.0	B		7	15	S6	1.2	324	PLE01
1996 10 15.85	&	S	6.3	S	11	L	7	32	&10	d3			CH001
1996 10 16.00		B	6.3	S	5.0	B		10	10				SIW01
1996 10 16.09		B	6.3:	AA	8.0	R	10	40	7.0	5			GER01
1996 10 16.11		B	6.2:	S	6.0	B		20	& 5	5			SCI
1996 10 16.13	—	B	6.2	S	5.0	B		10	6	s5/			MAR12
1996 10 16.15		I	5.8:	S	4.0	B		12	& 8	6/			WLO
1996 10 16.18		S	6.0	YF	5.0	B		10	10				ENT
1996 10 16.73	&	0	6.6	NP	5	R	6	20	2.5	s2/			JAR01
1996 10 16.75		B	6.0:	S	5.0	B		15	13	S1	0.1		FAJ
1996 10 16.75		S	5.7	S	5.0	B		10	&10	2			RES
1996 10 16.81					20.0	C	9	45	5.0	3	1.3	323	NAG04
1996 10 16.81		B	6.1	AA	7.0	B		10					NAG04
1996 10 16.82		S	5.7	YF	5.0	B		10	10				ENT
1996 10 16.83	&	M	6.1	S	8	R	7	35	12	6	1.1	315	KWI
1996 10 16.84		B	6.1	S	7.0	B		25	& 5	d5			SOC
1996 10 16.84	a	B	5.8	S	5.0	B		7	14	S6	1.0	331	PLE01
1996 10 17.78		P	5.5	SP	15	R	5		4	7	0.08	345	HEN
1996 10 17.83	a	B	5.9	S	5.0	B		7	12	S6	0.9	335	PLE01
1996 10 17.87	&	B	6.6	S	5.0	B		10	8				SIW01
1996 10 17.90	!	B	6.9	S	6.8	R	12	40	10	d3			CHR
1996 10 18.01		B	6.1	S	7.0	B		25	& 6	D5			SOC
1996 10 18.05		B	6.1	S	5.0	B		10	9		&0.50		SIW01
1996 10 18.12		B	7.0	S	5.0	B		10	5	s4			MAR12
1996 10 18.12		B	7.2	S	6.0	B		20	& 5	5			SCI
1996 10 18.15		I	6.0:	S	4.0	B		12	& 8	7			WLO
1996 10 18.85	a	B	6.5	S	5.0	B		7	11	S5/	0.8	339	PLE01
1996 10 19.76		S	5.9	S	5.0	B		10	10	2			RES
1996 10 20.71	&	B	8.0:	S	10	M	10	56	3	0			MAR12
1996 10 20.76		B[7.0	S	8.0	B		20	! 3				SPE01
1996 10 20.78	!	B	7.3	S	6.8	R	12	40	10	d3			CHR
1996 10 20.80	a	B	7.2	S	6.6	B		20	10	S5			PLE01
1996 10 20.84		S	6.5:	S	5.0	B		10	& 6	2/			RES
1996 10 23.74	a	B	8.0	S	10.0	B		25	8	s4			PLE01
1996 10 23.83		S	8.1	S	20.0	C	9	45	2.9	1	1.2	0	NAG04
1996 10 25.72		B	8.3	S	15.0	L	6	30	6.1	s0/			PID01
1996 10 25.72	\$	S	8.5:	S	35	M	10	90	& 6	s3			PLE01
1996 10 29.81	&	S	8.6	S	8	R	7	35	9	5			KWI
1996 10 30.81		S	7.6:	S	5.0	B		10	& 6	1			RES

April 1997

139

INTERNATIONAL COMET QUARTERLY

Comet C/1996 Q1 (Tabur) [cont].

DATE (UT)	N	MM	MAG.	RF	AP.	T	F/	PWR	COMA	DC	TAIL	PA	OBS.
1996 11 01.78		S	8.0:	S	5.0	B		10	& 5	1			RES
1996 11 03.72		S	8.5	AA	7.2	R	7	20	10	2	0.1	316	TUB
1996 11 04.74		B	9.8:	S	15.0	L	6	30	5.5	s1			PI001
1996 11 04.74		S	8.7	S	5.0	B		10	5	2			RES
1996 11 04.74		S	8.8	S	8	R	7	35	8	5			KWI
1996 11 04.75		S	9.0	AA	30	L	3	20	5	8			TUB
1996 11 04.76		B	7.8	S	5.0	B		15	8	DO/			FAJ
1996 11 06.77	\$	S	9.1:	S	35	M	10	90	& 5	s2/			PLE01
1996 11 08.72		B	9.8:	S	15.0	L	6	30	3.9	s1			PI001
1996 11 08.73		S	8.8	S	5.0	B		10	3	2			RES
1996 11 08.74		B	8.0	S	8.0	B		20	! 3.5				SPE01
1996 11 09.71		S	10.7	AA	27	L		100	2.5	0			SZA
1996 11 12.74		S	8.6	S	5.0	B		10	6	1			RES

Comet C/1997 A1 (NEAT)

DATE (UT)	N	MM	MAG.	RF	AP.	T	F/	PWR	COMA	DC	TAIL	PA	OBS.
1997 01 13.70		C	17.2	GA	60.0	Y	6	a240	0.5		0.9m	165	NAK01
1997 01 18.79		C	17.2	GA	60.0	Y	6	a240	0.6		0.7m	154	NAK01
1997 01 31.65		C	16.9	GA	60.0	Y	6	a240	0.75		1.1m	151	NAK01
1997 02 09.61		C	17.0	GA	60.0	Y	6	a240	0.7		1.1m	142	NAK01
1997 02 27.59		C	17.7	GA	60.0	Y	6	a120	0.4		1.5m	136	NAK01
1997 03 07.48		C	17.8	GA	60.0	Y	6	a240	0.4		0.8m	130	NAK01

Comet C/1997 BA6 (Spacewatch)

DATE (UT)	N	MM	MAG.	RF	AP.	T	F/	PWR	COMA	DC	TAIL	PA	OBS.
1997 02 13.70		C	19.3	GA	60.0	Y	6	a240		9			NAK01
1997 03 04.61		C	19.5	GA	60.0	Y	6	a240		9			NAK01

Comet C/1997 D1 (Mueller)

DATE (UT)	N	MM	MAG.	RF	AP.	T	F/	PWR	COMA	DC	TAIL	PA	OBS.
1997 02 20.56		C	15.1:	GA	60.0	Y	6	a120	0.65				NAK01
1997 02 22.77		C	14.7	GA	60.0	Y	6	a120	0.95				NAK01
1997 03 01.76		C	14.4	GA	60.0	Y	6	a120	1.3		1.6m	134	NAK01
1997 03 01.80		S	14.0	HS	35	L	5	237	0.7	2	1.9m	131	NAK01
1997 03 04.94		S	13.3	AC	25.4	L	5	104	0.5	4/			HOR02
1997 03 05.20		J	12.9	SC	25.4	T	4		0.43	d5	49.4s	130	MEY
1997 03 05.80		S	13.8	HS	35	L	5	158	1.1	2			ROQ
1997 03 06.11		S	13.7	HS	30	R	18	170	0.4	4			HOR02
1997 03 07.78		M	13.9	HS	35	L	5	158	0.9	3			SHA02
1997 03 07.81		S	14.0	HS	35	L	5	158	1.0	3/			HOR02
1997 03 07.98		S	13.4	AC	25.4	L	5	104	0.8	4			PLS
1997 03 08.13		S	13.7	HS	44.5	L	5	230	0.8	5			MEY
1997 03 08.13		S	14.0	HS	44.5	L	5	230	1	2/			SAR02
1997 03 08.81		S	14.3	HS	44.0	L	5	100	1.1	3			SZE02
1997 03 08.95		S	13.9	NP	44.5	L	5	100	0.75	1			HAS02
1997 03 09.15		S	14.2	HS	44.5	L	5	146	0.8	5			MAR02
1997 03 09.15		S	14.6	HS	44.5	L	5	146	1	3			SAR02
1997 03 09.27		J	13.1	SC	25.4	T	4		0.54	s5	54.7s	117	BAK01
1997 03 09.84	!	V	14.5	GA	36.0	T	7	a300	+ 0.7	8	& 4 m	110	ROQ
1997 03 09.85		S	13.2	GA	25.4	J	6	115	1.2	3/			MIK
1997 03 10.81		M	13.9	HS	35	L	5	158	1.1	3			BOU
1997 03 10.98		S	13.3	AC	25.4	L	5	104	0.7	3/			HOR02
1997 03 11.66		C	14.5	GA	60.0	Y	6	a120	1.0				MEY
1997 03 11.81		M	13.8	HS	35	L	5	158	1.1	3	2.8m	124	NAK01
1997 03 12.83		M	13.6	HS	35	L	5	104	1.3	2/			HOR02
1997 03 12.84		S	14.0	HS	35	L	5	104	0.9	2			HOR02
1997 03 13.00		S	13.1	HS	30	R	18	170	1.0	2			PLS
1997 03 13.15	!	J	12.6	SC	25.4	T	4		0.41	s5/	91.9s	114	SHA02
1997 03 18.16		J	12.1	SC	25.4	T	4		0.49	s5/	42.3s	116	ROQ
1997 03 20.20		J	12.9	SC	25.4	T	4		0.45	s5/	75.0s	104	ROQ
1997 03 27.14		J	11.8	SC	25.4	T	4		0.41	S6	98.7s	104	ROQ
1997 03 28.91		S	13.6	NP	44.5	L	5	167	1	0			MAR02

Comet C/1997 D1 (Mueller) [cont.]

DATE (UT)	N	MM	MAG.	RF	AP.	T	F/	PWR	COMA	DC	TAIL	PA	OBS.
1997 03 30.13		J	12.8	SC	25.4	T	4		0.31	s5/	78.5s	92	ROQ
1997 03 30.89		S	13.6:	NP	20	T	10	135	0.6	4			SHA02
1997 03 31.91		S	13.9:	VB	20	T	10	135	0.4	4			SHA02
1997 04 01.86		S	13.3	GA	25.4	J	6	143	1.0	1/			BOU
1997 04 02.83		M	13.6	HS	35	L	5	158	1	2			HOR02
1997 04 02.93		S	13.8:	HS	44.5	L	5	230	0.8	2			SAR02
1997 04 03.91		S	13.9:	HS	30	R	18	170	0.5	3			SHA02
1997 04 07.89		S	13.6:	VB	33	L	5	75	0.7	3			SHA02
1997 04 07.90		S	13.3	AC	25.4	J	6	143	1.0	1/			BOU
1997 04 09.92		S	[13.9	VB	20	T	10	135					SHA02
1997 04 10.91		S	13.6:	VB	33	L	5	100	1.1	3			SHA02
1997 04 13.15		J	13.1	SC	25.4	T	4		< 1	s6	65.2s	96	ROQ

Comet 4P/Faye

DATE (UT)	N	MM	MAG.	RF	AP.	T	F/	PWR	COMA	DC	TAIL	PA	OBS.
1991 10 19.80		S	10.5:	SC	6.0	R	10	30	& 1				MAN01
1991 11 09.80		S	10.0	SC	6.0	R	10	30	& 1		3m	90	MAN01

Comet 6P/d'Arrest

DATE (UT)	N	MM	MAG.	RF	AP.	T	F/	PWR	COMA	DC	TAIL	PA	OBS.
1995 07 29.04		S	12.1	NP	44.5	L	5	100	4	4			MAR02
1995 07 30.07		S	11.5	NP	44.5	L	5	100	3	3			ROD01
1995 07 30.07		S	11.9	NP	44.5	L	5	100	4	3			MAR02
1995 09 18.66		B	9.8	S	20.3	T	10	48	2.7	1			NAG04

Comet 22P/Kopff

DATE (UT)	N	MM	MAG.	RF	AP.	T	F/	PWR	COMA	DC	TAIL	PA	OBS.
1996 07 05.81		S	8.2	S	20	L	8	83		3			C0002
1996 07 14.89		S	8.7	S	15	L	9	50	4.0	3			SMI08
1996 07 15.84		S	8.6	S	20	L	8	83	2.0	3			C0002
1996 07 20.04		S	8.8	S	15	L	9	50	3.9	3			SMI08
1996 07 24.98		S	8.1	AA	8.0	B		11	6	4			DES01
1996 07 31.98		S	8.1	AA	8.0	B		11	6	3/			DES01
1996 08 01.99		S	8.2	AA	8.0	B		11	5	3			DES01
1996 08 02.98		S	8.2	AA	8.0	B		11	5	3			DES01
1996 08 03.98		S	8.3	AA	8.0	B		11	6	3/			DES01
1996 08 04.99		S	8.3	AA	8.0	B		11	6	3/			DES01
1996 08 05.99		S	8.5	AA	8.0	B		11	5	3			DES01
1996 08 06.79		S	8.9	S	20	L	8	83	0.7	3			C0002
1996 08 06.98		S	9.0	S	15	L	9	50	3.2	2			SMI08
1996 08 06.99		S	8.5	AA	8.0	B		11	5	3/			DES01
1996 08 07.98		S	8.6	AA	8.0	B		11	5	3/			DES01
1996 08 13.71		S	9.5	S	20	L	8	83		2			C0002
1996 08 13.98		S	9.6	S	15	L	9	80	3.0	1			SMI08
1996 08 31.76		S	[10	AA	20	L	8	83					C0002
1996 09 05.81		S	10.2	AA	20	L	8	83		1			C0002
1996 09 05.91		S	10.2	AA	15	L	9	80	1.0	0			SMI08
1996 09 15.78		S	10.5	AA	20	L	8	83		1			C0002
1997 01 12.42	a	C	14.3	GA	60.0	Y	6		2.2				NAK01
1997 02 09.41		C	15.8:	GA	60.0	Y	6		1.3				NAK01

Comet 29P/Schwassmann-Wachmann 1

DATE (UT)	N	MM	MAG.	RF	AP.	T	F/	PWR	COMA	DC	TAIL	PA	OBS.
1996 12 22.20		S	[13.0	AC	25.4	L	5	104	! 0.5				MEY
1997 02 02.19		S	11.6	TI	35	L	5	92	2.1	1/			HOR02
1997 02 02.20		S	11.7	HS	35	L	5	92	1.8	2			PLS
1997 02 03.19		S	12.0:	TI	35	L	5	104	1.6	1/			HOR02
1997 02 08.15		S	14.1:	VB	30	R	18	170	0.3	5			SHA02
1997 02 14.15		S	13.7	VB	30	R	18	170	0.7	s2			SHA02
1997 02 16.18		S	14.1	NP	44.5	L	5	100	1.5	0/			MAR02
1997 03 01.02		S	13.7	VB	30	R	18	210	0.6	2			SHA02

Comet 29P/Schwassmann-Wachmann 1 [cont.]

DATE (UT)	N	MM	MAG.	RF	AP.	T	F/	PWR	COMA	DC	TAIL	PA	OBS.
1997 03 06.13		S	[13.4	HS	30	R	18	170					SHA02
1997 03 07.96		S	[13.5	HS	44.5	L	5	230	1				SAR02
1997 03 08.96		S	[13.5	HS	44.5	L	5	230	1				SAR02
1997 03 10.93		S	13.5	HS	35	L	5	237	0.8	1			HOR02
1997 03 12.92		S	13.6	HS	35	L	5	237	0.8	1			HOR02
1997 03 13.02		S	13.6	VB	30	R	18	290	0.5	2			SHA02
1997 03 28.93		S	14.2	NP	44.5	L	5	100	< 1	0/			MAR02
1997 03 28.93		S	[12.9	HS	20	T	10	135					SHA02
1997 03 31.92		S	[13.8:	VB	20	T	10	135					SHA02
1997 04 01.92		S	[13.5	HS	44.5	L	5	230	1				SAR02
1997 04 02.93		S	[13.5	HS	44.5	L	5	230	1				SAR02
1997 04 07.91		S	[13.4	VB	33	L	5	75					SHA02
1997 04 09.94		S	[13.5	VB	20	T	10	135					SHA02

Comet 46P/Wirtanen

DATE (UT)	N	MM	MAG.	RF	AP.	T	F/	PWR	COMA	DC	TAIL	PA	OBS.
1997 02 01.75		S	11.8	AC	25.4	L	5	104	1.5	3			MEY
1997 02 02.72		S	11.5	TI	35	L	5	104	1.6	3			PLS
1997 02 02.73		M	11.4	TI	35	L	5	104	1.8	2/			HOR02
1997 02 03.71		S	[10.8	AC	11.0	L	7	50	1.5				BAR06
1997 02 06.74	!	S	11.0	HS	44.5	L	5	230	1.8	2			BAK01
1997 02 06.74	!	S	11.4	HS	44.5	L	5	230	1.8	4			SAR02
1997 02 06.75		M	10.9	TI	35	L	5	104	2.4	2/			HOR02
1997 02 07.77		S	10.5:	HS	30	R	18	170	0.7	2			SHA02
1997 02 07.77	a	S	11.3	AC	25.4	L	5	65	2	3			MEY
1997 02 09.42		C	12.1	GA	60.0	Y	6		3.0		2.4m	71	NAK01
1997 02 10.74		M	10.8:	TI	10	B		25	2.5	4			ZNO
1997 02 10.78	!	S	10.8	AC	30	R	18	100	1.8	3			SHA02
1997 02 14.75		M	10.2:	TI	35	L	5	92	3.6	2/			HOR02
1997 02 14.75		M	10.3:	TI	35	L	5	92	1.8	2/			PLS
1997 02 18.79		S	10.6	AC	20	R	14	90	1.2	2			SHA02
1997 02 22.75	—	S	10.4	TI	10	B		25	2.5	3			ZNO
1997 02 24.43	a	C	11.8	GA	60.0	Y	6		3.8		5.7m	72	NAK01
1997 02 24.71		B	9.7:	AC	11.0	L	7	50	6	1			ISH03
1997 02 24.72		B	10.0	AC	11.0	L	7	50	6	1			NAU
1997 02 24.73		S	9.9	AC	11	L	7	50	6	2/			BAR06
1997 02 25.73		S	9.8:	AC	11	L	7	50	6	2			BAR06
1997 02 27.75		M	9.4	TI	13	L	8	69	3.5	3			HOR02
1997 02 27.76		S	9.5	TI	13	L	8	69	3	2			PLS
1997 02 28.75		S	10.6	TI	10	B		25	3.0	2			ZNO
1997 02 28.76		M	9.4	TI	35	L	5	92	3.5	3			HOR02
1997 02 28.77		S	10.5	AC	11.0	L	7	50	6	3/			BAR06
1997 02 28.79		B	10.5	AC	11.0	L	7	50	4	2			ISH03
1997 03 01.42		S	10.5:	HS	25.4	T	6	60	1.3	4			YOS04
1997 03 01.44		S	10.2	A	41.0	L	6	80	3	3			KOB01
1997 03 01.75		S	10.2	TI	10	B		25	3.0	2/			ZNO
1997 03 01.76		M	9.3	TI	35	L	5	92	3	3			HOR02
1997 03 01.77		S	9.6	AC	25.4	L	5	65	2	3/			MEY
1997 03 04.77		M	9.6	TI	35	L	5	66	3.7	3			HOR02
1997 03 04.77		S	9.5	AC	25.4	L	5	65	1.5	3/			MEY
1997 03 04.77		S	10.0:	TI	35	L	5	66	2.2	1/			PLS
1997 03 05.75		B	10.2	AC	11.0	L	7	32	4	1			ISH03
1997 03 05.77		M	9.4	TI	35	L	5	66	3	3			HOR02
1997 03 06.77		S	10.3	AA	6.3	R	13	52	3	1			KOS
1997 03 06.78		S	9.9:	AC	15.2	L	5	42	3.5	2			MOE
1997 03 06.80		S	9.6	HS	25.4	J	6	58	2.2	2/			BOU
1997 03 07.42		C	10.9	GA	60.0	Y	6	a120	4.1				NAK01
1997 03 07.44		S	10.2:	HS	10.0	B		20	& 3				YOS02
1997 03 07.75		M	10.1	HS	44.5	L	5	72	5	5/	0.18	120	SZE02
1997 03 07.75		S	9.9	HS	44.5	L	5	72	4	5	0.1	150	BAK01
1997 03 07.75		S	10.0	HS	44.5	L	5	72	4	5	0.14	130	SAR02
1997 03 07.77		M	9.5	TI	20	L	5	48	3.5	2/			PLS
1997 03 07.77		S	9.4	TI	10	B		25	3.5	3			ZNO
1997 03 07.78		M	9.2	TI	20	L	5	48	3.5	3			HOR02

Comet 46P/Wirtanen [cont.]

DATE (UT)	N	MM	MAG.	RF	AP.	T	F/	PWR	COMA	DC	TAIL	PA	OBS.
1997 03 07.78		S	9.5	AC	25.4	L	5	65	2	3			MEY
1997 03 08.79		S	9.8	HS	44.0	L	5	63	1.4	3			HAS02
1997 03 09.80		S	9.7	HI	25.4	J	6	58	2.8	1/			BOU
1997 03 09.83	a	S	9.6	VF	25.3	L	6	58	& 2.5	2			PER01
1997 03 09.83	a	S	10.3	VF	25.3	L	6	58	& 2.1	2,			VIT01
1997 03 10.75		S	10.0	AA	6.3	R	13	52	3	2			KOS
1997 03 10.78		M	9.1	TI	20	L	5	48	3.6	3			HOR02
1997 03 10.78		S	9.4	AC	25.4	L	5	65	2	4			MEY
1997 03 10.87		S	10.0	AC	11.0	L	7	56	6	3			BAR06
1997 03 11.78		S	9.5:	AC	25.4	L	5	65	2	3			MEY
1997 03 11.79		M	9.0	TI	20	L	5	48	3.3	2/			HOR02
1997 03 11.79		M	9.5	TI	20	L	5	48	4	2/			PLS
1997 03 11.83	!	S	10.1	AC	20	R	14	90	2.5	1			SHA02
1997 03 12.80		M	9.5	TI	20	L	5	48	3.5	2			PLS
1997 03 12.81		M	9.0	TI	20	L	5	48	3	2/			HOR02
1997 03 26.75		S	10.0:	AC	20.0	L	5	71	3.5	2			BAR06
1997 03 28.86		M	9.7	NP	44.5	L	5	100	2	5			MAR02
1997 03 28.89	!	S	9.5	NP	20	T	10	75	2.5	2			SHA02
1997 03 29.84		M	9.8	NP	21.0	L	6	60	3	4/			MAR02
1997 03 29.85	a	S	9.3	PA	25.3	L	6	58	& 2.4	3			PER01
1997 03 29.85	a	S	9.5	PA	25.3	L	6	58	& 2	3/			VIT01
1997 03 30.75		S	10.8:	AC	11.0	L	7	32	2	1			BAR06
1997 03 30.78		M	10.1	TI	10	B		25	3	3			ZNO
1997 03 30.86	!	S	10.5	VB	20	T	10	75	2.3	3			SHA02
1997 03 31.84	a	S	10.0	GA	25.4	J	6	72	2.6	2			BOU
1997 03 31.85		M	9.7	NP	21.0	L	6	60	2	4			MAR02
1997 03 31.85	!	S	9.9	VB	20	T	10	75	3.1	2			SHA02
1997 03 31.85	a	S	9.6	PA	25.3	L	6	58	& 1.8	3/			PER01
1997 03 31.85	a	S	9.9	PA	25.3	L	6	58	& 1.3	2/			VIT01
1997 03 31.87		S	10.3	AC	28.0	T	6	68	2.5	2			MOE
1997 04 01.79		S	10.6:	HS	25.4	L	6	104	1.5	2			SAR02
1997 04 01.83	—	S	9.7	HS	20.3	T	10	80	1.7	2			KAM01
1997 04 01.84	a	S	10.1	GA	25.4	J	6	72	2.6	2			BOU
1997 04 02.79		S	10.0	HS	44.5	L	5	82	1.9	5			SAR02
1997 04 02.80		M	10.2	TI	10	B		25	2.5	2/			ZNO
1997 04 02.82		M	10.4	TI	35	L	5	104	1.5	2			HOR02
1997 04 03.78		S	9.7	HS	44.5	L	5	82	2.2	5/			SAR02
1997 04 03.85	!	S	9.5	VB	33	L	5	45	3.4	2			SHA02
1997 04 04.75		S	[10.7:	AC	11.0	L	7	50	!	2			BAR06
1997 04 04.78		S	10.4	HS	44.5	L	5	82	2.0	4			SAR02
1997 04 04.78		S	10.9	HS	44.5	L	5	82	3	2			DOB
1997 04 04.85	a	S	9.3	PA	25.3	L	6	58	> 2	3			PER01
1997 04 04.85	a	S	9.5	PA	25.3	L	6	58	& 2.5	3/			VIT01
1997 04 05.85		M	9.6	NP	21.0	L	6	60	> 3	4			MAR02
1997 04 06.84		S	9.6	HS	20.3	T	10	80	1.7	2			KAM01
1997 04 07.79		M	9.8	TI	10	B		25	3	2			ZNO
1997 04 07.84		S	9.4	HS	20.3	T	10	80	2.1	1/			KAM01
1997 04 07.84		S	10.5	AC	15.2	L	5	42	2	3			MOE
1997 04 07.85		S	10.3	GA	25.4	J	6	72	2.5	2			BOU
1997 04 07.86		S	10.5	VB	33	L	5	45	3.1	2			SHA02
1997 04 09.83		S	10.3	AC	15.2	L	5	42	2	2			MOE
1997 04 09.87	!	S	10.7	VB	20	T	10	75	2.4	2			SHA02
1997 04 10.88	!	S	11.4	VB	33	L	5	75	4.0	2			SHA02
1997 04 11.20		S	10.1	AC	20.0	T	10	125	2.1	2/			SPR
1997 04 13.79		M	10.2	TI	10	B		25	2.5	2/			ZNO
1997 04 15.13	!	J	10.1	SC	25.4	T	4		1.70	s5/	?		ROQ
1997 04 15.86		S	10.6	HS	20	R	14	90	2.0	2			SHA02
1997 04 23.87		S	[10.5	VB	20	R	14	90					SHA02
1997 04 26.88		S	10.5	AC	15.2	L	5	42	2	2			MOE
1997 04 27.79		S	[11.3	VF	20.0	L	7	71	!	2			BAR06

Comet 81P/Wild 2

DATE (UT)	N	MM	MAG.	RF	AP.	T	F/	PWR	COMA	DC	TAIL	PA	OBS.
1996 12 22.19		S	12.2	AC	25.4	L	5	104	1.3	4/			MEY

Comet 81P/Wild 2 [cont.]

DATE (UT)	N	MM	MAG.	RF	AP.	T	F/	PWR	COMA	DC	TAIL	PA	OBS.
1997 01 06.87		S	11.3	AC	25.4	L	5	65	1.3	s5/			MEY
1997 01 12.84		S	11.2	AC	25.4	L	5	65	2.3	s5/			MEY
1997 01 16.15		S	10.7	AC	20.0	T	10	102	1.5	4			SPR
1997 01 18.12		M	10.8	AC	25.4	L	5	65	2.0	S5/			MEY
1997 01 25.72		M	10.6	TI	35	L	5	92	1.5	5			HOR02
1997 01 25.73		M	10.6	TI	35	L	5	92	1.7	4			PLS
1997 01 26.73		M	10.3	TI	35	L	5	92	2	5			HOR02
1997 01 26.73		M	10.6	TI	35	L	5	92	1.8	4/			PLS
1997 01 26.77		M	10.4	AC	25.4	L	5	65	1.5	S6			MEY
1997 01 27.78		S	9.7	AA	11.0	L	7	32	4.5	4			VEL03
1997 01 29.75		S	9.9	AC	11	L	7	50	5	3/			BAR06
1997 01 29.81		B	10.0	AC	11	L	7	32	4	2			RED
1997 01 29.81		B	10.0	AC	11	L	7	32	4.5	2/			ISH03
1997 01 30.92		S	10.4	AC	20.3	T	10	50					ANZ
1997 01 30.96		M	10.7	AC	25.4	J	6	58	1.8	5			BOU
1997 01 31.80		M	10.0	TI	35	L	5	92	2.4	5			HOR02
1997 01 31.81		M	10.0	TI	35	L	5	92	1.8	5			PLS
1997 02 01.08		M	10.3	AC	25.4	L	6	108	2.0	6			GRA04
1997 02 01.56		C	10.2	GA	60.0	Y	6		5.1		> 6.8m	280	NAK01
1997 02 01.74		M	10.0	TI	10	B		25	2.5	5			ZNO
1997 02 01.77		S	10.3	AC	15.2	L	5	76	3.5	2			MOE
1997 02 01.80		M	10.1	AC	25.4	L	5	65	2	S5			MEY
1997 02 01.83		M	9.8	TI	35	L	5	92	2.5	5			HOR02
1997 02 01.90		M	10.4	AC	25.4	J	6	58	2.0	5			BOU
1997 02 01.96		S	10.5	AA	37.0	C	12	79	2	4			ANZ
1997 02 01.96		S	10.5:	AA	37.0	C	12	79	2	4			ANZ
1997 02 01.99		B	9.9	AC	11	L	7	50	4.5	3/			BAR06
1997 02 01.99		S	10.0	AC	11	L	7	50	4.5	3/			BAR06
1997 02 02.00		M	10.1	AC	25.4	L	6	108	2.5	6			GRA04
1997 02 02.75		S	9.7	TI	11	L	8	32	3	4			KYS
1997 02 02.77		M	9.7	TI	35	L	5	66	2.6	5/			PLS
1997 02 02.77		M	9.7	TI	35	L	5	66	2.7	6			HOR02
1997 02 02.82		S	9.9	AC	11	L	7	50		2			LUK04
1997 02 02.82		S	9.9	AC	11	L	7	50	4.5	3			BAR06
1997 02 02.84		S	9.6	AA	11.0	L	7	32	3.8	4			VEL03
1997 02 02.84		S	10.5	VB	30	R	18	100	1.1	s4			SHA02
1997 02 03.03		M	10.2	AC	25.3	L	6	58	2.0	5			PER01
1997 02 03.03		S	9.9	AC	25.3	L	6	58	2.0	5			PER01
1997 02 03.08		S	10.1	AC	11	L	7	50	4	3			BAR06
1997 02 03.09		S	10.3	AC	20.3	T	10	50	2	4			ANZ
1997 02 03.09		S	10.3:	AC	20.3	T	10	50	2	4			ANZ
1997 02 03.49		S	9.7	GA	10.0	B		25					SEA
1997 02 03.75		M	10.3	AC	11	L	7	50	4	4			LUK04
1997 02 03.77		S	10.3	AC	11	L	7	50	4.5	3/			BAR06
1997 02 03.88		S	9.9	AA	15.0	R	8	30	2	5			DIE02
1997 02 03.97		M	10.3	AC	25.3	L	6	58	1.4	5/			VIT01
1997 02 03.97		M	10.3	AC	25.3	L	6	58	2.3	5			PER01
1997 02 04.14		S	10.3	AC	11	L	7	50	3	2			BAR06
1997 02 04.42		M	9.9	GA	10.0	B		25	7	6			SEA
1997 02 04.66		S	9.6	AA	10.5	R	7	23		3			HAS08
1997 02 04.78		S	10.4	AA	11.0	L	7	115	1	3			IYA03
1997 02 04.86		B	9.9	AC	11	L	7	50	4.5	3			ISH03
1997 02 04.86		B	10.0	AC	11	L	7	50	5	3			RED
1997 02 05.00		S	9.9	AC	11	L	7	50	4.5	3			BAR06
1997 02 05.16		S	9.9	AC	20.0	T	10	64	3.0	4/			SPR
1997 02 05.47		S	10	: GA	10.0	B		25					SEA
1997 02 05.76		P	10.5:	AA	5.0	A	4		1				IYA03
1997 02 05.77		S	10.2	AC	15.2	L	5	42	3.5	3			MOE
1997 02 05.79		S	9.8	AA	15.0	R	8	30	2	6			DIE02
1997 02 05.83		S	10.4:	HS	30	R	18	100	4.2	s3			SHA02
1997 02 05.89		B	10.3	HS	25.6	L	5	42	3.5	7			BIV
1997 02 06.16		S	9.8	AA	20.0	T	10	64	2.5	4			SPR
1997 02 06.78		S	9.8	HS	25.4	L	6	104	2.5	5/			SAR02
1997 02 06.78		S	9.9	HS	25.4	L	6	104	3	6			BAK01
1997 02 06.80		M	9.2	TI	35	L	5	92	2.5	6			HOR02

Comet 81P/Wild 2 [cont.]

DATE (UT)	N	MM	MAG.	RF	AP.	T	F/	PWR	COMA	DC	TAIL	PA	OBS.
1997 02 06.88		B	10.1	HS	25.6	L	5	42	3	6			BIV
1997 02 06.90		S	9.8	AA	15.0	R	8	30	2	6			DIE02
1997 02 06.92		S	9.8	AC	11	L	7	32	5	3			BAR06
1997 02 07.06		S	10.1	AC	20.3	T	10	50	& 2	4/			ANZ
1997 02 07.20		B	10.2	NP	17.3	L	6	42	3	5			TRI
1997 02 07.55		E	9.8	GA	10.0	B		25					SEA
1997 02 07.55		S	9.7	GA	10.0	B		25					SEA
1997 02 07.73		S	10.3	AA	11.0	L	7	115	1.3	3			IVA03
1997 02 07.77		M	10.1	AC	25.4	L	5	65	2	S5/			MEY
1997 02 07.83		B	9.9	AC	11	L	7	50	5	3			ISH03
1997 02 07.85		S	9.9	AC	11	L	7	50	4	3			BAR06
1997 02 07.86		S	10.0	AC	11	L	7	50	5	3			CHU
1997 02 07.93		M	10.3	AC	25.4	J	6	58	2.2	5/			BOU
1997 02 07.94		S	10.6	VB	33	L	5	100	1.7	4		103	SHA02
1997 02 07.97		S	10.0	AC	15.2	L	5	42	3.5	3			MOE
1997 02 07.98		S	10.7	VB	30	R	18	100	1.4	5			SHA02
1997 02 08.21		B	10.5	NP	17.3	L	6	42	2.5	5			TRI
1997 02 08.72		S	10.2	AC	11	L	7	50	3.8	3			BAR06
1997 02 08.78		S	11.9:	VB	30	R	18	170	0.7	2			SHA02
1997 02 08.81		S	10.2	AA	11.0	L	7	115	1.3	3			IVA03
1997 02 08.92		S	9.8	AC	8.0	B		12	6	2			BAR06
1997 02 08.92		S	10.0:	AC	11	L	7	50	6	3			MAN01
1997 02 08.93		S	9.9	AC	15.2	L	5	42	3.5	4			MOE
1997 02 08.95		B	9.7	NP	44.5	L	5	100	4	4/			SAN04
1997 02 08.95		M	10.1	NP	44.5	L	5	100	3	5			MAR02
1997 02 09.02		M	10.2	AC	25.3	L	6	58	& 2.4	4/			PER01
1997 02 09.02		M	10.3	AC	25.3	L	6	58	& 1.3	4/			VIT01
1997 02 09.02		S	10.2	AC	25.3	L	6	58					PER01
1997 02 09.02		S	10.2	AC	25.3	L	6	58					VIT01
1997 02 09.16		B	10.5	HS	25.6	L	5	42	3	5			BIV
1997 02 09.20		B	10.4	NP	17.3	L	6	42	2	5			TRI
1997 02 09.54	—	S	9.7	GA	10.0	B		25	6				SEA
1997 02 09.57		C	9.8	GA	8.0	R	6		8.3		15	m 288	NAK01
1997 02 09.73		M	9.3	AA	12.0	B		20	6	3			WAS
1997 02 09.95		M	10.0	AC	25.4	L	5	65	3	S5			MEY
1997 02 09.96		S	10.2	AC	25.3	L	6	58	& 2.3	4/			PER01
1997 02 09.96		S	10.5	AC	25.3	L	6	58	& 1.3	3/			VIT01
1997 02 10.75		M	9.7	TI	10	B		25	3.5	6			ZNO
1997 02 10.81		M	9.8	TI	20	L	5	48	2.2	4			PLS
1997 02 10.83		S	11.1	VB	30	R	18	100	0.9	s4	0.02	110	SHA02
1997 02 10.89		M	9.2	TI	13	L	8	69	3	3/			HOR02
1997 02 10.91	!	V	10.3	GA	36.0	T	7		& 7	8	&10	m 270	MIK
1997 02 10.93		M	10.2	AC	25.4	J	6	58	2.3	4/			BOU
1997 02 11.10		S	9.9	AA	15.0	R	8	30	2	3			DIE02
1997 02 11.83		S	10.0	AC	11	L	7	50	5	3			BAR06
1997 02 11.83		S	10.2	AC	11	L	7	50	5	2			LUK04
1997 02 11.88		M	9.6	TI	20	L	5	48	3	3/			PLS
1997 02 11.88		S	9.7	AC	8.0	B		12	8.5	2			BAR06
1997 02 11.88		S	9.9	AC	8.0	B		12	6	2			BAR06
1997 02 11.89		S	10.1	AA	11.0	L	7	115	1.5	3			IVA03
1997 02 12.69		S	8.8	HS	10.0	B		20	5	5			YOS02
1997 02 12.94		S	9.9	AC	11	L	7	50	5.8	3	0.05	71	BAR06
1997 02 12.94		S	10.0	AC	11	L	7	50	6	2/	0.05	69	LUK04
1997 02 13.73		M	10.0	HS	12.5	L	6	60	2.0	4			TSU02
1997 02 13.74		S	9.1	HS	25.4	T	6	60	2.5	5			YOS04
1997 02 13.79		S	11.1	VB	30	R	18	100	1.3	s4			SHA02
1997 02 14.06		S	9.7	AA	15.0	R	8	30	2	7			DIE02
1997 02 14.77		M	9.6	TI	35	L	5	92	3.0	4/			PLS
1997 02 14.77		M	9.7	TI	35	L	5	92	3.0	6			HOR02
1997 02 15.02		S	9.9	AC	25.4	L	6	61	2.0	5			GRA04
1997 02 15.17		S	10.9	NP	10	B		14	2.3	3			SHA02
1997 02 15.79		S	9.9	AC	25.4	L	6	108	2.2	5			GRA04
1997 02 15.79		S	11.0	VB	30	R	18	100	1.0	s3			SHA02
1997 02 15.84		S	10.1	AA	11.0	L	7	80	1.5	3			IVA03
1997 02 15.94		S	10.2	AC	25.3	L	6	58	& 2	3/			PER01

April 1997

145

INTERNATIONAL COMET QUARTERLY

Comet 81P/Wild 2 [cont.]

DATE (UT)	N	MM	MAG.	RF	AP.	T	F/	PWR	COMA	DC	TAIL	PA	OBS.
1997 02 15.94	S	10.3	AC	25.3	L	6		58	& 1.3	3			VIT01
1997 02 16.13	M	9.8	NP	44.5	L	5		100	2.5	4			SAN04
1997 02 16.14	M	9.9	NP	44.5	L	5		100	3	6/			MAR02
1997 02 16.79	S	9.6	AA	6.3	R	13		52	4	0/			KOS
1997 02 22.74	M	9.7	TI	10	B			25	3.0	5/			ZNO
1997 02 23.72	B	9.7	AC	11.0	L	7		50	6	3			ISH03
1997 02 23.77	S	9.3	AA	6.3	R	13		52	4	0/			KOS
1997 02 23.94	S	10.0	AC	11	L	7		50	6	2			BAR06
1997 02 24.72	B	9.7	AC	11.0	L	7		50	6	3			ISH03
1997 02 24.73	K	9.5	AC	8.0	B			12		3			LUK04
1997 02 24.73	S	9.5	AC	8.0	B			12	9	3			BAR06
1997 02 24.73	S	9.6	AC	8.0	B			12	8	4			ISH03
1997 02 24.73	S	9.8	AC	11	L	7		50	7	3			BAR06
1997 02 24.76	S	9.2	AA	6.3	R	13		52	4	0/			KOS
1997 02 24.93	S	10.6	VB	30	R	18		100	1.4	3			SHAO2
1997 02 25.73	S	9.5	AC	11	L	7		50	4	2/	0.1	110	BAR06
1997 02 25.83	S	10.3	VB	20	R	14		40	1.7	s3			SHAO2
1997 02 26.83	M	9.8	TI	20	L	5		48	4	5			PLS
1997 02 26.90	S	10.0	AA	11.0	L	7		80	1.5	3			IVA03
1997 02 27.77	M	9.2	TI	8.0	B			10	5	4/			HOR02
1997 02 27.77	S	9.8	AC	15.2	L	5		42	3.5	2			MOE
1997 02 27.78	S	9.5	TI	8.0	B			10	6	3			PLS
1997 02 27.94	M	10.3	AC	25.3	L	6		58	& 2.3	4/			PER01
1997 02 27.94	M	10.5	AC	25.3	L	6		58	& 1.3	3/			VIT01
1997 02 27.94	S	9.9	AC	25.3	L	6		58	& 2.3	4/			PER01
1997 02 27.94	S	10.3	AC	25.3	L	6		58	& 1.3	3/			VIT01
1997 02 28.76	M	9.8	TI	10	B			25	3.0	4/			ZNO
1997 02 28.78	S	9.2	AC	8.0	B			12	10	3			ISH03
1997 02 28.79	S	9.1	AC	8.0	B			12	8	2			BAR06
1997 02 28.79	S	9.2	AC	11.0	L	7		50	6	3			BAR06
1997 02 28.81	B	9.3	AC	11.0	L	7		50	10	3	0.15	90	ISH03
1997 02 28.83	S	9.6	TI	11	L	8		32	3.5	2/			KYS
1997 02 28.99	S	10.6	VB	30	R	18		100	1.2	s3	0.02	20	SHAO2
1997 03 01.10	S	10.3	VB	20	R	14		110	1.3	3			SHAO2
1997 03 01.47	S	9.2	S	15.0	R	5		25	5	4/			NAG02
1997 03 01.49	S	9.3	AA	41.0	L	6		80	8	5			KOB01
1997 03 01.56	S	9.0	HS	25.4	T	6		60	4.2	5			YOS04
1997 03 01.76	M	9.7	TI	10	B			25	3.5	4			ZNO
1997 03 01.77	M	9.4	TI	35	L	5		92	3.6	5			HOR02
1997 03 01.77	S	9.3	AA	6.3	R	13		52	3	1			KOS
1997 03 01.83	M	9.6	AC	25.4	L	5		65	3	s5			MEY
1997 03 01.83	S	9.7	TI	8.0	B			10	4				POD
1997 03 01.86	S	10.8	AC	33.4	L	4		61	3	s4	0.2	90	SZE02
1997 03 01.93	S	10.3	AA	20	C			10	1.5	3			DAM
1997 03 02.76	S	9.5	AA	6.3	R	13		52	3	1			KOS
1997 03 02.78	M	9.4	TI	20	L	5		48	4.5	4/			PLS
1997 03 02.80	M	9.5	TI	20	L	5		48	3.6	5/			HOR02
1997 03 02.82	S	9.0	AC	8.0	B			12	9	2			BAR06
1997 03 02.82	S	9.2	AC	11.0	L	7		50	5.5	3			BAR06
1997 03 02.84	B	9.3	AC	11.0	L	7		50	7	3	0.1	90	ISH03
1997 03 02.84	S	9.2	AC	8.0	B			12	9	3	0.1	90	ISH03
1997 03 02.93	S	10.2	VB	30	R	18		100	1.3	4			SHAO2
1997 03 03.02	S	10.1	VB	20	T	10		75	1.6	3			SHAO2
1997 03 03.46	S	10.0	AA	10.0	B			25					SEA
1997 03 03.46	S	10.0	AA	10.0	B			25					SEA
1997 03 03.79	S	10.1	AC	15.2	L	5		42	2.5	3			MOE
1997 03 03.82	S	9.0	AC	8.0	B			12	9	3			BAR06
1997 03 03.82	S	9.2	AC	11.0	L	7		50	6.5	3			BAR06
1997 03 03.84	M	9.4	TI	35	L	5		92	3.2	5	0.07	115	HOR02
1997 03 03.88	S	9.9	AC	25.3	L	6		58	& 2.2	4			PER01
1997 03 03.88	S	10.3	AC	25.3	L	6		58	& 1.9	3/			VIT01
1997 03 04.04	M	9.2	S	8.0	B			10	4	5			GON05
1997 03 04.06	S	9.3	AC	11.0	L	7		50	6	2			BAR06
1997 03 04.77	S	9.8	AA	6.3	R	13		52	3	1			KOS
1997 03 04.78	M	9.3	TI	35	L	5		66	3.2	5	0.03	115	PLS

Comet 81P/Wild 2 [cont.]

DATE (UT)	N	MM	MAG.	RF	AP.	T	F/	PWR	COMA	DC	TAIL	PA	OBS.
1997 03 04.78		M	9.5	TI	35	L	5	66	3.5	5/	0.07	115	HOR02
1997 03 04.79		S	9.8	AC	25.4	L	5	65	2.5	D4			MEY
1997 03 04.83		S	10.1	AC	28.0	T	6	59	3	2			MOE
1997 03 04.86		S	9.0	AC	8.0	B		12	8	2			BAR06
1997 03 04.88		S	13.7	HS	44.0	L	5	156	0.3	5			HAS02
1997 03 05.06		S	9.1	AC	11.0	L	7	50	7	3			BAR06
1997 03 05.49		S	10.1	HS	40.0	L		96	2.1	5			NAG08
1997 03 05.50		S	9.8	AA	10.0	B		25					SEA
1997 03 05.52		S	8.9	VG	10.0	B		20	7.5	5			NAG08
1997 03 05.75		B	8.9	AC	8.0	B		12	12	3/	0.15	90	ISH03
1997 03 05.79		S	9.4	AA	11.0	L	7	32	6	3			VEL03
1997 03 05.83		M	9.3	TI	8.0	B		10	5.5	3/			HOR02
1997 03 05.85		S	9.5	AA	15.0	R	8	30	1.5	2			DIE02
1997 03 06.09		S	10.6	VB	30	R	18	100	1.6	3			SHA02
1997 03 06.76		S	10.0	AA	6.3	R	13	52	3	1			KOS
1997 03 06.81		S	9.9	AC	15.2	L	5	42	2.5	3			MOE
1997 03 06.82		M	9.8	GA	25.4	J	6	58	2.2	4			BOU
1997 03 07.51		S	9.2	HS	10.0	B		20	4	5			YOS02
1997 03 07.76		M	9.6	TI	10	B		25	4.5	3/			ZNO
1997 03 07.80		M	9.4	TI	20	L	5	48	4.5	5	0.05	105	PLS
1997 03 07.80		M	9.5	TI	20	L	5	48	4	4/			HOR02
1997 03 07.80		S	9.9	AC	25.4	L	6	104	4	s5	0.3	90	BAK01
1997 03 07.80		S	10.4	AC	25.4	L	6	104	4	s4	0.25	80	SAR02
1997 03 07.80		S	10.4	AC	25.4	L	6	104	6	s5	0.6	80	SZE02
1997 03 07.84		S	9.7	AA	15.0	R	8	30	2	4			DIE02
1997 03 07.84		S	9.7	AC	25.4	L	5	65	3	s4			MEY
1997 03 07.91		M	10.1	NP	21.0	L	6	60	4	6			MAR02
1997 03 08.75		M	9.7	TI	10	B		25	4	3			ZNO
1997 03 08.79		S	10.2	AC	33.4	L	5	61	4				SZE02
1997 03 08.88		S	9.5	AC	10.0	B		25	3.1	3			HAS02
1997 03 08.98		S	9.7	AC	6.0	B		20	10	2			SAR02
1997 03 08.99		M	9.9	NP	44.5	L	5	100	3	5/			MAR02
1997 03 09.00		S	10.0	AC	25.3	L	6	58	& 1.6	4/			PER01
1997 03 09.00		S	10.5	AC	25.3	L	6	58	& 1.6	5			VIT01
1997 03 09.77		S	9.4	AA	11.0	L	7	32	4.1	4			VEL03
1997 03 09.80		S	9.2	AC	11.0	L	7	32	9	5			ISH03
1997 03 09.82		M	9.8	GA	25.4	J	6	72	2.5	4/			BOU
1997 03 09.83		S	9.5	AC	20.3	T	10	50	1.9	5			KAM01
1997 03 09.85		S	9.7	AA	15.0	R	8	30	2	4			DIE02
1997 03 09.86		S	9.8	AC	25.3	L	6	58	& 2.2	4			PER01
1997 03 09.86		S	10.4	AC	25.3	L	6	58	& 1.9	4/			VIT01
1997 03 09.87		a	S	10.3	NP	25.3	L	6	58	& 2.2	4		PER01
1997 03 09.87		a	S	10.5	NP	25.3	L	6	58	& 1.9	4/		VIT01
1997 03 10.06		S	9.0	AC	11.0	L	7	32	7	3			BAR06
1997 03 10.75		S	10.4	AA	6.3	R	13	52	2	1			KOS
1997 03 10.80		S	9.8	AC	15.2	L	5	42	3	3			MOE
1997 03 10.80		S	10.0	AC	33.4	L	5	61	6	s6	0.5	95	SZE02
1997 03 10.81		S	9.3	AA	11.0	L	7	32	4	3			VEL03
1997 03 10.82		S	9.6	AC	25.4	L	5	65	3	s5			MEY
1997 03 10.86		M	9.2	TI	20	L	5	48	3.7	4/			HOR02
1997 03 11.46		S	9.6	AA	10.0	B		25					SEA
1997 03 11.77		M	9.8	TI	10	B		25	3.5	3/			ZNO
1997 03 11.79		S	9.2	AA	11.0	L	7	32	4	4			VEL03
1997 03 11.79		S	9.6	AC	25.4	L	5	65	2.5	4/			MEY
1997 03 11.84		M	9.1	TI	20	L	5	48	4	4/			HOR02
1997 03 11.85		S	10.6	VB	20	R	14	90	2.0	3		190	SHA02
1997 03 11.92		S	9.9	AC	25.3	L	6	58	& 3.2	4			PER01
1997 03 11.92		S	10.2	AC	25.3	L	6	58	& 2.2	4			VIT01
1997 03 11.93		a	S	9.9	NP	25.3	L	6	58	& 3.2	4		PER01
1997 03 11.93		a	S	10.4	NP	25.3	L	6	58	& 2.2	4		VIT01
1997 03 12.42		S	9.4	AA	10.0	B		25					SEA
1997 03 12.76		M	9.6	TI	10	B		25	4	4			ZNO
1997 03 12.81		M	9.1	TI	20	L	5	48	3.5	4/			HOR02
1997 03 12.82		M	9.6	TI	20	L	5	48	3.7	4			PLS
1997 03 12.97		M	9.8	AC	25.3	L	6	58	& 3.2	3/			PER01

Comet 81P/Wild 2 [cont.]

DATE (UT)	N	MM	MAG.	RF	AP.	T	F/	PWR	COMA	DC	TAIL	PA	OBS.
1997 03 12.97		S	9.7	AC	25.3	L	6	58	& 3.2	3/			PER01
1997 03 12.97		S	10.6	VB	30	R	18	100	1.6	s3			SHA02
1997 03 16.09		M	9.9	AC	25.3	L	6	58	& 3	3/			PER01
1997 03 16.09		S	9.8	AC	25.3	L	6	58	& 3	3/			PER01
1997 03 21.96		S	10.7	VB	30	R	18	170	0.8	3			SHA02
1997 03 22.81		S	9.9	AC	15.2	L	5	42	2.5	2			MOE
1997 03 26.81		S	9.5:	AC	20.0	L	5	70	5	2			BAR06
1997 03 26.94		S	10.2	VB	20	R	14	90	1.5	3			SHA02
1997 03 27.17		S	9.8	AA	20.0	T	10	64	2.2	3/			SPR
1997 03 27.85		S	9.4:	AC	5.0	B		20	5	2/			BAR06
1997 03 28.88		M	9.3	NP	44.5	L	5	100	2	5			SAN04
1997 03 28.88		M	9.9	NP	44.5	L	5	100	1.5	6			MAR02
1997 03 28.90		S	9.9	AA	15.0	R	8	30	2	6			DIE02
1997 03 28.91		S	9.8	VB	20	T	10	75	1.7	s4			SHA02
1997 03 29.84		S	9.8	AC	15.2	L	5	42	3	2			MOE
1997 03 29.85		M	9.7	NP	21.0	L	6	60	1	6	2.0m	70	MAR02
1997 03 29.85		S	10.5	AA	6.3	R	13	52	3	2			KOS
1997 03 29.87		S	9.7	AC	25.3	L	6	58	& 3	3			PER01
1997 03 29.87		S	10.1	AC	25.3	L	6	58	& 2	4			VIT01
1997 03 30.82		M	9.7	TI	10	B		25	2.5	5	0.08	110	ZNO
1997 03 30.84		M	9.3	TI	20	L	5	48	2.8	4/			HOR02
1997 03 30.84		S	9.3	AA	11.0	L	7	32	6	4			VEL03
1997 03 30.85		M	9.7	TI	20	L	5	48	3.5	4			PLS
1997 03 30.85		S	8.9	AA	11.0	L	7	32	6	4			BAR06
1997 03 30.86		S	9.0	AA	5.0	B		20	5	3			BAR06
1997 03 30.87		S	9.7	VB	20	T	10	75	2.0	4			SHA02
1997 03 30.89		S	9.7	GA	15.6	L	5	29	4.0	2/			BOU
1997 03 30.94		S	9.5	VB	10	B		14	2.8	3			SHA02
1997 03 30.94		S	11.3	HS	30	T	10	170	1	2			GOL02
1997 03 31.85		S	9.1	AA	5.0	B		20	5	3			BAR06
1997 03 31.86		M	9.9:	NP	21.0	L	6	60	3	5/	2.0m	80	MAR02
1997 03 31.86		S	9.8	GA	25.4	J	6	72	3.0	3/			BOU
1997 03 31.87		S	9.4	S	20.3	T	10	80	2.3	4/			KAM01
1997 03 31.88		S	9.6	AC	25.3	L	6	58	& 2.2	4			PER01
1997 03 31.88		S	9.9	AC	28.0	T	6	68	2.5	3			MOE
1997 03 31.88		S	10.0	AC	25.3	L	6	58	& 0.8	4			VIT01
1997 03 31.89		S	9.7	VB	20	T	10	75	2.7	s4			SHA02
1997 04 01.80		S	9.6	HD	44.5	L	5	146	2.5	s5	0.4	100	SAR02
1997 04 01.85		S	9.2	AA	11.0	L	7	32	6	4			BAR06
1997 04 01.86		S	9.1	AA	11.0	L	7	50	5.5	4			BAR06
1997 04 01.86		S	9.6	S	20.3	T	10	80	2.2	4/	0.02	100	KAM01
1997 04 01.87		S	8.9	AA	5.0	B		20	6	3			BAR06
1997 04 01.87		S	9.7	GA	25.4	J	6	58	3.3	3			BOU
1997 04 01.87		S	10.3	AA	15.0	R	8	30	1.5	6			DIE02
1997 04 02.81		M	9.6	TI	10	B		25	3	4	0.07	105	ZNO
1997 04 02.83		S	9.2:	AA	5.0	B		20	3	2			BAR06
1997 04 02.86		M	9.7	TI	35	L	5	66	3	3/	0.1	120	HOR02
1997 04 02.91		E	10.4	NP	30	L	5	60	3	4			NEV
1997 04 02.91		S	9.8	HD	44.5	L	5	82	5	5/	0.3	110	SAR02
1997 04 03.79		S	9.8	HD	6.0	B		20	4	2			SAR02
1997 04 03.79		S	9.9	HD	44.5	L	5	82	2	s6			SAR02
1997 04 03.80		S	10.0	HD	6.0	B		20	1	0			KIS02
1997 04 03.83		S	9.3	AA	11	L	7	32	5	3			BAR06
1997 04 03.86		S	9.5	VB	33	L	5	45	1.9	3			SHA02
1997 04 03.86		S	10.3	AA	15.0	R	8	30	1.5	6			DIE02
1997 04 04.83		S	9.3:	AA	5.0	B		20	3	2			BAR06
1997 04 04.88		S	9.6	AC	25.3	L	6	58	& 2.3	3/			PER01
1997 04 04.88		S	10.1	AC	25.3	L	6	58	& 1.3	4			VIT01
1997 04 05.86		M	9.9	NP	21.0	L	6	60	1.5	6			MAR02
1997 04 06.83		S	9.7	S	20.3	T	10	80	2.2	4/			KAM01
1997 04 07.80		M	9.7	TI	10	B		25	3	4/	0.07	100	ZNO
1997 04 07.85		S	9.7	S	20.3	T	10	80	2.1	4			KAM01
1997 04 07.86		S	10.0	AC	15.2	L	5	42	2.5	3			MOE
1997 04 07.88		E	10.4	NP	30	L	5	60	3	4/			NEV
1997 04 07.88		M	9.7	GA	25.4	J	6	58	3.0	3/			BOU

Comet 81P/Wild 2 [cont.]

DATE (UT)	N	MM	MAG.	RF	AP.	T	F/	PWR	COMA	DC	TAIL	PA	OBS.
1997 04 07.88		S	9.7	VB	33	L	5	45	1.8	3			SHA02
1997 04 07.89		S	11.3	HS	30	T	10	170	1.5	2			GOL02
1997 04 09.84		S	10.0	AC	15.2	L	5	42	2.5	3			MOE
1997 04 09.89		E	10.4	NP	30	L	5	60	3	4/			NEV
1997 04 09.90		S	10.1	VB	20	T	10	75	1.4	s3			SHA02
1997 04 10.89		S	10.2	VB	33	L	5	75	2.9	3			SHA02
1997 04 11.21		S	9.9	AC	20.0	T	10	125	2.3	3/			SPR
1997 04 11.84		S	10.2	TI	10	B		25	2	2			HYN
1997 04 11.88		S	10.6	VB	30	R	18	100	1.8	3			SHA02
1997 04 13.80		M	9.7	TI	10	B		25	3	4/	0.07	105	ZNO
1997 04 23.89		S	10.4	VB	20	R	14	90					SHA02
1997 04 24.83		S	9.3	VF	20	L	5	71	5.3	3			BAR06
1997 04 26.83		S	9.2	VF	20	L	5	71	8	2			BAR06
1997 04 26.85		S	10.2	AC	15.2	L	5	42	2	3			MOE
1997 04 27.22		S	10.3	AC	20.0	T	10	125	1.9	2/			SPR
1997 04 27.83		S	9.6:	VF	20	L	5	71	& 4	2/			BAR06
1997 04 28.83		S	9.6:	VF	20	L	5	71	5	2			BAR06
1997 04 29.90		S	10.2	AC	25.3	L	6	58	& 2	2/			PER01
1997 04 29.90		S	10.3	AC	25.3	L	6	58	& 2	3			VIT01

Comet 94P/Russell 4

DATE (UT)	N	MM	MAG.	RF	AP.	T	F/	PWR	COMA	DC	TAIL	PA	OBS.
1996 11 13.83		C	19.2	GA	60.0	Y	6	a240	0.25			295	NAK01
1997 01 18.88		C	17.0	GA	60.0	Y	6	a240	0.55		2.8m	292	NAK01
1997 02 04.84		C	16.7	GA	60.0	Y	6	a120	0.6		2.1m	291	NAK01
1997 03 01.74		C	16.3	GA	60.0	Y	6	a120	0.6		3.3m	288	NAK01
1997 03 11.71		C	16.1	GA	60.0	Y	6	a120	0.85		3.6m	287	NAK01

Comet 96P/Machholz 1

DATE (UT)	N	MM	MAG.	RF	AP.	T	F/	PWR	COMA	DC	TAIL	PA	OBS.
1996 08 13.70		S	11	AA	20	L	8	83					C0002
1996 08 31.74		S	11	AA	20	L	8	83					C0002

Comet 100P/Hartley 1

DATE (UT)	N	MM	MAG.	RF	AP.	T	F/	PWR	COMA	DC	TAIL	PA	OBS.
1997 01 18.85		C	19.1	GA	60.0	Y	6	a240	0.35		0.9m	297	NAK01
1997 01 19.87		C	19.1	GA	60.0	Y	6	a240	0.35		0.8m	293	NAK01
1997 02 04.85		C	18.4	GA	60.0	Y	6	a240	0.4		1.8m	289	NAK01
1997 03 05.71		C	16.9	GA	60.0	Y	6	a240	0.5		2.4m	285	NAK01
1997 03 11.77		C	16.9	GA	60.0	Y	6	a120	0.6			295	NAK01

Comet 109P/Swift-Tuttle

DATE (UT)	N	MM	MAG.	RF	AP.	T	F/	PWR	COMA	DC	TAIL	PA	OBS.
1992 11 12.82		S	5.2	AE	5.0	B		10	4.5	6/			DOH
1992 11 13.78		S	4.9	AE	5.0	B		10	4	6/	0.5	32	DOH
1992 11 18.90		S	4.8	AE	5.0	B		10	4	6/	0.33	42	DOH
1992 11 20.72		S	5.1	AE	5.0	B		10	3.7	6/	0.33	42	DOH
1992 11 23.83		S	5.0	AE	5.0	B		10	3.5	6	0.5	45	DOH
1992 11 26.73		S	4.9	AE	5.0	B		10	3.5	6	0.42	54	DOH

Comet 118P/Shoemaker-Levy 4

DATE (UT)	N	MM	MAG.	RF	AP.	T	F/	PWR	COMA	DC	TAIL	PA	OBS.
1996 12 28.78		S	12.9	AC	25.4	L	5	104	1.0	3			MEY
1997 01 06.84		S	12.4	AC	25.4	L	5	104	1.2	3/			MEY
1997 01 12.86		S	12.8	AC	25.4	L	5	104	1.1	2/			MEY
1997 01 25.74		S	13.0:	HS	35	L	5	237	1	2/			HOR02
1997 01 26.76		S	12.8	AC	25.4	L	5	104	0.8	3			MEY
1997 01 30.43		C	13.1	GA	60.0	Y	6	a120	2.5			70	NAK01
1997 02 01.78		S	12.9	AC	25.4	L	5	104	1.0	2/			MEY
1997 02 01.84		M	13.5	HS	35	L	5	158	0.8	3			HOR02

Comet 118P/Shoemaker-Levy 4 [cont.]

DATE (UT)	N	MM	MAG.	RF	AP.	T	F/	PWR	COMA	DC	TAIL	PA	OBS.
1997 02 01.89		S	13.1	AC	25.4	J	6	115	0.9	1			BOU
1997 02 02.75		M	12.7:	HS	35	L	5	104	1.6	2/			PLS
1997 02 02.75		M	12.8	HS	35	L	5	104	1.5	3			HOR02
1997 02 02.86		S	13.3:	VB	30	R	18	170	0.7	3			SHA02
1997 02 03.46		S	12.8	GA	25.4	L	4	71					SEA
1997 02 05.86		B	13.0	HS	25.6	L	5	42	1.5	5			BIV
1997 02 06.79		M	12.7	HS	35	L	5	104	1.4	3			HOR02
1997 02 06.80		S	13.7:	HS	25.4	L	6	104	1	4			SAR02
1997 02 07.75		S	13.2	HS	44.5	L	5	230	0.7	3/			SAR02
1997 02 07.78		S	12.9	AC	25.4	L	5	104	1.2	2			MEY
1997 02 07.92	a	S	12.9	AC	25.4	J	6	88	1.4	1/			BOU
1997 02 07.93		S	13.5:	VB	33	L	5	100	1.3	2			SHA02
1997 02 07.97		S	14.2:	VB	30	R	18	170	0.7	1			SHA02
1997 02 08.79		S	13.4	HS	44.5	L	5	230	0.5	2			SAR02
1997 02 08.79		S	13.5	HS	44.5	L	5	230					BAK01
1997 02 08.89		S	12.5	NP	44.5	L	5	100	1	2			MAR02
1997 02 08.89		S	12.7	NP	44.5	L	5	100	2	1			SAN04
1997 02 09.51		C	13.3	GA	60.0	Y	6	a120	2.2				NAK01
1997 02 09.94		S	12.9	AC	25.4	L	5	104	1.1	2			MEY
1997 02 10.82		S	13.5:	VB	30	R	18	290	0.3	2			SHA02
1997 02 10.91	a	S	13.0	AC	25.4	J	6	88	1.4	1			BOU
1997 02 14.78		M	12.7	HS	35	L	5	237	0.7	2			HOR02
1997 02 14.79		S	12.6	HS	35	L	5	237	0.7	1/			PLS
1997 02 24.44		C	13.6	GA	60.0	Y	6	a120	1.75		2.8m	94	NAK01
1997 02 25.85		S	14.1	VB	30	R	18	290	0.7	3			SHA02
1997 02 28.77		M	13.0	HS	35	L	5	158	0.9	2			HOR02
1997 03 01.78		S	13.5	HS	35	L	5	237	0.5	3			HOR02
1997 03 01.83		S	13.1:	AC	25.4	L	5	104	1.1	1			MEY
1997 03 02.92		S	[13.5	VB	30	R	18	290					SHA02
1997 03 05.78		M	13.3	HS	35	L	5	237	0.8	2/			HOR02
1997 03 07.77		S	13.3	HS	35	L	5	237	0.8	1/			HOR02
1997 03 07.78		M	13.2	HS	35	L	5	237	0.6	3			PLS
1997 03 07.81		S	14.5	HS	44.5	L	5	230	1	2/			SAR02
1997 03 07.81		S	14.6	HS	44.5	L	5	230	1	5			BAK01
1997 03 07.81		S	14.6	HS	44.5	L	5	230	1	5	0.03	90	SZE02
1997 03 08.83		S	13.7	HS	44.0	L	5	156	0.3	3			HAS02
1997 03 10.79		S	13.2	HS	35	L	5	237	0.9	1/			HOR02
1997 03 10.81		S	13.3	AC	25.4	L	5	104	0.8	2			MEY
1997 03 11.79		S	13.3:	HS	35	L	5	158	0.8	1/			HOR02
1997 03 12.80		S	13.1	HS	35	L	5	158	1.2	1/			HOR02
1997 03 12.81		M	12.9	HS	35	L	5	158	0.8	3			PLS
1997 03 31.88		S	13.8:	VB	20	T	10	135	0.5	2			SHA02
1997 04 01.84		S	14.5:	HS	44.5	L	5	230	0.5	3			SAR02
1997 04 02.85		S	13.2:	HS	35	L	5	237	0.7	2			HOR02
1997 04 02.92		S	[13.5	HS	44.5	L	5	230	0.5				SAR02
1997 04 09.88		S	[13.8	VB	20	T	10	135					SHA02

Comet 121P/Shoemaker-Holt 2

DATE (UT)	N	MM	MAG.	RF	AP.	T	F/	PWR	COMA	DC	TAIL	PA	OBS.
1997 01 31.66		C	14.9	GA	60.0	Y	6	a120	1.5		2.2m	254	NAK01
1997 02 02.90		S	14.3	HS	35	L	5	237	0.7	2/			HOR02
1997 02 07.04		S	13.7	HS	44.5	L	5	230	0.8	5			BAK01
1997 02 07.04		S	14.5:	HS	44.5	L	5	230	1	3			SAR02
1997 02 07.19		S	13.9:	HS	35	L	5	237	1	3			HOR02
1997 03 01.69		C	14.8	GA	60.0	Y	6	a120	1.3		1.7m	251	NAK01
1997 03 01.82		S	13.8:	HS	35	L	5	237	0.5	2			HOR02
1997 03 04.81		S	14.1	HS	35	L	5	237	0.7	2			HOR02
1997 03 04.85		S	9.5	AC	10.0	B		25	1.3	4			HAS02
1997 03 05.82		S	13.9	HS	35	L	5	158	0.7	2/			HOR02
1997 03 07.83		S	13.9	HS	35	L	5	237	0.9	2			HOR02
1997 03 07.84		S	13.9	HS	35	L	5	237	0.8	1/			PLS
1997 03 07.98		S	14.5	HS	44.5	L	5	230	0.5	6			SAR02
1997 03 07.98		S	14.7	HS	44.5	L	5	230	0.4	8			SZE02
1997 03 07.98		S	14.9	HS	44.5	L	5	230	0.5	s6			BAK01

Comet 121P/Shoemaker-Holt 2 [cont.]

DATE (UT)	N	MM	MAG.	RF	AP.	T	F/	PWR	COMA	DC	TAIL	PA	OBS.
1997 03 08.83		S	14.1	HS	44.0	L	5	156	0.6	3			HAS02
1997 03 08.99		S	14.6	HS	44.5	L	5	230	0.7	3			SAR02
1997 03 08.99		S	14.6	HS	44.5	L	5	230	1	5/			BAK01
1997 03 10.84		S	14.6	HS	35	L	5	237	0.6	2/			HOR02
1997 03 11.65		C	15.0	GA	60.0	Y	6	a120	1.0		1.8m	240	NAK01
1997 03 11.83		S	14.0	HS	35	L	5	237	0.9	1/			HOR02
1997 03 12.93		S	14.4	HS	35	L	5	237	0.8	1			HOR02
1997 04 02.92		S	13.7	HS	44.5	L	5	230	1	3/			SAR02

Comet 122P/de Vico

DATE (UT)	N	MM	MAG.	RF	AP.	T	F/	PWR	COMA	DC	TAIL	PA	OBS.
1995 10 03.78		B	5.8	AA	20.0	C	9	60	2.6	8	0.9	295	NAG04
1995 10 06.80		B	5.6	S	20.0	C	9	60		7	1.2	300	NAG04
1995 10 09.81		B	5.6	S	10.0	R	4	20	2.3	7	<1.0		NAG04
1995 10 25.18		S	6.0	SC	6.0	R	10	30	6				MAN01
1995 11 04.84		B	7.9	S	15.0	B		25	3.9	3			NAG04

Comet 126P/IRAS

DATE (UT)	N	MM	MAG.	RF	AP.	T	F/	PWR	COMA	DC	TAIL	PA	OBS.
1996 12 28.40		C	14.3	GA	60.0	Y	6	a120	1.2				NAK01
1997 01 12.43		C	14.2	GA	60.0	Y	6	a120	1.9		2.1m	77	NAK01
1997 01 30.42	a	C	15.0	GA	60.0	Y	6	a120	1.3		2.3m	69	NAK01
1997 02 09.43		C	15.0	GA	60.0	Y	6	a120	1.1			62	NAK01
1997 02 24.42	a	C	15.3	GA	60.0	Y	6	a120	1.0				NAK01
1997 03 08.80		S	14.0	HS	44.0	L	5	222					HAS02

Comet P/1997 B1 (Kobayashi)

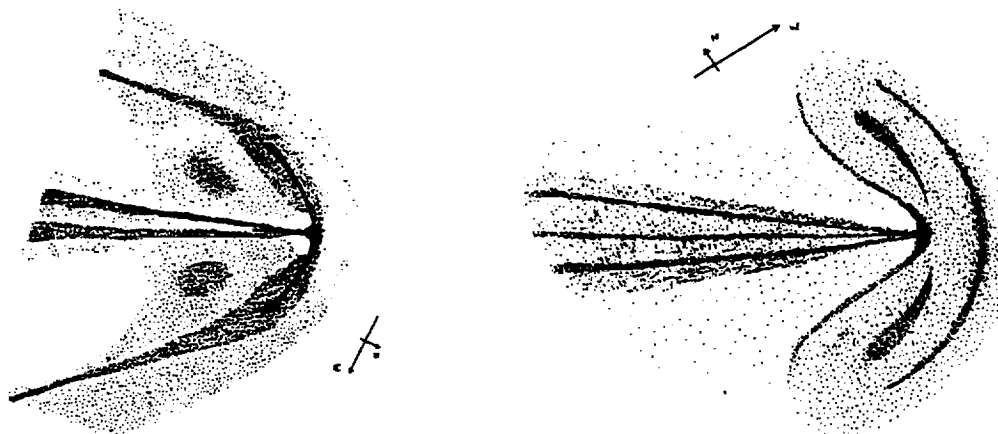
DATE (UT)	N	MM	MAG.	RF	AP.	T	F/	PWR	COMA	DC	TAIL	PA	OBS.
1997 02 04.75		C	17.5	GA	60.0	Y	6	a240	0.3	8/	0.6m	290	NAK01
1997 02 09.69		C	17.4	GA	60.0	Y	6	a240	0.4	8	0.6m	295	NAK01
1997 02 27.62		C	17.6	GA	60.0	Y	6	a240	0.4	8	1.0m	297	NAK01

Comet P/1997 C1 (Gehrels)

DATE (UT)	N	MM	MAG.	RF	AP.	T	F/	PWR	COMA	DC	TAIL	PA	OBS.
1997 02 04.71		C	17.4	GA	60.0	Y	6	a240	0.55		1.3m	291	NAK01
1997 02 09.66		C	17.9	GA	60.0	Y	6	a240	0.6		1.5m	290	NAK01
1997 02 24.45		C	18.4	GA	60.0	Y	6	a240	0.45		1.2m	298	NAK01
1997 03 01.60		C	18.4	GA	60.0	Y	6	a240	0.45		1.1m	298	NAK01
1997 03 05.56		C	18.4	GA	60.0	Y	6	a240	0.4		1.9m	294	NAK01

◇ ◇ ◇

Below: two drawings of comet C/1996 B2 (Hyakutake) by Martin Lehký at Hradec Králové, Czech Republic, as seen through a 42-cm f/5 L (75×), on 1996 Mar. 25.94 (left) and Mar. 27.81 (right).



Ground-Based Near-Infrared Imaging of Comet P/Halley 1986 III

CHARLES E. WOODWARD¹

Wyoming Infrared Observatory, Department of Physics and Astronomy, University of Wyoming, Laramie, Wyoming 82070-3905
E-mail: chelsea@kaya.uwyo.edu

MARK A. SHURE

Georgia State University, Center for High Angular Resolution Astronomy, 38 Peachtree Center Avenue, 1039GCB, Atlanta, Georgia 30303

WILLIAM J. FORREST¹

University of Rochester, Department of Physics and Astronomy, Rochester, New York 14627

T. J. JONES AND R. D. GEHRZ

Astronomy Department, School of Physics and Astronomy, 116 Church Street S.E., University of Minnesota, Minneapolis, Minnesota 55455

TETSUYA NAGATA¹

Nagoya University, Department of Physics, Nagoya 464-01, Japan

AND

ALAN T. TOKUNAGA

University of Hawaii, Institute for Astronomy, 2680 Woodlawn Drive, Honolulu, Hawaii 96822

Received September 24, 1993; revised August 12, 1996

We present an analysis of 1- to 5- μm , near-infrared broadband images of Comet P/Halley 1986 III covering a 10^4 -km square region of the inner coma obtained on three consecutive nights in 1986 March during post-perihelion passage. In all images, the coma is extended in the sunward direction and appears distinctly non-spherical, similar to morphology in the 10- μm made by Hayward *et al.* (1987) 3.0 days later during the *Giotto* encounter. Marked variation in the coma's overall structure and brightness also was apparent, including the presence of a jet feature which we associate with a short-term outburst of material from the comet nucleus. The observed coma surface brightness dependence upon nucleocentric distance (r) at all wavelengths in both the comet dust tail and in the jet deviates from the dependence predicted by the "steady state" model for comet nucleus ablation, with the radial decrease in surface brightness being slower than r^{-1} on the jet side of the nucleus and faster than r^{-1} on the tail side. The near-infrared colors of the coma are not constant as a function of nucleocentric distance, suggesting that the grain properties

are not uniform across the coma. Based on an elementary dynamical analysis of the trajectories of dust particles ablated from the nucleus we argue that these observations may be consistent with the hypothesis that particles emitted in jets fragments in the outflow on time scales of a few hours. © 1996 Academic Press, Inc.

I. INTRODUCTION

Infrared images of comets convey valuable information about the spatial distribution within the inner coma and tails of dust grains with various physical properties (e.g., Hanner and Tokunaga 1991, Campins *et al.* 1989). At wavelengths shortward of 2 μm , the observed light is primarily sunlight scattered by dust grains, while at longer wavelengths, thermal emission from the dust dominates the radiation. In addition, at near-infrared wavelengths many comets generally do not exhibit strong gaseous emission bands (Johnson *et al.* 1983), unlike the visual and ultraviolet spectral regions. Observations by Maillard *et al.* (1987) show that there were no such infrared emission lines in Comet P/Halley 1986 III. Thus, the imaging of comets in

¹ Visiting astronomer at the Infrared Telescope Facility, operated by the University of Hawaii, under contract from the National Aeronautics and Space Administration.

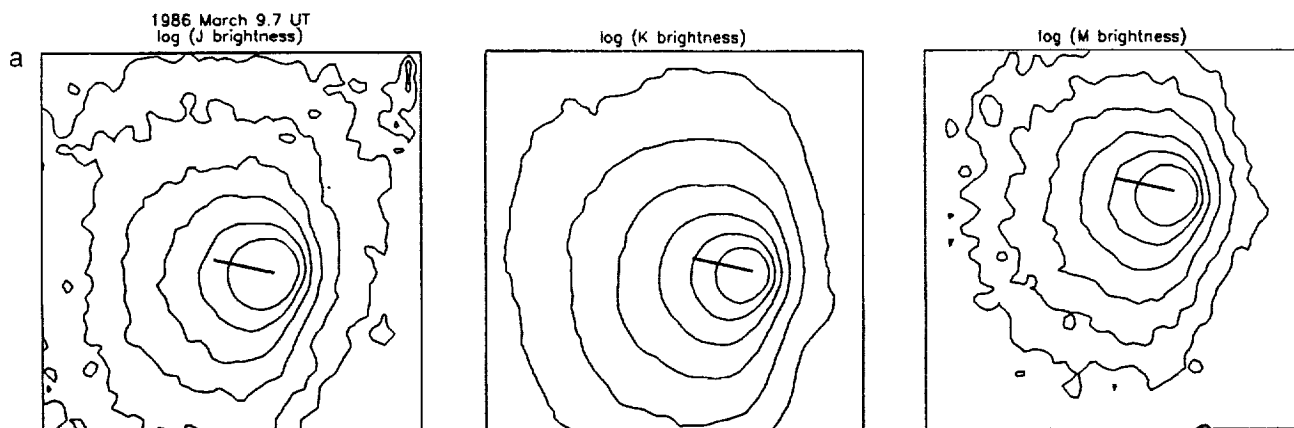


FIG. 1. Near-infrared images of Comet P/Halley 1986 III. The images are logarithm-scaled with contours at equal intervals. These images have been interpolated onto a grid of 63×63 pixels, each of which is $0.21''$ square (one-half the size of the original image pixels). The field of view is 13.2×13.2 arcsec. There is more than one image for each wavelength in some cases, to include data available beyond the 13.2×13.2 arcsec area. (a) 1986 March 9.7 UT (at J, K, and M'). (b) 1986 March 10.7 UT (at J, H, K, 3.3, L' , and M'). (c) 1986 March 11.7 UT (at K, and L').

the infrared can be a powerful method of studying spatial variations in the optical properties of the dust.

In particular, it is important to understand in detail what types of grains populate comet jets, classical dust tails, and anti-tails and how these structures are oriented with respect to the nucleus, the direction of the solar radiation field, and the projected orbital motion for a given comet. Such studies can yield important information about: the physical process of the ablation of comet nuclei; how grains of various sizes and compositions behave in the solar vicinity after their ablation from the nucleus; and the nature of the grains frozen into the nuclei during the formation of the primitive solar system. Among the grain properties that can be investigated with infrared techniques are scattered radiation, thermal emission, and albedo (see Gehrz and Ney 1992).

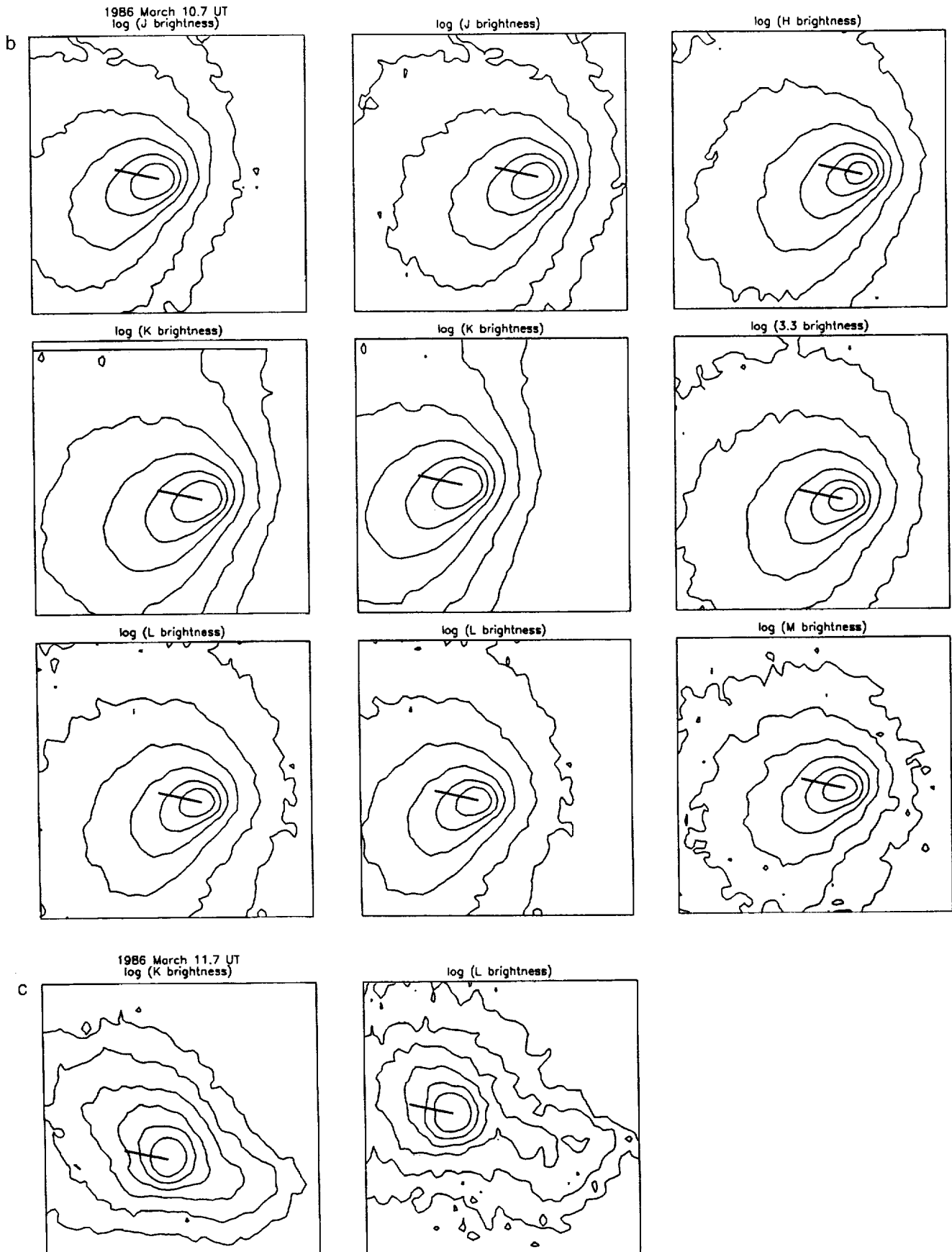
In this paper we present high-resolution 1- to $5\text{-}\mu\text{m}$ broadband images of P/Comet Halley 1986 III (hereafter referred to simply as P/Halley) taken in 1986 March and discuss the results of some simple model analyses. Dynamical studies of the trajectories of dust grains in the coma of P/Halley suggest that particles ablated from the nucleus are produced in a jet similar to those seen in the *Giotto* spacecraft images, and can produce the sunward extension of the coma observed near-infrared surface brightness.

II. OBSERVATIONS

The JHK $L'M'$ and $[3.3\text{-}\mu\text{m}]$ broadband observations of P/Halley were obtained at the NASA IRTF 3-m telescope on Mauna Kea, Hawaii on 1986 March 9.7, 10.7, and 11.7 UT, using the University of Rochester's 32×32 InSb infrared array camera. The observational epoch was approximately 30 days after perihelion passage (1986 Febru-

ary 9.5 UT) and three days before closest approach by the *Giotto* spacecraft. The observing techniques and data reduction procedures for this camera are described in Forrest *et al.* (1985) and Woodward (1987). The image pixel scale ($0.42''/\text{pixel}$) and rotation angle of the camera were calibrated using star pairs and star trails (obtained with the telescope drive switched off) as described in Forrest *et al.* (1986). A reference field for blank-sky background images was chosen $1000''$ south of the comet nucleus. Seeing varied from night to night; the average FWHM of star images at K was $1.0''$, $1.0''$, and $1.3''$ on March 9.7, 10.7, and 11.7 UT, respectively. The comet's heliocentric and geocentric distances were 0.9 and 1.1 AU, respectively, while the phase angle at the time of these observations was $\approx 60^\circ$. The image scale was ≈ 300 km/pixel with this geometry. Repeated observations of the standard star BS 7754 were used to derive a flux density calibration. We estimate an overall uncertainty of $\pm 10\%$ in the derived flux levels. This error estimate includes both systematic and photometric effects.

In order to take full advantage of the spatial resolution obtainable from multiple images taken at different positions for each wavelength, images were shifted and interpolated onto a 63×63 pixel grid before combining into the final mosaics. Small background variations observed in individual raw images (most likely due to the brightening morning twilight) were corrected by applying uniform offsets to each image before forming mosaics. These offsets were chosen such that they averaged to zero. The resulting 63×63 mosaics are presented in Figs. 1a through 1c. Solar illumination is from a position angle of 78° east of north (as indicated on the figures) and the projected comet velocity is toward a position angle of 241° . Distinct changes in the small-scale morphology are seen from night to night, and



all images are asymmetric about the nucleus. This is hardly surprising, as spectacular variations were also seen in optical images obtained on the preceding four nights (Jewitt 1991).

III. DISCUSSION

A. Spatial Morphology

The overall near-infrared morphology of the inner coma of P/Halley observed on each of the three nights (1986 March 9.7, 10.7, and 11.7 UT) varied, as can be seen by comparing the images made on the three nights at J (1.23 μm) and K (2.23 μm). All of the near-infrared images are asymmetric about the nucleus and show an extension at position angles (measured east of north) that varied with time ($\approx 90^\circ$ on March 9.7 UT; $\approx 115^\circ$ on March 10.7 UT; $\approx 50^\circ$ on March 11.7 UT). Hayward *et al.* (1987) obtained a 10- μm image on 1986 March 13.7 UT that exhibits a similar spatial morphology as that seen in our 1986 March 9.7 UT image (Fig. 1b; Fig. 4a). This feature is pointed about 40° southeast of the direction to the sun, and would at first glance appear to be an anti-tail similar to the one observed by Ney (1974a, 1974b) in Comet Kohoutek 1973 XII. Ney showed that the anti-tail had a smooth, featureless continuum energy distribution with no superheat (for a rigorous definition of superheat, see Gehrz and Ney 1992), and concluded that it was composed of dust grains larger than a few 10's of micrometers in radius. We argue below on dynamical grounds that it is difficult to understand how the extension we observed in Comet P/Halley could be produced by grains nearly as large as those in the anti-tail of Kohoutek, and that it is more probable that the extension is produced by emission from a jet of rather small particles. We refer to this feature hereafter as "the jet."

Our data set suggests that the jet apparently persisted in the same general spatial direction for a period of 48 hr from 1986 March 9.7 through 11.7 UT, and it pointed toward the sunward direction as did the jet observed on 1986 March 13.7 UT by Hayward *et al.* (1987). In view of this behavior, it seems unlikely that the jet seen during March 9.7–11.7 UT emanated from a single jet that was subject to the diurnal affects associated with a short rotation period. P/Halley's nucleus is believed to be tumbling in space, with periods between 2.2 to 7.4 days (Larson *et al.* 1987, Millis and Schleicher 1986). It seems likely that the direction of the jet would have changed substantially had the 2.2 days period been involved. Indeed computer enhanced visible CCD images obtained during the same period (Larson *et al.* 1987) covered by our infrared images suggest that the near-nuclear structure of the comet changed daily due to activity from one or more jets. The jets that are apparent in the near-infrared images could have been emitted from an area on a polar region the nucleus that is inertially pointed toward the sun for long periods of time.

Alternatively, there may be several spots on the nucleus that emit jets located in such a way that the effects of rotation are difficult to discern.

B. Surface Brightness Distribution

The radial and azimuthal infrared surface brightness variations derived from our images can be used to test models of dust grain production from cometary nuclei. If the rate of grain production from the nucleus is constant (i.e., steady-state) and spherically symmetric and if the coma optical depth is everywhere much less than unity, then standard models (cf. Gehrz and Ney 1992) predict that the surface brightness of the coma will fall off as r^{-1} (where r is the nucleocentric distance). The inner coma brightness profile of P/Halley has exhibited this behavior at some epochs (Gehrz and Ney 1992, Reitsemä *et al.* 1989); other comets often exhibit this behavior as well (Campins *et al.* 1989). When solar radiation pressure becomes important, the azimuthally-averaged surface brightness profile varies as $r^{-1.5}$ (cf., Jewitt 1991).

In order to describe the shapes of the brightness profiles, we define the logarithmic derivative $m = d \log B(r) / d \log r$, where $B(r)$ is the radial surface brightness profile and r is the projected angular distance from the photocenter of the image. Our assumption above of a steady-state, isotropic outflow yields $m = -1$, while the radiation pressure dominated case gives $m = -1.5$. Integrating the surface brightness over a circular aperture of angular radius r , we obtain the integrated brightness $B'(r)$, with a logarithmic slope of $m' = d \log B'(r) / d \log r = m + 2$. Thus, the steady-state, isotropic model predicts $m' = 1$; while the radiation-dominated pressure case predicts $m' = 0.5$.

In Table I, we present the integrated surface brightness as a function of increasing aperture size centered on the nucleus obtained from the images shown in Figs. 1a through 1c. These results are plotted in Figs. 2a through 2c. For the March 9.7 UT images the integrated brightness closely follows a slope of $m' = 1$, in agreement with the steady-state, isotropic grain production model. This is in agreement with the results of multi-aperture photometry of this comet obtained with a single detector (Gehrz and Ney 1992). On the following night, the slope increased slightly ($m' \approx 1.1$) and considerably more on the third night ($m' \approx 1.5$). On each of the three nights, all the wavelengths observed show the same slope. The slopes of integrated brightness on the last two nights suggest surface brightness profiles with $m \approx -0.9$ and -0.5 , respectively (averaged over all azimuth angles). These represent more uniform distributions of surface brightness (i.e., less peaked) than the predicted $B \propto r^{-1}$ steady-state isotropic model.

This trend in slopes inferred from the aperture photometry can be explained by deviation from a steady-state out-

TABLE I
Observational Summary of Image Data for Comet P/Halley 1986 III

FILTER	λ (μm)	$\Delta\lambda$ (μm)	1986 UT DATE	UT TIME OF OBSERVATIONS (hr:min)	INTEGRATED MAGNITUDE IN A SYNTHETIC APERTURE ^a					
					3.2"	4.0"	5.0"	6.3"	7.9"	10.0"
<i>J</i>	1.23	0.23	March 09	16:28–16:33	7.55	7.29	7.04	6.79	6.54	6.31
			March 10	16:22–16:23	8.12	7.83	7.55	7.27	6.97	6.68
<i>H</i>	1.65	0.32	March 10	16:25–16:26	7.44	7.15	6.87	6.59	6.29	5.99
<i>K</i>	2.23	0.41	March 09	16:20–17:08	6.76	6.48	6.22	5.96	5.70	5.45
			March 10	16:12–16:17	7.16	6.86	6.59	6.31	6.02	5.74
			March 11	16:36–16:41	8.66	8.28	7.91	7.55	7.18	6.83
3.3	3.26	0.20	March 10	16:28–16:30	5.35	5.06	4.78	4.50	4.20	3.91
<i>L'</i>	3.81	0.63	March 10	16:32–18:12	4.33	4.03	3.75	3.46	3.15	2.86
			March 11	16:55–18:24	5.79	5.43	5.07	4.70	4.32	3.94
<i>M'</i>	4.67	0.18	March 09	16:36–16:41	2.32	2.06	1.83	1.60	1.38	1.18
			March 10	16:35–16:41	2.76	2.47	2.20	1.92	1.64	1.36

^a Integrated magnitudes measured in an octagonal box with given diameter. The diameters were chosen to give 0.25 mag decrease per aperture for a r^{-1} brightness law (see text).

flow. As shown in Table I, the integrated *K*-band flux within the central 3.2" dropped by 0.4 mag between the first two nights (1986 March 09.7 UT and March 10.7 UT), and by an additional 1.6 mag on the following night (1986 March 11.7 UT). This drop in integrated surface brightness likely corresponded to a reduction in the dust production rate and thus to the decreasing slopes in the brightness distributions shown in Figs. 2a through 2c.

Variations in the level of activity during 1986 March 09 UT–12 UT also were recorded in observations at other wavelengths. The count rates of the *IUE* fine error sensor (FES) declined by a factor of 2.5 from 1986 March 9.6 UT to 11.6 UT (Festou *et al.* 1986, Feldman *et al.* 1987). Most of the signal is due to C_2 and continuum emission in a $12'' \times 12''$ area centered on the comet coma. Spectra obtained with the LWP camera of *IUE* over this same 3-day period showed that the brightness of the CS (0–0) molecular feature decreased by a factor of ≈ 3 (Festou *et al.* 1986). The *IUE* observations suggest that the dust production rate of P/Halley diminished over the temporal epoch covered by our observations. The 10- μm observations of Hanner *et al.* (1987a, 1987b) also suggest that dust emission rates and particle sizes present in the coma varied rapidly, on timescales of 3 to 7 days, during this same period in March 1986 UT.

A high production rate of C_2 on 1986 March 10.3 also was

observed in a 78 arcsec aperture by Millis and Schleicher (1986). The rate on March 10.3 ($\log Q \approx 27.5$) is about twice that observed on either 1986 March 9.3 or 1986 March 11.3, and a factor of three times larger than that observed on 1986 March 12.3. Indeed, the production rate of C_2 observed on March 10.3 corresponds to the first of two maxima in one period of the 7.4 days rotation rate of the nucleus proposed by Millis and Schleicher (1986) spanned by our infrared observations. Their data also indicate that the overall production rate of C_2 was steadily decreasing during this epoch. The variation in the observed near-infrared brightness measured from our images (Table I) also shows a similar temporal decline.

C. The Jet

The integrated flux in P/Halley's coma on 1986 March 9.7 and 10.7 UT, for circular diaphragms of diameter D centered on the nucleus (effectively averaging over all azimuthal angles), is proportional to D^{-1} (Table I). However, there is a wealth of detailed information in the azimuthal structure of the original images that is difficult to display in a gray-scale image due to the large dynamic range of the images. A close analysis of the surface brightness distribution of the near-infrared images of P/Halley (Fig. 3) shows that the radial surface brightness distribution of the

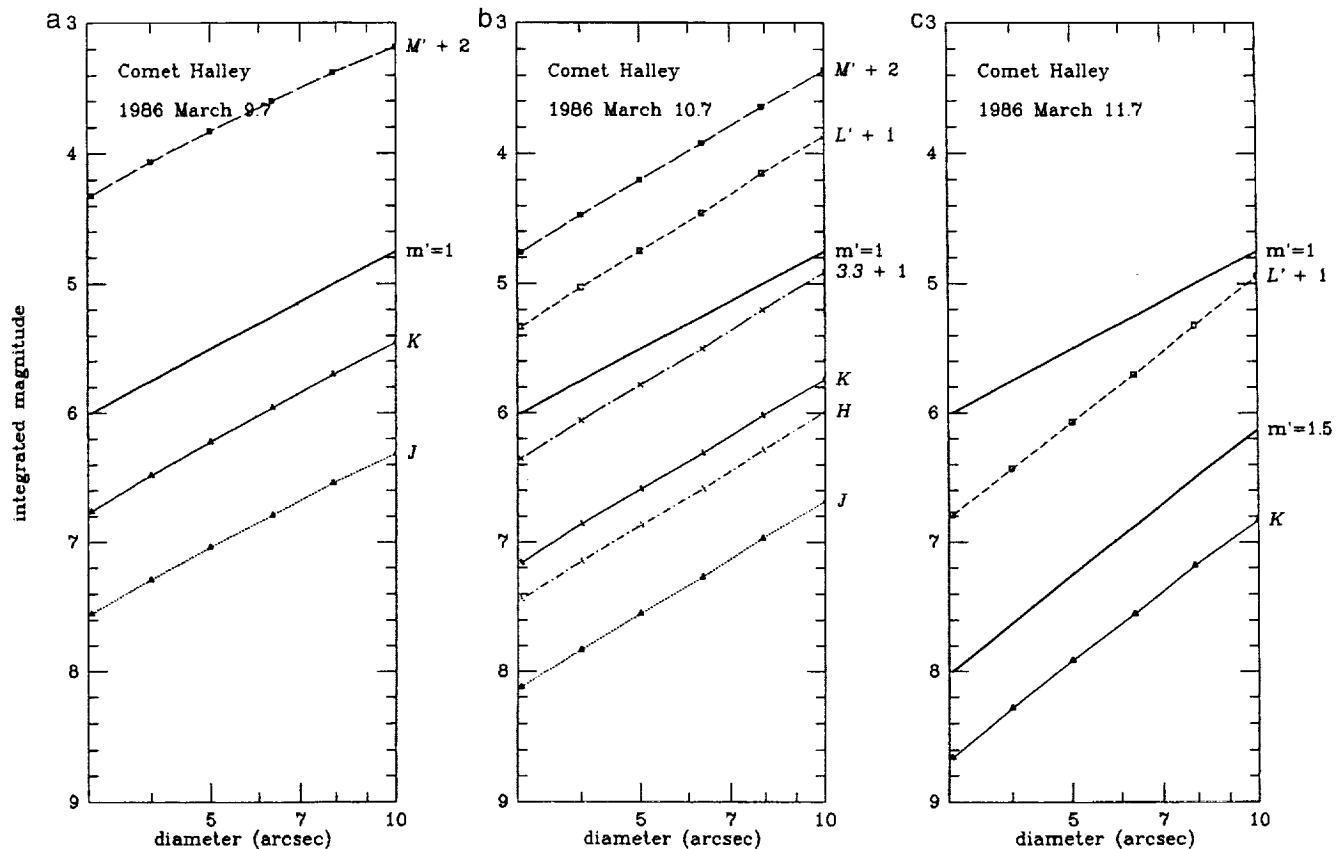


FIG. 2. Integrated surface brightness from images in Fig. 1. These were calculated using summed signal within octagonal apertures centered on the nucleus (see Table I). Aperture diameters were selected to give 0.25 mag decrease per aperture for r^{-1} surface brightness distribution (see text).

inner coma in the sunward and anti-sunward directions on 1986 March 10.7 UT deviates in detail at all near-infrared wavelengths from that predicted by the standard model. Specifically, the radial decrease in surface brightness is considerable shallower than r^{-1} on the jet side (east) of the nucleus and steeper than r^{-1} on the opposite (tail) side (west). These two gradients compensate for one another when the total flux is integrated within circular diaphragms centered on the nucleus. The resulting multi-aperture photometry (cf., Gehrz and Ney 1992), while presenting a generally valid indication of the integrated mass-loss characteristics of the nucleus, can lead to a misleading picture of the detailed surface brightness distribution within the coma.

The relatively flat surface brightness gradient on the jet side of the nucleus, compared to the r^{-1} law requires either that the distribution of dust grain sizes changes with nucleocentric distance from the nucleus, or the outflow velocity is not constant with nucleocentric distance. Analysis of the color gradients in Section III.E strongly implicate changes in grain size. Explanations for a change in grain size with radius fall into two broad categories. In one scenario, grains of different size are leaving the nucleus at

different velocities. Large grains, for example, may leave the nucleus at a slightly slower rate, causing a change in the ratio of large to small grains with nucleocentric distance. In the other scenario, the grains could be fragmenting to smaller grain size as they move out into the coma. Theoretical calculations suggest that the grains that fragment will do so within a few hundred kilometers of the nucleus, below the spatial resolution of our images (Combi 1994, Konno *et al.* 1993). Based on these calculations, we should see no effect as the grains would be fully fragmented outside of the inner resolution element of images. Nonetheless, the grain fragmentation model is sufficiently appealing that we will investigate its consequences if fragmentation can take place over longer time scales than recent theoretical work predicts.

In our grain fragmentation scenario, we assume that the total mass of material released from the coma in the form of solids remains constant in the outflow. An elementary argument suffices to demonstrate that the light scattering and thermal emission efficiency of a given mass of ejected solids increases under certain conditions in this scenario. Consider a mass M of ejected solid material with uniform density that is divided into a total of n spherical particles,

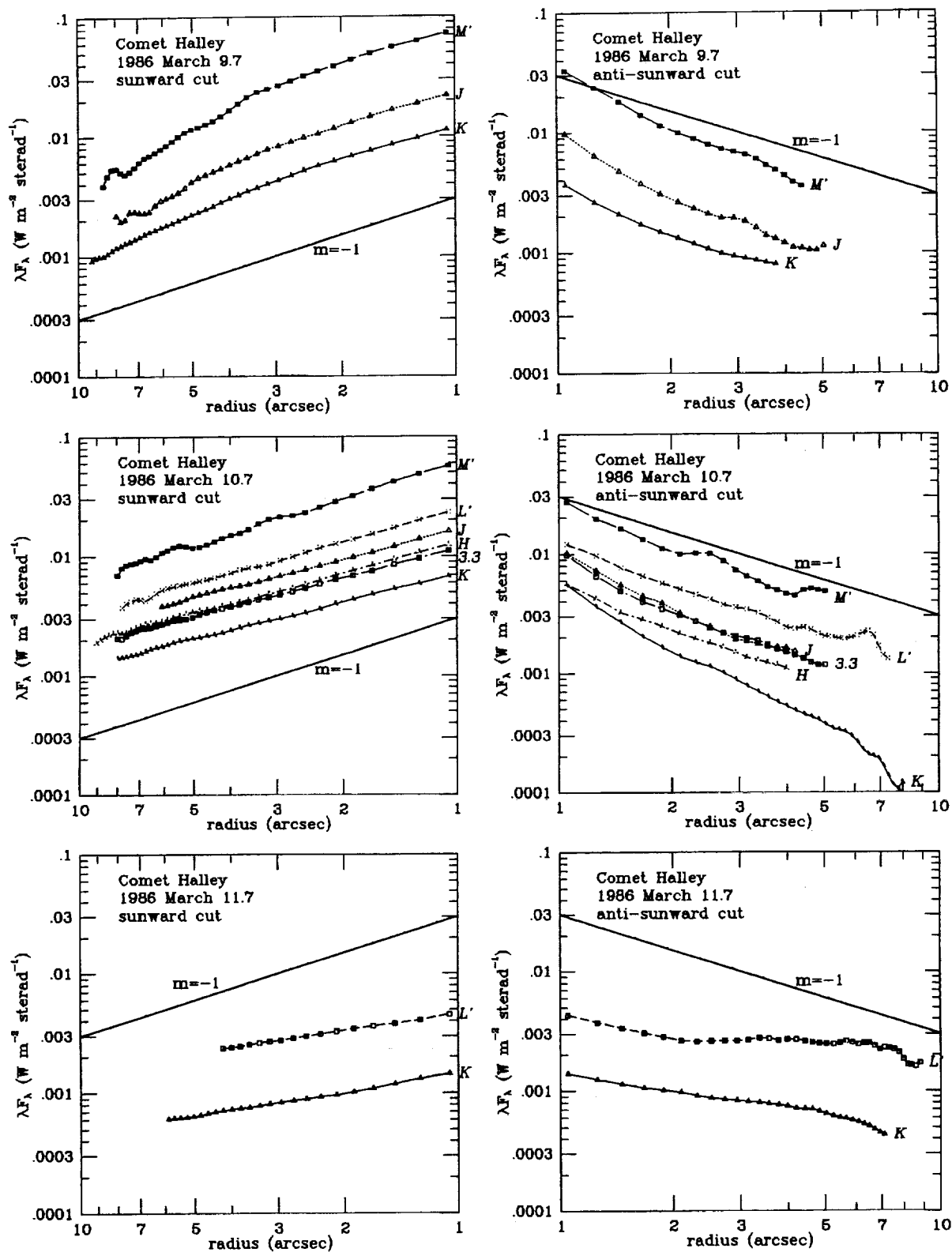


FIG. 3. Surface brightness profiles of Comet P/Halley 1986 III. These profiles represent cuts through the images in Fig. 1 in the sunward direction (PA = 78°) and in the anti-sunward direction (PA = 258°).

each with constant density r and radius $a(n)$, where $a(n) = [(3/(4\pi)M/(nr))]^{1/3}$ and $n = 1$ denotes the special case when the material is concentrated in a single large object. In this case, the total scattered radiation and thermal emission from this material respectively will be proportional to $L_{(s,a)} \propto Q_{(s,a)}n[a(n)]^2 \propto Q_{(s,a)}[m/r]^{2/3}n^{1/3}$, where $Q_{(s,a)}$ are the Planck mean scattering and absorption cross sections of the grains.

An examination of Gilman's (1974) calculations shows that $Q_{(s,a)} \approx 1$ for particles with radii on the order of or larger than $a(n) \approx \lambda = 1 \mu\text{m}$, and $Q_{(s,a)} \propto a(n)T_{\text{gr}}^2$ for particles smaller than $a(n) \approx (\lambda/2\pi) \approx 0.2 \mu\text{m}$, where T_{gr} is the grain temperature. Since $n \propto (m/a^3)$, $n^{1/3} \propto a^{-1}$, the scattering/emission efficiency of a given mass of material rises strongly as particles with radii in the range 1 to 10 μm break up into particles with radii as small as 0.5 to 1.0 μm . The $Q_{(s,a)} \propto a(n)T_{\text{gr}}^2$ dependency cancels the $n^{1/3} \propto a^{-1}$ dependency as the particles disintegrate further to sub-micrometer sizes, so that the scattering/emission efficiency no longer increases with further size reduction.

When the grain fragments, the emissivity drops at near infrared wavelengths, hence the grain temperature will increase to compensate (i.e., superheat). Thus, the emission at L' and M' will rise with the shift in the blackbody curve to shorter wavelengths, assuming that the grain albedo at visual wavelengths (where the bulk of the solar radiation is absorbed) remains essentially unchanged. At Sun-comet (heliocentric) distances of ≈ 1 AU, this amounts to a 15 to 20% effect at 3.8 and 5 μm , assuming the grains were not perfect blackbody radiators to begin with. Thus, grain fragmentation can explain the slow drop in surface brightness with radial distance both in the scattering and thermal regimes. We stress that our argument assumes that the total grain mass remains constant, and that evaporation of the grains is not an issue. The calculations presented below (see Section III.E) demonstrate that jet particles ejected at a velocity of $\leq 1 \text{ km s}^{-1}$ will travel out of the images in about 4 hr. This is the timescale over which the particles must fragment if fragmentation is the explanation of the radial color gradient of the jet side of the comet.

Gehrz and Ney (1992) argued on the basis of infrared photometry from 1.25 to 23 μm that the fluxes observed with 5" to 20" diaphragms were consistent with the interpretation that the typical radii of the optically important grains in P/Halley's coma were 0.5 to 1.0 μm . The near-infrared images of the jet show a gradual transition from a relatively flat surface brightness distribution inside 3" to one approaching r^{-1} at 5" to 10". This would imply that the solids ejected in the jet broke up in the outflow, and that the optically important particles subsequent to breakup were larger than about 1 μm in radius. We conclude that the grain fragmentation hypothesis can explain the radial color.

The rather steep surface brightness gradient on the anti-jet side of the nucleus is in the opposite sense to that expected from grain fragmentation. In this case, grains of different sizes may be traveling at different velocities, there is considerable evaporation of volatiles as a function of nucleocentric distance, or there is a velocity gradient in the outflow. Perhaps the particles in this portion of the coma decreased in radius by evaporation during their dynamical acceleration into the dust tail. In this scenario, the total mass in solids decreases in the outflow. Jewitt *et al.* (1982) and Jewitt and Meech (1987) reported similar behavior in several comets at large nucleocentric distances, and reasoned that the evaporation of volatile ices from grains could explain the effect. Because the particles on this side of the nucleus are initially moving much more slowly than are the particles in the jet (see Section III.E), the dwell time of these particles in the images is sufficiently long to expect that evaporation might be substantial. Another possible explanation is that changing particle size can change the solar radiation pressure on the particles and cause them to accelerate at different rates away from the nucleus.

D. Color Gradients in the Inner Coma

We have made cuts along the jet and in the anti-jet direction in the J (1.23 μm), K (2.23 μm), L' (3.8 μm), and M' (4.67 μm) images obtained on 1986 March 10.7 UT. The geometry of these cuts and their relation to the direction of the Sun and the motion of the comet are shown in Fig. 4a. In each image, the location of the nucleus of the comet was determined by an elliptical fit to the inner 3". In this manner the images at the different filters could be registered. The flux ratios with respect to the J band along these cuts are shown in Figs. 4b and 4c.

It is evident from Fig. 4 that there are color gradients along the jet and tail directions in the near-infrared images of the coma of P/Halley. In interpreting these gradients, it is important to recognize that the J and K images refer mainly to scattering properties of the grains, whereas the L' and M' images refer mainly to the absorption and emission characteristics of the grains. Along the jet (Fig. 4b) the observed J/K ratio remains constant, while the J/L' and J/M' ratios become bluer as a function of increasing nucleocentric distance r . This behavior is consistent with fragmentation and a decrease in grain radius (for grains with radii $\geq 0.5 \mu\text{m}$) with increasing r as hypothesized in Section III.C to explain the brightness gradient of the jet. As grains become smaller, they will scatter more efficiently at short wavelengths. At longer wavelengths the grain emissivity will decrease as grain size is reduced, but the grain temperature will increase. This could result in a net increase in

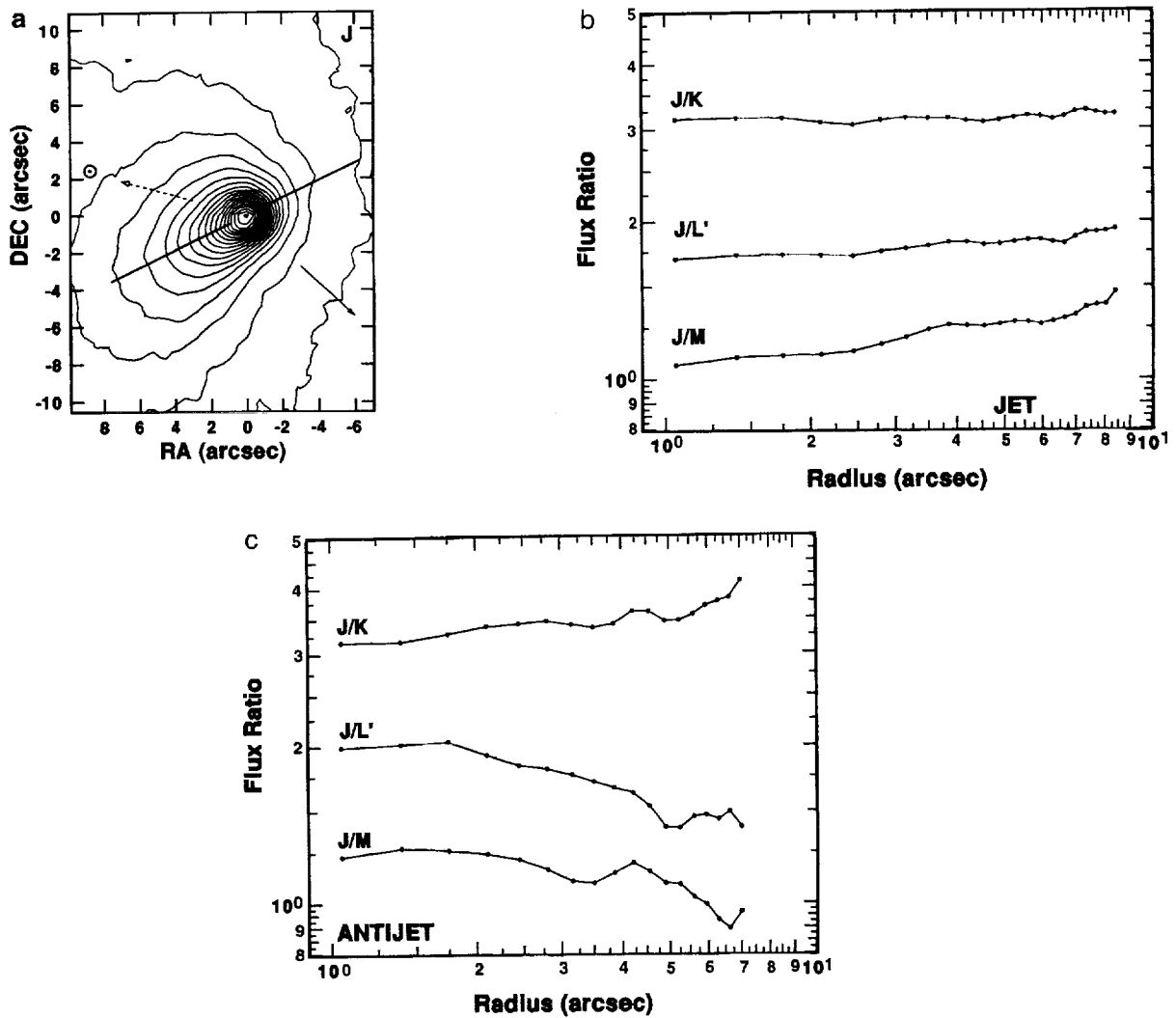


FIG. 4. (a) *J*-band image of comet Halley on 1986 March 10.7 UT with the locations of the one dimensional cuts (indicated by the solid lines to the southeast [along the jet] and to the northwest [anti-jet direction]) superposed on the isophotal contours. The projected directions of the sun and the orbital motion of the comet are indicated by dashed and solid arrows, respectively. (b) Flux ratios along the jet. (c) Flux ratios along the anti-jet.

flux at L' and M (assuming no change in the grain albedo in the visual where most of the Sun's flux is absorbed), but at heliocentric distances of ≈ 1 AU or less (i.e., $T \geq 300$ K) the effect is too small to compensate for the strong increase in the albedo at J . In other words, the surface brightness in the jet is falling off more slowly at both J and M' than expected from the standard model, just less so at M' .

In the anti-jet direction (Fig. 4c), we observe roughly the inverse behavior, with J/K increasing slightly and J/L' and J/M' decreasing with increasing radius. The decrease in J/L' and J/M' indicate that the average albedo of the grains is dropping with increasing radius. In Section III.C we suggested two scenarios for the steep

surface brightness gradient in the anti-jet direction. One scenario had the smaller particles being accelerated out of the inner tail by radiation pressure, depleting the small grain population that is most efficient at near-infrared scattering. This would explain the observed color gradient. The second scenario had volatiles evaporating from grains, making them darker and lowering their albedo (cf., Braum *et al.* 1992). This scenario also can explain the observed color gradient in the anti-jet direction. Both scenarios require that the grains are traveling more slowly away from the nucleus in the anti-jet direction, allowing more time for either the removal of small grains by radiation pressure, the evaporation of volatiles, or fragmentation.

E. Dynamics of Dust in the Coma

The near-infrared images convey information about the spatial distribution and physical properties of the grains in the coma. We assume that the observed infrared emission reflects the properties of the optically important grains (as defined by Gehrz and Ney 1992) along any given line of sight in the image data. Dust impact measurements from *Giotto* revealed a large range of particle sizes in the coma of P/Halley, and showed that the differential particle mass distribution followed a power law (McDonnell *et al.* 1987). Such a grain size distribution is consistent with the thermal emission from other comets (Hanner *et al.* 1985a, 1985b, 1985c). Jewitt and Meech (1986) and Jewitt (1991) argued that the effective grain radius of the optically important grains is given by the optically weighted mean grain size inferred from a power law differential grain radius distribution of the form $n(a)da = Ka^{-m}da$, where m is between 3 and 4.5. We assume in the discussion that follows that the grain properties that dominate the infrared scattering and emission refer to this optically weighted mean.

The spatial distribution of grains of various mineral and physical properties within cometary comas and tails can be determined by calculating the trajectories these particles will assume upon being ablated from the comet nucleus, using an elementary model (cf., Sekanina 1974a). We will assume that spherical grains of radius a , which are perfect absorbers, and uniform density are ejected at a thermal velocity from the nucleus by the heating due to insolation. In the absence of jet activity, the trajectory grains follow upon leaving the comet are, in general, determined by the ratio $\beta = F_{\text{rad}}/F_G$ of the radial radiative and gravitational forces (Burns *et al.* 1979).

The total acceleration vector \mathbf{a} on the grain obtained by combining the radiative acceleration (due to radial radiation pressure of the solar radiation field at the heliocentric distance r on a perfect absorber) and the acceleration due to gravity is

$$\mathbf{a} = -\frac{GM_{\odot}}{r^2} \left[\hat{\mathbf{r}} - \beta \left\{ \left(1 - \frac{v_r}{c} \right) \hat{\mathbf{r}} - \frac{\mathbf{v}}{c} \right\} \right].$$

Syndynes generated from this relation using a range of values of β are shown as dashed lines in Fig. 5. The orbit of the comet was assumed to be purely elliptical with no non-gravitational effects. For a wide range in β , material swept off of the comet by solar radiation pressure would appear to the west in any image of the comet taken on 1986 March 10.7 UT. The extension to the inner coma seen in the images however, are to the east. Therefore, some other mechanism such as jets must be responsible for creating the eastward extension to the image of the comet.

The effect of jets on particle trajectories is easily incorporated into our analysis. The solid lines in Fig. 5 are the

syndynes for particles ejected from the comet with a velocity vector pointing directly at the sun. Typical jet velocities observed in Comet P/Halley range from 0.2 to 1 km s⁻¹ (e.g., Watanabe *et al.* 1987). For simplification β was set to zero. The jet particles move ahead of the comet on an orbit that is initially interior to the comet orbit. Jet particles, then, would appear to the east in images of the comet on 1986 March 10.7 UT. We conclude that the eastern extension is caused by a jet of the type observed by *Giotto*, and seen in the 10 μ m images made during the *Giotto* encounter by Hayward *et al.* (1987). However, we note that whether or not the semi-major axis of the ejected particle's orbit is larger or smaller than the comet's depends on where in the comet orbit the particle was ejected. For non-zero values of β , jet particles will take more complicated trajectories than shown in the figure. However, on the spatial scale of our images, the jet velocity will initially dominate the motion. This can be seen by comparing the hourly intervals in Fig. 5b for the jet and the $\beta = 1$ anti-sunward tail.

The appearance of sunward anti-tails composed of very large grains (small β 's; Burns *et al.* 1979) such as the one reported for Comet Kohoutek 1973f by Ney (1974a, 1974b) can be explained as a projection effect (Sekanina 1974a, 1974b). Our dynamical analysis of the grain trajectories for P/Halley in mid-March 1986 shows that the large grains cannot extend in the sunward direction unless jet activity is involved in their ablation from the nucleus. Particles released with zero velocity with respect to the nucleus must, immediately begin trailing the nucleus because of the larger orbit dictated by the reduced gravity term that they feel. Those ejected with velocity vectors in the direction of the sun will precede the comet on the inside of the comet orbit. Particles released with zero velocity relative to the nucleus and very small values of β move away from the nucleus very slowly (Fig. 5b). If the grain characteristics change with time in such a way as to increase β , they will quickly accelerate further from the nucleus. Such an effect could explain the steep brightness gradient on the "tail" side of the comet. However, we caution that detailed interpretation of evaporation and/or fragmentation effects would require extensive quantitative modeling of the data (cf., Konno *et al.* 1993).

IV. CONCLUSIONS

Our near-infrared images of Comet Halley graphically demonstrate its very active behavior. We draw the following conclusions from our analysis presented here of post-perihelion near-infrared images of Comet P/Halley 1986 III.

(1) Both the scattered and thermal infrared components show that the dust in the coma is extended on the sunward side of the nucleus. The near-infrared coma morphology

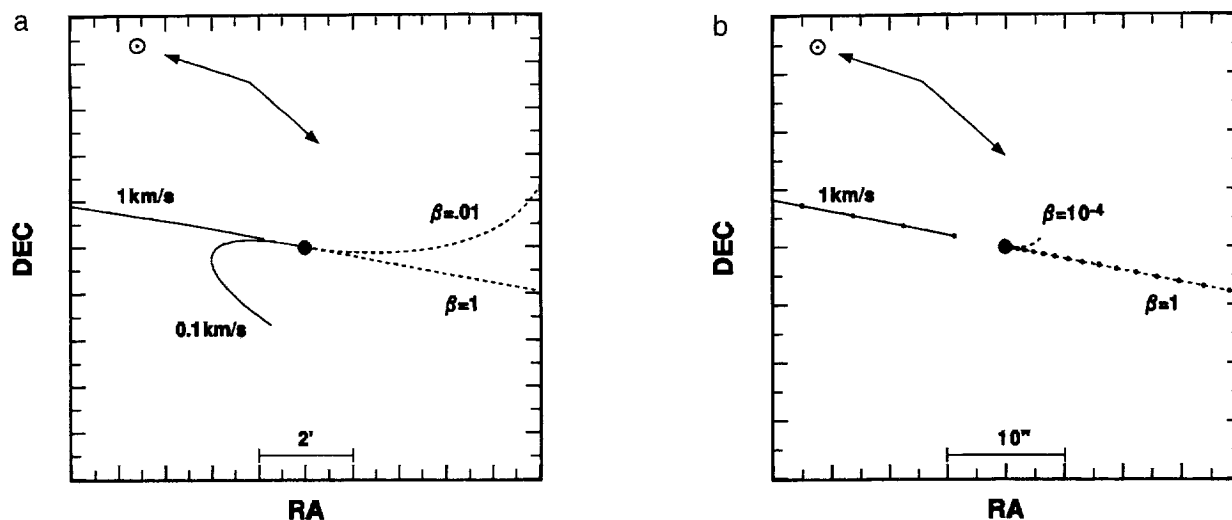


FIG. 5. Syndynes for dust particles lost from comet Halley as viewed from the Earth orbit on 1986 March 10.7 UT. Coordinates are RA and DEC. The solid arrows represent the projected directions of the sun (left) and the orbital motion of the comet (right). The dashed lines trace particles released with no initial velocity relative to the comet. Values for the parameter β (see text) are indicated. The solid lines trace particles ejected toward the sun (jet) with $\beta = 0$. The velocity of ejection is indicated. The dots along the lines in 5b correspond to hourly intervals in the loss of material from the comet. The dashed line with $\beta = 10^{-4}$ traces 30 days of ejection. The solid arrows represent (clockwise from the left) the projected directions of the orbital motion of the comet, the earth, and the sun.

resembles the $10\ \mu\text{m}$ morphology displayed in images made a few days later by Hayward *et al.* (1987).

(2) Our analysis of the trajectories of dust grains in the vicinity of the nucleus of P/Halley leads us to conclude that the sunward extension of the coma is produced by jets similar to those evident at visible wavelengths in the *Giotto* spacecraft images of the nucleus (Reitsema *et al.* 1989).

(3) The coma surface brightness dependence upon nucleocentric distance at all wavelengths in both the comet dust tail and in the jet deviates from the dependence predicted by the "steady state" model for comet nucleus ablation in which grains are ablated from the nucleus at a constant rate and flow outward from the nucleus at constant velocity.

(4) The near-infrared colors of the coma are not constant as a function of nucleocentric distance, suggesting that the grain properties are not uniform across the coma. The color profiles observed on the sunward side of the nucleus suggest that the grains fragment in the outflow of the jet on time scales of a few hours.

The changing structure we observe necessitates rapid evolution of dust production rates in different directions from the nucleus. However, dust observed within our small field of view might have originated in outbursts much earlier than those evident in our images. Thus, it will be important to obtain a continuous temporal series of images of comets in the future to fully explore dust production rates and mechanism. The increased fields of view available

with recent large format 256×256 infrared arrays will provide a more complete record of the evolution of dust grain distributions. As the present study demonstrates, it will be important to obtain images at wavelengths which span both the scattered and emitted thermal spectrum of coma dust grains.

ACKNOWLEDGMENTS

We thank the IRTF staff for helping to make this a useful observing run. We thank Nicholas Raines for assistance in reducing data and the referees whose comments improved the manuscript. The infrared array in the University of Rochester camera was on loan from the Santa Barbara Research Center. This research was supported by grants to the University of Rochester from the National Science Foundation, NASA/Ames, and the National Geographic Society. T. N. acknowledges the support of NSF Grant 84-20775 during the time of this work. C.E.W., T.J.J. and R.D.G. were supported during the analysis of these data by NASA Contract NAGW 2324.

REFERENCES

- BAUM, W. A., T. J. KREIDL, AND D. G. SCHLEICHER 1992. Cometary grains. *Astron. J.* **104**, 1216–1225.
- BURNS, J. A., P. L. LAMY, AND S. SOTER 1979. Radiation forces on small particles in the Solar System. *Icarus* **40**, 1–48.
- CAMPINS, H., M. J. RIEKE, AND G. H. RIEKE 1989. An infrared color gradient in the inner coma of Comet Halley. *Icarus* **78**, 54–62.
- COMBI, M. R. 1994. The fragmentation of dust in the innermost comae of comets: Possible evidence from ground-based images. *Astron. J.* **108**, 304–312.
- FELDMAN, P. D., M. C. FESTOU, M. F. A'HEARN, C. ARPIGNY, P. S.

- BUTTERWORTH, C. B., COSMOVICI, A. C., DANKS, R., GILMOZZI, W. M., JACKSON, L. A., MCFADDEN, P., PATRIARCHI, D. G., SCHLEICHER, G. P., TOZZI, M. K., WALLIS, H. A., WEAVER, AND T. N. WOODS 1987. IUE observations of comet P/Halley: Evolution of the ultraviolet spectrum between September 1985 and July 1986. *Astron. Astrophys.* **187**, 325–328.
- FESTOU, M. C., P. D. FELDMAN, M. F. A'HEARN, C. ARPIGNY, C. B. COSMOVICI, A. C. DANKS, L. A. MCFADDEN, R. GILMOZZI, G. P. TOZZI, M. K. WALLIS, AND H. A. WEAVER 1986. IUE observations of Comet Halley during the Vega and Giotto encounters. *Nature* **321**, 361–363.
- FORREST, W. J., J. L. PIPHER, AND W. STEIN 1986. Sagittarius A* and the positions of infrared sources in the galactic center. *Astrophys. J.* **301**, L49–L52.
- FORREST, W. J., A. MONETI, C. E. WOODWARD, J. L. PIPHER, AND A. HOFFMAN 1985. The new near-infrared array camera at the University of Rochester. *Publ. Astron. Soc. Pac.* **97**, 183–198.
- GEHRZ, R. D. AND E. P. NEY 1992. 0.7- to 23- μ m Photometric observations of P/Halley 1986 III and six recent bright comets. *Icarus* **100**, 162–186.
- GILMAN, R. C. 1974. Planck mean cross-sections for four grain materials. *Astrophys. J. Suppl. Ser.* **28**, 397–403.
- HANNER, M. S., AND A. T. TOKUNAGA 1991. Infrared techniques for comet observations. In *Comets in the Post-Halley Era*. (R. L. Newburn, Jr., M. Neugebauer, and J. Rahe, Eds.), Vol. 1 pp. 67–91. Kluwer, Dordrecht.
- HANNER, M. S., A. T. TOKUNAGA, W. F. GOLISCH, D. M. GRIEP, AND C. D. KAMINSKI 1987a. Infrared emission from P/Halley's dust coma during March 1986. *Astron. Astrophys.* **187**, 653–660.
- HANNER, M. S., P. N. KUPFERMANN, G. BAILEY, AND J. C. ZARNECKI 1987b. Infrared imaging with JPL's linear array camera. In *Infrared Astronomy with Arrays* (C. G. Wynn-Williams and E. E. Becklin, Eds.), pp. 205–211. Univ. of Hawaii, Honolulu.
- HANNER, M. S., D. K. AITKEN, R. KNACKE, S. McCORKLE, P. F. ROCHE, AND A. T. TOKUNAGA 1985a. Infrared spectrophotometry of Comet IRAS-Araki-Alcock (1983d): A bare nucleus revealed? *Icarus* **62**, 97–109.
- HANNER, M. S., R. KNACKE, Z. SEKANINA, AND A. T. TOKUNAGA 1985b. Dark grains in Comet Crommelin. *Astron. Astrophys.* **152**, 177–181.
- HANNER, M. S., E. TEDESCO, A. T. TOKUNAGA, G. J. VEEDER, D. LESTER, F. C. WITTEBORN, J. D. BREGMAN, J. GRADIE, AND L. LEBOSKY 1985c. The dust coma of periodic Comet Churyumov–Gerasimenko (1982 VIII). *Icarus* **64**, 11–19.
- HAYWARD, T. L., R. D. GHERZ AND G. L. GRASDALEN 1987. Ground-based infrared observations of Comet Halley. *Nature* **326**, 55–57.
- JEWITT, D. C. 1991. Cometary photometry. In *Comets in the Post-Halley Era*. (R. L. Newburn, Jr., M. Neugebauer, and J. Rahe, Eds.), Vol. 1 pp. 19–65. Kluwer, Dordrecht.
- JEWITT, D. C., AND K. J. MEECH 1987. Surface brightness profiles of 10 comets. *Astrophys. J.* **317**, 992–1001.
- JEWITT, D. C., AND K. J. MEECH 1986. Cometary grain scattering versus wavelength, or, "What color is comet dust?" *Astrophys. J.* **310**, 937–952.
- JEWITT, D. C., B. T. SOIFER, G. NEUGEBAUER, K. MATTHEWS, AND G. E. DANIELSON 1982. Visual and infrared observations of the distant Comets P/Stephan Oterma (1980g), Panther (1980u), and Bowell (1980b,a). *Astron. J.* **87**, 1854–1866.
- JOHNSON, J. R., U. FINK, AND H. P. LARSON 1983. The 0.9–2.5 micron spectrum of Comet West 1976 VI. *Astrophys. J.* **270**, 769–777.
- KONNO, I., W. F. HUEBNER, AND D. C. BOICE 1993. A model of dust fragmentation in near-nucleus jet-like features in Comet P/Halley. *Icarus* **101**, 84–94.
- LARSON, S., Z. SEKANINA, D. LEVY, AND M. SENAY 1987. Comet P/Halley near-nucleus phenomena in 1986. *Astron. Astrophys.* **187**, 639–644.
- MAILLARD, J. P., J. CROVISIER, T. ENCRENAZ, AND M. COMBES 1987. The spectrum of Comet P/Halley between 0.9- and 2.5- μ m. *Astron. Astrophys.* **187**, 398–404.
- MCDONNELL, J. A. M., W. M. ALEXANDER, W. M. BURTON, E. BUSSO-LETTI, G. C. EVANS, S. T. EVANS, J. G. FIRTH, R. J. L. GRARD, S. F. GREEN, E. GRUN, M. S. HANNER, D. W. HUGHES, E. IGENBERGS, J. KISSEL, H. KUCZERA, B. A. LINDBLAD, Y. LANGEVIN, J.-C. MANDEVILLE, S. NAPPO, G. S. A. PANKIEWICZ, C. H. PERRY, G. H. SCHWEHM, Z. SEKANINA, T. J. STEVENSON, R. F. TURNER, U. WEISHAUP, M. K. WALLIS, AND J. C. ZARNECKI 1987. The dust distribution within the inner coma of Comet P/Halley 1982i: Encounter by *Giotto's* impact detectors. *Astron. Astrophys.* **187**, 719–741.
- MILLIS, R. L., AND D. G. SCHLEICHER 1986. Rotational period of Comet Halley. *Nature* **324**, 646–649.
- NEY, E. P. 1974a. Infrared observations of Comet Kohoutek near perihelion. *Astrophys. J.* **189**, L141–L143.
- NEY, E. P. 1974b. Multiband photometry of Comets Kohoutek, Bennett, Bradfield, and Encke. *Icarus* **23**, 551–560.
- REITSEMA, H. J., W. A. DELAMERE, A. R. WILLIAMS, D. C. BOICE, W. F. HUEBNER, AND F. L. WHIPPLE 1989. Dust distribution in the inner coma of Comet Halley: Comparison with models. *Icarus* **81**, 31–40 (see also the cover illustration of *Planet. Rep.* **7**(5), 1987).
- SEKANINA, Z. 1974a. On the nature of the anti-tail of Comet Kohoutek (1973f) I. A working model. *Icarus* **23**, 502–518.
- SEKANINA, Z. 1974b. The prediction of anomalous tails of comets. *Sky and Telescope* **47**, 374–377.
- WATANABE, J., H. KAWAKAMI, K. TOMITA, H. KINOSHITA, T. NAKAMURA, AND Y. KOZAI 1987. The outburst of Comet P/Halley on December 12, 1985. *Astron. Astrophys.* **187**, 229–232.
- WOODWARD, C. E. 1987. High spatial resolution observations of dust and gas in NGC7027 and the M8 hourglass. Ph.D. dissertation, University of Rochester (Rochester, New York).

MID-INFRARED OBSERVATIONS OF THE NUCLEUS AND DUST OF COMET P/SWIFT-TUTTLE

M. N. FOMENKOVA

B. JONES, R. PINA, R. PUETTER, AND J. SARMECANIC

R. GEHRZ AND T. JONES

MID-INFRARED OBSERVATIONS OF THE NUCLEUS AND DUST OF COMET P/SWIFT-TUTTLE

M. N. FOMENKOVA

NASA Ames Research Center, MS 239-4, Moffett Field, California 94035-1000 and Center for Astrophysics and Space Sciences,
University of California San Diego, La Jolla, California 92093-0011
Electronic mail: mfomenko@ucsd.edu

B. JONES, R. PINA, R. PUETTER, AND J. SARMECANIC

Center for Astrophysics and Space Sciences, University of California San Diego, La Jolla, California 92093-0011

R. GEHRZ AND T. JONES

Astronomy Department, University of Minnesota, 116 Church st. SE, Minneapolis, Minnesota 55455

Received 1995 January 14; revised 1995 June 21

ABSTRACT

We report pre-perihelion observations of comet P/Swift-Tuttle obtained with the UCSD mid-infrared astronomical camera on 12 nights in November 1992. The images were taken through a $1\ \mu\text{m}$ wide filter centered at $11.65\ \mu\text{m}$. During the observing run, the heliocentric distance decreased from 1.13 to 0.98 AU, and the geocentric distance increased from 1.16 to 1.33 AU. The spatial scale of the images was 700–800 km per pixel. In addition, photometric data at wavelengths between 3.6 and $18.5\ \mu\text{m}$ were obtained on one night. The infrared images cover the cometary activity on time scales from hours to weeks and reveal large changes in the overall morphology of the coma. From periodic changes in the jet patterns we determined the period of nuclear rotation of 67.5 ± 0.4 h. Photometry indicates that the temperature of the coma was 35% higher than the blackbody temperature at the same heliocentric distance and, hence, that the coma was dominated by small particles of average radius of $0.7\ \mu\text{m}$. The dust mass loss rate varied with the heliocentric distance as $R^{-6.3}$ and displayed $\sim 40\%$ variation with the rotational phase. Two major jets were present in the images obtained on November 07–17, and a third area became active on November 24–29, increasing the average dust loss rate by a factor of 1.4. The relative positions of the three active areas on the surface of the nucleus are consistent with the positions of the most stable active zones identified by Sekanina [AJ, 86, 1741 (1981)] from the data on the P/Swift-Tuttle apparition in 1862. The radial brightness profiles suggest the radius of the nucleus is 15 ± 3 km. This implies that the nucleus of P/Swift-Tuttle is ~ 34 times more massive than the nucleus of P/Halley. © 1995 American Astronomical Society.

1. INTRODUCTION

Studies of the nature and evolution of comets depend crucially on our understanding of the mechanisms and characteristics of cometary activity. During perihelion passage, comets are heated by solar radiation and release gas and dust into the inner solar system, thus forming a coma. From observational studies, combined with extensive modeling, we know that the morphology of the coma is determined not only by the velocity and size distributions and the physical properties of the ejected material, but also by the geometry of jets and sources on the surface of the nucleus, its shape, and rotation geometry with respect to the Sun (review by Sekanina 1990).

Temporal and spatial variations in the distribution of both gas and dust in coma indicate highly anisotropic emission mechanisms which are due to the inhomogeneity of nucleus surface properties and also depend upon the local insolation history. Gas molecules and very small dust grains display semichaotic motion (Horanyi & Mendis 1985), but the motion of the optically efficient micron-sized and larger dust particles is much more collimated and predictable (Kitamura

1987; Rabinowitz 1988). Due to the quasi-coherent behavior of dust particle jet flows, the trajectories can be dynamically extrapolated back to the surface of the nucleus, resulting in location and identification of their sources (Sekanina & Larson 1986). This makes studies of the dust features in the coma an indispensable tool for probing the nature of cometary nuclei.

Imaging of comets in the mid infrared ($3\text{--}20\ \mu\text{m}$) is a very useful method for studying the morphology and the extent of the dust phenomena in the coma. The optical depth in the mid IR is very low ($\sim 10^{-5}$), which facilitates a straightforward interpretation of such images. The $10\ \mu\text{m}$ wavelength range is dominated by thermal radiation from the dust itself and is sensitive to the dust distribution and its physical properties. A few $10\ \mu\text{m}$ images of comets have been acquired to date and have demonstrated the importance of this wavelength range for an insight into cometary processes (P/Giacobini-Zinner—Telesco *et al.* 1986; P/Halley—Campins *et al.* 1987; Hayward *et al.* 1987; new comet Wilson—Campins *et al.* 1989; new comet Austin—Fomenkova *et al.* 1993). Analysis of these data has shown that the images are consistent with the premise that the over-

TABLE 1. Observational parameters for Comet P/Swift-Tuttle observations.

Date (UT)	Airmass	Number of images	R (AU)	Δ (AU)	Elongation (degrees)	Phase Angle (degrees)	Sun-Comet projection angle, North-to-East (degrees)	Linear Resolution (km/pixel)
1992 Nov 07.06-07.11	1.51-2.04	12	1.131	1.166	62.9	51.1	220.4	702
1992 Nov 08.07-08.11	1.58-2.00	8	1.122	1.165	62.4	51.3	221.2	701
1992 Nov 09.09-09.11	1.69-1.95	4	1.114	1.167	61.9	51.5	221.9	703
1992 Nov 12.06-12.11	1.48-2.05	9	1.089	1.174	59.5	51.7	223.9	707
1992 Nov 13.07-13.11	1.54-2.11	12	1.081	1.179	59.4	51.7	224.5	710
1991 Nov 14.06-14.11	1.47-2.18	14	1.073	1.184	58.7	51.7	225.1	713
1992 Nov 15.06-15.07	1.55-1.59	2 ^a	1.066	1.190	58.1	51.6	225.7	716
15.08	1.66-1.71	2 ^b						
15.09-15.11	1.90-2.25	6						
1992 Nov 17.05-17.12	1.44-2.51	18	1.052	1.205	56.7	51.5	226.8	725
1992 Nov 24.07-24.11	1.89-2.63	8	1.009	1.279	51.5	49.4	230.3	770
1992 Nov 26.07-26.11	1.80-2.85	10	0.998	1.305	49.9	48.5	231.2	786
1992 Nov 28.05-28.11	1.68-3.11	15	0.989	1.334	48.3	47.4	232.1	803
1992 Nov 29.05-29.10	1.67-2.77	11	0.985	1.349	47.5	46.9	232.6	812

a. Taken with a 4.8 μ filter.b. Taken with an 8.7 μ filter.

all maximum activity takes place on the sunlit side of a rotating nucleus. In dusty comets with jets, the ejection of dust is restricted to a few discrete active areas representing only a small fraction of the nuclear surface. These areas become dormant when they rotate out of direct sunlight. A temporal lag in sublimation due to thermal inertia also should be taken into account when interpreting the diurnal evolution of the coma.

In this paper we present 11–12 μ m images of comet P/Swift-Tuttle obtained pre-perihelion with the UCSD mid-IR astronomical camera. Comet P/Swift-Tuttle is a very active comet with a period of about 130 yr. It is the parent comet of the prominent Perseid meteor stream (Marsden 1973). Apparitions of this comet in the inner solar system have been traced back to the years AD 188 and 68 BC (Yau *et al.* 1994).

The observing run spanned the time period from 1992 November 7 (IAUC #5654) to November 28 with data taken on 12 nights. We show an extended sequence of high-resolution images revealing the distinctive outlines of prominent features in the morphology of the coma. The temporal evolution of these features is diagnostic of the nuclear rotation. We also discuss how this rotation affects the activity of the comet. For one of these nights, we have photometric data obtained with the University of Minnesota (UM) infrared photometer at the O'Brien 0.76 m telescope. These data are used to derive the temperature of the dust, to estimate the characteristic size of dust grains in the coma, and for comparison with other comets.

2. OBSERVATIONS

2.1 The Instrumentation

Infrared images of comet P/Swift-Tuttle were obtained with the UCSD mid-IR camera (the "Golden Gopher") on the UCSD/UM 1.5 m telescope at the Mt. Lemmon Observing Facility. The telescope is optimized for observing in the infrared. At 11 μ m, the image spatial resolution is diffraction limited to $\lambda/D \sim 1.5$ arcsec FWHM. The Golden Gopher

platescale of 0.83 arcsec/pixel samples the point spread function (PSF) with 2×2 pixels of the array. We used 64 columns \times 16 rows of the Si:As IBC array, which spanned 53×13 arcsec. On warm nights or when the humidity is high, only a subset of the array can be used since the pixel saturation time due to higher background becomes less than the electronics readout time of 2.7 ms for a full frame. The camera provides good sensitivity in the wavelength range from 5 to 27 μ m. At 11 μ m, the noise equivalent flux density is 40 mJy/arcsec² in 1 min (including both on and off source time) for a 1 μ m bandwidth. A detailed description of the instrument and observing procedure can be found in Pina *et al.* (1993).

Photometry was carried out with the 15 filter multiaperture infrared GaGe bolometer on the 0.76 m IR telescope of the UM O'Brien Observatory. The bandpasses, calibration, and operational characteristics of the photometer are described by Ney (1974) and Hanner *et al.* (1990). Calibrations for the silicate filters were obtained by interpolating the calibration scales given by Gehrz *et al.* (1974, 1992).

2.2 The Infrared Images and Photometric Data

In November 1992, comet P/Swift-Tuttle was imaged at a wavelength of 11–12 μ m during the 12 nights that weather permitted observations. On each night, from 4 to 18 images of the comet were acquired during 1–2 h of observing, the total number of images being 124. Table 1 summarizes the observing parameters and the Sun-comet-Earth geometry. During the observing run, the heliocentric distance R varied from 1.13 to 0.98 AU, and the geocentric distance Δ varied from 1.17 to 1.35 AU, resulting in a linear resolution at the comet of about 700–800 km/pixel (Table 1) or 840–960 km/arcsec. A typical chop throw between the sky and the object images was 1 arcmin, which was sufficiently large to avoid observable image contamination from a coma flux contribution in the reference beam.

If the dust in the coma is moving with velocity v_d , then a

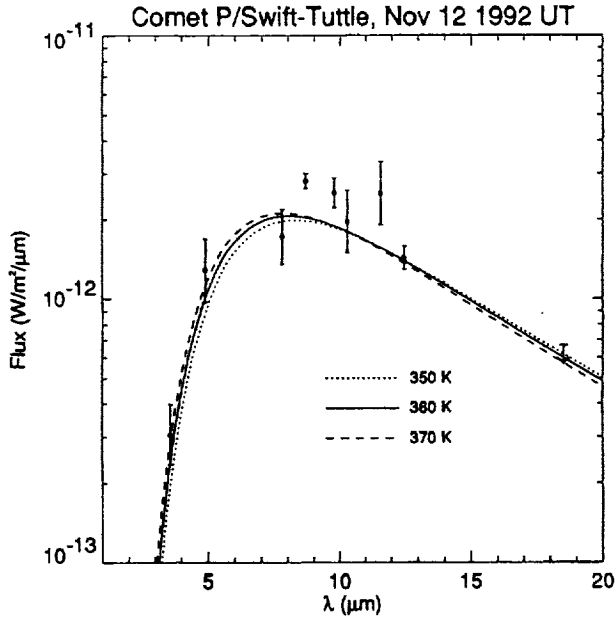


FIG. 2. The 2 to 20 μm energy distribution of P/Swift-Tuttle. A weak silicate feature is superimposed on a smooth continuum caused by thermal emission of small grains. The fitted blackbody curve yields the grain temperature of 360 K, which is 35% higher than the blackbody temperature at the heliocentric distance of 1.09 AU.

crossing time required for the dust particles to cross the minimal resolution element is:

$$\tau = \varphi \Delta / v_d,$$

where φ is an angular resolution and Δ is the geocentric distance. The crossing time defines an equivalent temporal resolution of the comet emission variability available from the images (Jewitt 1991). The terminal velocity v_{gas} of the gas entraining dust grains into the coma can be estimated from the Bobrovnikov–Delsemme relation (Delsemme 1982):

$$v_{\text{gas}} (\text{km/s}) = 0.58 R^{-1/2} (\text{AU}), \quad (1)$$

R being the heliocentric distance. Assuming that $v_d/v_{\text{gas}} \sim 0.5\text{--}0.8$ (Finson & Probstein 1968) the temporal resolution is given by (Fomenkova *et al.* 1993):

$$\tau (\text{h}) = 0.70 \varphi (\text{arcsec}) \Delta (\text{AU}) R^{1/2} (\text{AU}). \quad (2)$$

Typical values for comet Swift-Tuttle observations are: $\varphi = 2 \times 0.83''$ (two-pixel minimal resolution element), $R = 1$ AU, and $\Delta = 1.2$ AU. The resulting temporal resolution $\tau \sim 1$ h is comparable with the total observing time for each night, but is smaller than characteristic outburst duration of 2–3 h [as estimated by Sekanina (1981) for the previous apparition of P/Swift-Tuttle]. The typical time interval t_0 between successive images was 5–10 min, i.e., $t_0 \ll \tau$. Thus, images obtained on the same night were combined together to increase the signal-to-noise ratio and to extend the spatial coverage into the distant parts of the coma (Fig. 1, Plate 101).

The photometric measurements of the IR energy distribution of comet P/Swift-Tuttle were made on 1992 Nov 11.9–12.0 UT through narrowband filters at various wavelengths between 3.6 and 18.5 μm (Fig. 2), including a number of data points in the silicate emission band at 8–13 μm . For

these measurements, the beam size and chop throw between the source and reference beams were 9 and 45 arcsec, respectively. Corrections, as described by Gehrz & Ney (1992), were made for a coma flux contribution to the reference beam.

2.3 Flux Calibrations

For absolute flux calibration, we used the stars α Aql, β Peg, and α Tau. Calibrator images were obtained on each night, usually right before and right after the cometary observations. The absolute stellar fluxes were taken from the *IRAS* Point Source Catalog (PSC, 1988) with a quoted uncertainty range of 4%–8% for flux measurement at each wavelength. However, since the satellite data are not color corrected and the *IRAS* bandpasses are much wider than our filter bandpass of 1 μm , a correction factor needs to be applied. This factor depends on the spectral index of the star in question. The flux densities, $f(\lambda_0)$, quoted in the PSC for $\lambda_0 = 12, 25, 60$, and 100 μm , were derived assuming an intrinsic spectral index of -1 :

$$f_q(\lambda)/f_q(\lambda_0) = (\lambda/\lambda_0)^{-1},$$

or

$$\begin{aligned} F &= f_q(\lambda_0) \int f_q(\lambda)/f_q(\lambda_0) R_\lambda d\lambda \\ &= f_q(\lambda_0) \int (\lambda/\lambda_0)^{-1} R_\lambda d\lambda, \end{aligned}$$

where F is the flux measured by a detector through a given filter, and R_λ is the relative filter response (PSC, Table II.C.5). If the actual spectral dependence of flux is $\lambda^{-\beta}$ then

$$\begin{aligned} F &= f(\lambda_0) \int f(\lambda)/f(\lambda_0) R_\lambda d\lambda \\ &= f(\lambda_0) \int (\lambda/\lambda_0)^{-\beta} R_\lambda d\lambda, \end{aligned}$$

and the actual color-corrected value of the flux density is

$$f(\lambda_0) = f_q(\lambda_0)/K,$$

where the correction factor K equals

$$K = \left[\int (\lambda/\lambda_0)^{-\beta} R_\lambda d\lambda \right] / \left[\int (\lambda/\lambda_0)^{-1} R_\lambda d\lambda \right]. \quad (3)$$

This correction has a large effect (up to 50%) and yields the true 12 μm flux of the star.

For our calibration stars, the spectral index β was estimated from the *IRAS* flux values at 12 and 25 μm , assuming an average error of 6% for each flux measurement:

$$f(12)/f(25) = (12/25)^{-\beta}.$$

IRAS spectra of those stars were checked in the *IRAS* Atlas of Low-Resolution Spectra (Olson *et al.* 1986) to make sure that they are featureless. To obtain true calibration values for our filter centered at 11.65 μm , we applied an additional small correction (with the same index β) to the color-corrected flux densities $f(12)$. The resulting fluxes for the

calibration stars are 24.2 ± 1.5 Jy for α Aql, 286.1 ± 23.2 Jy for β Peg,¹ and 503.4 ± 31.2 Jy for α Tau.

Overall errors in the flux calibration of the cometary images are due to (i) the intrinsic uncertainties in the *IRAS* measurements, as given above, (ii) sky noise in the calibration star images, and (iii) airmass correction. Fluctuations in the sky emission are essentially random, and, since the raw sky flux is so large, the sky noise is very well described by a Gaussian distribution. Therefore, the uncertainty in the total flux in an aperture containing N pixels is equal to the average sky noise per pixel multiplied by the square root of N . On different nights, the sky noise contributes between 5% and 12% to the uncertainty in the raw flux measurement for images of α Aql, and about 1%–3% to the uncertainty in the fluxes of β Peg and α Tau. These errors, root-sum-squared with the errors in quoted *IRAS* fluxes given above, yield uncertainties in the flux calibrations between 9% and 15% for α Aql, 7%–11% for β Peg, and 5%–8% for α Tau.

To account for the atmospheric extinction, we used an exponential decay approximation of the flux dependence on the airmass. For each night, the calibration coefficients obtained were plotted vs airmass on a log-linear scale. The slope of a linear least-squares fit to these data points yields an extinction coefficient α , which, on different nights, ranged from 0.04 to 0.25 mag per airmass. The uncertainties in the best-fit parameters of the airmass correction increase the errors in the flux calibrations. (Usually, either the number of calibration stars was too low or the airmass range covered by them was too narrow to yield a tight fit.) The final uncertainties in the flux calibration of cometary images are between 9% and 18%.

3. RESULTS

3.1 Overall Morphology and Rotation of the Nucleus

During its previous apparition in 1862, comet P/Swift-Tuttle was noted for its spectacular activity and was extensively observed [see Sekanina (1981) for the references]. The comet exhibited the dynamical evolution of three types of structures: jets, envelopes, and tail bands, indicating distinctive dust phenomena. Based on drawings and micrometric measurements of the jets made by the 19th century astronomers, Sekanina (1981) derived a nuclear rotation period of 66.5 h and the obliquity of the orbit plane to the equator of 80° , i.e., the rotation axis is almost in the orbit plane. He estimated that no more than 1% of the nucleus surface area was active, located eight discrete emission spots, and inferred a typical ejection duration of ~ 2 –3 h for each of the source regions. Based on orbital calculations, Yau *et al.* (1994) noted a surprising absence of nongravitational perturbations in the P/Swift-Tuttle motion over an interval of more than two millennia. They suggested that either the comet has a very large nucleus, more massive than typical cometary nuclei, or that its emission pattern has been symmetric and extremely stable during this period. We will show later that our data support the notion of a very large nucleus.

Our infrared images cover the cometary activity on time scales from hours to weeks. The highly variable night-to-night activity of comet Swift-Tuttle is revealed in the coadded images (Fig. 1). Overall consistency of the images with an approximately 3 d period is immediately seen from the data and was noted by a number of other observers (Jorda *et al.* 1993; Feldman *et al.* 1993). To estimate the rotation period more accurately, we sequenced the images vs rotational phase assuming periods between 50 and 72 h. The most consistent succession of jet development with time (Fig. 3) is reconstructed for a period T of $67 < T < 68$ h. A period as long as 67 h, or as long as 68 h, changes the sequence in an unacceptable way. Therefore, our best estimate of the period is $T = 67.5 \pm 0.4$ h, which is slightly longer than the average period of 66.5 h derived by Sekanina (1981) from observations of the year 1862.

The sequence of images on Fig. 3 reveals that a drastic change in the activity of P/Swift-Tuttle occurred between Nov 17 and 24. Two dust jets are distinguishable in the cometary images obtained between Nov 07 and 17. The first, strongest jet J1 is apparent in the beginning of the period (Nov 07): contours of constant brightness are elongated westward. It rotates counterclockwise (Nov 13), and dies away in the northwest direction by the middle of the rotation period (Nov 08, 14, 17). In these images the outer contours, determined by the pattern of earlier emission, are elongated to the northwest, but the more recent innermost contours are either circular, or elongated to the southwest. The images of Nov 14 and 17 show that the second, weaker jet J2 becomes active and is directed Sunward. This jet also rotates counterclockwise (Nov 09), and disappears (Nov 12). At the end of the period (Nov 15) jet J1 is awakening again, pointing in the sunward direction.

The pattern of emission from these two major active areas is in good agreement with observations of gaseous species CN, C₂, and C₃ by Schulz *et al.* (1994) made on three nights in the beginning of October 1992. They estimated that, assuming that the nucleus of P/Swift-Tuttle is in a state of simple rotation, the two active areas producing gas jets are separated by 130° on the surface of the nucleus. From the measurements of dust continuum at 0.483 and 0.523 μm Schulz *et al.* (1994) also suggested that the gas and dust jets in P/Swift-Tuttle are correlated in some way. Since our observing run took place a month later than theirs, we cannot make a direct comparison of dust and gas emission. In our images, the time interval between the onset of jets J2 and J1 is ~ 22.5 h, which gives a distance between the active areas of $360^\circ \times (22.5 \text{ h} / 67.5 \text{ h}) \approx 120^\circ$. This result is consistent with the modeling by Sekanina (1981) based on the jet patterns observed during the previous apparition of P/Swift-Tuttle in 1862. He concluded that two most prominent emission areas A and B were separated by 120° in longitude in cometocentric equatorial coordinates. The same areas may be active during the 1992 apparition and responsible for correlated gas and dust production!

But the surface of P/Swift-Tuttle is not frozen permanently in the same, unchanging state. Images of Nov 24, 26, 28, and 29 show the presence of a new, very strong, third jet J3. It is directed southward and has maximum activity in the

¹The error for β Peg is larger because this is an irregular variable with a flux variation of 5% (Hanner 1994).

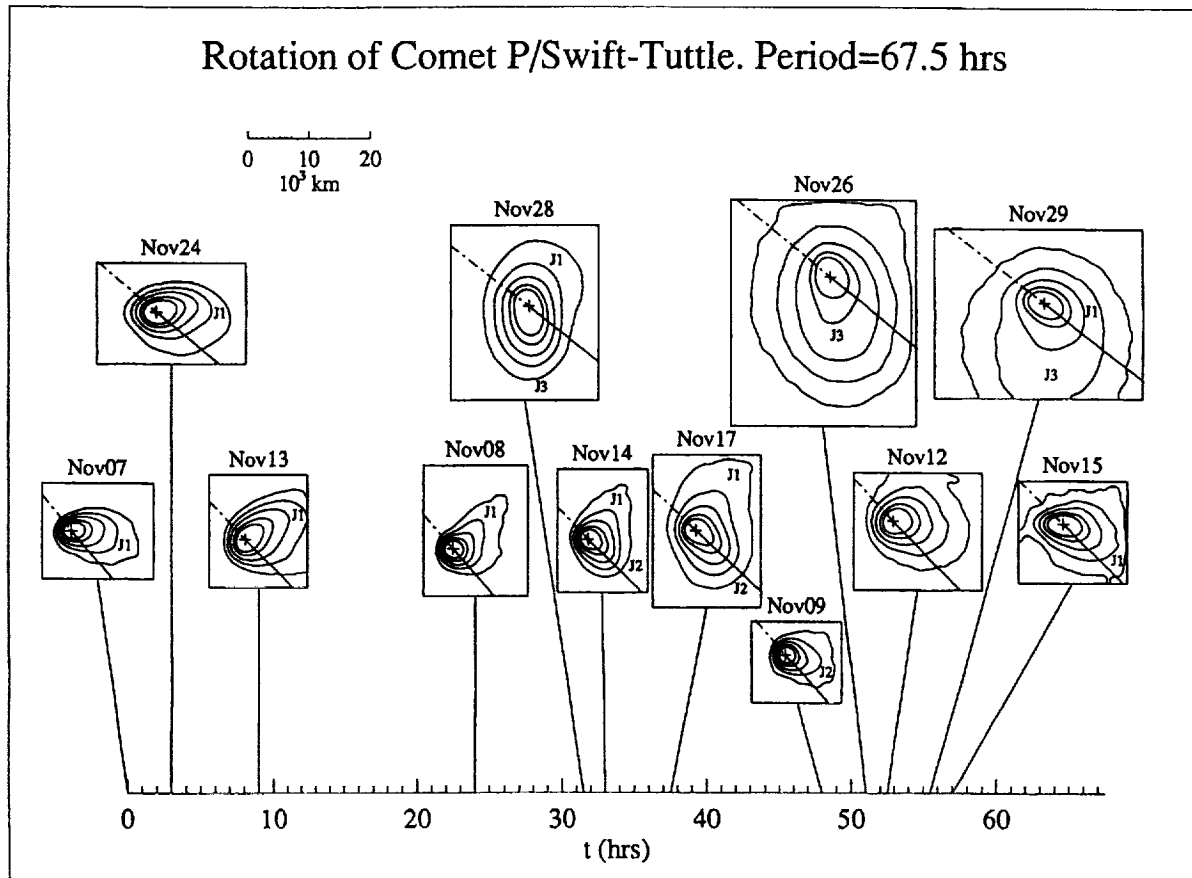


FIG. 3. Images vs rotational phase for a nuclear rotation period of 67.5 h. The brightest pixel of each image is marked by a cross. Contours are drawn at 60%, 40%, 30%, 20%, and 10% level of the peak. The solid line through the brightest pixel of each image shows the sunward direction.

beginning of the last quarter of the period (Nov 26), when it fully obscures the weaker jet J2. Then the activity of jet J3 decreases 5 h later (Nov 29), while jet J1 reappears. The remnants of jet J3 are still seen in the beginning of the period (Nov 24) where outer contours of the coma are slightly elongated southward. The jet J3 is separated from jet J1 by ~ 29 h in time or by $\sim 155^\circ$ and may correspond to the active zone C in the model by Sekanina (1981). In 1862, this zone became and stayed active closer to the perihelion than zones A and B.

The sudden activation of a new strong jet indicates that the mechanical and morphological surface properties of P/Swift-Tuttle are heterogeneous and evolve with time. Sekanina (1981) estimated that only about 1% of the surface area of the P/Swift-Tuttle nucleus was active during its 1862 apparition. If the active areas responsible for the jets we observed are indeed the same which were active in 1862, then our observations give evidence of both diurnal and seasonal variations in the activity of the comet. The closer to the perihelion, i.e., to the cometary "summer," the more areas on the surface change from a dormant to an active state. In Sekanina's (1981) model of the 1862 activity of P/Swift-Tuttle, the maximum number of active areas occurs right after the perihelion passage, during the peak of the cometary summer.

Alternatively, if the proximity of angular distances between the three active areas observed in the 1992 and in

1862 apparitions is a random coincidence, this would imply that the upper crust on the surface of the nucleus is unstable and subject to sudden openings of new crevices. Initiation of such a new active area would expose the inner, unmodified volatile-rich fresh material and result in a dramatic increase in the mass loss rate (see further). Fracturing of the surface may be caused by thermal stresses in cometary nuclei due to steep temperature gradients in the surface layer (Tauber & Kuhrt 1987). This explanation is also consistent with the observed jet activation at close heliocentric distance $R < 1$ AU.

3.2 Photometry and Comparison of Comet P/Swift-Tuttle with Other Comets

Photometric data obtained on 1992 Nov. 12 were used to estimate the coma temperature (Fig. 2). A blackbody fit to the continuum emission (excluding the silicate band) yields a coma temperature $T_{\text{obs}} = 360 \pm 10$ K. The blackbody temperature at a given heliocentric distance R can be determined from the energy balance between the power of absorbed solar radiation and the power emitted by grains in the thermal infrared:

$$\pi a^2 Q_a (L_{\text{Sun}} / 4 \pi R^2) = 4 \pi a^2 Q_e \sigma T_{\text{obs}}^4,$$

where Q_a and Q_e are the Planck mean absorption and emission coefficients, respectively, a is the average grain radius,

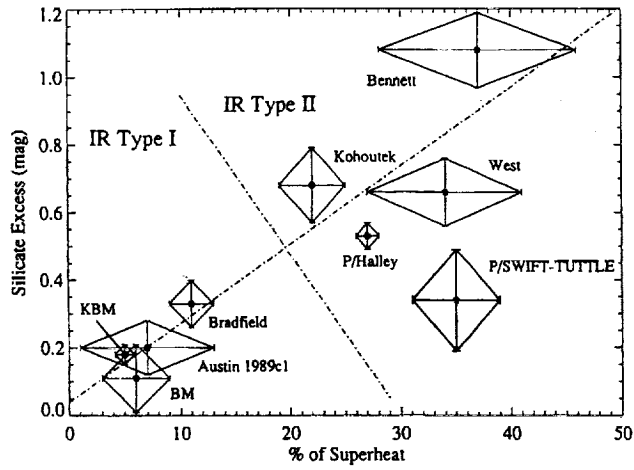


FIG. 4. Comparison of P/Swift-Tuttle with other recent bright comets. The data on superheat and silicate excess in other comets are from Gehrz & Ney (1992).

$L_{\text{Sun}} = 3.826 \times 10^{33}$ erg/s is the solar luminosity, and $\sigma = 5.6696 \times 10^{-5}$ erg/cm²/deg⁴ is the Stefan-Boltzmann constant. Assuming $Q_a = Q_e = 1$, the blackbody temperature is

$$T_{\text{bb}} \text{ (K)} = (L_{\text{Sun}} / 16 \pi \sigma R^2)^{1/4} = 278.3 R^{-1/2} \text{ (AU)}. \quad (4)$$

Following Gehrz & Ney (1992), we define the superheat of cometary dust as

$$S = T_{\text{obs}} / T_{\text{bb}} = (Q_a / Q_e)^{1/4}. \quad (5)$$

For the Nov 12 observations, $R = 1.09$ AU, $T_{\text{bb}} = 267$ K, $S = 1.35 \pm 0.04$, and $Q_e \leq 0.3 < Q_a$. The high superheat is indicative of small grains present in the coma. If the grains were as large as, or larger than the wavelength of the emitted radiation $10 \mu\text{m}$, then their emissivity Q_e would be close to unity, and their temperature would be close to that of a blackbody [Eq. (4)]. The temperature has to rise above T_{bb} in order for the grains to achieve radiative equilibrium.

The emission in the silicate band (the four points between 8.7 and $11.6 \mu\text{m}$) exceeds the continuum fit by an average of 0.34 ± 0.15 mag. To compare the P/Swift-Tuttle dust component with other comets, we used the data by Gehrz & Ney (1992) (Fig. 4). The observed combination of the superheat and silicate excess characterizes P/Swift-Tuttle as an IR Type II comet.² Using calculations by Gilman (1974), as presented in Fig. 5 of Gehrz & Ney (1992), we estimated the average grain size $a \approx 0.7 \pm 0.1 \mu\text{m}$. This is consistent with P/Swift-Tuttle classification as an IR Type II comet. For comet P/Halley, similar calculations confirmed that, usually, its coma was formed primarily by particles with radii of 0.5 – $1 \mu\text{m}$.

²The classification of comets into IR Type I and II was introduced by Gehrz *et al.* (1989). Type I comets have continuum emission with a low superheat, weak or absent silicate features and Type I (ion) tails. Type II comets have 10 and $20 \mu\text{m}$ silicate emission features superimposed on a superheated infrared continuum and prominent Type II (dust) tails. The observed differences between dust emission can be explained by different grain sizes: large (5 – $10 \mu\text{m}$) particles in comets of IR Type I and small (0.5 – $1 \mu\text{m}$) particles in comets of IR Type II.

3.3 Thermal Infrared Flux and the Mass Loss Rate

In the steady-state model approximation of cometary dust emission, the dust production rate and the particle velocity do not depend on time, and particles are isotropically emitted from the nucleus. In this case, radial brightness decreases as $1/r$ with the distance from the nucleus. The total thermal infrared flux F_{IR} in a square aperture is roughly proportional to the mass loss rate M :

$$F_{\text{IR}} = \ln(1 + \sqrt{2}) (\varphi / \Delta) (3 Q_e \sigma T_{\text{obs}}^4 / 4 \pi \rho a v_d) M, \quad (6)$$

OR

$$F_{\text{IR}} (\text{W/m}^2) = 1.16 \times 10^{-25} [\varphi (\text{arcsec}) / \Delta (\text{AU})] \\ \times [T_{\text{obs}}^4 (\text{K}) / a (\mu\text{m}) \rho (\text{g/cm}^3) \\ \times v_d (\text{km/s})] M (\text{kg/s}),$$

where φ is the size of a square aperture, a is the average grain size, ρ is the average density, and $Q_e = 0.3$. Obviously, comet Swift-Tuttle was not in a steady state as nonisotropic emission, temporal fluctuations in the dust production, and pronounced jets are clearly seen in the images. Many other parameters involved in these calculations are also very uncertain: the actual dust grain size, velocity and density distributions, the dependence of Q_e and T_{obs} on the particle size and composition, etc. Most important is the dependence on the assumed particle size distribution. A considerable amount of the dust mass in the coma is in the form of large particles ($> 100 \mu\text{m}$, McDonnell *et al.* 1991), which we do not detect in $10 \mu\text{m}$ images (Campins *et al.* 1989). Therefore, we can use the steady-state approximation only to obtain a rough measure of the lower limit of the dust mass loss. This estimate allows us a consistent study of short and long term variations in the dust activity of P/Swift-Tuttle during our observing run. Also, the dust production rate of other comets is usually estimated with similar assumptions, which makes the steady-state model a simple, but useful tool for comparing the productivity of different comets.

The total thermal flux F_{IR} can be estimated from our measurements of the flux f_{11} in a $1 \mu\text{m}$ wide filter centered on $11.65 \mu\text{m}$ as

$$F_{\text{IR}} = f_{11} \sigma T_{\text{obs}}^4 \left/ \left[\int_{11.15}^{12.15} B_{\text{bb}}(\lambda, T_{\text{obs}}) d\lambda \right] \right., \quad (7)$$

where λ is the wavelength in μm , and $B_{\text{bb}}(\lambda, T_{\text{obs}})$ is the Planck energy distribution. Assuming that on all dates the superheat of the cometary dust was the same as on Nov 12 (i.e., the temperature of the grains was 35% higher than the blackbody temperature at the same heliocentric distance: $T_{\text{obs}} = 375.7 R^{-1/2}$), we find that $F_{\text{IR}} \approx 16.26 f_{11}$. The mass loss rate shown in Figs. 5(a) and 5(b) was calculated from (6) for $a = 0.7 \mu\text{m}$, $\rho = 1.0 \text{ g/cm}^3$, $v_d = 0.46 R^{-1/2}$, and $Q_e = 0.3$.

Dust production in Fig. 5(a) varies approximately as $R^{-6.3}$, which agrees very well with the heliocentric dependence of the water production rate as derived by Hoban *et al.* (1993) from a vast set of independent observations. This heliocentric dependence is much steeper than a typical for comets R^{-2} – R^{-4} one (Gehrz & Ney 1992). The increment of the mass loss rate at $R < 1$ AU is caused by the activation of

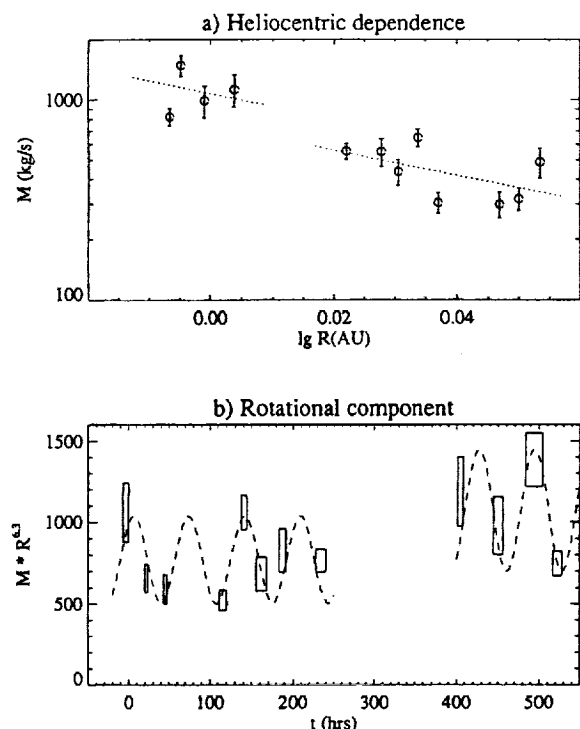


FIG. 5. Dust mass loss rate of P/Swift-Tuttle. (a) Heliocentric dependence. The heliocentric distance was decreasing with time. The dotted line is the least squares approximation showing the $R^{-0.3}$ dependence of the dust mass loss rate. (b) Rotational phase dependence. The sinusoidal curve is used as the simplest periodic function. The width of each box is determined by the angular size of the corresponding image as follows from Eq. (2): the mass loss rate obtained from our measurements is an average over this time interval. The height of each box shows the error of measurement.

jet J3 during the week between November 17 and 24 (cf. Sec. 3.1). Emission from the new area increased the average activity by a factor of 1.4. The overall activity is comparable with that of P/Halley ($\geq 10^3$ kg/s at $R=1$ AU) and is about an order of magnitude higher than in other comets (Gehrz & Ney 1992).

Day-to-day fluctuations in the mass loss rate [Fig. 5(b)] are roughly consistent with the suggested rotation period of 67.5 h. On November 7–17, the dust production achieved maximum when the jet J1 was active, and dropped to the minimum during the intervals of the jet J2 activity. The difference between maximum and minimum dust production is $\sim 40\%$, and similar variation in the water production was found from *IUE* observations (Feldman *et al.* 1993). The data presented by Schulz *et al.* (1994) show the following day-to-day abundance variations of gaseous species: 25% for CN, 26% for C_2 , and 40% for C_3 . This quantitative agreement confirms the hypothesis that, in contrast to comet P/Halley, the gas and dust jets in comet P/Swift-Tuttle are correlated. Remarkably, Feldman *et al.* observed a clear maximum in the water production on Nov 4. That is one rotation period earlier than our first observation of Nov 7, and, in accordance with the rotational dependence presented in Fig. 5(b), activity peaks at this rotational phase.

3.4 The Size of the Nucleus

Sudden activation of strong jets evidently contradicts the suggestion of a uniquely stable and symmetric pattern of

emission of P/Swift-Tuttle made by Yau *et al.* (1994). Seikanina (1981) also inferred from his model calculations that different areas had been active during different rotations of the nucleus, the total number of active areas being up to eight. We consider the alternative hypothesis by Yau *et al.* (1994): that a surprising absence of nongravitational perturbations in the orbital motion of this comet is due to a very large nucleus.

High-resolution infrared imaging gives us a key to direct observations of cometary nuclei even for highly active, Halley-type comets near perihelion. Consider an ideal “unit” comet producing $M=10^3$ kg/s of dust³ in $1\mu\text{m}$ size particles of the density $\rho=1$ g/cm³ at $R=\Delta=1$ AU. In accordance with Eq. (1), the velocity of dust grains is $v_d=0.5$ km/s, and, with a superheat of 1.35, the temperature of grains is 376 K. From Eq. (6) we estimate that the infrared flux of such a comet observed in a 1 arcsec square aperture equals: $I=4.6\times 10^{-12}$ W/m².

Suppose that the nucleus of the unit comet has an average radius x km (with a corresponding surface area of $4\pi x^2$ km²) and radiates as a point source at a blackbody temperature $T_{bb}=278$ K. The resulting infrared flux is given by

$$C=\sigma T_{bb}^4(x/\Delta)^2,$$

or

$$C(\text{W/m}^2)=2.534\times 10^{-24}T_{bb}^4(\text{K})x^2(\text{km}). \quad (8)$$

For $x=10$ km, C equals to 1.5×10^{-12} W/m², implying that the contribution from the nucleus to the central brightest pixel is at least comparable with the flux from the dust. Note that the smaller the size of the central pixel (that is the higher the angular resolution), the larger is the relative contribution of the nucleus flux.

In real images, however, the point source flux becomes spread out over some finite area described by the point spread function (PSF) of the instrument. Approximating our PSF with a Gaussian radial profile, $\text{PSF}=(1/2\pi\delta^2)\exp(-r^2/2\delta^2)$, the contribution of the point source flux to the central pixel is reduced and given by

$$C_{\text{PSF}}\leq C/2\pi\delta^2,$$

where δ is determined by the full-width half maximum (FWHM) of the PSF as

$$\delta^2=\text{FWHM}^2/8\ln 2$$

for a Gaussian approximation of the PSF. Computer modeling was applied to convolve the sum of the $1/r$ dust contribution and the point source contribution from the nucleus with the instrumental PSF. The FWHM was estimated for each night from the calibration star images. The ratio of the nuclear flux C to the dust flux in the central pixel was used as a free parameter in the model. Values of C obtained from the best fit between the model and experimental radial brightness profiles yield an average nucleus radius of $x=(15\pm 3)$ km. This result is consistent with photometric measure-

³This value of M is close to the average mass loss rate in P/Halley at 1 AU and is about an order of magnitude higher than in most comets (Gehrz & Ney 1992).

ments by Williams who suggested that P/Swift-Tuttle nucleus should be at least 24 km across [reported in News Notes, Sky and Telescope 89(1), 1995, page 13]. For comparison, the dimensions of the elongated comet P/Halley nucleus are $(15.3 \times 7.2 \times 7.22)$ km, thus giving an average radius of 4.8 km (Szego 1991).

We estimate that for the same density, the nucleus of P/Swift-Tuttle would be ~ 34 times more massive than the nucleus of P/Halley. Hughes & McBride (1989) showed that the mass of a meteor stream is proportional to the mass of its parent comet multiplied by its dust-to-gas mass ratio. The mass of the meteor stream Perseid associated with P/Swift-Tuttle is $(46 \pm 5) \times 10^{12}$ kg and the average mass of the meteor stream Orionid/Eta Aquarid associated with P/Halley is $(1.5 \pm 0.4) \times 10^{12}$ kg (Jenniskens 1994). Assuming the same dust-to-gas mass ratio in P/Halley and P/Swift-Tuttle, the ratio of masses of their meteor streams is 31, which is in excellent agreement with our result.

4. SUMMARY

Comet P/Swift-Tuttle at the heliocentric distance of 1 AU was one of the most active periodic comets after P/Halley and it demonstrated "Halley-type" behavior in some other respects too. Both P/Halley and P/Swift-Tuttle are old evolved comets having retrograde orbits (inclination $> 90^\circ$). Their comae are dominated by small ($\sim 1 \mu\text{m}$) particles. Images of both comets were consistent with the presence of anisotropic flows of ejecta emanating from discrete active regions (vents) on the rotating cometary nucleus. Moreover, it was suggested that the same vents have remained active since their previous apparitions in 1910 for P/Halley (Rabinowitz 1988) and in 1862 for P/Swift-Tuttle (Schulz *et al.* 1994; this work). This hypothesis, if true, implies a certain degree of stability and, hence, might be used to infer the physical strength of the upper crust on the nuclei of old evolved periodic comets. Future missions landing on the surface of a cometary nucleus would shed more light on this problem.

The activity of individual vents seems to remain stable from one apparition to another, but responds to the diurnal cycle and is affected by seasonal variations. To be fully addressed in the future, it requires a long series of observations of a comet which would provide comprehensive information on day-to-day temporal evolution of cometary activity pre- and post-perihelion. Our observations of P/Swift-Tuttle, as well as the interpretation of the 1862 observations by Sekanina (1981), show that the number of active areas tends to increase closer to perihelion. In our case, there were two sources of jets on November 07–17, and the third vent became active in the images on November 24–29. The mass loss rate depended on the heliocentric distance as $R^{-6.3}$. The initiation of strong emission from the new area increased the average mass loss rate by a factor of 1.4. From periodic changes in the jet pattern we determined the rotation period of P/Swift-Tuttle of 67.5 ± 0.4 h. The dust production varied by $\sim 40\%$ with rotational phase.

In contrast to P/Halley, the dust and gas jets appear to be correlated in P/Swift-Tuttle. Observations of both comets

give rise to speculations about possible heterogeneity of their nuclei (Mumma *et al.* 1990; Fomenkova & Chang 1993; Hoban *et al.* 1993), but there is not enough data to draw more certain conclusions.

The radial brightness profiles calculated for the mid-infrared images of P/Swift-Tuttle are consistent with the presence of a large nucleus, which contributes a non-negligible thermal infrared flux to the central part of each image. We estimated the radius of the nucleus to be 15 ± 3 km. If the densities of the two nuclei are equal, the nucleus of P/Swift-Tuttle is ~ 34 times more massive than the nucleus of P/Halley. This may provide an explanation of the absence of nongravitational perturbations in the motion of comet P/Swift-Tuttle.

We suggest that the differences in the general morphology of comae of new and old comets combined with the differences in the dust grain size distributions may be the principal physical parameters correlated with the dynamical age of comets. For example, images of dynamically new comet Austin (1989c1=1990V) obtained with the same UCSD camera did not reveal significant dust structures in the morphology of the coma, although the resolution was higher, < 300 km per pixel (Fomenkova *et al.* 1993). Either the dust emission was more or less uniform from the whole nucleus (with a slight prevalence on the sunlit side), or the dust grains were ejected in a large number of microjets indistinguishable as separate events from ground-based observations. The long history of apparitions in the inner solar system causes formation of a thick dusty mantle, possibly glued together by complex nonvolatile organics, on most of the surface of a comet (Brin & Mendis 1979). Such an impenetrable crust constraints the activity to a few active areas which are, probably, crevices reaching deeper volatile-rich layers. It effectively decreases and may be even completely prevents the dust emission from the rest of the surface. This scenario implies that the particle size distributions may be different in old and new comets. The coma of new comet Austin was dominated by larger particles ($10 \mu\text{m}$) with the size distribution $f(a) \sim a^{-1}$ (Lisse 1992), while the coma of P/Halley contained a larger fraction of small particles (0.5 – $1 \mu\text{m}$) with the size distribution $f(a) \sim a^{-3.7}$ (McDonnell *et al.* 1991). The photometric measurements of P/Swift-Tuttle indicate that the average size of dust grains in its coma is $\sim 0.7 \mu\text{m}$. A detailed modeling of dust emission processes in P/Swift-Tuttle to determine better its grain size distribution is a subject of our future work.

M. N. Fomenkova acknowledges the support of California Space Institute and thanks the National Research Council for a Resident Research Associateship at NASA Ames Research Center. B.J. and J.S. were supported under NASA Grant NGW-3127 from the Origin of Solar System Program. Partial support for R.P. was provided by NASA Graduate Student Fellowship. We thank Dr. P. Blanco for kindly providing his image processing routines. Comments by D. Cruickshank and by the reviewer S. Larson helped us to improve the manuscript.

REFERENCES

- Brin, G. D., & Mendis, D. A. 1979, *ApJ*, 229, 402
- Campins, H., Telesco, C. M., Decher, R., & Ramsey, B. D. 1987, *A&A*, 187, 601
- Campins, H., Lien, D., Decher, R., Telesco, C., & Clifton, K. 1989, *Icarus*, 80, 289
- Delsemme, A. H. 1982, in *Comets*, edited by L. L. Wilkening (University of Arizona, Tucson), pp. 85–130
- Finson, M. L., & Probst, R. F. 1968, *ApJ*, 154, 327
- Feldman, P. D., McPhate, J., A'Hearn, M. F., McFadden, L. A., & Haken, M. E. 1993, in *Asteroids, Comets, Meteors* (abstr.), IAU Symposium No. 160, 106
- Fomenkova, M. N., & Chang, S. 1993, in *Lunar Planet. Sci. Conf.*, 24, 501
- Fomenkova, M. N., Jones, B., Pina, P., Puetter, R. C., McFadden, L. A., Abney, F., & Gehrz, R. D. 1993, *Icarus*, 106, 489
- Gehrz, R. D., & Ney, E. P. 1992, *Icarus*, 100, 162
- Gehrz, R. D., Hackwell, J. A., & Jones, T. W. 1974, *ApJ*, 191, 675
- Gehrz, R. D., Ney, E. P., Piscatelli, J., Rosenthal, E., & Tokunaga, A. T. 1989, *Icarus*, 80, 280
- Gehrz, R. D., Grasdalén, G. L., & Hackwell, J. A. 1992, in *Encyclopedia of Physical Science & Technology*, 2, 125
- Gilman, R. C. 1974, *ApJS*, 28, 397
- Hanner, M. S. 1994, private communication
- Hanner, M. S., Newburn, R. L., Gehrz, R. D., Harrison, T., Ney, E. P., & Hayward, T. L. 1990, *ApJ*, 348, 312
- Hayward, T. L., Gehrz, R. D., & Grasdalén, G. L. 1987, *Nature*, 326, 55
- Hoban, S., Reuter, D., DiSanti, M., & Mumma, M. 1993, *Icarus*, 105, 548
- Horanyi, M., & Mendis, D. A. 1985, *ApJ*, 294, 357
- Hughes, D. W., & McBride, N. 1989, *MNRAS*, 240, 73
- IRAS Point Source Catalog, NASA RP-1190, 1988
- Jenniskens, P. 1994, *A&A*, 287, 990
- Jewitt, D. C. 1991, in *Comets in the Post-Halley Era*, edited by R. L. Newburn, M. Neugebauer, and J. Rahe (Kluwer, Dordrecht), pp. 19–65
- Jorda, L., Colas, F., & Lecacheux, J. 1993, in *Asteroids, Comets, Meteors* (abstr.), IAU Symposium No. 160, 150
- Kitamura, Y. 1987, *Icarus*, 72, 555
- Lisse, C. M. 1992, Ph.D. thesis, University of Maryland
- Marsden, B. G. 1973, *AJ*, 78, 654
- McDonnell, J. A. M., Lamy, P. L., & Pankiewicz 1991, in *Comets in the Post-Halley Era*, edited by R. L. Newburn, M. Neugebauer, and J. Rahe (Kluwer, Dordrecht), pp. 1043–1074
- Mumma, M., Reuter D., & Magee-Sauer K. 1990, *BAAS*, 22, 1088
- Ney, E. P. 1974, *ApJ*, 189, L141
- Olson, F. M., Raimond, E., & IRAS Science Team 1986, *IRAS Atlas of Low-Resolution Spectra*, *A&AS*, 65, 607
- Pina, R. K., Jones, B., & Puetter, R. C. 1993, in *Infrared Detectors and Instrumentation*, *SPIE Proc.*, 1946, 66
- Rabinowitz, D. L. 1988, *A&A*, 200, 225
- Schulz, R., McFadden, L. A., Chamberlin, A. B., A'Hearn, M. F., & Schleicher, D. G. 1994, *Icarus*, 109, 145
- Sekanina, Z. 1981, *AJ*, 86, 1741
- Sekanina, Z. 1990, *AJ*, 100, 1293
- Sekanina, Z., & Larson, S. 1986, *AJ*, 89, 1408; *AJ*, 92, 462
- Szego, K. 1991, in *Comets in the Post-Halley Era*, edited by R. L. Newburn, M. Neugebauer, and J. Rahe (Kluwer, Dordrecht), pp. 713–732
- Tauber, F., & Kuhrt, E. 1987, *Icarus*, 69, 83
- Telesco, C. M., *et al.* 1986, *ApJ*, 310, L61
- Yau, K., Yeomans, D., & Weissman, P. 1994, *MNRAS*, 266, 305

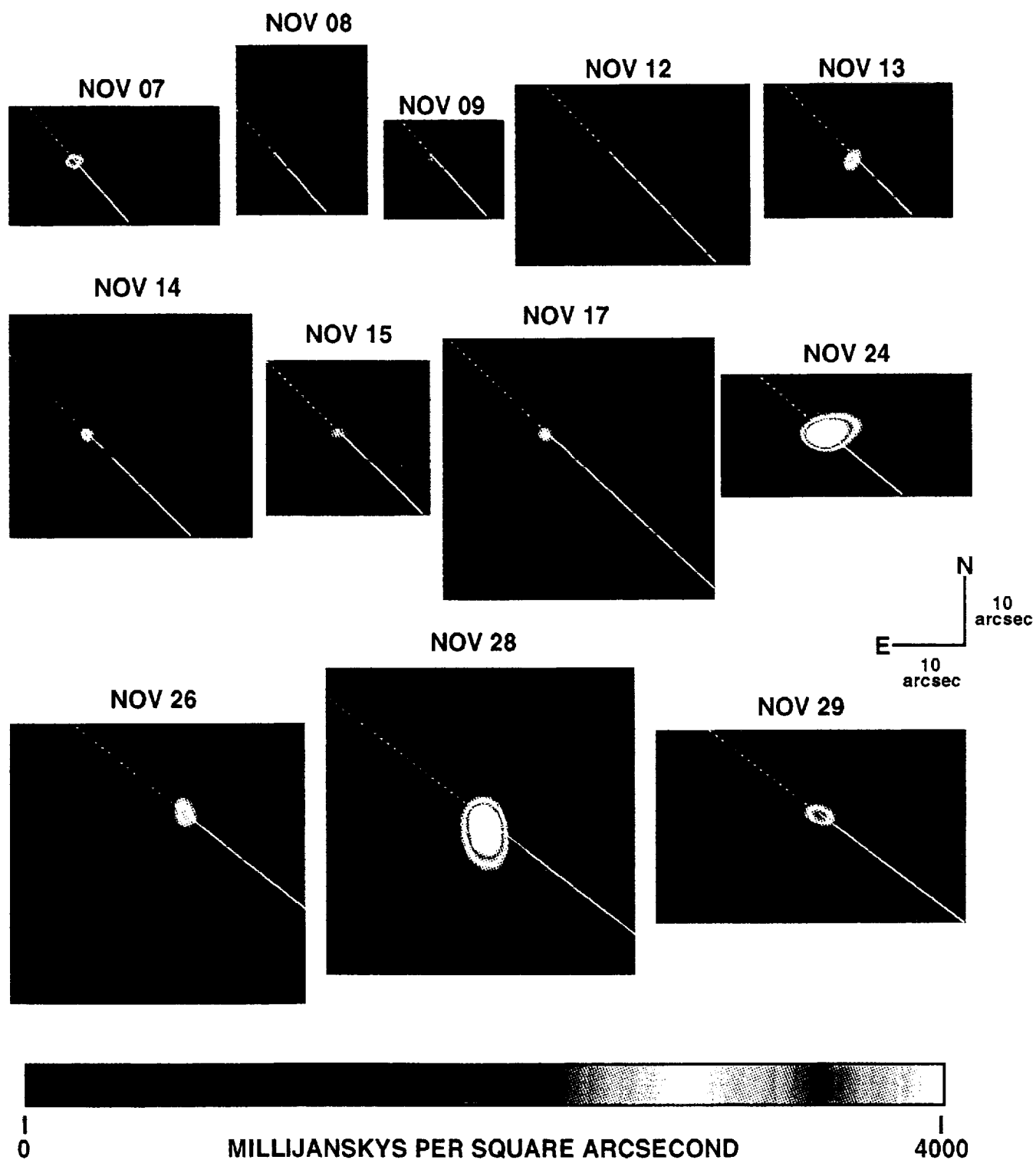


FIG. 1. Coadded thermal infrared images of comet P/Swift-Tuttle. North is upward, and east is leftward. The solid line through the brightest pixel of each image shows the Sunward direction.

Fomenkova *et al.* (see page 1868)

Infrared Observations of an Outburst of Small Dust Grains from the Nucleus of Comet P/Halley 1986 III at Perihelion

R. D. GEHRZ, C. H. JOHNSON, S. D. MAGNUSON, AND E. P. NEY

Astronomy Department, School of Physics and Astronomy, 116 Church Street SE, University of Minnesota, Minneapolis, Minnesota 55455
E-mail: gehrz@astl.spa.umn.edu

AND

T. L. HAYWARD

Center for Radiophysics and Space Research, Cornell University, Ithaca, New York 14853

Infrared Observations of an Outburst of Small Dust Grains from the Nucleus of Comet P/Halley 1986 III at Perihelion

R. D. GEHRZ, C. H. JOHNSON,¹ S. D. MAGNUSON,² AND E. P. NEY

Astronomy Department, School of Physics and Astronomy, 116 Church Street SE, University of Minnesota, Minneapolis, Minnesota 55455
E-mail: gehrz@astl.spa.umn.edu

AND

T. L. HAYWARD

Center for Radiophysics and Space Research, Cornell University, Ithaca, New York 14853

Received July 14, 1994; revised September 6, 1994

A close examination of the 0.7- to 23- μm infrared data base acquired by Gehrz and Ney (1992, *Icarus* 100, 162–186) suggests that the nucleus of Comet P/Halley 1986 III emitted a burst of small dust grains during a 3-day period commencing within hours of perihelion passage on 1986 February 9.46 UT. The outburst was characterized by significant increases in the coma's grain color temperature T_{obs} , temperature excess (superheat: $S = T_{\text{obs}}/T_{\text{BB}}$), infrared luminosity, albedo, and 10- μm silicate emission feature strength. These changes are all consistent with the sudden ejection from the nucleus of a cloud of grains with radii of approximately 0.5 μm . This outburst may have produced the dust that was responsible for some of the tail streamers photographed on 1986 February 22 UT. The peak of the dust outburst occurred about 3 days before a pronounced increase in the water production rate measured by the Pioneer Venus Orbiter Ultraviolet Spectrometer. We suggest that jets that release large quantities of small particles may be largely responsible for some of the variable infrared behavior that has been reported for P/Halley and other comets during the past two decades. Such jets may also account for some of the differences between IR Type I and IR Type II comets. © 1995

Academic Press, Inc.

I. INTRODUCTION

During its 1985–1986 apparition, Comet P/Halley 1986 III was studied extensively in the infrared by many observers who found it to be highly variable in several important ways (Tokunaga *et al.* 1986, 1988, Gehrz and Ney 1986, 1992, Hanner *et al.* 1987, Hanner 1988 and

references therein). Among the parameters that appeared to vary significantly on short time scales were the coma's infrared luminosity, grain temperature, albedo, and 10- μm silicate emission feature characteristics. We have recently reexamined the data base acquired by Gehrz and Ney (1992; Paper I hereafter) to look for systematic infrared variability in P/Halley during perihelion passage when the nucleus should have been the most active. In this paper, we report new evidence that the nucleus of P/Halley ejected a cloud of small grains during its February 1986 perihelion passage.

II. DATA DESCRIBING THE PERIHELION OUTBURST

In Paper I (Tables I–III), we reported the results of broadband optical/infrared photometry of Comet P/Halley 1986 III from 0.7 to 23 μm obtained between 1985 December 12 UT and 1986 May 6 UT using the University of Minnesota O'Brien 0.76-m telescope, the Wyoming Infrared Observatory 2.34-m telescope, and the University of Minnesota/University of California at San Diego Mount Lemmon Observing Facility 1.52-m telescope.

We recently digitized this data base using the TriMetrix, Inc. AXUM Technical Graphics and Data Analysis software to facilitate a detailed examination of the transient activity seen in the infrared and to expedite the comparison of our data with other data bases. An immediate product of this effort was our rediscovery of a pronounced short-lived outburst from P/Halley's nucleus during 1986 February 9–13 UT. Figure 1 shows the temporal evolution of six fundamental physical parameters, the first five of which are derived from the data in Paper I, that characterize this perihelion outburst as a function of time. Time is plotted in days from perihelion passage where $t = 0 =$

¹ Present address: Science Department, Breck Middle School, 123 Ottawa Avenue, North, Minneapolis, MN 55422.

² Present address: Science Department, Southwest Jr. High School, Southwest Highway 169, Albert Lea, MN 55607.

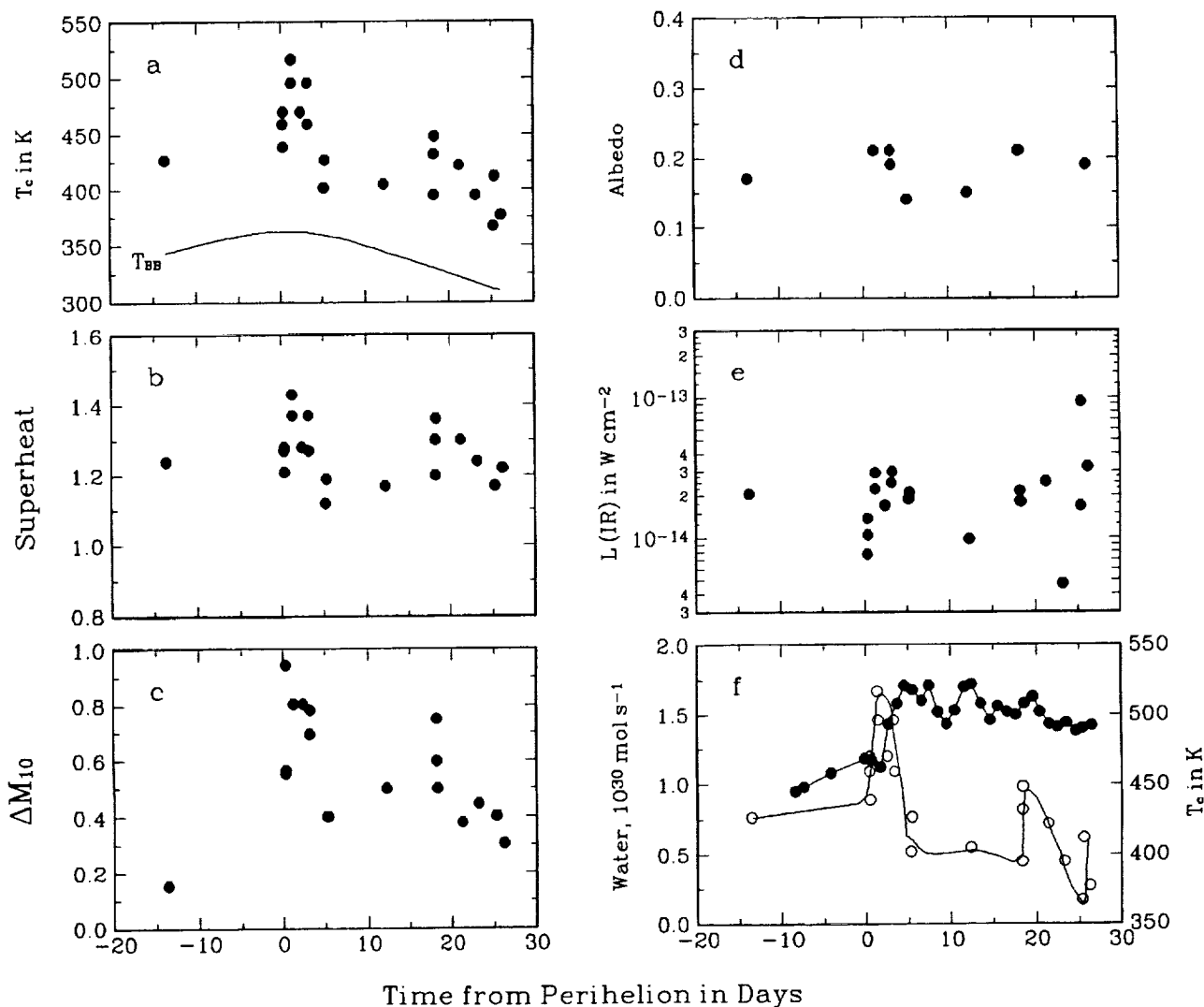


FIG. 1. Physical parameters characterizing the temporal development of the perihelion outburst of Comet P/Halley plotted as a function of days from perihelion passage ($t = 0$): (a) grain color temperature T_c in K; (b) temperature excess, or superheat S ; (c) strength of the $10\text{-}\mu\text{m}$ silicate emission feature relative to the continuum in magnitudes ΔM_{10} ; (d) grain albedo A ; (e) total infrared flux $L(\text{IR})$ emitted by the coma into a $20''$ circular diaphragm corrected for r and Δ ; and (f) water production rate as observed by the Pioneer Venus spacecraft (open circles, data from Stewart 1987) compared with grain color temperature. The solid line labeled T_{BB} in (a) shows the expected temporal evolution of the temperature of black grains as a function of the heliocentric distance r during the epoch of the observations. The fluxes in (e) were normalized to a $20''$ diaphragm and corrected for emission into the reference beam, r , and Δ as described in the text.

1986 February 9.4590 UT. The parameters are the grain color temperature T_c in K (Fig. 1a), the temperature excess as defined by the superheat S (Fig. 1b), the strength of the $10\text{-}\mu\text{m}$ silicate emission feature relative to the continuum in magnitudes ΔM_{10} (Fig. 1c), the albedo A of the coma (Fig. 1d), the total apparent infrared luminosity $L(\text{IR})$ emitted by the coma into a $20''$ circular diaphragm normalized to a heliocentric distance $r = 1$ AU and a geocentric distance $\Delta = 1$ AU (Fig. 1e), and the water production rate recorded by the Pioneer Venus spacecraft (Stewart 1987) compared with T_c (Fig. 1f). The fluxes given in Fig. 1e were scaled to a $20''$ diaphragm, corrected

for coma emission into the reference beam, and normalized to $r = \Delta = 1$ AU using the standard coma emission model described in the Paper I.

It is evident from Fig. 1 that a pronounced outburst commenced within hours of $t = 0$ and persisted for about 3 days thereafter. Activity of the nucleus appears to have returned to the preoutburst level by $t = +5$ days. We refer to this large outburst hereafter as the "primary outburst." There is evidence for a smaller secondary outburst around $t = +18$ days.

Table I summarizes the physical characteristics of the coma during the midpoint of the primary outburst and

TABLE I
Physical Parameters of the Coma during
the Perihelion Outburst

Parameter	Pre/Post Outburst	Midpoint of the primary outburst
r	0.59 AU	0.59 AU
Δ	1.52 AU	1.52 AU
Color temperature	420 K	510 K
Superheat	1.16	1.41
ΔM_{10}	0.35	0.85
Albedo A	0.16	0.22
Apparent luminosity	$6 \times 10^{-15} \text{ W cm}^{-2}$	$2.2 \times 10^{-14} \text{ W cm}^{-2}$
Water production rate	$1.2 \times 10^{30} \text{ mol sec}^{-1}$	$1.7 \times 10^{30} \text{ mol sec}^{-1}$
IR spectrum type	IR I	IR II
Grain radius a	$\geq 1 \mu\text{m}$	$\leq 0.5 \mu\text{m}$

during the pre/post-outburst “quiescent” period. During this outburst, the color temperature, superheat, 10- μm silicate emission feature strength, albedo, luminosity, and water production rate were all elevated with respect to the quiescent values. We argue in the discussion below that the elevations of the first five of these parameters strongly suggest that the primary outburst was characterized by the release of a burst of small grains. The secondary outburst appears to have been similar in this respect.

III. DISCUSSION

Consideration of the arguments we presented in Paper I leads us to conclude that the elevations in the color temperature, superheat, 10- μm silicate emission strength, albedo, and apparent luminosity of P/Halley’s coma during the primary outburst were caused by the release of a significant quantity of small grains with radii $a \leq 0.5 \mu\text{m}$. These physical parameters measure the properties of the optically important grains, and we have shown in Paper I that the mathematical characterization of these parameters is particularly straightforward when the grain radius distribution is assumed to be a power law. Observational evidence favors this assumption. Dust impact measurements from the Giotto spacecraft indicate that the differential particle mass distribution in the coma of P/Halley followed a power law (McDonnell *et al.* 1987), and Hanner *et al.* (1985a,b) found that power law grain size distributions enabled them to construct good model fits to the observed thermal energy distributions of other comets. Jewitt and Meech (1986) and Jewitt (1991) showed that a power law of the form $n(a) da = Ka^{-m} da$, where m lies between 3 and 4.5, can be used to compute the effective grain radius a for the optically important grains in typical comets. We assume in the discussion that follows that the grain radius measured by the infrared emission is the

optically weighted mean defined for such a power law distribution.

The elevated color temperature T_{obs} and the superheat S of the coma of P/Halley during the primary outburst strongly suggest that there was a sudden emission of a burst of relatively small dust grains from the comet nucleus. Following the arguments outlined in Paper I, we define the temperature excess or superheat S as

$$S = \frac{T_{\text{obs}}}{T_{\text{BB}}} = \left[\frac{Q_a}{Q_e} \right]^{1/4}, \quad (1)$$

where

$$T_{\text{BB}} = \left[\frac{L_{\odot}}{16\pi\sigma r^2} \right]^{1/4} = \frac{278}{\sqrt{r_A}} \text{ K} \quad (2)$$

is the temperature expected for a perfectly conducting black sphere at the heliocentric distance r_A (in AU), $T_{\text{obs}} = T_{\text{BB}}[Q_a/Q_e]^{1/4}$ is the observed color temperature of the coma, Q_a is the absorption efficiency of the grain averaged over the solar spectrum, and Q_e is the thermal emission efficiency of the grain at T_{obs} . Thus, T_{obs} and S measure the fourth root of the ratio of Q_a to Q_e , which is approximately unity for large grains, and becomes larger as the grain size decreases. S is a particularly useful parameter for evaluating temperature fluctuations due to grain size and composition because it eliminates to first order the $[r_A]^{-1/2}$ dependence of the grain temperature upon heliocentric distance. For very small grains where $2\pi a/\lambda < 1$, $Q_a/Q_e > 1$, and the grains are significantly superheated. In Paper I (see Paper I, Fig. 5), we examined in detail the parameter space relating S and a . We conclude from that analysis and the data in Table I that the optically important grains expelled during the primary perihelion outburst of P/Halley had mean radii of $a \leq 0.5 \mu\text{m}$ and that the mean grain radius in the coma during the quiescent pre/postoutburst phase was $\geq 1 \mu\text{m}$. Rises in T_{obs} and S also characterize the second outburst at $t \approx +18$ days, suggesting that this episode also was characterized by the emission of small grains.

The behavior of the 10- μm silicate emission feature was also consistent with the hypothesis that the small grains dominated the infrared emission from coma of P/Halley during the primary and secondary outbursts. In Paper I (see Table IV and Fig. 6), we showed that there is a strong correlation between S and the silicate emission excess for a number of comets and concluded that this behavior was consistent with the hypothesis that the strength of the silicate emission feature increases as grain size decreases. As shown in Fig. 1c, the emission feature was nearly a factor of two stronger relative to the continuum during the peak of the primary outburst than it was before and

after the outburst. We note that during quiescence before and between outbursts, the silicate feature was small and P/Halley had the energy distribution of an IR Type I comet. The optically important grains in the comae of IR Type I comets appear to have radii of $\geq 1 \mu\text{m}$ (see Paper I). The $10\text{-}\mu\text{m}$ emission feature was particularly weak on 1986 January 26.8 ($t = -13.6$) UT and 1986 February 14.67 UT ($t = 5.21$). During outburst, the values of S and ΔM_{10} were consistent with the behavior of the most extreme IR Type II comets such as Bennet 1969i (see Maas *et al.* 1970). The thermal infrared coma emission in IR Type II comets is produced primarily by grains with radii $a \leq 0.5 \mu\text{m}$ (see Paper I).

Figure 1d shows that the grain albedo A was about 50% higher during both the primary and the secondary outbursts than the albedo during the quiescent phase between the bursts. A straightforward argument shows that this increase is consistent with the interpretation that small grains were ejected in the outburst. We showed in Paper I that the bolometric albedo $A(\theta)$ as a function of scattering angle θ given by the integrated scattered and emitted energy distributions is

$$A(\theta) = \frac{f(\theta)}{1 + f(\theta)}, \quad (3)$$

where

$$f(\theta) = \frac{f_{\text{vis}}(\theta)}{f_{\text{IR}}(\theta)} = \frac{[\lambda f_{\lambda}(\text{vis}, \theta)]_{\text{max}}}{[\lambda f_{\lambda}(\text{IR}, \theta)]_{\text{max}}} \quad (4)$$

and $f_{\text{vis}}(\theta)$ and $f_{\text{IR}}(\theta)$ are the integrated apparent intensities in the scattered and thermal energy distributions of the coma, respectively, for the scattering angle θ . During the period from $t = -20$ days to $t = +30$ days, θ decreased from 166° to 118° . These scattering angles are in the side-scattering regime where the scattering phase function of comet dust is essentially flat (see Paper I, Fig. 8), and the albedo for a coma in which the grains are not varying in size and composition will be nearly constant such that $A(\theta) \approx A$. Therefore, we conclude that the variations in A for P/Halley that occurred during the outbursts represented actual changes in the mineral composition and/or the size distribution of the coma grains. Since $f(\theta) \ll 1$ for all the measurements in question here, $A(\theta) \approx f(\theta) \propto Q_{\text{scatt}}/Q_{\text{e}}$. As grain size decreases, the emission cross section Q_{e} decreases rapidly compared to the scattering cross section Q_{scatt} (see Gilman 1974). Therefore, $f(\theta)$ for the coma will increase as the optically important grains decrease in size. We conclude that the increase in A seen during the outbursts near perihelion in Comet P/Halley can be explained entirely by the dominance of the thermal infrared emission by small grains in the ejected material.

The increase in the infrared luminosity $L(\text{IR})$ during the primary outburst is generally consistent with an increase in the mass loss rate of solids with respect to the quiescent value. We note that the total IR luminosity rose again during the secondary outburst. In paper I we showed that for small silicate grains where the emission efficiency is proportional to the grain radius a (Gilman 1974), the apparent infrared intensity of the coma is directly proportional to the total mass M_{gr} of the grains,

$$f_{\phi}(\text{IR}) \propto \frac{M_{\text{gr}} \phi}{r^4 \Delta}, \quad (5)$$

where M_{gr} is the total mass of the coma in grains and ϕ is the diameter of the beam used to observe the coma. We conclude that the increase in infrared luminosity during outbursts is caused by increased mass loss. A remarkable aspect of the primary outburst is that it immediately preceded a pronounced increase in the water production rate observed by the Pioneer Venus spacecraft (Fig. 1f). Since the Pioneer Venus had a field of view of about 1° , and the travel time across the field for outflowing water molecules is many days, the ≈ 3 -day phase lag between the infrared outburst, which was observed in a beam ≈ 200 times smaller, and the increase in water production is not unexpected. We suggest that the primary outburst seen in the infrared commencing at $t \approx 0$ marked the onset of the increased water production rate which reached its peak value on Day 3 as seen by Pioneer Venus. Both the water production rate and the IR luminosity remained high for ≈ 30 days following perihelion. Green and Morris (1987) found that the integrated visible magnitude of P/Halley's coma varied asymmetrically with respect to perihelion passage, with the comet being significantly brighter for $t > 0$.

Our observation of outburst activity from the nucleus of P/Halley is consistent with the interpretation that the infrared variations in P/Halley result from rotation of the nucleus presenting active and passive surfaces to the Sun. Both Giotto images (Keller *et al.* 1986) and the groundbased $10\text{-}\mu\text{m}$ infrared images made during the Giotto passage by Hayward *et al.* (1986) suggest the presence of localized active jets on P/Halley's nucleus which could account for such behavior. Sekanina (1986) and Sekanina and Larson (1986) presented a photographic image of P/Halley taken on 1986 February 22 UT that shows multiple tail streamers. Sekanina's analysis of these structures suggested that they may have resulted from outbursts from discrete dust sources on the nucleus during the period from $t = -11.0 \pm 0.2$ days to $t = +3.2 \pm 0.1$ days, including events at $t = +0.3 \pm 0.2$ days and $t = +0.9 \pm 0.2$ days. It seems reasonable to conclude that the primary infrared outburst we report here was associated with the production of the dust in some of the stream-

ers that were eventually observed on 1986 February 22 UT. The physical properties of P/Halley's perihelion outburst are similar to those of the comae of IR Type II comets, suggesting that at least some of these comets may be characterized by persistent outburst activity as compared to IR Type I comets where the outburst activity may be low.

IV. CONCLUSIONS

We find that the nucleus of Comet P/Halley 1986 III emitted a large burst of small dust grains during a 3-day period commencing within hours of perihelion passage on 1986 February 9.46 UT. The outburst was characterized by significant increases in the coma's grain color temperature, superheat, 10- μm silicate emission feature strength, albedo, and infrared luminosity. These changes are all consistent with the sudden ejection from the nucleus of a cloud, or jet, of grains with radii smaller than a $\approx 0.5 \mu\text{m}$. This outburst may have produced the dust that was responsible for some of the tail-streamers photographed on 1986 February 22 UT. The peak of the dust outburst occurred about 3 days before a pronounced increase in the water production rate measured by the Pioneer Venus Orbiter Ultraviolet Spectrometer. A secondary outburst with similar infrared characteristics occurred about 18 days after perihelion passage. We suggest that jets that release large quantities of small particles may be largely responsible for some of the variable infrared behavior that has been reported for P/Halley and other comets during the past two decades. Such jets may also account for some of the differences between IR Type I and IR Type II comets.

ACKNOWLEDGMENTS

This research was supported by NASA, the National Science Foundation, the U.S. Air Force, the University of Minnesota Institute of Technology Dean's Office and Graduate School, and the University of Wyoming. We thank A. Knutson for assisting with the observations at O'Brien Observatory and are indebted to M. S. Hanner for pointing out the work of Sekanina (1986) and Sekanina and Larson (1986). C.H.J. and S.D.M. were supported by the Research Explorations (REX) for Teachers Program in Continuing Education and Extension at the University of Minnesota.

REFERENCES

- GEHRZ, R. D., AND E. P. NEY 1986. Infrared temporal development of P/Halley. In *Exploration of Halley's comet*, ESA SP-250, pp. 101–105. European Space Agency, Noordwijk.

- GEHRZ, R. D., AND E. P. NEY 1992. 0.7- to 23- μm photometric observations of P/Halley III and six recent bright comets. *Icarus* **100**, 162–186. (Paper I).
- GILMAN, R. C. 1974. Planck mean cross-sections for four grain materials. *Astrophys. J. Suppl.* **28**, 397–403.
- GREEN, D. W. E., AND C. S. MORRIS 1987. The visual brightness behavior of P/Halley during 1981–1987. *Astron. Astrophys.* **187**, 560–568.
- HANNER, M. S. 1988. Grain optical properties. In *Observations of Comets Halley and Wilson and Properties of the Grains* (M. S. Hanner, Ed.), NASA Conf. Pub. **3004**, pp. 22–49.
- HANNER, M. S., D. K. AITKEN, R. KNACKE, S. MCCORKLE, P. F. ROCHE, AND A. T. TOKUNAGA 1985a. Infrared spectrophotometry of Comet IRAS–Araki–Alcock (1983d): A bare nucleus revealed? *Icarus* **62**, 97–109.
- HANNER, M. S., E. TEDESCO, A. T. TOKUNAGA, G. J. VEEDER, D. F. LESTER, F. C. WITTEBORN, J. D. BREGMAN, J. GRADIE, AND L. LEBOWSKY 1985b. The dust coma of periodic Comet Churyumov–Gerasimenko (1982 VIII). *Icarus* **64**, 11–19.
- HANNER, M. S., A. T. TOKUNAGA, W. F. GOLISCH, D. M. GRIEP, AND C. D. KAMINSKI 1987. Infrared emission from P/Halley's dust coma during March 1986. *Astron. Astrophys.* **187**, 653–660.
- HAYWARD, T., R. D. GEHRZ, AND G. L. GRASDALEN 1986. Ground-based infrared observations of Comet Halley. *Nature* **326**, 55–57.
- JEWITT, D. 1991. Cometary Photometry. In *Comets in the Post-Halley Era*, (R. L. Newburn, Jr., M. Neugebauer, and J. Rahe, Kluwer, Eds.), Vol. 1, pp. 19–65. Dordrecht.
- JEWITT, D., AND K. J. MEECH 1986. Cometary grain scattering versus wavelength, or, "What color is comet dust?" *Astrophys. J.* **310**, 937–952.
- KELLER, H. U., *et al.* 1986. First Halley multicolor camera imaging results from Giotto. *Nature* **321**, 320–326.
- MAAS, R. W., E. P. NEY, AND N. J. WOOLF 1970. The 10 micron emission peak of Comet Bennett 1969i. *Astrophys. J. Lett.* **160**, L101–L104.
- MCDONNELL, J. A. M., and 27 coauthors 1987. The dust distribution within the inner coma of comet P/Halley 1982i: Encounter by Giotto's impact detectors. *Astron. Astrophys.* **187**, 719–741.
- SEKANINA, Z. 1986. Periodic Comet Halley (1982i). *IAU Circ.* 4187.
- SEKANINA, Z., AND S. M. LARSON 1986. Dust jets in Comet Halley observed by Giotto and from the ground. *Nature* **321**, 357–361.
- STEWART, A. I. F. 1987. Pioneer Venus measurements of H, O, and C Production in Comet P/Halley near perihelion. *Icarus* **187**, 369–374.
- TOKUNAGA, A. T., W. F. GOLISCH, D. M. GRIEP, C. D. KAMINSKI, AND M. S. HANNER 1986. The NASA Infrared Telescope Facility comet Halley monitoring program. I. Preperihelion results. *Astron. J.* **92**, 1183–1190.
- TOKUNAGA, A. T., W. F. GOLISCH, D. M. GRIEP, C. D. KAMINSKI, AND M. S. HANNER 1988. The NASA Infrared Telescope Facility comet Halley monitoring program. II. postperihelion results. *Astron. J.* **96**, 1971–1976.

Thermal–Infrared High-Resolution Imaging of Comet Austin

M. N. FOMENKOVA

California Space Institute, University of California San Diego, La Jolla, California 92093-0216
E-mail: marifo@macvax.ucsd.edu

B. JONES, R. K. PIÑA, AND R. C. PUETTER

Center of Astrophysics and Space Science, University of California San Diego, La Jolla, California 92093-0111

L. A. MCFADDEN

Department of Astronomy, University of Maryland, College Park, Maryland 20742

AND

F. ABNEY AND R. D. GEHRZ

Astronomy Department, University of Minnesota, Minneapolis, Minnesota 55455

Received May 17, 1993; revised August 30, 1993

We report postperihelion imaging of the dynamically new Comet Austin (1989c1 = 1990V) obtained with the UCSD mid-infrared astronomical camera (the “Golden Gopher”) during five nights in May 1990. The 64×16 array format of the camera covered 53×13 arcsec of the sky. The images were taken through a wide 9- to 12- μm filter and a narrower 8- to 9- μm filter. During the observing run, the heliocentric distances ranged from 0.8 to 0.9 AU and the geocentric distance ranged from 0.5 to 0.4 AU. The inner $(16 \times 4) \times 10^3$ km of the coma was sampled with a linear resolution of 290–220 km per pixel. The images obtained on the same night looked similar and were combined together to enhance the signal-to-noise ratio in the coadded images. No jet- or shell-like structures are observed. The coma is slightly elongated along the projected Sun–Comet direction, but there is no systematically higher intensity sunward over anti-sunward. Radial brightness profiles correspond to the steady-state model approximation of r^{-1} up to an angular distance of 4–5 arcsec ($1\text{--}1.5 \times 10^3$ km) from the nucleus but steepen to $r^{-1.25}$ at larger distances. This is consistent with the presence of fading grains in the close vicinity of the cometary nucleus. The thermal infrared flux measured in the images decreases as $R^{-5.5}$ with the heliocentric distance, suggesting a R^{-3} dependence of the dust production rate. The estimated mass loss rate was 1×10^6 g/sec on May 6 and 5.7×10^5 g/sec on May 12, giving a dust-to-gas ratio of 0.25. A map of the spatial behavior of the silicate emission in the coma was generated by comparison of the images obtained on May 12 through the two different filters. This shows a peak in the sunward direction at a distance of $1.5\text{--}2 \times 10^3$ km from the nucleus. The results presented here are the first application of the Golden Gopher camera in cometary research and they demonstrate the potential of mid-infrared array

technology, enabling further insight into the nature, properties, and evolution of comets. © 1993 Academic Press, Inc.

INTRODUCTION

Comets occupy a special place in the study of the cosmic history of the Solar System because they are believed to be the most primitive, least altered objects in the Solar System and contain volatile material from gold regions of the protosolar nebula and remnants of preserved interstellar material (Delsemme 1991). Comets also bear evidence of their own formation and evolution as building blocks of planetary material, thus providing information about the processes of the Solar System’s formation.

Two-dimensional imaging at visible wavelengths (0.4–1 μm) and infrared photometry (1–1000 μm) have proven to be very useful tools for studying comets (e.g., reviews by Jewitt 1991, Hanner 1988). Mid-infrared imaging (3–20 μm) is a relatively new technique (Telesco *et al.* 1986, Campins *et al.* 1987, 1989, Klavetter and Hoban 1992) which combines many of the advantages of both visible imaging and single detector infrared photometry (Hanner and Tokunaga 1991).

In the thermal IR the optical depth of cometary emission is very low (typically 10^{-5}). Mid-infrared imaging shows the morphology of structures in the coma which is directly related to the characteristics of the cometary nucleus. For

example, periodicity in the dust activity of a comet can be caused either by the rotation of active spots on the surface into sunlight or by different cross sections of an elongated rotating nucleus with uniform surface characteristics. The first scenario is more plausible for old evolved comets, and the second one for dynamically new comets. However, it is not yet known if a permanent nonvolatile crust over the nuclear surface can develop before the comet enters the inner Solar System (Weissman and Stern 1989). Comparative studies of the dust morphology in the comae of old and new comets can shed light on this problem.

Infrared imaging provides spatially resolved information about the temperature, size, physical properties, and composition of dust particles in the coma. Both remote (e.g., Chyba *et al.* 1989) and *in situ* (e.g., Fomenkova *et al.* 1992) measurements show cometary dust grains to be mixtures of silicates and organic material. They may represent preserved interstellar grains (Greenberg and Hage 1990), thus giving an opportunity to study this exotic material at close range when comets eject dust and gas into the inner Solar System during their passage near the Sun. At the same time, there is considerable evidence of complex transformations of dust in coma after ejection from the nucleus (e.g., extended sources of gaseous species—A'Hearn *et al.* 1986, Eberhardt *et al.* 1987, changes in the size spectrum of dust particles with the distance from the nucleus—McDonnell *et al.* 1986, steep surface brightness profiles in images of comets—Jewitt and Meech 1987). Spatial and compositional variations in the coma can be caused by (a) intrinsic heterogeneity of the cometary nucleus (possibly due to primary heterogeneity in the protosolar nebula, Fomenkova *et al.* 1993), (b) reworking and restructuring of cometary material after its accretion (crust/mantle formation, Houpin *et al.* 1985, Weissman 1986), and (c) disintegration or alteration of dust grains in the coma during the approach of a comet to the Sun (e.g., Mendis 1991, Fomenkova and Chang 1993). Remote observations of signatures of dust grains ejected from the nucleus may help to understand the influence and appearance of these processes in comets.

In this paper we present the first results of cometary work with the UCSD mid-IR astronomical camera. Fifteen images of the dynamically new Comet C/Austin 1989c1 = 1990V were obtained postperihelion in May 1990 (Rand *et al.* 1990) with a broad 9 to 12- μ m and narrower 8- to 9- μ m filter. We discuss the interpretation of the data in the context of the issues outlined above and compare our results with imaging of Comets C/Wilson 1987VII (Campins *et al.* 1989) and C/Levy 1990XX (Weaver *et al.* 1992).

OBSERVATIONS

The Instrument

The UCSD mid-infrared camera, known as the "Golden Gopher," uses a GenCorp Aerojet 64×20 element Si:As Impurity Band Conduction (IBC) array bonded to a direct readout MOS-FET multiplexer. The optics are gold-coated reflecting surfaces at liquid helium temperature and the array is operated at 10 K. A blocking filter at the Lyot stop defines the wavelength bandpass. The camera provides good sensitivity from 5 to 27 μ m with typical sensitivity of 25 mJy/arcsec² at 10 μ m using a 1- μ m bandwidth for S/N = 1 in 1 min. The platescale is 0.83 arcsec/pixel with the 64 columns \times 16 rows of the array in use, spanning 53×13 arcsec. A detailed description of the camera is given by Piña *et al.* (1993). The characteristics of this infrared camera (e.g., its spatial resolution and sensitivity) make its capabilities similar to those achieved for visible wavelength instrumentation and enable us to apply the data reduction techniques previously developed for optical wavelengths.

The data present in this paper were obtained with the Golden Gopher at the Mt. Lemmon Observing Facility (9000 feet, 30 miles north of Tucson, AZ) using the 1.5-m telescope operated jointly by the University of California San Diego and the University of Minnesota. The telescope is optimized for IR work and uses a standard thermal infrared observation sky-referencing technique (chopping the secondary mirror at 10 Hz and nodding the telescope every 20 sec—see Piña *et al.* (1993)) to subtract sky and telescope background. The image spatial resolution is limited by diffraction to $\lambda/D \sim 1.5$ arcsec FWHM at 10 μ m which is Nyquist sampled by two pixels at the given platescale.

The Infrared Images

The dynamically new Comet Austin (1989c1 = 1990V) was discovered at a heliocentric distance of 2.4 AU 4 months before its perihelion passage. Fifteen postperihelion images of the comet with a broad 9- to 12- μ m and a narrower 8- to 9- μ m filter were acquired during five nights in May 1990 (Rand *et al.* 1990). Table I summarizes the observing parameters and the Sun-C/Austin-Earth geometry. During the observing run, the heliocentric distance varied from 0.76 to 0.90 AU and the geocentric distance varied from 0.48 to 0.36 AU, resulting in a linear resolution at the comet of 290–220 km/pixel or 350–260 km/arcsec (Table I). The projection of the sunward direction onto the sky plane is shown in Figs. 1a–1f, where the solid line indicates the sunward direction.

Both the chop and the nod throw were 45 arcsec for all images. Given the exposure time of ~ 5 min the mean surface brightness at the reference position is below the

TABLE I
Parameters of Comet Austin Observations

	Date (UT)	Air mass	Filter (μm)	R (AU)	Δ (AU)	Elongation (degrees)	Phase angle (degrees)	Sun-comet projection angle, North-to-East (degrees)	Linear resolution (km/pixel)
1	1990 May 05.51	1.05	9-12	0.758	0.479	46.0	106.9	101.35	288
2	1990 May 05.53	1.20							
3	1990 May 06.49	1.05	9-12	0.779	0.461	47.9	106.0	98.76	277
4	1990 May 06.51	1.15							
5	1990 May 06.52	1.30							
6	1990 May 06.53	1.50							
7	1990 May 08.48	1.05	9-12	0.820	0.427	52.1	103.6	93.77	257
8	1990 May 08.50	1.15							
9	1990 May 08.51	1.30							
10	1990 May 08.53	1.52							
11	1990 May 11.49	1.10	9-12	0.880	0.377	59.4	98.9	86.58	227
12	1990 May 11.52	1.30							
13	1990 May 12.45	1.01	9-12	0.900	0.362	62.1	97.1	84.33	218
14	1990 May 12.47	1.05	8-9						
15	1990 May 12.50	1.15	8-9						

sensitivity of the camera and, hence, we do not expect this method of sky subtraction to bias our results.

The primary data reduction included a few technical operations which are basically the same for all images obtained with the "Golden Gopher": removal of bad pixels, removal of a half pixel shift between the upper and lower halves of the array, occasional background correction, and column noise rejection. The variations in pixel-to-pixel sensitivity of the array are $\sim 5\%$ and do not exceed 10% (Piña *et al.* 1993). Sky images simultaneous with cometary observations were used for producing flat fields to correct for these variations. Flux calibrations were obtained by imaging the stars β Peg, α Lyr, and α Sco. We used the data compiled in the Catalog of Infrared Observations (Gezari *et al.* 1984) for the magnitudes of these stars. During the observations, the air mass was ~ 1 , but varying atmospheric conditions limited the accuracy of absolute calibrations at 10–20%. However, none of our results depends on a precise knowledge of the absolute calibration.

The finite spatial resolution of cometary measurements puts a limit on the time scale of variability of cometary activity which can be detected. For an aperture of angular size ϕ centered on the nucleus, the "aperture escape time," $\tau(\phi)$, for dust ejected from the nucleus is (Jewitt 1991)

$$\tau(\phi) = \frac{1}{2} \frac{\phi \Delta}{v_d}, \quad (1)$$

where Δ is the geocentric distance and v_d is the velocity of dust grains dragged with the gas into the cometary coma. In accordance with (Delsemme 1981),

$$v_{\text{gas}} [\text{km/sec}] = 0.58 R^{-1/2} [\text{AU}], \quad (2)$$

with R being the heliocentric distance, and v_{gas} being the terminal gas velocity. Finson and Probst (1968) found

$$v_d/v_{\text{gas}} \cong 0.2 - 0.8, \quad (3)$$

depending on the particle size and density and the total dust-to-gas ratio. The terminal speed of dust particles is reached within 20 radii of the nucleus (~ 200 km), which is smaller than the linear pixel size (see Table I). Assuming $v_d/v_{\text{gas}} = 0.5$, we find

$$\tau(\phi) [\text{hr}] = 0.35 \times \phi [\text{arcsec}] \Delta [\text{AU}] R^{1/2} [\text{AU}]. \quad (4)$$

For the Comet Austin observations presented here $R = 0.8$ AU, $\Delta = 0.4$ AU (see Table I), and $\phi = 53 \times 13$ arcsec (RA \times Dec), yielding aperture escape times of 6.6 and 1.6 hr in each direction, respectively. Therefore, images obtained on different nights are not expected to appear the same, unless the dust ejection is isotropic and constant.

In accordance with Eq. (4), the two-pixel (minimal resolution element) crossing time is only 0.4 hr; i.e., each

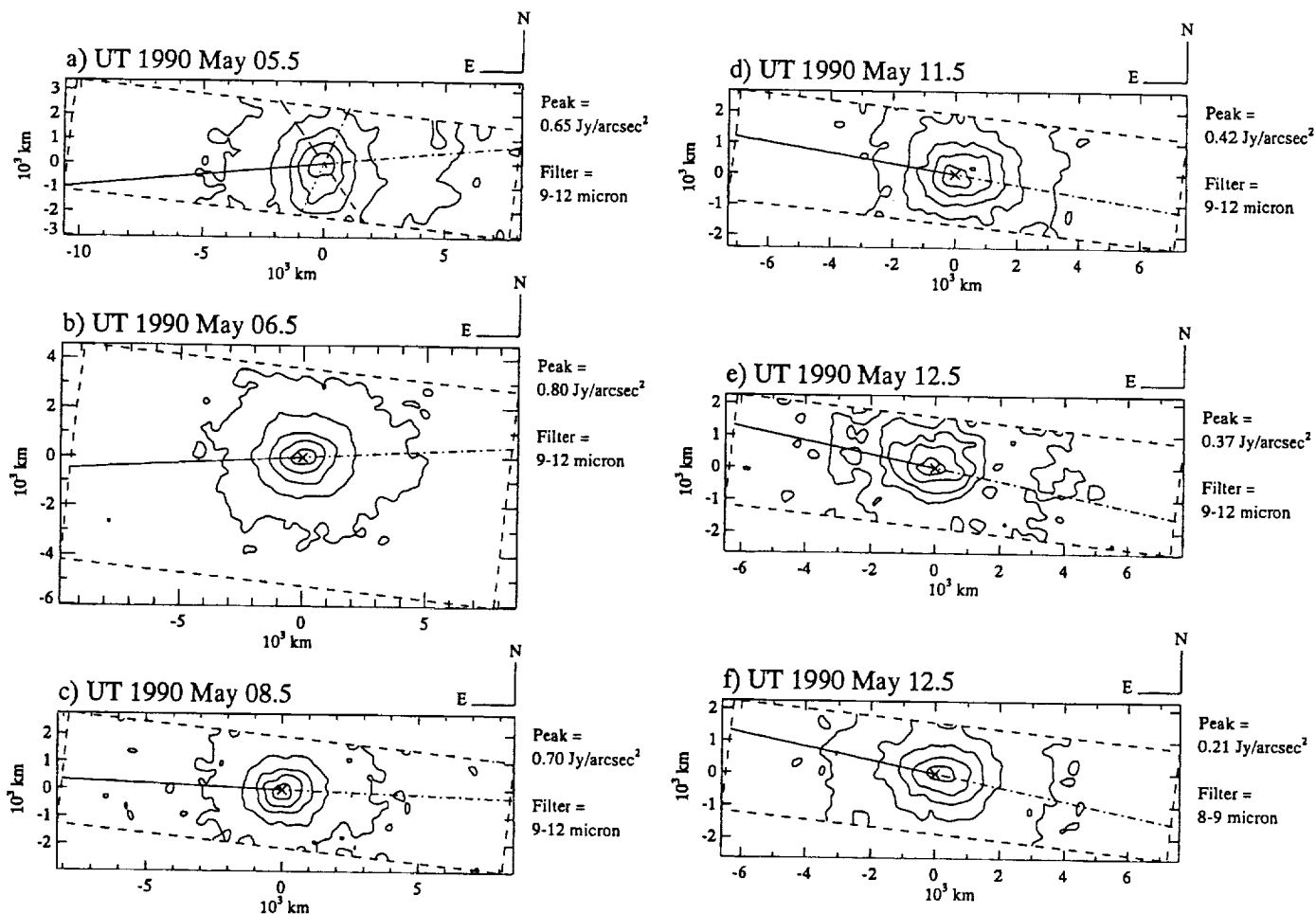


FIG. 1. (a-f) Coadded images of Comet Austin. Images are oriented north-up and east-left, with the length of the fiducial marks denoting 5 arcsec. The origin of coordinate system is located at the brightest pixel of each image and is marked by a cross. Contours are drawn at 90, 70, 50, 30, and 10% level of the peak. The solid line through the peak shows the sunward direction in each image. The cross cuts in (a) correspond to radial brightness profiles shown in Fig. 2a.

image represents a snapshot of the cometary activity for the previous 2–6 hr with a time resolution of 25 min. Images obtained on the same night with 35- to 40-min intervals (see Table I) appear similar within the accuracy of the data, which implies that the dust production rate did not exhibit variations or outbursts faster than time scales of a few hours. This enabled us to combine images from the same night together to enhance the signal-to-noise ratio in the resulting coadded images.

RESULTS

Overall Morphology

The combined images (see Fig. 1a–1f) sample the inner $(3.5\text{--}4.0 \times 14\text{--}18) \times 10^3 \text{ km}$ of the coma. At this distance, dust grains are decoupled from the gas. Dust particle trajectories are determined by their terminal velocities and by accelerations due to solar gravity and solar radia-

tion pressure. Comet Austin was noted by other observers as a “well-behaved” comet (Schleicher *et al.* 1990, Meredith *et al.* 1992), having a symmetric spherical coma in the UV and visible images and a smooth gas outflow. In contrast, our $10\text{-}\mu\text{m}$ images show a coma which is slightly elongated along the Sun–comet line. We believe that this asymmetry is real and not a result of imprecise telescope tracking. The comet was moving fast (1–2 arcsec in RA and 0.5–1 arcsec in Dec per nod period), and the position of the telescope on the comet was verified only between nods. However, the angle between the vector of the comet drift and the Sun–comet direction was about 30° during the observations and this does not coincide with the direction of the elongation.

Except for the coma elongation, the thermal infrared images exhibit a simple morphology similar to UV and visible images—there is no pronounced jet- or shell-like structures whose periodic occurrence could help in de-

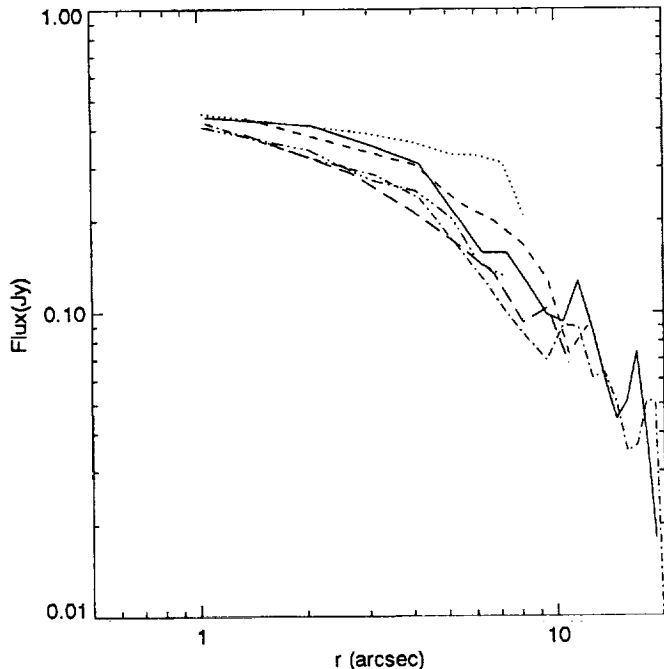


FIG. 2a. Radial brightness profiles for the cross cuts from Fig. 1a.

terminating the rotation period.¹ However, the images do look different from night to night and the shape of even the innermost brightest region appears to vary randomly. Fluctuations of the image morphology suggest that the emission from the surface of the nucleus was not uniform, but probably was rapidly changing as upper layers were blown away with the gas. The emission may have consisted of a large number of microjets indistinguishable as separate events from groundbased observations, but still influencing the overall appearance of the coma. Other evidence of a rapidly changing surface layer of the Comet Austin nucleus is given by Hoban *et al.* (1991), who found that mixing ratio of methanol to water was ~ 5 times larger in the beginning of May than 3 weeks later.

An absence of distinctive dust phenomena in Comet Austin may be intrinsic to all new comets. For example, the thermal infrared images of the dynamically new Comet Wilson obtained with the NASA/MSFC bolometer (Campins *et al.* 1989) with a linear resolution of ~ 5600 km/pixel, covering $\sim 10^5$ km of the coma, looked the same from night to night and did not show any irregular out-

bursts. However, this may be attributed to the large linear resolution and hence the large aperture crossing time (~ 25 hr) which make changes occurring on a comparable or shorter time scale impossible to detect (Jewitt 1991).

Radial Brightness Profiles

Six radial brightness profiles have been constructed for each of the combined images. The directions of the radial cuts through the coma are displayed in Fig. 1a as lines through the center of the image. The resulting profiles for this image are shown in the Fig. 2a. Despite the elongation of the coma in the sunward direction, no systematically higher intensity sunward over anti-sunward was observed. This is in contrast with other results of imaging of comets. Campins *et al.* (1989) argue that a model of dust emission in a 60° beam located 10° eastward from the subsolar point provides the best fit to their images of Comet Wilson. In the images of periodic Comet Levy (Weaver *et al.* 1992) obtained with the Hubble Space Telescope with a linear resolution of 78 km/pixel and covering $\sim 1.6 \times 10^4$ km of the coma, the intensity in the sunward quadrant was as much as two times higher than in the anti-sunward quadrant. Our data show no evidence of an azimuthal dependence of the emission.

Figure 2b shows the average radial brightness profile obtained by averaging all profiles from all images. It indi-

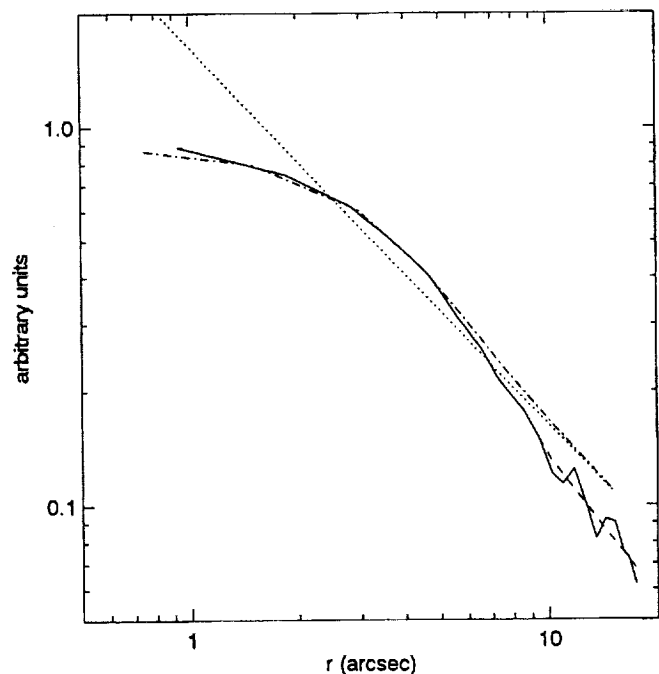


FIG. 2b. Average radial brightness profile. The dotted line shows a $1/r$ profile and the dash-dotted line shows a $1/r$ profile convolved with the instrumental point spread function. The dashed line shows $r^{-1.25}$ dependence.

¹ The image of May 05 (Fig. 1a) is an exception as it seems to have a jet or outburst stretching $\sim 60^\circ$ southward from the sunward direction. However, the somewhat marginal quality of the data which reflects the early engineering status of the camera at the time the observations were made mandates caution in interpretation of this data. The presence of this feature was not confirmed either by our subsequent observations or by other observers.

cates a r^{-1} brightness dependency on radial distance, consistent with a steady-state model (Gehrz and Ney 1992), up to an angular distance $r = 4\text{--}5$ arcsec ($1\text{--}1.5 \times 10^3$ km) from the nucleus. In the steady-state model approximation, the dust production rate and the particle velocity do not depend on time, and particles are isotropically emitted from the nucleus. The observed flattening of the profile near the center of the image is consistent with what is expected for a r^{-1} profile convolved with our instrumental point spread function.

At a larger distance from the nucleus, the profiles steepen to about $r^{-1.25}$, which is consistent with the number of grains in the coma decreasing faster than the steady-state model prediction of r^{-2} . A number of physical processes can be considered to explain the observed gradient of the brightness profiles, including the influence of solar radiation pressure, temporal variations in the dust loss rate, and the presence of fading grains in the coma. Jewitt and Meech (1987) have noted a steepening of profiles in many comets and explained it by shaping of the coma by solar radiation pressure. However, the radial distance at which this dynamical effect becomes important is typically $\sim 3\text{--}5 \times 10^4$ km. Since this scale is much larger than the spatial range covered by our images, solar radiation pressure could not cause the observed radial dependence. The resemblance of the profile gradients obtained on different nights practically rules out the possibility of significant changes in the dust loss rate. Thus, the more plausible hypothesis is that some of the grains are vanishing as they flow out from the comet. The presence of fading icy grains and processes of their sublimation in cometary comae have been considered by Delsemme and Miller (1971), Hanner (1981), Lichtenegger and Komle (1991).

Lichtenegger and Komle (1991) showed that the lifetime of $100\text{-}\mu\text{m}$ icy particles in the space environment at 1 AU from the Sun varies from 4.8 to 0.7 hr when the proportion of organic matter mixed with water ice varies from 1 to 50% and achieves 3000 years for a pure H_2O ice. This estimate is significantly longer than the results of Hanner (1981, based on another vapor pressure formula) and gives rise to the possibility of icy grains in comets surviving up to a radial extent of $\sim 1.0\text{--}1.5 \times 10^3$ km. However, to radiate effectively in the thermal infrared at $10\text{ }\mu\text{m}$, the fading grains should have a temperature of ~ 300 K. Lichtenegger and Komle (1991) estimated temperature of sublimating H_2O ice particles near 1 AU to be $\sim 180\text{--}200$ K, which makes their contribution too small in comparison with warmer mineral dust grains. On the other hand, the fading grains can be made up of organic polymers more refractory than water ice which can reach a higher temperature of ~ 300 K (see discussion by Mitchell *et al.* 1992). *In situ* studies of Comet Halley dust grains showed that stable cometary grains encountered at $1\text{--}5 \times 10^4$ km from the nucleus had a considerable organic component (Kissel

et al. 1986). The proportion of grain having organic component decreased with an increase of the distance from the nucleus (Fomenkova *et al.* 1993), which suggests the decomposition of organic matter in the coma. The evaporation of the organic grains in Comet Halley was proposed to provide an extended source of some gaseous species: C^+ (Balsiger *et al.* 1986), CO (Eberhardt *et al.* 1987), CN (A'Hearn *et al.* 1986), and more complex heavy ions (Mitchell *et al.* 1992). Meredith *et al.* (1992) discussed the possible presence of decomposing organic grains in Comet Austin to explain their observations of CN and C_2 abundances. We conclude that the observed brightness profiles represent evidence of evaporating organic grains in the coma of Comet Austin.

Heliocentric Dependence of the Thermal Flux

The majority of our images were obtained with a broad 9- to $12\text{-}\mu\text{m}$ filter bracketing the peak in blackbody emission. Thus, the integrated flux in the images should be roughly proportional to the total thermal emission,

$$f_{\text{IR}}(\phi) = \frac{\pi \phi}{4 \Delta} \dot{N} \int \frac{a^2 Q_e(a) \sigma T_{\text{obs}}^4(a)}{v_d(a)} f(a) da, \quad (5)$$

for a circle aperture of diameter ϕ (Gehrz and Ney 1992), or

$$r_{\text{IR}}(\phi) = \ln(1 + \sqrt{2}) \frac{\phi}{\Delta} \dot{N} \int \frac{a^2 Q_e(a) \sigma T_{\text{obs}}^4(a)}{v_d(a)} f(a) da \quad (6)$$

for a square aperture of size ϕ . Expressions (5) and (6) are derived for the steady state model, \dot{N} is the dust production rate, a is the grain radius, $Q_e(a)$ is the Planck emission coefficient of the grain, σ is the Stefan-Boltzmann constant, T_{obs} is the observed grain temperature, and $f(a)$ is the particle size distribution. Figure 3 presents the dependence of flux (multiplied by the geocentric distance) on the heliocentric distance for different aperture sizes. Typically, the total thermal infrared flux in comets is predicted to vary with the heliocentric distance as R^{-4} (Ney 1982). The measured flux in the Austin images varies as $R^{-5.5}$ and can be factored as follows. An R^{-2} dependence is caused by the temperature decrease resulting from the energy balance between the power of absorbed solar radiation and the power emitted by grains in the thermal infrared:

$$4\pi a^2 Q_e(a) \sigma T_{\text{gr}}^4 = \pi a^2 Q_a(a) \frac{L_{\text{sun}}}{4\pi R^2}. \quad (7)$$

Here L_{sun} is the solar luminosity, $Q_a(a)$ is the Planck mean absorption coefficient averaged over the energy distribution of the Sun, and T_{gr} is the local equilibrium tempera-

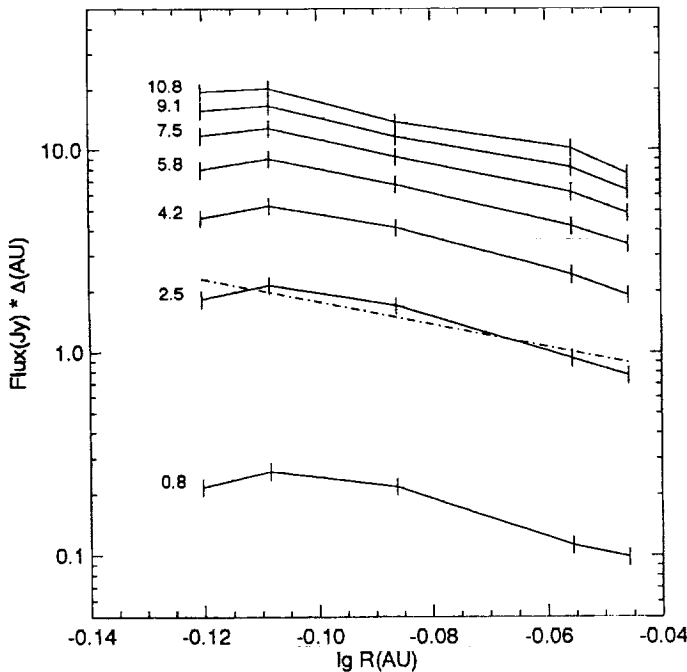


FIG. 3. Dependence of the thermal flux on the heliocentric distance for square apertures of a various size. Number at left of each curve is the length of the side of the square aperture in arcsec. Uncertainties in the flux are about 15%. The dash-dotted line is the least squares approximation to the slope of the curves showing the $R^{-5.5}$ dependence of the flux.

ture. Gehrz and Ney (1992) and Hanner *et al.* (1993) reported that for Comet Austin the observed temperature of dust grains T_{obs} was close to T_{gr} . An additional $R^{-0.5}$ dependence in the flux is expected due to the decrease of the grain terminal velocity as follows from Eqs. (2)–(3). The remaining heliocentric dependence of the flux can be accounted for if the dust production rate \dot{N} falls as R^{-3} . The slope of -3 of the dust production rate is consistent with the -2.75 value found by Schleicher *et al.* (1990) and with the -3.1 slope of the water production rate (Schultz *et al.* (1993). Hasegawa and Watanabe (1992) attributed such a fast drop of the activity postperihelion to a formation of a dust mantle layer on the surface of the Comet Austin nucleus. The low thermal conductivity of this mantle reduces the sublimation rate at the icy surface.

Mass Loss Rate

The mass loss rate \dot{M} can be estimated as

$$\dot{M} = \frac{4}{3} \pi \dot{N} \int \rho(a) a^3 f(a) da, \quad (8)$$

where $\rho(a)$ is the particle density.

It follows from Eqs. (6) and (8) that the mass production

rate depends on the assumed particle size, density, and velocity distributions. A number of observers (Gehrz and Ney 1992, Hanner 1993) have suggested that Comet Austin may have the bulk of its mass loss in large particles. This is based on the absence of strong silicate emission in its spectrum and the low excess of the grains' color temperature above the local equilibrium. Large spatial scale observations of the Comet Austin dust tail in the 3–100- μm range by COBE/DIRBE (Lisse 1992) demonstrated that the dust emission of Comet Austin was dominated by large dark particles $>10\text{--}100\ \mu\text{m}$, invisible at optical wavelengths. Such a size distribution, weighted toward larger grains, may correlate with the featureless coma. Laboratory simulation of cometary dust–gas emission (KOSI, Thiel *et al.* 1991) showed that highly active regions on the surface of their samples (the analog of jets) emit mostly small particles while large particles are more slowly and uniformly emitted. On the other hand, the relationship between the relatively high abundance of large particles in the coma and the previous processing history of the nucleus remains unclear. For example, the coma of new Comet Wilson was dominated by small particles (Hanner and Newburn 1989) as well as the coma of old Comet Halley (McDonnell *et al.* 1991).

To determine the mass loss rate of Comet Austin we used $f(a)$ and $\rho(a)$ from the model fit to the Comet Austin observation obtained by Lisse (1992):

$$f(a) \sim 1/a, \quad \rho(a) \sim a^{-0.27}, \quad 0.1\ \mu\text{m} < a < 10^4\ \mu\text{m}. \quad (9)$$

In comparison with the Halley dust size distribution (McDonnell *et al.* 1991), which varies as $a^{-3.7}$, this size distribution is highly dominated by large grains. The particle density ranges from $2.5\ \text{g/cm}^3$ for $0.1\ \mu\text{m}$ grains implying solid compact spheres at this end of the size distribution, to $0.1\ \text{g/cm}^3$ for $10^4\ \mu\text{m}$ grains implying that large particles are fluffy and highly porous. The latter is consistent with observations of anhydrous interplanetary dust particles of possibly cometary origin (Brownlee 1978) and with theoretical modeling of cometary dust properties (Greenberg and Hage 1990).

Lisse (1992) deduced a velocity distribution given by

$$v(a) \sim \frac{1}{\sqrt{R}} \frac{1}{\sqrt{\rho(a)a}} \quad (10)$$

as the best fit to his Comet Austin data. At the large scales ($10^6\ \text{km}$) measured by COBE/DIRBE on the Comet Austin tail, this velocity distribution is dominated by the interaction of dust particles with solar radiation and solar gravity. Thus, it is not applicable to our images which extend only over the inner part of the coma—a region in which dust particles interaction with the solar wind is insignificant.

Instead, the terminal velocity distribution from Finson and Probst (1968) was adopted. Also, we assumed that $Q_a = Q_e = 1$, which is appropriate for Comet Austin (Gehrz and Ney 1992) because of the predominance of large grains in its coma.

Having adopted the size distribution, particle density, and velocity distribution, the total mass loss rate can be calculated from Eqs. (6)–(8). The flux within a square aperture of 9×9 arcsec was used for calculations as it is the largest aperture for which the steady-state model is still applicable and the effect of grain fading is negligible (see Fig. 2b). The resulting calculated mass loss rate $\sim 1 \times 10^6$ g/sec on May 6 is 3 times larger than the lower limit estimate of Hanner *et al.* (1993) based on a Halley-type model of small absorbing grains. On May 12 we obtained $\dot{M} \sim 5.7 \times 10^5$ g/sec which is comparable with the value 5.1×10^5 g/sec from Lisse (1992) for May 15. Using the water production rate from Schultz *et al.* (1993) gives a dust-to-gas ratio of ~ 0.25 which characterizes Austin as a “dust-poor” comet. However, our mass loss rate estimate may also be underestimated because the size distribution (9) is cut off at $10^4 \mu\text{m}$ (0.5-g particles) while larger masses may have been emitted.

The Silicate Emission

Comet Austin had an unusually wide 9- to $12\text{-}\mu\text{m}$ silicate emission feature 15–20% above the continuum (Hanner *et al.* 1993) peaking at $11.06 \mu\text{m}$, which was quite different from that seen in Comet Halley and several other comets. In our set of data obtained on May 12, 1990, one image was acquired with the broad 9- to $12\text{-}\mu\text{m}$ filter and two images with a narrower 8- to $9\text{-}\mu\text{m}$ filter. We compared the total fluxes measured in the 11×11 -pixel (9.1×9.1 arcsec) square aperture in these images with the Comet Austin 9– $13\text{-}\mu\text{m}$ spectrum (Hanner *et al.* 1993) obtained on May 6, 1990, by using a 9.4-arcsec-diameter circular aperture and converted to the bandpasses of our filters. The ratios of 9- to $12\text{-}\mu\text{m}$ to 8- to $9\text{-}\mu\text{m}$ flux is 2.18 from the data of Hanner *et al.* (1993) and 1.79 from our data. This is adequate agreement because the uncertainties in our absolute flux calibration were $\sim 15\text{--}20\%$. Also, these measurements are separated by 6 days, and cometary spectra may be quite variable from date to date (Gehrz and Ney 1992).

The ratio of the 9- to $12\text{-}\mu\text{m}$ and 8- to $9\text{-}\mu\text{m}$ images was examined to determine the spatial distribution of the silicate emission in the coma (Fig. 4). Being normalized to the maximum, the ratio varies from 1 to ~ 0.3 , increasing within a $\sim 90^\circ$ angle in the sunward direction from the nucleus with the peak at a distance of $\sim 1.5\text{--}2 \times 10^3$ km. This implies an enhancement of silicate emission in this region. Small grains ($< 1 \mu\text{m}$) are responsible for the presence of the silicate emission

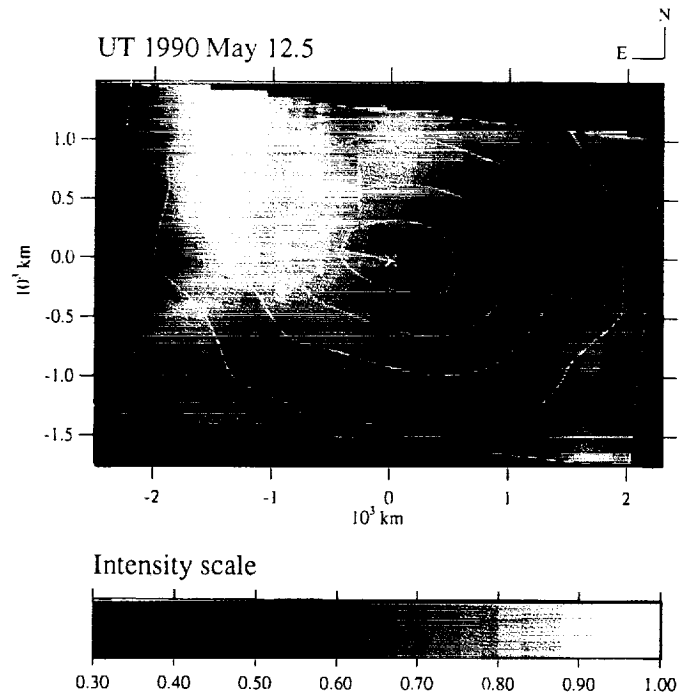


FIG. 4. Spatial behavior of the silicate emission feature. Halftone image shows the relative strength of the silicate emission. Contours show the position of the comet itself and are taken from Fig. 1f. That image was obtained through the 8- to $9\text{-}\mu\text{m}$ filter characterizing the thermal continuum emission. The length of fiducial marks denotes 0.83 arcsec (the pixel size).

feature in comets (Gehrz and Ney 1992). There is considerable evidence that these grains may be nonuniformly distributed in comae. Infrared photometry of Comet Kohoutek (Ney 1974) showed the silicate emission feature in its coma and tail (at 5 arcmin from the nucleus), but not in its anti-tail (at 11.3 arcmin from the nucleus). Imaging of the Comet Halley coma (Campins *et al.* 1987) at 10.8 and $12.8 \mu\text{m}$ indicated a stronger silicate emission in the sunward direction than in other directions which is consistent with our observations of Comet Austin, but they observed the peak emission located at the nucleus. We hypothesize that the small grains in Comet Austin are relatively more abundant in the fresh dust recently emitted from the dayside of the nucleus and later get blown away by radiation pressure. However, the data on the spatial distribution of particles of different size are controversial. Ney (1974) suggested that the anti-tail of Comet Kohoutek was made up of large particles while Telesco *et al.* (1986) explained the thermal infrared images of Comet Giacobini–Zinner by the presence of large particles in its tail. Further observations and modeling are required for a better understanding of the dust behavior in the inner part of cometary comae.

SUMMARY

The Comet Austin observations presented in this paper were the first application of the newly built Golden Gopher camera to cometary research. From these thermal infrared images obtained with a spatial resolution of 290–220 km/pixel we have determined the following:

1. The Comet Austin coma is slightly elongated sunward, but does not reveal systematically higher sublimation intensity in the sunward-facing hemisphere. No jets or other distinctive dust phenomena were observed.

2. The radial brightness profiles follow a $1/r$ dependence of the steady-state model approximation up to 4–5 arcsec from the nucleus and become steeper afterward which is consistent with the presence of fading grains in the coma.

3. The thermal infrared flux in the images decreases as $R^{-5.5}$ with the heliocentric distance which results in a R^{-3} dependence of the dust production rate.

4. The mass loss rate, estimated for a size distribution dominated by large grains, gives a dust-to-gas ratio of 0.25, which characterizes Comet Austin as a “dust-poor,” “gassy” comet. However, the estimate of dust mass loss is model dependent and represents a lower estimate since the grain size distribution was cut off at $10^4 \mu\text{m}$.

5. The ratio of the 9- to 12- μm image to the 8- to 9- μm image samples the spatial behavior of the thermal silicate emission. The silicate emission peaks at $1.5\text{--}2 \times 10^3 \text{ km}$ from the nucleus in the sunward direction, which suggests that the small silicate grains ($<1 \mu\text{m}$) responsible for the silicate feature prevail on the dayside of the nucleus. This is the only clearly asymmetrical feature observed in the coma of this comet.

High-resolution thermal infrared imaging of Comet Austin has provided spatially resolved information about the distribution of dust grains in its coma. How do these data specifically characterize Austin as a dynamically new comet making its first passage through the inner part of the Solar System? Smooth isotropic emission and the absence of jets may be a typical feature of a new comet if one suggests that repeated passages of the comet through the Solar System play a more important role in differentiating the surface of its nucleus than the time spent in the Oort cloud. The presence of fading, possibly volatile organic grains may also be expected for a new comet containing an outer layer of active fresh material. The sharp decrease in activity postperihelion is typical for many new comets and may be due to the formation of a dust mantle on the surface of their nuclei. Continuing work with mid-infrared array imaging will contribute further to our understanding of cometary origin and evolution.

ACKNOWLEDGMENTS

M. N. Fomenkova and L. A. McFadden acknowledge the support of California Space Institute. B. Jones and R. C. Puetter are partially supported by NSF Grant AST 9121784, and R. K. Piña acknowledges support from the NASA Graduate Student Researchers Program. We thank P. Blanco for kindly providing his image processing routines. Constructive comments of our reviewers M. Hanner and D. Jewitt helped us to improve the original manuscript.

REFERENCES

- A'HEARN, M. F., *et al.* 1986. CN jets in comet P/Halley. *Nature* **324**, 649–651.
- BALSIGER, H., *et al.* 1986. Ion composition and dynamics at comet Halley. *Nature* **321**, 330–334.
- BROWNLEE, D. 1978. Interplanetary dust: Possible implications for comets and presolar interstellar grains. In *Protostars and Planets* (T. Gehrels, Ed.), pp. 134–150. Univ. of Arizona Press, Tucson.
- CAMPINS, H., C. M. TELESKO, R. DECHER, AND B. D. RAMSEY 1987. Thermal infrared imaging of comet P/Halley. *Astron. Astrophys.* **187**, 601–604.
- CAMPINS, H., D. J., LIEN, R. DECHER, C. M. TELESKO, AND K. S. CLIFTON 1989. Infrared imaging of the coma of comet Wilson. *Icarus* **80**, 289–302.
- CHYBA, C. F., C. SAGAN, AND M. J. MUMMA 1989. The heliocentric evolution of cometary infrared spectra: results from an organic grain model. *Icarus* **79**, 362–381.
- DELSEMMÉ, A. H. 1982. Chemical composition of cometary nuclei. In *Comets* (L. L. Wilkening, Ed.), pp. 85–130, Univ. of Arizona, Tucson.
- DELSEMMÉ, A. H. 1991. Nature and history of organic compounds in comets: An astrophysical view. In *Comets in the Post-Halley Era* (R. L. Newburn, M. Neugebauer, and J. Rahe, Eds.), pp. 377–428. Kluwer Academic, The Netherlands.
- DELSEMMÉ, A. H., AND D. C. MILLER 1971. Physico-chemical phenomena in comets. III. The continuum of comet Burnham (1960 II). *Planet Space Sci.* **19**, 1229–1257.
- EBERHARDT, P., *et al.* 1987. The CO and N₂ abundance in Comet P/Halley. *Astr. Astrophys.* **187**, 481–484.
- FINSTON, M. L., AND R. F. PROBSTEN 1968. A theory of dust comets. *Astrophys. J.* **154**, 327–359.
- FOMENKOVA, M. N., S. CHANG, AND L. M. MUKHIN 1993. Carbonaceous Components in the Comet Halley dust. Submitted for publication.
- FOMENKOVA, M. N., AND S. CHANG 1993. Mass and spatial distribution of the carbonaceous components in Comet Halley. *Lun. Plan. Sci. Conf.* **24**, 501–502.
- FOMENKOVA, M. N., J. F. KERRIDGE, K. MARTI, AND L. A. MCFADDEN 1992. Compositional trends in rock-forming elements of comet Halley dust. *Science* **258**, 266–269.
- GEHRZ, R. D., AND E. P. NEY 1992. 0.7 to 23 micron photometric observations of P/Halley 1986 III and six recent bright comets. *Icarus* **100**, 162–186.
- GEZARI, D. Y., M. SCHMITZ, AND J. M. MEAD (Eds.) 1984. *Catalog of Infrared Observations*. NASA Ref. Publication 118.
- GREENBERG, J. M., AND J. I. HAGE 1990. From interstellar dust to comets: A unification of observational constraints. *Astrophys. J.* **361**, 260–274.
- HANNER, M. S. 1981. On the detectability of icy grains in the comae of comets. *Icarus* **47**, 342–350.

- HANNER, M. S., Ed. 1988. *Infrared Observations of Comets Halley and Wilson and Properties of the Grains*. NASA CP 3004.
- HANNER, M. S., AND R. L. NEWBURN 1989. Infrared photometry of Comet Wilson (19861) at two epochs. *Astron. J.* **97**, 254–261.
- HANNER, M. S., R. W. RUSSEL, D. K. LYNCH, AND T. Y. BROOKE 1993. Infrared spectroscopy and photometry of comet Austin 1990 V. *Icarus* **101**, 64–70.
- HANNER, M. S., AND A. T. TOKUNAGA 1991. Infrared techniques for comet observations. In *Comets in the Post-Halley Era* (R. L. Newburn, M. Neugebauer, and J. Rahe, Eds.), pp. 67–91. Kluwer Academic, Netherlands.
- HASEGAWA, H., AND J. WATANABE 1992. Lightcurve of Comet Austin (1989c1) and its dust mantle development. In *Asteroids, Comets, Meteors 1991* (A. W. Harris and E. Bowell, Eds.), pp. 231–234. Lunar and Planetary Institute, Houston.
- HOBAN, S., M. MUMMA, D. C. REUTER, M. DISANTI, R. R. JOYCE, AND A. STORRS 1991. A tentative identification of methanol as the progenitor of the 3.52- μ m emission feature in several comets. *Icarus* **93**, 122–134.
- HOUPIS, H. L., W.-H. IP, AND D. A. MENDIS 1985. The chemical differentiation of the cometary nucleus: The process and its consequences. *Astrophys. J.* **295**, 654–667.
- JEWITT, D. C. 1991. Cometary photometry. In *Comets in the Post-Halley Era* (R. L. Newburn, M. Neugebauer, and J. Rahe, Eds.), pp. 19–65. Kluwer Academic, Netherlands.
- JEWITT, D. C., AND K. J. MEECH 1987. Surface brightness profiles of 10 comets. *Astrophys. J.* **317**, 992–1001.
- KLAVETTER, J. J., AND S. HOBAN 1992. Imaging of 3.4 μ m feature in Comet Levy (1990c). *Icarus* **95**, 60–65.
- KISSEL, J., R. Z. SAGDEEV, J. BERTAUX, *et al.* 1986. Composition of comet Halley dust particles from Vega observations. *Nature* **321**, 280–282 and 336–338.
- LICHTENEGGER, H. I. M., AND N. I. KOMLE 1991. Heating and evaporation of icy particles in the vicinity of comets. *Icarus* **90**, 319–325.
- LISSE, C. M. 1992. *Infrared Observations of Cometary Dust by COBE*. Ph.D. thesis, University of Maryland.
- MCDONNELL, J. A. M. *et al.* 1986. In situ exploration of the dusty coma of Comet P/Halley at Giotto's encounter. *Nature* **321**, 338–340.
- MCDONNELL, J. A. M., P. L. LAMY, AND G. S. PANKIEWICZ 1991. Physical properties of cometary dust. In *Comets in the Post-Halley Era* (R. L. Newburn, M. Neugebauer, and J. Rahe, Eds.), pp. 1043–1074. Kluwer Academic, The Netherlands.
- MENDIS, D. A. 1991. The role of field emission in the electrostatic disruption of cosmic dust. *Astrophys. Space Sci.* **176**, 163–165.
- MEREDITH, N. P., M. K. WALLIS, AND D. REES 1992. Narrow-band IPD images of cometary CN and C₂: The effect of solar activity on coma scales. *Mon. Not. R. Astr. Soc.* **254**, 693–704.
- MITCHELL, D. L., *et al.* 1992. The origin of complex organic ions in the coma of comet Halley. *Icarus* **98**, 125–133.
- NEY, E. P. 1982. Optical and infrared observations of comets in the range 0.5 micron to 20 micron. In *Comets* (L. L. Wilkening, Ed.), pp. 323–340. Univ. of Arizona, Tucson.
- NEY, E. P. 1974. Infrared observations of Comet Kohoutek near perihelion. *Astrophys. J.* **189**, L141–L143.
- PIÑA, R. K., B. JONES, AND R. C. PUETTER 1993. Golden Gopher: UCSD's mid-IR astronomical camera. In *Infrared Detectors and Instrumentation*. SPIE Proc. 1946.
- RAND, W. M., L. A. MCFADDEN, B. JONES, R. C., PUETTER, AND R. K. PIÑA 1990. Two-dimensional thermal infrared images of comet Austin: May 5–12, 1990. *Bull. Am. Astron. Soc.* **22**, 1096.
- SCHLEICHER, D. G., D. J. OSIP, R. L. MILLIS, A. THOMPSON, AND L. M. SAUTER 1990. Photometric narrow-band CCD imaging of comets P/Brosen-Metcalf and Austin (1989c1). In *Workshop on Observations of Recent Comets* (W. F. Huebner, Ed.), pp. 8–12. Southwest Research Institute, Albuquerque.
- SCHULTZ, D., G. S. H. LI, F. SCHERB, AND F. L. ROESLER 1993. The O(1D) distribution of comet Austin 1989c1 = 1990V. *Icarus* **101**, 95–107.
- TELESCO, C. M., *et al.* 1986. Thermal-infrared and visual imaging of Comet Giacobini-Zinner. *Astrophys. J.* **310**, L61–L65.
- THIEL, K., G. KOLZER, AND H. KOHL 1991. Dust emission of mineral/ice mixtures: Residue structure and dynamical parameters. *Geophys. Res. Lett.* **18**, 281–284.
- WEAVER, H. A., *et al.* 1992. Inner coma imaging of Comet Levy (1990c) with the Hubble space telescope. *Icarus* **97**, 85–98.
- WEISSMAN, P. R. 1986. Are cometary nuclei really pristine? In *The Comet Nucleus Sample Return Mission*, pp. 15–25. ESA SP-249.
- WEISSMAN, P. R., AND S. A. STERN 1989. Physical processing of cometary nuclei. In *Proceedings of the Workshop on Analysis of Returned Comet Nucleus Samples*, Mipitas.

0.7- to 23- μ m Photometric Observations of P/Halley 1986 III and Six Recent Bright Comets

R. D. GEHRZ AND E. P. NEY

Astronomy Department, School of Physics and Astronomy, 116 Church Street S.E., University of Minnesota, Minneapolis, Minnesota 55455

Received March 30, 1992; revised July 23, 1992

We report 0.7- to 23- μ m observations of P/Halley 1986 III and six other recent bright comets. P/Halley was measured on 47 occasions between 1985 December 12 UT and 1986 May 6 UT, several times within hours of the perihelion passage on 1986 February 9 UT. Our data show that the strength of the 10- μ m silicate emission feature and the temperature excess (superheat; $S = T_{\text{obs}}/T_{\text{BB}}$) of the infrared continuum emission are strongly correlated. IR Type I comets have low continuum superheat and muted or undetectable silicate emission features, suggesting that the coma emission from these comets is produced by large grains with radii larger than 1 μ m. IR Type II comets have superheated thermal infrared continua and high-contrast silicate emission features, indicating that the coma emission is from small grains with radii between 0.5 and 1 μ m. Both types of behavior were exhibited by Comet P/Halley at various times. The relationship between superheat and 10- μ m silicate emission may be complex, for although the strength of these quantities was generally strongly correlated, several comets exhibited occasional episodes when superheat and silicate emission were not correlated. P/Halley's dust coma had an average albedo of 0.20 at a scattering angle of 130°. Our data show that the scattering phase function for typical comet dust is characterized by a moderately strong forward scattering peak, no appreciable backscattering peak, a mean bolometric albedo of ≈ 0.32 , and an albedo of ≈ 0.15 for scattering angles between 120° and 180°. These characteristics are consistent with laboratory and theoretical results for nonspherical and "fluffy" core-mantle aggregate grains. P/Halley's 10- μ m silicate signature showed significant variations in strength and was occasionally weak or absent at heliocentric distances both smaller and larger than 1 AU. Simultaneous measurements of P/Halley and Bradfield 1980 XV with different diaphragms are generally consistent with the steady-state model for nuclear ablation. P/Halley's coma luminosity fluctuated by a factor of nearly 10 on time scales of 1 to 2 days. These variations are consistent with jet-like activity probably associated with nuclear rotation. Dust mass loss rates for the comets studied here are estimated, and we conclude that P/Halley was losing $\geq 10^6$ g sec⁻¹ of dust at a heliocentric distance of 1 AU. © 1992 Academic Press, Inc.

I. INTRODUCTION

Infrared observations of comets can yield fundamental information about the composition and structure of astro-

physical dust grains. Comet nuclei are believed to contain samples of the primary solid and condensable constituents of the primitive Solar System frozen in the state in which they were trapped during the epoch of comet nucleus formation. During perihelion passage, this primordial material can be studied by modern-day observers as the nucleus is ablated by sunlight to form the coma and tail. More than 20 years ago, observations of Comet Ikeya-Seki by Becklin and Westphal (1966) first showed that comets are strong infrared sources because of thermal emission from dust grains that are driven away from the nucleus by the evaporation of volatiles such as water and carbon dioxide ices. We subsequently observed many bright comets to define the properties of cometary grains and study the characteristics of the ablation of comet nuclei (Maas *et al.* 1970, Ney 1974a, 1974b, 1982a, Gehrz *et al.* 1989, and Hanner *et al.* 1990). Our investigations were based on measurements of the reflected and thermally reradiated energy from grains in comet comae, tails, and the antitail of Comet Kohoutek. Comets are especially important because they present the only case in which the light scattering phase function of astrophysical grains can be determined with reasonable certainty. Their heliocentric and geocentric distances, and hence their scattering angles, can be determined.

In this paper, we present 0.7- to 23- μ m infrared photometry of P/Halley 1986 III and six other recent bright comets, and we discuss the data in the context of our previous infrared studies of comets.

II. THE OBSERVATIONS

We used broadband optical/infrared photometers that measure from 0.7 to 23 micrometers mounted on the University of Minnesota (UM1, UM2) O'Brien 0.76-m telescope, the Wyoming Infrared Observatory (WIRO) 2.34-m telescope, and the UM Mount Lemmon Observing Facility (MLOF) 1.52-m telescope to measure Comet P/Halley 47 times between 1985 December 12 UT and 1986 May 6 UT. Data for six other recent bright comets that we observed near perihelion passage are presented

here for comparison. These were Comets Kobayashi–Berger–Milon 1975 IX (KBM), Bradfield 1980 XV (1980t), Austin 1984 XIII (1984i), Machholz 1985 VIII (1985e), Austin 1989c, (designated 1990 V after this paper went to press), and Brorson–Metcalf 1989 X (BM). The photometric results and important parameters related to the analysis presented below are summarized in Tables I–IV, and Appendix C (Table C-I). The photometric systems, magnitude scales, and absolute flux calibrations for the UM and MLOF measurements were described by Ney (1974a). Gehrz *et al.* (1974, 1987) described these parameters for the photometric system used at WIRO. Comments on a preliminary reduction of a subset of the P/Halley data were presented by Gehrz and Ney (1986). Ney (1982a) discussed the initial analysis of the data on Comets KBM and Bradfield 1980 XV. On three occasions, simultaneous measurements were obtained with the UM and WIRO telescopes using different beam diameters. The O'Brien and WIRO telescopes were the *only* infrared telescopes in the world that monitored P/Halley from mid January to late February 1986 III during its perihelion passage.

Nearly all the measurements made at WIRO were obtained using a telephone observing link enabling us to control the computer-operated Wyoming Infrared Telescope (Gehrz and Hackwell 1978) remotely from the University of Minnesota. All data acquisition parameters and telescope control functions were commanded by the remote observer over two 2400-Baud telephone lines, and a third telephone line was used to communicate with an on-site assistant whose main task was to center offset guide stars on a reticle upon request. A continuous stripchart of the infrared-detector output enabled the remote observer to center sources in the photometer beam and monitor data acquisition. Automatic searching and peaking routines were used to find bright objects and to keep them centered. This system is, to our knowledge, the first substantial demonstration of the routine use of remote control to obtain data from a groundbased optical/infrared telescope.

Data in Table II are raw magnitudes corrected only for atmospheric extinction. These data are uncorrected for the contribution of the coma emission in the reference beam. Since the coma is extended, the beam-switching technique we employed in taking our data automatically subtracts the coma emission in the reference beam from the coma emission in the source beam. Correction factors which must be applied to reconstruct the full signal that would have been observed in the source beam if the reference beam had been placed off the coma depend on the surface brightness distribution of the coma. The correction factors used in the quantitative analysis described below are derived in detail in Appendixes A and B and are supplied in Tables I and III. Several of the photome-

ters had square diaphragms as noted in the footnotes to Tables I and II. We derived the equivalent circular aperture diameters cited in Table I (column 12) and Table II (column 6) by comparing the integrated fluxes that would be observed in circular and square diaphragms using the r^{-1} coma surface brightness distribution given by the steady-state model described in Appendix A.

All three tables contain five identical leading columns that serve to characterize the observations on each date: column 1, a chronological observation number; 2, the UT observation date; 3, the Julian date of the observation; 4, the UT time of each observation in decimal days with respect to perihelion passage ($t = 0$) where negative and positive values indicate pre- and postperihelion observations, respectively; and 5, the photometric system in use at the time of each observation. The remaining columns in Table I give the physical parameters of the comet orbit computed using the orbital elements given in Appendix C, the photometer configuration, and the correction factors required to normalize the observations: 6, the heliocentric distance r in AU; 7, the geocentric distance Δ in AU; 8, the multiplier to correct the observed coma emission to $r = 1$ and $\Delta = 1$; 9, the elongation (Sun–Earth–comet) angle θ_{el} ; 10, the scattering (Sun–comet–Earth) angle θ , (11), the phase angle θ_{ph} ($\theta_{ph} = 180^\circ - \theta$); 12, the beam diameter ϕ in arcseconds (the equivalent circular diameter is given for photometers with square beams); 13, the chopper throw ψ between the source and reference beams in arcseconds; 14, the multiplier required to correct for coma emission in the reference beam; 15, the multiplier to normalize the coma emission to a circular diaphragm of 20-arcsec diameter; and 16, the multiplier that gives the coma emission in a standard beam of diameter 20 arcsec corrected for emission into the reference beam. The remaining columns in Table II give: 6, the diaphragm diameter ϕ in arcseconds (the equivalent circular diameter is given for photometers with square beams); 7, the chopper throw ψ between the source and the reference beams in arcseconds, and columns 8 through 21, the raw photometric magnitudes corrected only for atmospheric extinction. The remaining columns in Table III summarize physical quantities derived from the data given in Table II, orbital parameters computed using the orbital elements given in Appendix C (Table C-I), and the correction factors derived in Appendixes A and B: 6, r ; 7, Δ ; 8, the temperature T_{BB} of a black conducting sphere at heliocentric distance r ; 9, the measured infrared color temperature T_{obs} of the comet's continuum emission; 10, the superheat S of the continuum emission; 11, the observed apparent maximum emission from the infrared continuum $[\lambda f_\lambda(IR)]_{max}$ in $W\ cm^{-2}$; 12, the observed apparent maximum emission from the scattered solar component $[\lambda f_\lambda(V)]_{max}$ in $W\ cm^{-2}$; 13, the albedo $A(\theta)$ of the coma at the scattering angle θ from Eq. (6); 14, the equivalent blackbody angular

TABLE I
Optical and Observational Parameters for Comet P/Halley and Six Other Bright Comets

(1)	(2)	(3)	(4)	(5)	(6)	(7)	(8)	(9)	(10)	(11)	(12)	(13)	(14)	(15)	(16)
#	UT DATE	JD 2,440,000+	Days from Perihelion	SYSTEM	r AU	Δ AU	$\frac{1}{r^2 \Delta}$	θ_a deg	θ deg	θ_p deg	ϕ arcsec ¹	ψ arcsec	$\frac{4\psi}{4\psi - \phi}$	$\frac{2\phi}{\phi}$	$\left[\frac{4\psi}{4\psi - \phi} \right] \frac{2\phi}{\phi}$
<u>Comet P/Halley 1986 III</u>															
1	12.11 Dec, 1985	6411.61	-59.35	UM2	1.32	0.77	0.43	97	132	48	22.5	30	1.23	0.89	1.09
2	13.06 Dec, 1985	6412.56	-58.40	UM2	1.30	0.79	0.44	94	131	49	22.5	30	1.23	0.89	1.09
3	14.01 Dec, 1985	6413.51	-57.45	UM2	1.29	0.80	0.45	92	130	50	22.5	30	1.23	0.89	1.09
4	25.00 Dec, 1985	6424.50	-46.46	UM2	1.11	1.02	0.65	68	125	55	22.5	30	1.23	0.89	1.09
5	30.00 Dec, 1985	6429.50	-41.46	UM2	1.04	1.12	0.76	59	126	54	22.5	30	1.23	0.89	1.09
6	1.01 Jan, 1986	6431.51	-39.45	UM2	1.01	1.16	0.83	56	127	53	22.5	30	1.23	0.89	1.09
7	7.89 Jan, 1986	6438.39	-32.57	UM2	0.90	1.29	1.18	44	130	50	22.5	30	1.23	0.89	1.09
8	11.1 Jan, 1986	6441.60	-29.36	WIRO	0.86	1.34	1.36	40	133	47	5	16	1.08	4.00	4.32
9	11.9 Jan, 1986	6442.40	-28.56	WIRO	0.85	1.35	1.42	38	134	46	5	17	1.08	4.00	4.32
10	12.0 Jan, 1986	6442.50	-28.46	UM2	0.84	1.48	1.48	38	134	46	22.5	30	1.23	0.89	1.09
11	12.7 Jan, 1986	6443.20	-27.76	WIRO	0.84	1.36	1.48	40	135	45	5	18	1.07	4.00	4.28
12	12.7 Jan, 1986	6443.20	-27.76	WIRO	0.84	1.36	1.48	40	135	45	5	18	1.07	4.00	4.28
13	12.8 Jan, 1986	6443.30	-27.66	WIRO	0.84	1.36	1.48	40	135	45	2.2	18	1.03	9.09	9.36
14	12.8 Jan, 1986	6443.30	-27.66	WIRO	0.84	1.36	1.48	40	135	45	3.3	18	1.05	6.06	6.36
15	12.9 Jan, 1986	6443.40	-27.56	WIRO	0.84	1.36	1.48	40	135	45	8.3	18	1.13	2.41	2.72
16	26.8 Jan, 1986	6457.30	-13.60	UM2	0.66	1.54	3.42	17	154	26	22.5	30	1.23	0.89	1.09
17	9.75 Feb, 1986	6471.25	+00.29	UM2	0.59	1.54	5.36	8.5	166	14	22.5	30	1.23	0.89	1.09
18	9.83 Feb, 1986	6471.33	+00.37	WIRO	0.59	1.54	5.36	8.5	166	14	8.3	18	1.13	2.41	2.72
19	9.85 Feb, 1986	6471.35	+00.39	UM2	0.59	1.54	5.36	8.5	166	14	22.5	30	1.23	0.89	1.09
20	10.72 Feb, 1986	6472.22	+01.26	UM2	0.59	1.54	5.36	9.5	164	16	22.5	30	1.23	0.89	1.09
21	10.77 Feb, 1986	6472.27	+01.31	UM2	0.59	1.54	5.36	9.5	164	16	22.5	30	1.23	0.89	1.09
22	11.88 Feb, 1986	6473.38	+02.42	WIRO	0.59	1.53	5.39	11	162	18	8.3	20	1.12	2.41	2.70
23	12.67 Feb, 1986	6474.17	+03.21	UM2	0.59	1.52	5.43	12	160	20	22.5	30	1.23	0.89	1.09
24	12.74 Feb, 1986	6474.24	+03.28	UM2	0.59	1.52	5.43	12	160	20	22.5	30	1.23	0.89	1.09
25	14.67 Feb, 1986	6476.17	+05.21	UM2	0.60	1.50	5.14	15	156	24	22.5	30	1.23	0.89	1.09
26	14.79 Feb, 1986	6476.29	+05.33	UM2	0.60	1.50	5.14	15	156	24	22.5	30	1.23	0.89	1.09
27	21.7 Feb, 1986	6483.20	+12.24	UM2	0.65	1.40	4.00	24	141	39	22.5	30	1.23	0.89	1.09
28	27.69 Feb, 1986	6489.19	+18.23	UM2	0.71	1.30	3.03	33	130	50	22.5	30	1.23	0.89	1.09
29	27.70 Feb, 1986	6489.20	+18.24	WIRO	0.71	1.29	3.05	33	130	50	8.3	17.5	1.13	2.41	2.72
30	27.75 Feb, 1986	6489.25	+18.29	UM2	0.71	1.29	3.05	33	130	50	22.5	30	1.23	0.89	1.09
31	2.71 Mar, 1986	6492.21	+21.25	WIRO	0.75	1.22	2.59	37	126	54	5	5	1.33	4.00	5.32
32	2.71 Mar, 1986	6492.21	+21.25	WIRO	0.75	1.22	2.59	37	126	54	5	43	1.03	4.00	4.12
33	4.64 Mar, 1986	6494.14	+23.18	UM2	0.76	1.20	2.50	40	125	55	22.5	30	1.23	0.89	1.09
34	6.74 Mar, 1986	6496.24	+25.28	WIRO	0.80	1.13	2.16	43	122	58	5	40	1.03	4.00	4.12
35	7.61 Mar, 1986	6497.11	+26.15	UM2	0.81	1.12	2.17	45	120	60	22.5	30	1.23	0.89	1.09
36	13.62 Mar, 1986	6503.12	+32.16	WIRO	0.90	0.97	1.57	54	116	64	5	5	1.33	4.00	5.32
37	13.62 Mar, 1986	6503.12	+32.16	WIRO	0.90	0.97	1.57	54	116	64	5	20	1.07	4.00	4.28
38	15.63 Mar, 1986	6505.13	+34.17	UM2	0.92	0.92	1.50	58	115	65	22.5	30	1.23	0.89	1.09
39	20.58 Mar, 1986	6510.08	+39.12	UM2	1.00	0.80	1.25	67	114	66	22.5	30	1.23	0.89	1.09
40	23.5 Mar, 1986	6513.00	+42.04	UM2	1.05	0.72	1.14	73	115	65	22.5	30	1.23	0.89	1.09
41	25.5 Mar, 1986	6515.00	+44.04	MLOF	1.08	0.68	1.08	76	115	65	15.2	23	1.20	1.32	1.58
42	28.55 Mar, 1986	6518.05	+47.09	WIRO	1.13	0.60	1.04	86	118	62	5	17	1.08	4.00	4.32
43	27.3 Apr, 1986	6547.80	+76.84	MLOF	1.57	0.69	0.24	81	153	27	10	20	1.14	2.00	2.28
44	28.3 Apr, 1986	6548.80	+77.84	MLOF	1.59	0.72	0.22	136	153	27	10	20	1.14	2.00	2.28
45	1.21 May, 1986	6551.71	+80.75	WIRO	1.63	0.80	0.18	129	151	29	5	20	1.07	4.00	4.28
46	5.2 May, 1986	6555.70	+84.74	UM2	1.69	0.92	0.13	122	150	30	22.5	30	1.23	0.89	1.09
47	6.2 May, 1986	6556.70	+85.74	UM2	1.71	0.96	0.12	121	149	31	22.5	30	1.23	0.89	1.09
<u>COMET KOBAYASHI-BERGER-MILON 1975 IX</u>															
1	27.7 July, 1975	2621.2	-39.6	UM1	1.02	0.32	2.89	82.5	100.1	79.9	30.3	30	1.34	0.66	0.88
2	27.7 Aug, 1975	2652.2	-08.6	UM1	0.48	0.99	19.0	27.9	101.0	79.0	30.3	30	1.34	0.66	0.88
3	31.9 Aug, 1975	2656.4	-04.4	UM1	0.44	1.09	24.5	24.0	111.8	68.2	30.3	30	1.34	0.66	0.88
4	1.9 Sep, 1975	2657.4	-03.4	UM1	0.44	1.11	24.0	23.2	114.3	65.7	30.3	30	1.34	0.66	0.88

TABLE I—Continued

(1)	(2)	(3)	(4)	(5)	(6)	(7)	(8)	(9)	(10)	(11)	(12)	(13)	(14)	(15)	(16)
#	UT DATE	JD 2,440,000+	Days from Perihelion	SYSTEM	r AU	Δ AU	$\frac{1}{r^2\Delta}$	θ_n deg	θ deg	θ_{ps} deg	ϕ arcsec ¹	ψ arcsec	$\frac{4\psi}{4\psi-\phi}$	$\frac{20}{\phi}$	$\left[\frac{4\psi}{4\psi-\phi}\right]\left[\frac{20}{\phi}\right]$
5	2.7 Sep, 1975	2658.2	-02.6	UM1	0.43	1.12	26.1	22.8	115.3	64.7	30.3	30	1.34	0.66	0.88
6	3.9 Sep, 1975	2659.4	-01.4	UM1	0.43	1.15	25.4	21.7	119.4	60.6	30.3	30	1.34	0.66	0.88
7	5.3 Sep, 1975	2660.8	-0.0	UM1	0.43	1.17	25.0	20.8	122.8	57.2	30.3	30	1.34	0.66	0.88
8	8.8 Sep, 1975	2664.3	+3.5	UM1	0.44	1.24	21.5	19.1	130.6	49.4	30.3	30	1.34	0.66	0.88
<u>COMET BRADFIELD 1980 XV (1980i)</u>															
1	1.8 Jan, 1981	4606.3	+03.3	UM2	0.28	0.73	222.9	8.4	30.6	149.3	22.5	30	1.23	0.89	1.09
2	2.8 Jan, 1981	4607.3	+4.3	UM2	0.30	0.75	164.6	11.8	42.7	137.3	22.5	30	1.23	0.89	1.09
3	3.8 Jan, 1981	4608.3	+5.3	UM2	0.31	0.77	140.6	14.9	53.7	126.3	22.5	30	1.23	0.89	1.09
4	9.7 Jan, 1981	4614.2	+11.2	UM2	0.44	0.96	27.8	26.2	99.7	80.3	22.5	30	1.23	0.89	1.09
5	11.9 Jan, 1981	4616.4	+13.4	UM2	0.49	1.04	16.7	28.0	110.4	69.6	22.5	30	1.23	0.89	1.09
6	16.8 Jan, 1981	4621.3	+18.3	UM2	0.61	1.23	5.9	29.5	127.3	52.7	22.5	30	1.23	0.89	1.09
7	17.9 Jan, 1981	4622.4	+19.4	UM2	0.64	1.27	4.7	29.6	130.1	49.9	22.5	30	1.23	0.89	1.09
8	18.8 Jan, 1981	4623.3	+20.3	UM2	0.66	1.30	4.1	29.5	132.4	47.6	22.5	30	1.23	0.89	1.09
9	21.8 Jan, 1981	4626.3	+23.3	UM2	0.72	1.41	2.6	29.0	138.7	41.3	22.5	30	1.23	0.89	1.09
10	22.9 Jan, 1981	4627.4	+24.4	WIRO	0.75	1.44	2.2	28.8	140.7	39.3	8.3	20	1.13	2.41	2.72
11	22.9 Jan, 1981	4627.4	+24.4	WIRO	0.75	1.44	2.2	28.8	140.7	39.3	5	20	1.07	4.00	4.28
12	24.8 Jan, 1981	4629.3	+26.3	UM2	0.79	1.51	1.7	28.4	143.8	36.2	22.5	30	1.23	0.89	1.09
<u>COMET AUSTIN 1984 XIII (1984i)</u>															
1	8.8 Aug, 1984	5921.3	-03.3	UM2	0.31	1.16	93.3	14.5	124.9	55.0	22.5	30	1.23	0.89	1.09
2	9.8 Aug, 1984	5922.3	-02.3	UM2	0.30	1.19	103.7	12.8	132.0	48.0	22.5	30	1.23	0.89	1.09
3	10.8 Aug, 1984	5923.3	-01.3	UM2	0.30	1.22	101.2	10.9	139.4	40.6	22.5	30	1.23	0.89	1.09
<u>COMET MACHHOLZ 1985 VIII (1985e)</u>															
1	24.75 Jun, 1985	6241.25	-4.0	UM2	0.22	1.09	391.6	11.2	115.9	64.1	22.5	30	1.23	0.89	1.09
<u>COMET AUSTIN (1989c)</u>															
1	23.83 Mar, 1990	7974.33	-17.14	UM2	0.59	1.36	6.07	23.0	138.4	41.6	22.5	30	1.23	0.89	1.09
2	3.71 Apr, 1990	7985.21	-6.26	UM2	0.39	1.16	37.3	19.1	123.8	56.2	22.5	30	1.23	0.89	1.09
3	12.78 Apr, 1990	7994.28	+2.81	UM2	0.36	0.96	62.0	21.0	93.2	86.8	22.5	30	1.23	0.89	1.09
4	15.79 Apr, 1990	7997.29	+5.82	WIRO	0.39	0.88	49.1	22.7	83.8	96.2	5	50	1.03	4.00	4.12
<u>COMET BRORSON-METCALF 1989 X (1989o)</u>															
1	15.8 Sep, 1989	7785.3	+3.86	WIRO	0.49	1.23	14.10	22.5	127.9	52.1	5	27	1.04	4.00	4.22
2	16.7 Sep, 1989	7786.2	+4.76	WIRO	0.49	1.25	13.88	22.1	129.9	50.1	5	24	1.05	4.00	4.20

¹Notes to Table 1:

UM1 had a 27" square beam which is equivalent to a 30.3" circular aperture;

UM2 had a 20" square beam which is equivalent to a 22.5" circular aperture; MLOF on 25 March, 1986 UT had a 13.5" square beam which is equivalent to a 15.2" circular aperture.

radius θ_r of the coma continuum in milliarcseconds; 15, the upper limit to radius of the nucleus, in kilometers, from the thermal emission maximum; 16 and 17, the correction factors (see Appendixes A and B) applied in reducing the photometric data to a common distance, beam diameter, and throw; and 18, the activity index as defined by the total infrared emission corrected for beam size, throw, and distance effects as described by Eqs. (11), (B-1), and (B-2). The quantities in columns 14 and 15 were calculated assuming that all the emission is from a nucleus that is

point-like with respect to the beam (see Gehrz *et al.* 1989). In this case, the correction factors given by Eqs. (11), (B-1), and (B-2) do not apply.

III. DISCUSSION

The photometric data we report here for recent bright comets reveal some of the physical properties of the dust grains released by comet nuclei and help to define the nature of the nuclear ablation process.

TABLE II
Infrared Magnitudes for Comet P/Halley and Six Other Recent Bright Comets

(1)	(2)	(3)	(4)	(5)	(6)	(7)	(8)	(9)	(10)	(11)	(12)	(13)	(14)	(15)	(16)	(17)	(18)	(19)	(20)	(21)
#	UT DATE	JD 2,440,000+	Days from Perihelion	SYSTEM	ϕ arcsec	ψ arcsec	[0.7]	[1.2]	[1.6]	[2.X] ²	[3.6]	[4.X] ²	[8.X] ²	N	[10.X] ²	[11.X] ²	[12.X] ²	[18]	[19.5]	[23]
COMET P/HALLEY 1986 III																				
1	12.11 Dec, 1985	6411.61	-59.35	UM2	22.5	30	-	-	-	+6.8	+6.1	-	-0.5	-	-1.9	-	-1.9	-3.4	-	-
2	13.06 Dec, 1985	6412.56	-58.40	UM2	22.5	30	-	-	-	-	-	-	+0.9	-	-0.9	-	-1.4	-2.0	-	-
3	14.01 Dec, 1985	6413.51	-57.45	UM2	22.5	30	-	-	-	-	-	-	+0.9	-	-0.8	-	-	-2.2	-	-
4	25.00 Dec, 1985	6424.50	-46.46	UM2	22.5	30	-	+6.7	-	+7.0	+5.2	+2.8	-0.5	-	-1.6	-	-1.6	-3.3	-	-
5	30.00 Dec, 1985	6429.50	-41.46	UM2	22.5	30	-	-	+7.5	+7.5	+6.2	+3.2	-0.1	-	-0.9	-	-1.3	-3.2	-	-
6	1.01 Jan, 1986	6431.51	-39.45	UM2	22.5	30	-	-	-	-	-	-	-	-	-1.5	-	-1.0	-	-	-
7	7.89 Jan, 1986	6438.39	-32.57	UM2	22.5	30	-	-	+5.9	+6.1	+4.1	+1.5	-1.6	-	-2.8	-	-2.8	-4.4	-	-
8	11.1 Jan, 1986	6441.60	-29.36	WIRO	5	16	-	-	-	+7.6	+5.1	+3.6	+0.8	-0.3	-1.0	-0.1	-0.8	-	-2.4	-
9	11.9 Jan, 1986	6442.40	-28.56	WIRO	5	17	-	-	-	+7.56	+5.02	+2.80	-0.72	-1.16	-1.24	-1.61	-1.46	-	-2.41	-2.4
10	12.0 Jan, 1986	6442.50	-28.46	UM2	22.5	30	-	+5.7	+6.3	+6.1	+3.6	+1.3	-2.1	-	-3.1	-	-3.2	-3.3	-	-
11	12.7 Jan, 1986	6443.20	-27.76	WIRO	5	18	-	-	-	+6.69	+4.02	+2.04	-1.11	-1.58	-1.92	-2.19	-2.15	-	-3.17	-3.4
12	12.7 Jan, 1986	6443.20	-27.76	WIRO	5	18	-	-	-	+6.92	+4.34	+2.17	-1.01	-1.40	-1.90	-2.10	-2.10	-	-3.10	-3.4
13	12.8 Jan, 1986	6443.30	-27.66	WIRO	2.2	18	-	-	-	+7.67	+5.35	+3.40	+0.16	-	-0.73	-0.97	-1.05	-	-1.86	-
14	12.8 Jan, 1986	6443.30	-27.66	WIRO	3.3	18	-	-	-	+7.05	+5.43	+3.18	+0.18	-	-1.14	-1.45	-1.29	-	-2.08	-
15	12.9 Jan, 1986	6443.40	-27.56	WIRO	8.3	18	-	-	-	+6.39	+3.56	+1.54	-1.20	-	-2.24	-2.58	-2.33	-	-3.48	-
16	26.8 Jan, 1986	6457.30	-13.60	UM2	22.5	30	-	+4.5	+4.4	+4.5	+1.2	-0.8	-3.6	-	-4.2	-	-4.3	-5.4	-	-
17	9.75 Feb, 1986	6471.25	+00.29	UM2	22.5	30	-	-	-	+3.7	+2.0	-0.3	-2.8	-	-3.9	-	-3.9	-5.1	-	-
18	9.83 Feb, 1986	6471.33	+00.37	WIRO	8.3	18	-	-	-	+4.33	+1.58	-0.28	-2.54	-3.01	-3.84	-3.71	-3.46	-	-	-4.5
19	9.85 Feb, 1986	6471.35	+00.39	UM2	22.5	30	-	-	-	+3.5	+1.8	-1.0	-3.3	-	-4.3	-	-4.2	-5.7	-	-
20	10.72 Feb, 1986	6472.22	+01.26	UM2	22.5	30	-	-	+3.0	+2.6	+0.2	-1.7	-3.8	-	-5.1	-	-4.9	-6.3	-	-
21	10.77 Feb, 1986	6472.27	+01.31	UM2	22.5	30	+4.3	+3.3	+3.0	+2.3	+0.2	-2.1	-4.2	-	-5.5	-	-5.2	-6.6	-	-
22	11.88 Feb, 1986	6473.38	+02.42	WIRO	8.3	20	-	-	-	+3.80	+1.25	-0.54	-2.73	-3.20	-3.94	-3.63	-3.64	-	-4.56	-4.7
23	12.67 Feb, 1986	6474.17	+03.21	UM2	22.5	30	+4.6	+3.7	+3.5	+2.3	-0.2	-1.8	-4.1	-	-5.2	-	-5.1	-6.5	-	-
24	12.74 Feb, 1986	6474.24	+03.28	UM2	22.5	30	+4.2	+4.2	+3.0	+2.3	-0.1	-1.8	-4.2	-	-5.5	-	-5.3	-6.5	-	-
25	14.67 Feb, 1986	6476.17	+5.21	UM2	22.5	30	-	+4.3	+4.5	+3.1	+1.1	-0.9	-3.8	-	-4.7	-	-4.8	-6.3	-	-
26	14.79 Feb, 1986	6476.29	+05.33	UM2	22.5	30	-	-	-	+0.7	-1.3	-3.9	-	-4.8	-	-4.8	-6.0	-	-	-
27	21.7 Feb, 1986	6483.20	+12.24	UM2	22.5	30	-	-	+5.2	+4.5	+2.1	+0.0	-2.8	-	-3.8	-	-3.9	-5.2	-	-
28	27.69 Feb, 1986	6489.19	+18.23	UM2	22.5	30	+4.9	+4.7	+4.5	+4.1	+1.8	-0.4	-3.5	-	-4.5	-	-4.3	-5.5	-	-
29	27.70 Feb, 1986	6489.20	+18.24	WIRO	8.3	17.5	-	-	-	+4.95	+2.10	+0.24	-2.43	-3.10	-3.52	-3.56	-3.46	-	-3.91	-3.3
30	27.75 Feb, 1986	6489.25	+18.29	UM2	22.5	30	-	-	+4.3	+3.7	+1.3	-0.7	-3.3	-	-4.2	-	-4.0	-5.8	-	-
31	2.71 Mar, 1986	6492.21	+21.25	WIRO	5	5	-	-	-	-	-	-	-	-1.87	-	-	-	-	-	-
32	2.71 Mar, 1986	6492.21	+21.25	WIRO	5	43	-	-	-	+5.84	+3.07	+1.00	-1.71	-2.24	-2.47	-2.94	-2.77	-	-3.57	-3.2
33	4.64 Mar, 1986	6494.14	+23.18	UM2	22.5	30	-	-	-	+5.7	+3.9	+1.4	-1.7	-	-2.5	-	-2.3	-3.2	-	-
34	6.74 Mar, 1986	6496.24	+25.28	WIRO	5	40	-	-	-	+7.65	+4.08	+1.73	-1.40	-1.87	-	-2.64	-2.09	-	-	-
35	7.61 Mar, 1986	6497.11	+26.15	UM2	22.5	30	-	-	+4.2	+4.1	+1.9	-0.4	-3.5	-	-4.2	-	-4.3	-5.6	-	-
36	13.62 Mar, 1986	6503.12	+32.16	WIRO	5	5	-	-	-	+5.70	-	-	-	-0.80	-1.14	-	-	-	-	-
37	13.62 Mar, 1986	6503.12	+32.16	WIRO	5	20	-	-	-	+7.46	+5.23	+2.68	-0.53	-1.27	-1.45	-1.71	-1.58	-	-2.83	-2.8
38	15.63 Mar, 1986	6505.13	+34.17	UM2	22.5	30	-	-	+5.5	+6.0	+3.8	+1.5	-2.2	-	-3.3	-	-3.3	-3.7	-	-
39	20.58 Mar, 1986	6510.08	+39.12	UM2	22.5	30	-	+6.2	-	-	+4.2	+1.8	-1.2	-	-2.5	-	-2.6	-3.8	-	-
40	23.5 Mar, 1986	6513.00	+42.04	UM2	22.5	30	-	-	-	+6.4	+5.0	+2.3	-1.6	-	-2.5	-	-3.2	-	-	-
41	25.5 Mar, 1986	6515.00	+44.04	MLOF	15.2	23	-	+7.49	+7.27	+7.31	+4.93	+2.76	-1.27	-2.03	-1.92	-2.32	-2.70	-3.2	-	-
42	28.55 Mar, 1986	6518.05	+47.09	WIRO	5	17	-	-	-	+7.94	+6.14	+3.42	+0.03	-0.83	-1.15	-1.49	-1.60	-	-2.65	-2.58
43	27.3 Apr, 1986	6547.80	+76.84	MLOF	10	20	-	-	-	$\geq +8.1$	-	-	+0.8	-	-0.2	-	-0.6	-	-	-
44	28.3 Apr, 1986	6548.80	+77.84	MLOF	10	20	-	-	+9.2	-	$\geq +6.0$	+1.1	-	-0.1	-	-	-0.7	-1.5	-	-
45	1.21 May, 1986	6551.71	+80.75	WIRO	5	20	-	-	-	+9.81	+8.44	+5.67	+2.44	+1.15	+0.85	+0.39	-0.21	-	-0.96	-0.81
46	5.2 May, 1986	6555.70	+84.74	UM2	22.5	30	-	-	-	-	-	-	+0.4	-	-0.7	-	-1.2	-	-	-
47	6.2 May, 1986	6556.70	+85.74	UM2	22.5	30	-	-	$\geq +7.6$	-	$\geq +6.0$	$\geq +3.7$	+1.0	-	-0.0	-	-0.9	-	-	-
COMET KOBAYASHI-BERGER-MILON 1975 IX																				
1	27. Jul, 1975	2621.2	-39.6	UM1	30.3	30	-	-	-	-	-	-	+1.1	-	0.0	-	-0.7	-	-	-
2	27.7 Aug, 1975	2652.2	-08.6	UM1	30.3	30	-	+5.1	+5.3	+5.6	+2.6	+0.5	-2.1	-	-2.8	-	-3.1	-	-	-
3	31.9 Aug, 1975	2656.4	-04.4	UM1	30.3	30	-	+5.6	+5.7	+5.3	+2.0	+0.2	-2.3	-	-3.0	-	-3.1	-	-	-
4	1.9 Sep, 1975	2657.4	-03.4	UM1	30.3	30	-	+5.3	+5.1	+5.0	+2.1	+0.5	-2.1	-	-2.8	-	-3.1	-	-	-

TABLE II—Continued

(1)	(2)	(3)	(4)	(5)	(6)	(7)	(8)	(9)	(10)	(11)	(12)	(13)	(14)	(15)	(16)	(17)	(18)	(19)	(20)	(21)
#	UT DATE	JD 2,440,000+	Days from Perihelion	SYSTEM	ϕ arcsec	ψ arcsec	[0.7]	[1.2]	[1.6]	[2.X] ²	[3.6]	[4.X] ²	[8.X] ²	N	[10.X] ²	[11.X] ²	[12.X] ²	[18]	[19.5]	[23]
5	2.7 Sep, 1975	2658.2	-02.6	UM1	30.3	30	-	+5.2	+5.0	+5.2	+2.0	+0.3	-2.2	-	-2.9	-	-3.2	-	-	-
6	3.9 Sep, 1975	2659.4	-01.4	UM1	30.3	30	-	+5.6	+5.7	+5.0	+1.8	-0.4	-2.6	-	-3.0	-	-3.5	-	-	-
7	5.3 Sep, 1975	2660.8	-00.0	UM1	30.3	30	-	-	-	+5.4	+2.0	+0.4	-2.1	-	-2.9	-	-3.2	-	-	-
8	8.8 Sep, 1975	2664.3	+3.5	UM1	30.3	30	-	+6.5	+6.3	+6.0	+2.0	+0.5	-2.2	-	-2.9	-	-3.1	-	-	-
COMET BRADFIELD 1980 XV (1980i)																				
1	1.8 Jan, 1981	4606.3	+03.3	UM2	22.5	30	-	+2.2	+1.8	+1.4	-0.6	-1.9	-3.6	-	-4.6	-	-4.6	-4.6	-	-
2	2.8 Jan, 1981	4607.3	+04.3	UM2	22.5	30	+4.1	+3.0	+2.7	+1.7	-0.5	-1.9	-3.7	-	-4.5	-	-4.5	-4.9	-	-
3	3.8 Jan, 1981	4608.3	+05.3	UM2	22.5	30	+4.9	+3.8	+3.3	+2.6	0.0	-1.6	-3.7	-	-4.4	-	-4.4	-5.0	-	-
4	9.7 Jan, 1981	4614.2	+11.2	UM2	22.5	30	+7.8	+6.4	+6.2	+5.7	+2.7	+0.6	-2.2	-	-2.9	-	-2.9	-3.4	-	-
5	11.9 Jan, 1981	4616.4	+13.4	UM2	22.5	30	+8.2	+7.1	+7.1	+6.3	+3.5	+1.2	-1.7	-	-2.3	-	-2.4	-3.2	-	-
6	16.8 Jan, 1981	4621.3	+18.3	UM2	22.5	30	-	+6.2	+6.3	+6.2	+3.5	+1.1	-2.1	-	-2.7	-	-2.9	-3.7	-	-
7	17.9 Jan, 1981	4622.4	+19.4	UM2	22.5	30	+8.5	+7.2	-	+6.5	+4.1	+1.9	-1.5	-	-2.2	-	-2.4	-2.7	-	-
8	18.8 Jan, 1981	4623.3	+20.3	UM2	22.5	30	-	+6.8	+7.5	+6.8	+4.3	+2.1	-1.2	-	-1.9	-	-2.1	-3.2	-	-
9	21.8 Jan, 1981	4626.3	+23.3	UM2	22.5	30	-	-	-	+7.6	+5.4	+3.2	-0.6	-	-1.2	-	-1.5	-2.5	-	-
10	22.9 Jan, 1981	4627.4	+24.4	WIRO	8.3	20	-	-	-	-	+6.53	+4.21	+1.02	+0.66	-	+0.18	-0.05	-	-1.27	-
11	22.9 Jan, 1981	4627.4	+24.4	WIRO	5	20	-	-	-	-	+7.01	+4.66	+1.56	+1.09	-	+0.55	+0.20	-	-0.49	-
12	24.8 Jan, 1981	4629.3	+26.3	UM2	22.5	30	-	-	-	-	+6.0	+3.1	+0.4	-	-0.7	-	-0.8	-	-	-
COMET AUSTIN 1984 XIII (1984i)																				
1	8.8 Aug, 1984	5921.3	-03.3	UM2	22.5	30	-	-	-	-	-	-0.66	-3.05	-	-3.63	-	-3.77	-	-	-
2	9.8 Aug, 1984	5922.3	-02.3	UM2	22.5	30	-	+5.00	+4.84	+3.55	+0.65	-1.07	-2.98	-	-3.42	-	-3.66	-	-	-
3	10.8 Aug, 1984	5923.3	-01.3	UM2	22.5	30	-	+4.8	+4.5	+3.51	+0.42	-1.16	-3.16	-	-3.62	-	-3.89	-	-	-
COMET MACHHOLZ 1985 VIII (1985e)																				
1	24.75 Jan, 1985	6241.25		UM2	22.5	30	-	+4.2	\geq +5.6	+4.4	+1.5	-0.1	-1.3	-	-1.9	-	-2.0	-	-	-
COMET AUSTIN (1989c)																				
1	23.83 Mar, 1990	7974.33	-17.14	UM2	22.5	30	-	-	-	-	-	-	-1.0	-	-	-	-	-	-	-
2	3.71 Apr, 1990	7985.21	-6.26	UM2	22.5	30	-	-	+5.6	+5.2	+2.1	-0.1	-2.3	-	-2.9	-	-3.1	-3.5	-	-
3	12.78 Apr, 1990	7994.28	+2.81	UM2	22.5	30	-	-	-	+5.3	+1.5	-0.3	-2.7	-	-3.5	-	-3.7	-	-	-
4	15.79 Apr, 1990	7997.29	+5.82	WIRO	5	50	-	+6.91	-	+5.88	+2.89	+1.04	-0.65	-1.12	-1.48	-1.38	-1.84	-2.06	-	-
COMET BRORSON-METCALF X (1989o)																				
1	15.8 Sep, 1989	7785.3	+3.86	WIRO	5	27	-	-	-	\geq +7.6	+5.58	+4.16	+1.27	+0.87	+0.90	+0.89	+0.92	-0.62	-	-
2	16.7 Sep, 1989	7786.2	+4.76	WIRO	5	24	-	\geq +8.1	\geq +8.7	-	+6.36	+3.92	+1.69	+1.07	+1.15	+0.60	+0.59	+0.30	-	-
PRIMARY CALIBRATOR																				
VEGA				WIRO	5	-	0.00	-0.01	-0.01	-0.02	-0.03	-0.03	-0.03	-0.03	-0.03	-0.03	-0.03	-0.03	-0.03	-0.03
VEGA				UM1,2	22.5	-	0.0	0.0	0.0	0.0	0.0	0.0	0.0	0.0	0.0	0.0	0.0	0.0	0.0	0.0

¹UM1 had a 27" square beam which is equivalent to a 30.3" circular aperture; UM2 had a 20" square beam which is equivalent to a 22.5" circular aperture; MLOF on 25 March, 1986 UT had a 13.5" square beam which is equivalent to a 15.2" circular aperture.

²Effective wavelengths for the UM system are 2.2, 4.8, 8.5, 10.6, and 12.5 μ m; effective wavelengths for the WIRO system are 2.3, 4.9, 8.7, 10, 11.4 and 12.6 μ m; effective wavelengths for the MLOF system are 2.3, 4.9, 8.6, 10.3, 11.3, and 12.8 μ m.

Many of the arguments in the analysis below are based upon the assumption that the infrared energy distributions measure the properties of the optically important grains. It is known from dust impact measurements with the *Giotto* spacecraft that there was a large range of particle sizes in the coma of P/Halley, and that the differential particle mass distribution followed a power law (see McDonnell *et al.* 1987). A power law grain-size distribution has also

been found to be consistent with the thermal emission from other comets (see Hanner *et al.* 1985a, 1985c). Jewitt and Meech (1986) and Jewitt (1991) have argued that the effective grain radius a for the grains that are optically important can be determined by computing the optically weighted mean grain size, assuming that the differential grain distribution follows a power law of the form $n(a)da = Ka^{-m}da$, where m lies between 3 and 4.5. If one

TABLE III
Measured Properties of Comet P/Halley and Six Other Recent Bright Comets

(1)	(2)	(3)	(4)	(5)	(6)	(7)	(8)	(9)	(10)	(11)	(12)	(13)	(14)	(15)	(16)	(17)	(18)
#	UT Date	JD 2,440,000+	Days from Perihelion	SYSTEM	r AU	Δ AU	T_{BB} K	T_{color} K	S	$[\lambda f_{\lambda}(IR)]_{max}$	$[\lambda f_{\lambda}(V)]_{max}$	A(θ)	θ mas	a km	$\frac{1}{r^2 \Delta}$	$\left[\frac{4\psi}{4\psi - \phi} \right] \left[\frac{20}{\phi} \right]$	$\times r^2 \Delta \left[\frac{4\psi}{4\psi - \phi} \right] \left[\frac{20}{\phi} \right]$
COMET P/HALLEY 1986 III																	
1	12.11 Dec, 1985	6411.61	-59.35	UM	1.32	0.77	242	331	1.37	3.5×10^{-15}	8.4×10^{-16}	0.19	54	30.5	0.43	1.09	8.88×10^{-15}
2	13.06 Dec, 1985	6412.56	-58.40	UM	1.30	0.79	244	306	1.25	1.0×10^{-15}	-	-	34	19.6	0.44	1.09	2.47×10^{-15}
3	14.01 Dec, 1985	6413.51	-57.45	UM	1.29	0.80	245	-	-	1×10^{-15}	-	-	-	-	0.45	1.09	2.42×10^{-15}
4	25.00 Dec, 1985	6424.50	-46.46	UM	1.12	1.02	263	382	1.45	2.9×10^{-15}	1.1×10^{-15}	0.28	37	27.6	0.62	1.09	5.09×10^{-15}
5	30.00 Dec, 1985	6429.50	-41.46	UM	1.04	1.12	273	328	1.20	2.6×10^{-15}	6.5×10^{-16}	0.20	48	39.0	0.76	1.09	3.73×10^{-15}
6	1.01 Jan, 1986	6431.51	-39.45	UM	1.01	1.16	277	-	-	1.8×10^{-15}	-	-	-	-	0.83	1.09	2.36×10^{-15}
7	7.89 Jan, 1986	6438.39	-32.57	UM	0.90	1.29	293	382	1.30	9×10^{-15}	2.1×10^{-15}	0.19	66	61.6	1.18	1.09	8.31×10^{-15}
8	11.1 Jan, 1986	6441.60	-29.36	WIRO	0.86	1.34	300	-	-	-	-	-	-	-	1.36	4.32	-
9	11.9 Jan, 1986	6442.40	-28.56	WIRO	0.85	1.35	302	370	1.21	3×10^{-15}	-	-	40	39.4	1.42	4.32	9.13×10^{-15}
10	12.0 Jan, 1986	6442.50	-28.46	UM	0.85	1.36	302	399	1.32	1×10^{-14}	2.2×10^{-15}	0.18	63	62.7	1.48	1.09	7.37×10^{-15}
11	12.7 Jan, 1986	6443.20	-27.76	WIRO	0.84	1.36	304	375	1.22	5×10^{-15}	-	-	51	50.2	1.48	4.28	1.45×10^{-14}
12	12.7 Jan, 1986	6443.20	-27.76	WIRO	0.84	1.36	304	375	1.22	5×10^{-15}	-	-	51	50.2	1.48	4.28	1.45×10^{-14}
13	12.8 Jan, 1986	6443.30	-27.66	WIRO	0.84	1.36	304	375	1.22	2×10^{-15}	-	-	32	31.8	1.48	9.36	1.26×10^{-14}
14	12.8 Jan, 1986	6443.30	-27.66	WIRO	0.84	1.36	304	375	1.22	2×10^{-15}	-	-	32	31.8	1.48	6.36	8.59×10^{-15}
15	12.9 Jan, 1986	6443.40	-27.56	WIRO	0.84	1.36	304	375	1.22	6×10^{-15}	-	-	56	55	1.48	2.72	1.10×10^{-14}
16	26.8 Jan, 1986	6457.30	-13.60	UM	0.66	1.54	343	427	1.24	5×10^{-14}	1×10^{-14}	0.17	124	139	3.42	1.04	1.52×10^{-14}
17	9.75 Feb, 1986	6471.25	+00.29	UM	0.59	1.54	362	459	1.27	2.9×10^{-14}	-	-	82	91	5.36	1.04	5.63×10^{-15}
18	9.83 Feb, 1986	6471.33	+00.37	WIRO	0.59	1.54	362	470	1.28	2×10^{-14}	-	-	65	73	5.36	2.72	1.01×10^{-14}
19	9.85 Feb, 1986	6471.35	+00.39	UM	0.59	1.54	362	439	1.21	3.8×10^{-14}	-	-	102	114	5.36	1.09	7.73×10^{-15}
20	10.72 Feb, 1986	6472.22	+01.26	UM	0.59	1.54	362	517	1.43	8×10^{-14}	-	-	106	120	5.36	1.09	1.64×10^{-14}
21	10.77 Feb, 1986	6472.27	+01.31	UM	0.59	1.54	362	496	1.37	1.05×10^{-13}	2.8×10^{-14}	0.21	133	150	5.36	1.09	2.14×10^{-14}
22	11.88 Feb, 1986	6473.38	+02.42	WIRO	0.59	1.53	362	470	1.28	2.5×10^{-14}	-	-	72	80	5.39	2.70	1.25×10^{-14}
23	12.67 Feb, 1986	6474.17	+03.21	UM	0.59	1.52	362	496	1.37	9.1×10^{-14}	2.36×10^{-14}	0.21	124	137	5.43	1.09	1.82×10^{-14}
24	12.74 Feb, 1986	6474.24	+03.28	UM	0.59	1.52	362	459	1.27	1.09×10^{-13}	2.58×10^{-14}	0.19	158	175	5.43	1.09	2.19×10^{-14}
25	14.67 Feb, 1986	6476.17	+5.21	UM	0.60	1.50	359	402	1.12	6.51×10^{-14}	1.07×10^{-14}	0.14	159	174	5.14	1.09	1.38×10^{-14}
26	14.79 Feb, 1986	6476.29	+05.33	UM	0.60	1.50	359	427	1.19	7.3×10^{-14}	-	-	150	163	5.14	1.09	1.55×10^{-14}
27	21.7 Feb, 1986	6483.20	+12.24	UM	0.65	1.40	345	405	1.17	2.64×10^{-14}	4.44×10^{-15}	0.15	100	102	4.00	1.09	7.19×10^{-15}
28	27.69 Feb, 1986	6489.19	+18.23	UM	0.71	1.29	330	395	1.20	4.44×10^{-14}	1.2×10^{-14}	0.21	136	128	3.05	1.09	1.59×10^{-14}
29	27.70 Feb, 1986	6489.20	+18.24	WIRO	0.71	1.29	330	432	1.30	1.5×10^{-14}	-	-	66	62	3.05	2.72	1.34×10^{-14}
30	27.75 Feb, 1986	6489.25	+18.29	UM	0.71	1.29	330	448	1.36	3.7×10^{-14}	1×10^{-14}	0.21	97	91	3.05	1.09	1.32×10^{-14}
31	2.71 Mar, 1986	6492.21	+21.25	WIRO	0.75	1.22	321	-	-	-	-	-	-	-	2.59	5.32	-
32	2.71 Mar, 1986	6492.21	+21.25	WIRO	0.75	1.22	321	422	1.30	9×10^{-15}	-	-	54	48	2.59	4.12	1.85×10^{-14}
33	4.64 Mar, 1986	6494.14	+23.18	UM	0.76	1.20	319	395	1.24	7.94×10^{-15}	-	-	58	50	2.50	1.09	3.46×10^{-15}
34	6.74 Mar, 1986	6496.24	+25.28	WIRO	0.80	1.13	311	367	1.17	6.5×10^{-15}	-	-	60	50	2.16	4.12	1.24×10^{-14}
35	7.61 Mar, 1986	6497.11	+26.15	UM	0.81	1.12	309	377	1.22	4.64×10^{-14}	1.05×10^{-14}	0.19	153	125	2.13	1.09	2.37×10^{-14}
36	13.62 Mar, 1986	6503.12	+32.16	WIRO	0.90	0.97	293	334	1.13	3.3×10^{-15}	-	-	52	37	1.57	5.32	1.12×10^{-14}
37	13.62 Mar, 1986	6503.12	+32.16	WIRO	0.90	0.97	293	367	1.25	3.5×10^{-15}	-	-	44	31	1.57	4.28	9.53×10^{-15}
38	15.63 Mar, 1986	6505.13	+34.17	UM	0.92	0.92	290	363	1.25	1.2×10^{-14}	2.7×10^{-15}	0.19	84	56	1.50	1.09	8.72×10^{-15}
39	20.58 Mar, 1986	6510.08	+39.12	UM	1.00	0.80	278	375	1.35	6.5×10^{-15}	2.01×10^{-15}	0.24	58	34	1.25	1.09	5.66×10^{-15}
40	23.5 Mar, 1986	6513.00	+42.04	UM	1.05	0.72	272	338	1.24	1.0×10^{-14}	-	-	88	46	1.14	1.09	9.57×10^{-15}
41	25.5 Mar, 1986	6515.00	+44.04	MLOF	1.08	0.68	268	322	1.19	7×10^{-15}	6.0×10^{-16}	0.08	81	40	1.08	1.58	1.06×10^{-14}
42	28.55 Mar, 1986	6518.05	+47.09	WIRO	1.13	0.60	262	322	1.22	2.5×10^{-15}	-	-	47	21	1.04	4.32	1.04×10^{-14}
43	27.3 Apr, 1986	6547.80	+76.84	MLOF	1.57	0.69	222	-	-	1.3×10^{-15}	-	-	-	-	0.24	2.28	1.24×10^{-14}
44	28.3 Apr, 1986	6548.80	+77.84	MLOF	1.59	0.72	220	-	1.46	1.1×10^{-15}	-	-	35	17.6	0.22	2.28	1.35×10^{-14}
45	1.21 May, 1986	6551.71	+80.75	WIRO	1.63	0.80	218	291	1.32	7×10^{-16}	-	-	32	18.4	0.18	4.28	1.66×10^{-14}
46	5.2 May, 1986	6555.70	+84.74	UM	1.69	0.92	214	-	-	1.7×10^{-15}	-	-	-	-	0.13	1.09	1.44×10^{-14}
47	6.2 May, 1986	6556.70	+85.74	UM	1.71	0.96	213	280	1.31	1.06×10^{-15}	-	-	42	29	0.12	1.09	9.63×10^{-15}

TABLE III—Continued

(1)	(2)	(3)	(4)	(5)	(6)	(7)	(8)	(9)	(10)	(11)	(12)	(13)	(14)	(15)	(16)	(17)	(18)
#	UT Date	JD 2,440,000+	Days from Perihelion	SYSTEM	r AU	Δ AU	T_{BB} K	T_{color} K	S	$[\lambda f_{\lambda}(\text{IR})]_{\text{max}}$	$[\lambda f_{\lambda}(\text{V})]_{\text{max}}$	$A(\theta)$	θ mas	a km	$\frac{1}{r^4 \Delta}$	$\left[\frac{-4\Phi}{4\Phi-1} \right] \frac{20}{\Phi}$	$\frac{[\lambda f_{\lambda}(\text{IR})]_{\text{max}}}{r^4 \Delta} \left[\frac{-4\Phi}{4\Phi-1} \right] \frac{20}{\Phi}$
<u>COMET KOBAYASHI-BERGER-MILON 1975 IX</u>																	
1	27.7 Jul, 1975	2621.2	-39.6	UM1	1.02	0.32	275	-	-	-1.1×10^{-15}	-	-	-	-	2.89	0.88	3.35×10^{-16}
2	27.7 Aug, 1975	2652.2	-08.6	UM1	0.48	0.99	401	427	1.06	1.4×10^{-14}	5.5×10^{-15}	0.28	66	48	19.0	0.88	6.48×10^{-16}
3	31.9 Aug, 1975	2656.4	-04.4	UM1	0.44	1.09	419	459	1.10	1.7×10^{-14}	3.2×10^{-15}	0.16	62	50	24.5	0.88	6.11×10^{-16}
4	1.9 Sep, 1975	2657.4	-03.4	UM1	0.44	1.11	419	432	1.03	1.5×10^{-14}	5.2×10^{-15}	0.26	66	53	24.0	0.88	5.50×10^{-16}
5	2.7 Sep, 1975	2658.2	-02.6	UM1	0.43	1.12	424	432	1.02	1.5×10^{-14}	5.5×10^{-15}	0.27	66	54	26.1	0.88	6.02×10^{-16}
6	3.9 Sep, 1975	2659.4	-01.4	UM1	0.43	1.15	424	459	1.08	2.4×10^{-14}	3.2×10^{-15}	0.12	74	62	25.4	0.88	8.32×10^{-16}
7	5.3 Sep, 1975	2660.8	-0.0	UM1	0.43	1.17	424	432	1.02	1.7×10^{-14}	-	-	71	61	25.0	0.88	5.98×10^{-16}
8	8.8 Sep, 1975	2664.3	+3.5	UM1	0.44	1.24	419	432	1.03	1.5×10^{-14}	1.7×10^{-15}	0.10	66	60	21.5	0.88	6.14×10^{-16}
<u>COMET BRADFIELD 1980 XV (1980c)</u>																	
1	1.8 Jan, 1981	4606.3	+03.3	UM2	0.28	0.73	525	592	1.13	7×10^{-14}	10^{-15}	0.59	76	40	222.9	1.09	3.43×10^{-16}
2	2.8 Jan, 1981	4607.3	+4.3	UM2	0.30	0.75	508	573	1.13	7×10^{-14}	3.6×10^{-14}	0.34	81	44	164.6	1.09	4.63×10^{-16}
3	3.8 Jan, 1981	4608.3	+5.3	UM2	0.31	0.77	499	510	1.02	6.5×10^{-14}	1.5×10^{-14}	0.19	99	55	140.6	1.09	5.04×10^{-16}
4	9.7 Jan, 1981	4614.2	+11.2	UM2	0.44	0.96	419	432	1.03	1.2×10^{-14}	1.6×10^{-15}	0.12	59	41	27.8	1.09	4.71×10^{-16}
5	11.9 Jan, 1981	4616.4	+13.4	UM2	0.49	1.04	397	427	1.08	8×10^{-15}	8×10^{-16}	0.09	50	44	16.7	1.09	5.22×10^{-16}
6	16.8 Jan, 1981	4621.3	+18.3	UM2	0.61	1.23	356	386	1.08	1.2×10^{-14}	1.9×10^{-15}	0.14	74	66	5.9	1.09	2.22×10^{-15}
7	17.9 Jan, 1981	4622.4	+19.4	UM2	0.64	1.27	348	367	1.05	5.5×10^{-15}	6×10^{-16}	0.10	56	51	4.7	1.09	1.28×10^{-15}
8	18.8 Jan, 1981	4623.3	+20.3	UM2	0.66	1.30	342	386	1.13	5×10^{-15}	8×10^{-16}	0.14	48	45	4.1	1.09	1.33×10^{-15}
9	21.8 Jan, 1981	4626.3	+23.3	UM2	0.72	1.41	328	367	1.12	3.2×10^{-15}	-	-	42	44	2.6	1.09	1.34×10^{-15}
10	22.9 Jan, 1981	4627.4	+24.4	WIRO	0.75	1.44	321	376	1.17	6.5×10^{-16}	-	-	18	19	2.2	2.72	10^{-16}
11	22.9 Jan, 1981	4627.4	+24.4	WIRO	0.75	1.44	321	367	1.14	5×10^{-16}	-	-	17	17.6	2.2	4.28	10^{-16}
12	24.8 Jan, 1981	4629.3	+26.3	UM2	0.79	1.51	313	380	1.21	1.6×10^{-15}	-	-	28	37	1.7	1.09	1.03×10^{-15}
<u>COMET AUSTIN 1984 XIII (1984i)</u>																	
1	8.8 Aug, 1984	5921.3	-03.3	UM2	0.31	1.16	499	-	-	3×10^{-14}	-	-	79	67	93.3	1.09	3.50×10^{-16}
2	9.8 Aug, 1984	5922.3	-02.3	UM2	0.30	1.19	508	540	1.06	3.4×10^{-14}	6.8×10^{-15}	0.17	64	55	103.7	1.09	3.57×10^{-16}
3	10.8 Aug, 1984	5923.3	-01.3	UM2	0.30	1.22	508	524	1.03	4×10^{-14}	8×10^{-15}	0.17	74	65	101.2	1.09	4.31×10^{-16}
<u>COMET MACHHOLZ 1985 VIII (1985e)</u>																	
1	24.75 Jun, 1985	6241.25	-4.0	UM2	0.22	1.09	593	667	1.12	10^{-14}	-	-	23	18	391.6	1.09	2.79×10^{-17}
<u>COMET AUSTIN (1989c)</u>																	
1	23.83 Mar, 1990	7974.33	-17.14	UM2	0.59	1.36	362	-	-	5×10^{-15}	-	-	-	-	6.07	1.09	8.98×10^{-16}
2	3.71 Apr, 1990	7985.21	-6.26	UM2	0.39	1.16	445	459	1.03	1.6×10^{-14}	3.4×10^{-15}	0.17	61	51	37.3	1.09	4.67×10^{-16}
3	12.78 Apr, 1990	7994.28	+2.81	UM2	0.36	0.96	463	458	0.99	2.4×10^{-14}	-	-	75	52	62.0	1.09	4.22×10^{-16}
4	15.79 Apr, 1990	7997.29	+5.82	WIRO	0.39	0.88	445	524	1.18	4.5×10^{-15}	1.2×10^{-15}	0.21	25	15.8	49.1	4.12	3.78×10^{-16}
<u>COMET BRORSON-METCALFE 1989 X (1989o)</u>																	
1	15.8 Sep, 1989	7785.3	+3.86	WIRO	0.49	1.23	398	408	1.03	6×10^{-16}	-	-	15	13.3	14.10	4.22	1.8×10^{-16}
2	16.7 Sep, 1989	7786.2	+4.76	WIRO	0.49	1.25	398	432	1.09	4×10^{-16}	-	-	11	9.8	13.88	4.20	1.21×10^{-16}

assumes that there is a lower limit a_{min} to the grain radius and that the value of m lies close to 4.5 or even 5 (see Hayward *et al.* 1986), then the optically weighted mean grain size is given by $2a_{\text{min}} \leq a \leq 3a_{\text{min}}$. The effective radius of the optically important grains in comets is nearly an order of magnitude larger than the effective radius of the grains responsible for the general interstellar extinction. Jewitt and Meech (1986) suggest that the grains incorporated in comet nuclei during the formation of the Solar System could have grown to the larger radii characteristic of comet grains by accretion in the cores of molecular clouds. In fact, optical/infrared extinction and polariza-

tion studies provide strong evidence that the grains in the Orion nebula (Breger *et al.* 1981) and the Ophiuchus Dark Cloud (Castelaz *et al.* 1985) are larger than interstellar grains. Small grains were detected in the coma of P/Halley by the *Giotto* dust detectors, but the differential size distribution flattens out below grain radii of $\approx 0.5 \mu\text{m}$ (McDonnell *et al.* 1987, 1991), so that the small grains do not contribute significantly to the optical scattering and emission from the coma (see also Hanner 1988, Jewitt 1991). We assume in the discussion that follows that the grain radius measured by the infrared emission is the optically weighted mean defined above.

We have assumed in our analysis that the grains in the coma are radiatively cooled, and that heat losses by conduction to the gas are negligible. In the steady-state model (see Appendix A), the grains are accelerated to terminal velocity by momentum coupling to the gas. The hydrodynamic coupling is through the viscosity of the plasma. Since the transport properties of viscosity and thermal conductivity are proportional to each other (and to $T^{1/2}$), the grains are thermally coupled to the gas as long as they are being accelerated by the gas. The density of the gas in the outflow decreases inversely as the square of the distance from the nucleus. When the gas mean free path, which is inversely proportional to the gas density, approaches the size of the grains, the coupling to the gas is reduced and both the thermal conductivity and the viscosity become proportional to the pressure. In general, we do not know the coma radius at which this condition occurs, but from this point outward the grains cool radiatively, and the relationship between flux and diaphragm diameter is linear (see Eq. A-4). Visible images of Comet Levy 1990c with the Hubble Space Telescope show that this linear relationship holds to diaphragm radii as small as 0.1 arcsec (Weaver *et al.* 1992). We therefore believe that it is safe to assume that cooling of the grains by thermal conduction to the gas can be ignored for the coma in the observing diaphragms we used in this study (radii of 1.1 to 13.5 arcsec).

A. General Morphology of the Energy Distributions

Figures 1–3 display typical infrared energy distributions exhibited by P/Halley and the six other recent comets measured in this study. We have included the energy distributions of the coma, tail, and anti-tail of Comet Kohoutek (Ney 1974a) in Fig. 1 for comparison. In all cases (except Machholz, which was too faint for our O'Brien detector at short wavelengths) there was a clearly defined visible/near-infrared continuum due to reflected sunlight and a thermal-infrared component due to thermal emission from dust. Both these components have been observed previously in many comets (see Ney 1982a). The comets in our study appear to fall into two basic classes based upon their thermal infrared dust emission (Figs. 2 and 4–6): I, those that show continuum emission with low superheat and weak or muted silicate emission features (designated IR Type I by Gehrz *et al.* 1989), and II, those that have optically thin 10- and 20- μ m silicate emission features (Woolf and Ney 1969) superimposed on a superheated thermal infrared continuum believed to be caused by emission from small carbon or iron grains (designated IR Type II by Gehrz *et al.* 1989). The IR Type I/II designation assigned by Gehrz *et al.* (1989) was based upon the fact that the IR Type I comets had Type I (ion) tails, and the IR Type II comets were characterized by the presence

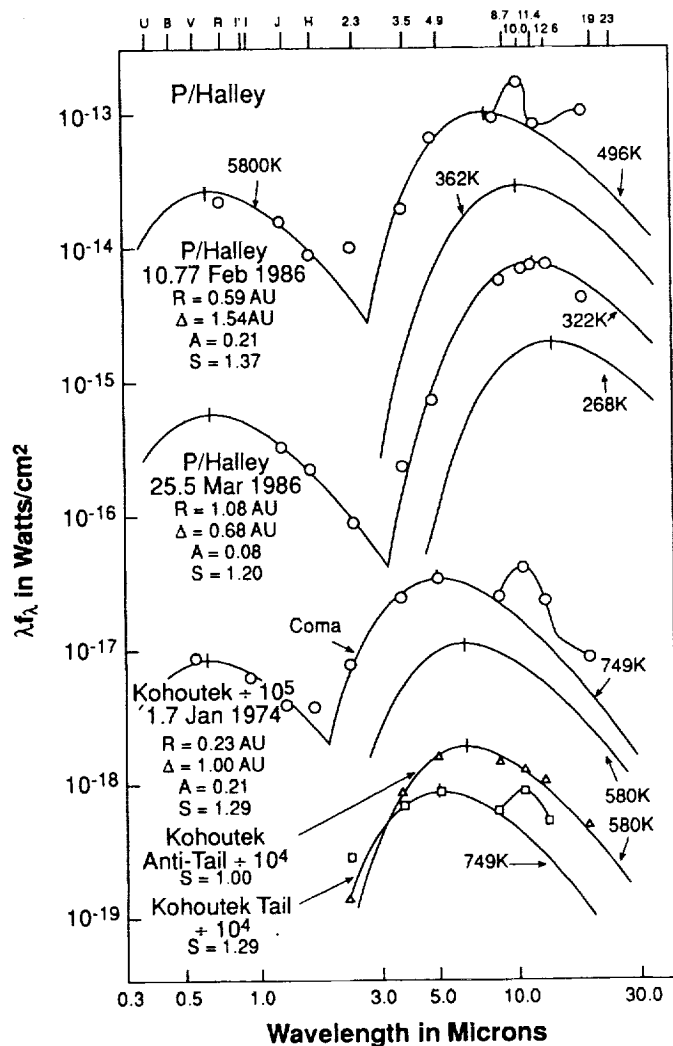


FIG. 1. Typical coma energy distributions for P/Halley when the 10- μ m silicate emission feature was present (10.77 February 1986 UT) and absent (25.5 March 1986 UT) showing the scattered solar and thermal continua. Statistical errors are smaller than the plotting symbols. R is the heliocentric distance in AU, Δ is the geocentric distance in AU, A is the albedo, and S is the superheat. The energy distributions of the coma, dust tail, and antitail of Comet Kohoutek are included for comparison (data for Ney 1974a). Also shown are blackbody energy distributions corresponding to the black sphere temperature at the heliocentric distance of each comet as given by Eq. (3).

of prominent Type II (dust) tails. It is evident from Figs. 1 and 3 that there were occasions upon which P/Halley, normally an IR Type II comet, became an IR Type I comet.

The differences between the dust emission from IR Types I and II comets could be caused by effects that are dependent upon grain size. The energy distributions of the IR Type II comets are similar to those of Kohoutek's Type II dust tail and coma which were composed of small

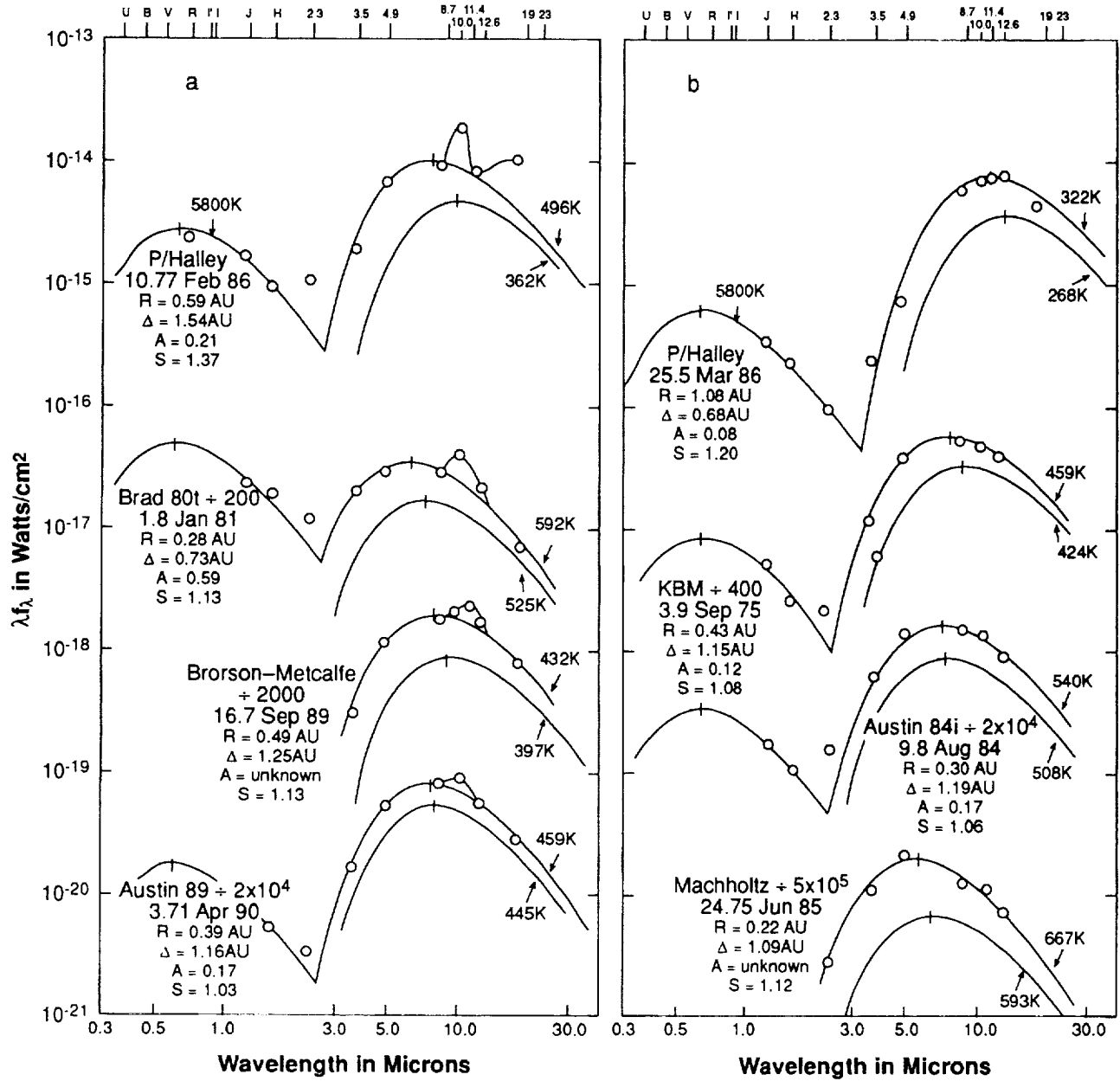


FIG. 2. The energy distributions of six recent bright comets compared to P/Halley. The quantities R , Δ , A , and S are as defined in Fig. 1. Statistical errors are smaller than the plotting symbols. Panel (a) shows comets whose energy distributions are characterized by 10- and 20- μ m silicate features superimposed on a smooth continuum caused by thermal emission from carbon or iron grains. Panel (b) shows the IR Type I comets in our survey.

grains (less than 1 μ m in diameter) with an optically thin silicate component. IR Type I comets have energy distributions more like that of the anti-tail of Comet Kohoutek. Ney (1974a) has argued that the anti-tail is composed of "gravel" (diameters greater than 1 mm) in the plane of the comet orbit (see also Sekanina 1974a,b, 1976). The coma and dust-tail grains of Kohoutek and the coma grains of the IR Type II comets are superheated as defined in

Section B, the anti-tail grains of Kohoutek are not superheated at all, and the superheat of the coma grains of the IR Type I comets is small.

B. Comet Grain Properties

Spectral energy distributions of the comets in our sample (Table II and Figs. 1-7) can be used to determine:

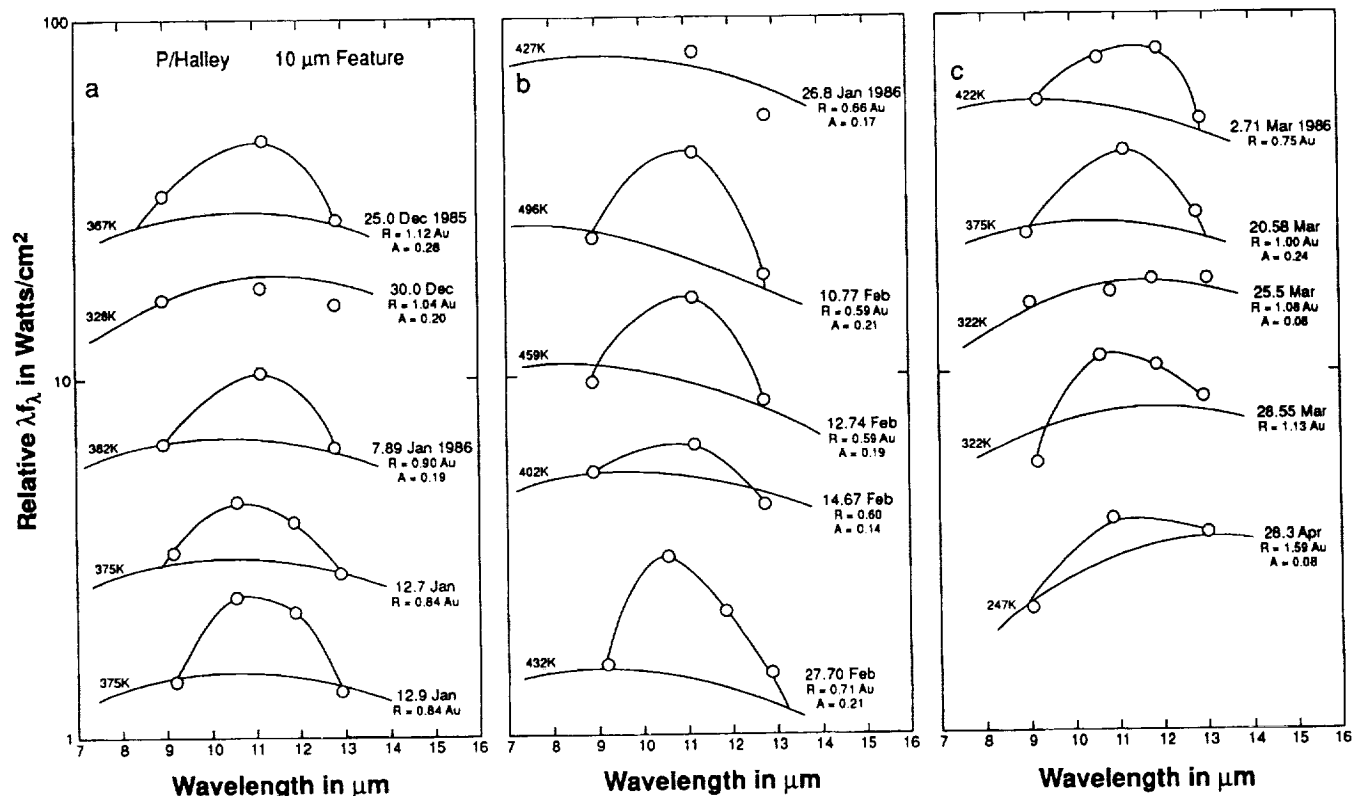


FIG. 3. The 7- to 14- μ m energy distribution of P/Halley showing temporal variations observed in the contrast of the 10- μ m silicate emission feature. R and S are as defined in Fig. 1. Statistical errors are smaller than the plotting symbols. The silicate feature was occasionally weak or absent for heliocentric distances both less than and larger than 1 AU. On 25.5 March, when the signature was absent, the albedo of P/Halley fell to about 0.08. The blackbody curves were determined from the continuum outside the feature.

1, the mineral content of the grains; 2, the rough size distribution of the grains responsible for the thermal infrared emission; 3, some structural properties of the grains; and 4, the temporal variability of these properties.

The mineral composition of comet grains. The 10- and 20- μ m emission features in the IR Type II comets indicate that there is an optically thin silicate dust component in the coma. These features, observed first in a comet (Bennett 1969i) by Maas *et al.* (1970), suggest that IR Type II comets contain the same type of silicate materials observed in the circumstellar shells of cool supergiant stars (Woolf and Ney 1974). Silicate emission features are usually, though not always, present in P/Halley spectra as discussed below (Figs. 1 and 3). Recent determinations of the composition of P/Halley's coma grains by the *Giotto* PIA mass spectrometer appear to confirm the presence of iron-magnesium silicate material in the inner coma (Kissel *et al.* 1986). The thermal continuum radiation from 3 to 8 μ m that is present in both IR Type I and IR Type II comets is believed to be due to carbon or iron (Ney 1982a); we assume in the following discussion that the material responsible for this thermal continuum emission is carbon.

P/Halley is the only periodic comet among the seven observed in this study; the remainder are new comets. Although previous studies (Ney 1974a, 1982a) had suggested that silicate signatures were muted or missing in periodic comets and that new comets usually have strong 10- and 20- μ m emission features indicating the presence of small silicate grains, the additional data we present here leads to the conclusion that the presence or absence of small silicate grains does not necessarily depend upon the processing history of the nucleus. Indeed, as shown in Fig. 2, the old Comet P/Halley has stronger silicate emission than any of the new comets in our sample, and there are at least two examples of new comets (KBM and Austin 1984) that have no small silicate grain component. The superheat of the continuum emission from these last two is quite small, suggesting that they have large grains like the anti-tail of Comet Kohoutek (Fig. 1); the grains in this case may be larger than hundreds of micrometers. Telesco *et al.* (1986) have concluded that the dust tail of Comet Giacobini-Zinner was composed of dust grains with radii as large as $\approx 300 \mu$ m. In the case of the comets with optically thin silicate emission features, the super heat is high enough to signify that grains with radii as small as

TABLE IV
Mean Properties of Selected Bright Comets¹

NAME	SPECIAL SELECTION CRITERIA, COMMENTS	SILICATE EMISSION EXCESS IN MAGNITUDES	% ($\lambda > 1$ X100)
1975 IX	Extreme IR Type I Comet	0.18 ± 0.03	5 ± 1
1980 XV	IR Type I Comet	0.33 ± 0.07	11 ± 2
1984 XIII	Extreme IR Type I Comet	0.13 ± 0.03	5 ± 2
1985 VIII	IR Type I Comet	0.25	7
1989C ₁	IR Type I Comet	0.20 ± 0.08	7 ± 6
1989 X	IR Type I Comet	0.11 ± 0.11	6 ± 3
Bennett	Extreme IR Type II Comet	1.08 ± 0.11	37 ± 9
Kohoutek	IR Type II Comet	0.68 ± 0.11	22 ± 3
West	IR Type II Comet	0.66 ± 0.10	34 ± 7
IR Type I	Average over all IR Type Comets above	0.24 ± 0.03	8 ± 1
IR Type II	Average over all IR Type II's above	0.76 ± 0.08	29 ± 3
P/Halley	Average of all days	0.53 ± 0.04	27 ± 1

¹ The errors quoted here are the standard deviation of the mean σ_x , of all measurements of a given comet, or grouping of comets.

0.5 to 1 μm dominate the emission from the center of the coma.

A key issue is whether the continuum emission and the silicate emission features are from separate grain distributions, or whether both spectral components are emitted by composite, fluffy aggregate grains having either the "cluster-of-grapes" morphology exhibited by interplanetary dust particles (IDPs) collected in the atmosphere and oceans of the Earth (Brownlee 1987, Brownlee *et al.* 1980, Fraundorf *et al.* 1982) or the core/mantle structure as proposed by Hanner *et al.* (1981), Greenberg (1982, 1986), and Greenberg and Hage (1990). Gehrz *et al.* (1989) have argued that the presence or absence of the 10- and 20- μm emission features can be explained by grain size effects alone. We present evidence in the discussion below that our albedo measurements and the correlation between superheat and 10- μm silicate emission strength (Table IV, Fig. 6) appear to favor the composite grain hypothesis.

Superheat as a grain size indicator. P/Halley and other IR Type II comets are characterized by an elevation of the temperature of the thermal infrared continuum considerably above the black-sphere temperature appropriate to the comet's heliocentric distance. Ney (1974a, 1982a) has suggested that the grains in these comets are superheated because they are too small to radiate like blackbodies. A quantitative measure of the relationship between the grain radius and the grain temperature T_{gr} can be established by setting the power absorbed by the grain from the solar radiation field equal to the power emitted by the grain in the thermal infrared,

$$\frac{L_{\odot}}{4\pi r^2} \pi a^2 Q_a = 4\pi a^2 Q_e \sigma T_{\text{gr}}^4, \quad (1)$$

where r is the heliocentric distance, a is the grain radius in centimeters, $L_{\odot} = 3.826 \times 10^{33} \text{ erg sec}^{-1}$ is the solar luminosity, $\sigma = 5.6696 \times 10^{-5} \text{ erg cm}^{-2} \text{ deg}^{-4}$ is the Stefan-Boltzmann constant, and $Q_a(a, T)$ and $Q_e(a, T)$ are the Planck mean absorption and emission coefficients (see Gilman 1974). Q_a is the absorption efficiency of the grain averaged over the energy distribution of the illuminating source (the Sun), and Q_e is the thermal emission efficiency of the grain at T_{gr} . Solving Eq. (1) for the grain temperature yields

$$T_{\text{gr}} = \left[\frac{L_{\odot} Q_a}{16\pi \sigma r^2 Q_e} \right]^{1/4}, \quad (2)$$

which gives the black sphere temperature T_{BB} ,

$$T_{\text{BB}} = \frac{278}{\sqrt{r_A}} \text{ K}, \quad (3)$$

in the case when $Q_a = Q_e = 1$, where r_A is the heliocentric distance in AU (1 AU = $1.4960 \times 10^{13} \text{ cm}$). Equation (2) demonstrates that for small grains where $Q_e < Q_a$, the grain temperature must rise above the black-sphere temperature in order for the grain to come to radiative equilibrium. Equation (3) defines a lower limit to the temperature that comet grains can assume as a function of heliocentric distance.

We define the superheat $S = T_{\text{obs}}/T_{\text{BB}}$ as the ratio of the observed carbon-grain temperature to that expected for a perfectly conducting black sphere at the same heliocentric distance. Assuming that the infrared color temperature of the grains T_{obs} measures the physical temperature of the grain T_{gr} , Eqs. (2) and (3) can be combined to show that S measures the fourth root of the ratio of Q_a to Q_e ,

$$S = \frac{T_{\text{obs}}}{T_{\text{BB}}} = \left[\frac{Q_a}{Q_e} \right]^{1/4}, \quad (4)$$

where the right-hand side is unity for large grains and becomes progressively larger as the grain size decreases. T_{obs} and T_{gr} are equivalent in cases where the grain emissivity does not vary significantly over the spectral region used to define the color temperature. Our determination of the carbon continuum color temperature was heavily weighted by measurements in the 2.3- to 8.7- μm spectral region where the emissivity is approximately constant for small carbon grains with radii larger than about 0.5 μm (see Temi *et al.* 1989), and we believe that the color tem-

peratures given in column 9 of Table III are representative of the physical grain temperatures. Some comets, including P/Halley, show weak hydrocarbon emission at 3.28 μm (Brooke *et al.* 1986, 1988, 1991), and silicates can contribute weakly to the 8.6- μm emission. Neither of these emission contributions significantly affects the continuum color temperature for the cases studied here.

We calculated the superheat as a function of grain radius a and temperature T_{gr} for small carbon grains illuminated by the solar radiation field using the Planck mean absorption cross sections for graphite grains published by Gilman (1974). The Sun was assumed to radiate like a blackbody with an effective temperature of 5800 K. Our results are plotted in Figs. 4–6.

The dependence of the grain temperature on heliocentric distance (Fig. 4) shows that the grains in P/Halley (Fig. 4b) were superheated compared to those in the remaining comets in this survey (Fig. 4a). In both cases, it is evident that the grain temperature falls as the square root of the heliocentric distance. All of the comets plotted in Fig. 4a are IR Type I, which have relatively large grains. We believe that the comparison of various comets presented in Fig. 4c provides a powerful demonstration that Eq. (3) defines the lower limit to the temperature of comet dust. The comet dust trails detected by the Infrared Astronomical Satellite IRAS (Sykes *et al.* 1986, Sykes and Walker 1992) and the anti-tail of Comet Kohoutek (Ney 1974a) are included in the summary comparison presented in Fig. 4c. The particles in comet dust trails and Kohoutek's anti-tail are expected to be large compared to the grains in the inner coma, and they therefore provide an excellent indication of the lowest temperatures that can be attained by cometary solids.

The cross-hatched region in Fig. 5 shows the range of grain temperatures and superheats recorded for P/Halley (Table III). We conclude that P/Halley's coma continuum emission was usually produced by grains with radii between 0.5 and 1 μm . There were occasional episodes when P/Halley's grains appeared to be as large as 5 μm (Fig. 5). It is apparent from Fig. 5 that grains larger than 6–7 μm probably populate the comae of the average IR Type I comet.

An examination of similar data on the thermal emission from other extreme IR Type II comets (Maas *et al.* 1970, Ney 1974a,b, 1982a) leads us to conclude that their comae have small grains similar to those in the coma of P/Halley. On the other hand, the thermal emission from the comae of the most extreme IR Type I comets observed in the current study appears from Table III and Fig. 5 to be predominantly from large grains. The superheat in Comets KBM, Bradfield 1980 XV, Austin 1984 XIII, and Austin 1989c₁ was frequently low enough to imply that the coma grains were as large as 20 μm . The absence of strong silicate emission in the IR Type I comets (Fig. 2b) may

also indicate the presence of large silicate grains. Ordinarily, the absence of the 10- μm silicate emission feature is taken to indicate that the grains are carbon or iron. However, Rose (1979) reported laboratory experiments demonstrating that olivine grains with radii ≈ 10 –20 μm had weak 10- μm emission features and that grains larger than 37 μm exhibited no feature at all.

Although there is no reason to believe a priori that the size distributions of the carbon and silicate grains in comets are related, our data show that there is a fairly strong correlation between superheat and 10- μm silicate emission excess (Table IV and Fig. 6), with silicate emission increasing as superheat increases. Ney (1982a) noted a similar tendency among a smaller sample of comets. Several interpretations of this result appear plausible. It is possible that the grain-size distributions of the carbon and silicate particles are quite similar, so that the processes that apparently deplete the small particles in the IR Type I comets affect both types of particle similarly. Alternatively, the comet grains may be highly irregular fluffy aggregates of silicate and carbonaceous grains. Two possible forms for these aggregates are the "cluster-of-grapes" morphology exhibited by the IDPs described by Brownlee (1987), Brownlee *et al.* (1980), and Fraundorf *et al.* (1982) and the silicate-core/carbon-mantle particles suggested by Greenberg (1982, 1986). In the case of aggregate particles, both the continuum emission and the silicate emission arise from the same particles, and increasing particle size naturally leads to a suppression of both the superheat and the silicate emission feature (see the discussion of the large grains in Comet P/Encke by Gehrz *et al.* 1989). Both scenarios require that the IR Type I comets be relatively depleted of small particles.

We have plotted values averaged over all measurements of each comet in Fig. 6. Despite the strong correlation between superheat and silicate excess, there were occasional episodes for some comets when low superheat was accompanied by strong silicate emission (e.g., Bradfield 1980 XV, Days +3.3 and 4.3), and vice versa (e.g., Austin 1989c₁, Day +5.82). There may be conditions under which the carbon and silicate components can be affected independently.

The albedo of comet dust and the structure of the grains. Following the arguments presented by Van de Hulst (1957), Hanner *et al.* (1981), and Eaton (1984), we define a bolometric albedo A for small grains by the relationship

$$\frac{f_{\text{vis}}}{f_{\text{IR}}} = \frac{A}{1 - A}, \quad (5)$$

where the left-hand side of Eq. (5) is the ratio of the energy scattered in all directions to the total energy removed

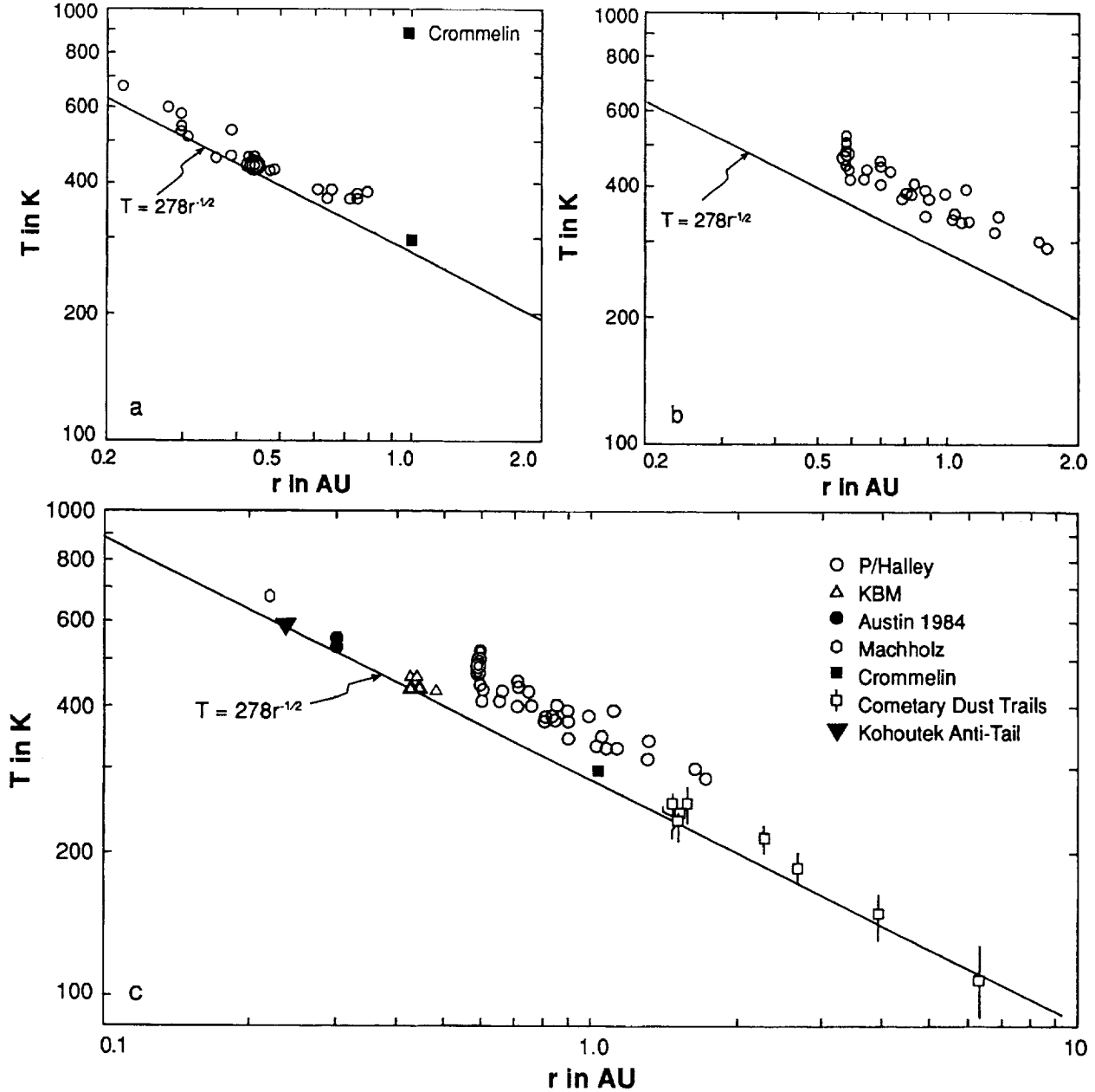


FIG. 4. The observed coma continuum temperature T_{obs} plotted as a function of heliocentric distance for (a) the six comparison IR Type I comets observed in the present survey (open circles) and comet Crommelin 1983n (datum from Hanner *et al.* 1985b), (b) Comet P/Halley, and (c) Comet P/Halley compared with the IR Type I comets with the lowest superheat from this survey, Comet Crommelin 1983n, the anti-tail of Comet Kohoutek, and the cometary dust trails detected by the Infrared Astronomical Satellite IRAS (data from Sykes and Walker 1992). Crommelin 1983n is the darkest comet known. The comet dust trails detected by IRAS (Sykes *et al.* 1986, Sykes and Walker 1992) and the anti-tail of Comet Kohoutek (Ney 1974a) shown in panel (c) are believed to be composed of large particles and therefore provide an indication of the lowest temperatures that can be attained by cometary solids. The solid line given by Eq. (3) evidently sets the lower limit to the temperature that comet grains assume as a function of heliocentric distance. It is apparent that P/Halley shows a much larger temperature excess on the average than do the comparison comets. In both cases, the data are consistent with an $r^{-1/2}$ dependence for the temperature.

from the incident beam, f_{vis} is the apparent intensity integrated over all scattering angles due to scattering of solar radiation, and f_{IR} is the integrated apparent thermal emission due to reradiation of the absorbed component. In the case of small comet grains, the quantity in the numerator

of the left-hand side of Eq. (5) must be derived from measurements of the visible/near-infrared energy distribution of the coma at all phase angles, because the scattering phase function is highly anisotropic (see Van de Hulst 1957, Bohren and Hufmann 1983, Hanner *et al.* 1981).

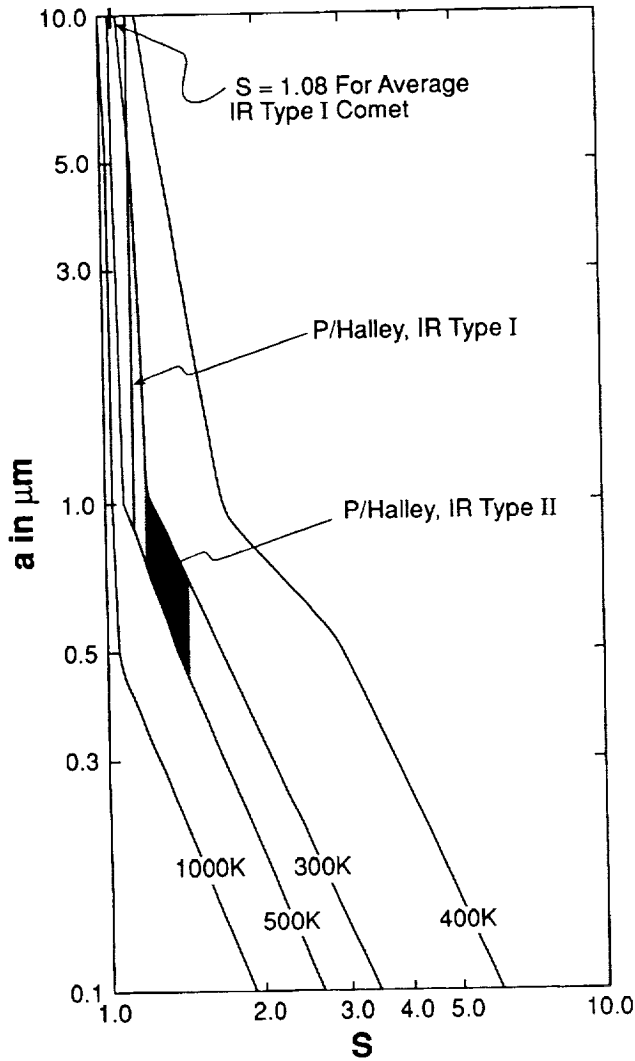


FIG. 5. The superheat S plotted as a function of grain radius a and temperature T_g for small carbon grains illuminated by the solar radiation field, assuming that the Sun has an effective temperature of 5800 K. Curves are based on Gilman's (1974) calculations of the Planck mean absorption cross sections for graphite grains. The range of grain temperatures and superheats recorded for P/Halley confirm that its coma continuum emission was usually produced primarily by particles with radii between 0.5 and 1 micrometer. When P/Halley exhibited IR Type I characteristics, its coma grains may have been as large as 5 μm . Typical IR Type I comets as characterized by the remaining comets in this survey have an average superheat of $S = 1.08$, suggesting the presence of grains with radii as large as 10 μm .

Since the energy removed from the beam is that absorbed by the grains and therefore reemitted by them in the infrared, the quantity in the denominator can be determined by measurements of the thermal infrared energy distribution of the coma. For a scattering angle θ , the bolometric albedo as a function of scattering angle $A(\theta)$ given by the integrated scattered and emitted energy distributions follows from Eq. (5) as

$$A(\theta) = \frac{f(\theta)}{1 + f(\theta)}, \quad (6)$$

where

$$f(\theta) = \frac{f_{\text{vis}}(\theta)}{f_{\text{IR}}(\theta)} = \frac{[\lambda f_{\lambda}(\text{vis}, \theta)]_{\text{max}}}{[\lambda f_{\lambda}(\text{IR}, \theta)]_{\text{max}}}. \quad (7)$$

In Eq. (7), $f_{\text{vis}}(\theta)$ and $f_{\text{IR}}(\theta)$ are the integrated apparent intensities in the scattered and thermal energy distributions of the coma, respectively, for the scattering angle θ .

The mean bolometric albedo A averaged over all scattering angles is then given by

$$A = \frac{1}{\pi} \int_0^{\pi} A(\theta) d\theta. \quad (8)$$

The scattered and thermal energy distributions of comets can be closely approximated by blackbody energy distributions. We show in Appendix A that, for black body radiation, the integrated intensity F is related to the maximum of the (λF_{λ}) function by $F \approx 1.36(\lambda F_{\lambda})_{\text{max}}$. The quantities $[\lambda f_{\lambda}(\text{vis})]_{\text{max}}$ and $[\lambda f_{\lambda}(\text{IR})]_{\text{max}}$ for P/Halley are plotted as a function of r in Fig. 7.

We have examined the scattering phase function of comet grains for a number of comets by measuring the ratio of the solar energy reflected by the grains to the absorbed solar energy reemitted by the grains as a function of phase angle (Fig. 8). Comets West 1976 VI (1975h) (Ney and Merrill 1976) and Bradfield 1980 XV (Tables I–III) passed between the Earth and the Sun, enabling us to make an excellent determination of $A(\theta)$ for typical comet grains at scattering angles between 30° and 150° (Fig. 8a). Our observations of these comets near inferior conjunction showed that typical comet grains have a moderately strong forward-scattering peak as would be expected for small particles (Fig. 8b). There is no evidence in our comet data for a backscattering peak that would be expected for spherical particles (Fig. 8b), and the forward-scattering lobe for comet dust is lower than that expected for spherical particles (Fig. 8b). Typical comet grains as defined by the data on Comets West and Bradfield 1980 XV have a mean bolometric albedo of $A \approx 0.32$, and $A(\theta) \approx 0.15$ for scattering angles between 120° and 180° .

The flattened forward-scattering lobe and the absence of a pronounced backscattering peak in $A(\theta)$ for comet dust (Fig. 8a) strongly suggest that the comet grains are nonspherical and, perhaps, fluffy aggregates as suggested by Hanner *et al.* (1981), Greenberg (1982, 1986), Greenberg and Hage (1989). Figure 8b shows $A(\theta)$ derived from laboratory data for small cloud chamber droplets (from the data presented by Webb 1935 and Wilson 1951), nonspherical particles (Bohren and Hufmann 1983), and

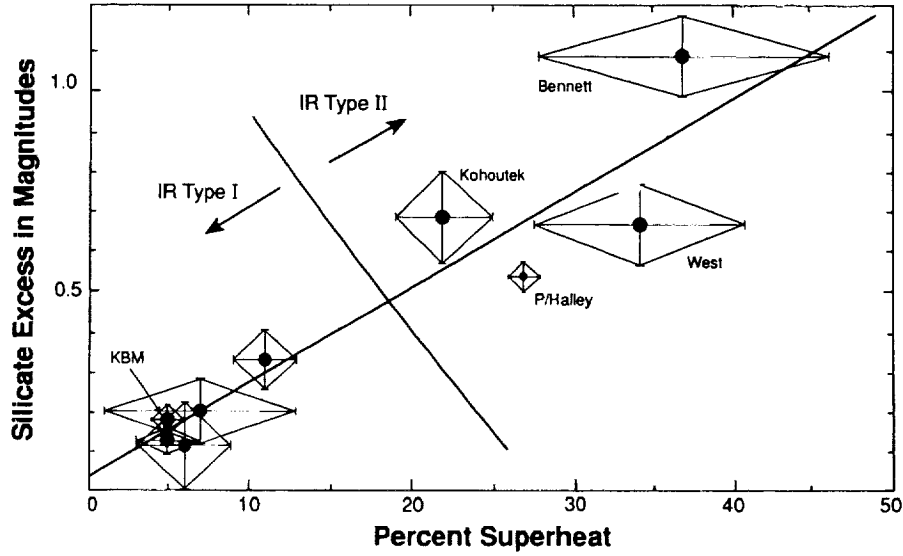


FIG. 6. The silicate excess (in magnitudes) plotted as a function of percent superheat ($[S - 1] \times 100$; see Eq. (4) for the definition of S) for recent bright comets (data in Table IV). The linear relation (solid line) is $y = 0.0233x + 0.0394$. The correlation coefficient is 0.94.

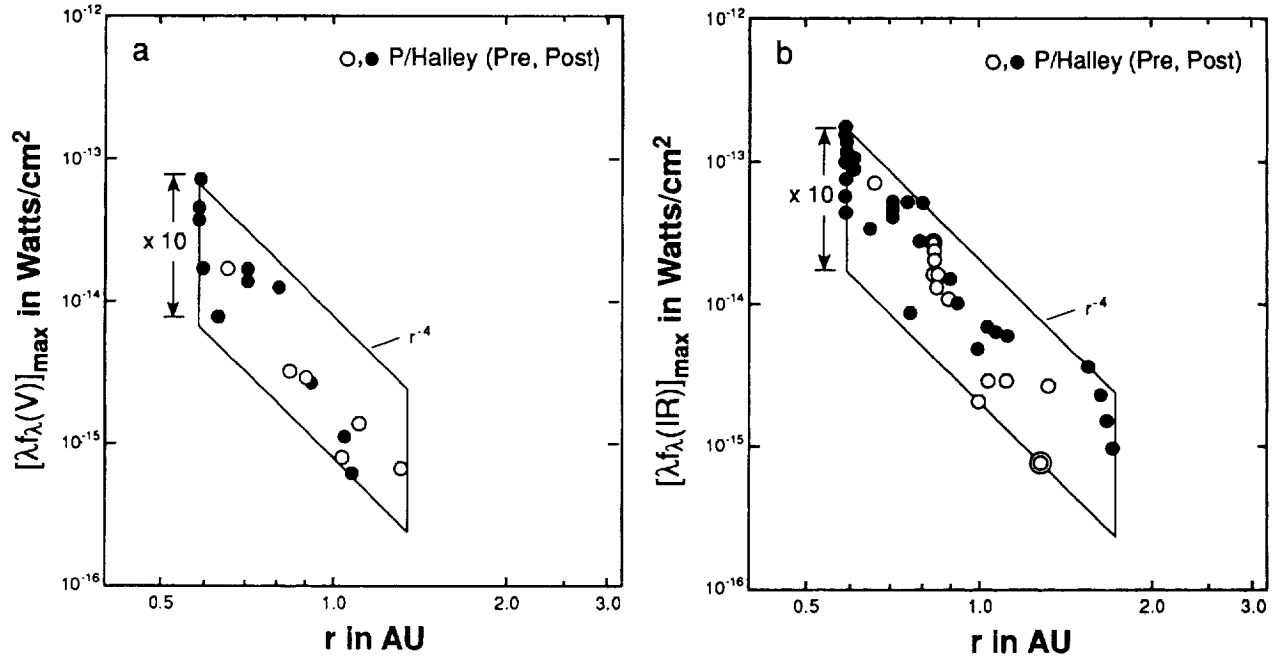


FIG. 7. The activity of the nucleus of P/Halley as a function of heliocentric distance at (a) visible and (b) infrared wavelengths as measured by variations of the apparent intensities $[\lambda f_{\lambda}(V)]_{\max}$ and $[\lambda f_{\lambda}(\text{IR})]_{\max}$, respectively. The coma model described in Appendix A has been used to correct the data for emission in the reference beam and to normalize the apparent intensities to a geocentric distance of $\Delta = 1$ AU and a beam diameter of 20 arcsec. Statistical errors are smaller than the plotting symbols. The parallelograms superimposed on panels (a) and (b) show that P/Halley generally brightened proportionally to r^{-4} as predicted by the theory of nuclear activity described by Eqs. (9) through (12), but varied by almost a factor of 10 on short time scales.

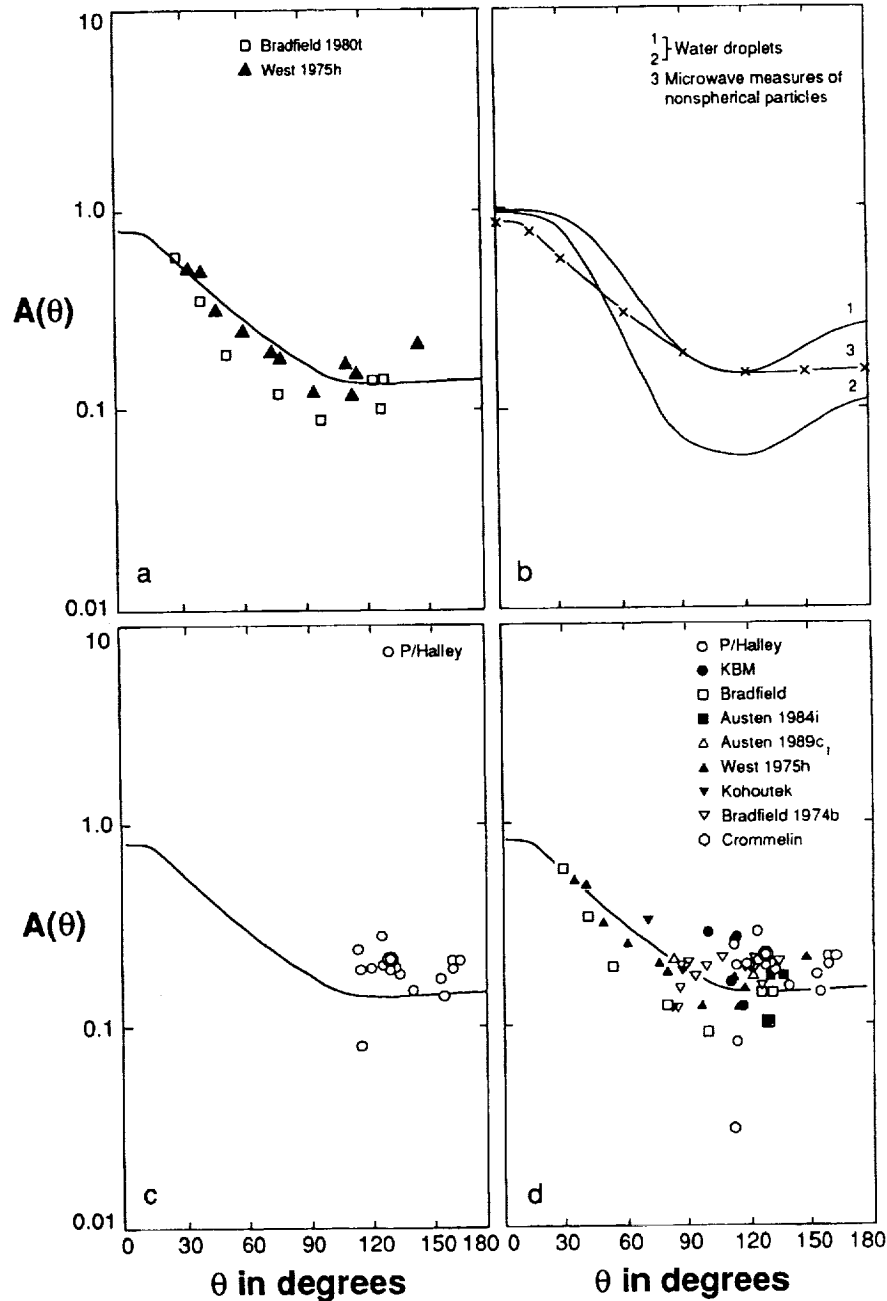


FIG. 8. The albedo of comet grains as a function of scattering angle as measured by the ratio of the scattered to the reemitted (absorbed) radiation. Panel (a) shows data for West 1975h (data for Ney and Merrill 1976) and Bradfield 1980 XV (data from this paper) that define the albedo of cometary grains for scattering angles between 30° and 150°. The flattened forward scattering lobe and the absence of a pronounced backscattering peak suggest that the comet grains are nonspherical and, perhaps, fluffy. Panel (b) shows laboratory data for small water droplets in cloud chambers (from the data presented by Webb 1935 and Wilson 1951) and nonspherical particles (Bohren and Hufmann 1983, Hanner *et al.* 1981). Panel (c) shows data for P/Halley for scattering angles between 114° and 165°, illustrating that P/Halley's grains were highly variable in albedo, but on the average were about the same as the grains of the comets in panel (a). Panel (d) shows data for Comet West 1975h (data from Ney and Merrill 1976), Crommelin 1983n (datum from Hanner *et al.* 1985b), and all the comets for which new data are reported in this paper with curve 3 from Fig. 5b superimposed for comparison. The side scattering albedo of comet grains generally lies in the range $0.1 \leq A \leq 0.3$, and the grains of individual comets can display a high degree of variability in albedo. To our knowledge, Crommelin is the darkest comet on record.

fluffy aggregates (Hanner *et al.* 1981). The comet data are consistent with the curves for nonspherical particles and fluffy aggregates. These characteristics are also consistent with theoretical results for "fluffy" aggregates (Greenberg 1982, 1986).

Figure 8c shows $A(\theta)$ for P/Halley for scattering angles between 114° and 165° , indicating that P/Halley's grains were highly variable in albedo, but on the average had a side-scattering albedo similar to that of the grains of the comets in Fig. 8a. We were able to observe P/Halley at backscattering angles out to 165° near perihelion passage. Any backscattering increase appeared to be small. P/Halley's dust coma had an average albedo of $A(\theta) \approx 0.20$ at a scattering angle of 130° , making it slightly brighter than the comae of average comets at phase angles from 120° to 165° . This would be expected for an extreme IR Type II comet with a significant small silicate grain component. We note that the lowest side-scattering albedo we observed for P/Halley ($A(\theta) \approx 0.08$) occurred when the $10\text{-}\mu\text{m}$ silicate emission feature was absent. Both of these indicators are consistent with a coma at these times that was populated predominantly by large grains.

Figure 8d shows $A(\theta)$ for Comet West, Comet Crommelin 1983n, and all the comets for which data are reported in this paper. We conclude that the side-scattering albedo of comet grains generally lies in the range $0.1 \leq A \leq 0.3$, but that the grains of individual comets can display a high degree of temporal variability in albedo during an apparition.

Variations in the silicate emission feature and albedo. Variations in several grain composition indicators were observed for P/Halley. Our data (Fig. 3) and additional infrared data obtained by Hanner *et al.* (1987) and Tokunaga *et al.* (1986 and 1988) at the NASA Infrared Telescope Facility (IRTF) show that P/Halley's silicate emission feature was occasionally weak or absent. Although this behavior usually occurred at heliocentric distances greater than 1 AU, there were several occasions when this behavior occurred at small heliocentric distances (e.g., 26.8 January 1986 UT and 14.67 February 1986 UT). Furthermore, our data show that the strength of the $10\text{-}\mu\text{m}$ silicate emission feature varied significantly when P/Halley was inside a heliocentric distance of 1 AU (Fig. 3). Ryan and Campins (1991) reached a similar conclusion based upon a more limited data set.

The disappearance of the silicate signature for distances greater than 1 AU was previously noted for Comet Kohoutek by Rieke *et al.* (1974). Comet Bradfield 1980 XV (Ney 1982a and Tables I–III of this paper) clearly was an IR Type II comet near perihelion (Fig. 2a), but showed no silicate emission beyond $r = 0.6$ AU.

On one occasion when P/Halley's silicate feature was

missing, the dust albedo fell as low as 0.08 (Fig. 8). A similar correlation between silicate signature strength and dust albedo is clearly evident for Comet Bradfield 1980 XV (this paper, Table III) and was noted in Comet Bradfield 1974b by Ney (1974b).

C. The Physics of the Nuclear Ablation Process

Our observations provide information about the nature of the nuclear ablation process by (i) showing that production rate and outflow of grains from the nucleus nominally conforms with the steady-state model, (ii) establishing the amplitude of short-term temporal variations in the activity of the nucleus, and (iii) measuring the mass loss rate of the solid material.

Constraints on models of the production and outflow of coma grains. We made nearly simultaneous observations of P/Halley with several diaphragms on four separate occasions using the O'Brien and WIRO telescopes and obtained multiaperture photometry of Comet Bradfield 1980 XV during a time span of about 1 hr on one occasion from Wyoming. These multiaperture measurements can be interpreted in terms of the steady-state model of nuclear activity described in Appendix B. In this model, grains are released from the nucleus at a constant rate and flow outward from the nucleus at constant velocity. Reitsema *et al.* (1989), in an elegant study, showed that the visible images of the inner coma of P/Halley by *Giotto* were consistent with the interpretation that the individual active areas on the nucleus behave according to the steady-state model.

Our multidaphragm observations of P/Halley and Comet Bradfield 1980 XV (Fig. 9) show that the coma flux was usually proportional to ϕ and that the steady-state grain production model was valid for times as great as 0.25 days (6 hr) on most occasions. Possible jet-like activity developing rapidly on time scales of a few hours is suggested by our P/Halley observations on 9.83 February 1986 UT, when the average flux recorded in a 20-arcsec beam at O'Brien was less than that expected from the flux recorded in an 8.3-arcsec beam at WIRO. The sudden activation of an intense gas jet, similar to those seen in the *Giotto* images (Keller *et al.* 1986), appears to provide a plausible explanation for the 9.83 February measurements. One set of infrared imaging observations, obtained a few hours prior to the *Giotto* encounter by Hayward *et al.* (1986), tends to confirm the hypothesis that the infrared variations may be profoundly affected by jets releasing material on the sunward side of the nucleus.

Activity in comet nuclei. Figures 7 and 10 summarize the activity of the nuclei of P/Halley and the six other recent bright comets studied in this work as measured by the infrared luminosities of their comae. In Fig. 10, we have included schematic representations of the average

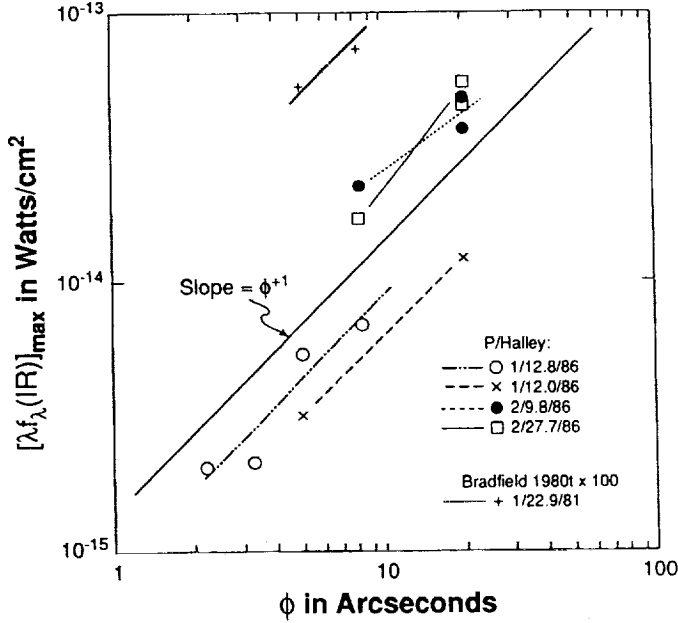


FIG. 9. Coma brightnesses of P/Halley and Bradfield 1980 XV as a function of aperture diameter. The coma model described in Appendix A has been used to correct the data for emission in the reference beam. The data are generally consistent with a constant production rate of grains in a constant velocity outflow (the steady-state model described in Appendix A).

activity of some of the other bright comets we have measured previously (Ney 1982a, Gehrz *et al.* 1989). The activity in most comets is proportional to r^{-4} both preceding and following perihelion passage with small superimposed variations. Comet West 1976 VI (1975h) brightened significantly after perihelion because the nucleus broke into four parts. Encke probably behaves differently than most comets because of an appreciable contribution to the thermal emission by the nucleus itself (Gehrz *et al.* 1989).

The apparent infrared intensity $f_\phi(\text{IR})$ of an optically thin comet coma in a beam of angular diameter ϕ radians that is much smaller than the angular extent of the coma follows from Eqs. (2), (A-4), and (A-6), to be

$$f_\phi(\text{IR}) = 1.3586(\lambda f_\lambda)_{\text{max}} = \left[\frac{\pi a^2 Q_e \sigma T_{\text{obs}}^4}{4V_0} \right] \frac{\phi}{\Delta} \frac{dN}{dt} = \left[\frac{a^2 Q_a L_\odot}{64V_0} \right] \frac{\phi}{r^2 \Delta} \frac{dN}{dt}, \quad (9)$$

where Q_a and Q_e are, respectively, the Planck mean absorption and emission coefficients for the grains as defined by Gilman (1974), where r and Δ are the heliocentric and geocentric distances in centimeters. If the grain production rate as a function of heliocentric distance $dN(r)/dt$ is

directly proportional to the intensity of the solar radiation incident upon the nucleus, then

$$\frac{dN(r)}{dt} = \frac{dN(r_p)}{dt} \left[\frac{r_p}{r} \right]^2, \quad (10)$$

where r_p is the perihelion distance, $dN(r_p)/dt$ is the grain production rate in grains sec^{-1} at perihelion, and r is the heliocentric distance. Combining Eqs. (9) and (10), we find that the apparent coma intensity is

$$f_\phi(\text{IR}) = \left[\frac{a^2 Q_a L_\odot}{64V_0} \right] \frac{\phi}{r^4 \Delta} \frac{dN(r_p)}{dt} \propto \frac{\phi}{r^4 \Delta}. \quad (11)$$

An interesting variation of the relationship expressed by Eq. (11) occurs in the case when the luminosity of the coma is generated by emission from small silicate grains for which the emission efficiency is proportional to the grain radius a (Gilman 1974). In this case, the apparent infrared intensity of the coma is directly proportional to the total mass M_{gr} of the grains,

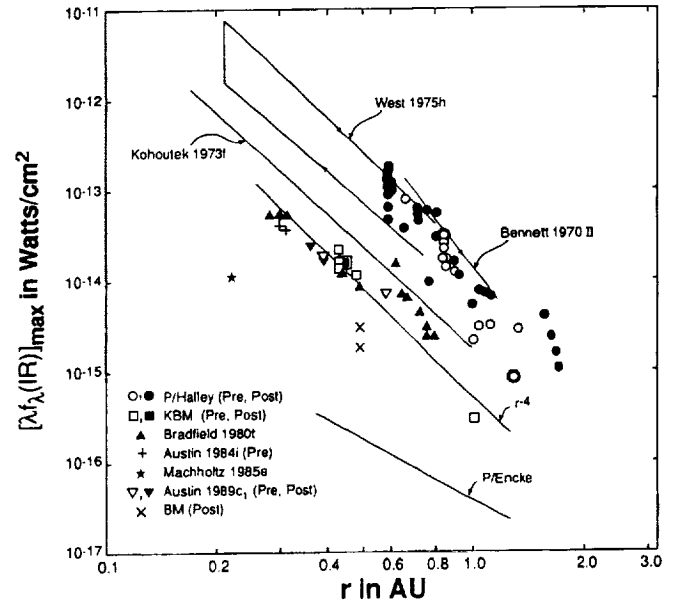


FIG. 10. The infrared activity of the nucleus of P/Halley compared to that of the nuclei of other recent bright comets as a function of heliocentric distance as measured by variations in the quantity $[\lambda f_\lambda(\text{IR})]_{\text{max}}$. The coma model described in Appendix A has been used to correct the data for emission in the reference beam and to normalize the apparent intensities to a geocentric distance of $\Delta = 1$ AU and a beam diameter of 20 arcsec. Comets Bennett 1970 II, Kohoutek 1973f, West 1975h (Ney 1982a), and P/Encke (Gehrz *et al.* 1987) are shown for comparison; the step function in activity for West near perihelion was caused by the breakup of the nucleus. An r^{-4} activity model adequately describes the heliocentric brightening of almost all comets. P/Halley exhibited large variations about the canonical law.

$$f_{\psi}(\text{IR}) \propto \frac{M_{\text{gr}} \phi}{r^4 \Delta}. \quad (12)$$

It is evident from Eq. (11) that the approximation quantified in Eq. (10) for the apparent luminosity of comets implies a dependence of r^{-4} for both the energy absorbed and the energy reemitted. The quantity $(\lambda f_{\lambda})_{\text{max}}$ for the thermal emission is a measure of the energy reradiated and is equal to the energy absorbed. It is a better measure of a comet's intrinsic brightness than short-wavelength reflected light measurements because of the variation in albedo with phase angle.

Both short-term and long-term variations in comet nucleus activity that are superimposed upon the r^{-4} radial dependence can be readily evaluated by examination of the quantity given in column 18 of Table III. This quantity has been normalized using Eqs. (11), (B-1), and (B-2) to give the flux expected in a standard circular 20-arcsec diameter diaphragm for an infinite reference beam throw with the comet at a standard heliocentric distance of $r = 1$ AU and a standard geocentric distance of $\Delta = 1$ AU.

In the comparison with the six other comets observed in this work (Fig. 10), P/Halley (Fig. 7) is seen to exhibit more frequent large-amplitude variations about the r^{-4} brightening law than is usually the case. Overall, we found that P/Halley varied in brightness by a factor of up to 7 on time scales of a few hours and days and by a factor of 10 overall compared to the expected rate of brightening with changing heliocentric distance; its thermal emission was as dim on some occasions as that of Kohoutek 1973f and as bright as that of Comets Bennett 1970 II and West 1975h on others. The large variations of P/Halley are also apparent in the scattered component (Fig. 7).

Our data enable us to draw several conclusions with regard to the activity of the nucleus and coma of P/Halley:

(1) Neither the large short-term variations nor the long-term variations in the bolometric infrared emission from P/Halley appear to correlate in any detail with the visible variations reported by Green and Morris (1987) and Millis and Schleicher (1986). Green and Morris (1987) found that the heliocentric dependence of the integrated visible magnitude of P/Halley's coma varied asymmetrically about perihelion passage, with the comet being significantly brighter postperihelion. Our data show that both the heliocentric dependence of the scattered light (Fig. 7a) and the thermal emission within a 20-arcsec beam were comparable pre- and postperihelion. Both our data and those of Green and Morris show large-amplitude short-term variations, but there is no detailed correlation between the intensity variations seen in our small beam with those exhibited by the entire coma.

(2) Millis and Schleicher (1986) and Schleicher *et al.* (1990) reported visual photometry showing periodic varia-

tions on a time scale of 7.4 days that they attributed to activity associated with the illumination of different regions of the nucleus. Although there is no obvious tight correlation between the variations exhibited in our data and those reported during overlapping periods by Millis and Schleicher (1986), both our data sets appear to be consistent with the inner coma being fainter in visible emission around 20 March 1986 and brighter around March 15, 23, and 25.5. We conclude that our data are consistent with the interpretation that the infrared variations in P/Halley result from rotation of the nucleus, presenting active and passive surfaces to the Sun. Both *Giotto* images (Keller *et al.* 1986) and the groundbased 10- μm infrared images made during the *Giotto* passage by Hayward *et al.* (1986) suggest the presence of localized active jets on P/Halley's nucleus which could account for such behavior.

(3) McFadden *et al.* (1987) and Rettig *et al.* (1987) noted a marked brightening of P/Halley in several visible emission bands during 23–25 March 1986 UT. Our data do not show any conclusive evidence of unusual brightening in either the scattered or the thermal emission from the inner 20 arcsec of the coma at the beginning and end of this period.

Dust mass loss rates of comet nuclei. The dust mass loss rate dM_D/dt caused by the ablation of dN/dt grains sec^{-1} from the comet nucleus, each having density ρ_{gr} and radius a , is

$$\frac{dM_D}{dt} = m_{\text{gr}} \frac{dN}{dt} = \frac{4\pi}{3} \rho_{\text{gr}} a^3 \frac{dN}{dt}, \quad (13)$$

where m_{gr} is the mass of a single grain. Combining Eqs. (9) and (13), we find that

$$\frac{dM_D}{dt} = [1.3586(\lambda f_{\lambda})_{\text{max}}] \frac{256\pi}{3} \frac{a \rho_{\text{gr}}}{L_{\odot} Q_a} V_0 \frac{r^2 \Delta}{\phi}, \quad (14)$$

where V_0 is the grain ejection velocity and $(\lambda f_{\lambda})_{\text{max}}$ is obtained by correcting the intensity given in Table III, column 11, for beam throw effects using Eq. (B-1). Presuming that the grains are accelerated to terminal velocity by momentum coupling to the gas, V_0 is of the order of the sonic velocity in the gas (Finson and Probst 1968) which is given with the aid of Eq. (3) by

$$V_0 = 5 \times 10^4 \left[\frac{T_{\text{bb}}}{278} \right]^{1/2} \\ = \frac{5 \times 10^4}{r_A^{1/4}} \text{ cm sec}^{-1} \approx 0.5 \text{ km sec}^{-1}, \quad (15)$$

where T_{BB} is the blackbody temperature at the heliocentric

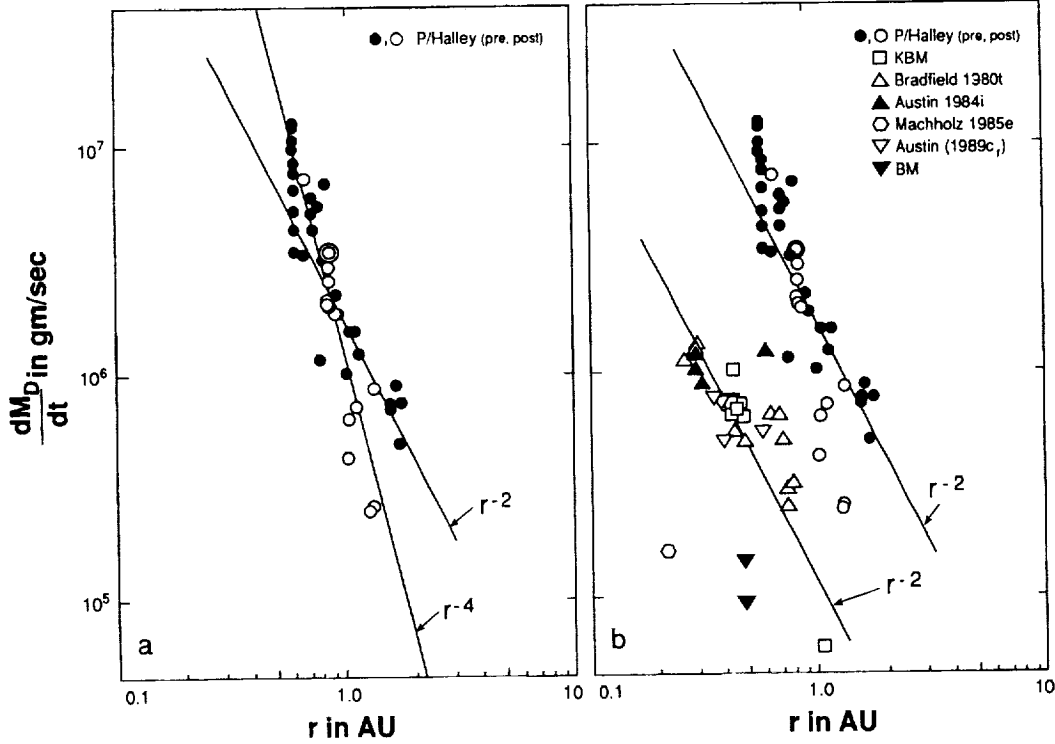


FIG. 11. The dust mass loss rates (normalized to a grain radius of $1 \mu\text{m}$ and a geocentric distance of $\Delta = 1 \text{ AU}$) as a function of heliocentric distance (a) from the nucleus of P/Halley and (b) from the nucleus of P/Halley in comparison with the nuclei of the IR Type I comets in this survey. The coma model described in Appendix A has been used to correct the data for emission in the reference beam and to normalize the apparent intensities to a geocentric distance of $\Delta = 1 \text{ AU}$ and a beam diameter of 20 arcsec. P/Halley showed substantial bursts of activity superimposed on the canonical r^{-2} law. The dust mass loss rates of the IR Type I comets shown here may be multiplied by a factor of 10 if it is presumed that their comae are composed primarily of $10 \mu\text{m}$ grains. In this case, their dust mass loss rates are equivalent to the rates inferred for dusty IR Type II comets like P/Halley.

distance r_A in AU of the comet. Given the very weak dependence of V_0 on r , we use the approximation that $V_0 \approx 0.5 \text{ km sec}^{-1}$ in the analysis that follows. We concluded above that the observed superheat S for the IR Type II comets discussed herein suggests a typical grain radius of $a \approx 1 \mu\text{m} = 10^{-4} \text{ cm}$ for the carbon grains responsible for the continuum emission. Typical IDP aggregates have a density of $\leq 1 \text{ g cm}^{-3}$, while pure carbon and silicate grains would have densities of $\approx 2\text{--}3 \text{ g cm}^{-3}$. We conclude that a typical comet grain can be presumed to have a density of $\approx 1 \text{ g cm}^{-3}$ (see also Hanner 1988). Using Eqs. (14) and (15) with $a = 1 \mu\text{m}$, $\rho_{gr} = 1 \text{ g cm}^{-3}$, and $Q_a = 1$, the dust mass loss rate becomes

$$\frac{dM_D}{dt} = 7 \times 10^{21} (\lambda f_\lambda)_{\text{max}} \frac{r_A^2 \Delta_A}{\phi_s} \text{ g sec}^{-1}, \quad (16)$$

where r_A and Δ_A are the heliocentric and geocentric distances in AU, ϕ_s is the beam diameter in arcseconds, and $(\lambda f_\lambda)_{\text{max}}$ is the integrated apparent infrared intensity in watts per square centimeter. We emphasize that the mass

loss rates calculated above refer only to the emission from the optically important particles. Since a considerable amount of the dust mass is in large particles that do not contribute significantly to the infrared emission (see Jewitt 1991), the mass loss rates given by Eq. (16) are lower limits. Sykes and Walker (1992) suggest that the mass loss in large particles may be more than double that estimated by other means.

The observational results for our sample of comets, normalized to a grain radius of $1 \mu\text{m}$, is summarized in Fig. 11, and it is clear from these that the dust mass loss rates for individual comets vary approximately as r_A^{-2} . This heliocentric distance dependency is readily understood by combining Eqs. (11) and (14) to yield:

$$\frac{dM_D}{dt} \propto r_A^{-2}. \quad (17)$$

Applying Eq. (16) to the data for P/Halley, we find that its average mass loss normalized to a heliocentric distance of 1 AU is $\geq 10^6 \text{ g sec}^{-1}$. P/Halley's mass loss rate varied

about this mean value by up to a factor of 7 on short time scales (Fig. 11a). For the remaining comets in this study (all IR Type I), Eq. (16) gives a mean loss rate that is a factor of ≈ 10 lower than that for P/Halley (see Fig. 11b). If it is assumed that the IR Type I comets have grains as large as $10 \mu\text{m}$, their mass loss rates would be increased by a factor of 10 and would become comparable to the mass loss rate deduced for P/Halley.

IV. CONCLUSIONS

The 0.7- to $23\text{-}\mu\text{m}$ observations reported in this paper for P/Halley and six other bright comets lead to several conclusions about the nature of comet grains and the physics of comet nuclear activity.

(1) Comets can be classified by their thermal infrared energy distributions. IR Type I comets have low continuum superheat and the $10\text{-}\mu\text{m}$ silicate emission is muted or absent. IR Type II comets have large continuum superheat and strong silicate emission features. The differences may be due to grain size.

(2) Simultaneous measurements of P/Halley and Bradfield 1980 XV with different diaphragms using telescopes in Minnesota and Wyoming are generally consistent with the steady-state model for nuclear ablation.

(3) P/Halley's dust coma had an average albedo of 0.20 at a scattering angle of 130° . Our data show that the scattering phase function for typical comet dust is characterized by a moderately strong forward-scattering peak, no appreciable backscattering peak beyond angles of 150° , a mean bolometric albedo of ≈ 0.32 , and a sidescattering albedo of ≈ 0.15 .

(4) The correlation between superheat and $10\text{-}\mu\text{m}$ silicate excess, the flattened forward-scattering peak of the albedo curve, and the relatively low backscattering albedo are all consistent with laboratory and theoretical results for nonspherical and fluffy grains. These results appear to be especially consistent with core-mantle grain models such as have been proposed by J. M. Greenberg and his collaborators (Greenberg and Hage 1989, Hage and Greenberg 1989).

(5) P/Halley's $10\text{-}\mu\text{m}$ silicate signature showed significant variations in strength and was occasionally weak or absent at heliocentric distances both smaller and larger than 1 AU.

(6) P/Halley's coma luminosity fluctuated by a factor of nearly 10 on time scales of 1 to 2 days. These variations are consistent with the jet-like activity associated with nuclear rotation.

(7) The mass loss rate for P/Halley was highly variable and averaged $\geq 10^6 \text{ g sec}^{-1}$ at $r = 1 \text{ AU}$. The mass loss rates for the IR Type I comets would be comparable to that deduced for P/Halley if it is assumed that their comae are composed of grains of radius $a \approx 10 \mu\text{m}$.

APPENDIX A: THE STEADY-STATE MODEL FOR INFRARED EMISSION FROM COMA DUST GRAINS

In the so-called "steady-state" model of nuclear activity (see Jewitt 1991), the thermal emission from the coma results from dust grains ablated from the nucleus at a constant rate of dN/dt grains sec^{-1} and flowing away from the nucleus at a constant velocity V_0 . Assuming that the coma is optically thin to thermal infrared radiation (see Ney 1982b, Jewitt 1991), the contribution to the apparent infrared intensity of the coma $f(\text{IR})$ by N dust grains is given by

$$f(\text{IR})_{\text{IR}} = \frac{L_{\text{IR}}}{4\pi\Delta^2} = \frac{N4\pi a^2 Q_c \sigma T_{\text{obs}}^4}{4\pi\Delta^2} = \frac{Na^2 Q_c \sigma T_{\text{obs}}^4}{\Delta^2}, \quad (\text{A-1})$$

where L_{IR} is the coma luminosity, a is the grain radius, Q_c is the Planck mean emission cross section of the grain (Gilman 1974), σ is the Stefan-Boltzmann constant, T_{obs} is the grain temperature, and Δ is the geocentric distance. Assuming that the dust grain distribution is isotropic, the total number of grains in a spherically symmetric coma within a radius r of the nucleus is given by

$$N = 4\pi \int_0^r n(r)r^2 dr = \frac{dN}{dt} t = \frac{dN}{dt} \frac{r}{V_0}, \quad (\text{A-2})$$

where $t = r/V_0$ is the time required for grains to flow out to radius r at constant velocity V_0 , and $n(r)$ is the radial number density distribution of grains in the coma. Our multiaperture measurements typically occurred when Δ was between 1 and 1.5 AU, so that the residence time of grains with $V_0 = 0.5 \text{ km sec}^{-1}$ in the beams we used was between 0.6 hr (2.2-arcsec beam) and 6 hr (20-arcsec beam). By inspection of Eq. (A-2), it follows that the steady-state model leads to a radial grain density distribution in the coma of

$$n(r) = \frac{1}{4\pi r^2 V_0} \frac{dN}{dt}. \quad (\text{A-3})$$

Integrating this density distribution over the cylindrical volume V of the coma that is intercepted by a photometer beam of angular diameter ϕ to obtain the number N_ϕ of grains emitted into the beam, and substituting the result into Eq. (A-1), we find that the apparent infrared intensity $f_\phi(\text{IR})$ measured in the beam is

$$\begin{aligned} f_\phi(\text{IR}) &= \frac{a^2 Q_c \sigma T_{\text{obs}}^4}{\Delta^2} N_\phi \\ &= \frac{a^2 Q_c \sigma T_{\text{obs}}^4}{\Delta^2} \int \int_V n(r) d^3r = \left[\frac{\pi a^2 Q_c \sigma T_{\text{obs}}^4}{4V_0} \right] \frac{\phi}{\Delta} \frac{dN}{dt}, \end{aligned} \quad (\text{A-4})$$

where the result on the extreme right-hand side is for the case where the angular diameter of the beam is much smaller than the angular diameter of the coma. It can be seen from Eq. (A-2) that $f_\phi(\text{IR}) \propto \phi\Delta^{-1}$, leading to the correction terms specified in Eqs. (B-1) and (B-2) that we derive in Appendix B.

The determination of $f_\phi(\text{IR})$ is particularly straightforward when the continuum emission from the dust approximates that of a blackbody as is the case with all the comets observed here. In this case, the ratio of the maximum of the λF_λ function to the total blackbody emission F is given by

TABLE C-I
Orbital Elements for the Comets

COMET	KBM 1975 IX	Bradfield 1980 XV	Austin 1984 XIII	Machholz 1985 VIII	Austin 1989c ₁	BM 1989X	P/Halley 1986 III
EQUINOX	1950.0	1950.0	1950.0	1950.0	J2000.0	J2000.0	J2000.0
EPOCH	5 Sep 25	80 Dec 27	84 Aug 8	-	90 Apr 19	89 Oct 1	86 Feb 19
T	75 Sep 5.3348	80 Dec 29.5417	84 Aug 12.1371	85 Jun 28.7388	90 Apr 9.96745	89 Sep 11.9384	86 Feb 9.4590
q	0.425561	0.259823	0.291284	0.106252	0.349775	0.478742	0.587104
e	1.000095	0.999725	0.999846	1.000000	1.000225	0.971959	0.967277
P	-	-	-	-	-	-	76.00
PERI (ω)	116.9756	358.2855	353.12701	274.0831	61.5763	129.6111	111.8657
NODE (Ω)	295.6526	114.6465	170.87724	194.7292	75.9255	311.5878	58.8601
INCL (i)	80.7779	138.5882	164.15979	16.2827	58.95639	19.3357	162.2422

$$\frac{(\lambda F_\lambda)_{\max}}{F} = \frac{2\pi hc^2}{\sigma(\lambda_m T)^4} \left[\frac{1}{e^{hc/(k\lambda_m T)} - 1} \right] = \frac{1}{1.3586}, \quad (\text{A-5})$$

$$\frac{f_1}{f_2} = \frac{\phi_1 \Delta_2}{\phi_2 \Delta_1}, \quad (\text{B-2})$$

where λ_m is the wavelength of maximum emission in λF_λ , $\lambda_m T = 0.3670$ cm deg is Wien's law for λF_λ , $h = 6.6262 \times 10^{-27}$ erg sec, $c = 2.9979 \times 10^{10}$ cm sec $^{-1}$, $\sigma = 5.6696 \times 10^{-5}$ erg cm $^{-2}$ deg $^{-4}$ sec $^{-1}$ and $k = 1.3806 \times 10^{-16}$ erg deg $^{-1}$. Thus, the apparent infrared intensity $f_\phi(\text{IR})$ of the coma is given by

$$f_\phi(\text{IR}) = 1.3586(\lambda f_\lambda)_{\max}, \quad (\text{A-6})$$

where $(\lambda f_\lambda)_{\max}$ is the observed apparent emission maximum of the infrared continuum.

APPENDIX B: CORRECTIONS FOR BEAM DIAMETER, THROW, AND GEOCENTRIC DISTANCE

Comet comae are extended sources of infrared emission and are large enough so that coma emission is present in the reference beam used for background cancellation. The total emission into a beam of a given angular diameter depends upon the volume of coma material intercepted by the beam. Therefore, analysis and interpretation of the infrared photometry require correction of the data for the effects of beam diameter, reference beam throw, and geocentric distance. The correction is straightforward for comets that obey a steady-state model where the coma is produced by material ablated from the nucleus at a constant rate and flowing away from the nucleus at a constant velocity. We describe this model quantitatively in Appendix A, concluding that it leads to a ϕ^{+1} dependence for the flux from the coma, where ϕ is the radius of the coma, and a Δ^{-1} dependence of the coma brightness on geocentric distance. In this case, the apparent intensity f_z that would be measured in a beam of angular diameter ϕ for a throw large enough so that the reference beam falls off the coma and the apparent intensity f_ψ observed in the same beam with a throw of angular diameter ψ such that the reference beam falls on the coma are related by

$$\frac{f_z}{f_\psi} = \frac{4\psi}{4\psi - \phi}. \quad (\text{B-1})$$

Furthermore, the apparent intensities, f_1 and f_2 measured in two different apertures with diameters ϕ_1 and ϕ_2 with the comet at geocentric distances of Δ_1 and Δ_2 , respectively, will be related by

These correction factors have been applied where appropriate in the analysis above using a standard reference beam diameter of $\phi_1 = 20$ arcsec and a standard geocentric distance of $\Delta_1 = 1$ AU.

APPENDIX C: ORBITAL ELEMENTS FOR THE COMETS OBSERVED

We present in Table C-I the orbital elements we used for deriving the orbital parameters of the comets for which we report infrared observations here. These have been gleaned from the *Catalog of Cometary Orbits* (Marsden 1982) and The Central Bureau for Astronomical Telegrams (Marsden 1992). The data tabulated by row are (1) the comet name, (2) the equinox for Ω , ω , and the orbital inclination (i), (3) the osculation date in decimal days (Universal, or Ephemeris, Time), (4) the perihelion time (Ephemeris Time), (5) the perihelion distance q in astronomical units, (6) the orbital eccentricity, (7) the revolution period in years (no entry signifies $p > 1000$ years), (8) the argument of perihelion ω in decimal degrees, (9) the longitude of the ascending node Ω in decimal degrees, and (10) the orbital inclination i in decimal degrees.

ACKNOWLEDGMENTS

We are especially grateful to D. Hufmann for giving freely of his time to discuss with us the characteristics of the phase function of comet dust particles; his comments weighed heavily in the framing of our conclusions. M. S. Hanner helpfully provided us with her insightful lecture notes on defining albedos for small particles, and T. J. Jones gave us guidance on the definition of albedos. T. W. Jones confirmed the conversion factors between square and circular apertures for an r^{-1} surface brightness distribution. We thank B. Jones for a critical reading of the manuscript and for suggesting several improvements in the presentation. T. Williams, L. R. Shaw, T. Hayward, C. Jaworosky, and L. Chisholm assisted with the observations at WIRO. Hayward's contributions were especially valuable and included a crucial last-minute repair of the photometer at WIRO during the remote observations of P/Halley on perihelion day. He also obtained the 15.79 April 1990 UT observation of Comet Austin 1989c, for us at WIRO. A. Knutson provided invaluable assistance with observations at O'Brien Observatory. We thank T. J. Jones for obtaining the 27.3 and 28.3 April 1986 UT observations of P/Halley at MLOF for us. Finally, A. Tokunaga and A. Storrs, who

refereed the manuscript, made several useful suggestions that improved the clarity of the presentation. This research was supported by NASA, the National Science Foundation, the U.S. Air Force, and the University of Minnesota Institute of Technology Dean's Office and Graduate School, and the University of Wyoming.

REFERENCES

- BECKLIN, E. E., AND J. A. WESTPHAL 1966. Infrared observations of comet 1965f. *Astrophys. J.* **145**, 445–453.
- BOHREN, C. F., AND D. R. HUFMANN 1983. *Absorption and Scattering of Light by Small Particles*, pp. 399–401. Wiley, New York.
- BREGER, M., R. D. GEHRZ, AND J. A. HACKWELL 1981. Interstellar grain size. II. Infrared photometry and polarization in Orion. *Astrophys. J.* **248**, 963–976.
- BROOKE, T. Y., R. F. KNACKE, AND R. R. JOYCE 1986. Near-infrared studies of comet Halley: polarization and color. In *Exploration of Halley's Comet*, ESA SP-250, pp. 87–89. European Space Agency, Noordwijk.
- BROOKE, T. Y., R. F. KNACKE, T. C. OWEN, AND A. T. TOKUNAGA 1988. Spectroscopy of emission features near 3 μm in comet Wilson (1986l), submitted for publication.
- BROOKE, T. Y., A. T. TOKUNAGA, AND R. F. KNACKE 1991. Detection of the 3.4 μm emission feature in comets P/Brorson–Metcalf and Okazaki–Levy–Rudenko (1989R) and an observational summary. *Astron. J.* **101**, 268–278.
- BROWNEE, D. E. 1987. A comparison of Halley dust with meteorites, interplanetary dust, and interstellar grains. In *Observations of Comets Halley and Wilson and Properties of the Grains*, (M. S. Hanner, Ed.), NASA Conference Publ. 3004, pp. 66–67.
- BROWNEE, D. E., L. PILACHOWSKI, E. OLSZEWSKI, AND P. W. HODGE 1980. Analysis of interplanetary dust collections. In *Solid Particles in the Solar System* (I. Halliday and B. A. McIntosh, Eds.), pp. 333–342. Reidel, Dordrecht.
- CASTELAZ, M. W., J. A. HACKWELL, G. L. GRASDALEN, R. D. GEHRZ, AND C. GULLIXSON 1985. GSS 30: an infrared reflection nebula in the Ophiuchus dark cloud. *Astrophys. J.* **290**, 261–272.
- EATON, N. 1984. Comet dust—Applications of Mie scattering. *Vistas Astron.* **27**, 111–129.
- FINSON, M. L., AND R. F. PROBSTEN 1968. A theory of dust comets: I. Model and equations and II. Results for Comet Arend–Roland. *Astrophys. J.* **154**, 327.
- FRAUNDORF, P., D. E. BROWNEE, AND R. M. WALKER 1982. Laboratory studies of interplanetary dust. In *Comets*, (L. Wilkening, Ed.), pp. 323–340. Univ. of Arizona Press, Tucson.
- GEHRZ, R. D., AND J. A. HACKWELL 1978. Exploring the infrared universe from Wyoming. *Sky Telescope* **55**, 466–473.
- GEHRZ, R. D., AND E. P. NEY 1986. Infrared temporal development of P/Halley. In *Exploration of Halley's Comet*, ESA SP-250, pp. 101–105. European Space Agency, Noordwijk.
- GEHRZ, R. D., G. L. GRASDALEN, AND J. A. HACKWELL 1987. Infrared astronomy. In *Encyclopedia of Physical Science and Technology*, Vol. 2, pp. 53–80. Academic Press, New York.
- GEHRZ, R. D., J. A. HACKWELL, AND T. W. JONES 1974. Infrared observations of Be stars from 2.3 to 19.5 microns. *Astrophys. J.* **191**, 675–684.
- GEHRZ, R. D., E. P. NEY, J. PISCATELLI, E. ROSENTHAL, AND A. T. TOKUNAGA 1989. Infrared photometry and spectroscopy of Comet P/Encke 1987. *Icarus* **80**, 280–288.
- GILMAN, R. C. 1974. Planck mean cross-sections for four grain materials. *Astrophys. J. Suppl. Ser.* **28**, 397–403.
- GREEN, D. W. E., AND C. S. MORRIS 1987. The visual brightness behavior of P/Halley during 1981–1987. *Astron. Astrophys.* **187**, 560–568.
- GREENBERG, J. M. 1982. In *Comets* (L. L. Wilkening, Ed.), pp. 131–163. Univ. of Arizona Press, Tucson.
- GREENBERG, J. M. 1986. Predicting that comet Halley is dark. *Nature* **321**, 385.
- GREENBERG, J. M., AND J. I. HAGE 1990. From interstellar dust to comets: A unification of observational constraints. *Astrophys. J.* **361**, 260–274.
- HAGE, J. I., AND J. M. GREENBERG 1990. A model for the optical properties of porous grains. *Astrophys. J.* **361**, 251–259.
- HANNER, M. S. 1988. Grain optical properties. In *Observations of Comets Halley and Wilson and Properties of the Grains* (M. S. Hanner, Ed.), pp. 22–49. NASA Conference Publ. 3004.
- HANNER, M. S., R. H. GIESE, K. WEISS, AND R. ZERULL 1981. On the definition of albedo and application to irregular particles. *Astron. Astrophys.* **104**, 42–46.
- HANNER, M. S., D. K. AITKEN, R. KNACKE, S. MCCORKLE, P. F. ROCHE, AND A. T. TOKUNAGA 1985a. Infrared spectrophotometry of Comet IRAS–Araki–Alcock (1983d): A bare nucleus revealed? *Icarus* **62**, 97–109.
- HANNER, M. S., R. KNACKE, Z. SEKANINA, AND A. T. TOKUNAGA 1985b. Dark grains in Comet Crommelin. *Astron. Astrophys.* **152**, 177–181.
- HANNER, M. S., E. TEDESCO, A. T. TOKUNAGA, G. J. VEEDER, D. F. LESTER, F. C. WITTEBORN, J. D. BREGMAN, J. GRADIE, AND L. LEBOWSKY 1985c. The dust coma of periodic Comet Churyumov–Gerasimenko (1982 VIII). *Icarus* **64**, 11–19.
- HANNER, M. S., A. T. TOKUNAGA, W. F. GOLISCH, D. M. GRIEP, AND C. D. KAMINSKI 1987. Infrared emission from P/Halley's dust coma during March 1986. *Astron. Astrophys.* **187**, 653–660.
- HANNER, M. S., R. L. NEWBURN, R. D. GEHRZ, A. T. HARRISON, AND E. P. NEY 1990. The infrared spectrum of comet Bradfield (1987s) and the silicate emission feature. *Astrophys. J.* **348**, 312–321.
- HAYWARD, T., R. D. GEHRZ, AND G. L. GRASDALEN 1986. Ground-based infrared observations of comet Halley. *Nature* **326**, 55–57.
- JEWITT, D. 1991. Cometary photometry. In *Comets in the Post-Halley Era* (R. L. Newburn, Jr., M. Neugebauer, and J. Rahe, Eds.), Vol. 1, pp. 19–64. Kluwer, Dordrecht.
- JEWITT, D., AND K. J. MEECH 1986. Cometary grain scattering versus wavelength, or, "What color is comet dust?" *Astrophys. J.* **310**, 937–952.
- KELLER, H. U., *et al.* 1986. First Halley multicolor camera imaging results from Giotto. *Nature* **321**, 320–326.
- KISSEL, J., *et al.* 1986. Composition of comet Halley dust particles from Giotto observations. *Nature* **321**, 336–337.
- MAAS, R. W., E. P. NEY, AND N. J. WOOLF 1970. The 10 micron emission peak of comet Bennett 1969i. *Astrophys. J.* **160**, L101–L104.
- MARSDEN, B. G. 1982. *Catalog of Cometary Orbits*, 4th ed. Minor Planet Center, Smithsonian Astrophysical Observatory, Cambridge, MA.
- MARSDEN, B. G. 1992. *IAU Circulars, e-mail service*.
- MCDONNELL, J. A. M., *et al.* 1987. The dust distribution within the inner coma of comet P/Halley 1982i: Encounter by Giotto's impact detectors. *Astron. Astrophys.* **187**, 719–741.
- MCDONNELL, J. A. M., P. L. LAMY, AND G. S. PANKIEWICZ 1991. Physical properties of cometary dust. In *Comets in the Post-Halley Era* (R. L. Newburn, Jr., M. Neugebauer, and J. Rahe, Eds.), Vol. 2, pp. 1043–1073. Kluwer, Dordrecht.
- McFADDEN, L. A., M. F. A'HEARN, P. D. FELDMAN, E. E. ROETTGER, D. M. EDSALL, AND P. S. BUTTERWORTH 1987. Activity of Comet

- P/Halley 23–25 March, 1986: IUE observations. *Astron. Astrophys.* **187**, 333–338.
- MILLIS, R. L., AND D. G. SCHLEICHER 1986. Rotational period of comet Halley. *Nature* **324**, 646–649.
- NEY, E. P. 1974a. Infrared observations of comet Kohoutek near perihelion. *Astrophys. J.* **189**, L141–L143.
- NEY, E. P. 1974b. Multiband photometry of comets Kohoutek, Bennett, Bradfield, and Encke. *Icarus* **23**, 551–560.
- NEY, E. P. 1977. Star Dust. *Science* **195**, 541–546.
- NEY, E. P. 1982a. Optical and infrared observations of bright comets in the range 0.5 μm to 20 μm . In *Comets* (L. Wilkening, Ed.), pp. 323–340. Univ. of Arizona Press, Tucson.
- NEY, E. P. 1982b. Visibility of comet nuclei. *Science* **215**, 397–398.
- NEY, E. P., AND K. M. MERRILL 1976. Comet West and the scattering function of cometary dust. *Science* **194**, 1051–1053.
- REITSEMA, H. J., W. A. DELAMERE, A. R. WILLIAMS, D. C. BOICE, W. F. HUEBNER, AND F. L. WHIPPLE 1989. Dust distribution in the inner coma of Comet Halley: Comparison with models. *Icarus* **81**, 31–40 (see also the cover illustration of *Planetary Rep.* **VII**(5), Sept./Oct. 1987).
- RETTIG, T. W., J. R. KERN, R. RUCHTI, B. BAUMBAUGH, A. E. BAUMBAUGH, K. L. KNICKERBOCKER, AND J. DAWE 1987. Observations of the coma of Comet P/Halley and the outburst of 1986 March 24–25 (UT). *Astron. Astrophys.* **187**, 249–255.
- RIEKE, G. H., F. J. LOW, T. A. LEE, AND W. W. WISNIEWSKI 1974. Infrared observations of comet Kohoutek. In *Comet Kohoutek*, NASA-SP 355, pp. 175–182. NASA, Washington DC.
- ROSE, L. A. 1979. Laboratory simulation of infrared astrophysical features. *Astrophys. Space Sci.* **65**, 47–67.
- RYAN, E. V., AND H. CAMPINS 1991. Comet Halley: Spatial and temporal variability of the silicate emission feature. *Astron. J.* **101**, 695–705.
- SCHLEICHER, D. G., R. L. MILLIS, D. T. THOMPSON, P. V. BIRCH, R. MARTIN, D. J. THOLEN, J. R. PISCITELLI, N. L. LARK, AND H. B. HAMMEL 1990. Periodic variations in the activity of comet P/Halley during the 1985/1986 apparition. *Astron. J.* **100**, 896–912.
- SEKANINA, Z. 1974a. On the nature of the anti-tail of Comet Kohoutek (1973f) I. a working model. *Icarus* **23**, 502–518.
- SEKANINA, Z. 1974b. The prediction of anomalous tails of comets. *Sky Telescope* **47**, 374–377.
- SEKANINA, Z. 1976. In *The Study of Comets* (B. Donn, M. Mumma, W. Jackson, M. A'Hearn, and R. Harrington, Eds.), NASA SP-393, pp. 893–933. U.S. G.P.O., Washington, D.C.
- SYKES, M. V., L. A. LEBOWSKY, D. M. HUNTEN, AND F. LOW 1986. The discovery of dust trails in the orbits of periodic comets. *Science* **232**, 1115–1117.
- SYKES, M. V., AND R. G. WALKER 1992. Cometary dust trails. *Icarus* **95**, 180–210.
- TELESCO, C. M., R. DECHER, C. BAUGHER, H. CAMPINS, D. MOZURKEWICH, H. A. THRONSON, D. P. CRUIKSHANK, H. B. HAMEL, S. LARSON, AND Z. SEKANINA 1986. Thermal-infrared and visual imaging of comet Giacobini-Zinner. *Astrophys. J.* **310**, L61–L65.
- TEMI, P., P. DE BERNARDS, S. MASI, G. MORENO, AND A. SALAMA 1989. Infrared emission from interplanetary dust. *Astrophys. J.* **337**, 528–535.
- TOKUNAGA, A. T., W. F. GOLISCH, D. M. GRIEP, C. D. KAMINSKI, AND M. S. HANNER 1986. The NASA Infrared Telescope Facility comet Halley monitoring program. I. Preperihelion results. *Astron. J.* **92**, 1183–1190.
- TOKUNAGA, A. T., W. F. GOLISCH, D. M. GRIEP, C. D. KAMINSKI, AND M. S. HANNER 1988. The NASA Infrared Telescope Facility comet Halley monitoring program. II. Postperihelion results. *Astron. J.* **96**, 1971–1976.
- VAN DE HULST, H. C. 1957. *Light Scattering by Small Particles*, pp. 183 and 449. Dover, New York.
- WALKER, R. M. 1987. Comparison of laboratory determined properties of interplanetary dust with those of comet Halley particles: What are comets made of? In *Infrared Observations of Comets Halley and Wilson and Properties of the Grains* (M. Hanner, Ed.), NASA Conference Publ. 3004, pp. 53–63.
- WEAVER, H. A., M. F. A'HEARN, P. D. FELDMAN, C. ARPIGNY, W. A. BAUM, J. C. BRANDT, R. M. LIGHT, AND J. A. WESTPHAL 1992. Inner coma imaging of Comet Levy (1990C) with the Hubble Space Telescope. *Icarus*, in press.
- WEBB, C. G. 1935. The scattering of light by drops in a Wilson chamber. *Philos. Mag.* **19**, 927–933.
- WILSON, J. G. 1951. *The Principles of Cloud-Chamber Technique*, p. 59. Cambridge Univ. Press, Cambridge.
- WOOLF, N. J., AND E. P. NEY 1969. Circumstellar emission from cool stars. *Astrophys. J.* **155**, L181–L184.

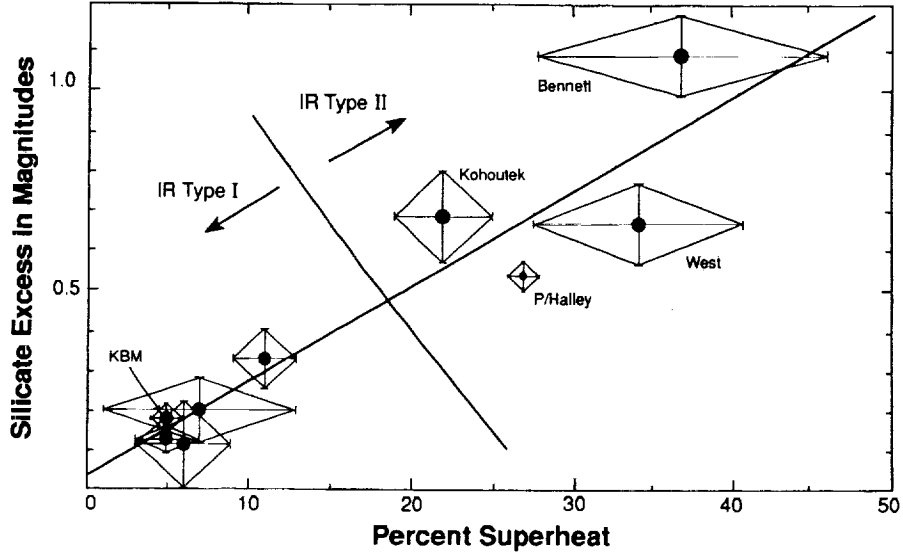


FIG. 6. The silicate excess (in magnitudes) plotted as a function of percent superheat $[(S - 1) \times 100]$; see Eq. (4) for the definition of S for recent bright comets (data in Table IV). The linear relation (solid line) is $y = 0.0233x + 0.0394$. The correlation coefficient is 0.94.

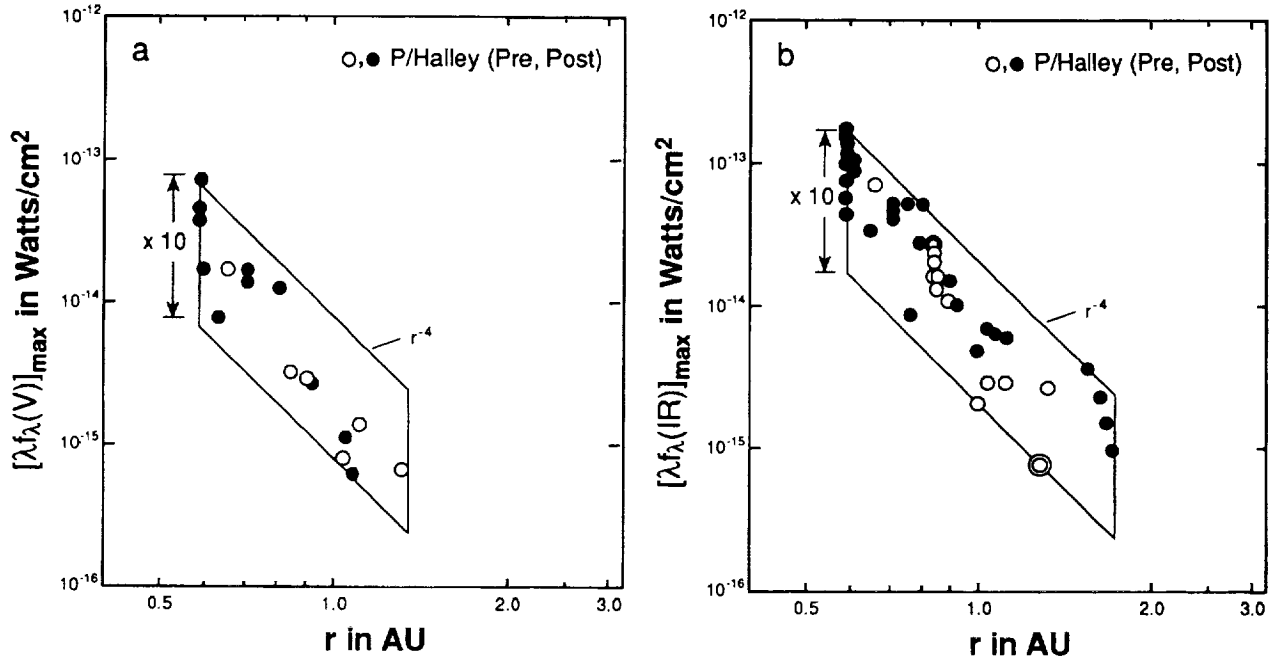


FIG. 7. The activity of the nucleus of P/Halley as a function of heliocentric distance at (a) visible and (b) infrared wavelengths as measured by variations of the apparent intensities $[\lambda f_{\lambda}(V)]_{\max}$ and $[\lambda f_{\lambda}(IR)]_{\max}$, respectively. The coma model described in Appendix A has been used to correct the data for emission in the reference beam and to normalize the apparent intensities to a geocentric distance of $\Delta = 1$ AU and a beam diameter of 20 arcsec. Statistical errors are smaller than the plotting symbols. The parallelograms superimposed on panels (a) and (b) show that P/Halley generally brightened proportionally to r^{-4} as predicted by the theory of nuclear activity described by Eqs. (9) through (12), but varied by almost a factor of 10 on short time scales.

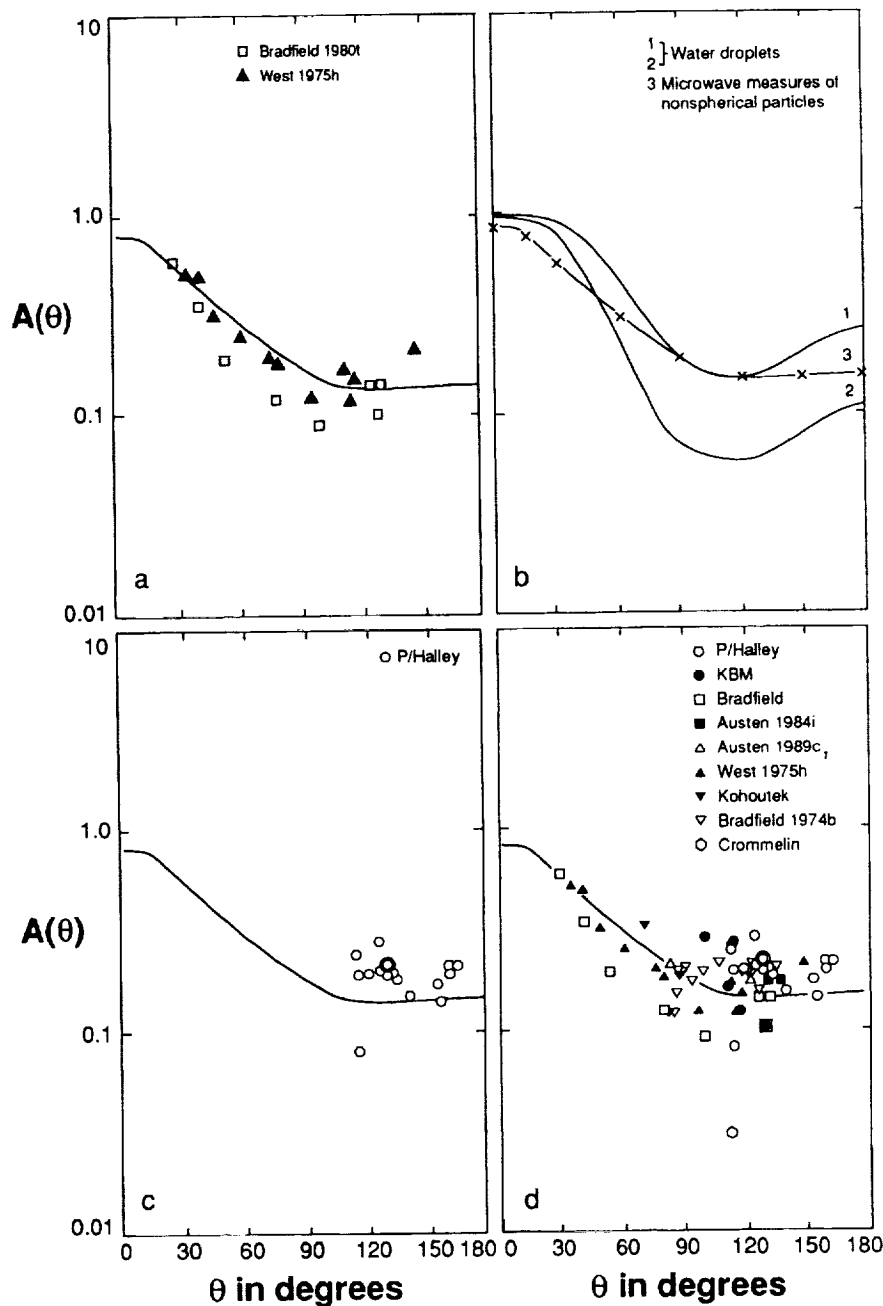


FIG. 8. The albedo of comet grains as a function of scattering angle as measured by the ratio of the scattered to the reemitted (absorbed) radiation. Panel (a) shows data for West 1975h (data for Ney and Merrill 1976) and Bradfield 1980 XV (data from this paper) that define the albedo of cometary grains for scattering angles between 30° and 150° . The flattened forward scattering lobe and the absence of a pronounced backscattering peak suggest that the comet grains are nonspherical and, perhaps, fluffy. Panel (b) shows laboratory data for small water droplets in cloud chambers (from the data presented by Webb 1935 and Wilson 1951) and nonspherical particles (Bohren and Hufmann 1983, Hanner *et al.* 1981). Panel (c) shows data for P/Halley for scattering angles between 114° and 165° , illustrating that P/Halley's grains were highly variable in albedo, but on the average were about the same as the grains of the comets in panel (a). Panel (d) shows data for Comet West 1975h (data from Ney and Merrill 1976), Crommelin 1983n (datum from Hanner *et al.* 1985b), and all the comets for which new data are reported in this paper with curve 3 from Fig. 5b superimposed for comparison. The side scattering albedo of comet grains generally lies in the range $0.1 \leq A \leq 0.3$, and the grains of individual comets can display a high degree of variability in albedo. To our knowledge, Crommelin is the darkest comet on record.

fluffy aggregates (Hanner *et al.* 1981). The comet data are consistent with the curves for nonspherical particles and fluffy aggregates. These characteristics are also consistent with theoretical results for "fluffy" aggregates (Greenberg 1982, 1986).

Figure 8c shows $A(\theta)$ for P/Halley for scattering angles between 114° and 165° , indicating that P/Halley's grains were highly variable in albedo, but on the average had a side-scattering albedo similar to that of the grains of the comets in Fig. 8a. We were able to observe P/Halley at backscattering angles out to 165° near perihelion passage. Any backscattering increase appeared to be small. P/Halley's dust coma had an average albedo of $A(\theta) \approx 0.20$ at a scattering angle of 130° , making it slightly brighter than the comae of average comets at phase angles from 120° to 165° . This would be expected for an extreme IR Type II comet with a significant small silicate grain component. We note that the lowest side-scattering albedo we observed for P/Halley ($A(\theta) \approx 0.08$) occurred when the $10\text{-}\mu\text{m}$ silicate emission feature was absent. Both of these indicators are consistent with a coma at these times that was populated predominantly by large grains.

Figure 8d shows $A(\theta)$ for Comet West, Comet Crommelin 1983n, and all the comets for which data are reported in this paper. We conclude that the side-scattering albedo of comet grains generally lies in the range $0.1 \leq A \leq 0.3$, but that the grains of individual comets can display a high degree of temporal variability in albedo during an apparition.

Variations in the silicate emission feature and albedo. Variations in several grain composition indicators were observed for P/Halley. Our data (Fig. 3) and additional infrared data obtained by Hanner *et al.* (1987) and Tokunaga *et al.* (1986 and 1988) at the NASA Infrared Telescope Facility (IRTF) show that P/Halley's silicate emission feature was occasionally weak or absent. Although this behavior usually occurred at heliocentric distances greater than 1 AU, there were several occasions when this behavior occurred at small heliocentric distances (e.g., 26.8 January 1986 UT and 14.67 February 1986 UT). Furthermore, our data show that the strength of the $10\text{-}\mu\text{m}$ silicate emission feature varied significantly when P/Halley was inside a heliocentric distance of 1 AU (Fig. 3). Ryan and Campins (1991) reached a similar conclusion based upon a more limited data set.

The disappearance of the silicate signature for distances greater than 1 AU was previously noted for Comet Kohoutek by Rieke *et al.* (1974). Comet Bradfield 1980 XV (Ney 1982a and Tables I–III of this paper) clearly was an IR Type II comet near perihelion (Fig. 2a), but showed no silicate emission beyond $r = 0.6$ AU.

On one occasion when P/Halley's silicate feature was

missing, the dust albedo fell as low as 0.08 (Fig. 8). A similar correlation between silicate signature strength and dust albedo is clearly evident for Comet Bradfield 1980 XV (this paper, Table III) and was noted in Comet Bradfield 1974b by Ney (1974b).

C. The Physics of the Nuclear Ablation Process

Our observations provide information about the nature of the nuclear ablation process by (i) showing that production rate and outflow of grains from the nucleus nominally conforms with the steady-state model, (ii) establishing the amplitude of short-term temporal variations in the activity of the nucleus, and (iii) measuring the mass loss rate of the solid material.

Constraints on models of the production and outflow of coma grains. We made nearly simultaneous observations of P/Halley with several diaphragms on four separate occasions using the O'Brien and WIRO telescopes and obtained multiaperture photometry of Comet Bradfield 1980 XV during a time span of about 1 hr on one occasion from Wyoming. These multiaperture measurements can be interpreted in terms of the steady-state model of nuclear activity described in Appendix B. In this model, grains are released from the nucleus at a constant rate and flow outward from the nucleus at constant velocity. Reitsemä *et al.* (1989), in an elegant study, showed that the visible images of the inner coma of P/Halley by *Giotto* were consistent with the interpretation that the individual active areas on the nucleus behave according to the steady-state model.

Our multidaphragm observations of P/Halley and Comet Bradfield 1980 XV (Fig. 9) show that the coma flux was usually proportional to ϕ and that the steady-state grain production model was valid for times as great as 0.25 days (6 hr) on most occasions. Possible jet-like activity developing rapidly on time scales of a few hours is suggested by our P/Halley observations on 9.83 February 1986 UT, when the average flux recorded in a 20-arcsec beam at O'Brien was less than that expected from the flux recorded in an 8.3-arcsec beam at WIRO. The sudden activation of an intense gas jet, similar to those seen in the *Giotto* images (Keller *et al.* 1986), appears to provide a plausible explanation for the 9.83 February measurements. One set of infrared imaging observations, obtained a few hours prior to the *Giotto* encounter by Hayward *et al.* (1986), tends to confirm the hypothesis that the infrared variations may be profoundly affected by jets releasing material on the sunward side of the nucleus.

Activity in comet nuclei. Figures 7 and 10 summarize the activity of the nuclei of P/Halley and the six other recent bright comets studied in this work as measured by the infrared luminosities of their comae. In Fig. 10, we have included schematic representations of the average

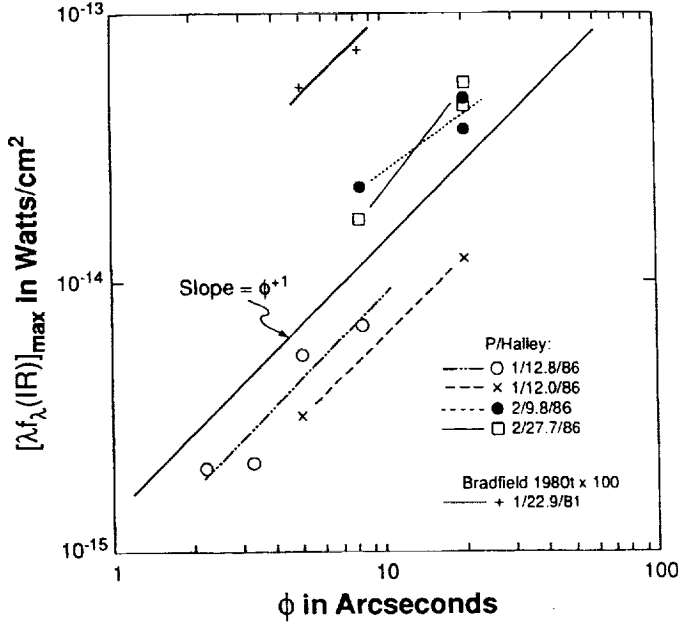


FIG. 9. Coma brightnesses of P/Halley and Bradfield 1980 XV as a function of aperture diameter. The coma model described in Appendix A has been used to correct the data for emission in the reference beam. The data are generally consistent with a constant production rate of grains in a constant velocity outflow (the steady-state model described in Appendix A).

activity of some of the other bright comets we have measured previously (Ney 1982a, Gehrz *et al.* 1989). The activity in most comets is proportional to r^{-4} both preceding and following perihelion passage with small superimposed variations. Comet West 1976 VI (1975h) brightened significantly after perihelion because the nucleus broke into four parts. Encke probably behaves differently than most comets because of an appreciable contribution to the thermal emission by the nucleus itself (Gehrz *et al.* 1989).

The apparent infrared intensity $f_\phi(\text{IR})$ of an optically thin comet coma in a beam of angular diameter ϕ radians that is much smaller than the angular extent of the coma follows from Eqs. (2), (A-4), and (A-6), to be

$$f_\phi(\text{IR}) = 1.3586(\lambda f_\lambda)_{\max} = \left[\frac{\pi a^2 Q_e \sigma T_{\text{obs}}^4}{4V_0} \right] \frac{\phi}{\Delta} \frac{dN}{dt} = \left[\frac{a^2 Q_a L_\odot}{64V_0} \right] \frac{\phi}{r^2 \Delta} \frac{dN}{dt}, \quad (9)$$

where Q_a and Q_e are, respectively, the Planck mean absorption and emission coefficients for the grains as defined by Gilman (1974), where r and Δ are the heliocentric and geocentric distances in centimeters. If the grain production rate as a function of heliocentric distance $dN(r)/dt$ is

directly proportional to the intensity of the solar radiation incident upon the nucleus, then

$$\frac{dN(r)}{dt} = \frac{dN(r_p)}{dt} \left[\frac{r_p}{r} \right]^2, \quad (10)$$

where r_p is the perihelion distance, $dN(r_p)/dt$ is the grain production rate in grains sec^{-1} at perihelion, and r is the heliocentric distance. Combining Eqs. (9) and (10), we find that the apparent coma intensity is

$$f_\phi(\text{IR}) = \left[\frac{a^2 Q_a L_\odot}{64V_0} \right] \frac{\phi}{r^4 \Delta} \frac{dN(r_p)}{dt} \propto \frac{\phi}{r^4 \Delta}. \quad (11)$$

An interesting variation of the relationship expressed by Eq. (11) occurs in the case when the luminosity of the coma is generated by emission from small silicate grains for which the emission efficiency is proportional to the grain radius a (Gilman 1974). In this case, the apparent infrared intensity of the coma is directly proportional to the total mass M_{gr} of the grains,

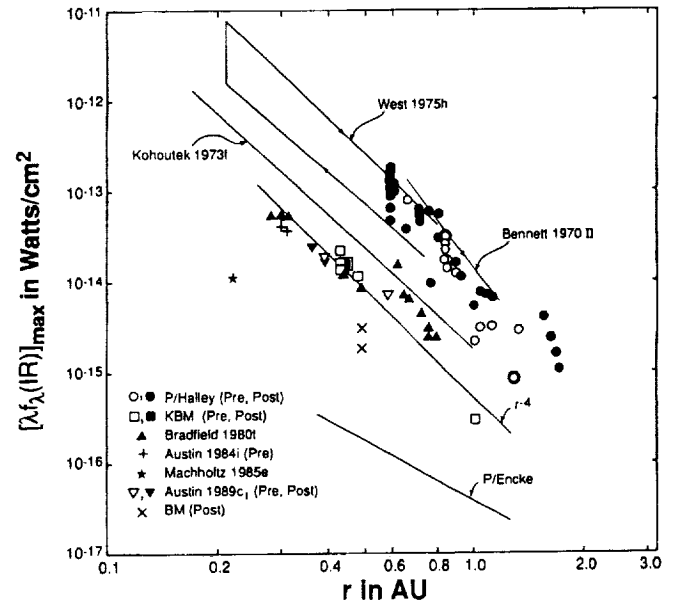


FIG. 10. The infrared activity of the nucleus of P/Halley compared to that of the nuclei of other recent bright comets as a function of heliocentric distance as measured by variations in the quantity $[\lambda f_\lambda(\text{IR})]_{\max}$. The coma model described in Appendix A has been used to correct the data for emission in the reference beam and to normalize the apparent intensities to a geocentric distance of $\Delta = 1$ AU and a beam diameter of 20 arcsec. Comets Bennett 1970 II, Kohoutek 1973f, West 1975h (Ney 1982a), and P/Encke (Gehrz *et al.* 1987) are shown for comparison; the step function in activity for West near perihelion was caused by the breakup of the nucleus. An r^{-4} activity model adequately describes the heliocentric brightening of almost all comets. P/Halley exhibited large variations about the canonical law.

$$f_{\phi}(\text{IR}) \propto \frac{M_{\text{gr}} \phi}{r^4 \Delta}. \quad (12)$$

It is evident from Eq. (11) that the approximation quantified in Eq. (10) for the apparent luminosity of comets implies a dependence of r^{-4} for both the energy absorbed and the energy reemitted. The quantity $(\lambda f_{\lambda})_{\text{max}}$ for the thermal emission is a measure of the energy reradiated and is equal to the energy absorbed. It is a better measure of a comet's intrinsic brightness than short-wavelength reflected light measurements because of the variation in albedo with phase angle.

Both short-term and long-term variations in comet nucleus activity that are superimposed upon the r^{-4} radial dependence can be readily evaluated by examination of the quantity given in column 18 of Table III. This quantity has been normalized using Eqs. (11), (B-1), and (B-2) to give the flux expected in a standard circular 20-arcsec diameter diaphragm for an infinite reference beam throw with the comet at a standard heliocentric distance of $r = 1$ AU and a standard geocentric distance of $\Delta = 1$ AU.

In the comparison with the six other comets observed in this work (Fig. 10), P/Halley (Fig. 7) is seen to exhibit more frequent large-amplitude variations about the r^{-4} brightening law than is usually the case. Overall, we found that P/Halley varied in brightness by a factor of up to 7 on time scales of a few hours and days and by a factor of 10 overall compared to the expected rate of brightening with changing heliocentric distance; its thermal emission was as dim on some occasions as that of Kohoutek 1973f and as bright as that of Comets Bennett 1970 II and West 1975h on others. The large variations of P/Halley are also apparent in the scattered component (Fig. 7).

Our data enable us to draw several conclusions with regard to the activity of the nucleus and coma of P/Halley:

(1) Neither the large short-term variations nor the long-term variations in the bolometric infrared emission from P/Halley appear to correlate in any detail with the visible variations reported by Green and Morris (1987) and Millis and Schleicher (1986). Green and Morris (1987) found that the heliocentric dependence of the integrated visible magnitude of P/Halley's coma varied asymmetrically about perihelion passage, with the comet being significantly brighter postperihelion. Our data show that both the heliocentric dependence of the scattered light (Fig. 7a) and the thermal emission within a 20-arcsec beam were comparable pre- and postperihelion. Both our data and those of Green and Morris show large-amplitude short-term variations, but there is no detailed correlation between the intensity variations seen in our small beam with those exhibited by the entire coma.

(2) Millis and Schleicher (1986) and Schleicher *et al.* (1990) reported visual photometry showing periodic varia-

tions on a time scale of 7.4 days that they attributed to activity associated with the illumination of different regions of the nucleus. Although there is no obvious tight correlation between the variations exhibited in our data and those reported during overlapping periods by Millis and Schleicher (1986), both our data sets appear to be consistent with the inner coma being fainter in visible emission around 20 March 1986 and brighter around March 15, 23, and 25.5. We conclude that our data are consistent with the interpretation that the infrared variations in P/Halley result from rotation of the nucleus, presenting active and passive surfaces to the Sun. Both *Giotto* images (Keller *et al.* 1986) and the groundbased 10- μm infrared images made during the *Giotto* passage by Hayward *et al.* (1986) suggest the presence of localized active jets on P/Halley's nucleus which could account for such behavior.

(3) McFadden *et al.* (1987) and Rettig *et al.* (1987) noted a marked brightening of P/Halley in several visible emission bands during 23–25 March 1986 UT. Our data do not show any conclusive evidence of unusual brightening in either the scattered or the thermal emission from the inner 20 arcsec of the coma at the beginning and end of this period.

Dust mass loss rates of comet nuclei. The dust mass loss rate dM_D/dt caused by the ablation of dN/dt grains sec^{-1} from the comet nucleus, each having density ρ_{gr} and radius a , is

$$\frac{dM_D}{dt} = m_{\text{gr}} \frac{dN}{dt} = \frac{4\pi}{3} \rho_{\text{gr}} a^3 \frac{dN}{dt}, \quad (13)$$

where m_{gr} is the mass of a single grain. Combining Eqs. (9) and (13), we find that

$$\frac{dM_D}{dt} = [1.3586(\lambda f_{\lambda})_{\text{max}}] \frac{256\pi}{3} \frac{a \rho_{\text{gr}}}{L_{\odot} Q_a} V_0 \frac{r^2 \Delta}{\phi}, \quad (14)$$

where V_0 is the grain ejection velocity and $(\lambda f_{\lambda})_{\text{max}}$ is obtained by correcting the intensity given in Table III, column 11, for beam throw effects using Eq. (B-1). Presuming that the grains are accelerated to terminal velocity by momentum coupling to the gas, V_0 is of the order of the sonic velocity in the gas (Finson and Probst 1968) which is given with the aid of Eq. (3) by

$$V_0 = 5 \times 10^4 \left[\frac{T_{\text{bb}}}{278} \right]^{1/2} \\ = \frac{5 \times 10^4}{r_A^{1/4}} \text{ cm sec}^{-1} \approx 0.5 \text{ km sec}^{-1}, \quad (15)$$

where T_{BB} is the blackbody temperature at the heliocentric

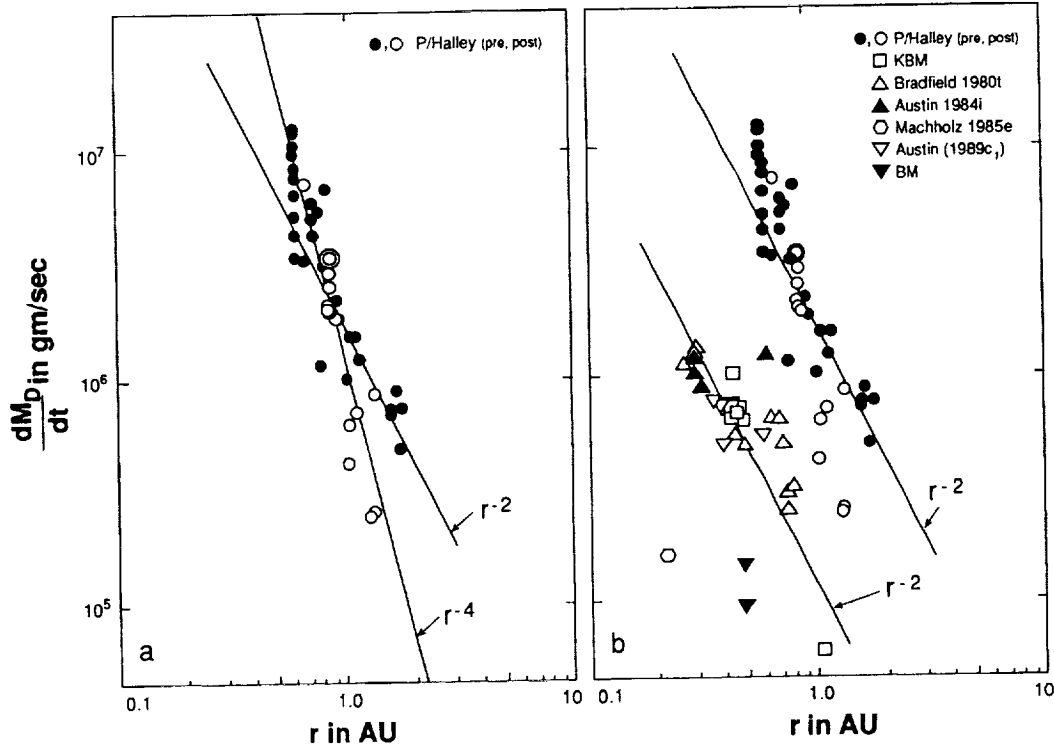


FIG. 11. The dust mass loss rates (normalized to a grain radius of $1 \mu\text{m}$ and a geocentric distance of $\Delta = 1 \text{ AU}$) as a function of heliocentric distance (a) from the nucleus of P/Halley and (b) from the nuclei of the IR Type I comets in this survey. The coma model described in Appendix A has been used to correct the data for emission in the reference beam and to normalize the apparent intensities to a geocentric distance of $\Delta = 1 \text{ AU}$ and a beam diameter of 20 arcsec. P/Halley showed substantial bursts of activity superimposed on the canonical r^{-2} law. The dust mass loss rates of the IR Type I comets shown here may be multiplied by a factor of 10 if it is presumed that their comae are composed primarily of $10 \mu\text{m}$ grains. In this case, their dust mass loss rates are equivalent to the rates inferred for dusty IR Type II comets like P/Halley.

distance r_A in AU of the comet. Given the very weak dependence of V_0 on r , we use the approximation that $V_0 \approx 0.5 \text{ km sec}^{-1}$ in the analysis that follows. We concluded above that the observed superheat S for the IR Type II comets discussed herein suggests a typical grain radius of $a \approx 1 \mu\text{m} = 10^{-4} \text{ cm}$ for the carbon grains responsible for the continuum emission. Typical IDP aggregates have a density of $\leq 1 \text{ g cm}^{-3}$, while pure carbon and silicate grains would have densities of $\approx 2\text{--}3 \text{ g cm}^{-3}$. We conclude that a typical comet grain can be presumed to have a density of $\approx 1 \text{ g cm}^{-3}$ (see also Hanner 1988). Using Eqs. (14) and (15) with $a = 1 \mu\text{m}$, $\rho_{gr} = 1 \text{ g cm}^{-3}$, and $Q_a = 1$, the dust mass loss rate becomes

$$\frac{dM_D}{dt} = 7 \times 10^{21} (\lambda f_\lambda)_{\text{max}} \frac{r_A^2 \Delta_A}{\phi_s} \text{ g sec}^{-1}, \quad (16)$$

where r_A and Δ_A are the heliocentric and geocentric distances in AU, ϕ_s is the beam diameter in arcseconds, and $(\lambda f_\lambda)_{\text{max}}$ is the integrated apparent infrared intensity in watts per square centimeter. We emphasize that the mass

loss rates calculated above refer only to the emission from the optically important particles. Since a considerable amount of the dust mass is in large particles that do not contribute significantly to the infrared emission (see Jewitt 1991), the mass loss rates given by Eq. (16) are lower limits. Sykes and Walker (1992) suggest that the mass loss in large particles may be more than double that estimated by other means.

The observational results for our sample of comets, normalized to a grain radius of $1 \mu\text{m}$, is summarized in Fig. 11, and it is clear from these that the dust mass loss rates for individual comets vary approximately as r_A^{-2} . This heliocentric distance dependency is readily understood by combining Eqs. (11) and (14) to yield:

$$\frac{dM_D}{dt} \propto r_A^{-2}. \quad (17)$$

Applying Eq. (16) to the data for P/Halley, we find that its average mass loss normalized to a heliocentric distance of 1 AU is $\geq 10^6 \text{ g sec}^{-1}$. P/Halley's mass loss rate varied

about this mean value by up to a factor of 7 on short time scales (Fig. 11a). For the remaining comets in this study (all IR Type I), Eq. (16) gives a mean loss rate that is a factor of ≈ 10 lower than that for P/Halley (see Fig. 11b). If it is assumed that the IR Type I comets have grains as large as $10 \mu\text{m}$, their mass loss rates would be increased by a factor of 10 and would become comparable to the mass loss rate deduced for P/Halley.

IV. CONCLUSIONS

The 0.7- to $23\text{-}\mu\text{m}$ observations reported in this paper for P/Halley and six other bright comets lead to several conclusions about the nature of comet grains and the physics of comet nuclear activity.

(1) Comets can be classified by their thermal infrared energy distributions. IR Type I comets have low continuum superheat and the $10\text{-}\mu\text{m}$ silicate emission is muted or absent. IR Type II comets have large continuum superheat and strong silicate emission features. The differences may be due to grain size.

(2) Simultaneous measurements of P/Halley and Bradfield 1980 XV with different diaphragms using telescopes in Minnesota and Wyoming are generally consistent with the steady-state model for nuclear ablation.

(3) P/Halley's dust coma had an average albedo of 0.20 at a scattering angle of 130° . Our data show that the scattering phase function for typical comet dust is characterized by a moderately strong forward-scattering peak, no appreciable backscattering peak beyond angles of 150° , a mean bolometric albedo of ≈ 0.32 , and a sidescattering albedo of ≈ 0.15 .

(4) The correlation between superheat and $10\text{-}\mu\text{m}$ silicate excess, the flattened forward-scattering peak of the albedo curve, and the relatively low backscattering albedo are all consistent with laboratory and theoretical results for nonspherical and fluffy grains. These results appear to be especially consistent with core-mantle grain models such as have been proposed by J. M. Greenberg and his collaborators (Greenberg and Hage 1989, Hage and Greenberg 1989).

(5) P/Halley's $10\text{-}\mu\text{m}$ silicate signature showed significant variations in strength and was occasionally weak or absent at heliocentric distances both smaller and larger than 1 AU.

(6) P/Halley's coma luminosity fluctuated by a factor of nearly 10 on time scales of 1 to 2 days. These variations are consistent with the jet-like activity associated with nuclear rotation.

(7) The mass loss rate for P/Halley was highly variable and averaged $\geq 10^6 \text{ g sec}^{-1}$ at $r = 1 \text{ AU}$. The mass loss rates for the IR Type I comets would be comparable to that deduced for P/Halley if it is assumed that their comae are composed of grains of radius $a \approx 10 \mu\text{m}$.

APPENDIX A: THE STEADY-STATE MODEL FOR INFRARED EMISSION FROM COMA DUST GRAINS

In the so-called "steady-state" model of nuclear activity (see Jewitt 1991), the thermal emission from the coma results from dust grains ablated from the nucleus at a constant rate of dN/dt grains sec^{-1} and flowing away from the nucleus at a constant velocity V_0 . Assuming that the coma is optically thin to thermal infrared radiation (see Ney 1982b, Jewitt 1991), the contribution to the apparent infrared intensity of the coma $f(\text{IR})$ by N dust grains is given by

$$f(\text{IR})_{\text{IR}} = \frac{L_{\text{IR}}}{4\pi\Delta^2} = \frac{N4\pi a^2 Q_c \sigma T_{\text{obs}}^4}{4\pi\Delta^2} = \frac{Na^2 Q_c \sigma T_{\text{obs}}^4}{\Delta^2}, \quad (\text{A-1})$$

where L_{IR} is the coma luminosity, a is the grain radius, Q_c is the Planck mean emission cross section of the grain (Gilman 1974), σ is the Stefan-Boltzmann constant, T_{obs} is the grain temperature, and Δ is the geocentric distance. Assuming that the dust grain distribution is isotropic, the total number of grains in a spherically symmetric coma within a radius r of the nucleus is given by

$$N = 4\pi \int_0^r n(r)r^2 dr = \frac{dN}{dt} t = \frac{dN}{dt} \frac{r}{V_0}, \quad (\text{A-2})$$

where $t = r/V_0$ is the time required for grains to flow out to radius r at constant velocity V_0 , and $n(r)$ is the radial number density distribution of grains in the coma. Our multiaperture measurements typically occurred when Δ was between 1 and 1.5 AU, so that the residence time of grains with $V_0 = 0.5 \text{ km sec}^{-1}$ in the beams we used was between 0.6 hr (2.2-arcsec beam) and 6 hr (20-arcsec beam). By inspection of Eq. (A-2), it follows that the steady-state model leads to a radial grain density distribution in the coma of

$$n(r) = \frac{1}{4\pi r^2 V_0} \frac{dN}{dt}. \quad (\text{A-3})$$

Integrating this density distribution over the cylindrical volume V of the coma that is intercepted by a photometer beam of angular diameter ϕ to obtain the number N_ϕ of grains emitted into the beam, and substituting the result into Eq. (A-1), we find that the apparent infrared intensity $f_\phi(\text{IR})$ measured in the beam is

$$\begin{aligned} f_\phi(\text{IR}) &= \frac{a^2 Q_c \sigma T_{\text{obs}}^4}{\Delta^2} N_\phi \\ &= \frac{a^2 Q_c \sigma T_{\text{obs}}^4}{\Delta^2} \int \int_V n(r) d^3r = \left[\frac{\pi a^2 Q_c \sigma T_{\text{obs}}^4}{4V_0} \right] \frac{\phi}{\Delta} \frac{dN}{dt}, \end{aligned} \quad (\text{A-4})$$

where the result on the extreme right-hand side is for the case where the angular diameter of the beam is much smaller than the angular diameter of the coma. It can be seen from Eq. (A-2) that $f_\phi(\text{IR}) \propto \phi\Delta^{-1}$, leading to the correction terms specified in Eqs. (B-1) and (B-2) that we derive in Appendix B.

The determination of $f_\phi(\text{IR})$ is particularly straightforward when the continuum emission from the dust approximates that of a blackbody as is the case with all the comets observed here. In this case, the ratio of the maximum of the λF_λ function to the total blackbody emission F is given by

TABLE C-I
Orbital Elements for the Comets

COMET	KBM 1975 IX	Bradfield 1980 XV	Austin 1984 XIII	Machholz 1985 VIII	Austin 1989c ₁	BM 1989X	P/Halley 1986 III
EQUINOX	1950.0	1950.0	1950.0	1950.0	J2000.0	J2000.0	J2000.0
EPOCH	5 Sep 25	80 Dec 27	84 Aug 8	-	90 Apr 19	89 Oct 1	86 Feb 19
T	75 Sep 5.3348	80 Dec 29.5417	84 Aug 12.1371	85 Jun 28.7388	90 Apr 9.96745	89 Sep 11.9384	86 Feb 9.4590
q	0.425561	0.259823	0.291284	0.106252	0.349775	0.478742	0.587104
e	1.000095	0.999725	0.999846	1.000000	1.000225	0.971959	0.967277
p	-	-	-	-	-	-	76.00
PERI (ω)	116.9756	358.2855	353.12701	274.0831	61.5763	129.6111	111.8657
NODE (Ω)	295.6526	114.6465	170.87724	194.7292	75.9255	311.5878	58.8601
INCL (i)	80.7779	138.5882	164.15979	16.2827	58.95639	19.3357	162.2422

$$\frac{(\lambda F_\lambda)_{\max}}{F} = \frac{2\pi hc^2}{\sigma(\lambda_m T)^4} \left[\frac{1}{e^{hc/k(\lambda_m T)} - 1} \right] = \frac{1}{1.3586}, \quad (\text{A-5})$$

$$\frac{f_1}{f_2} = \frac{\phi_1 \Delta_2}{\phi_2 \Delta_1}. \quad (\text{B-2})$$

where λ_m is the wavelength of maximum emission in λF_λ , $\lambda_m T = 0.3670$ cm deg is Wien's law for λF_λ , $h = 6.6262 \times 10^{-27}$ erg sec, $c = 2.9979 \times 10^{10}$ cm sec $^{-1}$, $\sigma = 5.6696 \times 10^{-5}$ erg cm $^{-2}$ deg $^{-4}$ sec $^{-1}$ and $k = 1.3806 \times 10^{-16}$ erg deg $^{-1}$. Thus, the apparent infrared intensity $f_\phi(\text{IR})$ of the coma is given by

$$f_\phi(\text{IR}) = 1.3586(\lambda F_\lambda)_{\max}, \quad (\text{A-6})$$

where $(\lambda F_\lambda)_{\max}$ is the observed apparent emission maximum of the infrared continuum.

APPENDIX B: CORRECTIONS FOR BEAM DIAMETER, THROW, AND GEOCENTRIC DISTANCE

Comet comae are extended sources of infrared emission and are large enough so that coma emission is present in the reference beam used for background cancellation. The total emission into a beam of a given angular diameter depends upon the volume of coma material intercepted by the beam. Therefore, analysis and interpretation of the infrared photometry require correction of the data for the effects of beam diameter, reference beam throw, and geocentric distance. The correction is straightforward for comets that obey a steady-state model where the coma is produced by material ablated from the nucleus at a constant rate and flowing away from the nucleus at a constant velocity. We describe this model quantitatively in Appendix A, concluding that it leads to a ϕ^{+1} dependence for the flux from the coma, where ϕ is the radius of the coma, and a Δ^{-1} dependence of the coma brightness on geocentric distance. In this case, the apparent intensity f_∞ that would be measured in a beam of angular diameter ϕ for a throw large enough so that the reference beam falls off the coma and the apparent intensity f_ϕ observed in the same beam with a throw of angular diameter ψ such that the reference beam falls on the coma are related by

$$\frac{f_\infty}{f_\psi} = \frac{4\psi}{4\psi - \phi}. \quad (\text{B-1})$$

Furthermore, the apparent intensities, f_1 and f_2 measured in two different apertures with diameters ϕ_1 and ϕ_2 with the comet at geocentric distances of Δ_1 and Δ_2 , respectively, will be related by

These correction factors have been applied where appropriate in the analysis above using a standard reference beam diameter of $\phi_1 = 20$ arcsec and a standard geocentric distance of $\Delta_1 = 1$ AU.

APPENDIX C: ORBITAL ELEMENTS FOR THE COMETS OBSERVED

We present in Table C-I the orbital elements we used for deriving the orbital parameters of the comets for which we report infrared observations here. These have been gleaned from the *Catalog of Cometary Orbits* (Marsden 1982) and The Central Bureau for Astronomical Telegrams (Marsden 1992). The data tabulated by row are (1) the comet name, (2) the equinox for Ω , ω , and the orbital inclination (i), (3) the osculation date in decimal days (Universal, or Ephemeris, Time), (4) the perihelion time (Ephemeris Time), (5) the perihelion distance q in astronomical units, (6) the orbital eccentricity, (7) the revolution period in years (no entry signifies $p > 1000$ years), (8) the argument of perihelion ω in decimal degrees, (9) the longitude of the ascending node Ω in decimal degrees, and (10) the orbital inclination i in decimal degrees.

ACKNOWLEDGMENTS

We are especially grateful to D. Hufmann for giving freely of his time to discuss with us the characteristics of the phase function of comet dust particles; his comments weighed heavily in the framing of our conclusions. M. S. Hanner helpfully provided us with her insightful lecture notes on defining albedos for small particles, and T. J. Jones gave us guidance on the definition of albedos. T. W. Jones confirmed the conversion factors between square and circular apertures for an r^{-1} surface brightness distribution. We thank B. Jones for a critical reading of the manuscript and for suggesting several improvements in the presentation. T. Williams, L. R. Shaw, T. Hayward, C. Jaworosky, and L. Chisholm assisted with the observations at WIRO. Hayward's contributions were especially valuable and included a crucial last-minute repair of the photometer at WIRO during the remote observations of P/Halley on perihelion day. He also obtained the 15.79 April 1990 UT observation of Comet Austin 1989c, for us at WIRO. A. Knutson provided invaluable assistance with observations at O'Brien Observatory. We thank T. J. Jones for obtaining the 27.3 and 28.3 April 1986 UT observations of P/Halley at MLOF for us. Finally, A. Tokunaga and A. Storrs, who

refereed the manuscript, made several useful suggestions that improved the clarity of the presentation. This research was supported by NASA, the National Science Foundation, the U.S. Air Force, and the University of Minnesota Institute of Technology Dean's Office and Graduate School, and the University of Wyoming.

REFERENCES

- BECKLIN, E. E., AND J. A. WESTPHAL 1966. Infrared observations of comet 1965f. *Astrophys. J.* **145**, 445–453.
- BOHREN, C. F., AND D. R. HUFMANN 1983. *Absorption and Scattering of Light by Small Particles*, pp. 399–401. Wiley, New York.
- BREGER, M., R. D. GEHRZ, AND J. A. HACKWELL 1981. Interstellar grain size. II. Infrared photometry and polarization in Orion. *Astrophys. J.* **248**, 963–976.
- BROOKE, T. Y., R. F. KNACKE, AND R. R. JOYCE 1986. Near-infrared studies of comet Halley: polarization and color. In *Exploration of Halley's Comet*, ESA SP-250, pp. 87–89. European Space Agency, Noordwijk.
- BROOKE, T. Y., R. F. KNACKE, T. C. OWEN, AND A. T. TOKUNAGA 1988. Spectroscopy of emission features near 3 μm in comet Wilson (1986I), submitted for publication.
- BROOKE, T. Y., A. T. TOKUNAGA, AND R. F. KNACKE 1991. Detection of the 3.4 μm emission feature in comets P/Brorson–Metcalf and Okazaki–Levy–Rudenko (1989R) and an observational summary. *Astron. J.* **101**, 268–278.
- BROWNEE, D. E. 1987. A comparison of Halley dust with meteorites, interplanetary dust, and interstellar grains. In *Observations of Comets Halley and Wilson and Properties of the Grains*, (M. S. Hanner, Ed.), NASA Conference Publ. 3004, pp. 66–67.
- BROWNEE, D. E., L. PILACHOWSKI, E. OLSZEWSKI, AND P. W. HODGE 1980. Analysis of interplanetary dust collections. In *Solid Particles in the Solar System* (I. Halliday and B. A. McIntosh, Eds.), pp. 333–342. Reidel, Dordrecht.
- CASTELAZ, M. W., J. A. HACKWELL, G. L. GRASDALEN, R. D. GEHRZ, AND C. GULLIXSON 1985. GSS 30: an infrared reflection nebula in the Ophiuchus dark cloud. *Astrophys. J.* **290**, 261–272.
- EATON, N. 1984. Comet dust—Applications of Mie scattering. *Vistas Astron.* **27**, 111–129.
- FINSON, M. L., AND R. F. PROBSTEN 1968. A theory of dust comets: I. Model and equations and II. Results for Comet Arend–Roland. *Astrophys. J.* **154**, 327.
- FRAUNDORF, P., D. E. BROWNEE, AND R. M. WALKER 1982. Laboratory studies of interplanetary dust. In *Comets*, (L. Wilkening, Ed.), pp. 323–340. Univ. of Arizona Press, Tucson.
- GEHRZ, R. D., AND J. A. HACKWELL 1978. Exploring the infrared universe from Wyoming. *Sky Telescope* **55**, 466–473.
- GEHRZ, R. D., AND E. P. NEY 1986. Infrared temporal development of P/Halley. In *Exploration of Halley's Comet*, ESA SP-250, pp. 101–105. European Space Agency, Noordwijk.
- GEHRZ, R. D., G. L. GRASDALEN, AND J. A. HACKWELL 1987. Infrared astronomy. In *Encyclopedia of Physical Science and Technology*, Vol. 2, pp. 53–80. Academic Press, New York.
- GEHRZ, R. D., J. A. HACKWELL, AND T. W. JONES 1974. Infrared observations of Be stars from 2.3 to 19.5 microns. *Astrophys. J.* **191**, 675–684.
- GEHRZ, R. D., E. P. NEY, J. PISCATELLI, E. ROSENTHAL, AND A. T. TOKUNAGA 1989. Infrared photometry and spectroscopy of Comet P/Encke 1987. *Icarus* **80**, 280–288.
- GILMAN, R. C. 1974. Planck mean cross-sections for four grain materials. *Astrophys. J. Suppl. Ser.* **28**, 397–403.
- GREEN, D. W. E., AND C. S. MORRIS 1987. The visual brightness behavior of P/Halley during 1981–1987. *Astron. Astrophys.* **187**, 560–568.
- GREENBERG, J. M. 1982. In *Comets* (L. L. Wilkening, Ed.), pp. 131–163. Univ. of Arizona Press, Tucson.
- GREENBERG, J. M. 1986. Predicting that comet Halley is dark. *Nature* **321**, 385.
- GREENBERG, J. M., AND J. I. HAGE 1990. From interstellar dust to comets: A unification of observational constraints. *Astrophys. J.* **361**, 260–274.
- HAGE, J. I., AND J. M. GREENBERG 1990. A model for the optical properties of porous grains. *Astrophys. J.* **361**, 251–259.
- HANNER, M. S. 1988. Grain optical properties. In *Observations of Comets Halley and Wilson and Properties of the Grains* (M. S. Hanner, Ed.), pp. 22–49. NASA Conference Publ. 3004.
- HANNER, M. S., R. H. GIESE, K. WEISS, AND R. ZERULL 1981. On the definition of albedo and application to irregular particles. *Astron. Astrophys.* **104**, 42–46.
- HANNER, M. S., D. K. AITKEN, R. KNACKE, S. MCCORKLE, P. F. ROCHE, AND A. T. TOKUNAGA 1985a. Infrared spectrophotometry of Comet IRAS–Araki–Alcock (1983d): A bare nucleus revealed? *Icarus* **62**, 97–109.
- HANNER, M. S., R. KNACKE, Z. SEKANINA, AND A. T. TOKUNAGA 1985b. Dark grains in Comet Crommelin. *Astron. Astrophys.* **152**, 177–181.
- HANNER, M. S., E. TEDESCO, A. T. TOKUNAGA, G. J. VEEDER, D. F. LESTER, F. C. WITTEBORN, J. D. BREGMAN, J. GRADIE, AND L. LEBOSKY 1985c. The dust coma of periodic Comet Churyumov–Gerasimenko (1982 VIII). *Icarus* **64**, 11–19.
- HANNER, M. S., A. T. TOKUNAGA, W. F. GOLISCH, D. M. GRIEP, AND C. D. KAMINSKI 1987. Infrared emission from P/Halley's dust coma during March 1986. *Astron. Astrophys.* **187**, 653–660.
- HANNER, M. S., R. L. NEWBURN, R. D. GEHRZ, A. T. HARRISON, AND E. P. NEY 1990. The infrared spectrum of comet Bradfield (1987s) and the silicate emission feature. *Astrophys. J.* **348**, 312–321.
- HAYWARD, T., R. D. GEHRZ, AND G. L. GRASDALEN 1986. Ground-based infrared observations of comet Halley. *Nature* **326**, 55–57.
- JEWITT, D. 1991. Cometary photometry. In *Comets in the Post-Halley Era* (R. L. Newburn, Jr., M. Neugebauer, and J. Rahe, Eds.), Vol. 1, pp. 19–64. Kluwer, Dordrecht.
- JEWITT, D., AND K. J. MEECH 1986. Cometary grain scattering versus wavelength, or, "What color is comet dust?" *Astrophys. J.* **310**, 937–952.
- KELLER, H. U., *et al.* 1986. First Halley multicolor camera imaging results from Giotto. *Nature* **321**, 320–326.
- KISSEL, J., *et al.* 1986. Composition of comet Halley dust particles from Giotto observations. *Nature* **321**, 336–337.
- MAAS, R. W., E. P. NEY, AND N. J. WOOLF 1970. The 10 micron emission peak of comet Bennett 1969i. *Astrophys. J.* **160**, L101–L104.
- MARSDEN, B. G. 1982. *Catalog of Cometary Orbits*, 4th ed. Minor Planet Center, Smithsonian Astrophysical Observatory, Cambridge, MA.
- MARSDEN, B. G. 1992. *IAU Circulars, e-mail service*.
- MCDONNELL, J. A. M., *et al.* 1987. The dust distribution within the inner coma of comet P/Halley 1982i: Encounter by Giotto's impact detectors. *Astron. Astrophys.* **187**, 719–741.
- MCDONNELL, J. A. M., P. L. LAMY, AND G. S. PANKIEWICZ 1991. Physical properties of cometary dust. In *Comets in the Post-Halley Era* (R. L. Newburn, Jr., M. Neugebauer, and J. Rahe, Eds.), Vol. 2, pp. 1043–1073. Kluwer, Dordrecht.
- McFADDEN, L. A., M. F. A'HEARN, P. D. FELDMAN, E. E. ROETTGER, D. M. EDSALL, AND P. S. BUTTERWORTH 1987. Activity of Comet

- P/Halley 23–25 March, 1986: IUE observations. *Astron. Astrophys.* **187**, 333–338.
- MILLIS, R. L., AND D. G. SCHLEICHER 1986. Rotational period of comet Halley. *Nature* **324**, 646–649.
- NEY, E. P. 1974a. Infrared observations of comet Kohoutek near perihelion. *Astrophys. J.* **189**, L141–L143.
- NEY, E. P. 1974b. Multiband photometry of comets Kohoutek, Bennett, Bradfield, and Encke. *Icarus* **23**, 551–560.
- NEY, E. P. 1977. Star Dust. *Science* **195**, 541–546.
- NEY, E. P. 1982a. Optical and infrared observations of bright comets in the range 0.5 μm to 20 μm . In *Comets* (L. Wilkening, Ed.), pp. 323–340. Univ. of Arizona Press, Tucson.
- NEY, E. P. 1982b. Visibility of comet nuclei. *Science* **215**, 397–398.
- NEY, E. P., AND K. M. MERRILL 1976. Comet West and the scattering function of cometary dust. *Science* **194**, 1051–1053.
- REITSEMA, H. J., W. A. DELAMERE, A. R. WILLIAMS, D. C. BOICE, W. F. HUEBNER, AND F. L. WHIPPLE 1989. Dust distribution in the inner coma of Comet Halley: Comparison with models. *Icarus* **81**, 31–40 (see also the cover illustration of *Planetary Rep.* **VII**(5), Sept./Oct. 1987).
- RETTIG, T. W., J. R. KERN, R. RUCHTI, B. BAUMBAUGH, A. E. BAUMBAUGH, K. L. KNICKERBOCKER, AND J. DAWE 1987. Observations of the coma of Comet P/Halley and the outburst of 1986 March 24–25 (UT). *Astron. Astrophys.* **187**, 249–255.
- RIEKE, G. H., F. J. LOW, T. A. LEE, AND W. W. WISNIEWSKI 1974. Infrared observations of comet Kohoutek. In *Comet Kohoutek*, NASA-SP 355, pp. 175–182. NASA, Washington DC.
- ROSE, L. A. 1979. Laboratory simulation of infrared astrophysical features. *Astrophys. Space Sci.* **65**, 47–67.
- RYAN, E. V., AND H. CAMPINS 1991. Comet Halley: Spatial and temporal variability of the silicate emission feature. *Astron. J.* **101**, 695–705.
- SCHLEICHER, D. G., R. L. MILLIS, D. T. THOMPSON, P. V. BIRCH, R. MARTIN, D. J. THOLEN, J. R. PISCITELLI, N. L. LARK, AND H. B. HAMMEL 1990. Periodic variations in the activity of comet P/Halley during the 1985/1986 apparition. *Astron. J.* **100**, 896–912.
- SEKANINA, Z. 1974a. On the nature of the anti-tail of Comet Kohoutek (1973f) I. a working model. *Icarus* **23**, 502–518.
- SEKANINA, Z. 1974b. The prediction of anomalous tails of comets. *Sky Telescope* **47**, 374–377.
- SEKANINA, Z. 1976. In *The Study of Comets* (B. Donn, M. Mumma, W. Jackson, M. A'Hearn, and R. Harrington, Eds.), NASA SP-393, pp. 893–933. U.S. G.P.O., Washington, D.C.
- SYKES, M. V., L. A. LEBOSKY, D. M. HUNTEN, AND F. LOW 1986. The discovery of dust trails in the orbits of periodic comets. *Science* **232**, 1115–1117.
- SYKES, M. V., AND R. G. WALKER 1992. Cometary dust trails. *Icarus* **95**, 180–210.
- TELESCO, C. M., R. DECHER, C. BAUGHER, H. CAMPINS, D. MOZURKEWICH, H. A. THRONSON, D. P. CRUIKSHANK, H. B. HAMEL, S. LARSON, AND Z. SEKANINA 1986. Thermal-infrared and visual imaging of comet Giacobini-Zinner. *Astrophys. J.* **310**, L61–L65.
- TEMI, P., P. DE BERNARDS, S. MASI, G. MORENO, AND A. SALAMA 1989. Infrared emission from interplanetary dust. *Astrophys. J.* **337**, 528–535.
- TOKUNAGA, A. T., W. F. GOLISCH, D. M. GRIEP, C. D. KAMINSKI, AND M. S. HANNER 1986. The NASA Infrared Telescope Facility comet Halley monitoring program. I. Preperihelion results. *Astron. J.* **92**, 1183–1190.
- TOKUNAGA, A. T., W. F. GOLISCH, D. M. GRIEP, C. D. KAMINSKI, AND M. S. HANNER 1988. The NASA Infrared Telescope Facility comet Halley monitoring program. II. Postperihelion results. *Astron. J.* **96**, 1971–1976.
- VAN DE HULST, H. C. 1957. *Light Scattering by Small Particles*, pp. 183 and 449. Dover, New York.
- WALKER, R. M. 1987. Comparison of laboratory determined properties of interplanetary dust with those of comet Halley particles: What are comets made of? In *Infrared Observations of Comets Halley and Wilson and Properties of the Grains* (M. Hanner, Ed.), NASA Conference Publ. 3004, pp. 53–63.
- WEAVER, H. A., M. F. A'HEARN, P. D. FELDMAN, C. ARPIGNY, W. A. BAUM, J. C. BRANDT, R. M. LIGHT, AND J. A. WESTPHAL 1992. Inner coma imaging of Comet Levy (1990C) with the Hubble Space Telescope. *Icarus*, in press.
- WEBB, C. G. 1935. The scattering of light by drops in a Wilson chamber. *Philos. Mag.* **19**, 927–933.
- WILSON, J. G. 1951. *The Principles of Cloud-Chamber Technique*, p. 59. Cambridge Univ. Press, Cambridge.
- WOOLF, N. J., AND E. P. NEY 1969. Circumstellar emission from cool stars. *Astrophys. J.* **155**, L181–L184.

THE INFRARED SPECTRUM OF COMET BRADFIELD (1987s) AND THE SILICATE EMISSION FEATURE

M. S. HANNER¹ AND R. L. NEWBURN¹
 Jet Propulsion Laboratory

R. D. GEHRZ, T. HARRISON, AND E. P. NEY
 Astronomy Department, School of Physics and Astronomy, University of Minnesota

AND

T. L. HAYWARD
 Wyoming Infrared Observatory, Department of Physics and Astronomy, University of Wyoming
 Received 1989 March 13; accepted 1989 July 1

ABSTRACT

Infrared (1–20 μm) observations of comet Bradfield (1987s) from three observatories are reported. Silicate emission is prominent in all the data, from heliocentric distance $r = 0.87$ to 1.45 AU. A CVF spectrum at $r = 1.45$ AU shows a peak at 11.3 μm identified as crystalline olivine; the spectral shape is similar to that in Halley. Dust optical properties are similar to those of the grains in Halley's jets. Dust production rate near perihelion was $\sim 10^6 \text{ g s}^{-1}$ and varied $\propto r^{-2}$. We suggest that some differences in grain properties among comets could result from differences in the thermal history of the nuclear surface and the relative fraction of the dust particles originating in the subsurface icy layer versus the devolatilized mantle.

Subject headings: comets — infrared: spectra — interstellar: grains

I. INTRODUCTION

Comets almost certainly contain interstellar grains in some form. The extent to which the grains have been altered since their existence in the interstellar medium has to be inferred from the properties of the comet grains. For example, the outer few meters of comet nuclei must have been heavily processed by cosmic rays in the Oort cloud. Two key spectral features were discovered in comet Halley—a possible signature of processed organic material near 3.4 μm (Combes *et al.* 1986, 1988; Baas, Geballe, and Walther 1986; Danks *et al.* 1987; Knacke, Brooke, and Joyce 1986; Wickramasinghe and Allen 1986) and a peak in the silicate emission feature at 11.3 μm identified with crystalline olivine (Bregman *et al.* 1987; Campins and Ryan 1989). Both are puzzling because they differ from the corresponding spectral features arising from interstellar grains. Now one wishes to know whether the grains in other comets are similar to those in Halley and whether differences in grain properties among comets can provide clues to their processing history.

Comet Bradfield (1987s) is a long-period comet, but certainly not a dynamically new comet. It was discovered at $r = 1.7$ AU and reached perihelion on 1987 November 7 at $r = 0.87$ AU. The comet exhibited a visual light curve nearly symmetric about perihelion. With a 34° inclination and eccentricity of 0.995, the orbit is fairly stable, and the comet probably had a similar perihelion distance last time (D. K. Yeomans, private communication). In this paper we report our infrared observations of Bradfield from 1987 September to 1988 January, compare the dust optical properties with the dust in Halley, and discuss the nature of the silicate grains.

II. OBSERVATIONS

Infrared observations of the dust coma were obtained at three observatories: the 3 m NASA Infrared Telescope Facility (IRTF), Mauna Kea; the 2.34 m Wyoming Infrared Observatory telescope (WIRO), and the University of Minnesota's O'Brien Observatory 0.76 m telescope (UM). A journal of the observations is given in Table 1, and the observed magnitudes are presented in Table 2. Because of the comet's southern declination and the small angular distance from the Sun, all of the 1987 observations were done at large air mass; thus, extinction is the main source of error.

The UM and WIRO observations used broad-band optical/infrared photometers constructed at the University of Minnesota (Ney 1974; Gehrz, Hackwell, and Jones 1974; Gehrz, Grasdalen, and Hackwell 1987). The same photometer at UM was used for extensive observations of comet Halley (Gehrz and Ney 1986). The UM photometer employs filters centered at 8.5, 10.6, and 12.5 μm , with $\lambda/\Delta\lambda \simeq 10$, while the Minnesota photometer at WIRO contains the set of six intermediate bandpass silicate filters from OCLI, identical to the set in use at the IRTF (Tokunaga *et al.* 1986). Vega (α Lyr) was used to calibrate the October 21 measurements at WIRO, and β Peg was the calibrator for all of the other UM data. The magnitudes of β Peg are shown in Table 3. Beta Peg is apparently variable at the 5%–10% level (Tokunaga *et al.* 1986). The values in Table 3 are consistent with our measurement of β Peg versus α Lyr at the IRTF on 1987 July 19. Mean extinction coefficients were applied in reducing the data.

The WIRO measurements were obtained with a new telephone observing link enabling us to control the computer-operated WIRO telescope remotely from the University of Minnesota (see Gehrz and Hackwell 1978). Data and control functions are transmitted by two 2400 baud telephone lines. A third telephone line provides voice communication with the WIRO technical staff.

¹ Visiting Astronomer, Infrared Telescope Facility, operated by the University of Hawaii under contract from the National Aeronautics and Space Administration.

TABLE 1
COMET BRADFIELD (1987s): JOURNAL OF OBSERVATIONS

Date UT	r^a (AU)	Δ^b (AU)	ϵ^c (deg)	Θ^d (deg)	Telescope	Beam Diameter (arcsec)	Throw (arcsec)	Sky Quality	Observations
1987 Sep 21.2	1.21	1.45	55	43	3 m IRTF	6.8	20	Cirrus	8.7–12.5 μm
Oct 21.1	0.92	1.24	48	52	2.3 m WIRO	5	20	Clear	1–18 μm
Oct 22.0	0.92	1.23	48	53	2.3 m WIRO	3	60	Clear	8–12 μm images
Nov 7.0	0.87	1.07	50	60	0.8 m UM	20	30	Cirrus	8.5–12.5 μm
Nov 9.0	0.87	1.05	50	61	0.8 m UM	20	30	Clear	1–18 μm
Nov 13.0	0.88	1.01	52	63	0.8 m UM	20	30	Clear	1.6–18 μm
Nov 18.0	0.89	0.96	54	64	0.8 m UM	20	30	Clear	1–18 μm
Nov 19.0	0.90	0.95	55	64	0.8 m UM	20	30	Clear	1–18 μm
Dec 4.0	1.00	0.85	65	64	0.8 m UM	20	30	Poor	4.8–18 μm
1988 Jan 12.15	1.44	1.08	88	43	3 m IRTF	6.8	20	Clear/day	4.8–20 μm
Jan 13.25	1.45	1.10	88	43	3 m IRTF	7.1	20	Clear	10 μm CVF
Jan 14.15	1.46	1.11	88	42	3 m IRTF	Var. ^e	20	Clear/day	1.2–3.8 μm

^a Heliocentric distance.

^b Geocentric distance.

^c Sun-Earth-comet angle.

^d Sun-comet-Earth angle.

^e J, H: 7"6; K: 7"4; L: 6"1; L': 5"8.

Bradfield was observed at the IRTF using the facility InSb (1–3.8 μm) and bolometer (4.8–20 μm) systems. On September 21 the comet was observed at air mass 2.0–2.6 shortly after sunset, while in 1988 January it was observed before sunset near the zenith. Extinction was determined at each wavelength each night by following standard stars over a range in air mass. Magnitudes of the 4.8–20 μm standard stars are given in Table 3. The magnitudes of α Boo and β And at 7.8 and 12.5 μm have been measured relative to α Lyr on one or more nights; the estimated uncertainties are 3%–5%. SJ 9503 was the standard at 1.2–3.8 μm (Elias *et al.* 1982). The aperture diameters listed in Table 1 are the full width at half-maximum obtained by scanning the telescope across a bright star. The field lens in the InSb photometer causes the effective aperture size to decrease with wavelength; the FWHM is 7"6 at J and H, 7"4 at K, 6"1 at L, and 5"8 arcsec at L' (Tokunaga *et al.* 1988).

There will be a small contribution from the comet's outer coma at the position of the reference ("sky") beam. For spherically symmetric radial outflow of dust, the coma brightness in the reference beam will be $I_0(\phi/4\alpha)$, where ϕ = aperture diameter, α = chopping throw, and I_0 = true brightness centered on the comet. The true brightness is therefore approximately $1.06 I_{\text{obs}}$ for the WIRO data, $1.10 I_{\text{obs}}$ for the IRTF data, and $1.20 I_{\text{obs}}$ for the UM data, and, to first order, is independent of wavelength. The magnitudes in Table 2 are given without correction.

Comet observations through the broad, L, L', M, N, and Q filters require a temperature-dependent correction to account for the difference in spectral shape between the radiation from the warm comet dust and the hot standard stars. Corrections of -0.05 and -0.04 mag have been applied to the N and Q magnitudes, respectively (Hanner *et al.* 1984). The corrections for the L and M bandpasses are negligible compared to the observational uncertainties. Because the L bandpass contains both scattered and thermal radiation, the correction is model-dependent. No correction has been applied to our L magnitudes in Table 2. A more detailed discussion of photometric systems is given by Hanner and Tokunaga (1989).

The infrared fluxes are plotted in Figures 1 and 2. The solid curves are dust models discussed in § IV. Excess emission attributed to small silicate grains is present near 10 and 18 μm

in all of the data sets. The color temperature of the underlying continuum between 8 and 12.5 μm is about 15% higher than that of a blackbody in equilibrium with the incident solar flux,

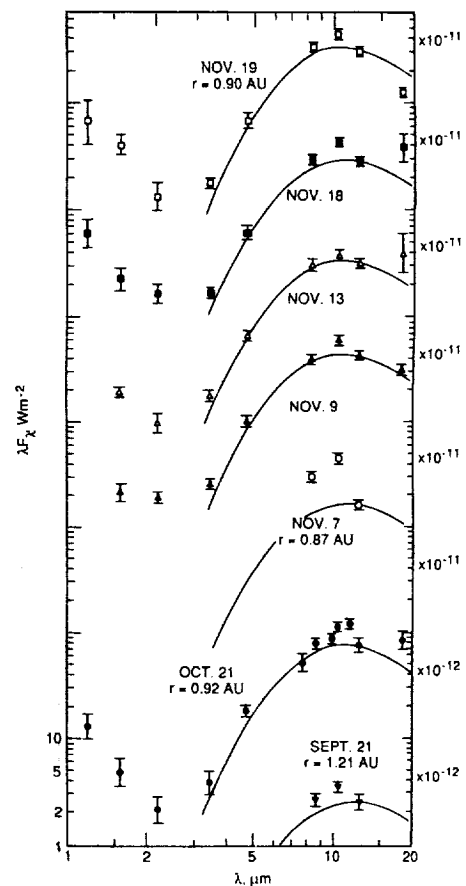


FIG. 1.—Observed spectral energy distribution of comet Bradfield (1987s) in 1987. Data sets are offset by a factor of 10. Solid curves are the predicted continuum emission from dust model 1 (§ IV), normalized to the 12.5 μm flux.

TABLE 2
PHOTOMETRIC OBSERVATIONS OF COMET BRADFIELD (1987s)

Wavelength (μm)	1987 Sep 21.2 ^a IRTF ^b 7 ^c $r = 1.21^d$	1987 Oct 21.06 WIRO 5 $r = 0.87$	1987 Nov 7.0 UM 20 $r = 0.87$	1987 Nov 9.0 UM 20 $r = 0.87$	1987 Nov 13.0 UM 20 $r = 0.88$	1987 Nov 18.0 UM 20 $r = 0.89$	1987 Nov 19.0 UM 20 $r = 0.90$	1987 Dec 4.0 UM 20 $r = 1.00$	1988 Jan 12.15 IRTF 7 $r = 1.44$	1988 Jan 14.15 IRTF ^e $r = 1.46$
J	1.2	8.72 \pm 0.26	...	6.30 \pm 0.20	...	7.04 \pm 0.33	6.93 \pm 0.50	10.79 \pm 0.02
H	1.6	9.00 \pm 0.34	...	7.37 \pm 0.20	...	7.32 \pm 0.25	6.67 \pm 0.20	10.34 \pm 0.02
K	2.2	9.08 \pm 0.31	...	6.71 \pm 0.11	7.42 \pm 0.20	6.86 \pm 0.20	7.11 \pm 0.33	10.24 \pm 0.02
L	3.5	6.99 \pm 0.26	...	4.95 \pm 0.10	5.35 \pm 0.11	5.42 \pm 0.10	5.34 \pm 0.11	9.57 \pm 0.03
L	3.8	9.19 \pm 0.03
M	4.7	4.36 \pm 0.14	...	2.51 \pm 0.10	2.97 \pm 0.10	3.04 \pm 0.11	2.92 \pm 0.17	3.65 \pm 0.25	6.86 \pm 0.03	...
N	10.1	0.30 \pm 0.05	1.66 \pm 0.02	...
	7.8	1.69 \pm 0.21	3.43 \pm 0.05	...
	8.5	-0.73 \pm 0.10	-0.47 \pm 0.10	-0.41 \pm 0.10	-0.54 \pm 0.10	-0.82 \pm 0.25	2.42 \pm 0.02	...
	8.7	0.90 \pm 0.05	1.63 \pm 0.02	...
	9.8	0.40 \pm 0.05	1.48 \pm 0.03	...
	10.3	-0.03 \pm 0.05
	10.6	-1.93 \pm 0.10	-1.43 \pm 0.10	-1.55 \pm 0.10	-1.58 \pm 0.10	-1.80 \pm 0.10
	11.6	-0.47 \pm 0.10	1.06 \pm 0.03	...
	12.5	-0.14 \pm 0.10	...	-1.04 \pm 0.10	-1.73 \pm 0.10	-1.61 \pm 0.10	-1.70 \pm 0.10	-1.42 \pm 0.10	1.23 \pm 0.07	...
	18.1	-0.26 \pm 0.06	...
	185	-1.6 \pm 0.15	...	-2.97 \pm 0.15	-3.20 \pm 0.45	-3.19 \pm 0.34	-1.97 \pm 0.15
Q	20.0	-0.44 \pm 0.03	...

^a UT date.

^b System.

^c Beam diameter in arcseconds.

^d r in AU.

^e Beam diameter = J, H: 7".6; K: 7".4; L: 6".1; L: 5".8.

TABLE 3
STANDARD STAR MAGNITUDES

Star	Spectral Type	M 4.8 μm	7.8	8.7	9.8	N 10.1	10.3	11.6	12.5	18.1	Q 20.0	System
5340 α Boo	K2 III	-2.92 ^a	-3.08 ^b	-3.17 ^b	-3.17	-3.17 ^c	-3.17	-3.26	-3.26 ^b	-3.13	-3.13 ^c	IRTF
337 β And	MO III	-1.76 ^a	-1.95 ^b	-1.97	-2.03	-2.04 ^c	-2.04	-2.10	-2.10 ^b	-2.09	-2.09 ^c	IRTF
6406 α Her	M5 II		-3.64 ^b	-3.83	-3.97	-3.94 ^c	-4.02	-4.13	-4.20 ^b			WIRO
8775 β Peg	M2 II	-2.30 ^d		-2.46 ^d		-2.51 ^d			-2.59 ^d	-2.61 ^c		UM

^a Sinton and Tittermore 1984.

^b Uncertainty $\geq \pm 0.03$ mag.

^c Tokunaga 1984.

^d Gehrz *et al.* 1987.

implying that the emission arises mainly from small absorbing grains.

On January 13, a 2% circular variable filter was used with the IRTF Si:As photoconductor to obtain a 16 point spectrum of Bradfield between 7.8 and 12.8 μm . Spectra of the comet were alternated with spectra of β And at air mass 1.0–1.8, and α Tau and α CMa were observed after the comet set. Extinction was determined separately for each of the 16 wavelengths from the three β And spectra. Each individual measurement was reduced to unit air mass before conversion to absolute flux. A high-resolution spectrum of the telluric ozone band at 9.58 μm was used for wavelength calibration.

Bradfield was imaged in the 7–14 μm spectral region on 1987 October 22 UT using a prism array spectrometer with a 3"0 beam and a 60" reference throw. The spectrometer, described by Gehrz, Hackwell, and Smith (1976), was mounted at the Cassegrain focus of the Wyoming infrared telescope. The flux is simultaneously recorded in six channels, centered at 7.92, 8.45, 9.45, 10.69, 11.54, and 12.70 μm . The image was constructed by scanning the chopping secondary in declination at a rate of 7 arcsec s^{-1} , sampling at 1" (chopping frequency is 7 Hz), then stepping the telescope 1" in R.A. and repeating. Four successive images were obtained; the mean air mass was 1.67. Calibration star was α Her, located just 20° from the comet.

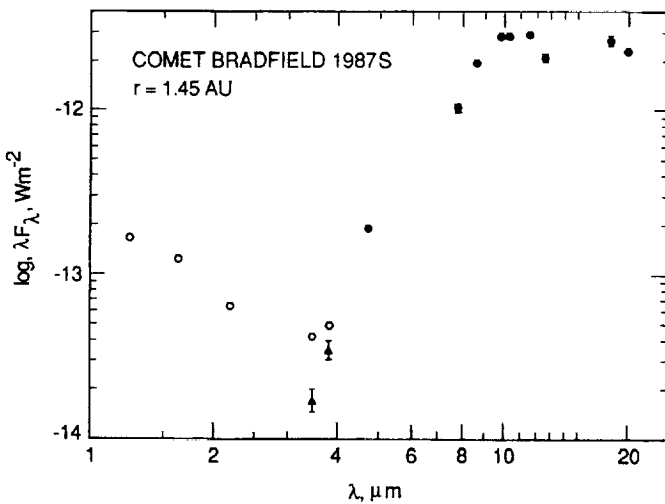


FIG. 2.—Spectral energy distribution of comet Bradfield on Jan 12 (●) and Jan 14 (○) 1988. The InSb data (○) have been scaled to the 6.8 arcsec bolometer beam size assuming flux $\propto \phi$. The triangles are the thermal emission component obtained by subtracting scattered light flux assuming solar spectrum from 2.2 to 3.8 μm .

III. THE SILICATE FEATURE

The CVF spectrum obtained on January 13 is shown in Figure 3. The uncertainty in the absolute flux level is $\sim 10\%$. The filter photometry from the previous night is also plotted in the figure, at the effective wavelengths determined by convolving each filter function with the spectral shape from the CVF spectrum and the sky. The agreement between the filter photometry and the spectrum demonstrates that careful filter photometry can accurately measure the strength of the silicate feature, although of course not its detailed shape. The agreement in the absolute flux levels indicates that the comet did not change its dust output from January 12 to 13.

To compare the shape of the emission feature with other sources, the CVF spectrum was divided by the continuum defined by the dust models in Figure 5. This procedure is physically correct if the silicate grains are at the temperature implied by the continuum. Since the Planck function from 8 to 13 μm is fairly flat in the relevant temperature range, this normalization is unlikely to distort the shape of the silicate feature. Our three Bradfield spectra were individually divided by the continuum normalized to 12.81 μm .

The average of the three normalized spectra and the standard deviations are presented in Figure 4a. Two peaks are apparent, one at 9.7–10.0 μm , similar to the interstellar feature, and one near 11.24 μm . This spectrum is remarkably similar to that of comet Halley at smaller r (Bregman *et al.* 1987; Campins and Ryan 1989), as illustrated in Figure 4b. Bregman *et al.* and Campins and Ryan identify the peak at 11.3 μm with

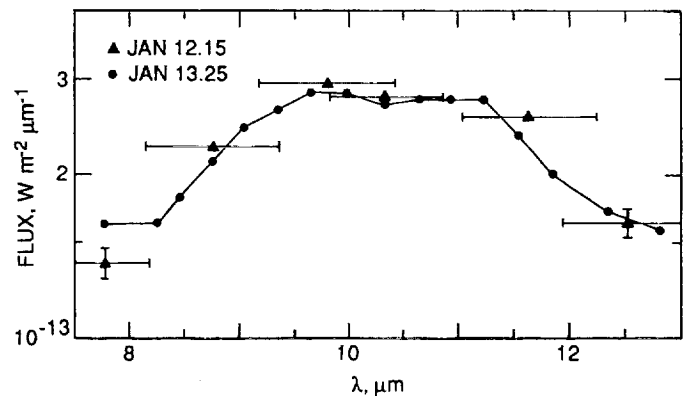


FIG. 3.—CVF spectrum of the dust coma on 1988 Jan 13, (●) compared with filter photometry on January 12 (▲). Horizontal bars are the filter band-passes convolved with comet spectrum (FWHM).

crystalline olivine. Our spectrum, although the spectral resolution is poorer, indicates the presence of crystalline olivine in Bradfield at 1.45 AU. A higher resolution spectrum of Bradfield at $r = 1.0$ AU, recorded by Russell, Lynch, and Chatelain (1988) clearly shows this peak as well.

Other possible explanations for the peak at $11.3 \mu\text{m}$, such as SiC or PAHs, can be ruled out from the width of the peak, on abundance arguments, or for lack of corresponding features, such as the $8.6 \mu\text{m}$ feature present when an $11.3 \mu\text{m}$ peak is associated with the set of unidentified interstellar infrared bands (Campins and Ryan 1989).

While emission by small crystalline olivine particles matches the $10.5\text{--}12.5 \mu\text{m}$ portion of the spectrum well (see discussion in Campins and Ryan), other silicates are required to account for the peak near $10 \mu\text{m}$ and the steep rise from 8 to $9 \mu\text{m}$. There are three main possibilities.

1. *Mix of crystalline silicate minerals.*—Chondritic interplanetary dust particles (IDPs) examined by Sandford and Walker (1985) fall into three distinct classes based on their $10 \mu\text{m}$ transmission spectra, corresponding to olivines, pyroxenes,

and hydrated silicates. Bregman *et al.* fitted their Halley spectrum with a mixture of these three IDP spectral types—primarily olivine for the $11.3 \mu\text{m}$ peak and pyroxenes to fit the $9\text{--}10 \mu\text{m}$ peak. This approach has the advantage of relating the comet dust directly to the IDPs thought to originate in comets. The disadvantage is that we do not know the history of the IDPs—whether all chondritic IDPs are cometary and whether they could have annealed during their years in the inner solar system or during atmospheric entry.

2. *Partially annealed grains.*—Interstellar silicate grains are thought to be amorphous, because no structure is apparent in the silicate feature. From the laboratory emission spectra recorded by Stephens and Russell (1979), amorphous olivine can explain the broad peak near $10 \mu\text{m}$ in both the cometary and interstellar spectra while amorphous enstatite particles can account for the steep rise from 8 to $9 \mu\text{m}$. The comet grains could have a wide range in their degree of structural order, as a result of partial annealing via heating in the solar nebula. Day (1974) showed that the $11.3 \mu\text{m}$ peak first appeared in the spectrum of an amorphous olivine sample when heated to ~ 800 K, although long-range structural order did not develop until the grains were heated to ~ 1000 K. Small crystalline silicate grains have a higher mass absorption coefficient than amorphous grains, by a factor of 3 to 10 (Day 1981). Thus, only a small fraction by mass of crystalline olivine grains could give rise to the observed $11.3 \mu\text{m}$ peak. Moreover, Aitken *et al.* (1988) have now found evidence for annealed olivine grains in at least one interstellar source.

Partial crystallinity could also explain why no distinct peaks are seen shortward of $22 \mu\text{m}$ in the $16\text{--}30 \mu\text{m}$ spectrum of Halley published by Herter, Campins, and Gull (1987), for narrow peaks will show up in the $10 \mu\text{m}$ stretching mode vibrations for a lesser degree of structural order than required to produce peaks in the $20 \mu\text{m}$ bending mode vibration (cf. Hanner 1987).

3. *Hydrated silicates.*—Hydrated silicates dominate the composition of type I carbonaceous chondrites; they are the result of low-temperature aqueous alteration. Type II carbonaceous chondrites have about equal proportions of hydrated silicates and olivine; in fact, their spectra look quite similar to the comet Halley and Bradfield spectra, with a small $11.3 \mu\text{m}$

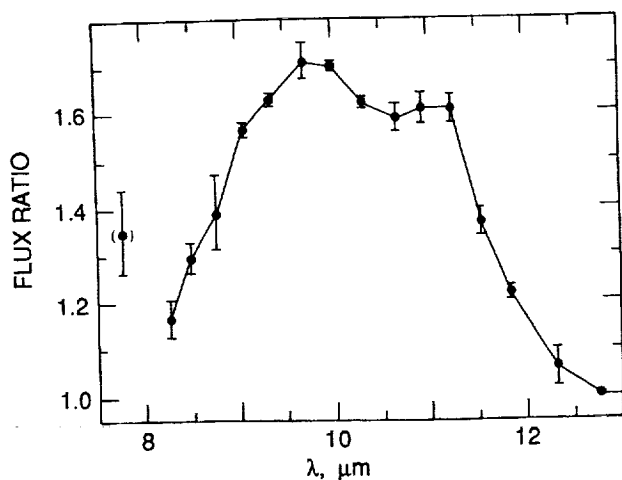


FIG. 4a

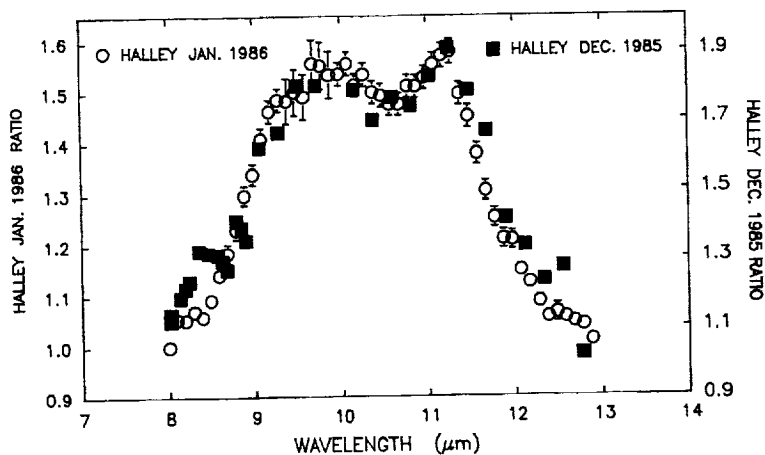


FIG. 4b

FIG. 4.—(a) Spectrum of Bradfield (1987s) divided by the continuum and normalized at $12.81 \mu\text{m}$. Error bars are the standard deviations from the mean of the three spectra. (b) $8\text{--}13 \mu\text{m}$ spectra of comet Halley: observed flux divided by continuum. ■ Bregman *et al.* (1987) $r = 1.25$ AU; ○ Campins and Ryan (1989) $r = 0.79$ AU. Figure courtesy of H. Campins.

peak (Zaikowski, Knacke, and Porco 1975). Based on their experiments on the formation of hydrated silicates, Nelson, Nuth, and Donn (1987) suggest that amorphous silicate grains residing on the surface of a comet nucleus could absorb one or more monolayers of water molecules from the outflowing gas and could be converted to hydrated silicates if exposed to temperatures of 300 K or above for a few weeks.

Lawler *et al.* (1988) compared the heterogeneity in the Mg/Fe/Si abundances in the dust grains sampled by the PIA and PUMA experiments on the Halley probes with various classes of meteorites and IDPs. They concluded that only the anhydrous chondritic aggregate IDPs match the Mg-rich silicates and the very wide range in Fe/Si seen in Halley samples; i.e., that there is no positive evidence for the mineralogy of hydrated silicates in the Halley particles. However, PIA and PUMA sampled only the smallest (most numerous) grains with masses $\sim 10^{-16}$ – 10^{-12} g. Whether these grains are representative of the larger grains, which contain most of the mass, is unknown.

Based on present data, then, there is not a unique interpretation of the state of cometary silicates. The three possibilities listed here have, of course, different implications for the evolutionary history of silicate grains since their existence in the interstellar medium. The possibility that the grains are only partially annealed requires the least departure from the interstellar grains. Indeed, with the discovery of annealed grains in astronomical sources, further processing of interstellar silicates may not be required at all. However, annealing of grains after leaving the comet is then required to explain the state of the IDPs.

It would be very helpful to have high-resolution spectra of the silicate feature in comets at $r \sim 0.3$ AU, where the temperature of small grains will be greater than 500 K and one might expect to see further evidence of annealing. It is ironic that the sole spectrum of Kohoutek at $r = 0.31$ AU suffered a data outage from 10.3 to 11 μm (Merrill 1974). However, the smooth slope in the data from 11.1 to 12 μm indicates that an olivine peak was not present. Campins and Ryan showed that their Halley spectrum was very similar in shape to the Kohoutek spectrum except for the 11.3 μm peak. They concluded that thermal processing alone cannot account for the difference between comets; rather, some diversity in the initial cometary material is likely.

IV. DUST PRODUCTION RATE

The rate of dust-mass loss from the nucleus can be estimated from the thermal emission, within the uncertainties discussed below. We have modeled the continuum emission, based on the temperatures for small absorbing grains from Hanner (1983). The temperature is a strong function of size for absorbing grains $\lesssim 2 \mu\text{m}$ in radius; larger grains have a temperature close to that appropriate for a blackbody in equilibrium with the solar radiation. Two slightly different size distribution functions were applied. The first one, described by Hanner (1984) and Hanner *et al.* (1985) has been used to compute dust production rates in several short-period comets. The second model adopts the analytical form proposed by Divine and Newburn (1987) to fit the dust impact data from the *Giotto* Halley probe (McDonnell *et al.* 1987). Both functions have $n(a) \propto a^{-N}$ at large a , with $N = 3.7$ and 3.8, respectively, and both have a free parameter to adjust the peak in the size distribution, in order to match the observed spectral energy distribution. Model 2 has more (hot) submicron grains. The

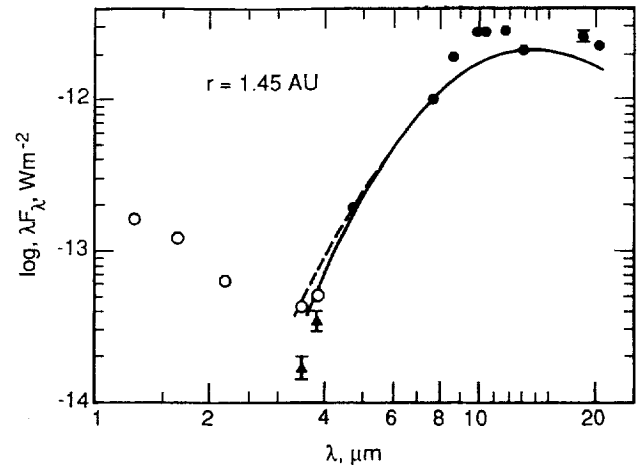


FIG. 5.—Thermal emission on 1988 Jan 12 fitted with models of the continuum emission. Solid line: $n(a) = (1 - a_0/a)^M (a_0/a)^N$, with $a_0 = 0.1 \mu\text{m}$, $M = 14$, $N = 3.7$ (model 1); dashed line: Divine and Newburn (1987) mass distribution function, $\alpha = 0.94$, $\beta = 0.19$, $\gamma = 1.0$, $m_i = 7.5 \times 10^{-12}$ g (model 2).

parameter values giving the best fit to Bradfield at 1.44 AU also gave the best match to Halley at 0.9 AU (Hanner *et al.* 1987).

Figure 5 shows the predicted thermal emission fit to the January 12 data. At 10 μm , approximately 75% of the flux is produced by grains with $a > 1 \mu\text{m}$, while at 4.8 μm , the grains with $a < 1 \mu\text{m}$ contribute 75% of the flux. The corresponding size distributions in the coma are shown in Figure 6, plotted as cumulative number versus particle mass. For $m \geq 10^{-10}$ g, $N(m) \propto m^{-\alpha}$, where $\alpha = (N - 1)/3$. For our models, $\alpha < 1$, and the mass is concentrated toward the large particles. Thus, the total mass in the field of view depends upon the unknown abundance of large particles, which contribute only a small fraction of the 3–20 μm thermal emission. The dust impact detector on *Giotto* measured a high concentration of large particles ($m > 10^{-6}$ g), above the extrapolated slope in Figure 6 (McDonnell *et al.* 1987, 1989). The radar echo from Halley also implied the presence of centimeter-size or larger debris (Campbell, Harmon, and Shapiro 1989). Because of their low

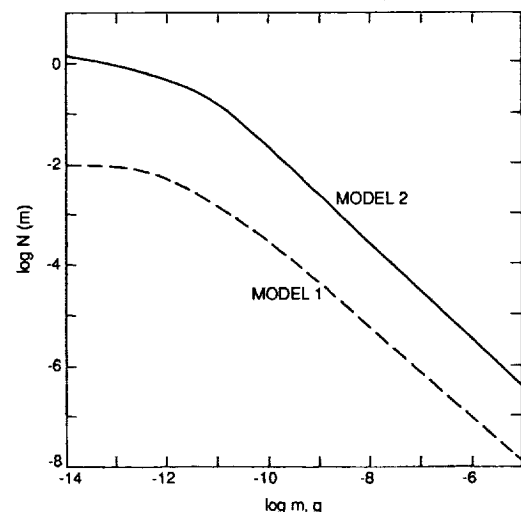


FIG. 6.—Cumulative mass distribution functions fitting the thermal emission on January 12. Solid curve: model 2; dashed curve: model 1.

velocity, however, a high concentration of large dust grains in the coma does not necessarily imply that they dominate the mass flux from the nucleus. One interpretation of the *Giotto* data is that the larger grains were the remnant of an earlier outburst. The predicted continuum based on these dust models, normalized to the 12.5 μm flux, is shown for the other data sets in Figure 1.

To obtain the mass-loss rate, we compute the weighted mean velocity,

$$\bar{v} = \frac{\int a^3 n(a) v(a) da}{\int a^3 n(a) da} \quad (1)$$

following Hanner (1984). For Bradfield at $r = 1.44$ AU, we used the dust velocities, $v(a)$, from Gombosi (1987). These were computed for Tempel 2 at $r = 1.48$ AU from a time-dependent dusty gas dynamical model (Gombosi, Cravens, and Nagy 1985). For other dates, the gas flux per unit surface area was assumed to vary in direct proportion to the total dust production rate, and the velocities were scaled via the relationship shown in Hanner (1984), Figure 4, resulting in a distance dependence, $\bar{v} \propto r^{-1}$. At large particle sizes, $v(a) \propto a^{-0.5}$; thus $\alpha \approx 1.1$ for the mass distribution leaving the nucleus, and the mass is concentrated toward small grains, near the "knee" in the cumulative mass distribution.

Table 4 presents the computed dust production rates, integrated up to a maximum grain radius of 1 cm. The uncertainty in these numbers is at least a factor of 2, due to the uncertainties in velocities, mean grain density (we assumed $\rho = 1 \text{ g cm}^{-3}$), observed flux, and the abundance of large grains. Models 1 and 2 differed by $\sim 20\%$. If Bradfield has an excess of large particles compared to our assumed $n(a)$, the Q_d computed here could be a lower limit. The method of scaling the velocities accentuates the fluctuations in Q_d . If we had assumed a constant mean velocity for October 21–November 19 ($r = 0.87\text{--}0.93$ AU); i.e., if higher Q_d implied a larger active surface area, rather than a higher gas and dust flux per unit area, then Q_d on October 21 and November 9 would be $\sim 1.5 \times 10^6 \text{ g s}^{-1}$. A production rate of $\sim 10^6 \text{ g s}^{-1}$ implies an active area of $\sim 10 \text{ km}^2$, assuming a dust/gas mass ratio of 0.5 and a gas flux of $2 \times 10^{-5} \text{ g cm}^{-2} \text{ s}^{-1}$. This gives a lower limit of 1.3 km radius for a spherical nucleus if the entire sunward hemisphere were active.

D. G. Schleicher and R. L. Millis (private communication) derived an OH production rate of $\sim 2.5 \times 10^{28} \text{ s}^{-1}$ on 1988 January 14 and 15. Our dust production rate on January 12–13 was $4 \times 10^5 \text{ g s}^{-1}$. Thus, the dust/water mass ratio was ~ 0.5

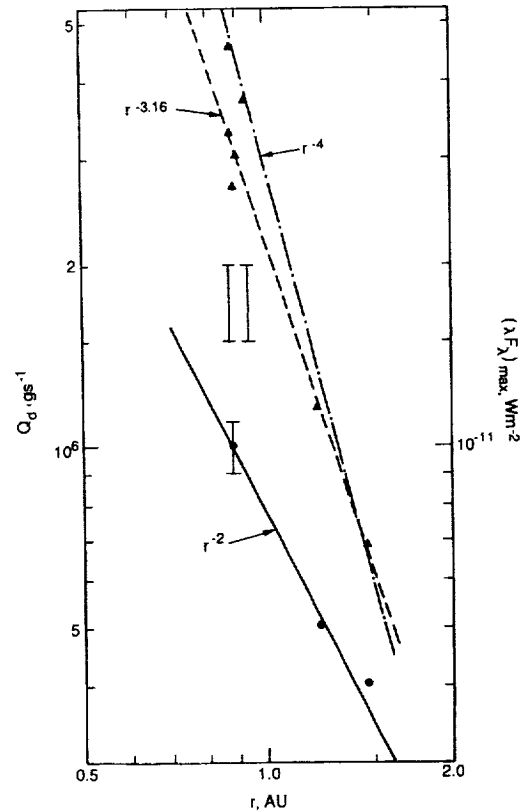


FIG. 7.—Dust production rate, Q_d , (●) and $(\lambda F_\lambda)_{\text{max}}$ (▲) vs. heliocentric distance. The $(\lambda F_\lambda)_{\text{max}}$ have been normalized to 1 AU and to $20''$ beam, assuming isotropic radial outflow. The bar from 1.5 to $2 \times 10^6 \text{ g s}^{-1}$ refers to Q_d on Oct. 21 and Nov. 9, while the bar on the point at 10^6 g s^{-1} displays the range in computed values from Nov. 7 to Dec. 4.

and the total rate of mass loss for comet Bradfield at $r = 1.45$ AU was $\geq 10^6 \text{ g s}^{-1}$.

In contrast, comet Halley was losing $\sim 2 \times 10^6 \text{ g s}^{-1}$ of small dust grains at 1.5–1.3 AU preperihelion and $\sim 10^7 \text{ g s}^{-1}$ at 0.9 AU pre- and post-perihelion, based on similar dust models (Tokunaga *et al.* 1986; Hanner *et al.* 1987). The fluctuations of a factor 1.5–2 in comet Bradfield's dust production near perihelion indicate nonuniform activity across the nuclear surface, either due to outbursts from pockets of more volatile material or to different active areas rotating into sunlight.

The dust production rates and the quantity $\Delta(\lambda F_\lambda)_{\text{max}}$, which is proportional to the total infrared luminosity (Ney 1982), are plotted versus r in Figure 7. Excluding the two outbursts, Q_d varied approximately as r^{-2} , similar to the new comets Kohoutek (1973 XII) and West (1976 VI) (Ney 1982), but much less steeply than in the case of some short-period comets, such as P/Churyumov-Gerasimenko (Hanner *et al.* 1985). This suggests that the sublimating ice layer is closer to the surface in the new comets and Bradfield and is responding more directly to the incident solar energy than is the case for the more evolved short-period comets.

The infrared luminosity is related to the temperature of the radiating grains and the total number of grains within the field of view by the following equation:

$$L = 4\pi \int a^2 n(a) Q_{\text{abs}} \sigma T^4(a, r) da, \quad (2)$$

TABLE 4
DUST PRODUCTION RATES

Date	$Q_d (\text{g s}^{-1})$
Sep 21.2	5×10^5
Oct 21.0	2×10^6 ^a
Nov 7.0	1×10^6
Nov 9.0	2×10^6 ^a
Nov 13.0	1×10^6
Nov 18.0	1×10^6
Nov 19.0	1×10^6
Dec 4.0	1×10^6
Jan 12.15	4×10^5
Jan 13.2	4×10^5

^a $1.5 \times 10^6 \text{ g s}^{-1}$ if \bar{v} remains constant.

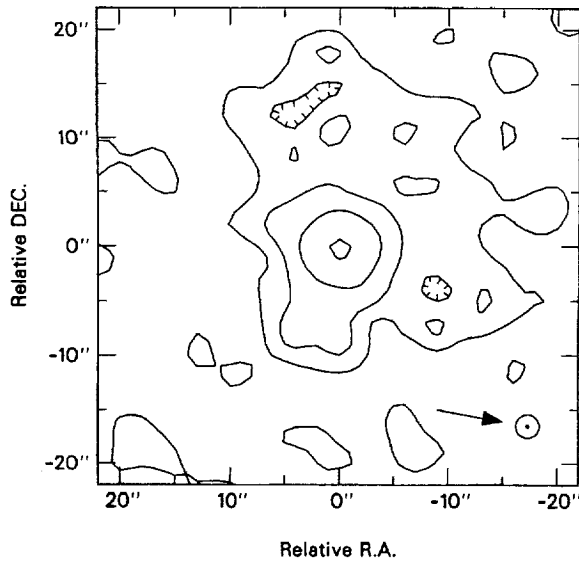


FIG. 8.—Image of the inner dust coma on 1987 October 22. This composite 8.5–11.5 μm image was created by co-adding the fluxes from four spectral channels and four successive images. Beam diameter is 3".0 and reference throw is 60". The sunward direction is indicated. The contour levels are at 0.2, 0.4, and 0.8 and 1.6 Jy per square arcsec.

where Q_{abs} is the appropriate wavelength-averaged absorption efficiency for a grain of radius a . Since the grain temperature $T(a, r) \propto r^{-1/2}$ (if the grains are not too small), then, $T^4 \propto r^{-2}$ and, for constant outflow velocity, $Q_d \propto r^{-2}$ would give $(\lambda F_\lambda)_{\text{max}} \propto L \propto r^{-4}$. However, in our case, if $\bar{v} \propto r^{-1}$, then the number of grains in the field of view varies as $Q_d/\bar{v} \propto r^{-1}$, and $(\lambda F_\lambda)_{\text{max}} \propto r^{-3}$, close to the $r^{-3.16}$ slope shown in Figure 7.

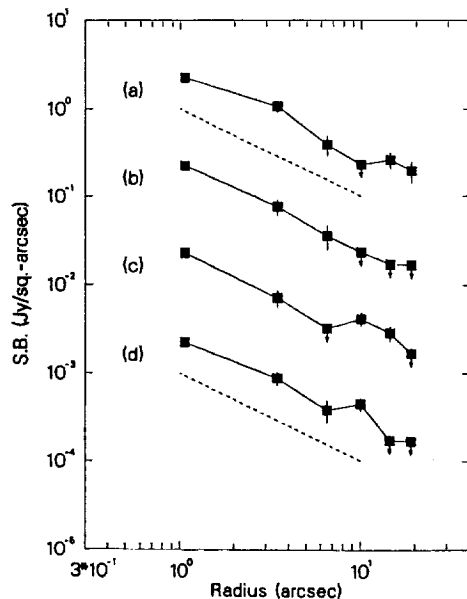


FIG. 9.—Radial brightness gradients as measured from the co-added map. The four curves are at position angles (degrees east of north): (a) 260°, the direction to the Sun; (b) 80° (anti-sunward); (c) 350°; (d) 170°. The first point of each curve is the mean surface brightness within the 3×3 pixel centered on the nucleus. The remaining points are the mean surface brightnesses within arcs 60° wide, with the outward radii of successive arcs at 5", 8", 12", 17", and 21" from the nucleus. Dashed line is $1/d$ dependence.

V. 10 MICRON IMAGE

Figure 8 displays a composite image of the inner coma on October 22.0, created by summing channels 2–5 (8.45–11.54 μm), then summing the four images obtained. The beam-switching technique described in Grasdaen *et al.* (1984) was used to subtract the background. There is evidence for a fan-shaped coma in the sunward hemisphere, consistent with the main dust emission occurring from the illuminated side of the nucleus. Dust emission may also be occurring toward the south. The radial gradients in the sunward, anti-sunward, and perpendicular directions are compared in Figure 9. Within the uncertainties the brightness gradient approximates the $1/d$ decrease expected for uniform radial outflow.

A silicate feature was present at all positions within $\sim 12''$ of the center; the signal/noise ratio is not sufficient to detect differences in the shape of the feature. Figure 10 presents the spectrum centered on the brightness peak, at 13" south, and integrated over the inner 19 square arcsec.

VI. DUST ALBEDO

Since the total cross section of the dust in the field of view can be derived from the dust model fitting the thermal emission, the average near-infrared albedo of the grains can be computed. We define $A_p(\theta)$ as the ratio of the scattered flux at phase angle θ to that scattered by a white Lambert disk with the same geometric cross section; i.e., $A_p(\theta)$ is the geometric albedo times the normalized phase function (Hanner *et al.* 1981). Assuming that the amount of dust in the field of view did not change from the previous two nights, we find $A_p(\theta) = 0.043$ at J and 0.057 at K on January 14, at phase angle 42° . The albedos at K computed for the other data sets are similar within the $\pm 20\%$ observational uncertainties. The albedos at J

Comet Bradfield 22.0 October 1987

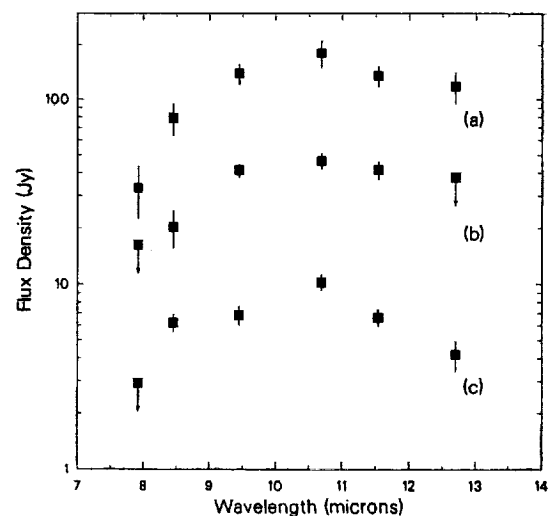


FIG. 10.—Spectra taken with the six-channel spectrometer. The top spectrum (a) was measured from the six images with a 19" square centered on the nucleus. Spectra (b) and (c) were measured using standard beam-switched photometry just prior to taking the images. Spectrum (b) was taken with the 3" beam centered on the nucleus and (c) was taken 13" south of the nucleus.

are considerably higher for the other data sets and, particularly on October 21 and November 9, are beyond what can reasonably be ascribed to measurement or extinction uncertainty.

The albedos at J and K are higher than the albedos derived for other periodic comets via similar dust models, including Halley preperihelion (Tokunaga *et al.* 1986) and P/Churyumov-Gerasimenko (Hanner *et al.* 1985) or even new comet Wilson (1986) at $r = 1.35$ AU (Hanner and Newburn 1989).

Bradfield's colors of $J-H = 0.45$ and $H-K = 0.10$ on January 14 are toward the neutral (less red) end of the range we have measured at the IRTF for comets at $r \leq 2.8$ AU (Hanner and Newburn 1989).

The quantity γ , defined by

$$\frac{(\lambda F_\lambda)_{\max}^{\text{VIS}}}{(\lambda F_\lambda)_{\max}^{\text{IR}}} = \frac{\gamma}{1 - \gamma} \quad (3)$$

is also a useful measure of the average albedo of the grains, since $(\lambda F_\lambda)_{\max}$ is proportional to the total energy under the Planck curve. We find $\gamma = 0.20$ – 0.25 for comet Bradfield, compared with 0.14 – 0.20 for comet Kohoutek at similar phase angles (Ney 1982). If the scattered radiation were isotropic, γ would be a measure of the single scattering albedo. Because the scattering function is strongly peaked in the forward direction, γ represents a lower limit to the single scattering albedo (Ney and Merrill 1976).

VII. DISCUSSION

Do the grains in comet Bradfield differ from those in comet Halley? We have seen that the shape of the silicate feature was similar in the two comets. A similar emission feature at $3.36 \mu\text{m}$, thought to be a signature of organic material, was detected in Bradfield at $r = 0.9$ AU by Brooke *et al.* (1988). Bradfield was unusual in displaying a strong silicate feature at $r = 1.45$ AU, a distance where Halley and other comets have, at most, a broader, weaker feature.

The picture in Halley was complicated by its extreme variability. The strength of the silicate feature varied from day to day (Gehrz and Ney 1986) and with position in the coma (Campins *et al.* 1987; Hanner *et al.* 1987). A higher albedo, and perhaps bluer color as well, were associated with brightness increases (Tokunaga *et al.* 1986; Campins and Tokunaga 1987). The mean $A_p(\theta)$ we derive for Bradfield on January 14 is slightly larger than the maximum Halley values.

Kikuchi *et al.* (1988) measured higher polarization of the scattered light in comet Bradfield than in the quiescent coma of Halley at phase angles $38^\circ < \theta < 65^\circ$. In Halley, higher polarization was observed in the inner coma ("fresh dust") than in the outer coma (Dollfus *et al.* 1988) and increased polarization was associated with outbursts (Kikuchi *et al.* 1987).

In general, then, the optical properties of the dust in Bradfield are similar to the active jets in Halley.

Higher polarization, less red color, higher albedo, and stronger silicate feature could be caused by (1) a higher proportion of small grains, $a \ll \lambda$; (2) a larger relative abundance of silicates; or (3) a difference in the way that the silicate and absorbing material are mixed. For example, it takes only a small fraction of absorbing material by mass to alter the color and albedo of a dielectric such as silicate, if the dark material is physically mixed with the silicate on a fine scale.

The dust detectors on the Halley space probes measured

changes in the size distribution along the probe trajectories, with steeper slope (more small grains) within dust jets (McDonnell *et al.* 1987). The dust composition experiment (PIA, PUMA) recorded differences in the mix of particle compositions along the trajectory, although this instrument sampled only the smallest dust particles (Clark, Mason, and Kissel 1987).

Halley and several low-activity comets detected in the infrared have hot, dark nuclear surfaces, too hot to be compatible with ice sublimation directly from the surface (see review by A'Hearn 1988). The ices sublimate below this mantle and the gas escapes either through cracks and local "bare" areas or directly through the porous mantle. From the *Giotto* images of Halley and the ratio of total gas production to surface area in the comets with known nuclear radii, it appears that most of the gas and dust is emitted from limited active areas.

Where, then, does the dust originate? Are the dust particles from the icy layer below the mantle, entrained by the sublimed gas, or are they dislodged from the surface by the outflowing gas? Surely, the size distribution will differ for these two cases and perhaps the composition as well, particularly if the surface has been altered by cosmic-ray bombardment or solar heating. Silicate grains in such a processed mantle are likely to be physically clumped into larger particles and coated with dark carbonaceous residue of processed organic material. The size distribution of the particles dislodged from the mantle will depend on the friability of the material (see, e.g., Gombosi *et al.* 1985) and may differ for different components.

Therefore, observed differences in dust properties among comets could reflect differences in the properties of the mantle (whether the mantle is primordial, recent thermal history, porosity, friability) and in the relative fraction of the grains coming from the mantle versus the "pristine" interior. One would expect the particles originating in the icy interior to be related more closely to interstellar grains than the dust from the mantle.

Possible interpretations of the similarities and differences between Halley and Bradfield are:

1. The jets in comet Halley and the dust in comet Bradfield contained a higher proportion of particles originating in the subsurface icy layer, including a population of small silicate grains with less carbonaceous material adhering to them than the grains in the mantle. The crystalline olivine grains were present initially in the comet nucleus; the perihelion temperature of Bradfield and Halley is not sufficient to anneal grains exposed on the nucleus surface. In Halley's quiescent periods, or when the jet activity subsided at larger r , grains from the mantle dominated the optical properties.

The more evolved short-period comets which lack a distinct silicate feature may shed their dust mainly from the mantle.

2. The volatility of the organic component in the grains may also have differed. The organic material "gluing" the dust in Bradfield and in the Halley jets may have volatilized readily when exposed to solar heating, causing the grains to fragment, whereas the grains on Halley's nuclear surface contained a more stable, carbonaceous residue, similar to that seen in interplanetary dust particles.

Loss of organic coatings on silicate grains due to heating at smaller r can explain why the silicate feature appears to be stronger in most comets at $r < 1$ AU, but cannot alone explain differences between comets at the same r , without prior thermal processing which makes the mantle material less volatile.

3. There were initial differences in the composition and/or clumping of the grains in the nucleus, perhaps due to formation at different heliocentric distances in the solar nebula.

VII. SUMMARY

In summary, Bradfield was unusual in displaying a prominent silicate feature in our CVF spectrum at 1.45 AU post-perihelion. The shape of the feature was very similar to that observed in Halley at smaller r , with a peak at $11.3 \mu\text{m}$ identified as crystalline olivine. The silicate feature was strong in all of our data sets near perihelion. The optical properties of the grains were similar to those in comet Halley's dust jets. The peak grain size derived by fitting the infrared spectral energy distribution at $r = 1.44$ AU is the same as that derived for Halley at 0.9 AU. The observed quantity $(\lambda F_\lambda)_{\text{max}}$, which measures the total infrared radiation from the dust coma, varied approximately as r^{-3} rather than r^{-4} . On the plausible assumption that the weighted mean dust grain velocity is proportional to the gas flux, $\bar{v} \propto r^{-1}$ and $Q_d \propto r^{-2}$.

We suggest that the differences in grain properties between comets could result from differences in the thermal history of the nuclear surface and in the relative fraction of the dust particles originating in the subsurface icy layer versus the devolatilized surface.

We thank the staff of the WIRO and the IRTF for their support. Don Yeomans kindly provided updated ephemerides. We thank Humberto Campins for discussing his Halley data with us prior to publication and providing Figure 4b. The University of Minnesota infrared astronomy program is supported by NASA, the United States Air Force, the National Science Foundation, and the University of Minnesota Graduate School. Part of this research was carried out at the Jet Propulsion Laboratory, California Institute of Technology, under contract with the National Aeronautics and Space Administration (Planetary Astronomy Program).

REFERENCES

- A'Hearn, M. F. 1988, in *Ann. Rev. Earth and Planetary Sci.*, **16**, 273.
 Aitken, D. K., Roche, P. F., Smith, C. H., James, S. D., and Hough, J. H. 1988, *M.N.R.A.S.*, **230**, 629.
 Baas, F., Geballe, T. R., and Walther, D. M. 1986, *Ap. J. (Letters)*, **311**, L97.
 Bregman, J. D., Campins, H., Witteborn, F. C., Wooden, D. H., Rank, D. M., Allamandola, L. J., Cohen, M., and Tielens, A. G. G. M. 1987, *Astr. Ap.*, **187**, 616.
 Brooke, T. Y., Knacke, R. F., Owen, T. C., Tokunaga, A. T., Mumma, M., Reuter, D., and Storrs, A. 1988, *Bull. AAS*, **20**, 819.
 Campbell, D. B., Harmon, J. K., and Shapiro, I. I. 1989, *Ap. J.*, **338**, 1094.
 Campins, H. C., and Ryan, E. V. 1989, *Ap. J.*, **341**, 1059.
 Campins, H. C., Telesco, C. M., Decher, R., and Ramsey, B. D. 1987, *Astr. Ap.*, **187**, 601.
 Campins, H., and Tokunaga, A. 1987, in *Infrared Observations of Comets Halley and Wilson and Properties of the Grains*, ed. M. S. Hanner (NASA C.P. 3004), p. 1.
 Clark, B. C., Mason, L. W., and Kissel, J. 1987, *Astr. Ap.*, **187**, 779.
 Combes, M., et al. 1986, *Nature*, **321**, 266.
 Combes, M., et al. 1988, *Icarus*, **76**, 404.
 Danks, A. C., Encrenaz, T., Bouchet, P., LeBertre, T., and Chababiev, A. 1987, *Astr. Ap.*, **184**, 329.
 Day, K. L. 1974, *Ap. J. (Letters)*, **192**, L15.
 ———, 1981, *Ap. J.*, **246**, 110.
 Divine, T. N., and Newburn, R. L. 1987, *Astr. Ap.*, **187**, 867.
 Dollfus, A., Bastien, P., Le Borgne, J.-F., Levasseur-Regourd, A. C., and Mukai, T. 1988, *Astr. Ap.*, **206**, 348.
 Elias, J. H., Frogel, J. A., Matthews, K., and Neugebauer, G. 1982, *A.J.*, **87**, 1029.
 Gehr, R. D., Grasdalén, G. L., and Hackwell, J. A. 1987, in *Encyclopedia of Physical Science and Technology*, **2**, 53.
 Gehr, R. D., and Hackwell, J. A. 1978, *Sky Tel.*, **55**, 466.
 Gehr, R. D., Hackwell, J. A., and Jones, T. W. 1974, *Ap. J.*, **191**, 675.
 Gehr, R. D., Hackwell, J. A., and Smith, J. R. 1976, *Pub. A.S.P.*, **88**, 971.
 Gehr, R. D., and Ney, E. P. 1986, in *Exploration of Halley's Comet* (ESA SP-250), Vol. II, p. 101.
 Gombosi, T. I. 1987, preprint.
 Gombosi, T. I., Cravens, T. E., and Nagy, A. F. 1985, *Ap. J.*, **293**, 328.
 Grasdalén, G. L., Hackwell, J. A., and Gehr, R. D. 1984, *Pub. A.S.P.*, **96**, 1017.
 Hanner, M. S. 1983, in *Cometary Exploration*, ed. T. I. Gombosi, Vol. 2, p. 1.
 ———, 1984, *Adv. Space Res.*, **4**, No. 9, 189.
 ———, ed. 1987, *Infrared Observations of Comets Halley and Wilson and Properties of the Grains* (NASA C.P. 3004).

- Hanner, M. S., Giese, R. H., Weiss, K., and Zerull, R. 1981, *Astr. Ap.*, **104**, 42.
 Hanner, M. S., and Newburn, R. L. 1989, *A.J.*, **97**, 254.
 Hanner, M. S., Tedesco, E., Tokunaga, A. T., Veeder, G. J., Lester, D. F., Witteborn, F. C., Bregman, J. D., Gradie, J., and Lebofsky, L. 1985, *Icarus*, **64**, 11.
 Hanner, M. S., and Tokunaga, A. T. 1989, in *Comets in the Post-Halley Era*, ed. R. L. Newburn, M. M. Neugebauer, and J. Rahe (Dordrecht: Kluwer), in press.
 Hanner, M. S., Tokunaga, A. T., Golisch, W. F., Griep, D. M., and Kaminski, C. D. 1987, *Astr. Ap.*, **187**, 653.
 Hanner, M. S., Tokunaga, A. T., Veeder, G. J., and A'Hearn, M. F. 1984, *A.J.*, **89**, 162.
 Hayward, T., Gehr, R. D., and Grasdalén, G. L. 1986, *Nature*, **326**, 55.
 Herter, T., Campins, H., and Gull, G. E. 1987, *Astr. Ap.*, **187**, 629.
 Kikuchi, S., Mikami, Y., Mukai, T., and Mukai, S. 1988, *Astr. Ap.*, in press.
 Kikuchi, S., Mikami, Y., Mukai, T., Mukai, S., and Hough, J. H. 1987, *Astr. Ap.*, **187**, 689.
 Knacke, R. F., Brooke, T. Y., and Joyce, R. R. 1986, *Ap. J. (Letters)*, **310**, L49.
 Lawler, M. E., Brownlee, D. E., Temple, S., and Wheelock, M. M. 1988, *Icarus*, **80**, 225.
 McDonnell, J. A. M., et al. 1987, *Astr. Ap.*, **187**, 719.
 McDonnell, J. A. M., Green, S. F., Nappo, S., Pankiewicz, G. S., Perry, C. H., and Zarnecki, J. C. 1989, Paper presented at Conference on Comets in the Post-Halley Era, Bamberg FRG 1989 April 24-28.
 Merrill, K. 1974, *Icarus*, **23**, 566.
 Nelson, R., Nuth, J. A., and Donn, B. 1987, *Proc. 17th Lunar Planetary Sci. Conf., J. Geophys. Res.* (**92**, No. B4), p. E657.
 Ney, E. P. 1974, *Icarus*, **23**, 551.
 ———, 1982, in *Comets*, ed. L. L. Wilkening (Tucson: University of Arizona Press), p. 323.
 Ney, E. P., and Merrill, K. M. 1976, *Science*, **194**, 1051.
 Russell, R. W., Lynch, D. K., and Chatelain, M. A. 1988, in preparation.
 Sandford, S. A., and Walker, R. M. 1985, *Ap. J.*, **291**, 838.
 Sinton, W. M., and Tittmore, W. C. 1984, *A.J.*, **89**, 1366.
 Stephens, J. R., and Russell, R. W. 1979, *Ap. J.*, **228**, 780.
 Tokunaga, A. T. 1984, *A.J.*, **89**, 172.
 Tokunaga, A. T., Golisch, W. F., Griep, D. M., Kaminski, C. D., and Hanner, M. S. 1986, *A.J.*, **92**, 1183.
 ———, 1988, *A.J.*, **96**, 1971.
 Wickramasinghe, D. T., and Allen, D. A. 1986, *Nature*, **323**, 44.
 Zalkowski, A., Knacke, R. F., and Porco, C. C. 1975, *Ap. Space Sci.*, **35**, 97.

R. D. GEHRZ, T. HARRISON, and E. P. NEY: Department of Astronomy, University of Minnesota, 116 Church St., S.E., Minneapolis, MN 55455

M. S. HANNER and R. L. NEWBURN, JR.: Jet Propulsion Laboratory, Mail Stop 169-237, 4800 Oak Grove Drive, Pasadena, CA 91109

T. L. HAYWARD: Box 3905, University of Wyoming, University Station, Laramie, WY 82071

